

V/STOL TILT ROTOR AIRCRAFT STUDY

VOLUME X

PERFORMANCE AND STABILITY TEST OF A 1/4.622 FROUDE SCALED BOEING VERTOL MODEL 222 TILT ROTOR AIRCRAFT (PHASE I)

F.J. McHUGH

W. EASON

H. R. ALEXANDER

H. MUTTER

OCTOBER 1973

PREPARED UNDER CONTRACT NO. NAS2-6598 PHASE 3 (TASK C)

FOR

NATIONAL AERONAUTICS AND SPACE ADMINISTRATION
AMES RESEARCH CENTER

BY

BOEING VERTOL COMPANY

A DIVISION OF THE BOEING COMPANY

P. O. BOX 16858

PHILADELPHIA, PENNSYLVANIA 19142

THE **BOEING** COMPANY

VERTOL DIVISION • PHILADELPHIA, PENNSYLVANIA

CODE IDENT. NO. 77272

NUMBER D222-10053-1

V/STOL TILT ROTOR AIRCRAFT STUDY
VOLUME X

TITLE PERFORMANCE AND STABILITY TEST OF A

1/4.622 FROUDE SCALED BOEING VERTOL

MODEL 222 TILT ROTOR AIRCRAFT (PHASE I)

ORIGINAL RELEASE DATE _____. FOR THE RELEASE DATE OF
SUBSEQUENT REVISIONS, SEE THE REVISION SHEET. FOR LIMITATIONS
IMPOSED ON THE DISTRIBUTION AND USE OF INFORMATION CONTAINED
IN THIS DOCUMENT, SEE THE LIMITATIONS SHEET.

MODEL 222 CONTRACT NAS2-6598

ISSUE NO. _____ ISSUED TO: _____

PREPARED BY E. J. MC HUGH

DATE 8/10/73

PREPARED BY

~~APPROVED BY~~

W. EASON

DATE _____

PREPARED BY

~~APPROVED BY~~

H. ALEXANDER

DATE 11/1/73

PREPARED BY

~~APPROVED BY~~

H. MITTER

DATE 8/10/73

APPROVED BY

K. GILLMORE

DATE 8/10/73

APPROVED BY

D. RICHARDSON

DATE 8/10/73

LIMITATIONS

This document is controlled by Organization 7040

All revisions to this document shall be approved by the
above noted organization prior to release.

ACTIVE SHEET RECORD

SHEET NUMBER	REV LTR	ADDED SHEETS				SHEET NUMBER	REV LTR	ADDED SHEETS			
		SHEET NUMBER	REV LTR	SHEET NUMBER	REV LTR			SHEET NUMBER	REV LTR	SHEET NUMBER	REV LTR
1						46					
2						47					
3						48					
4						49					
5						50					
6						51					
7						52					
8						53					
9						54					
10						55					
11						56					
12						57					
13						58					
14						59					
15, 15A						60					
16						61					
17						62					
18						63					
19						64					
20						65					
21						66					
22						67					
23						68					
24						69					
25						70					
26						71					
27						72					
28						73					
29						74					
30						75					
31						76					
32						77					
33						78					
34						79					
35						80					
36						81					
37						82					
38						83					
39						84					
40						85					
41						86					
42						87					
43						88					
44						89					
45						90					

ACTIVE SHEET RECORD

SHEET NUMBER	REV LTR	ADDED SHEETS				SHEET NUMBER	REV LTR	ADDED SHEETS			
		SHEET NUMBER	REV LTR	SHEET NUMBER	REV LTR			SHEET NUMBER	REV LTR	SHEET NUMBER	REV LTR
91						136					
92						137					
93						138					
94						139					
95						140					
96						141					
97						142					
98						143					
99						144					
100						145					
101						146					
102						147					
103						148					
104						149					
105						150					
106						151					
107						152					
108						153					
109						154					
110						155					
111						156					
112						157					
113						158					
114						159					
115						160					
116						161					
117						162					
118						163					
119						164					
120						165					
121						166					
122						167					
123						168					
124						169					
125						170					
126						171					
127						172					
128						173					
129						174					
130						175					
131						176					
132						177					
133						178					
134						179					
135						180					

ACTIVE SHEET RECORD

SHEET NUMBER	REV LTR	ADDED SHEETS				SHEET NUMBER	REV LTR	ADDED SHEETS			
		SHEET NUMBER	REV LTR	SHEET NUMBER	REV LTR			SHEET NUMBER	REV LTR	SHEET NUMBER	REV LTR
181						226					
182						227					
183						228					
184						229					
185						230					
186						231					
187						232					
188						233					
189						234					
190						235					
191						236					
192						237					
193						238					
194						239					
195						240					
196						241					
197						242					
198						243					
199						244					
200						245					
201						246					
202						247					
203						248					
204						249					
205						250					
206						251					
207						252					
208						253					
209						254					
210						255					
211						256					
212						257					
213						258					
214						259					
215						260					
216						261					
217						262					
218						263					
219						264					
220						265					
221						266					
222						267					
223						268					
224						269					
225						270					

ACTIVE SHEET RECORD

SHEET NUMBER	REV LTR	ADDED SHEETS				SHEET NUMBER	REV LTR	ADDED SHEETS			
		SHEET NUMBER	REV LTR	SHEET NUMBER	REV LTR			SHEET NUMBER	REV LTR	SHEET NUMBER	REV LTR
271						316					
272						317					
273						318					
274						319					
275						320					
276						321					
277						322					
278						323					
279						324					
280						325					
281						326					
282						327					
283						328					
284						329					
285						330					
286						331					
287						332					
288						333					
289						334					
290						335					
291						336					
292						337					
293						338					
294						339					
295						340					
296						341					
297						342					
298						343					
299						344					
300						345					
301						346					
302						347					
303						348					
304						349					
305						350					
306						351					
307						352					
308						353					
309						354					
310						355					
311						356					
312						357					
313						358					
314						359					
315						360					

ACTIVE SHEET RECORD

SHEET NUMBER	REV LTR	ADDED SHEETS				SHEET NUMBER	REV LTR	ADDED SHEETS			
		SHEET NUMBER	REV LTR	SHEET NUMBER	REV LTR			SHEET NUMBER	REV LTR	SHEET NUMBER	REV LTR
361						406					
362						407					
363						408					
364						409					
365						410					
366						411					
367						412					
368						413					
369						414					
370						415					
371						416					
372						417					
373						418					
374						419					
375						420					
376						421					
377						422					
378						423					
379						424					
380						425					
381						426					
382						427					
383						428					
384						429					
385						430					
386						431					
387						432					
388						433					
389						434					
390						435					
391						436					
392						437					
393						438					
394						439					
395						440					
396						441					
397						442					
398						443					
399						444					
400						445					
401						446					
402						447					
403						448					
404						449					
405						450					

ACTIVE SHEET RECORD

SHEET NUMBER	REV LTR	ADDED SHEETS				SHEET NUMBER	REV LTR	ADDED SHEETS			
		SHEET NUMBER	REV LTR	SHEET NUMBER	REV LTR			SHEET NUMBER	REV LTR	SHEET NUMBER	REV LTR
451											
452											
453											
454											
455											
456											
457											
458											
459											
460											

FOREWORD

This report is one of a series prepared by The Boeing Vertol Company, Philadelphia, Pennsylvania for the National Aeronautics and Space Administration, Ames Research Center, Moffett Field, California under contract NAS2-6598. The studies reported under Volumes I through IV and VIII through X were jointly funded by NASA and the U.S. Army Air Mobility Research and Development Laboratory, Ames Directorate. Volumes V through VII were funded by the U. S. Air Force Flight Dynamics Laboratory, Wright Patterson Air Force Base, Ohio.

This contract was administered by the National Aeronautics and Space Administration. Mr. Richard J. Abbott was the Contract Administrator, Mr. Gary B. Churchill, Tilt Rotor Research Aircraft Project Office, was the Technical Monitor, and coordination and liaison with the U.S. Air Force Flight Dynamics Laboratory was through Mr. D. Fraga. The Boeing Vertol Project Engineer for the work reported in Volume X was Mr. F.J. McHugh.

The complete list of reports published under this contract is as follows:

- Volume I -- Conceptual Design of Useful Military and/or Commercial Aircraft, NASA CR-114437
- Volume II -- Preliminary Design of Research Aircraft, NASA CR-114438
- Volume III -- Overall Research Aircraft Project Plan, Schedules, and Estimated Cost, NASA CR-114439
- Volume IV -- Wind Tunnel Investigation Plan for a Full Scale Tilt Rotor Research Aircraft, CR-114440
- Volume V -- Definition of Stowed Rotor Research Aircraft, NASA CR-114598
- Volume VI -- Preliminary Design of a Composite Wing for Tilt Rotor Aircraft, NASA CR-114599
- Volume VII -- Tilt Rotor Flight Control Program Feedback Studies, NASA CR-114600
- Volume VIII - Mathematical Model for a Real Time Simulation of a Tilt Rotor Aircraft (Boeing Vertol Model 222), NASA CR-114601
- Volume IX -- Piloted Simulator Evaluation of the Boeing Vertol Model 222 Tilt Rotor Aircraft, NASA CR-114602
- Volume X -- Performance and Stability Test of a 1/4.622 Froude Scaled Boeing Vertom Model 222 Tilt Rotor Aircraft (Phase I), NASA CR-114603

ABSTRACT

Wind tunnel test data obtained from a 1/4.622 Froude scale Boeing Model 222 with a full span, two prop, tilt rotor, powered model in the Boeing V/STOL wind tunnel are reported. Data were taken in transition and cruise flight conditions and include performance, stability and control and blade loads information. The effects of the rotors, tail surfaces and airframe on the performance and stability are isolated as are the effects of the airframe on the rotors.

The rotors are dynamically representative of the full scale aircraft rotor tested under NASA Contract NAS2-6505. Predicted rotor frequencies were verified, both static and rotating, and since they influence rotor response characteristics, correlation for stability and blade load data is included.

TABLE OF CONTENTS

	<u>PAGE</u>
FOREWORD	ix
ABSTRACT	x
SUMMARY	xiii
PERFORMANCE	xiii
STABILITY & CONTROL	xiv
ROTOR LOADS	xvii
DYNAMICS	xviii
LIST OF ILLUSTRATIONS	xxxi
LIST OF TABLES	LVI
LIST OF SYMBOLS	LVII
1.0 INTRODUCTION	1
2.0 OBJECTIVES	3
3.0 TEST INSTALLATION	9
3.1 Model Description	9
3.2 Tunnel Installation	17
3.3 Data Reduction	23
3.4 Test Program	25
3.5 Model Problems	27
4.0 PERFORMANCE	34
4.1 Transition Performance	35
4.1.1 Rotor Performance	35
4.1.2 Aircraft Performance	49
4.2 Cruise Performance	55
4.2.1 Rotor Performance	55
4.2.2 Aircraft Performance	74
4.3 Comparison of Test and Theory	82
5.0 STABILITY AND CONTROL	85
5.1 Transition Stability and Control	86

TABLE OF CONTENTS

	<u>PAGE</u>
5.1.1 Rotor Stability Derivatives	87
5.1.2 Aircraft Stability Derivatives	115
5.1.3 Control Power and Mixing	137
5.1.4 Comparison of Test and Theory in Transition	199
5.2 Cruise Stability	211
5.2.1 Rotor Stability Derivatives	211
5.2.2 Aircraft Stability Derivatives	253
5.2.3 Control Effectiveness	283
5.2.4 Comparison of Test & Theory in Cruise.	326
6.0 ROTOR LOADS	341
6.1 Blade Frequency	342
6.1.1 Non-Rotating Frequency	342
6.1.2 Rotating Frequency	342
6.2 Transition Blade Loads	348
6.2.1 Attitude Effects	348
6.2.2 Effects of Nacelle Incidence	349
6.2.3 Cyclic Pitch Effects	349
6.3 Cruise Blade Loads	357
6.3.1 Attitude Effects	357
6.3.2 Effect of Forward Speed	357
6.3.3 Cyclic Pitch Effects	358
7.0 DYNAMICS	369
7.1 Model Frequencies	370
7.2 Aeroelastic Stability and Damping	372
7.2.1 Cruise	372
7.2.2 Hover	373
7.2.3 Transition	373
8.0 CONCLUSIONS AND RECOMMENDATIONS	381
9.0 REFERENCES	383
APPENDICES	384
A - RUN LOG	384
B - DEFLECTION TESTS	401
C - MODEL WEIGHTS AND BALANCE	429
D - HUB TARES	436
E - RESULTS OF FLOW VISUALIZATION OF THE 1/4.622 SCALE MODEL 222 - BVWT 096	445

SUMMARY

The primary objective of this wind tunnel test program was to obtain steady state rotor and aircraft loads, aerodynamic and aeroelastic characteristics of a tilt rotor model. A 1/4.622 scale full span, powered model that was dynamically scaled from the Model 222 Tilt Rotor Research Aircraft was utilized.

Testing accomplished was only a portion of the first program of Phase IV of NASA contract NAS2-6598. Model mechanical and instrumentation problems prevented completion of the program. This report summarizes the test data obtained, from mid transition into the cruise regime, and is divided into performance, stability and control, rotor loads and dynamics.

Performance

Performance data was obtained for the rotor, airframe and aircraft showing the effects of pitch and yaw attitude as well as the effects of flap deflection, rotor cyclic and rotor collective in transition. Flap deflection and lateral cyclic have a slight effect on rotor performance in mid transition and cruise. Longitudinal cyclic produces an effect equivalent to 40 percent of that produced by collective in transition, but has a negligible effect on cruise rotor performance. The airframe characteristics presented in Figure 1, indicate that wing stall occurs at approximately 14-degrees while the tail provides sufficient lift to delay total airframe stall to 17-degrees. Total aircraft performance in transition is presented in Figure 2, defining the lift and propulsive force characteristics. Imposed on the figure is an aircraft lift coefficient of 2.45 which represents the full scale vehicle at a gross weight of 13,500 pounds.

Accounting for the difference in drag between the model and the aircraft ($\Delta C_D = 0.1$) indicates that "lg" transition flight can easily be achieved. Similar data was obtained in cruise up to 182 feet per second (225 knots equivalent full scale speed) and is presented in Section 4.

Stability and Control

In conjunction with the performance testing, stability and control data was obtained showing the effects of pitch and yaw attitude as well as the effects of aircraft control, rotor cyclic and collective in transition. The effect of flap deflection on rotor normal force and pitching moment is very slight for the mid transition speed of 72 feet per second (90 knots equivalent full scale speed) with a nacelle incidence of 41.6-degrees. Rotor longitudinal stability characteristics were obtained for a nacelle incidence of 30-degrees at this same speed and indicates that the rotor stability derivatives are increasing as the nacelle incidence decreases. During transition from hover to cruise the major portion of control is obtained from rotor cyclic and collective pitch. Summarized in Section 5 are the rotor force and moment derivatives with cyclic at the mid transition test condition.

The rotor stability derivatives obtained during the yaw testing in cruise were not significantly effected by flap deflection. The effect of lift is quite evident in Figure 3 by the distinct change in rotor normal force level. Data obtained from the pitch sweeps, define the stability derivatives including the wing lift variation with angle of attack as well as the flap effect.

Figure 4 presents this comparison, including the testing performed at all speeds or advance ratios. The area between the trends obtained from yaw sweeps and pitch sweeps is a result of the wing lift influence and is indicated by the shaded area. The lift influence on the force derivatives appears to be an advance ratio squared (μ^2) and the influence on the moment derivatives appears to be a μ^4 effect. As seen in the normal force and pitching moment trend the wing lift effect on the rotor produces a destabilizing contribution to the aircraft stability and must be accounted for in analyzing the aircraft.

Figure 4 presents a concise summary of the rotor derivatives as influenced by forward speed. It indicates a significant increase in normal force derivative with speed while the pitching moment derivative is decreasing and becoming stable at an advance ratio of approximately 0.66.

Cyclic effectiveness was investigated in the cruise regime to define inputs into the low rate feedback system for blade load alleviation. A summary of the cyclic derivatives is presented in Section 5.

Stability and control data were obtained for the transition condition at a tunnel speed of 72 fps representing a full scale equivalent velocity of 90 knots. Results of the tests indicate adequate longitudinal and directional stability at all conditions tested.

Generally the lift curve slope C_{L_α} is lower than estimated and $\frac{dC_m}{dC_L}$ indicates a neutral point location much further aft than predicted at the test Reynolds number of 0.6×10^6 for the rotors off

airframe with tail on as indicated in Figure 5. Addition of the rotors results in a forward shift of neutral point and a substantial increase in lift curve slope. Directional stability is decreased with addition of rotors but is still adequate. The tail contribution to directional stability is higher than predicted.

Control effectiveness is indicated to be good in transition. The combination of aircraft and rotor controls yields quite high control power at all conditions. Spoiler effectiveness with flaps extended is indicated to be lower than predicted, $C_{l_{\max}} = 0.0706$ at 45-degrees δ_F compared to 0.100. This is believed to result at least partially from the low Reynolds number resulting in flow separation over the flap upper surface with the spoiler closed. Rudder effectiveness agrees well with predictions and elevator effectiveness is indicated to be lower than predicted, $C_{m_{\delta_e}} = -.023$ compared to $-.031$ predicted. Change in pitching moment coefficient with longitudinal cyclic, $C_{m_{B_1}}$, is, however, higher than predicted, $-.122$ compared to $-.0837$ predicted.

Aircraft stability derivatives derived from test data for the cruise configuration follow the same trends as for the transition configurations. The longitudinal stability is presented in Figure 6 indicating the increments of stability resulting from the horizontal tail and rotor. An adequate longitudinal stability level is indicated for the tail on configurations at all conditions tested. Lateral/directional stability data indicates an adequate level of stability.

Control power about all axes is indicated to be high in the cruise configuration where all control for maneuver is derived from the airplane control surfaces. Elevator effectiveness is indicated to be lower than predicted, $C_{m\delta_e} = -.0242$ compared to $-.0310$ predicted. Adequate longitudinal control power, with ± 20 -degrees elevator deflection, is available for all cruise trim and maneuver requirements. Spoiler rolling moment effectiveness is indicated to be higher than predicted and aileron rolling moment lower than predicted. Rudder yawing moment effectiveness, $C_{n\delta_r}$, and flap lift effectiveness, C_{L_F} , agree well with predictions. The application of the cyclic for blade load minimization as would be achieved with low rate feedback produces a stabilizing effect on the rotor as indicated by the normal force trend in Figure 7.

Rotor Loads

A definition of the blade frequency characteristics obtained during this model test program are presented in Figure 8 together with the prediction for hover and cruise collectives. First mode bending is in-plane and the prediction is approximately the same as the characteristics obtained from blade flap bending tweaks. Second mode bending prediction is out of plane and is lower than the chord bending tweaks. Data obtained during hover checkout define the 1 per rev and 2 per rev crossings. From the data of Section 7.2 minimum damping of the wing vertical bending mode occurs at 1030 RPM indicating that, in cruise, lower blade lag and wing vertical bending coalesce at this point. This indicates that the blade lag frequency is 742 CPM and verifies the cruise mode bending frequency prediction.

In transition the effect of flap deflection on blade loads is equivalent to decreasing the angle of attack by 5-degrees for minimum blade loads and increasing the minimum blade loads by the equivalent to 2-degrees angle of attack. Cyclic pitch effects on flap bending loads are small but the impact on chord bending loads is significant, being 15 times more effective than angle of attack.

In cruise the blade load data obtained from a yaw sweep is representative of an isolated rotor. When comparing this data with that obtained from a pitch sweep indicates a decrease of approximately 20 percent in blade loads, further verification that increased lift has the effect equivalent to reducing the angle of attack.

Cyclic effectiveness data was obtained in cruise as baseline data for the low rate feedback, blade load alleviation systems. A summary of these effects is shown in Figure 9 with the manual simulation of the feedback. The blade loads are maintained at the minimum level over a wider range of angle of attack than for the constant cyclic case.

Dynamics

The dynamic data obtained for the model indicate that its characteristics are substantially different than the full scale Model 222 and the stand upon which it was mounted introduced additional modes which significantly alter the dynamic behavior of the model. It is evident that this data can only be used as a base for verifying the analytical techniques. The dynamics data has been converted to full scale in this report.

The predicted cruise aeroelastic stability boundaries are shown in Figure 10 indicating that the conditions tested were stable and fall within the region predicted to be stable. At 90 knots the rotor speed was increased from 386 RPM (cruise) to 551 RPM (hover) and the measured damping was stable. Figure 11 presents this data showing a minimum damping of 1.5 percent as compared to 0.5 percent for the theory. The theory has indicated it is conservative in hover and transition in the lightly damped regions.

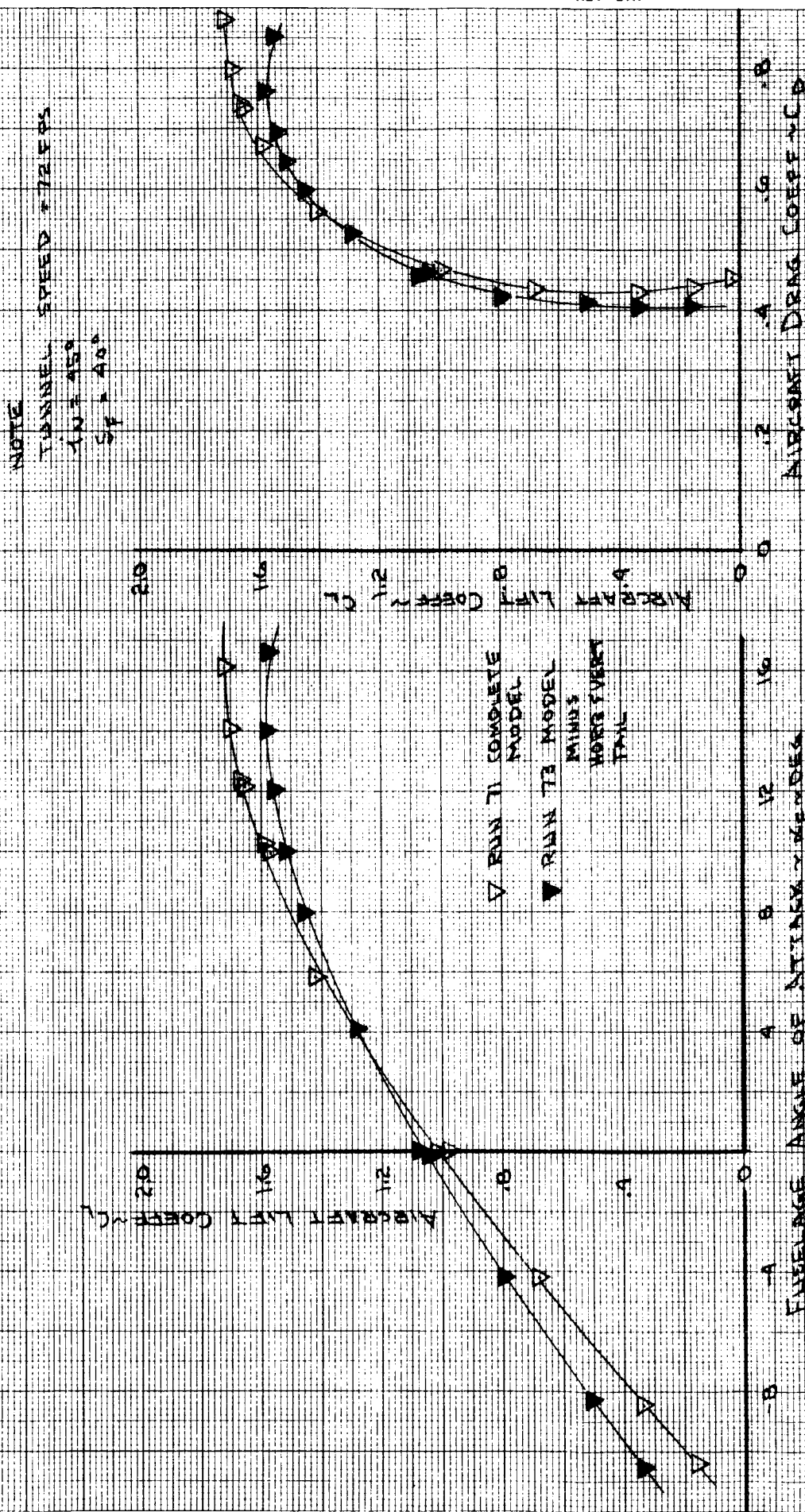


FIGURE 1 AIRFRAME PERFORMANCE CHARACTERISTICS IN TRANSITION

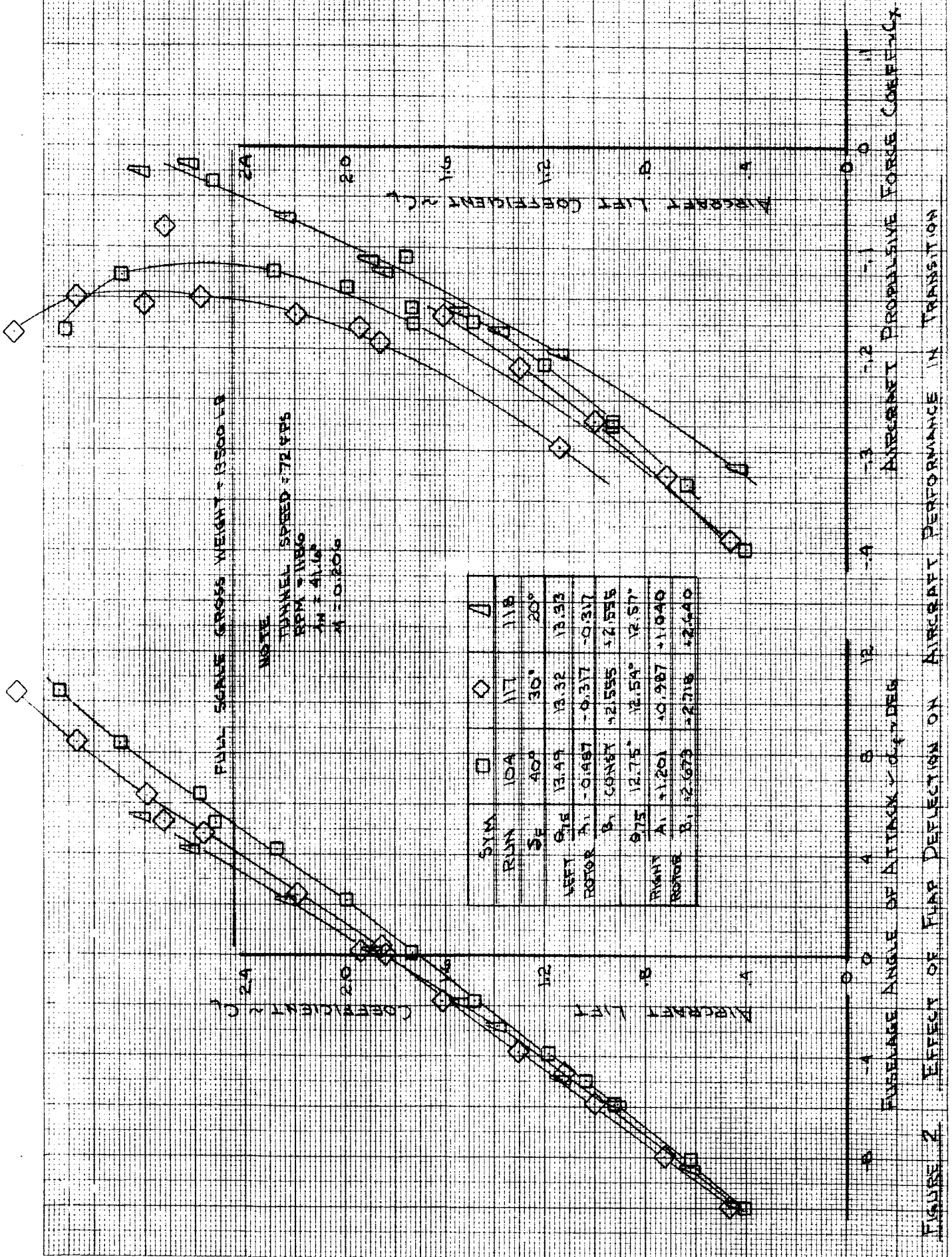


FIGURE 2 EFFECT OF FLAP DEFLECTION ON AIRCRAFT PERFORMANCE IN TRANSITION

RIGHT ROTOR

RUN	SYM	Sc	$\frac{C_{Np}}{2\psi}$
32	▽	0	0.000003
34	□	40	0.000003
36	○	20	0.000003

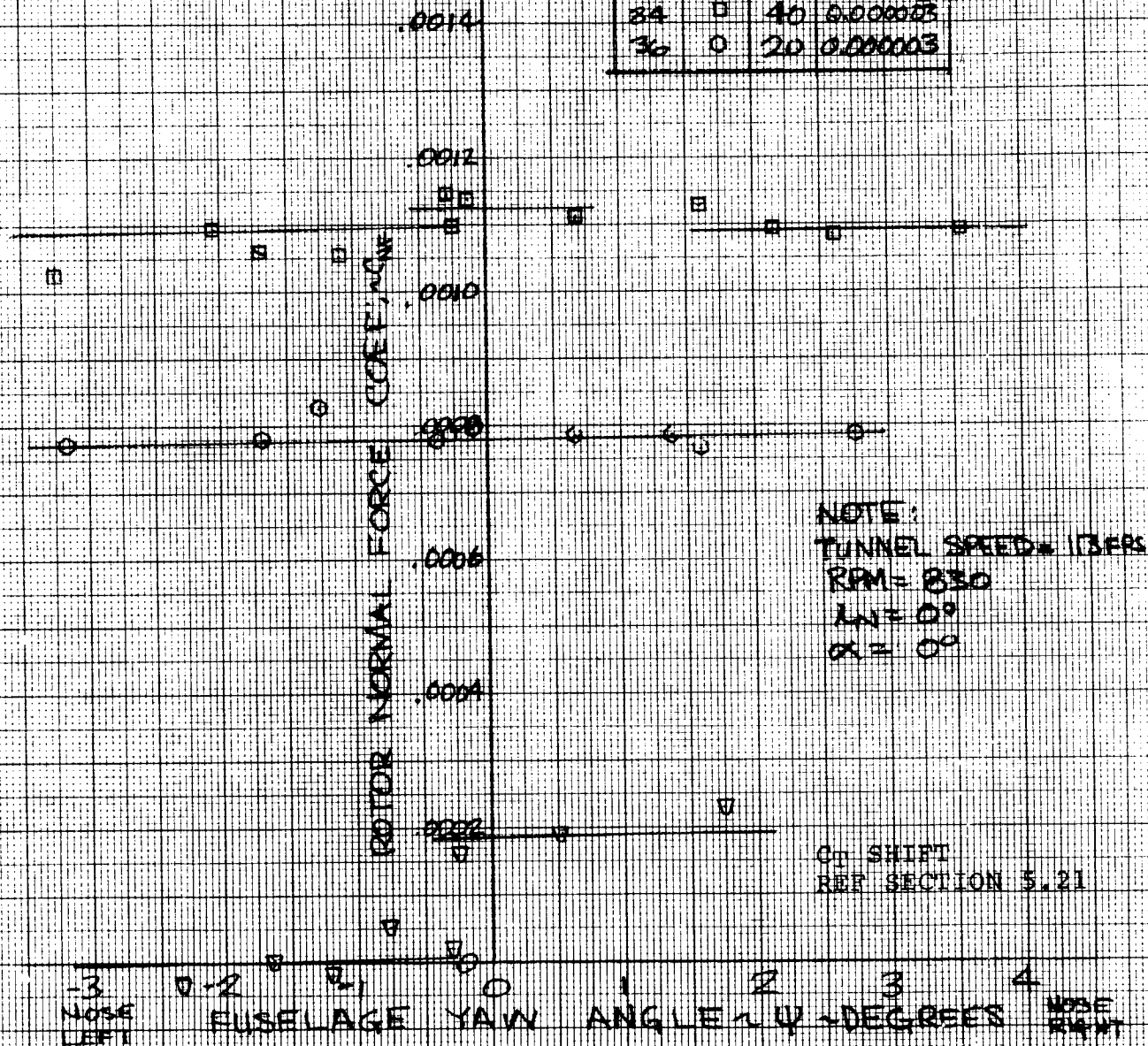


FIGURE 3 EFFECT OF FUSELAGE YAW ANGLE AND FLAP DEFLECTION ON ROTOR NORMAL FORCE COEFFICIENT IN CRUISE

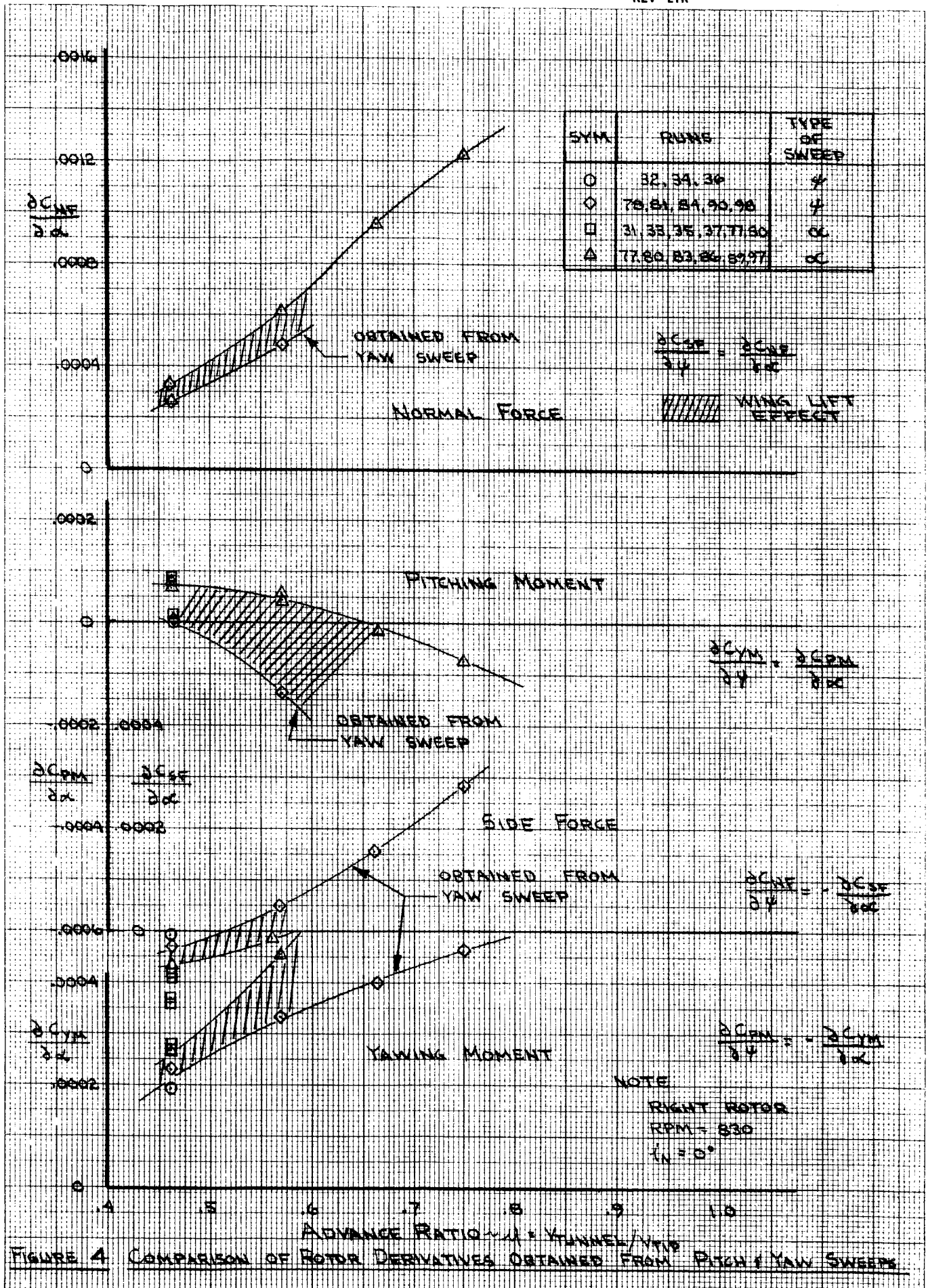


FIGURE 4 COMPARISON OF ROTOR DERIVATIVES OBTAINED FROM PITCH/YAW SWEEPS

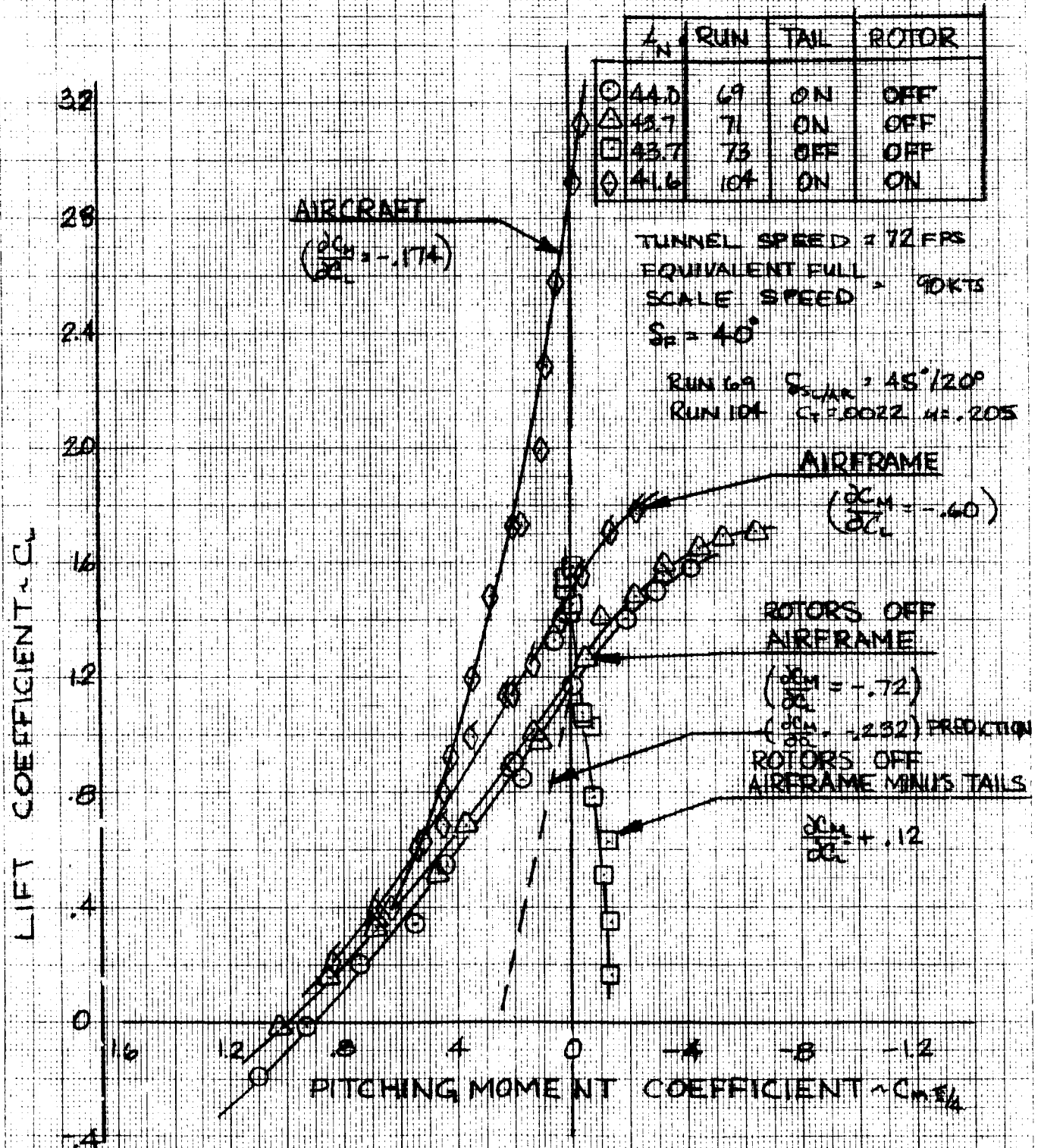


FIGURE 5 LONGITUDINAL STABILITY IN TRANSITION
VARIATION OF PITCHING MOMENT WITH
LIFT COEFFICIENT

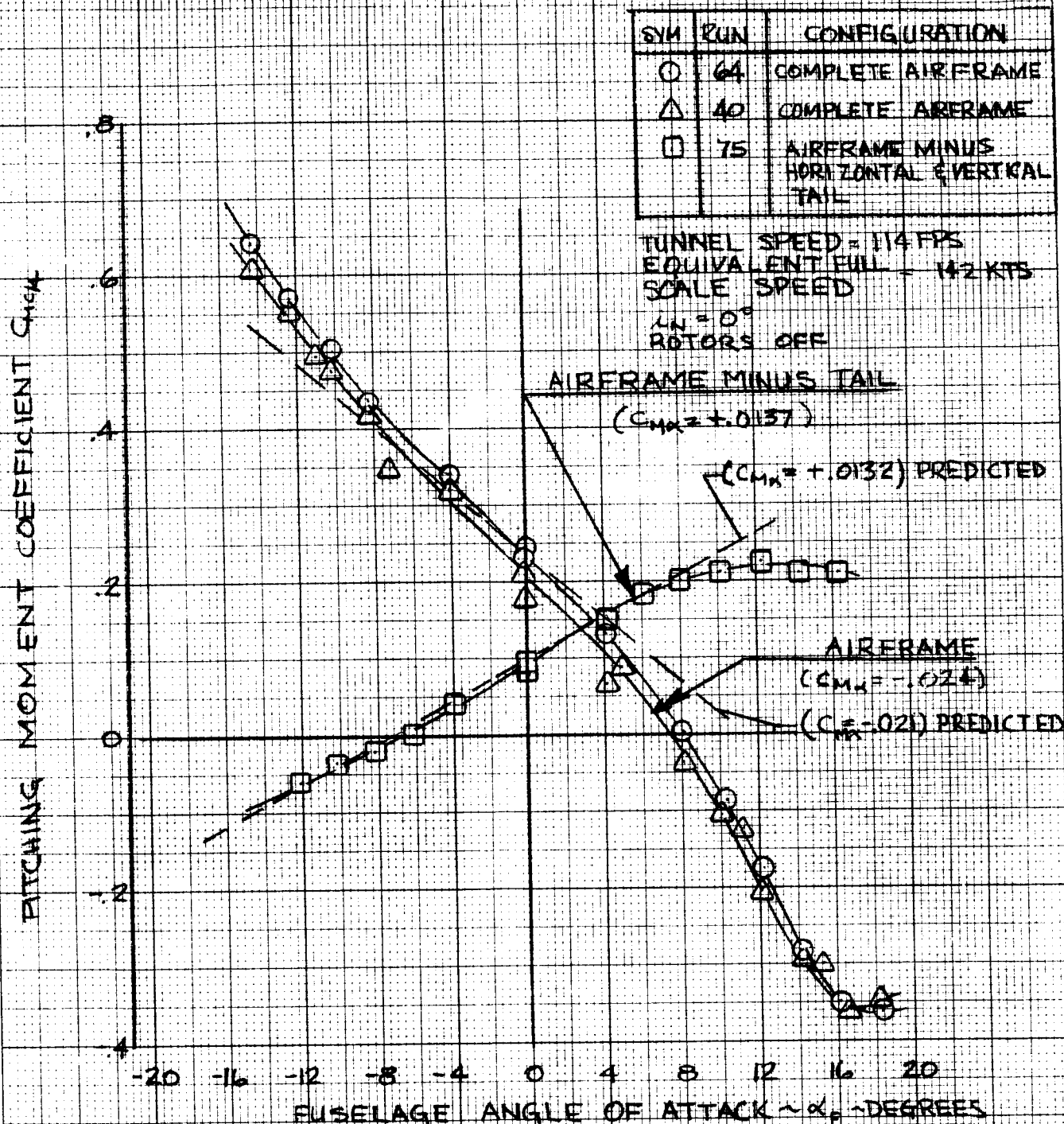


FIGURE 6 LONGITUDINAL STABILITY IN CRUISE
EFFECT OF HORIZONTAL AND VERTICAL TAIL
ON PITCHING MOMENT COEFFICIENT

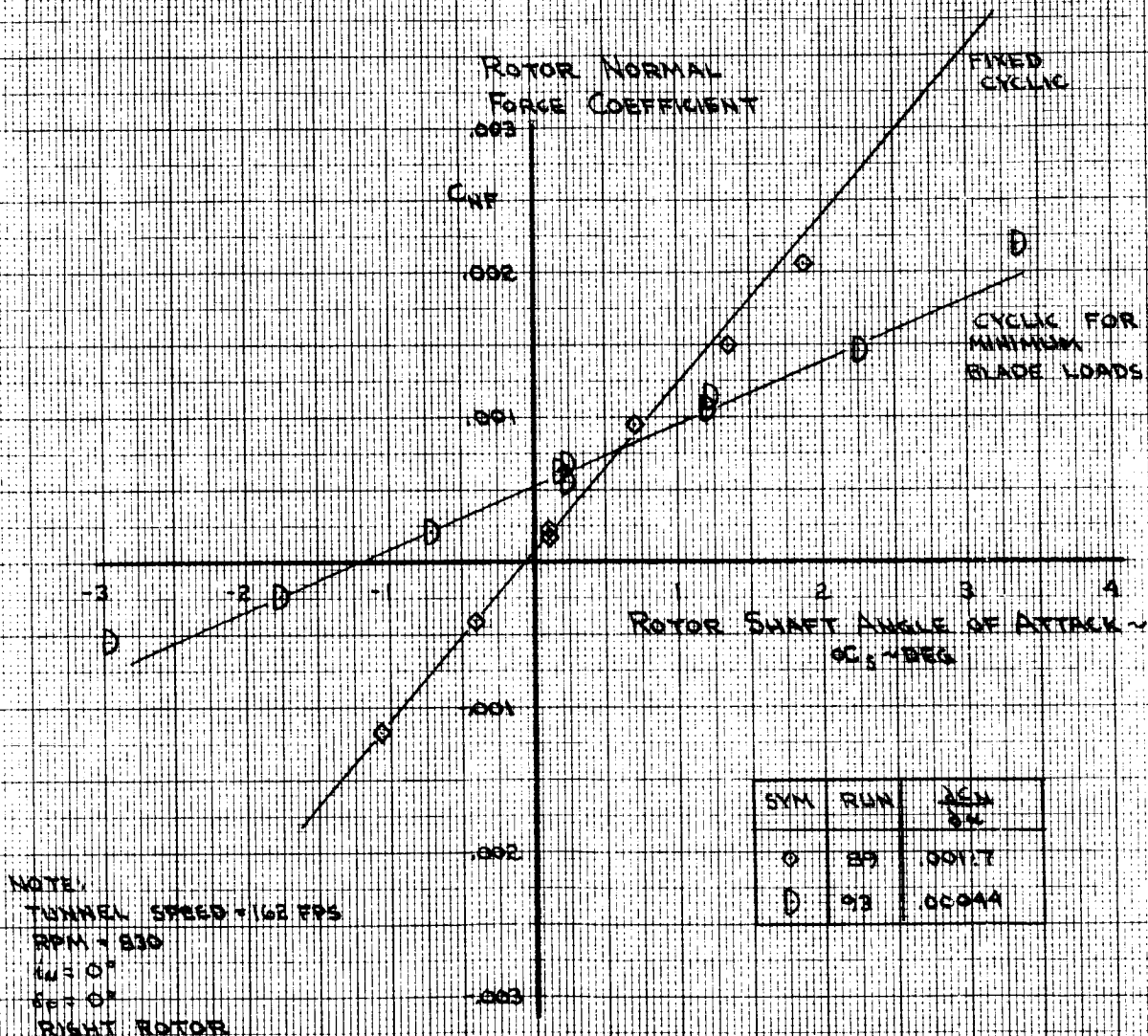


FIGURE 7

EFFECT OF BLADE LOAD MINIMIZATION ON ROTOR
NORMAL FORCE CHARACTERISTICS IN CRUISE

- STATIC BLADE TWEAKS
- MAX 1/REV BLADE LOADS (SEE FIG 6-2)
- ◇ MAX 3/REV BLADE LOADS (SEE FIG 6-3)
- △ ω_L INDICATED BY MIN AIR RESONANCE MODE DAMPING AT CROSSING OF $(2-\omega_L)$ AND WING VERT BEND. FREQ

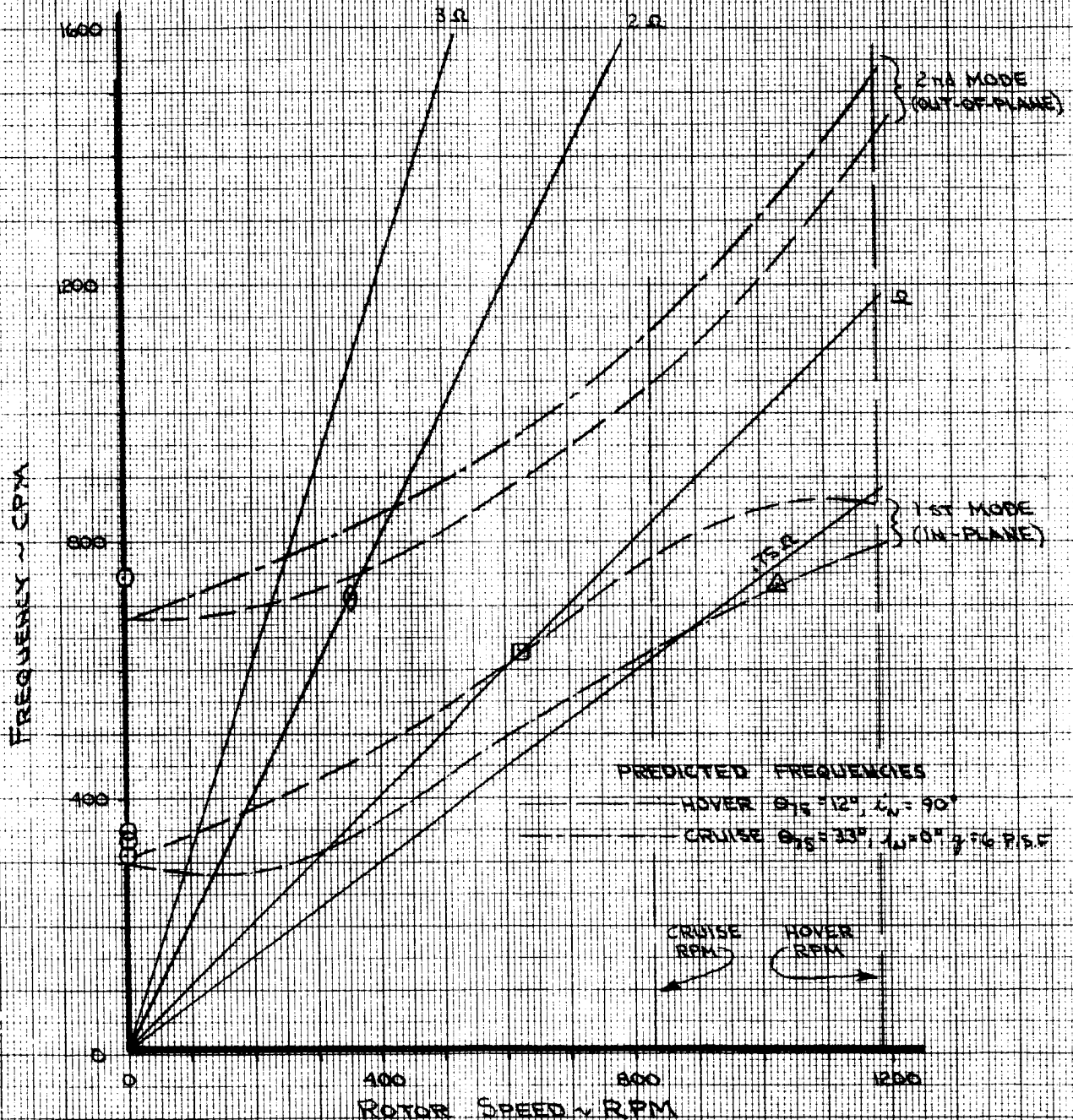


FIGURE 8 SUMMARY OF BLADE ROTATING NATURAL FREQUENCIES

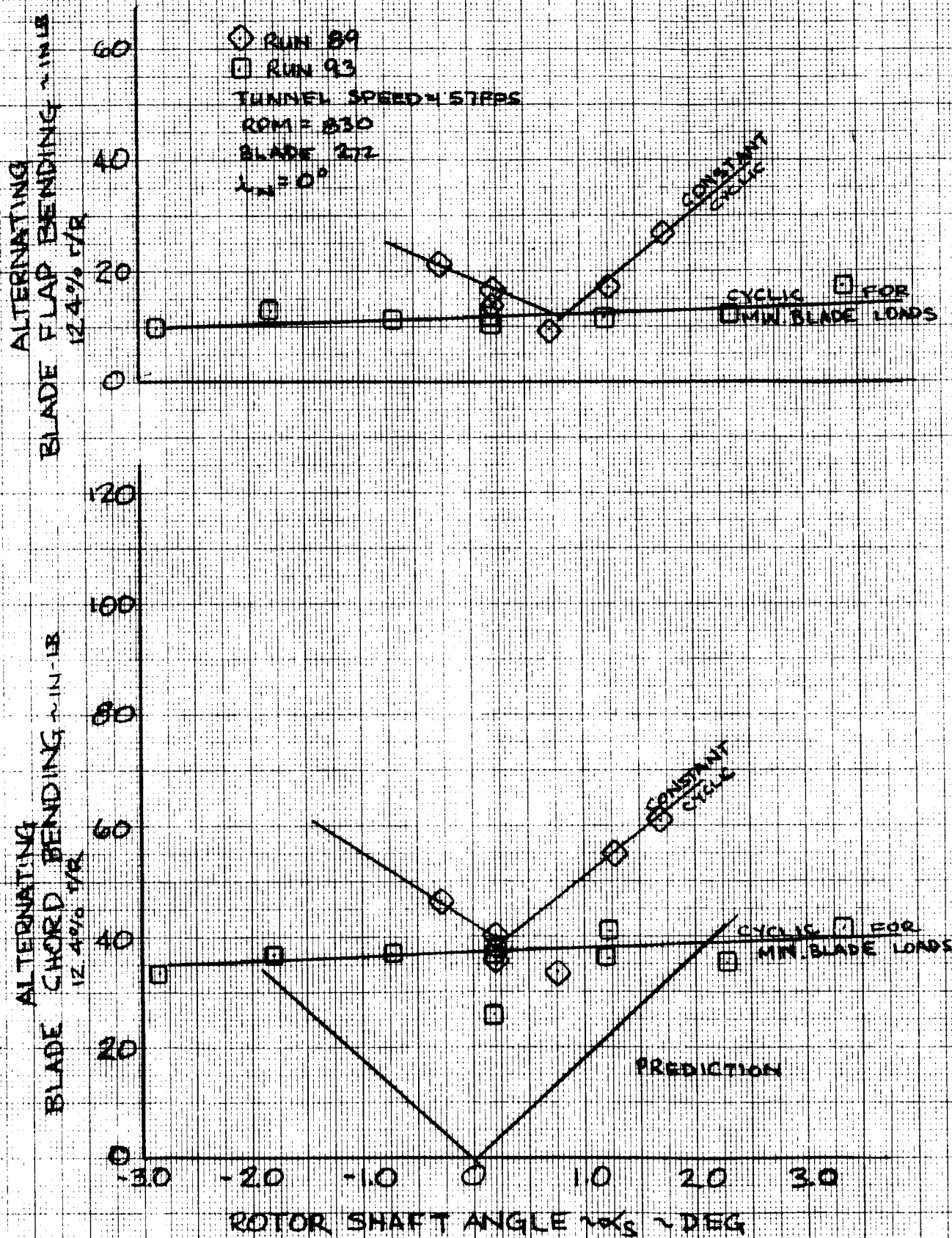
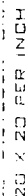


FIGURE 9 EFFECT OF CYCLIC ON ALTERNATING BLADE LOADS IN CRUISE



CRUISE STABILITY BOUNDARIES PREDICTED
WITH ACTUAL MODEL FREQUENCIES $\lambda_n = 0$

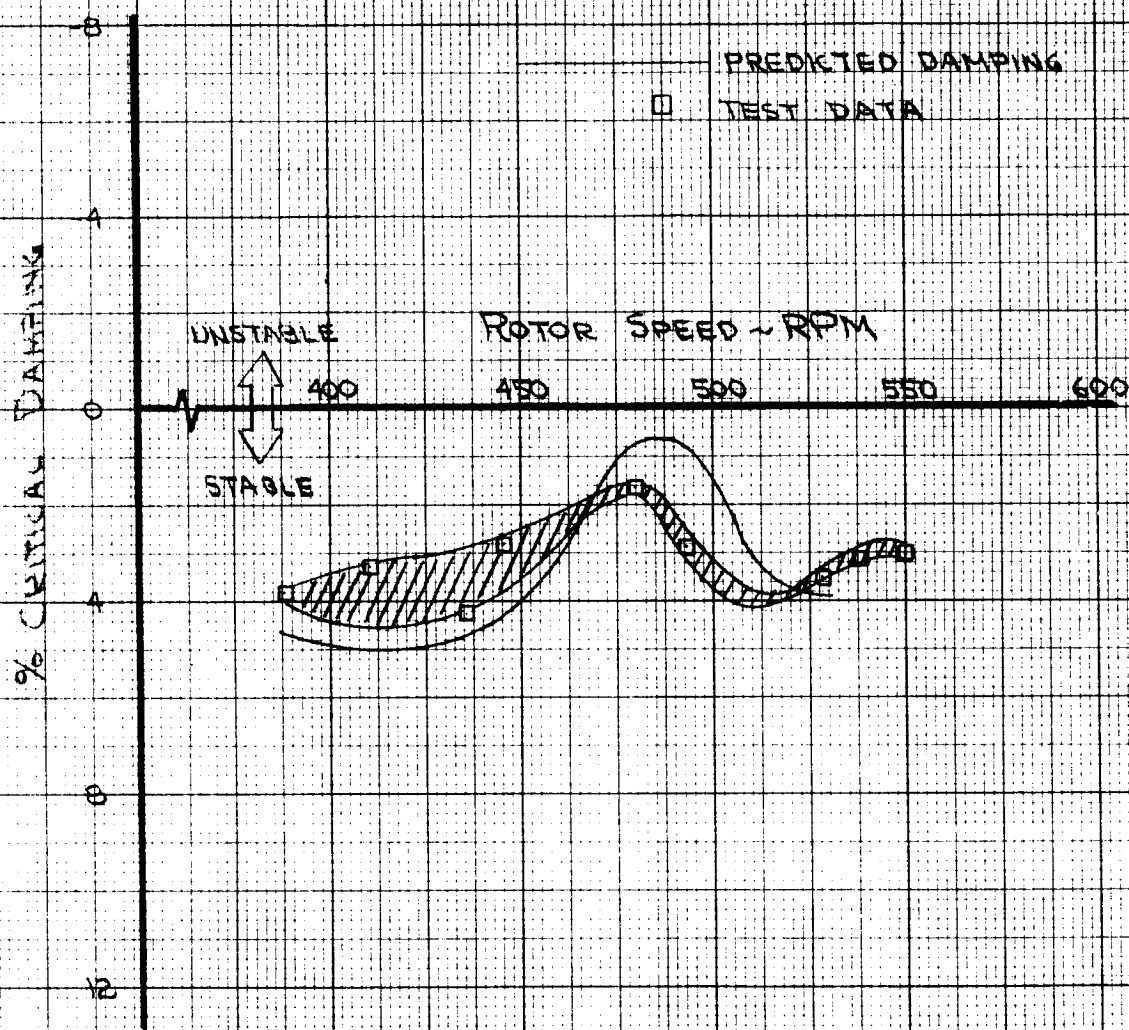


FIGURE 11 DAMPING IN AIR RESONANCE MODE $V_{\text{FORWARD}} = 90 \text{ KTS}$
 $\pm 1^\circ \text{N} \pm 10^\circ$

LIST OF ILLUSTRATIONS

<u>FIGURE</u>		<u>PAGE</u>
1	Airframe Performance Characteristics in Transition	xx
2	Effect of Flap Deflection on Aircraft Performance in Transition	xxi
3	Effect of Fuselage Yaw Angle and Flap Deflection on Rotor Normal Force Coefficient in Cruise . .	xxii
4	Comparison of Rotor Derivatives Obtained from Pitch and Yaw Sweeps	xxiii
5	Longitudinal Stability in Transition - Variation of Pitching Moment with Lift Coefficient	xxiv
6	Longitudinal Stability in Cruise - Effect of Vertical and Horizontal Tails on Pitching Moment Coefficient	xxv
7	Effect of Blade Load Minimization on Rotor Normal Force Characteristics in Cruise	xxvi
8	Summary of Blade Rotating Natural Frequencies	xxvii
9	Effect of Cyclic on Alternating Blade Loads in Cruise	xxviii
10	Cruise Stability Boundaries Predicted with Actual Model Frequencies - 1/4.622 Scale Model Full Scale Data	xxix
11	Damping in Air Resonance Mode - Cruise 1/4.622 Scale Model Full Scale Parameters	xxx
12	1/4.622 Froude Scale Wind Tunnel Model	14
13	1/4.622 Froude Scale Model 222 Blade Definition	15
14	Model 222 Control Display	15A
15	1/4.622 Scale Model 222 Installed in the Wind Tunnel Test Section	
16	The Boeing V/STOL Wind Tunnel General Arrangement	19
17	Model 222 Wind Tunnel Installation	21
18	Model 222 Lowered to Working Height	

LIST OF ILLUSTRATIONS

<u>FIGURE</u>		<u>PAGE</u>
19	Model 222 Balance Arrangement	24
20	Model 222 Sign Convention	32
21	Model Force and Moment Sign Convention	33
22	Effect of Flap Deflection in Transition on Rotor Thrust Characteristics $\left\{ \begin{array}{l} 40^\circ \\ 30^\circ \\ 20^\circ \end{array} \right.$ $(i_N = 41.6^\circ, \delta_F = 30^\circ, V=72 \text{ FPS}) . . .$	37
23	Blade Collective, Longitudinal, Lateral Cyclic Variation during Flap Deflection Investigation in Transition $\left\{ \begin{array}{l} 40^\circ \\ 30^\circ \\ 20^\circ \end{array} \right.$ $(i_N=41.6^\circ, \delta_F=30^\circ, V=72 \text{ FPS}) . . .$	38
24	Effect of Flap Deflection in Transition on Rotor Performance $\left\{ \begin{array}{l} 40^\circ \\ 30^\circ \\ 20^\circ \end{array} \right.$ $(i_N=41.6^\circ, \delta_F=30^\circ, V=72 \text{ FPS}) . . .$	39
25	Rotor Thrust and Power Characteristics in Yaw Angle Investigation in Transition $(i_N=41.6^\circ, \delta_F=40^\circ, V= 72 \text{ FPS}) . . .$	40
26	Collective and Lateral and Longitudinal Cyclic During Yaw Angle Investigation in Transition $(i_N=41.6^\circ, \delta_F=40^\circ, V=72 \text{ FPS}) . . .$	41
27	Rotor Thrust and Power Characteristics in Yaw Angle Investigation in Transition $(i_N=30^\circ, \delta_F=30^\circ, V=73 \text{ FPS}) . . .$	42
28	Collective and Lateral and Longitudinal Cyclic During Yaw Angle Investigation in Transition $(i_N=30^\circ, \delta_F=30^\circ, V=73 \text{ FPS})$	43
29	Effect of Nacelle incidence on Rotor Thrust and Power $(\delta_F=40^\circ, V=72 \text{ FPS})$	44
30	Rotor Thrust and Power Characteristics in Angle of Attack Investigation in Transition $(i_N=30^\circ, \delta_F=30^\circ, V=73 \text{ FPS}) . . .$	45

LIST OF ILLUSTRATIONS

<u>FIGURE</u>		<u>PAGE</u>
31	Collective and Lateral and Longitudinal Cyclic During Pitch Angle Investigation in Transition ($i_N=30^\circ$, $\delta_F=30^\circ$, $V=73$ FPS)	46
32	Effect of Cyclic in Transition on Rotor Per- formance Characteristics ($i_N=41.6^\circ$, $\delta_F=40^\circ$, $V=72$ FPS)	47
33	Effect of Collective in Transition on Rotor Performance Characteristics ($i_N=41.6^\circ$, $\delta_F=40^\circ$, $V=72$ FPS)	48
34	Airframe Performance Characteristics in Transition ($i_N=45^\circ$, $\delta_F=40^\circ$, $V = 72$ FPS)	51
35	Effect of Flap Deflection on Aircraft Performance in Transition ($i_N=41.6^\circ$, $\delta_F=\begin{cases} 40^\circ \\ 30^\circ \\ 20^\circ \end{cases}$, $V=72$ FPS)	52
36	Effect of Nacelle Incidence on Aircraft Performance ($\delta_F = \begin{cases} 40^\circ \\ 30^\circ \end{cases}$, $V=72$ FPS)	53
37	Effect of Nacelle Incidence on Aircraft Performance in Yaw in Transition ($i_N=\begin{cases} 41.6^\circ \\ 30^\circ \end{cases}$, $\delta_F=\begin{cases} 40^\circ \\ 30.0^\circ \end{cases}$, $V=72$ FPS)	54
38	Effect of Rotor Shaft Angle and Flap Deflection on Rotor Power and Thrust in Cruise ($i_N=0^\circ$, $V = 113$ FPS)	57
39	Collective and Lateral and Longitudinal Cyclic Changes During Yaw Angle Investigation in Cruise ($i_N=0^\circ$, $V=113$ FPS)	58
40	Collective and Lateral and Longitudinal Cyclic Changes during Yaw Angle Investigation in Cruise ($i_N=0^\circ$, $V=113$ FPS)	59
41	Effect of Forward Speed in Cruise on Rotor Thrust and Power ($i_N=0$, $V=113, 139, 162, 182$ FPS)	60

LIST OF ILLUSTRATIONS

<u>FIGURE</u>		<u>PAGE</u>
42	Effect of Lateral and Longitudinal Cyclic and Blade Collective on Shaft Angle	61
43	Effect of Lateral and Longitudinal Cyclic and Blade Collective on Rotor Shaft Angle ($i_N=0^\circ$, $V=139$ FPS)	62
44	Effect of Lateral and Longitudinal Cyclic and Blade Collective on Rotor Shaft Angle ($i_N=0^\circ$, $V=162, 182$ FPS)	63
45	Effect of Forward Speed in Cruise on Rotor Performance ($i_N=0^\circ$, $\delta_F=30^\circ$, $V=113, 139, 157, 182$ FPS)	64
46	Effect of Fuselage Yaw Angle and Flap Deflection on Rotor Thrust and Power Characteristics in Cruise ($i_N=0^\circ$, $\delta_F=\begin{cases} 0^\circ \\ 20^\circ \\ 40^\circ \end{cases}$, $V=113$ FPS)	65
47	Collective and Lateral and Longitudinal Cyclic Changes during Yaw Angle Investigation in Cruise ($i_N=0^\circ$, $\delta_F=\begin{cases} 0^\circ \\ 20^\circ \\ 40^\circ \end{cases}$, $V=113$ FPS)	66
48	Effect of Fuselage Yaw Angle and Forward Speed on Rotor Thrust and Power Characteristics in Cruise ($i_N=0^\circ$, $\delta_F=0^\circ$, $V=113, 161, 182$ FPS)	67
49	Collective and Lateral and Longitudinal Cyclic Changes during yaw angle investigation in Cruise ($i_N=0^\circ$, $\delta_F=0^\circ$, $V=113, 139, 161, 182$ FPS)	68
50	Effect of Lateral Cyclic and Forward Speed in Cruise on Rotor Power and Thrust Characteristics ($i_N=0^\circ$, $\delta_F=0^\circ$, $V=113, 161$ FPS)	69
51	Collective and Longitudinal Cyclic Changes during Lateral Cyclic Investigation ($i_N=0^\circ$, $\delta_F=0^\circ$, $V=113, 161$ FPS)	70

LIST OF ILLUSTRATIONS

<u>FIGURE</u>		<u>PAGE</u>
52	Effect of Longitudinal Cyclic and Forward Speed in Cruise on Rotor Power and Thrust Character- istics ($i_N=0^\circ$, $\delta_F=0^\circ$, $V=113$, 161 FPS)	71
53	Collective and Lateral Cyclic Changes during Longitudinal Cyclic Investigation ($i_N=0^\circ$, $\delta_F=0^\circ$, $V=113$ FPS)	72
54	Effect of Blade Load Minimization on Rotor Thrust and Power in Cruise ($i_N=0^\circ$, $\delta_F=0^\circ$, $V=162$ FPS).	73
55	Aircraft Lift Characteristics Rotors Off ($i_N=0^\circ$, $\delta_F=0^\circ$, $V=113$ FPS).	75
56	Definition of Induced Drag and Airplane Efficiency, Rotors Off	76
57	Effect of Fuselage Angle of Attack and Flap Deflection on Aircraft Performance in Cruise ($i_N=0^\circ$, $\delta_F=0^\circ, 10^\circ, 20^\circ, 40^\circ$, $V=113$ FPS)	78
58	Effect of Fuselage Yaw Angle and Flap Deflection on Aircraft Performance in Cruise ($i_N=0^\circ$, $\delta_F=0^\circ, 20^\circ, 40^\circ$, $V=113$ FPS)	79
59	Effect of Forward Speed in Cruise on Aircraft Performance ($i_N=0^\circ$, $\delta_F=0^\circ$, $V=113, 139, 162-182$ FPS)	80
60	Effect of Fuselage Yaw Angle and Forward Speed on Aircraft Performance in Cruise ($i_N=0^\circ$, $\delta_F=0^\circ$, $V=113, 139, 162, 182$ FPS). . . .	81
61	Comparison of Theory and Test Data in Transition on Rotor Performance Characteristics ($i_N=41.6^\circ$, $\delta_F=40^\circ$, $V=72$ FPS)	83
62	Comparison of Test Data and Pre-test Prediction of Power Required ($i_N=0^\circ$, $\delta_F=0^\circ$)	84
63	Effect of Flap Deflection in Transition on Aircraft Lift Coefficient ($i_N=41.6^\circ$, $\delta_F=\begin{cases} 20^\circ \\ 30^\circ \\ 40^\circ \end{cases}$, $V=72$ FPS)	91

LIST OF ILLUSTRATIONS

<u>FIGURE</u>		<u>PAGE</u>
64	Effect of Flap Deflection in Transition on Airframe Lift Coefficient $(i_N=41.6^\circ, \delta_F=\begin{cases} 20^\circ \\ 30^\circ \\ 40^\circ \end{cases}, V=72 \text{ FPS})$	92
65	Effect of Flap Deflection in Transition on Rotor Thrust Characteristics $(i_N=41.6^\circ, \delta_F=\begin{cases} 20^\circ \\ 30^\circ \\ 40^\circ \end{cases}, V=72 \text{ FPS}).$	93
66	Effect of Flap Deflection in Transition on Rotor Normal Force Coefficient $(i_N=41.6^\circ, \delta_F=\begin{cases} 20^\circ \\ 30^\circ \\ 40^\circ \end{cases}, V=72 \text{ FPS})$	94
67	Effect of Flap Deflection in Transition on Rotor Pitching Moment Coefficient $(i_N=41.6^\circ, \delta_F=\begin{cases} 20^\circ \\ 30^\circ \\ 40^\circ \end{cases}, V=72 \text{ FPS}).$	95
68	Effect of Flap Deflection in Transition on Rotor Side Force Coefficient $(i_N=41.6^\circ, \delta_F=\begin{cases} 20^\circ \\ 30^\circ \\ 40^\circ \end{cases}, V=72 \text{ FPS}).$	96
69	Effect of Flap Deflection in Transition on Rotor Yawing Moment Coefficient $(i_N=41.6^\circ, \delta_F=\begin{cases} 20^\circ \\ 30^\circ \\ 40^\circ \end{cases}, V=72 \text{ FPS}).$	97
70	Blade Collective, Longitudinal and Lateral Cyclic Variation during Flap Deflection Investigation in Transition $(\delta_F=\begin{cases} 20^\circ \\ 30^\circ \\ 40^\circ \end{cases}, V=72 \text{ FPS}).$	98
71	Effect of Fuselage Yaw Angle on Aircraft Lift Coefficient in Transition $(i_N=41.6^\circ, \delta_F=0^\circ, V=72 \text{ FPS})$	99
72	Effect of Fuselage Yaw Angle on Rotor Normal Force in Transition $(i_N=41.6^\circ, \delta_F=0^\circ, V=72 \text{ FPS})$	100

LIST OF ILLUSTRATIONS

<u>FIGURE</u>		<u>PAGE</u>
73	Effect of Fuselage Yaw Angle on Rotor Pitching Moment in Transition ($i_N=41.6^\circ$, $\delta_F=0^\circ$, $V=72$ FPS)	101
74	Effect of Fuselage Yaw Angle on Rotor Side Force in Transition ($i_N=41.6^\circ$, $\delta_F=0^\circ$, $V=72$ FPS)	102
75	Effect of Fuselage Yaw Angle on Rotor Yawing Moment in Transition ($i_N=41.6^\circ$, $\delta_F=0^\circ$, $V=72$ FPS)	103
76	Rotor Normal Force Characteristics in Yaw Angle Investigation in Transition ($i_N=30^\circ$, $\delta_F=30^\circ$, $V=72$ FPS)	104
77	Rotor Pitching Moment Characteristics in Yaw Angle Investigation in Transition ($i_N=30^\circ$, $\delta_F=30^\circ$, $V=73$ FPS)	105
78	Rotor Side Force Characteristics in Yaw Angle Investigation in Transition ($i_N=30^\circ$, $\delta_F=30^\circ$, $V=73$ FPS)	106
79	Rotor Yawing Moment Characteristics in Yaw Angle Investigation in Transition ($i_N=30^\circ$, $\delta_F=30^\circ$, $V=73$ FPS)	107
80	Rotor Normal Force Characteristics in Angle of Attack Investigation in Transition ($i_N=30^\circ$, $\delta_F=30^\circ$, $V=73$ FPS)	108
81	Rotor Pitching Moment Characteristics in Angle of Attack Investigation in Transition ($i_N=30^\circ$, $\delta_F=30^\circ$, $V=73$ FPS)	109
82	Rotor Side Force Characteristics in Angle of Attack Investigation in Transition ($i_N=30^\circ$, $\delta_F=30^\circ$, $V=73$ FPS)	110
83	Rotor Yawing Moment Characteristics in Angle of Attack Investigation in Transition ($i_N=30^\circ$, $\delta_F=30^\circ$, $V=73$ FPS)	111

LIST OF ILLUSTRATIONS

<u>FIGURE</u>		<u>PAGE</u>
84	Effect of Nacelle Incidence on Aircraft Lift Coefficient in Mid Transition Speed ($\delta_F=40^\circ$, $V=72$ FPS)	112
85	Effect of Nacelle Incidence on Pitching Moment and Normal Force ($\delta_F=40^\circ$, $V=72$ FPS)	113
85	Effect of Nacelle Incidence on Side Force and Yawing Moment ($\delta_F=40^\circ$, $V=72$ FPS)	114
87	Variation of Lift Coefficient with Angle of Attack in Transition ($V=72$ FPS, $i_N \approx 43^\circ$)	124
88	Variation of Pitching Moment Coefficient with Angle of Attack in Transition ($V=72$ FPS, $i_N \approx 43^\circ$)	125
89	Longitudinal Stability - Variation of Pitching Moment with Lift Coefficient in Transition ($V=72$ FPS, $i_N \approx 43^\circ$)	126
90	Variation of Aircraft Lift Coefficient with Angle of Attack in Transition ($V=72$ FPS, $i_N = 30^\circ$, 41.6°)	127
91	Variation of Aircraft Pitching Moment Coefficient with Angle of Attack in Transition ($V=72$ FPS, $i_N = 30^\circ$, 41.6°)	128
92	Variation of Aircraft Pitching Moment Coefficient with Lift Coefficient in Transition ($V = 72$ FPS, $i_N = 30^\circ$, 41.6°)	129
93	Variation of Airframe Lift Coefficient with Angle of Attack in Transition ($V=72$ FPS, $i_N = 30^\circ$, 41.6°)	130
94	Longitudinal Stability - Variation of Airframe Pitching Moment Coefficient with Lift Coefficient in Transition ($V=72$ FPS, $i_N = 30^\circ$, 41.6°)	131
95	Variation of Airframe Pitching Moment Coefficient with Angle of Attack in Transition ($V=72$ FPS, $i_N = 30^\circ$, 41.6°)	132

LIST OF ILLUSTRATIONS

<u>FIGURE</u>		<u>PAGE</u>
96	Effect of Nacelle Incidence on Lift and Pitching Moment Coefficients in Transition (V=72 FPS)	133
97	Directional Stability - Variation of Yawing Moment Coefficient with Sideslip Angle in Transition (V=72 FPS, $i_N = 43^\circ$)	134
98	Dihedral Effect - Variation of Rolling Moment Coefficient with Sideslip Angle in Transition (V=72 FPS, $i_N = 43^\circ$)	135
99	Variation of Side Coefficient with Sideslip Angle in Transition (V=72 FPS, $i_N = 43^\circ$)	136
100	Effect of Cyclic in Transition on Rotor Normal Force Characteristics ($i_N = 41.6^\circ$, $\delta_F = 40^\circ$, V=72 FPS)	147
101	Effect of Cyclic in Transition on Rotor Pitching Moment Characteristics ($i_N = 41.6^\circ$, $\delta_F = 40^\circ$, V=72 FPS)	148
102	Effect of Cyclic in Transition on Rotor Side Force Characteristics ($i_N = 41.6^\circ$, $\delta_F = 40^\circ$, V=72 FPS)	149
103	Effect of Cyclic in Transition on Rotor Yawing Moment Characteristics ($i_N = 41.6^\circ$, $\delta_F = 40^\circ$, V=72 FPS)	150
104	Longitudinal Cyclic and Blade Collective Changes during Lateral Cyclic Sweep ($i_N = 41.6^\circ$, $\delta_F = 40^\circ$, V=72 FPS)	151
105	Lateral Cyclic and Blade Collective Changes during Longitudinal Cyclic Sweep ($i_N = 41.6^\circ$, $\delta_F = 40^\circ$, V=72 FPS)	152
106	Effect of Collective in Transition on Rotor Normal Force Characteristics ($i_N = 41.6^\circ$, $\delta_F = 40^\circ$, V=72 FPS)	153

LIST OF ILLUSTRATIONS

<u>FIGURE</u>		<u>PAGE</u>
107	Effect of Collective in Transition on Rotor Pitching Moment Characteristics ($i_N=41.6^\circ$, $\delta_F=40^\circ$, $V=72$ FPS)	154
108	Effect of Collective in Transition on Rotor Side Force Characteristics ($i_N=41.6^\circ$, $\delta_F=40^\circ$, $V=72$ FPS)	155
109	Effect of Collective in Transition on Rotor Yawing Moment Characteristics ($i_N=41.6^\circ$, $\delta_F=40^\circ$, $V=72$ FPS)	156
110	Longitudinal and Lateral Cyclic Changes during Differential Collective ($i_N=41.6^\circ$, $\delta_F=40^\circ$, $V=72$ FPS)	157
111	Effect of Aileron Deflection on Aircraft Rolling Moment ($V=72$ FPS, $i_N=41.6^\circ$)	158
112	Effect of Aileron Deflection on Aircraft Yawing Moment ($V=72$ FPS, $i_N=41.6^\circ$)	159
113	Effect of Aileron Deflection on Aircraft Lateral Stability ($V=72$ FPS, $i_N=41.6^\circ$)	160
114	Effect of Aileron Deflection on Aircraft Lift ($V=72$ FPS, $i_N=41.6^\circ$)	161
115	Effect of Aileron Deflection on Aircraft Pitching Moment ($V=72$ FPS, $i_N=41.6^\circ$)	162
116	Blade Collective, Longitudinal and Lateral Cyclic During Aileron Deflection Run ($V=72$ FPS, $i_N=41.6^\circ$)	163
117	Effect of Aileron on Rotor Thrust and Power ($V=72$ FPS, $i_N=41.6^\circ$)	164
118	Effect of Aileron Deflection on Rotor Normal Force and Pitching Moment ($V=72$ FPS, $i_N=41.6^\circ$)	165
119	Effect of Aileron Deflection on Rotor Side Force and Yawing Moment ($V=72$ FPS, $i_N=41.6^\circ$)	166
120	Effect of Spoiler Deflection on Aircraft Rolling Moment ($V=72$ FPS, $i_N=41.6^\circ$)	167

LIST OF ILLUSTRATIONS

<u>FIGURE</u>		<u>PAGE</u>
121	Effect of Spoiler Deflection on Aircraft Yawing Moment (V=72 FPS, $i_N = 41.6^\circ$)	168
122	Effect of Spoiler Deflection on Aircraft Lift (V=72 FPS, $i_N = 41.6^\circ$).	169
123	Effect of Spoiler Deflection on Aircraft Pitching Moment (V=72 FPS, $i_N = 41.6^\circ$)	170
124	Effect of Spoiler Deflection on Aircraft Lateral Stability (V=72 FPS, $i_N = 41.6^\circ$)	171
125	Blade Collective, Longitudinal and Lateral Cyclic during Spoiler Deflection Run (V=72 FPS, $i_N = 41.6^\circ$).	172
126	Effect of Spoiler Deflection on Thrust and Power (V=72 FPS, $i_N = 41.6^\circ$).	173
127	Effect of Spoiler Deflection on Rotor Normal Force and Pitching Moment (V=72 FPS, $i_N = 41.6^\circ$).	174
128	Effect of Spoiler Deflection on Rotor Side Force an Yawing Moment (V=72 FPS, $i_N = 41.6^\circ$).	175
129	Schedule of Aileron Deflection versus Spoiler Deflection (V=72 FPS, $i_N = 41.6^\circ$).	176
130	Effect of Aileron and Spoiler Deflection on Aircraft Rolling Moment (V=72 FPS, $i_N=41.6^\circ$)	177
131	Effect of Aileron and Spoiler Deflection on Yawing Moment (V=72 FPS, $i_N=41.6^\circ$)	178
132	Effect of Aileron and Spoiler Deflection on Aircraft Lift (V=72fps, $i_N=41.6^\circ$)	179
133	Effect of Aileron and Spoiler Deflection on Aircraft Pitching Moment (V=72 FPS, $i_N=41.6^\circ$).	180
134	Blade Collective, Longitudinal and Lateral Cyclic during Combined Aileron and Spoiler Run (V=72 FPS, $i_N = 41.6^\circ$).	181
135	Effect of Aileron and Spoiler Deflection on Rotor Thrust and Power (V=72 FPS, $i_N = 41.6^\circ$).	182
136	Effect of Aileron and Spoiler Deflection on Rotor Normal Force and Pitching Moment (V= 72 FPS, $i_N= 41.6^\circ$).	183

LIST OF ILLUSTRATIONS

<u>FIGURE</u>		<u>PAGE</u>
137	Effect of Aileron and Spoiler Deflection on Rotor Side Force and Yawing Moment ($V=72$ FPS, $i_N = 41.6^\circ$)	184
138	Effect of Differential Thrust, Spoiler and Aileron Deflection and Rudder Deflection on Rolling Moment Coefficient in Transition ($V=72$ FPS, $i_N = 42^\circ$)	185
139	Effect of Differential Thrust, Spoiler and Aileron Deflection and Rudder Deflection on Yawing Moment Coefficient in Transition ($V=72$ FPS, $i_N = 42^\circ$)	186
140	Effect of Differential Thrust, Spoiler and Aileron Deflection and Rudder Deflection on Side Force Coefficient in Transition ($V=72$ FPS, $i_N = 42^\circ$)	187
141	Effect of Differential Thrust on Yawing Moment Coefficients in Transition ($V=72$ FPS, $i_N = 42^\circ$)	188
142	Effect of Differential Collective - Aircraft Rolling Moment Coefficient versus Yawing Moment Coefficient	189
143	Change in Thrust Coefficient with Collective Pitch ($V=72$ FPS, $i_N = 41.6^\circ$)	190
144	Elevator Effectiveness in Transition -Aircraft Pitching Moment ($V=72$ FPS, $i_N = 41.6^\circ$)	191
145	Elevator Effectiveness in Transition - Aircraft Lift Coefficient ($V=72$ FPS, $i_N = 41.6^\circ$)	192
146	Longitudinal Cyclic Effectiveness - Variation of Lift and Pitching Moment Coefficients with Longitudinal Cyclic in Transition (Right Rotor B_1) ($V=72$ FPS, $i_N = 41.6^\circ$)	193
147	Longitudinal Cyclic Effectiveness - Variation of Rolling and Yawing Moment Coefficients with Longitudinal Cyclic in Transition (Right Rotor B_1) ($V=72$ FPS, $i_N = 41.6^\circ$)	194
148	Lateral Cyclic Effectiveness - Variation of Rolling and Yawing Moment Coefficients with Lateral Cyclic in Transition (Left Rotor A_1) ($V=72$ FPS, $i_N = 41.6^\circ$)	195

LIST OF ILLUSTRATIONS

<u>FIGURE</u>		<u>PAGE</u>
149	Lateral Cyclic Effectiveness - Variation of Rolling and Yawing Moment Coefficients with Lateral Cyclic in Transition (Right Rotor A ₁) (V=172 FPS, $i_N = 41.6^\circ$)	196
150	Lateral Cyclic Effectiveness - Variation of Lift and Pitching Moment Coefficients with Lateral Cyclic in Transition (Left Rotor A ₁) (V= 72 FPS, $i_N = 41.6^\circ$)	197
151	Lateral Cyclic Effectiveness - Variation of Lift and Pitching Moment Coefficients with Lateral Cyclic in Transition (Right Rotor A ₁) (V=72 FPS, $i_N = 41.6^\circ$)	198
152	Comparison of Theory and Test Data in Transition on Rotor Normal Force Characteristics ($i_N=41.6^\circ$, $\delta_F = 40^\circ$, V= 72 FPS).	207
153	Comparison of Theory and Test Data in Transition on Rotor Pitching Moment Characteristics ($i_N = 41.6^\circ$, $\delta_F = 40^\circ$, V=72 FPS)	208
154	Comparison of Test and Theory for Lateral Cyclic Rotor Derivatives in Transition ($i_N = 41.6^\circ$, $\delta_F = 40^\circ$, V=72 FPS)	209
155	Comparison of Test and Theory for Longitudinal Cyclic Rotor Derivatives in Transition	210
156	Effect of Fuselage Yaw Angle and Flap Deflection on Airframe Lift Characteristics in Cruise ($i_N=0^\circ$, $\delta_F = \begin{cases} 0^\circ \\ 20^\circ \\ 40^\circ \end{cases}$, V=113 FPS)	219
157	Collective and Lateral and Longitudinal Cyclic Changes during Yaw Angle Investigation in Cruise ($i_N=0^\circ$, $\delta_F = 0^\circ, 20^\circ, 40^\circ$, V=113 FPS)	220
158	Effect of Fuselage Yaw Angle and Flap Deflection on Rotor Thrust and Power Characteristics in Cruise ($i_N=0^\circ$, $\delta_F = 0^\circ, 20^\circ, 40^\circ$, V=113 PFS)	221
159	Effect of Fuselage Yaw Angle and Flap Deflection on Rotor Normal Force in Cruise ($i_N=0^\circ$, $\delta_F = 0^\circ, 20^\circ, 40^\circ$, V=113 FPS).	222
160	Effect of Fuselage Yaw Angle and Flap Deflection on Rotor Pitching Moments in Cruise ($i_N=0^\circ$, $\delta_F = 0^\circ, 20^\circ, 40^\circ$, V=113 FPS)	223

LIST OF ILLUSTRATIONS

<u>FIGURE</u>		<u>PAGE</u>
161	Effect of Fuselage Yaw Angle and Flap Deflection on Rotor Side Force in Cruise ($i_N=0^\circ, \delta_F=0^\circ, 20^\circ, 40^\circ, V=113 \text{ FPS}$)	224
162	Effect of Fuselage Yaw Angle and Flap Deflection on Rotor Yawing Moment in Cruise ($i_N=0^\circ, \delta_F=0^\circ, 20^\circ, 40^\circ, V=113 \text{ FPS}$)	225
163	Effect of Fuselage Yaw Angle and Speed on Rotor Normal Force in Cruise ($i_N=0^\circ, \delta_F=0^\circ, V=113, 139, 161, 182 \text{ FPS}$)	226
164	Effect of Fuselage Yaw Angle and Speed on Rotor Pitching Moment in Cruise ($i_N=0^\circ, \delta_F=0^\circ, V=113, 139, 161 \text{ FPS}$)	227
165	Effect of Fuselage Yaw Angle on Rotor Pitching Moment in Cruise ($i_N=0^\circ, \delta_F=0^\circ, V=182 \text{ FPS}$)	228
166	Effect of Fuselage Yaw Angle and Speed on Rotor Side Force in Cruise ($i_N=0^\circ, \delta_F=0^\circ, V=113, 139 \text{ FPS}$)	229
167	Effect of Fuselage Yaw Angle and Speed on Rotor Yawing Moment in Cruise ($i_N=0^\circ, \delta_F=0^\circ, V=113, 139 \text{ FPS}$)	230
168	Effect of Rotor Shaft Angle and Flap Deflection on Airframe Lift Coefficient in Cruise ($i_N=0^\circ, \delta_F=0^\circ, 10^\circ, 20^\circ, 40^\circ, V=113 \text{ FPS}$)	231
169	Effect of Rotor Shaft Angle & Flap Deflection on Rotor Normal Force in Cruise ($i_N=0^\circ, \delta_F=0^\circ, 10^\circ, 20^\circ, 40^\circ, V=113 \text{ FPS}$)	232
170	Effect of Rotor Shaft Angle and Flap Deflection on Rotor Pitching Moment in Cruise ($i_N=0^\circ, \delta_F=0^\circ, 10^\circ, 20^\circ, 40^\circ, V=113 \text{ FPS}$)	233
171	Effect of Rotor Shaft Angle and Flap Deflection on Rotor Side Force in Cruise ($i_N=0^\circ, \delta_F=0^\circ, 10^\circ, 20^\circ, 40^\circ, V=113 \text{ FPS}$)	234
172	Effect of Rotor Shaft Angle and Flap Deflection on Rotor Yawing Moment in Cruise ($i_N=0^\circ, \delta_F=0^\circ, 10^\circ, 20^\circ, 40^\circ, V=113 \text{ FPS}$)	235
173	Effect of Wing Lift in Cruise on Rotor Normal Force and Pitching Moment ($i_N=0^\circ, \delta_F=0^\circ, 10^\circ, 20^\circ, 40^\circ, V=113 \text{ FPS}$)	236

LIST OF ILLUSTRATIONS

<u>FIGURE</u>		<u>PAGE</u>
174	Effect of Wing Lift in Cruise on Rotor Side Force and Yawing Moment ($i_N=0^\circ, \delta_F=0^\circ, 10^\circ, 20^\circ, 40^\circ, V=113 \text{ FPS}$)	237
175	Effect of Forward Speed in Cruise on Rotor Normal Force Characteristics ($i_N=0^\circ, \delta_F=0^\circ, V=113, 139, 162-182 \text{ FPS}$)	238
176	Effect of Forward Speed in Cruise on Rotor Pitching Moment Characteristics ($i_N=0^\circ, \delta_F=0^\circ, V=113, 139, 162, 182 \text{ FPS}$)	239
177	Effect of Forward Speed in Cruise on Rotor Side Force Characteristics ($i_N=0^\circ, \delta_F=0^\circ, V=113, 139 \text{ FPS}$)	240
178	Effect of Forward Speed in Cruise on Rotor Yawing Moment ($i_N=0^\circ, \delta_F=0^\circ, V=113, 139 \text{ FPS}$)	241
179	Comparison of Rotor Derivatives Obtained From Pitch and Yaw Sweeps ($i_N=0^\circ$).	242
180	Effect of Lateral Cyclic and Forward Speed in Cruise on Rotor Normal Force Characteristics ($i_N=0^\circ, \delta_F=0^\circ, V=113, 161 \text{ FPS}$)	243
181	Effect of Lateral Cyclic and Forward Speed in Cruise on Rotor Pitching Moment Characteristics ($i_N=0^\circ, \delta_F=0^\circ, V=113, 161 \text{ FPS}$)	244
182	Effect of Lateral Cyclic in Cruise on Rotor Side Force Characteristics ($i_N=0^\circ, \delta_F=0^\circ, V=113 \text{ FPS}$)	245
183	Effect of Lateral Cyclic in Cruise on Rotor Yawing Moment Characteristics	246
184	Effect of Longitudinal Cyclic and Forward Speed in Cruise on Rotor Normal Force Characteristics ($i_N=0^\circ, \delta_F=0^\circ, V=113, 161 \text{ FPS}$)	247
185	Effect of Longitudinal Cyclic and Forward Speed in Cruise on Rotor Pitching Moment Characteristics ($i_N=0^\circ, \delta_F=0^\circ, V=113, 161 \text{ FPS}$)	248
186	Effect of Longitudinal Cyclic in Cruise on Rotor Side Force Characteristics ($i_N=0^\circ, \delta_F=0^\circ, V=113 \text{ FPS}$)	249

LIST OF ILLUSTRATIONS

<u>FIGURE</u>		<u>PAGE</u>
187	Effect of Longitudinal Cyclic and Forward Speed in Cruise on Rotor Yawing Moment Characteristics ($i_N=0^\circ, \delta_F=0^\circ, V=113 \text{ FPS}$)	250
188	Effect of Blade Load Minimization on Rotor Normal Force Characteristics in Cruise ($i_N=0^\circ, \delta_F=0^\circ, V=162 \text{ FPS}$)	251
189	Effect of Blade Load Minimization on Rotor Pitching Moment Characteristics in Cruise ($i_N=0^\circ, \delta_F=0^\circ, V=162 \text{ FPS}$)	252
190	Lift Curve Slope - Effect of Vertical and Horizontal Tails ($V=115 \text{ FPS } i_N=0^\circ$)	261
191	Pitching Moment Coefficient - Effect of Vertical and Horizontal Tails ($V=115 \text{ FPS, } i_N=0^\circ$)	262
192	Longitudinal Stability - Effect of Vertical and Horizontal Tails ($V=115 \text{ FPS, } i_N=0^\circ$)	263
193	Horizontal Tail Effectiveness ($V=115 \text{ FPS, } i_N=0^\circ$).	264
194	Effect of Dynamic Pressure on Longitudinal Characteristics Aircraft Lift and Pitching Moment Coefficients ($i_N=0^\circ$)	265
195	Effect of Dynamic Pressure on Longitudinal Stabili- ty - Aircraft ($i_N=0^\circ$)	266
196	Effect of Dynamic Pressure on Longitudinal Characteristics Airframe Lift and Pitching Moment Coefficients ($i_N=0^\circ$)	267
197	Effect of Dynamic Pressure on Longitudinal Stability - Airframe ($i_N=0^\circ$)	268
198	Effect of Horizontal Tail on Longitudinal Characteristics in Cruise ($V=113 \text{ FPS, } i_N=0^\circ$).	269
199	Effect of Horizontal Tail on Longitudinal Stability ($V=113 \text{ PFS, } i_N=0^\circ$)	270
200	Lift Curve Slope Variation with Velocity - Rotors on and Off ($i_N=0^\circ$)	271
201	Static Longitudinal Stability Summary ($i_N=0^\circ$).	272

LIST OF ILLUSTRATIONS

<u>FIGURE</u>		<u>PAGE</u>
202	Variation of Side Force Coefficient with Sideslip Angle in Cruise ($V=113$ FPS, $i_N=0^\circ$)	273
203	Variation of Yawing Moment Coefficient with Sideslip Angle in Cruise ($V=113$ FPS, $i_N=0^\circ$)	274
204	Variation of Rolling Moment Coefficient with Sideslip Angle - Tails on and Tails Off ($V=113$ FPS, $i_N=0^\circ$).	275
205	Effect of Dynamic Pressure on Yawing and Rolling Moment Coefficients versus Sideslip Angle ($i_N=0^\circ$).	276
206	Effect of Dynamic Pressure on Side Force Coefficient versus Sideslip Angle ($i_N=0^\circ$)	277
207	Variation of Yawing and Rolling Moment Coefficients with Sideslip Angle Tails on and Tails Off ($V=113$ FPS, $i_N=0^\circ$)	278
208	Variation of Side Force Coefficients with Sideslip Angle Tails on and Tails off ($V=113$ FPS, $i_N=0^\circ$)	279
209	Directional Stability Summary - Directional Stability Derivative versus Velocity ($V=113$ FPS, $i_N=0^\circ$)	280
210	Dihedral Effect Summary - Lateral Stability Derivative versus Velocity ($i_N=0^\circ$)	281
211	Side Force Summary - Side Force Derivative versus Velocity ($i_N=0^\circ$)	282
212	Lateral Cyclic Effectiveness - Variation of Aircraft Lift and Pitching Moment Coefficient with Lateral Cyclic - Right Rotor ($V=161$ FPS, $i_N=0^\circ$)	292
213	Lateral Cyclic Effectiveness - Variation of Aircraft Side Force and Yawing Moment Coefficients with Lateral Cyclic - Right Rotor ($V=161$ FPS, $i_N=0^\circ$)	293
214	Longitudinal Cyclic Effectiveness - Variation of Lift and Pitching Moment Coefficients with Longitudinal Cyclic ($V=161$ FPS, $i_N=0^\circ$)	294

LIST OF ILLUSTRATIONS

<u>FIGURE</u>		<u>PAGE</u>
215	Longitudinal Cyclic Effectiveness - Variation of Aircraft Side Force and Yawing Moment Coefficients with Longitudinal Cyclic (V=161 FPS, $i_N=0^\circ$)	295
216	Longitudinal Cyclic Effectiveness - Variation of Yawing Moment Coefficients with Longitudinal Cyclic (V=161 FPS, $i_N=0^\circ$)	296
217	Elevator Effectiveness in Cruise - Aircraft Pitching Moment versus Elevator Deflection (V=113 FPS, $i_N=0^\circ$)	297
218	Variation of Lift Coefficient with Elevator Deflection in Cruise (V=113 FPS, $i_N=0^\circ$)	298
219	Elevator Effectiveness - Incremental Lift Coefficient and Incremental Pitching Moment Coefficient (V=113 FPS, $i_N=0^\circ$)	299
220	Elevator Effectiveness in Cruise - Airframe Lift Coefficient versus Angle of Attack - Rotors Off (V=113 FPS; $i_N=0^\circ$; $\delta_e=0^\circ$ & 10.4°)	300
221	Elevator Effectiveness in Cruise Airframe Pitching Moment versus Angle of Attack (V=113 FPS; $i_N=0^\circ$; $\delta_e=0^\circ$ & 10.4°) Rotors Off	301
222	Elevator Effectiveness Airframe Lift versus Pitching Moment Coefficients (V=113 FPS; $i_N=0^\circ$; $\delta_e=0^\circ$ & 10.4°)	302
223	Elevator Effectiveness in Yaw (V=113FPS; $i_N=0^\circ$; $\delta_e=0^\circ$ & 10°)	303
224	Schedule of Spoiler Deflection versus Aileron Deflection (V=113 FPS $i_N=0^\circ$)	304
225	Roll Control Effectiveness in Cruise - Variation of Rolling and Yawing Moment Coefficients with Combined Aileron and Spoiler Deflections (V=113 FPS, $i_N=0^\circ$)	305
226	Roll Control Effectiveness in Cruise - Variation of Rolling and Yawing Moment Coefficients with Spoiler and Aileron Deflection (V=113 FPS; $i_N=0^\circ$)	306

LIST OF ILLUSTRATIONS

<u>FIGURE</u>		<u>PAGE</u>
227	Roll Control Effectiveness in Cruise - Variation of Rolling and Yawing Moment Coefficients with Spoiler and Aileron Deflection (V=113 FPS $i_N = 0^\circ$)	307
228	Roll Control Effectiveness - Variation of Rolling and Yawing Moment Coefficients with Angle of Attack in Cruise (V=113 FPS, $i_N = 0^\circ$)	308
229	Effect of Roll Control on Lift - Variation of Lift Coefficient with Angle of Attack (V=113 FPS, $i_N = 0^\circ$, $\delta_{S/A} = 0/0$ and $\delta_{S/A} = 50/26$)	309
230	Effect of Roll Control on Pitching Moment Coefficient Variation with Angle of Attack (V=113 FPS, $i_N = 0^\circ$, $\delta_{S/A} = 0/0$, and $\delta_{S/A} = 50/26$)	310
231	Effect of Roll Control on Longitudinal Stability (V=113 FPS, $i_N = 0^\circ$, $\delta_{S/A} = 0/0$, and $\delta_{S/A} = 50/26$)	311
232	Rudder Effectiveness - Variation of Yawing Moment Coefficient with Rudder Deflection (V = 113 FPS, $i_N = 0^\circ$)	312
233	Rudder Effectiveness in Yaw - Effect of Sideslip Angle on Yawing Moment Coefficient due to Rudder Deflections (V=113 FPS, $i_N = 0^\circ$)	313
234	Effect of Rudder on Rolling Moment Coefficient versus Sideslip Angle (V=113 FPS, $i_N = 0^\circ$)	314
235	Variation of Rolling Moment Coefficient with Rudder Deflection (V=113 FPS, $i_N = 0^\circ$)	315
236	Effect of Flap Deflection on Variation of Lift Coefficient with Angle of Attack (V=113 FPS, $i_N = 0^\circ$, $\delta_F = 0^\circ, 10^\circ, 20^\circ, 40^\circ$)	316
237	Effect of Flap Deflection on Variation of Pitching Moment with Angle of Attack (V=113 FPS, $i_N = 0^\circ$, $\delta_F = 0^\circ, 10^\circ, 20^\circ, 40^\circ$)	317

FIGURE	LIST OF ILLUSTRATIONS	PAGE
238	Effect of Flap Deflection on Static Longitudinal Stability ($V=113$ FPS, $i_N=0^\circ$, $\delta_F=0^\circ, 10^\circ, 20^\circ, 40^\circ$)	318
239	Effect of Flap Deflection on Lift Coefficient Variation with Angle of Attack ($V=113$ FPS, $i_N=0^\circ$, $\delta_F=0^\circ, 10^\circ, 20^\circ, 40^\circ$)	319
240	Effect of Flap Deflection on Pitching Moment Coefficient Variation with Angle of Attack ($V=113$ FPS, $i_N=0^\circ$, $\delta_F=0^\circ, 10^\circ, 20^\circ, 40^\circ$)	320
241	Effect of Flap Deflection on Longitudinal Stability ($V=113$ FPS, $i_N=0^\circ$, $\delta_F=0^\circ, 10^\circ, 20^\circ, 40^\circ$)	321
242	Effect of Flap Deflection on Yawing and Rolling Moment Coefficient Variation with Sideslip ($V=113$ FPS, $i_N=0^\circ$, $\delta_F=0^\circ, 20^\circ, 40^\circ$)	322
243	Flap Effectiveness - Aircraft Lift and Pitching Moment Coefficient - Rotors Off ($V=113$ FPS, $i_N=0^\circ$)	323
244	Flap Effectiveness Aircraft Lift and Pitching Moment Coefficient - Rotors On ($V=113$ FPS, $i_N=0^\circ$)	324
245	Comparison of Test and Theory for Angle of Attack Rotor Derivatives in Cruise ($i_N=0^\circ$)	336
246	Comparison of Test and Theory for Lateral Cyclic Rotor Derivatives in Cruise ($i_N=0^\circ$, $\delta_F=0^\circ$)	337
247	Comparison of Test and Theory for Lateral Cyclic Rotor Derivatives in Cruise ($i_N=0^\circ$, $\delta_F=0^\circ$)	338
248	Comparison of Test and Theory for Longitudinal Cyclic Rotor Derivatives in Cruise ($i_N=0^\circ$, $\delta_F=0^\circ$)	339
249	Comparison of Test and Theory for Longitudinal Cyclic Rotor Derivatives in Cruise ($i_N=0^\circ$, $\delta_F=0^\circ$)	340
250	Summary of Blade Rotating Natural Frequency	345

LIST OF ILLUSTRATIONS

<u>FIGURE</u>		<u>PAGE</u>
251	1/Rev Content of Alternating 12.5%R Blade Loads in Hover ($i_N=90^\circ$, $\theta_{75}=12^\circ$)	346
252	2/Rev Content of Alternating 12.5%R Blade Loads in Hover ($i_N=90^\circ$, $\theta_{75}=12^\circ$)	347
253	Effect of Flap Deflection in Transition on Alternating Blade Loads ($i_N=41.6^\circ$, $\delta_F=20,30,40$, $V=113$ FPS)	350
254	Effect of Fuselage Yaw Angle on Alternating Blade Loads ($i_N=41.6^\circ$, $\delta_F=0^\circ$, $V=72$ FPS)	351
255	Effect of Nacelle Incidence in Transition on Alternating Blade Loads ($i_N=30.0^\circ$, 41.6° , $\delta_F=30^\circ$, 40° $V=113$ FPS)	352
256	Effect of Nacelle Incidence on Alternating Blade Loads ($V=72$ FPS)	353
257	Cyclic Required to Minimize Blade Loads During Nacelle Incidence Sweep ($V=72$ FPS)	354
258	Effect of Longitudinal Cyclic in Transition on Alternating Blade Loads ($i_N=41.6^\circ$, $\delta_F=40^\circ$, $V=72$ FPS)	355
259	Effect of Lateral Cyclic in Transition on Alternating Blade Loads ($i_N=41.6^\circ$, $\delta_F=40^\circ$, $V=72$ FPS)	356
260	Effect of Forward Speed in Cruise on Alternating Blade Loads ($i_N=0^\circ$, $\delta_F=0^\circ$, $V=113,139,162$ FPS)	359
261	Effect of Fuselage Yaw Angle on Alternating Blade Loads ($i_N=0^\circ$, $V=113,139,161,182$ FPS)	360
262	Effect of Flap Deflection on Alternating Blade Loads in Cruise ($i_N=0^\circ$, $\delta_F=0,10,20,40^\circ$, $V=113$ FPS)	361
263	Effect of Tunnel Dynamic Pressure on Alternating Blade Loads ($i_N=0^\circ$)	362

LIST OF ILLUSTRATIONS

<u>FIGURE</u>		<u>PAGE</u>
264	Effect of Tunnel Dynamic Pressure on Alternating Blade Loads ($i_N=0^\circ$)	363
265	Cyclic Required to Minimize Blade Loads from 71 to 183 FPS Tunnel Speed ($i_N=0^\circ$)	364
266	Effect of Longitudinal Cyclic in Cruise on Alternating Blade Loads ($i_N=0^\circ$)	365
267	Effect of Lateral Cyclic in Cruise on Alternating Blade Loads ($i_N=0^\circ$, $\delta_F=0^\circ$, $V=161$ FPS)	366
268	Effect of Cyclic on Alternating Blade Loads in Cruise ($i_N=0^\circ$, $V=157$ FPS)	367
269	Cyclic Required to Minimize Blade Loads at Tunnel Cruise Speed = 161 FPS ($i_N=0^\circ$)	368
270	1/4.622 Scale Model Cruise Stability Boundaries Predicted with Actual Model Frequencies for the Full Scale Aircraft ($i_N=0^\circ$)	375
271	1/4.622 Scale Model Damping in Air Resonance Mode for the Full Scale Aircraft at 90 Knots ($i_N=0^\circ$) ,	376
272	1/4.622 Scale Model Predicted Coupled Frequencies for the Full Scale Aircraft in Hover ($i_N=90^\circ$)	377
273	1/4.622 Scale Model Damping in Resonance Mode for the Full Scale Aircraft in Hover ($i_N=90^\circ$)	378
274	1/4.622 Scale Model Damping in Resonance Mode for the Full Scale Aircraft at 90 Knots ($i_N=45^\circ$)	379
275	1/4.622 Scale Model Coupled Frequencies from Analysis for the Full Scale Aircraft at 90 Knots ($i_N=45^\circ$)	380

	<u>PAGE</u>
<u>APPENDIX A</u>	
RUN LOG	384
<u>APPENDIX B</u>	401
B-1 Deflection Test Wing Deflection due to Wing Lift ($i_N=0^\circ$)	404
B-2 Deflection Test Wing Deflection due to Wing Lift ($i_N=0^\circ$)	405
B-3 Deflection Test Wing Deflection due to Rotor Normal Force ($i_N=0^\circ$)	406
B-4 Deflection Test Wing Deflection due to Rotor Normal Force ($i_N=45^\circ$)	407
B-5 Deflection Test-Wing Deflection due to Rotor Pitching Moment ($i_N=0^\circ$)	408
B-6 Wing Deflection due to Rotor Thrust ($i_N=0^\circ$)	409
B-7 Wing Chordwise Deflections with 40 LBS rotor Thrust ($i_N=0^\circ$).	410
B-8 Deflection Test-Wing Rotation due to Rotor Normal Force ($i_N=0^\circ$).	411
B-9 Deflection Test-Wing Rotation due to Rotor Normal Force ($i_N=45^\circ$)	412
B-10 Deflection Test-Wing Rotation due to Rotor Pitching Moment ($i_N=0^\circ$)	413
B-11 Deflection Test-Wing Rotation due to Rotor Pitching Moment ($i_N=0^\circ$)	414
B-12 Deflection Test-Wing Rotation due to Rotor Thrust ($i_N=0^\circ$).	415
B-13 Deflection Test-Rotor Disc Rotation due to Rotor Pitching Moment ($i_N=0^\circ$).	416
B-14 Deflection Test-Rotor Disc Rotation due to Rotor Pitching Moment ($i_N=0^\circ$).	417
B-15 Deflection Test-Rotor Disc Rotation due to Rotor Pitching Moment ($i_N=45^\circ$)	418

PAGEAPPENDIX B

B-16	Deflection Test-Rotor Disc Rotation due to Rotor Pitching Moment ($i_N=90^\circ$)	419
B-17	Deflection Test-Rotor Disc Rotation due to Rotor Normal Force ($i_N=0^\circ$)	420
B-18	Deflection Test-Rotor Disc Rotation due to Rotor Normal Force ($i_N=45^\circ$)	421
B-19	Deflection Test-Rotor Disc Rotation due to Rotor Normal Force ($i_N=90^\circ$)	422
B-20	Deflection Test-Rotor Disc Deflection due to Rotor Yawing Moment ($i_N=0^\circ$)	423
B-21	Deflection Test-Rotor Disc Deflection due to Rotor Yawing Moment ($i_N=0^\circ$)	424
B-22	Deflection Test-Rotor Disc Rotation due to Rotor Yawing Moment ($i_N=45^\circ$)	425
B-23	Deflection Test-Rotor Disc Rotation due to Rotor Yawing Moment ($i_N=90^\circ$)	426
B-24	Deflection Test-Nacelle Deflection due to Rotor Side Force ($i_N=45^\circ$)	427
B-25	Deflection Test-Rotor Disc Plane Rotation due to Rotor Side Force ($i_N=90^\circ$)	428

APPENDIX C

C-1	Wing Weight and Balance	430
C-2	1/4 Scale Model 222 Fuselage	431
C-3	1/4 Scale Model 222 Nacelles	432
C-4	1/4 Scale Model 222 Horizontal Stabilizer.	433
C-5	1/4 Scale Model 222 Vertical Stabilizer	434
C-6	1/4 Scale Model 222 Flaps	435

APPENDIX D

D-1	Rotor Hub Tares Transition ($i_N=45^\circ$, $\delta_F=40^\circ$, $V=72$ FPS)	437
D-2	Rotor Hub Tares Transition ($i_N=45^\circ$, $\delta_F=40^\circ$, $V\neq 72$ FPS)	438

PAGEAPPENDIX D

D-3	Rotor Hub Tares Transition ($i_N=45^\circ$, $\delta_F=40^\circ$, $V=73$ FPS)	439
D-4	Rotor Hub Tares Transition ($i_N=45^\circ$, $\delta_F=40^\circ$, $V=72$ FPS)	440
D-5	Rotor Hub Tares Cruise ($i_N=0^\circ$, $V=113$ FPS).	441
D-6	Rotor Hub Tares Cruise ($i_N=0^\circ$, $V=113$ FPS).	442
D-7	Rotor Hub Tares Cruise ($i_N=0^\circ$, $V=113$ FPS).	443
D-8	Rotor Hub Tares Cruise ($i_N=0^\circ$, $V=113$ FPS).	444

APPENDIX E

		445
E-1	Flow Visualization Test Run Log	450
E-2	Initial Flow Survey at 0° Fuselage Attitude	452
E-3	Flow Survey at 10° Fuselage Attitude Modified Fillet of Run 3	453
E-4	Flow Survey at 10° Fuselage Attitude Modified Fillet of Run 3	454
E-5	Flow Survey at 7° Fuselage Attitude Final Fillet Modification	455
E-6	Flow Survey at 0° Fuselage Attitude 15° Nose Left Yaw	456
E-7	Flow Survey at 0° Fuselage Attitude 15° Nose Right Yaw	457
E-8	Pressure Survey at Tail	458
E-9	Pressure Survey at Tail Plane	459
E-10	Pressure Survey at Tail Plane	460

LIST OF TABLES

<u>TABLE</u>		<u>PAGE</u>
1	PHASE I TEST PROGRAM EVALUATION	7
2	MODEL DIMENSIONS	12
3	BOEING V/STOL WIND TUNNEL PERTINENT DATA	18
4	WIND TUNNEL DATA REDUCTION INPUT CONSTANTS	30
5	LONGITUDINAL STABILITY DERIVATIVES IN TRANSITION	116
6	LATERAL/DIRECTIONAL STABILITY DERIVATIVES IN TRANSITION	121
7	LONGITUDINAL STABILITY DERIVATIVES IN CRUISE	254
8	LATERAL/DIRECTIONAL STABILITY DERIVATIVES IN CRUISE	260
9	EFFECT OF LATERAL CYCLIC ON AIRCRAFT STABILITY	284
10	EFFECT OF LONGITUDINAL CYCLIC ON AIRCRAFT STABILITY PARAMETERS (RIGHT ROTOR)	286
11	BLADE FREQUENCIES FROM STATIC TWEAK TESTS	344
12	MODEL FREQUENCIES	371

LIST OF SYMBOLS

<u>SYMBOL</u>		<u>UNITS</u>
A_1	Lateral cyclic pitch	Deg
B_1	Longitudinal cyclic pitch	Deg
C_D	Airframe drag = $\frac{D}{qs}$	-
C	Chord	Ft
C_L	Aircraft lift coefficient = $\frac{L}{qs}$	-
C_ℓ	Aircraft rolling moment coefficient $\frac{RM}{qsb}$	-
C_{L_α}	Lift curve slope $\partial C_L / \partial \alpha$	1/Deg
C_{ℓ_β}	Rolling moment derivative with side slip angle	1/Deg
C_m	Aircraft pitching moment coefficient $\frac{PM}{qs\bar{c}}$	-
$C_{m_{\delta_e}}$	Pitching moment derivative with elevator deflection	1/Deg
C_n	Aircraft yawing moment coefficient $\frac{YM}{qsb}$	-
C_{nA_1}	Yawing moment derivative with lateral cyclic	1/Deg
C_P	Rotor power coefficient $\frac{HP \times 550}{\rho \pi R^2 V_T^3}$	-
C_{PM}	Rotor pitching moment coefficient $\frac{PM}{\rho \pi R^3 V_T^2}$	-
C_{SF}	Rotor side force coefficient $\frac{SF}{\rho \pi R^2 V_T^2}$	-
C_T	Rotor thrust coefficient $\frac{T}{\rho \pi R^2 V_T^2}$	-
C_X	Aircraft propulsive force coefficient $\frac{x}{qs}$	-
C_Y	Aircraft side force coefficient $\frac{SF}{qs}$	-
C_{Y_β}	Side force derivative with side slip angle	1/Deg
C_{YM}	Rotor yawing moment $\frac{YM}{\rho \pi R^3 V_T^2}$	-
$c/4$	Wing quarter chord	-
D	Airframe drag	LB

LIST OF SYMBOLS

<u>SYMBOL</u>		<u>UNITS</u>
GW	Gross weight	LB
HP	Rotor horsepower	HP
I_{xx}, I_{yy}, I_{zz}	Mass moment of inertia about the three axes	IN-LB SEC ²
I_{PIVOT}	Moment of inertia - polar	LB-FT
i_N	Nacelle incidence	Deg
i_{NS}	Nacelle shaft angle of incidence	Deg
i_w	Wing incidence	Deg
L	Lift	LB
P	Per rotor revolution	-
PM, m	Pitching moment	FT LB
q	Freestream dynamic pressure $1/2\rho V^2$	LB/FT ²
R	Rotor radius	FT
r	Radial location to a blade station	FT
RM, l	Rolling moment	FT LB
S	Wing area	FT ²
SF	Side Force	LB
T	Rotor thrust	LB
t	Airfoil thickness	FT
V	Freestream velocity	FT/SEC
V_T	Rotor tip speed	FT/SEC
X	Aircraft propulsive force	LB
YM, n	Yawing moment	FT LB
θ_{75}	Rotor blade collective pitch at the three quarter radius	Deg
α_f	Fuselage pitch deflection	Deg

LIST OF SYMBOLS

<u>SYMBOL</u>		<u>UNITS</u>
α_s	Nacelle shaft pitch deflection	Deg
β	Side slip angle	Deg
ψ	Fuselage yaw angle (rotor azimuth angle)	Deg
μ	Advance ratio V/V_T	-
ω_c	Wing chordwise bending frequency	cps
ω_l	Blade lag rotational frequency	cps
ω_β	First mode, flapwise blade natural frequency	cps
ω_p	Aircraft pitch frequency	cps
ω_v	Wing vertical bending frequency	cps
ω_α	Wing torsional frequency	cps
$\Omega - \omega_l$	Lower blade lag rotational frequency	cps
$\omega + \omega_\beta$	Upper blade flap rotational frequency	cps
$\Omega - \omega_\beta$	Lower blade flap rotational frequency	cps
ρ	Density of air	LB SEC ² /FT ⁴
Ω	Rotor angular velocity	-
$1\Omega, 2\Omega$	Integer frequency ratio	-
σ	Rotor solidity $\frac{bcR}{\pi R^2}$	-
δ_A	Aileron deflection	Deg
δ_F	Flap deflection	Deg
δ_S	Spoiler deflection	Deg
Δ	Increment in coefficient	

1.0 INTRODUCTION

During the technical assessment phase of Task 1 of Contract NAS2-6598 several areas were defined where additional research is desirable. These included definition of aircraft characteristics and the effects of feedback control systems, ground effect, transient rotor loads, autorotation and descent, and free-free aeroelastic tests.

To permit experimental investigations in these areas, Boeing fabricated a 1/4.622 Froude scale wind tunnel model of the M-222 Research Aircraft. The selection of this scale was the result of meeting the following ground rules:

1. Develop one model that will provide performance and dynamic testing capability.
2. The scale factor must be large enough to provide a Reynolds number of greater than 500,000 at the three-quarter blade radius to achieve meaningful rotor performance.
3. The model span must be less than 75% of the test section to avoid being significantly affected by wind tunnel wall effects.
4. The model must be capable of properly representing the dynamics of the full scale airplane at 400 KTS.

Boeing was awarded a contract from NASA to conduct a wind tunnel program with this model in two phases directed at the following:

- o Obtain steady state rotor and aircraft loads,
aerodynamic and aeroelastic characteristics
- o Obtain the dynamic characteristics and boundaries
with four degrees of freedom testing

The testing accomplished was only a portion of the first program above when model mechanical and instrumentation problems prevented any further useful testing until they were fixed. Further testing is recommended to provide data directed at achieving the basic research objectives of the original program.

2.0 TEST OBJECTIVES

The overall objective of this test program was to provide performance, stability and control data from hover through transition and cruise. The testing defines the unaccelerated rotor and aircraft characteristics and loads including the elastic and dynamic interactions associated with the full-scale aircraft. A list of the specific test objectives is presented in Table 1 with an estimate of the percent completion achieved during this test program.

A cross reference between the objectives that were accomplished and the section of the report containing the applicable data is listed here for rapid reference.

1. Conduct Flow Visualization Testing on Model to Determine the Flow at the Horizontal and Vertical Stabilizer and Develop a Satisfactory Fairing at the Wing Fuselage Junction

Data was obtained from a flow visualization test conducted prior to the fabrication of the model fuselage skins.

This is presented in Appendix E as a reprint of the memo report summarizing the test.

2. Determine Basic Aircraft Performance and Static Stability throughout Transition and in the Airplane Mode

Rotor, airframe and total aircraft performance is presented in Sections 4.1 and 4.2 for the transition and cruise regime. Static stability is presented in Sections 5.1 and 5.2 for rotor, airframe and total aircraft characteristics in transition and cruise.

3. Determine the Control Power Available throughout Transition and Cruise and Define the Control Scheduling Required to Minimize Cross Coupling Between Axes

Section 5.1.3 provides data summarizing the control power and mixing in transition. Control effectiveness in cruise is presented in Section 5.2.3.

4. Determine the Effect of Flap Setting on Performance, Trim Requirements and Control through Transition

The effect of flap deflection on rotor performance in transition is shown in Section 4.1.1 and on the aircraft performance in Section 4.1.2. Flap effects on rotor and aircraft performance is presented in Sections 4.2.1 and 4.2.2 for the beginning of the cruise regime. The effects of flap deflection on trim and control are defined in Sections 5.1.2 and 5.1.3 in transition. Flap effects are also examined at the beginning of the cruise regime and Sections 5.2.2 and 5.2.3 present these effects on trim and control.

5. Investigate the Variation of Blade Loads through Transition as a Function of Nacelle Incidence, Speed, Cyclic Pitch

The blade load data in transition is presented in Section 6.2 for transition. Additional data is provided in Section 6.3 defining the effects of attitude, forward speed and cyclic pitch on blade loads in cruise.

6. Investigate the Effects of Ground Proximity, during Low Speed Transition Flight, on Static Stability, Control Power and Blade Loads. Investigate any Non-Periodic or Random Load Variations Associated with Ground Effect

No data was obtained for this objective.

7. Determine Inception and Boundaries for Wing Stall and Tail Stall through Transition and Cruise Modes

Wing stall data was obtained and is presented in Section 4.1.2 for transition and 4.2.2 for cruise with the rotors removed.

8. Develop Input Signals, Signal Shaping and Output Mixing for a Feedback System Aimed at:

- (a) Minimizing Blade Loads through Transition
- (b) Improving Aircraft Static Stability in Transition and Cruise
- (c) Minimizing Blade Load Variation with Speed and Angle of Attack in the Cruise Mode

Cyclic effectiveness data was obtained in transition and cruise which can be used for defining the gains and signal shaping for the low rate feedback system

The effects of cyclic on blade loads are presented in Sections 6.2.3 and 6.3.3. The effects on aircraft stability is a result of changes in the rotor stability characteristics shown in Sections 5.1.3 and 5.2.3. The impact on total aircraft stability is shown in 5.2.2.

9. Examine the Lightly Damped Air Resonance Mode and Determine the Effect of Cyclic Feedback on this Mode

Dynamic data acquired during this testing addresses the lightly damped modes and is discussed in Section 7.2

10. Examine the Compatibility of the Feedback Characteristics to Meet the Various Objectives of Item 8 and 9 and Develop a Single Compromise System

No testing was accomplished with the feedback systems operating.

TABLE 1

PHASE I - TEST PROGRAM EVALUATION

TEST OBJECTIVES	% COMPLETE	
	Flight Modes	
	Transition	Cruise
1. Conduct Flow Visualization Testing on Model to Determine the Flow at the Horizontal and Vertical Stabilizer and Develop a Satisfactory Fairing at the Wing Fuselage Junction	0%	Completed Prior to Model Fabrication
2. Determine Basic Aircraft Performance and Static Stability throughout Transition and in the Airplane Mode	50% 50%	50% 80%
3. Determine the Control Power Available throughout Transition and Cruise and Define the Control Scheduling Required to Minimize Cross Coupling Between Axes	50%	80%
4. Determine the Effect of Flap Setting on Performance, Trim Requirements and Control through Transition	50%	
5. Investigate the Variation of Blade Loads throughout Transition as a Function of <u>Nacelle Incidence</u> <u>Speed</u> <u>Cyclic Pitch</u>	50% 50% 50%	
6. Investigate the Effects of Ground Proximity, during Low Speed Transition Flight, on Static Stability, Control Power and Blade Loads. Investigate any Non-Periodic or Random Load Variations Associated with Ground Effect	0%	
7. Determine Inception and Boundaries for <u>Wing Stall</u> and <u>Tail Stall</u> through Transition and Cruise Modes	50% 50%	75% 50%
8. Develop Input Signals, Signal Shaping and Output Mixing for a Feedback System Aimed at:		
(a) Minimizing Blade Loads through Transition	15%	
(b) Improving Aircraft Static Stability in Transition and Cruise	15%	25%
(c) Minimizing Blade Load Variation with Speed and Angle of Attack in the Cruise Mode		25%

TABLE 1 (continued)		
PHASE I - TEST PROGRAM EVALUATION		
TEST OBJECTIVES	% COMPLETE	
	Flight Modes	
	Transition	Cruise
9. Examine the <u>Lightly Damped Air Resonance Mode and Determine the Effect of Cyclic Feedback on this Mode</u>	50%	100%
	0%	0%
10. Examine the Compatibility of the Feedback Characteristics to Meet the Various Objectives of Item 8 and 9 and Develop a Single Compromise System	0%	0%
SUMMARY	<u>40%</u>	<u>60%</u>

3.0 TEST INSTALLATION

This section provides a description of the model, its installation in the wind tunnel and the data reduction methods utilized in this test program.

3.1 MODEL DESCRIPTION

The model is a 1/4.622 scale full span, powered configuration that is Froude scaled from the Model 222 Tilt Rotor Research aircraft as described in Reference 1 dated March 1972. It incorporates the 26 ft. diameter soft in-plane prop/rotor designed and tested under NASA contract. This model, shown in Figure 12, was provided by the contractor for this test program and has the following major dynamically-scaled components.

1. Two 3-bladed rotors
2. Two nacelles
3. Full span wing
4. Fuselage
5. Tail

Essential model dimensions are shown in Table 2. The rotors are defined in Figure 13 and have the same aerodynamic and aeroelastic characteristics as the full scale rotor built under NASA contract NAS2-6505. It has remote controlled fast acting collective pitch and two axes fast acting cyclic pitch actuation systems.

The nacelles are joined to the wing by a pivot and have remote pitch actuation.

The wing is crown mounted and has full span flaps and leading edge

umbrellas for download alleviation. Flaps are used during transition to provide additional lift and the outboard section of the flap is used as an aileron for control in conjunction with outboard spoilers.

The wing, fuselage, and empennage are dynamically scaled from the Model 222 aircraft and the rudder and elevator are remotely controlled. The model was supported on a pedestal mount with pitch and yaw capability.

The primary instrumentation included strain gages to obtain flap, chord and torsion loads at the blade root. A six component balance in each nacelle measured the rotor forces moments and torque. A six component main balance located in the fuselage measured aircraft forces and moments. Strain gages were located at the wing root to measure the flap and chord bending and torsion to define the aerodynamic and load characteristics. Position indicators were connected to meters to provide a visual display of the aircraft control positions which were remotely controlled as schematically shown in Figure 14. Each rotor has an RPM and 1/rev output. Twelve thermocouple readouts provided safety monitoring of critical motor, gearbox and cross shaft bearing temperatures.

The model is powered by a 20 HP, 11,375 RPM electric motor manufactured by Task Corporation. The motor drives a 3.04:1 reduction gear box in the center fuselage which is connected by cross shafts in the wing to a 3.09:1 reduction gear box in each nacelle. This provides a total gear reduction from the electric motor to rotor of 9.39:1.

A photograph of the model under test in the cruise configuration is shown in the top of Figure 15 and the lower portion is a left rear quarter view showing details of the strakes, sponsons and flaps.

TABLE 2
MODEL DIMENSIONS

ROTOR

Number of Blades	3
Radius	33.75 IN.
Chord	4.078 IN.
Twist	42.5 DEG.
Airfoil Section	23021/23010-1.58
Solidity	0.115
Rotor Speed (Hover)	1185 RPM
Rotor Speed (Cruise)	825 RPM
Collective Pitch Available	-5 to 65 DEG.
Cyclic Pitch Available	+ 10 DEG.

NACELLE

Nacelle Pivot Position (in % of Wing Chord)	40%
Rotor Disc Nacelle Pivot Distance	12.33 IN.

WING

Airfoil Section	634221 Modified
Span (Rotor ξ to Rotor ξ)	86.76 IN.
chord	15.53 IN.
Area	9.36 FT. ²
Aspect Ratio	5.61
Flap in % of Chord	30%
Wing Incidence	2 DEG.
Thickness - Chord Ratio	0.21

FUSELAGE

Diameter	14.69 IN.
Length	102.50 IN.

TAIL - HORIZONTAL

Area	2.73 FT. ²
Span	10.89 IN.
Aspect Ratio	4.25
Taper Ratio (C _{TIP} /C _{ROOT})	.384
Root Chord	14.05 IN.
Airfoil Section	64A010
Elevators in % of Chord	44.1%

TABLE 2 (continued)TAIL - VERTICAL

Area	2.03 FT ²
Span	22.75 IN.
Aspect Ratio	1.77
Taper Ratio (C_{TIP}/C_{ROOT})	.35
Root Chord	20.98 IN.
Airfoil Section	64A008
Rudder in % of Chord	50.6

Figure 12. 1/4 622 Froude Scale Wind Tunnel Model

WING

Span 86.76 In.
 Chord 15.53 In.
 Area 9.36 FT²
 Aspect Ratio 5.61
 Thickness-Chord Ratio 0.21

VERTICAL TAIL

Span 22.72 In.
 Area 2.03 FT²

HORIZONTAL TAIL

Span 40.89 In.
 Area 2.73 FT²

ROTOR

Diameter 67.50 In.
 Solidity .115
 No. Blades 3

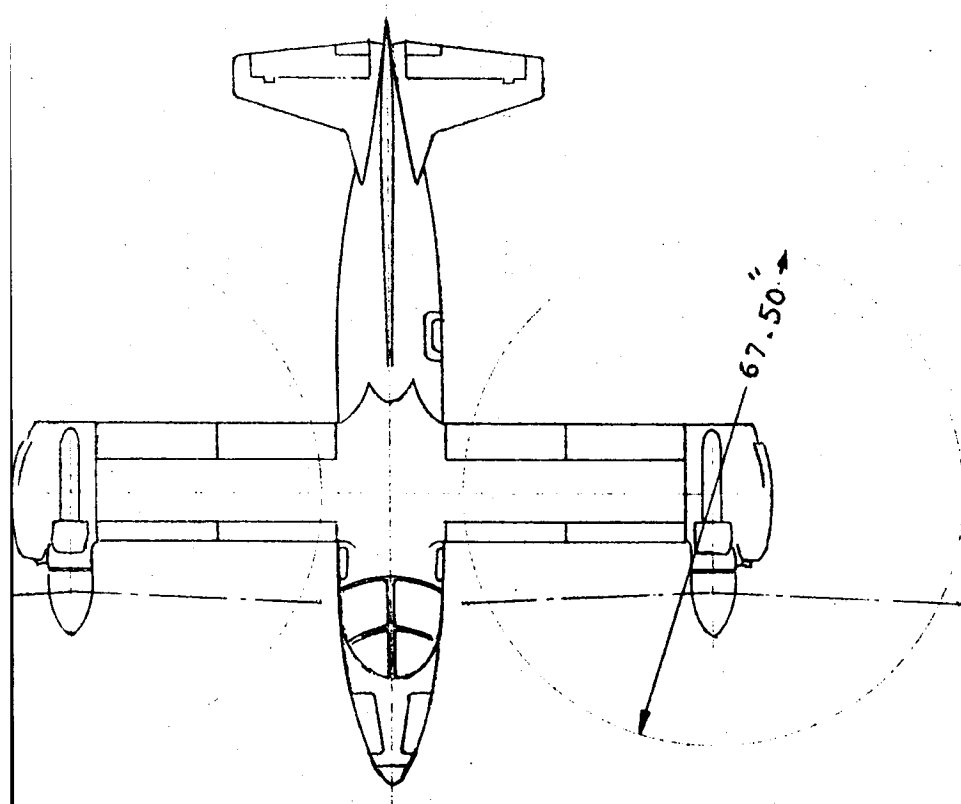
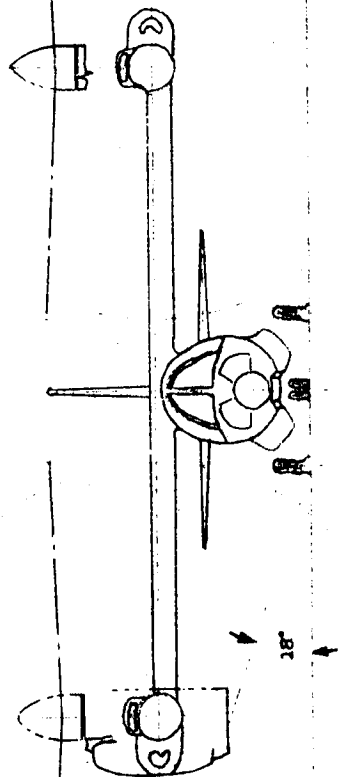
WEIGHTS

Design Gross Wt 122. LBS

14.

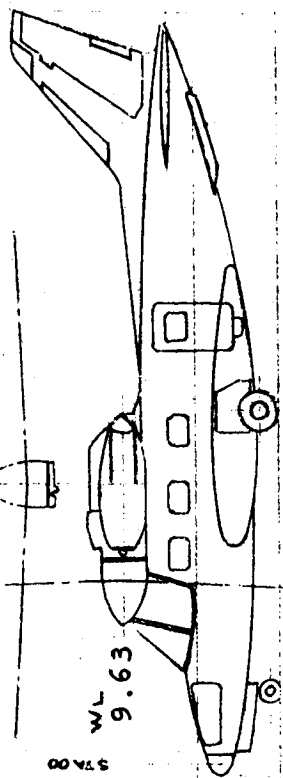
154.26"

86.76"



WL 9.63

102.50"



V4622 FROUDE SCALE MODEL 222
BLADE DEFINITION

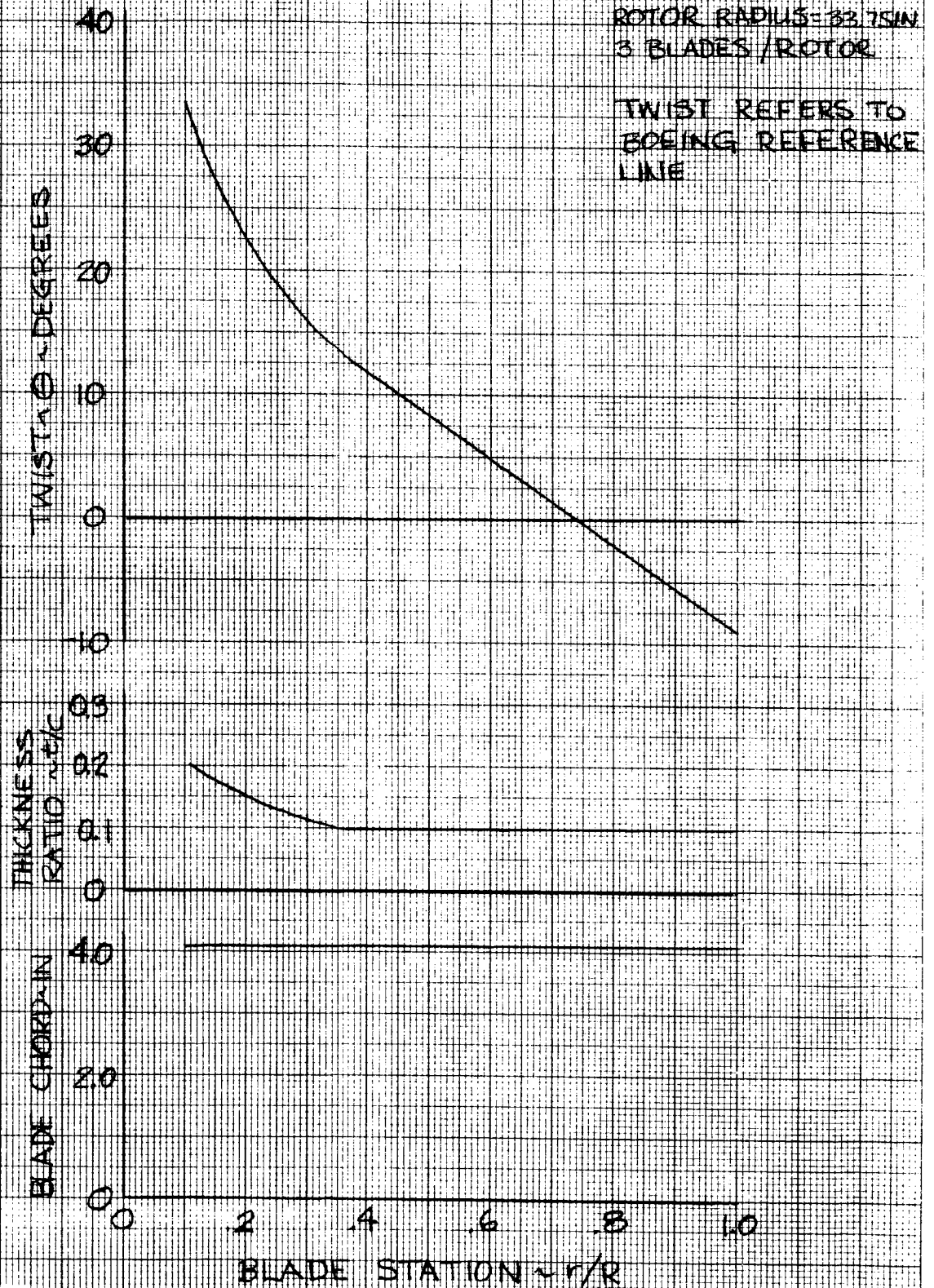


Figure 13

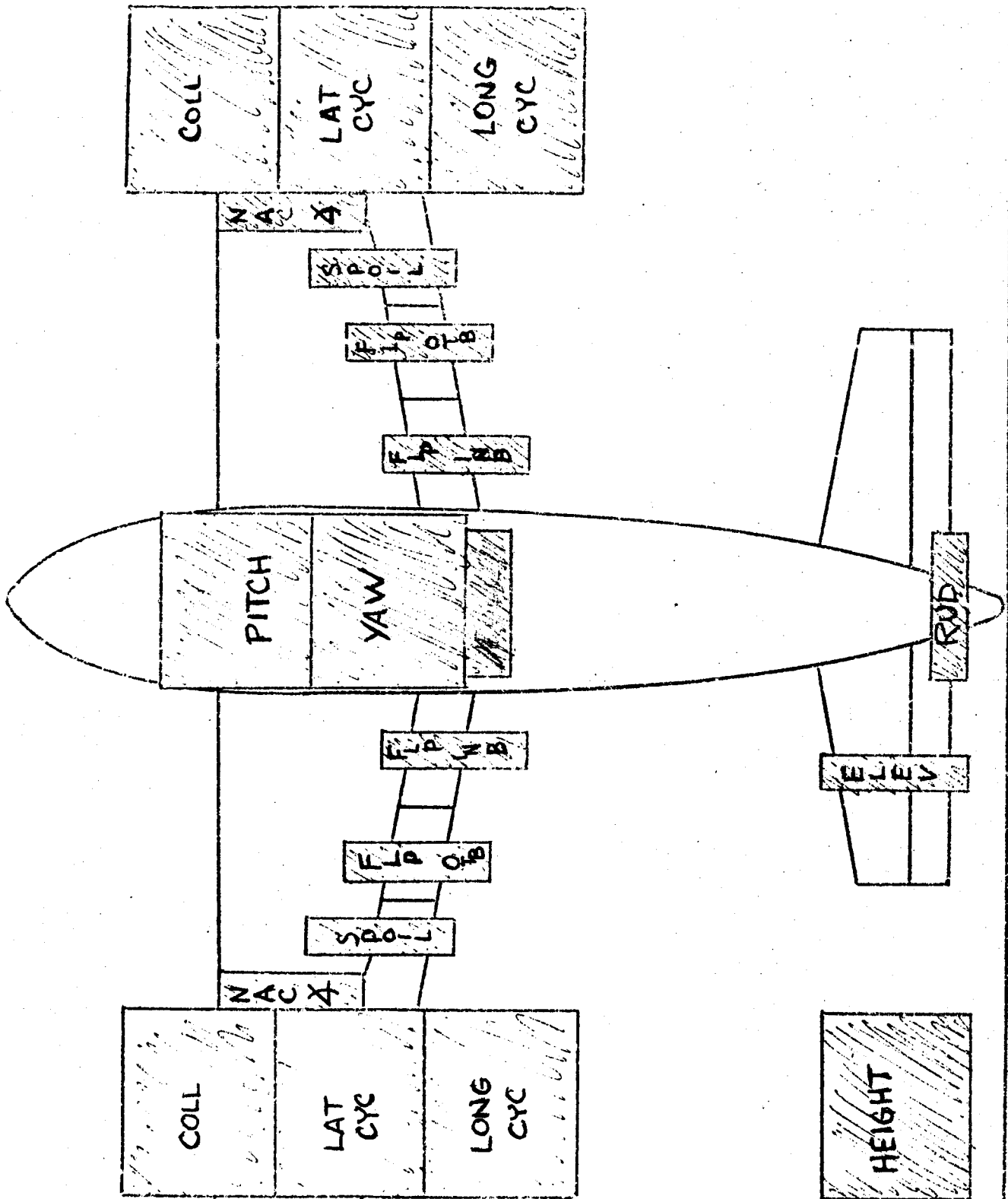
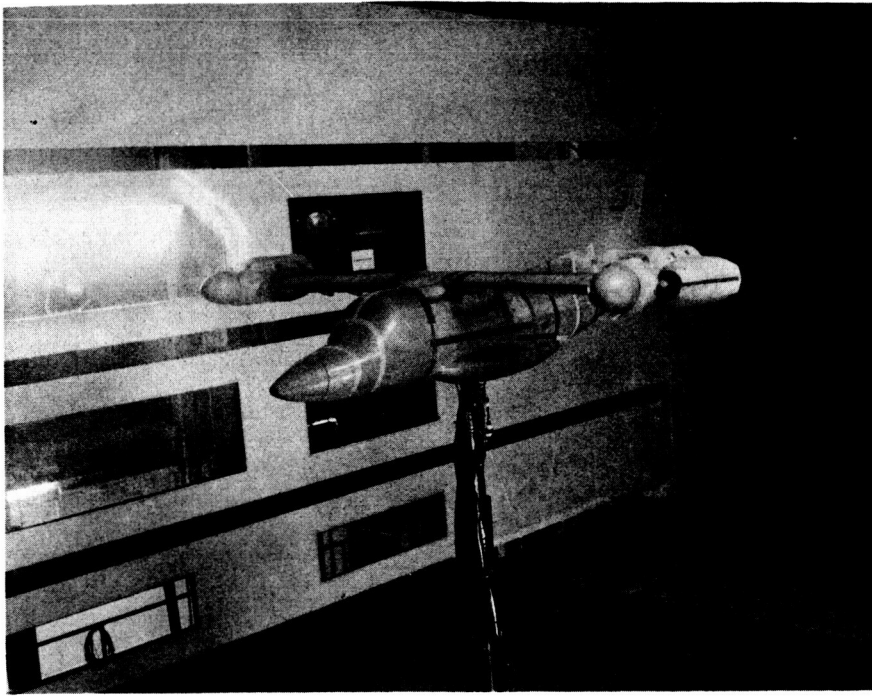
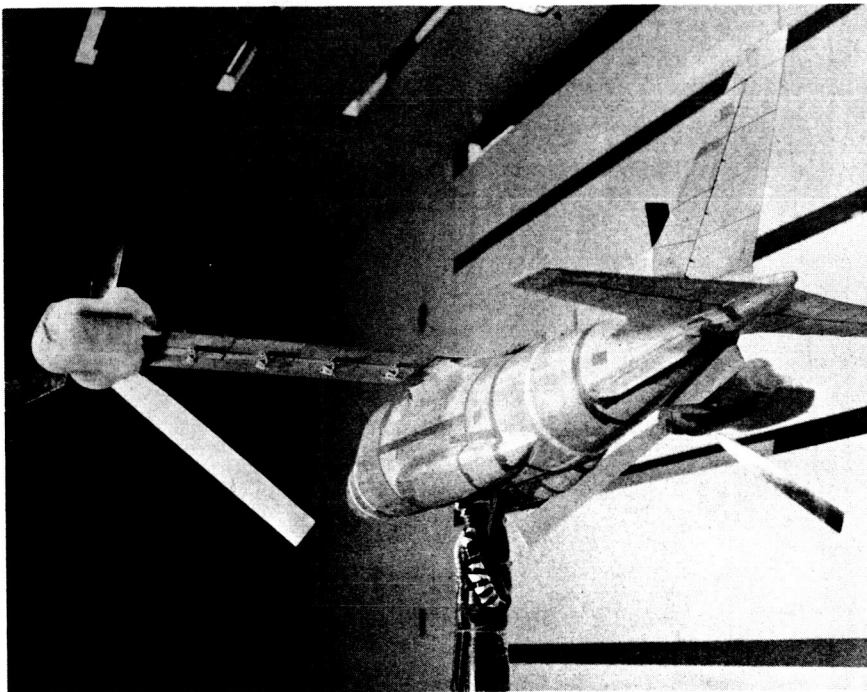


FIGURE 14 MODEL 222 CONTROL DISPLAY



MODEL 222 IN CRUISE TESTING



MODEL 222 REAR QUARTER VIEW

FIGURE 15 - 1/4 622 SCALE MODEL 222 INSTALLED IN THE WIND TUNNEL TEST SECTION

3.2 TUNNEL INSTALLATION

3.2.1 Boeing V/STOL Wind Tunnel

This closed circuit, continuous flow facility contains nine fixed-pitch blades, 39 feet in diameter, which provide wind speeds up to 240 knots. The fan is powered by a 15,000 horsepower motor package consisting of two separate motors located in a nacelle. Air travels through the 742 foot closed circuit tunnel and is turned by vanes into the test section which is 20 feet wide, 20 feet high and 45 feet long. Models can be positioned in the wind tunnel test section on a sting or pedestal mount. A pedestal mount was used for the Model 222 test. The tunnel is equipped with an air exchange system which reduces tunnel temperature and also removes the turbulent air boundary layer before it enters the test section. New air is pulled into the wind tunnel through the inlet section of the air exchange system located downstream from the test section. Pertinent wind tunnel data are shown in Table 3 and the wind tunnel general arrangement is shown in Figure 16.

TABLE 3 BOEING V/STOL WIND TUNNEL PERTINENT DATA

CIRCUIT DIMENSIONS

Length (overall)	347 feet (approx. square in cross section)
Width (overall)	120 feet
Height (ground)	50 feet

TEST SECTION DIMENSIONS

Closed	20 feet square by 45 feet long
Slotted	20 feet square by 45 feet long; 10 percent porosity
Open Throat	20 feet square by 23 feet long
Contraction Ratio	6:1
Diffuser Angle	6 degrees equivalent cone (maximum)

FAN DESCRIPTION

Diameter	39 feet
Blades	9, fixed pitch
Motors (horsepower)	13,500 AC, 1,500 DC: 15,000 total
Nacelle	18 feet maximum diameter by 72 feet long, 272 design rpm

MODEL SUPPORT SYSTEM

Floor Mount	12 feet by 16 feet floor insert, custom installation
-------------	---

AUXILIARY SYSTEMS

Data Acquisition	120-channel system using an IBM 1800 computer which operates independently or linked to a central IBM 360 system
------------------	--

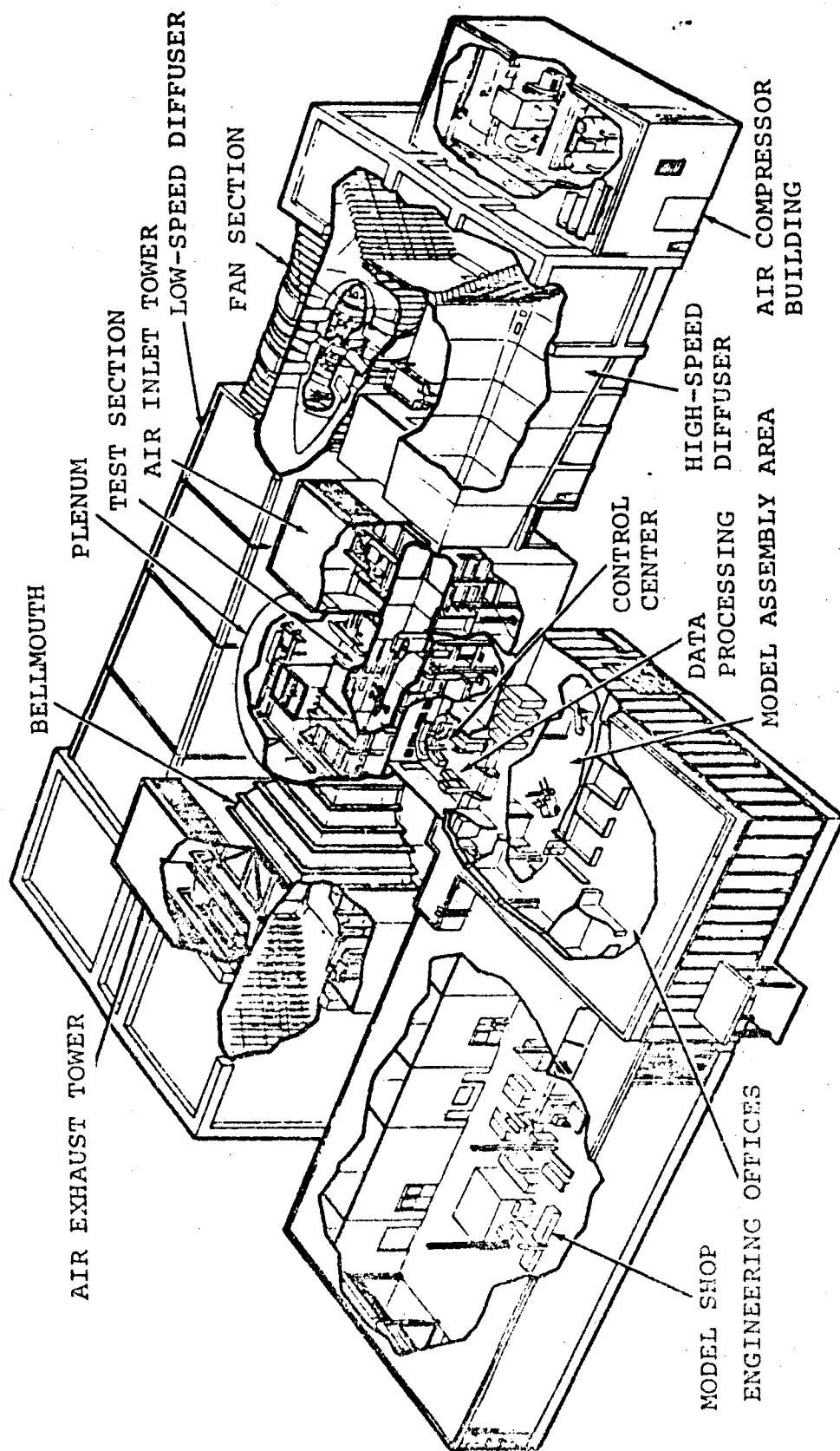


Figure 16 The Boeing V/STOL Wind Tunnel
General Arrangement

3.2.2 Model Installation

The 1/4.622 dynamically scaled Model 222 was installed in the Boeing V/STOL wind tunnel on a pedestal mount attached to a yaw table located on an elevator below the test section floor. The nominal test location of the model within the test section is shown in Figure 17. Installation of the yaw table on the elevator permitted lowering of the model to a working height for model maintenance. The rotor centerline (in cruise) was nominally at a 10 foot height during test but was lowered to approximately 5 feet for maintenance as shown in the photograph in Figure 18. The capability of being able to raise and lower the model also permits testing of the model in ground effect; however, no in ground effect testing was conducted on the Model 222 during the test period covered by the report.

A fixed ground plane 20 feet wide by 16 feet long and 13 inches high was installed in the test section. The ground plane provides a more stable boundary layer near the floor for in ground effect testing and also provides a solid work platform when the yaw table is lowered to position the model at a working height.

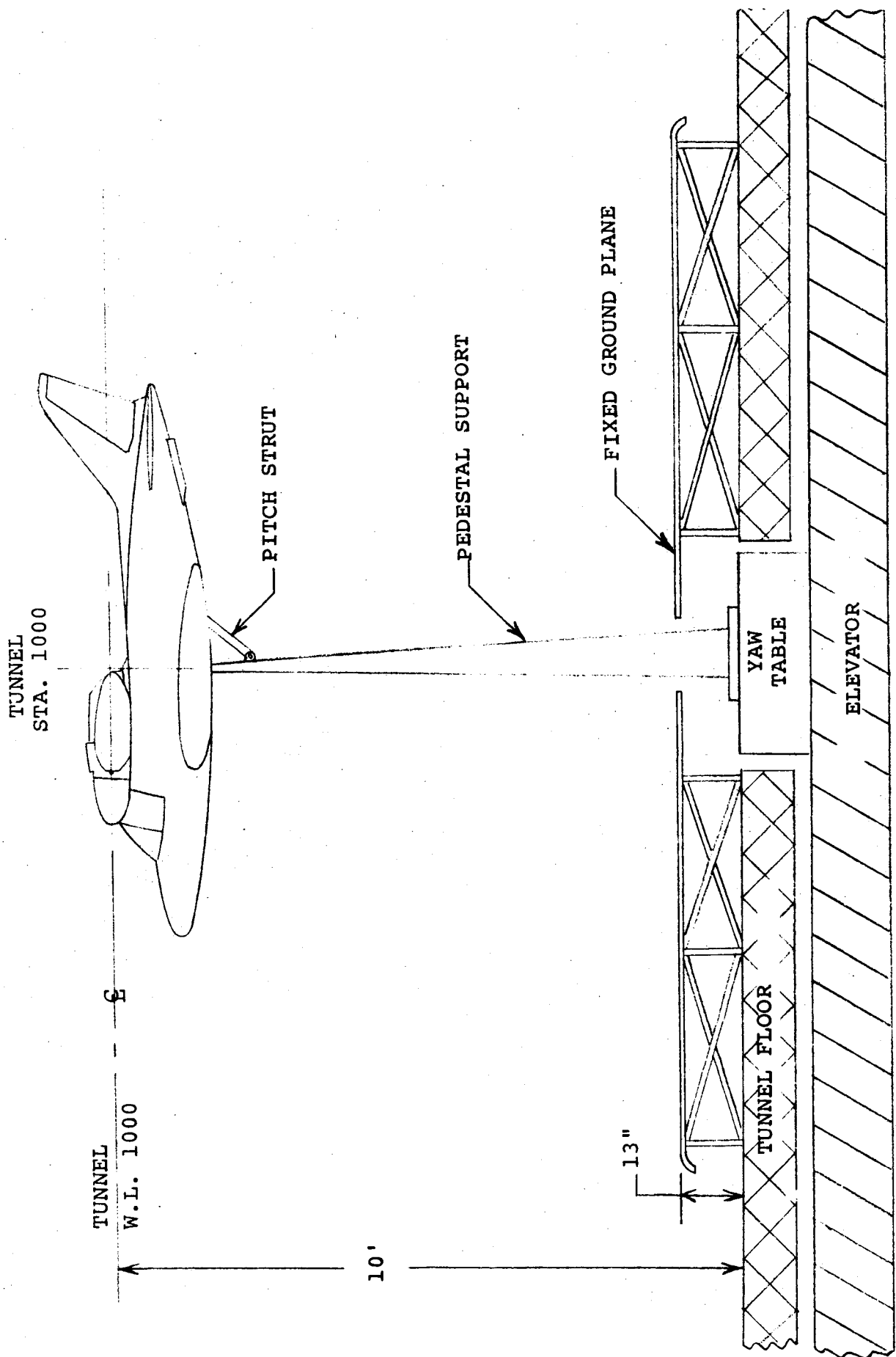


FIGURE 17 MODEL 222 WIND TUNNEL INSTALLATION

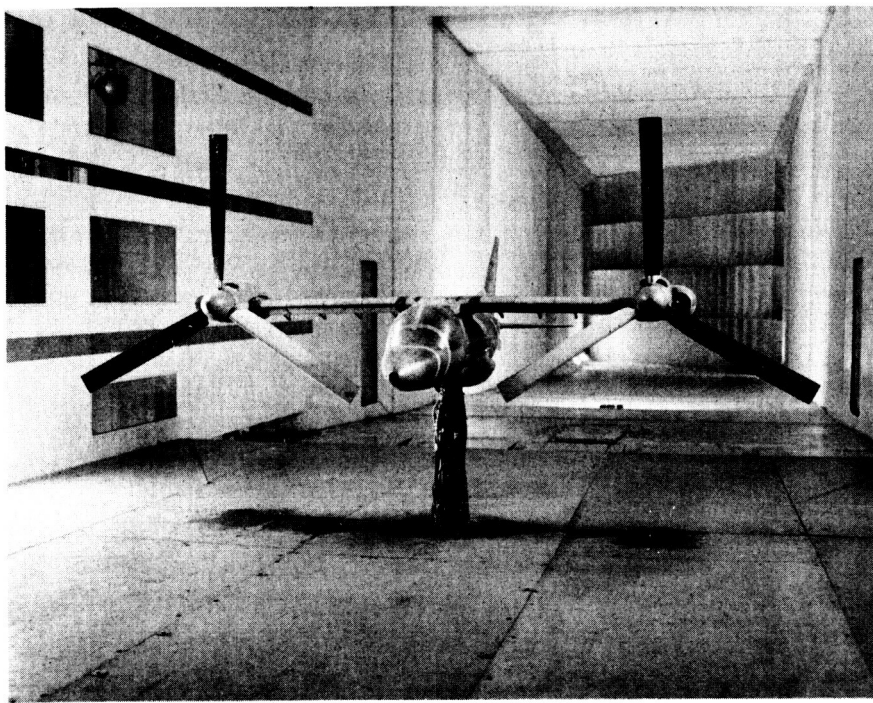


FIGURE 18 - MODEL 222 LOWERED TO WORKING HEIGHT

3.3 DATA REDUCTION

The summary of the data reduction program is on file at the wind tunnel for BVWT 105. The critical dimensions used as input data for this program are presented in Table 4 and a sketch of the balance arrangement is shown in Figure 19.

To account for model flexibility in the pitch direction the equations presented below are integrated in the data reduction program.

Wing Pitch Deflections

$$\begin{aligned} \Delta \alpha_{w1} = & [NF_{1MB} - (NF_{2RB} + NF_{3RB}) \cos i_{N2} - (T_{2RB} + T_{3RB}) \sin i_{N2}] K_1 \\ & + [FM_{1MB} + .29 AF_{1MB} + .591 (T_{2RB} - T_{3RB}) \cos i_{N2} + .408 (T_{2RB} + T_{3RB}) \sin i_{N2} \\ & - PM_{2RB} - PM_{3RB} - (NF_{2RB} + NF_{3RB}) \sin i_{N2} (.375 + .365 \sin i_{N2}) \\ & - (NF_{2RB} + NF_{3RB}) \cos i_{N2} (.365 \cos i_{N2} - .192)] K_2 \end{aligned}$$

Nacelle Pitch Deflections

$$\begin{aligned} \Delta \alpha_{i_{N2}} = & (K_3 - K_4 \cos i_{N2}) NF_{2RD} + K_5 PM_{2RB} \\ & - K_6 T_{2RB} \cos i_{N2} + \Delta \alpha_{w1} \\ \Delta \alpha_{i_{N3}} = & (K_3 - K_4 \cos i_{N3}) NF_{3RB} + K_5 PM_{3RB} \\ & - K_6 T_{3RB} \cos i_{N3} + \Delta \alpha_{w1} \end{aligned}$$

$$i_{N2 \text{ corr}} = i_{N2} + \Delta \alpha_{i_{N2}}$$

$$i_{N3 \text{ corr}} = i_{N3} + \Delta \alpha_{i_{N3}}$$

K_1 = wing rotation due to pitching moment applied by the wing

K_2 = wing rotation due to pitching moment applied by the rotor

K_3 = rotor disc rotation due to rotor normal force

MODEL 222 BALANCE ARRANGEMENT

- BVWT 104
- ALL DIMENSIONS IN INCHES

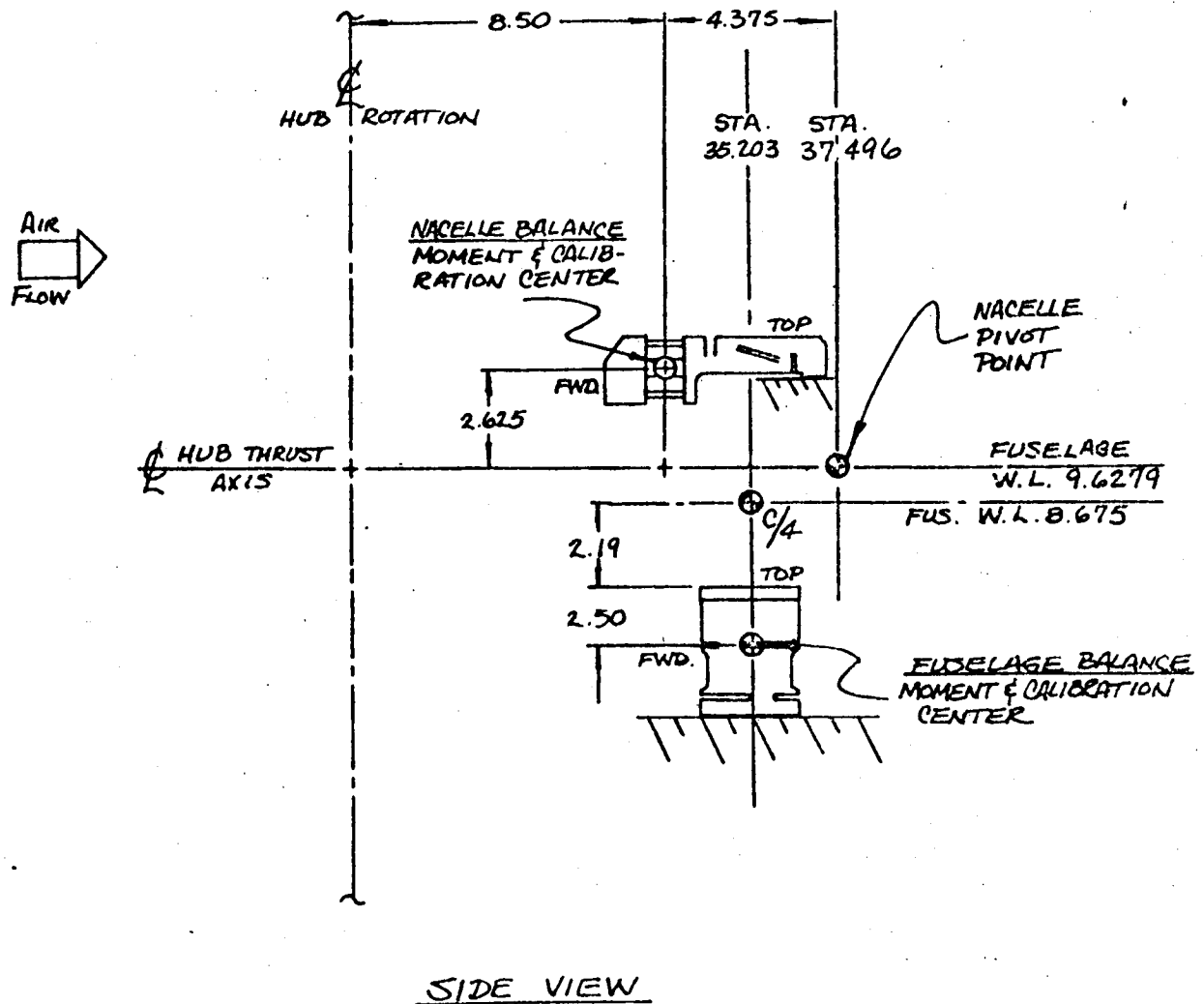


FIGURE 19

K_4 = nacelle incidence correction to rotor disc rotation
due to rotor normal force

K_5 = rotor disc rotation due to rotor pitching moment

K_6 = rotor disc rotation due to ~~rotor~~ thrust

The sign convention utilized for the model controls is presented in Figure 20 and a sign convention for the measured forces and moments is defined in Figure 21.

3.4 TEST PROGRAM

The testing accomplished in the program is briefly summarized here and the detail run schedule is presented in Appendix A.

- 1-16 End to end system check (no nacelle fairings)
- 17-39 Complete model with non-aerodynamic nacelle fairings in cruise regime
- 40-63 Complete model with non-aerodynamic nacelle fairings minus rotor blades in cruise and transition regime
- 64-72 Complete model with new nacelle fairings minus rotor blades in cruise and transition regime
- 73-76 Complete model with new nacelle fairings minus rotor blades and horizontal and vertical tail in cruise and transition regime

77-119 Complete model with new nacelle fairings in
cruise and transition regime

120-121 Complete model with new nacelle fairings minus
horizontal and vertical tail in cruise regime

2

3.5 MODEL PROBLEMS

During the assembly checkout and testing of the 1/4.622 Froude Scale Model 222 numerous problems were encountered. This section will summarize reasons for the delay in the test and also the termination of the testing.

1. MODEL PROBLEMS IDENTIFIED IN ASSEMBLY AND FIXED
 - a. Blade retention pin drilled off center in hubs
 - b. Redesign control system position pot supports
 - c. Fit all shells (very time consuming)
 - d. Balance main gearbox gear at Tinius Olsen
2. MODEL TRANSDUCER READOUT LIMITED IN CHECKOUT ROOM,
INCREASING FUNCTIONAL CHECKOUT TIME
3. MODEL FREQUENCIES NOT COMPATIBLE WITH SAFE OPERATION
WHILE ON PEDESTAL
 - a. Increased fuselage/pedestal pitch
 - b. Reduced fuselage/pedestal roll and yaw
 - c. Increased wing vertical bending
 - d. Increased vertical tail lateral bending
4. MODEL AIRRESONANCE PROBLEM ENCOUNTERED IN HOVER -
REQUIRED MODIFYING THE BLADES AND REINSTRUMENTING THEM
5. MODEL ELECTRONIC'S (BLACK BOX) WAS BEHIND SCHEDULE
AND THE COMPLEXITY WAS UNDERESTIMATED
6. MODEL PROBLEMS IDENTIFIED IN CHECKOUT AND TESTING
AND FIXED

- a. Leaking gearbox oil seals
- b. Nacelle gearbox fouling
- c. Rework blade pitch arms to provide proper indexing
- d. Add spacers to right blade pitch arms to provide clearance for pitch arms
- e. Grind away hubs locally to provide collective travel range
- f. Grind away locally on control position pot support to provide clearance for swashplate screw heads to get full cyclic range (even this is most restricted)
- g. Build and fit new nacelle covers
- h. Remove gearbox to replace oil jets after accident
- i. Balance hubs without blades
- j. Balance hubs with blades
- k. Rebuild blades after instability in checkout room
- l. Repair main balance side force
- m. Modified both nacelle balances to correctly account for the rotor torque loads acting through the balance
- n. Remove slop in flaps (not successful)
- o. Replace inboard gages on RH blades and one LH blade after starting with cyclic in tunnel
- p. Replaced Roulin bushing on control system readout
- q. Control system short; elevator shake put in reduced LH collective
- r. Replaced clutch motor to reduce speed for manual operation
- s. Replaced several clutch coils downstairs

- t. Rebuilt clutches in tunnel to provide proper clearance
 - u. Constant repair of broken instrumentation wiring (replaced one wing wirepack for RH nacelle balance)
 - v. Oil in 1/rev and 60/rev cover behind gearbox
 - w. Relocated 1/rev pickup to permit removal without pulling gearbox from model
 - x. Sizing of oil return lines from gearboxes to balance oil flow
 - y. Water leaks on nacelle balances - removed and sealed
 - z. Remade blade retention pins after they were reamed out to fit blades before hubs were reworked to position pins
7. Model Modification Defined from Testing (see conclusions for subsequent action).
- a. Redesign and fabricate new nacelle upper controls including limit switch support bracketry. Design should permit $\pm 10^\circ$ cyclic (longitudinal and lateral) with mechanical stops which can be preset as a safety feature. Also provide position feedback.
 - b. Replace all model wiring with Markel wiring.
 - c. Repair blade root instrumentation.
 - d. Model control console position meters inadequate. Replace with digital readout or some other improvements.
 - e. Rework flap/ailerons to eliminate slop and relocate position pots to provide direct position reading.
 - f. Clear gearbox - nacelle balance fouling
 - g. Determine proper model wing/pedestal, wing/monkey pole stiffness properties. Modify model accordingly.

TABLE 4 - WIND TUNNEL DATA REDUCTION INPUT CONSTANTS

RDINC	SYM		ALL DIMENSIONS PER PRINT	
			UNITS	
1	x_2	Horiz. Dist. from Left Nacelle Bal. Axis ζ to Ref. Body Axis	FT	.7083
2	y_2	Lat. Dist. from Left Nacelle Bal. Axis ζ to Ref. Body Axis	FT	0.0
3	z_2	Vert. Dist. from Left Nacelle Bal. Axis ζ to Ref. Body Axis	FT	-.2188
4	x_3	Horiz. Dist. from Right Nacelle Bal. Axis ζ to Ref. Body Axis	FT	.7083
5	y_3	Lat. Dist. from Right Nacelle Bal. Axis ζ to Ref. Body Axis	FT	0.0
6	z_3	Vert. Dist. from Right Nacelle Bal. Axis ζ to Ref. Body Axis	FT	-.2188
7	d_2	Left Torque Directional Sign i.e. as CW Rotation (Blade) = -1 view from		-1
8	d_3	Right Torque Directional Sign i.e. pilot CCW Rotation (Blade) = +1 seat		+1
9	l_2	Horiz. Dist. from Left Nacelle Ref. Body Axis to Nacelle Pivot Point	FT	-1.0729
10	m_2	Lat. Dist. from Left Nacelle Ref. Body Axis to Nacelle Pivot Point	FT	0.0
11	n_2	Vert. Dist. from Left Nacelle Ref. Body Axis to Nacelle Pivot Point	FT	0.0
12	l_3	Horiz. Dist. from Right Nacelle Ref. Axis to Nacelle Pivot Point	FT	-1.0729
13	m_3	Lat. Dist. from Right Nacelle Ref. Body Axis to Nacelle Pivot Point	FT	0.0
14	n_3	Vert. Dist. from Right Nacelle Ref. Body Axis to Nacelle Pivot Point	FT	0.0
15	e_1	Horiz. Dist. from Aircraft Balance Axis ζ to Model Body Axis	FT	0.0
16	f_1	Lat. Dist. from Aircraft Balance Axis ζ to Model Body Axis	FT	0.0

TABLE 4
INPUT CONSTANTS (continued)ALL DIMENSIONS
PER PRINT

RDINC	SYM		UNITS	
17	g_1	Vert. Dist. from Aircraft Balance Axis to Model Body Axis	FT	.3908
18	e_2	Horiz. Dist. from Left Nacelle Pivot Axis to Model Body Axis	FT	+.1911
19	f_2	Lat. Dist. from Left Nacelle Pivot Axis to Model Body Axis (neglecting droop and/or bent spar)	FT	+3.6150
20	g_2	Vert. Dis. from Left Nacelle Pivot Axis to Model Body Axis	FT	-.0794
21	e_3	Horiz. Dist. from Right Nacelle Pivot Axis to Model Body Axis	FT	+.1911
22	f_3	Lat. Dist. from Right Nacelle Pivot Axis to Model Body Axis (neglecting droop and/or best spar)	FT	-3.6150
23	g_3	Vert. Dist. from Right Nacelle Pivot Axis to Model Body Axis	FT	-.0794
24	S	Wing Area	FT ²	9.360
25	b	Wing Span	FT	7.230
26	c	Wing Chord	FT	1.294
27	R_2	Left Rotor Radius	FT	2.8125
28	R_3	Right Rotor Radius	FT	2.8125
29	ΔAL_2	Left Nacelle Lateral Cyclic Ratio (Left Lat.)		
30	ΔAR_2	Left Nacelle Lateral Cyclic Ratio (Right Lat.)		
31	ΔB_2	Left Nacelle Longitudinal Cyclic Ratio		
32	ΔAL_3	Right Nacelle Lateral Cyclic Ratio (Left Lat.)		
33	ΔAR_3	Right Nacelle Lateral Cyclic Ratio (Right Lat.)		
34	ΔB_3	Right Nacelle Longitudinal Cyclic Ratio		

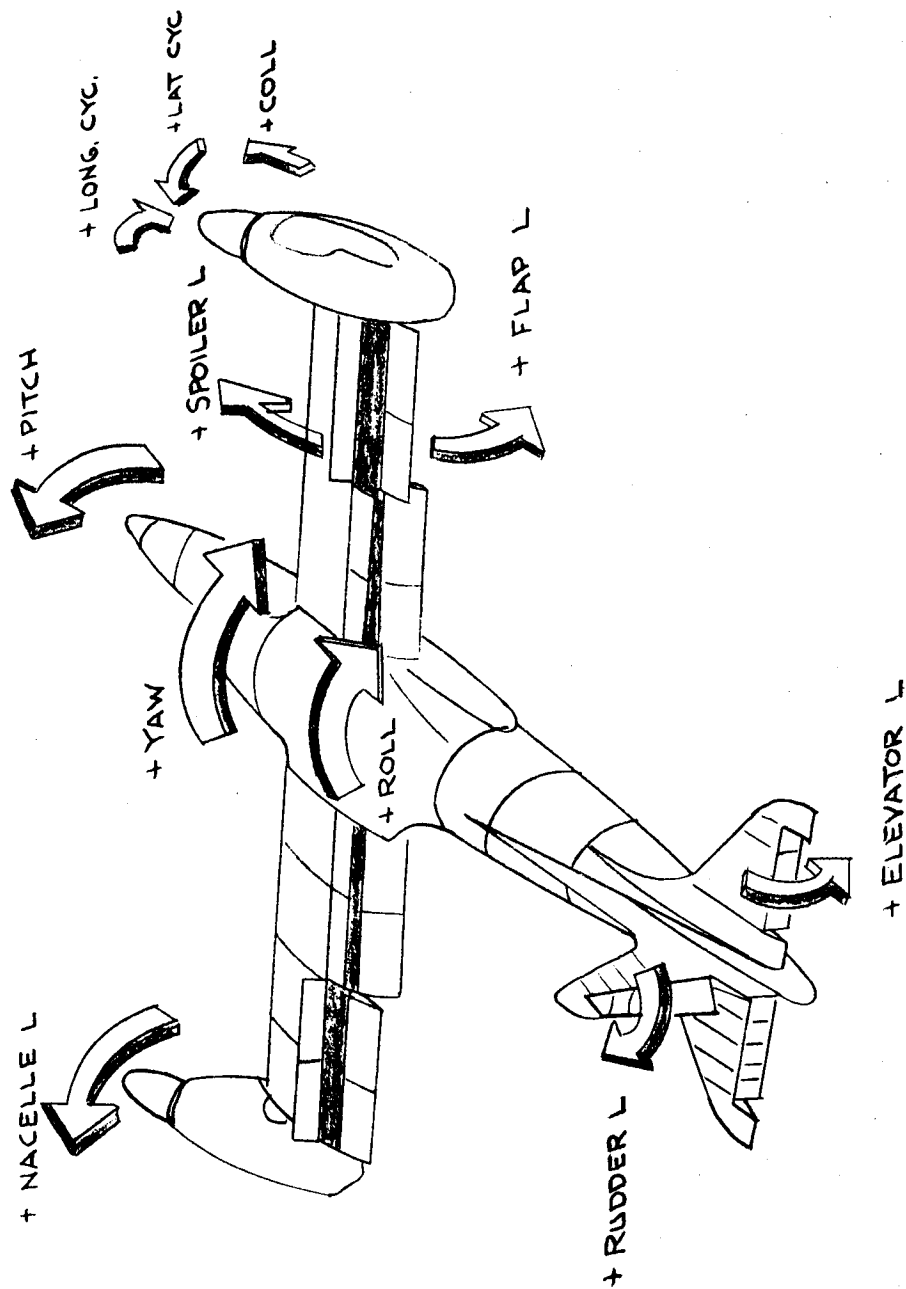


FIGURE 20 MODEL 222 SIGN CONVENTION

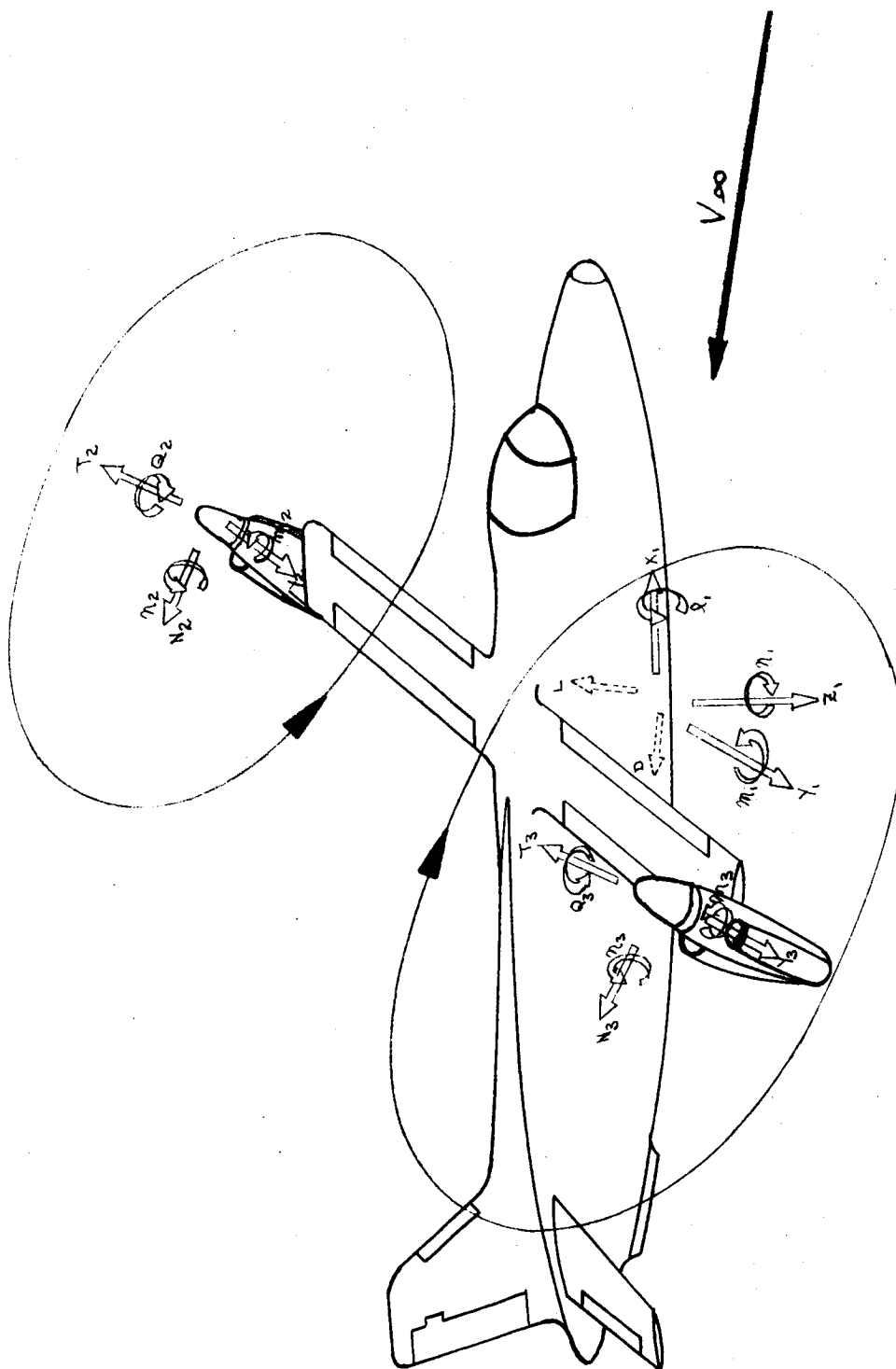


FIGURE 2/ - MODEL FORCE & MOMENT SIGN CONVENTION

4.0 PERFORMANCE

The performance testing conducted during this program starts at mid transition and continues into the cruise regime. Data is presented for the rotor, airframe and the aircraft, showing the effects of pitch and yaw attitude as well as the effects of flap deflection, rotor cyclic and rotor collective on performance. Owing to mechanical problems in the model control system, control settings could not be held constant during a run. Therefore to correctly analyze the data obtained, it was necessary to first plot the rotor control positions and rotor thrust and power during each run. Careful examination of each of these five quantities would permit a data fairing with fixed rotor controls or at least a linear interaction between collective and longitudinal cyclic. This requirement was the result of having slop in the rotor controls as well as the interactions between collective and longitudinal cyclic. The following sections will address these items as they were covered in the testing directed at Objectives 2, 4 and 7 presented in Section 2.0.

4.1 Transition Performance

Transition performance was obtained at 72 ft/sec and 1185 RPM rotor speed. This is equivalent to 90 kts and 551 RPM rotor speed for the full scale aircraft.

4.1.1 Rotor Performance

Rotor performance is presented first at a nacelle incidence of 41.6 degrees, the normal transition value at 90 kts for the full scale aircraft. Figure 22 presents the rotor thrust coefficient (C_T) variation with rotor shaft angle of attack for flap deflections of 20, 30 and 40 degrees. The collective, longitudinal and lateral cyclic variation during this series of runs are presented in Figure 23 and indicate that the collective for run 104, 40 degrees flap deflection, is higher than for 30° or the initial part of 20° deflections. There is an apparent zero shaft in the collective between Run 104 and Runs 117 and 118. Presenting the thrust-power coefficient variation as shown in Figure 24 indicates a similar trend but at a lower thrust level. Comparing the thrust and power at a fixed shaft angle indicates that the thrust and power are both lower for the 40 degrees flap deflection indicating that the collective must be lower and not higher. This is indicative that individual runs or back to back runs should provide satisfactory data but great care must be taken when trying to extract absolute data levels from this test data but the slopes (derivatives) are consistent and valid. Figure 25 presents the rotor performance in yawed flight for the flap deflection of 40 degrees. The thrust and power increase as the yaw angle is increased and the rotor collective and cyclic for this case are presented in Figure 26.

Yawed flight at a nacelle incidence of 30 degrees is presented in Figure 27. The flight speed was again 72 ft/sec with a rotor speed of 1186 and an attempt was made to maintain the thrust coefficient of approximately 0.0024. Thrust is slightly higher but power is significantly higher at a nacelle incidence of 30 degrees. This is a result of the much higher collective, $\theta = 15.85^\circ$ for $i_N = 30^\circ$ and $\theta = 12.75$ for $i_N = 41.6$ as indicated in Figure 28. To examine the variation of this change in performance with nacelle incidence, data was taken at intermediate values and is presented in Figure 29. Thrust and attitude were held constant as the nacelle angle was reduced and the power variation is linear. At a nacelle angle of 30 degrees standard angle of attack performance was obtained and is presented in Figure 30 with the collective and cyclic presented in Figure 31.

The effect of longitudinal and lateral cyclic and collective on rotor performance is shown in Figures 32 and 33 respectively. This data was obtained during the definition of the rotor control power in transition and also the cyclic effectiveness to be utilized for the low rate feedback. Lateral cyclic has a very slight effect on rotor performance but longitudinal produces large changes in both thrust and power. Comparing its effect to that of collective shown in Figure 33 positive longitudinal cyclic produces approximately 40 percent of the change in thrust and power that negative collective does.

C-2

FIGURE 22. EFFECT OF FLAP DEFLECTION IN TRANSITION
ON
ROTOR THRUST CHARACTERISTICS

RIGHT ROTOR

NOTE:

TUNNEL SPEED = 72 FPS

RPM = 1186

$\lambda_{tip} = 4.6^\circ$

$\mu = 0.206$

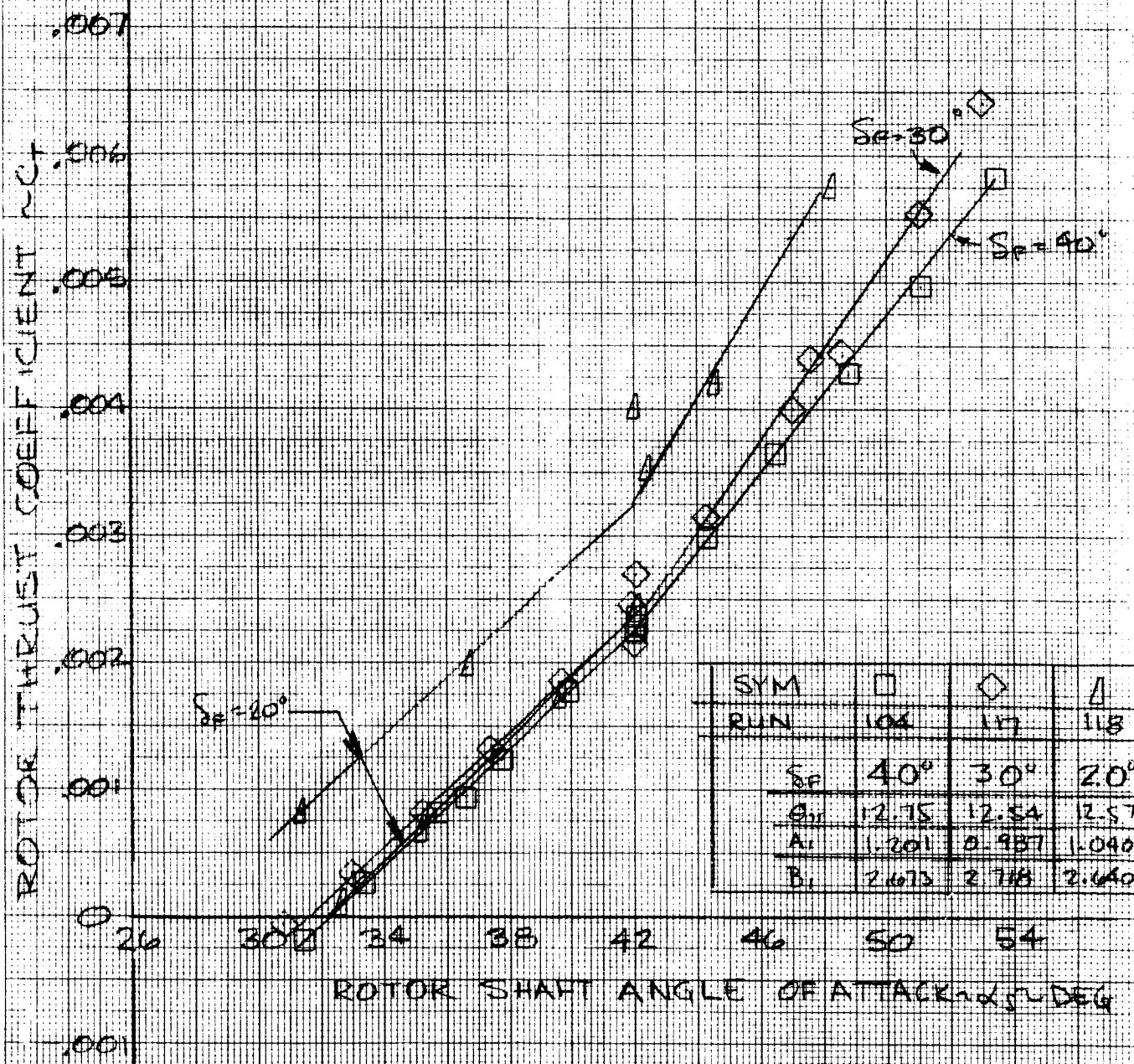


FIGURE 23

BLADE COLLECTIVE, LONGITUDINAL & LATERAL CYCLIC
VARIATION DURING FLAP DEFLECTION INVESTIGATION
TRANSITION

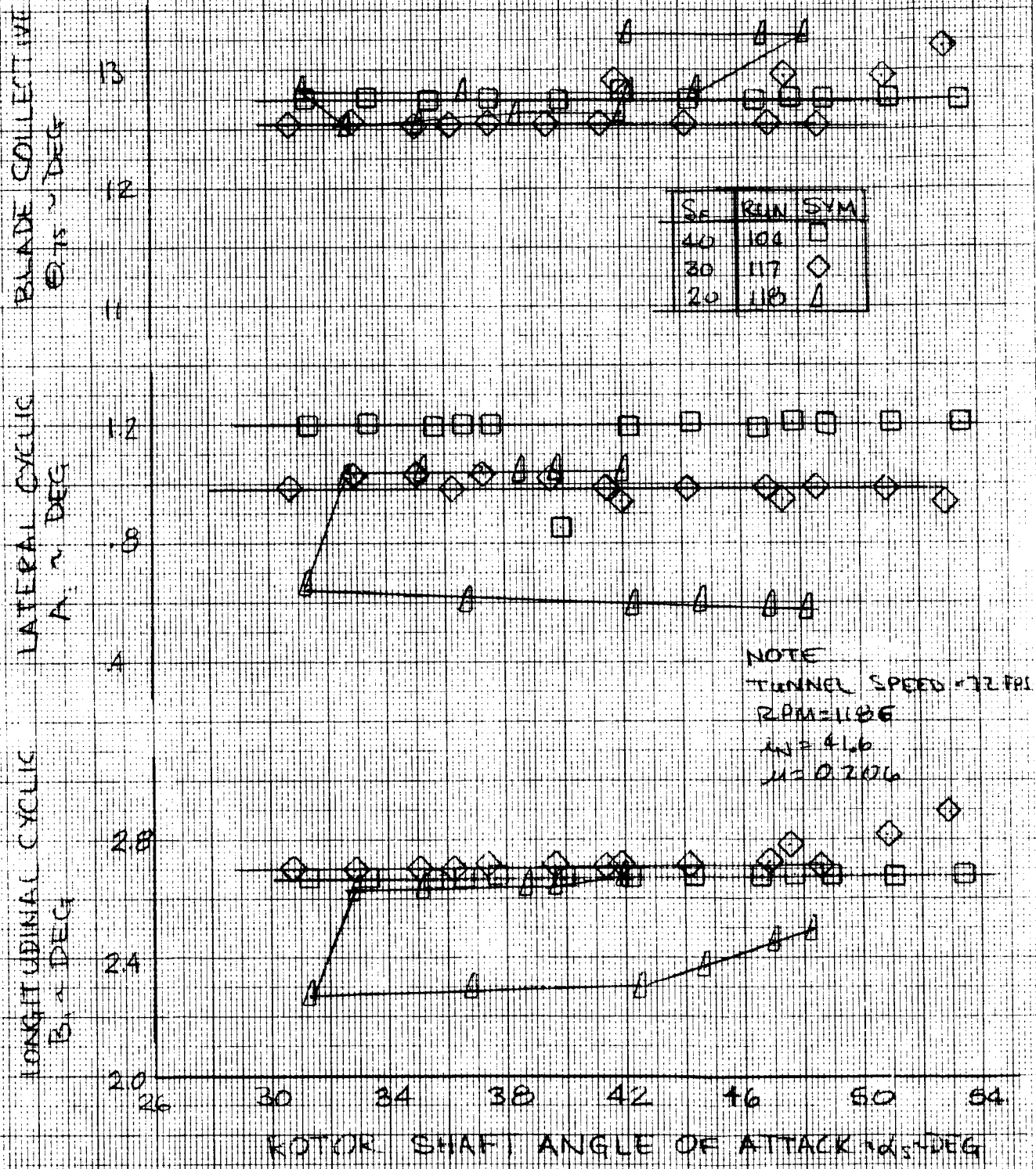


FIGURE 24 EFFECT OF FLAP DEFLECTION IN TRANSITION
ON
ROTOR PERFORMANCE

RIGHT ROTOR

NOTE
TUNNEL SPEED = 72 FPS
RPM = 1185
 $L/D = 41.6^\circ$
 $M = 0.206$
FULL SCALE
EQUIVALENT = 90 KTS
SPEED

ROTOR THRUST COEFFICIENT $\sim C_T$

.007
.006
.005
.004
.003
.002
.001
0
-.001

0 .0002 .0004 .0006 .0008 .0010 .0012

ROTOR POWER COEFFICIENT $\sim C_P$

SYM	□	◇	△
RUN	104	117	118
SE	40°	30°	20°
B_{∞}	12.75	12.54	12.57
A	-1.201	-0.987	-1.040
B	-2.673	-2.718	-2.640

EUGENE DIEZGEN CO.
MADE IN U. S. A.
MILLIMETER

FIGURE 25 ROTOR THRUST AND POWER CHARACTERISTICS
IN YAW ANGLE INVESTIGATION

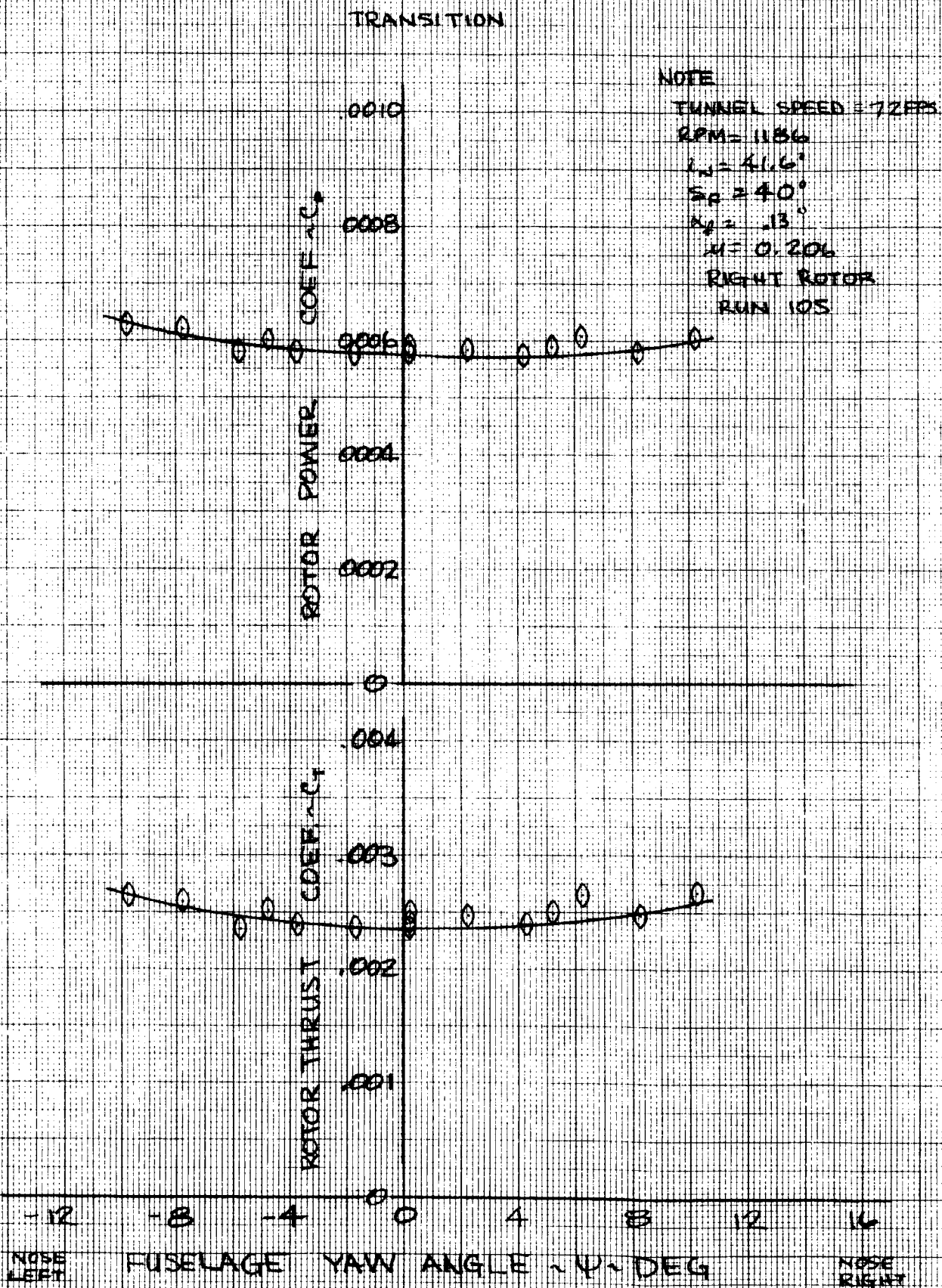


FIGURE 26

COLLECTIVE & LATERAL AND LONGITUDINAL CYCLIC
DURING YAW ANGLE INVESTIGATION

TRANSITION

NOTE

TUNNEL SPEED = 72 FPS

RPM = 1186

$L_N = 41.6^\circ$

$S_F = 40^\circ$

$\alpha_F = 13^\circ$

U = 0.206

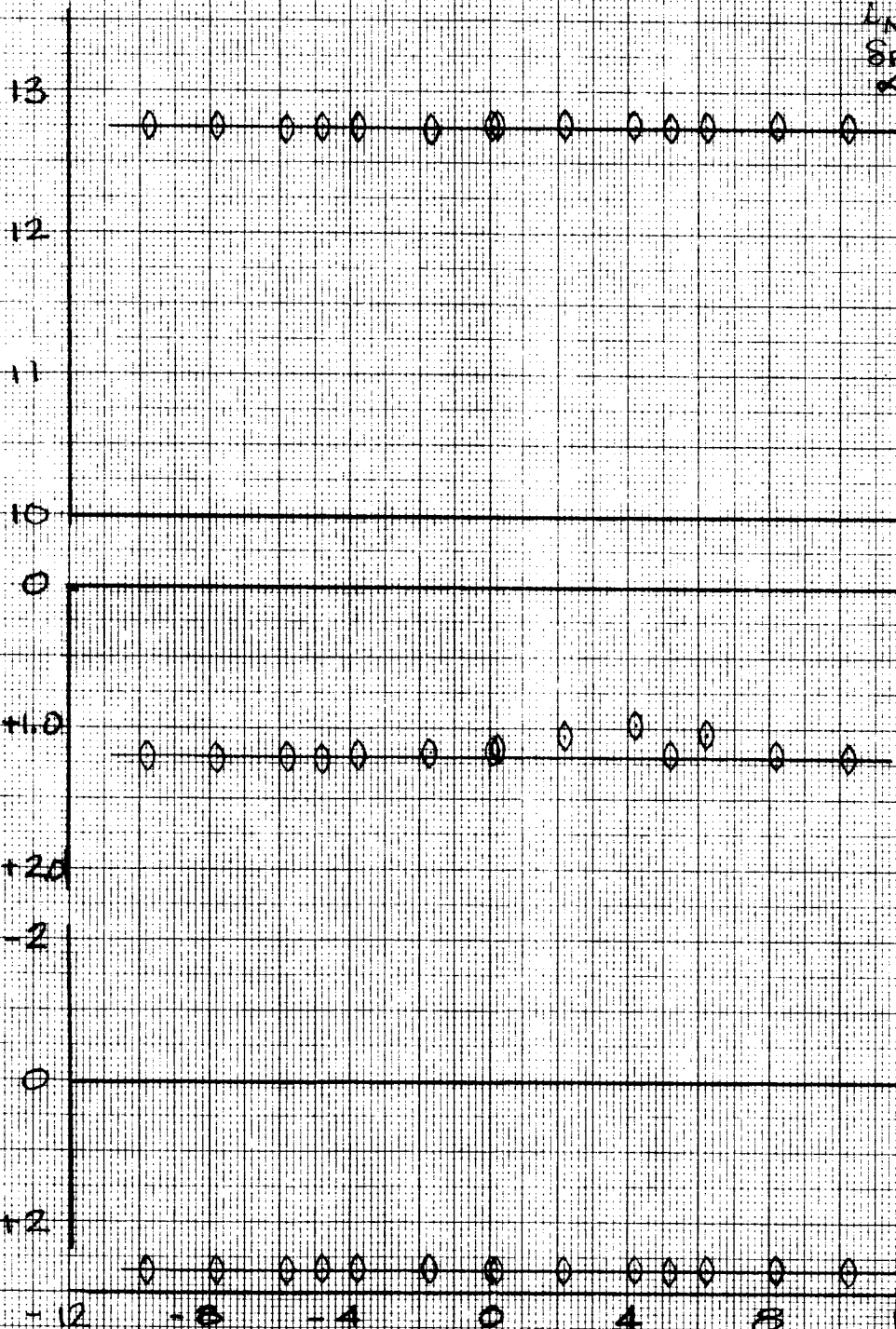
RIGHT ROTOR

RUN 105

BLADE COLLECTIVE PITCH ~ DEG

LATERAL CYCLIC ~ DEG

LONGITUDINAL CYCLIC ~ DEG



NOSE LEFT

FUSELAGE

YAW ANGLE ~ DEG

NOSE RIGHT

FIGURE 27

ROTOR THRUST AND POWER CHARACTERISTICS IN YAW ANGLE INVESTIGATION

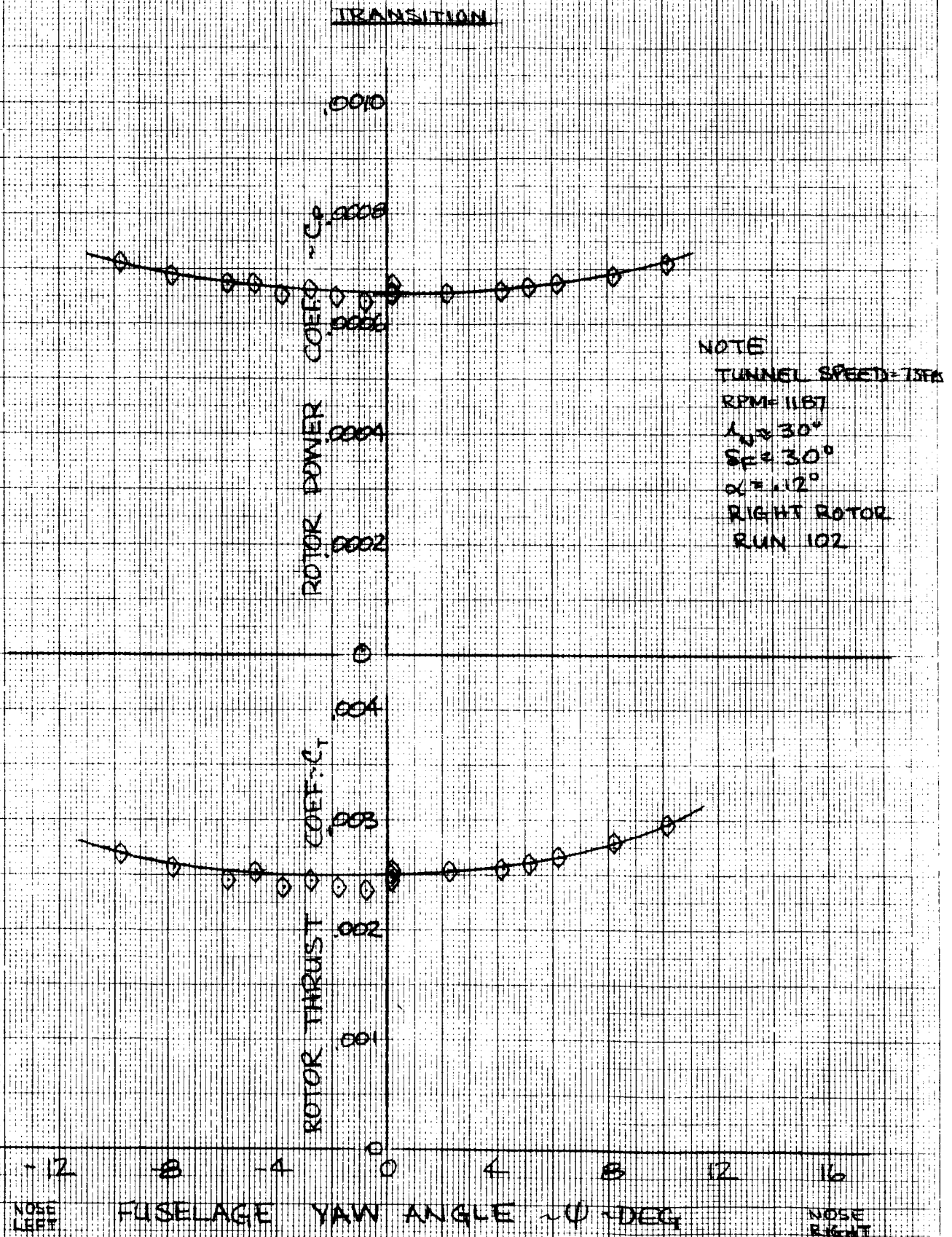


FIGURE 28

COLLECTIVE & LATERAL AND LONGITUDINAL CYCLIC
DURING YAW ANGLE INVESTIGATION

TRANSITION

NOTE

TUNNEL SPEED = 73 FPS

RPM = 1187

$\beta = 30^\circ$

$\delta = 30^\circ$

$\alpha = 12^\circ$

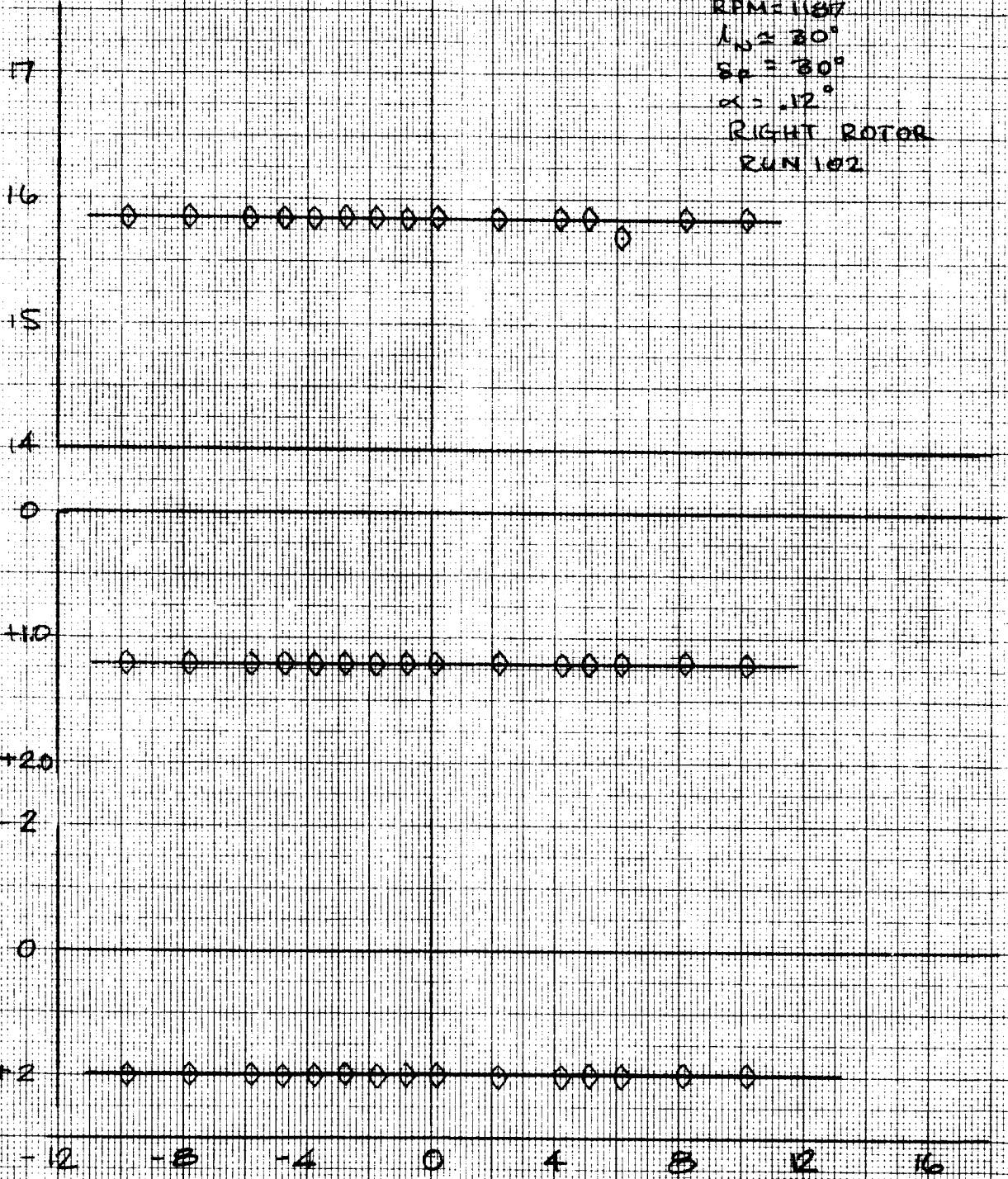
RIGHT ROTOR

RUN 102

BLADE COLLECTIVE PITCH - %

LATERAL CYCLIC - %

LONGITUDINAL CYCLIC - %



NOSE
LEFT

FUSELAGE YAW ANGLE - ψ - DEG

NOSE
RIGHT

FIGURE 29

EFFECT OF NACELLE INCIDENCE
ON
ROTOR THRUST AND POWER

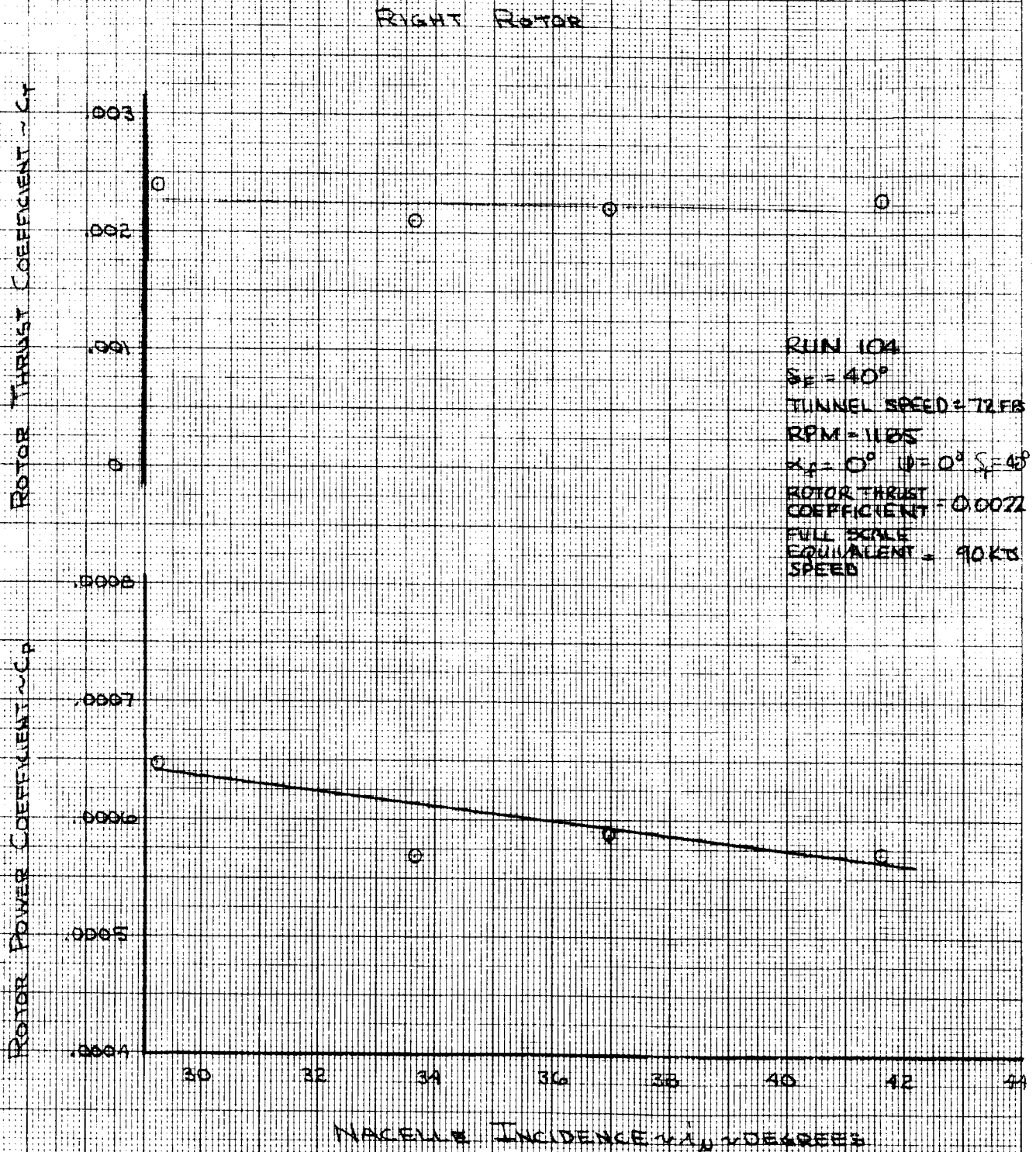


FIGURE 30

ROTOR THRUST AND POWER CHARACTERISTICS IN ANGLE OF ATTACK INVESTIGATION

TRANSITION

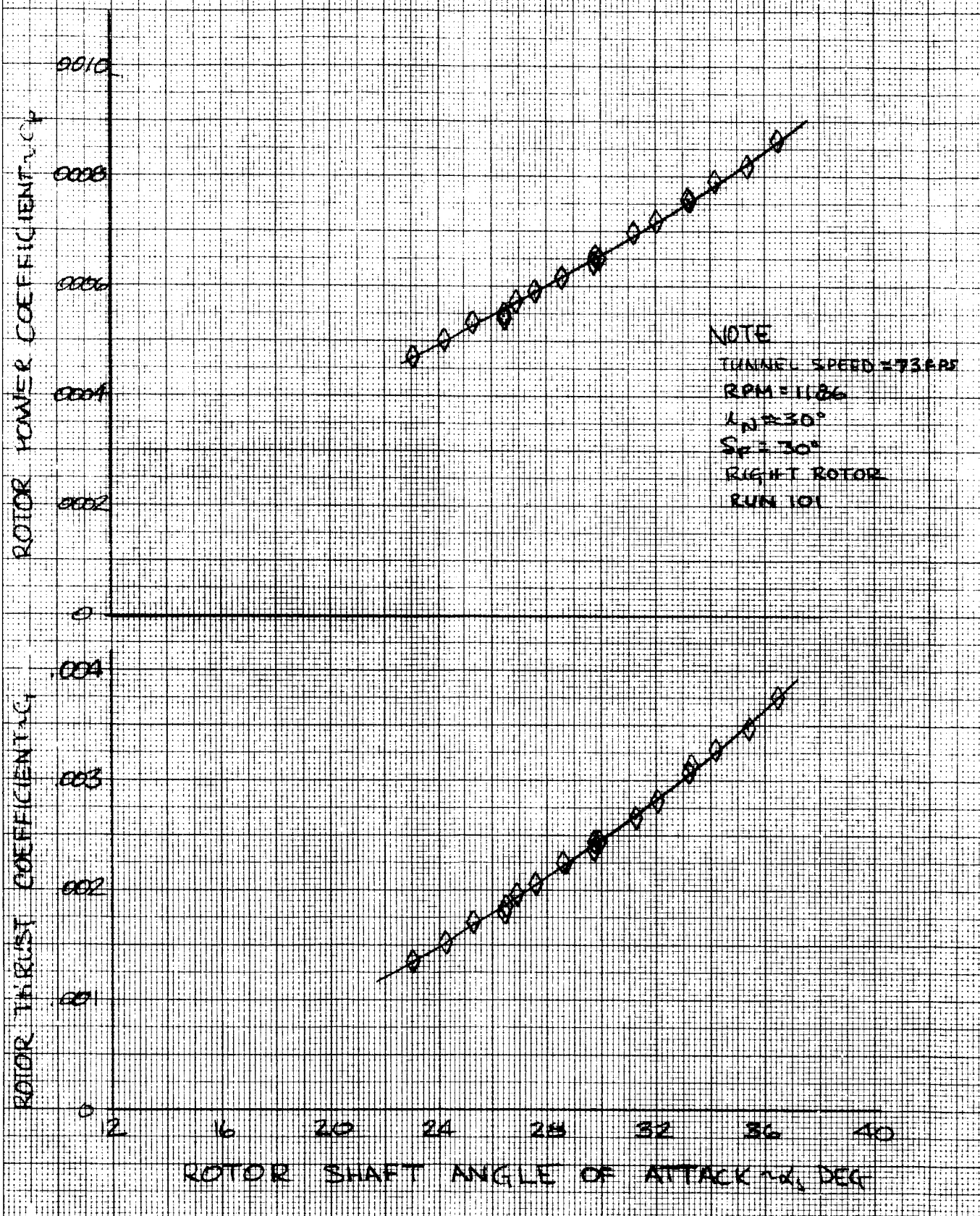


FIGURE 31

COLLECTIVE & LATERAL AND LONGITUDINAL CYCLIC
DURING PITCH ANGLE INVESTIGATION
IN TRANSITION

NOTE:

TUNNEL SPEED = 73 FPS
RPM = 1184
 $N_{\alpha} \approx 30^\circ$
 $S_{\alpha} \approx 30^\circ$
RIGHT ROTOR
RUN 101

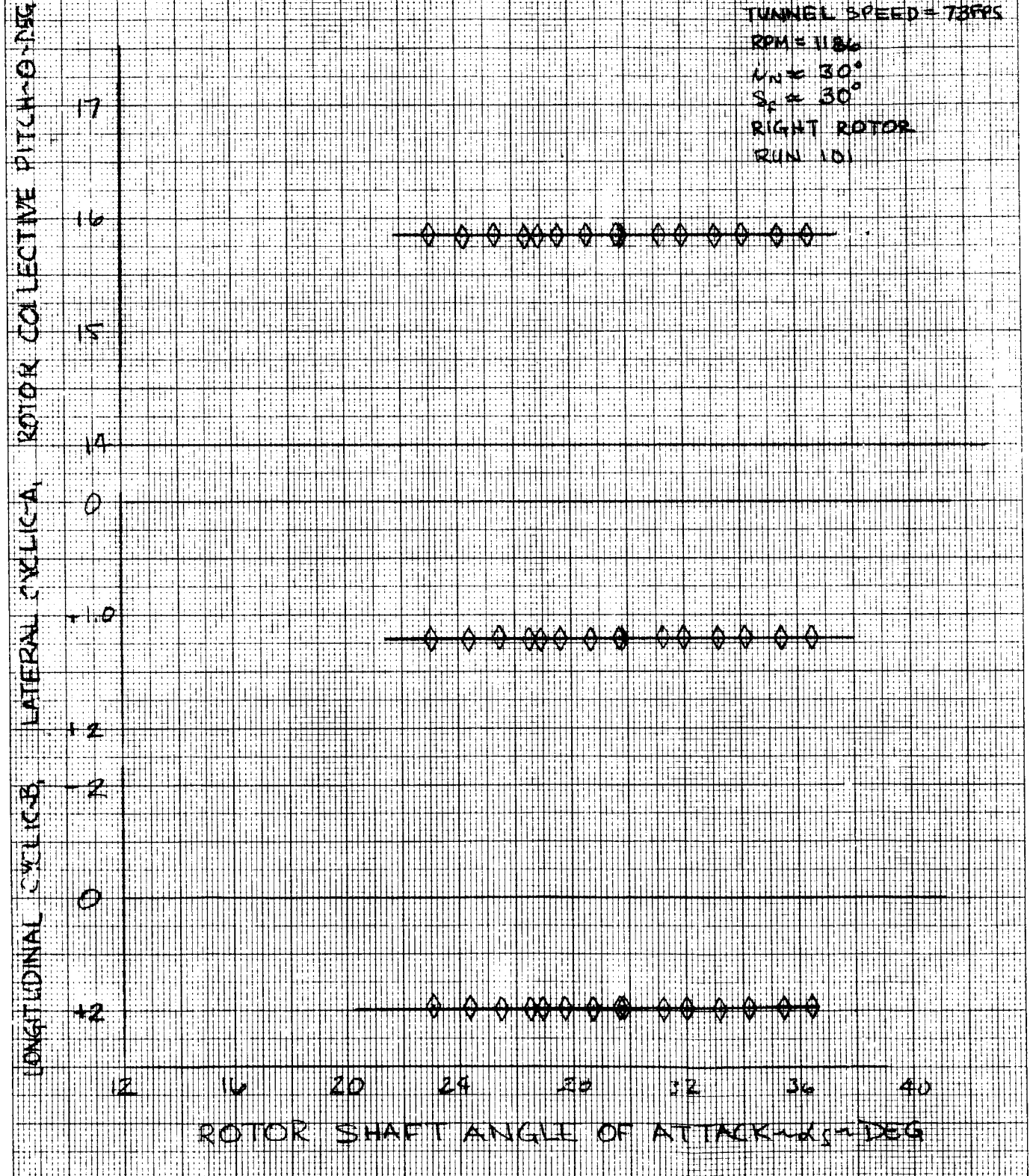


FIGURE 32

EFFECT OF CYCLIC IN TRANSITION ON ROTOR PERFORMANCE CHARACTERISTICS

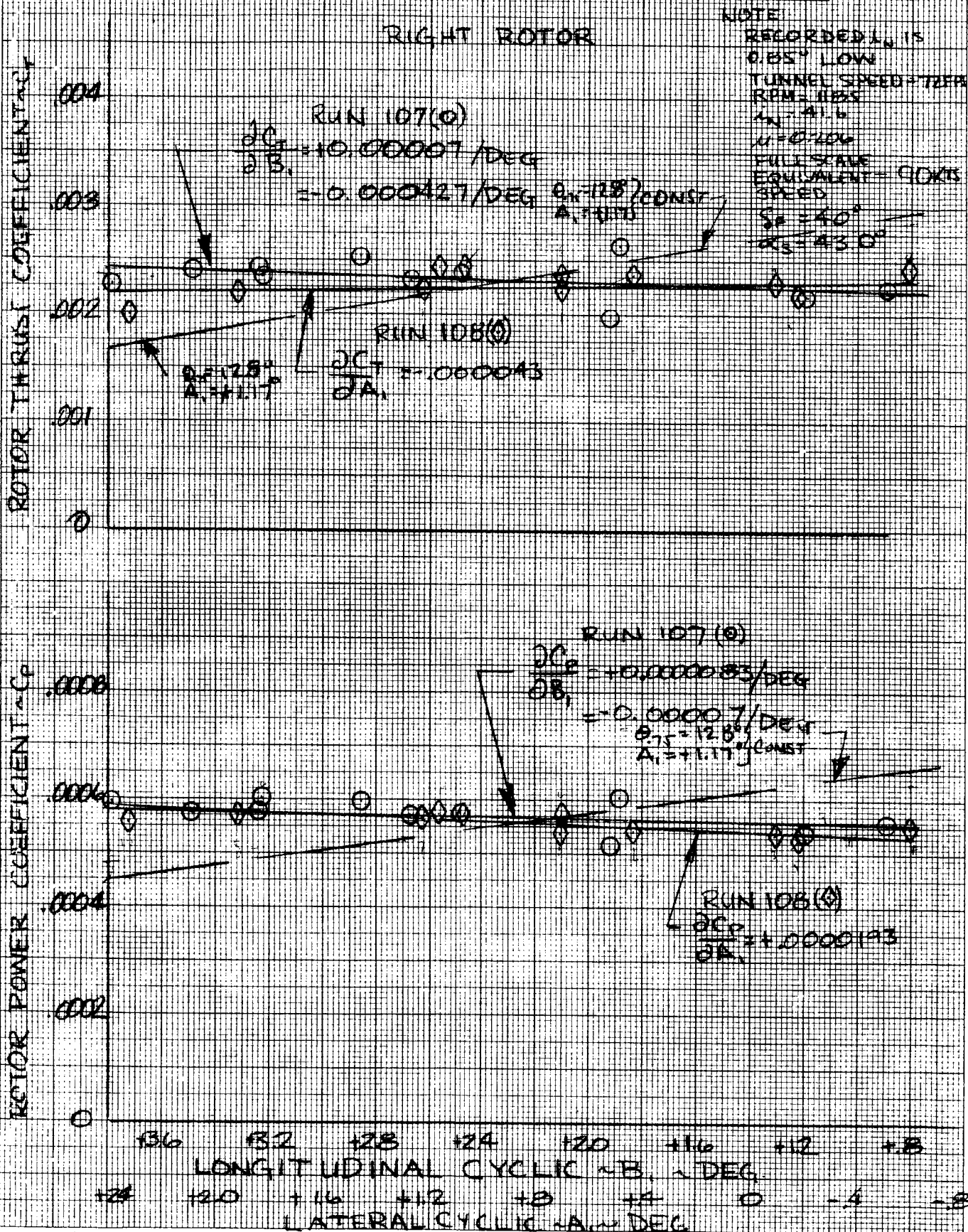
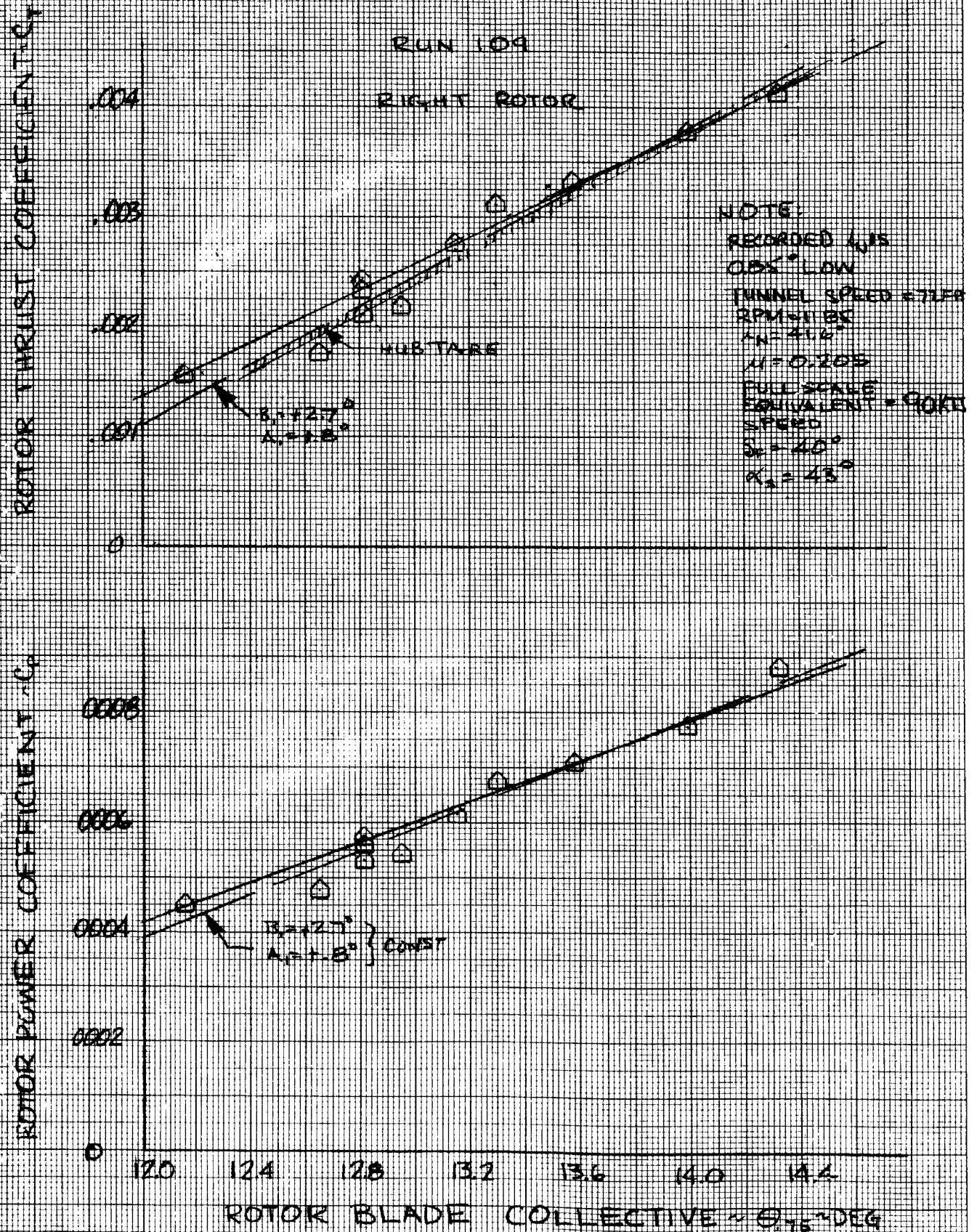


FIGURE 33 - EFFECT OF COLLECTIVE IN TRANSITION
ON
ROTOR PERFORMANCE CHARACTERISTICS



4.1.2 Aircraft Performance

A summary of the aircraft performance in the transition regime is presented here. Figure 34 presents the rotors off airframe performance characteristics for the mid transition flight condition of 72 ft/sec with the nacelle incidence of 45 degrees and a flap deflection of 40 degrees. The angle at which stall occurs for the complete aircraft is approximately 17 degrees. Removing the horizontal and vertical tail reduces this angle to approximately 14 degrees indicating wing stall occurs at this angle and the tail continues to provide sufficient lift to delay total aircraft stall to 17 degrees. Figure 35 presents the effect of flap deflection on total aircraft (rotors on) performance at a tunnel speed of 72 ft/sec and a rotor speed of 1186 RPM. As pointed out earlier there is some question as to the relationship of the rotor data obtained at 40 degrees flap deflection and it was assumed that there was a zero shift in collective and it was actually lower than was measured and therefore the thrust was lower. The total aircraft lift reflects the lower thrust but the aircraft propulsive force does not. It is approximately the same as that for 30 degrees flap deflection run.

Imposed on Figure 35 is an aircraft lift coefficient of 2.45 which represents the full scale aircraft at a gross weight of 13,500 LB. Accounting for the difference in the drag of the model and the aircraft ($C_D = 0.1$ as discussed in Section 4.2.2), indicates that a trim "1g" transition flight can be achieved over a range of flap angles. Figure 36 shows the relationship of the aircraft performance for a nacelle incidence of 41.6 and 30 degrees. It indicates that the lower nacelle incidence provides approximately ".08 g"

acceleration for approximately 10 percent increase in power.

Performance in yawed flight is shown in Figure 37 for nacelle incidence of 41.6 and 30 degrees. There is no significant change in lift but there is an increase in propulsive force as the aircraft is yawed for both nacelle incidence.

AIRFRAME PERFORMANCE CHARACTERISTICS
IN TRANSITION.

NOTE:

TUNNEL SPEED 0.7249
 $\alpha_N = 4.5^\circ$
 $S_F = 40^\circ$

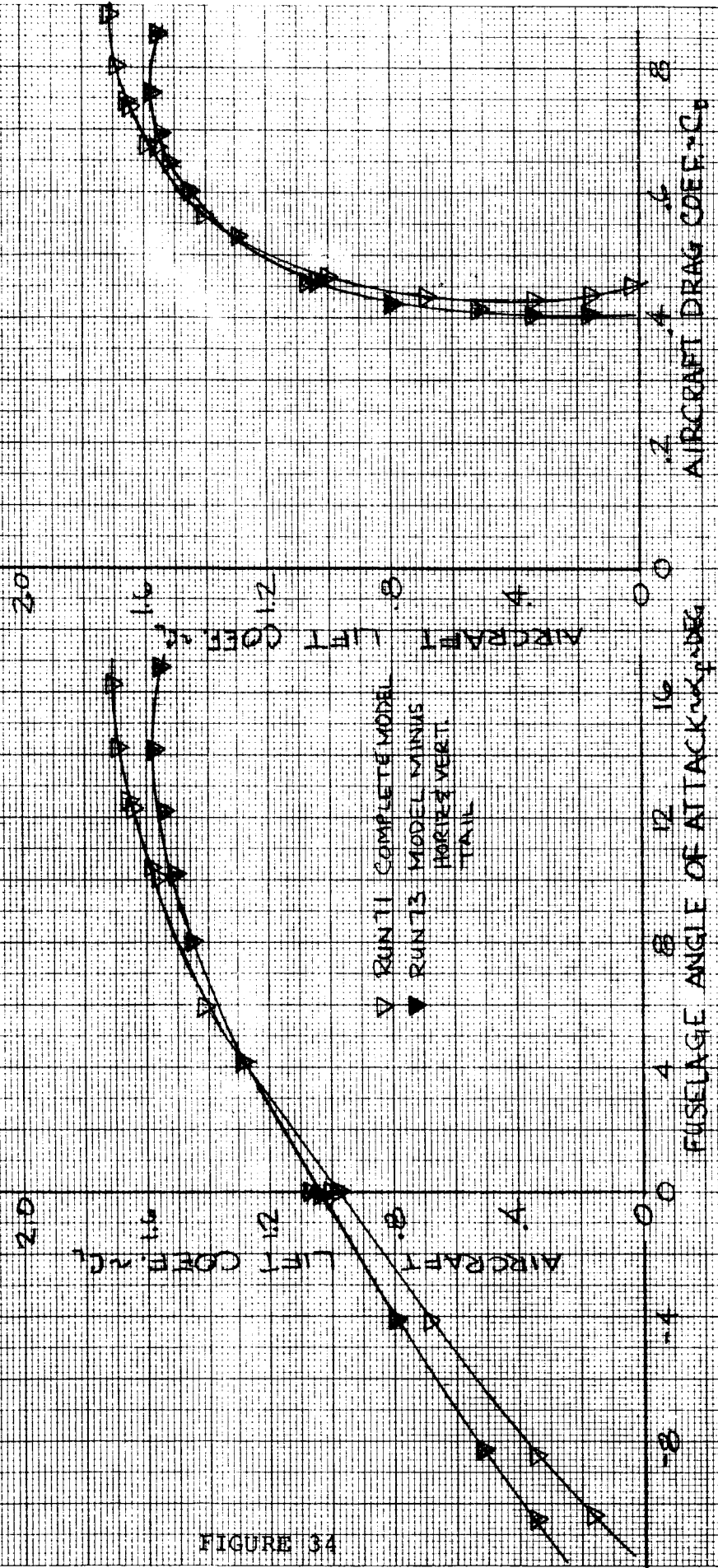


FIGURE 34

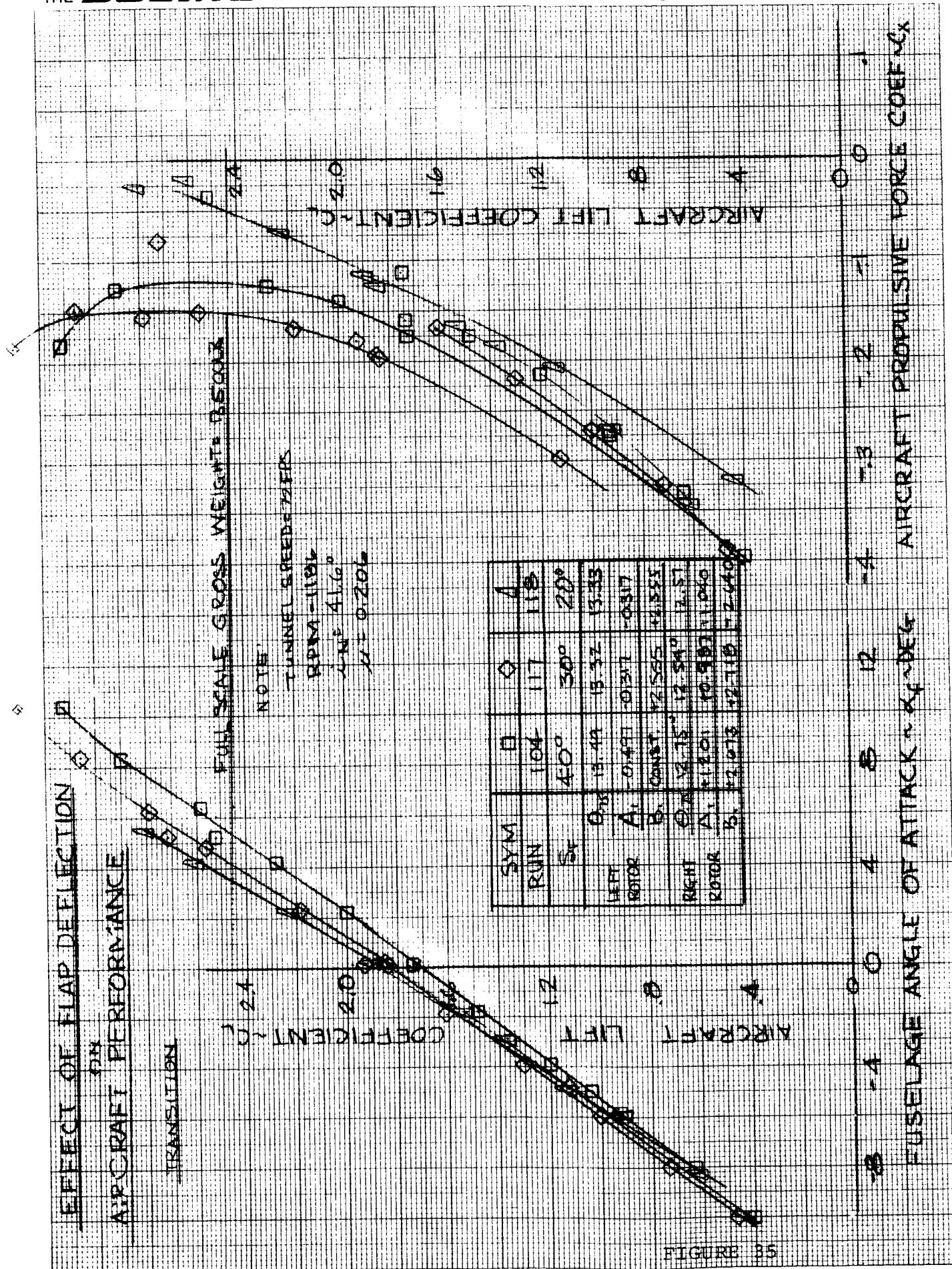


FIGURE 35

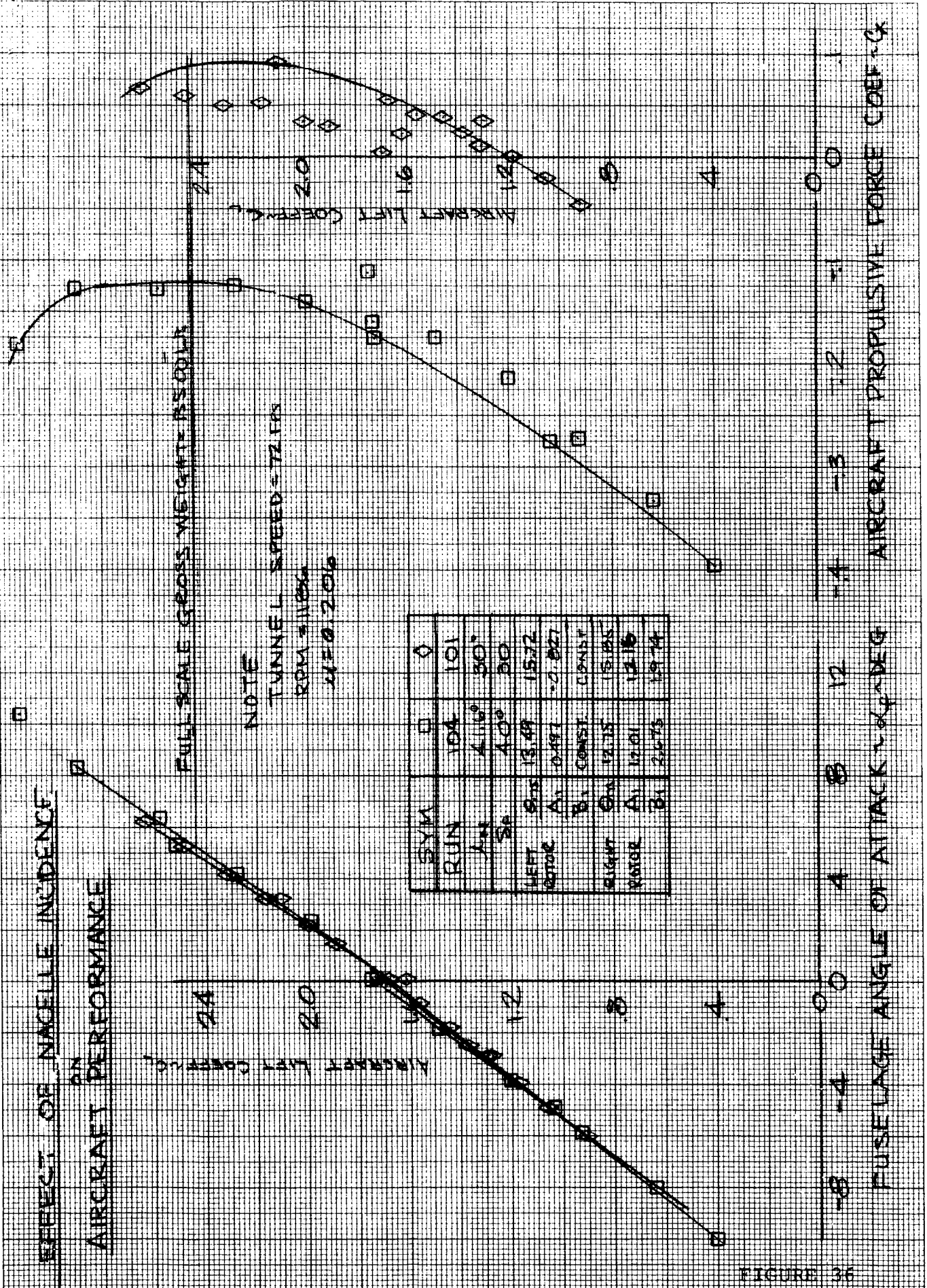


FIGURE 36

EFFECT OF NACELLE INCIDENCE

ON

AIRCRAFT PERFORMANCE

IN YAW

TRANSITION

NOTE

TUNNEL SPEED = 72 FPS

RPM = 1186

$M = 0.206$

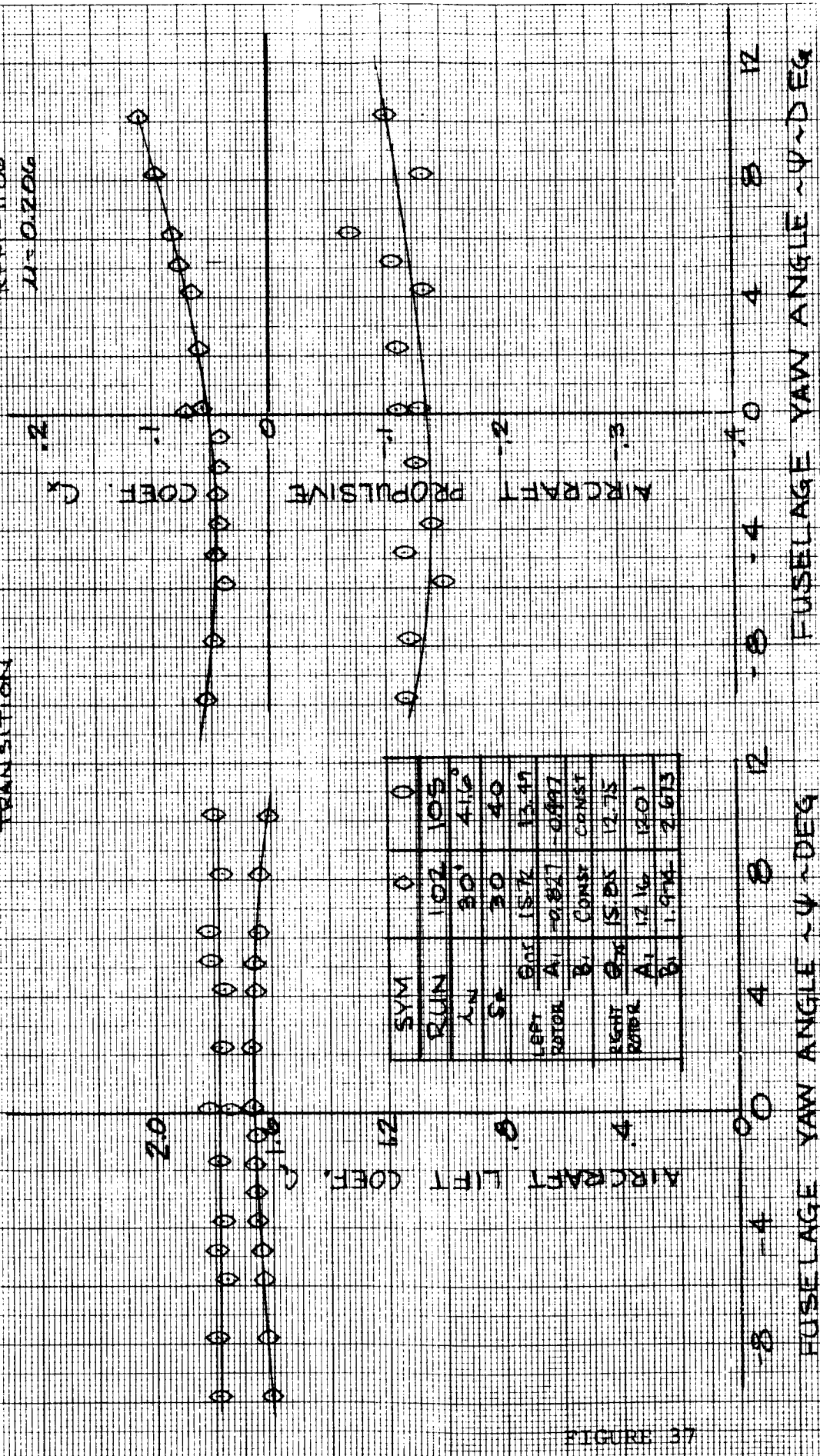


FIGURE 37

4.2 Cruise Performance

Cruise performance was obtained at speeds of 113 ft/sec to 182 ft/sec at a rotor speed of 830 RPM with the nacelle incidence of zero. This represents a speed range from the end of transition, 142 kts, to 225 kts, in cruise for the full scale aircraft.

4.2.1 Rotor Performance

At the end of transition 113 ft/sec a flap deflection investigation was made. Figure 38 presents the thrust and power coefficients for these runs while Figures 39 and 40 define the collective and cyclic variations. There is a trend indicated in the data that shows that flap deflection decreases thrust and power. The variation of the collectives and cyclics in addition to back lash in the rotor control system prohibit quantifying this trend.

In the cruise mode, the airframe test variables were fixed and the rotor controls were then set to minimize blade loads with cyclic at the rotor thrust coefficient estimated for the full scale aircraft. Figure 41 presents the performance for cruise conditions with a flap deflection of zero at speeds of 113 ft/sec to 182 ft/sec. There is a distinct increase in power with speed but the associated thrust levels overlap each other. The associated collective and cyclic values are presented in Figures 42 through 44. To obtain a better understanding of the performance in cruise, a thrust power presentation was made and is shown in Figure 45.

Yaw performance at the end of transition is presented in Figure 46. Also shown is the effect of flap deflection of 20 and 40 degrees indicating that rotor performance decreases as the flaps are

deflected. Figure 47 presents the rotor collective and cyclic associated with this performance. Yawed flight performance was obtained across the speed range of 113 ft/sec to 182 ft/sec. The thrust and power data presented in Figure 48 show small changes with yaw and the collective and cyclic variations during these runs are presented in Figure 49.

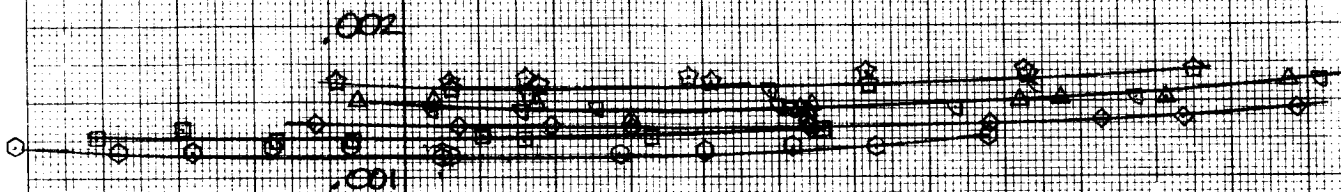
Performance data obtained from the cyclic effectiveness investigation in the cruise regime are shown in Figures 50 to 53. This data indicates that there is no effect of longitudinal or lateral cyclic on rotor thrust or power in cruise. An additional verification of this, is the rotor thrust and power obtained from the manual simulation of low rate cyclic feedback shown in Figure 54.

EFFECT OF ROTOR SHAFT ANGLE & FLAP DEFLECTION ON ROTOR POWER & THRUST IN CRUISE

ROTOR POWER
COEFFICIENT

C_P .004
.003
.002
.001

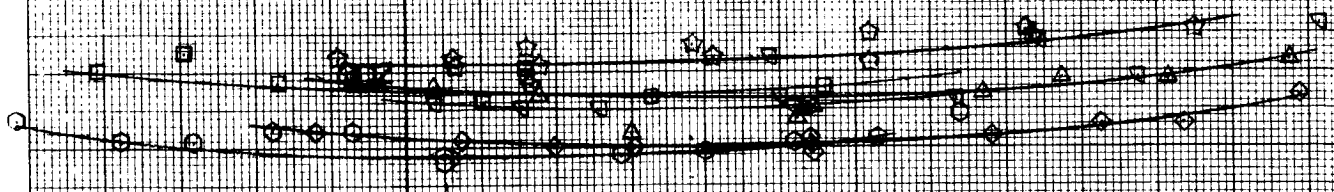
SYM	RUN	δ_c
☆	31	0°
◇	33	40°
△	35	20°
▽	37	10°
□	77	0
○	80	0



ROTOR THRUST
COEFFICIENT

C_T .004
.003
.002
.001

NOTE
TUNNEL SPEED: 113 KTS
 $\alpha_N = 0^\circ$
330 RPM



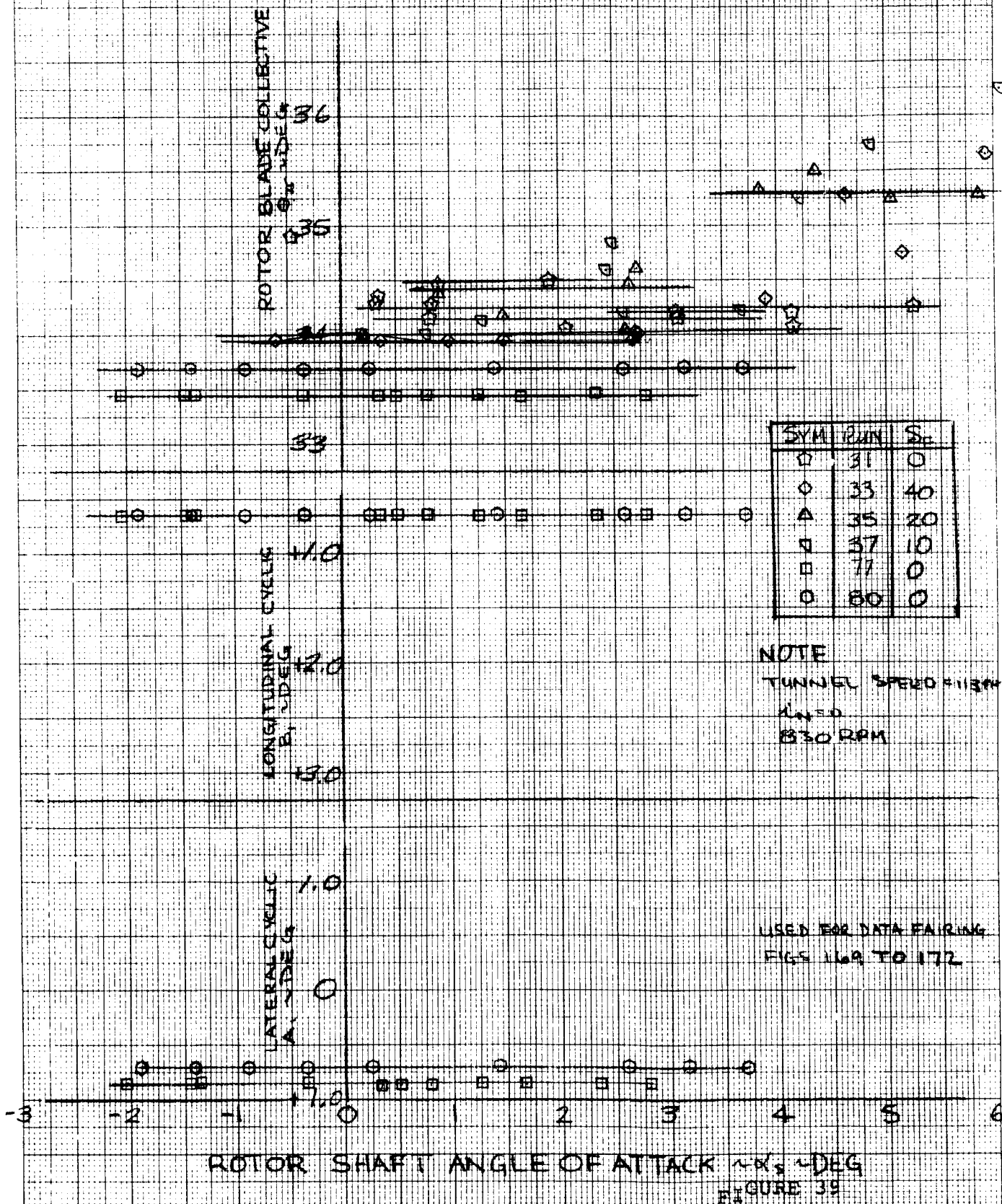
USED FOR DATA FAIRING
FIGS 169 TO 172

-2 -1 0 1 2 3 4 5 6

ROTOR SHAFT ANGLE OF ATTACK α , DEG

FIGURE 38

COLLECTIVE & LATERAL AND LONGITUDINAL CYCLIC CHANGES DURING YAW ANGLE INVESTIGATION IN CRUISE



COLLECTIVE & LATERAL AND LONGITUDINAL CYCLIC CHANGES
DURING YAW ANGLE INVESTIGATION
IN CRUISE

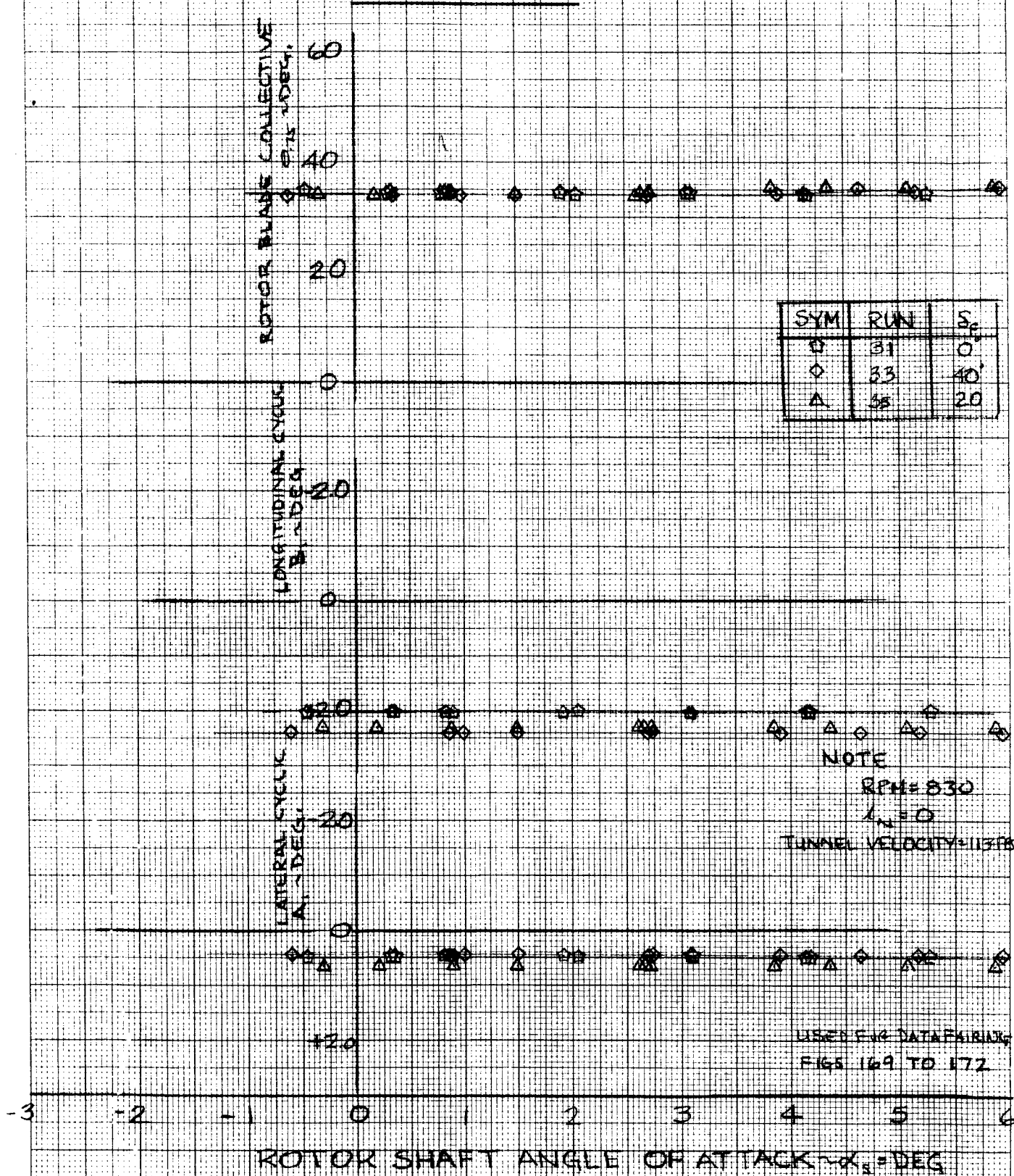


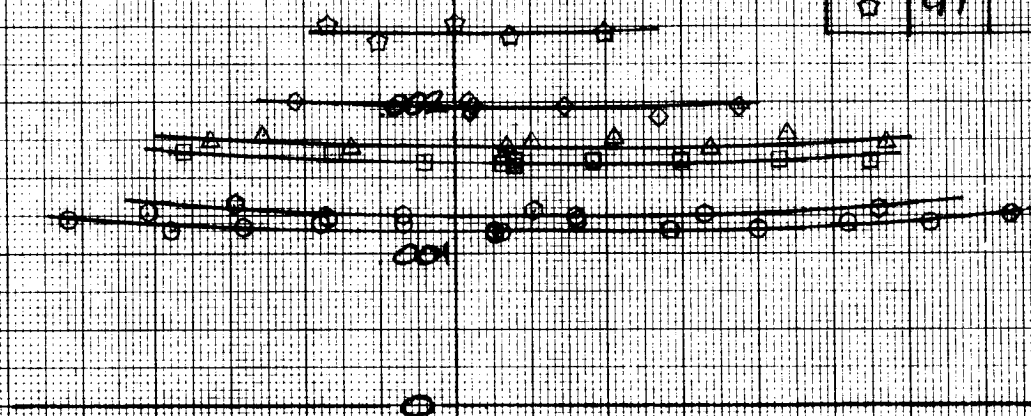
FIGURE 40

EFFECT OF FORWARD SPEED IN CRUISE ON ROTOR THRUST AND POWER

ROTOR POWER COEFFICIENT

SYM	RUN	TUNNEL SPEED (FPS)
○	77	113
○	80	113
□	83	139
△	86	139
◇	89	162
☆	97	182

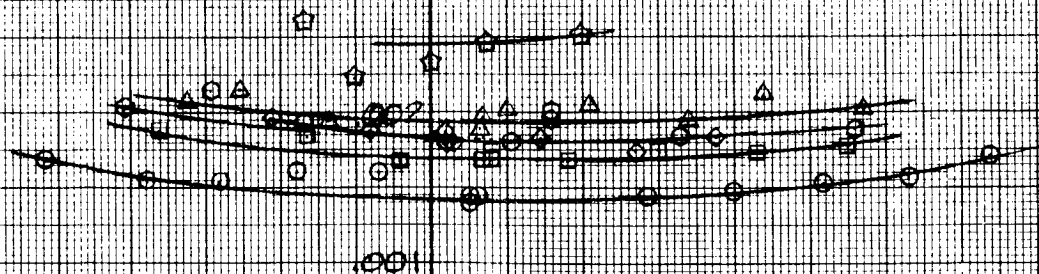
C_P .003



ROTOR THRUST COEFFICIENT

NOTE:
830 RPM
 $i_n = 0$
RIGHT ROTOR

C_T .003



USED FOR DATA FAIRING
FILES 174 TO 176

ROTOR SHAFT ANGLE OF ATTACK α , DEG.

FIGURE 41

EFFECT OF LATERAL, LONGITUDINAL CYCLIC AND BLADE COLLECTIVE ON SHAFT ANGLE

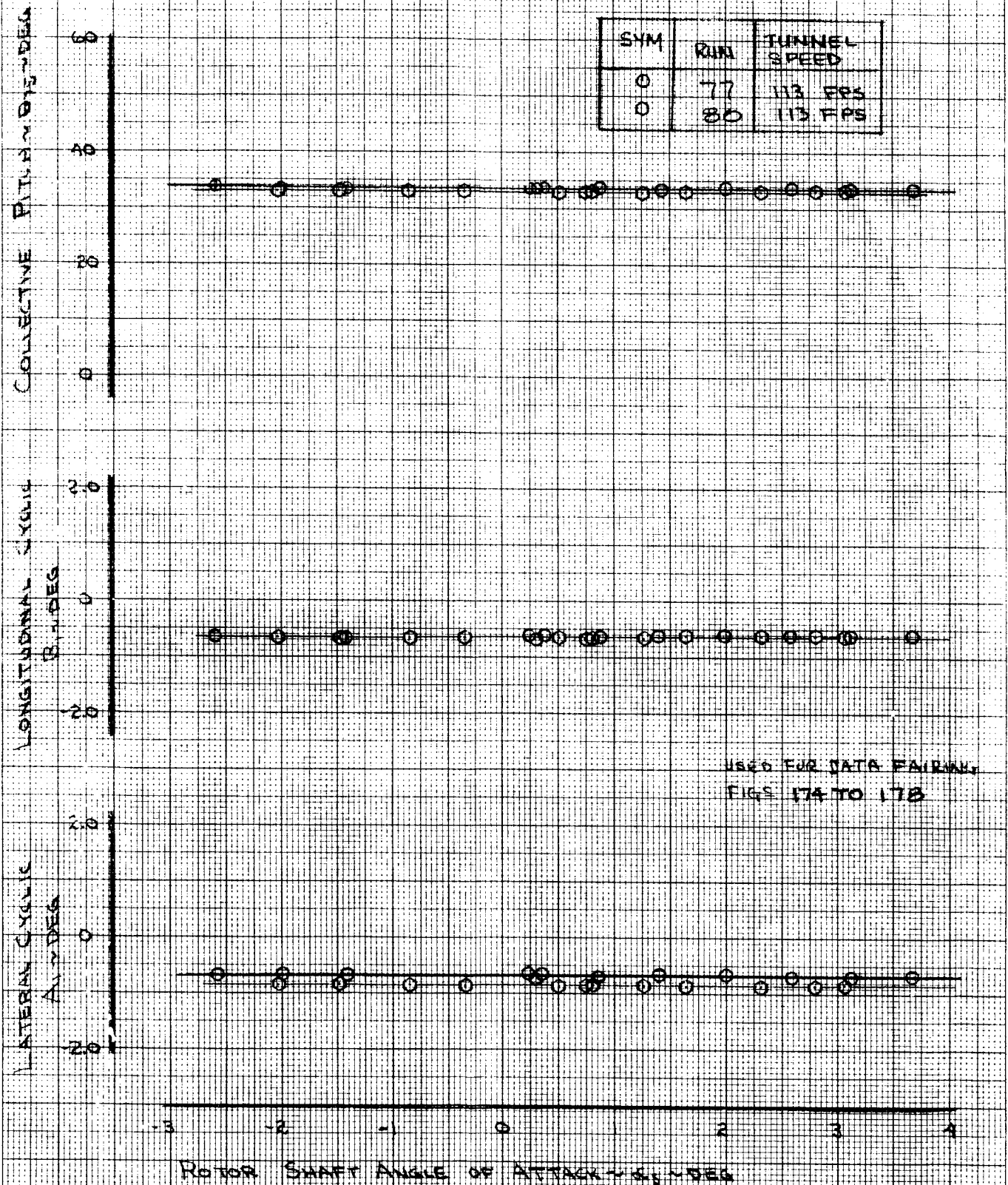
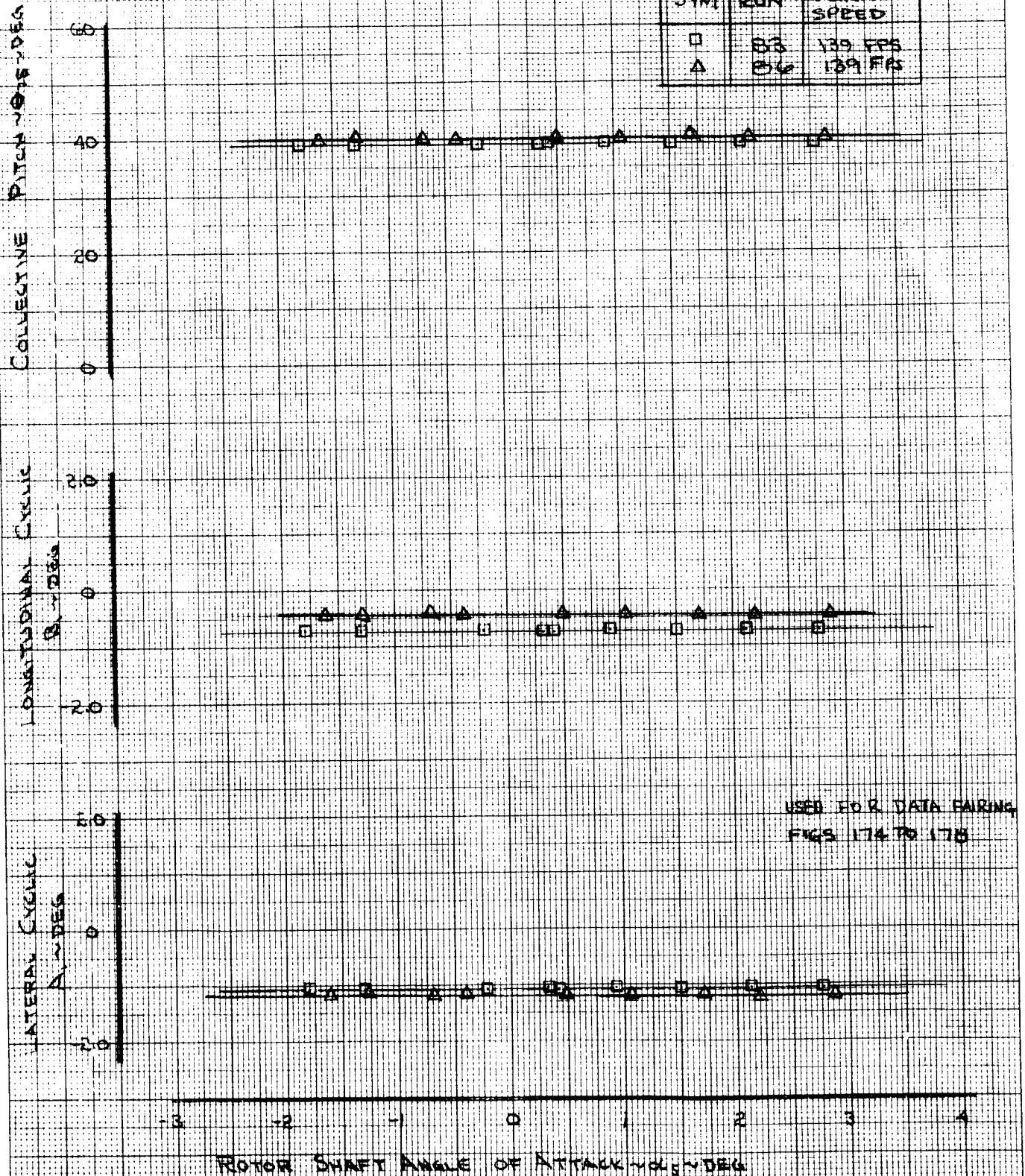


FIGURE 42

EFFECT OF LATERAL LONGITUDINAL CYCLIC
AND BLADE COLLECTIVE ON ROTOR SHAFT ANGLE

SYM	RUN	TUNNEL SPEED
□	83	139 FPS
△	86	139 FPS



USED FOR DATA FAIRING
FIGS 174 TO 178

FIGURE 43

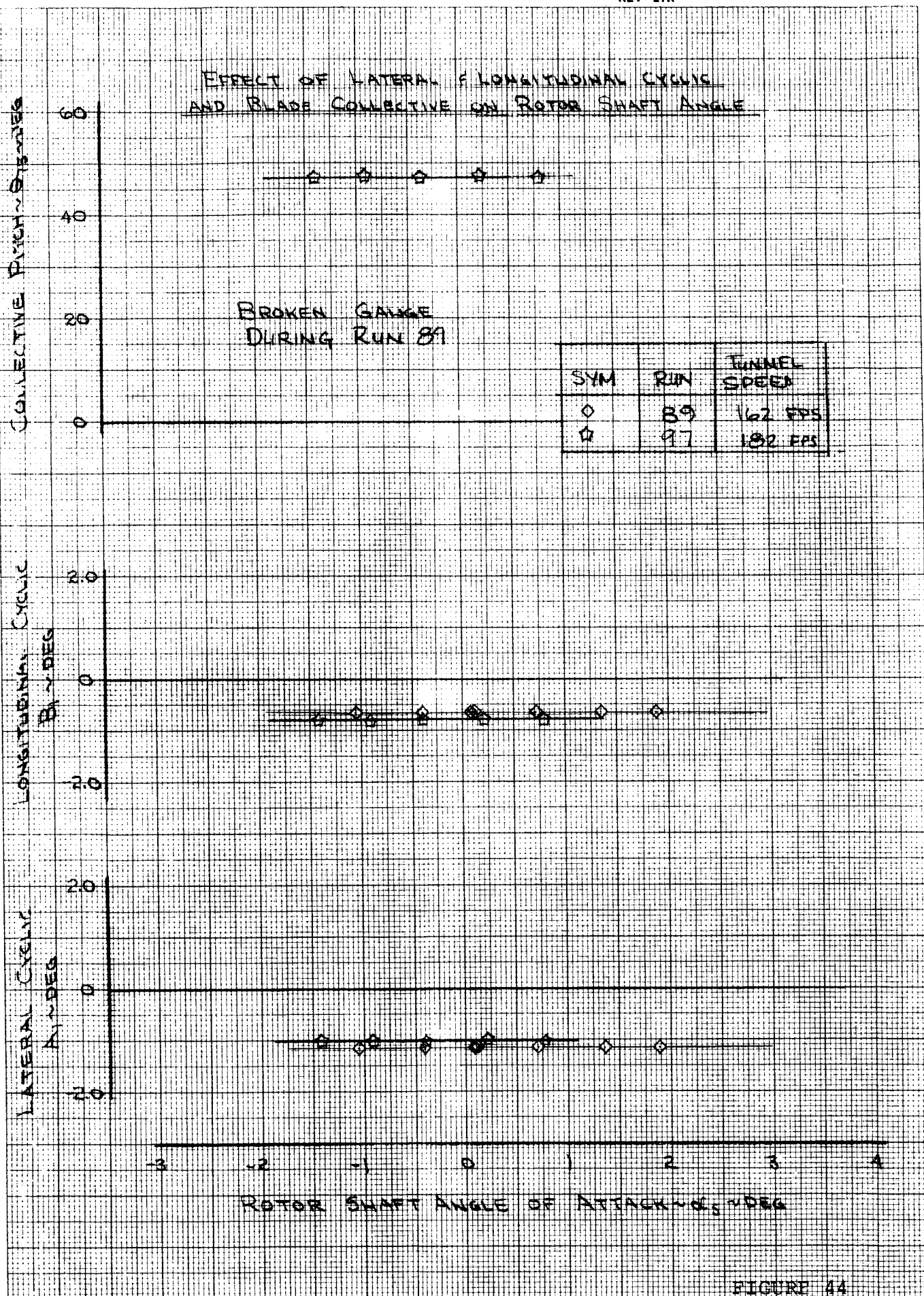


FIGURE 44

EFFECT OF FORWARD SPEED IN CRUISE
ON
ROTOR PERFORMANCE

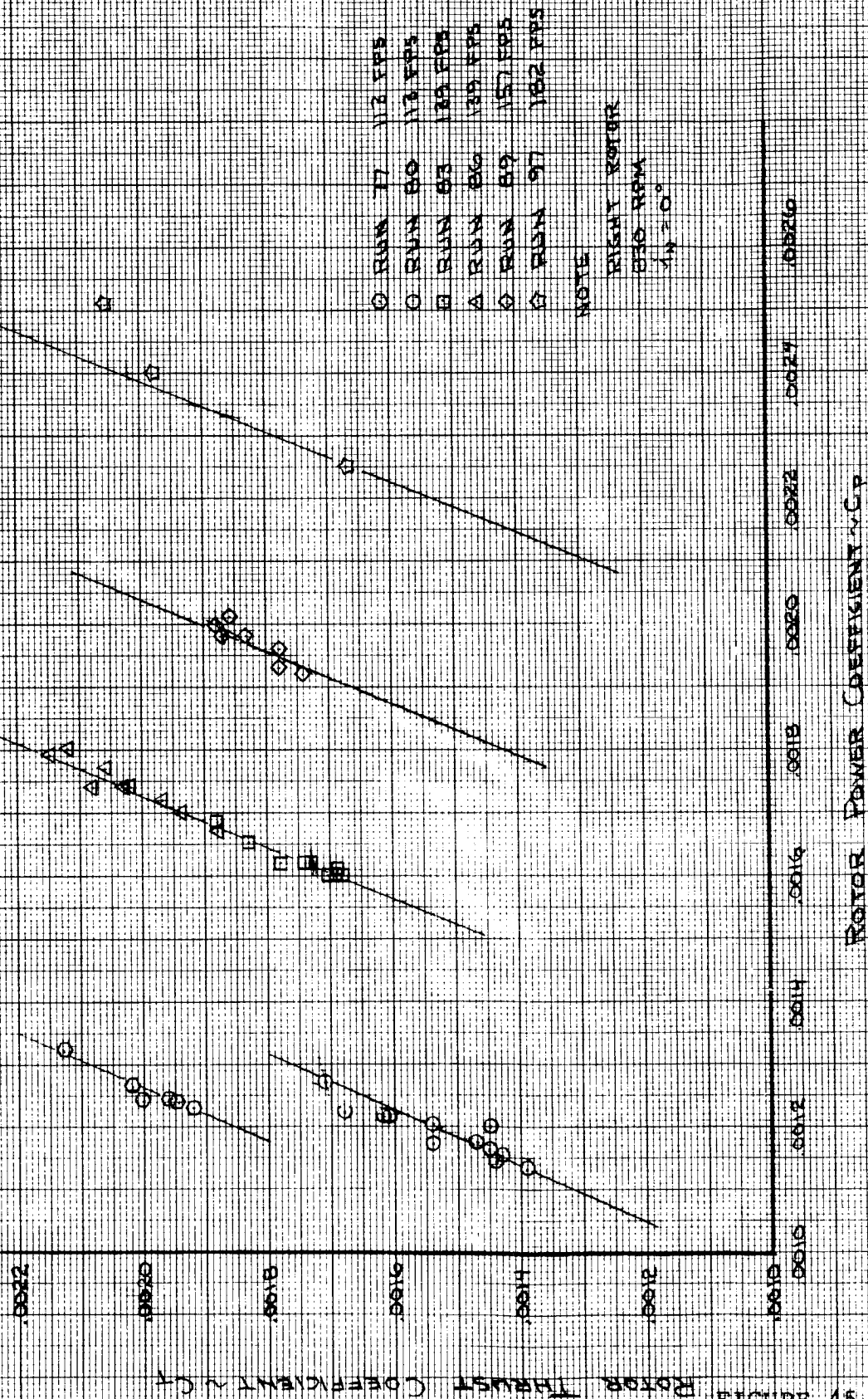


FIGURE 45

EFFECT OF FUSELAGE YAW ANGLE & FLAP DEFLECTION ON ROTOR THRUST & POWER CHARACTERISTICS IN CRUISE

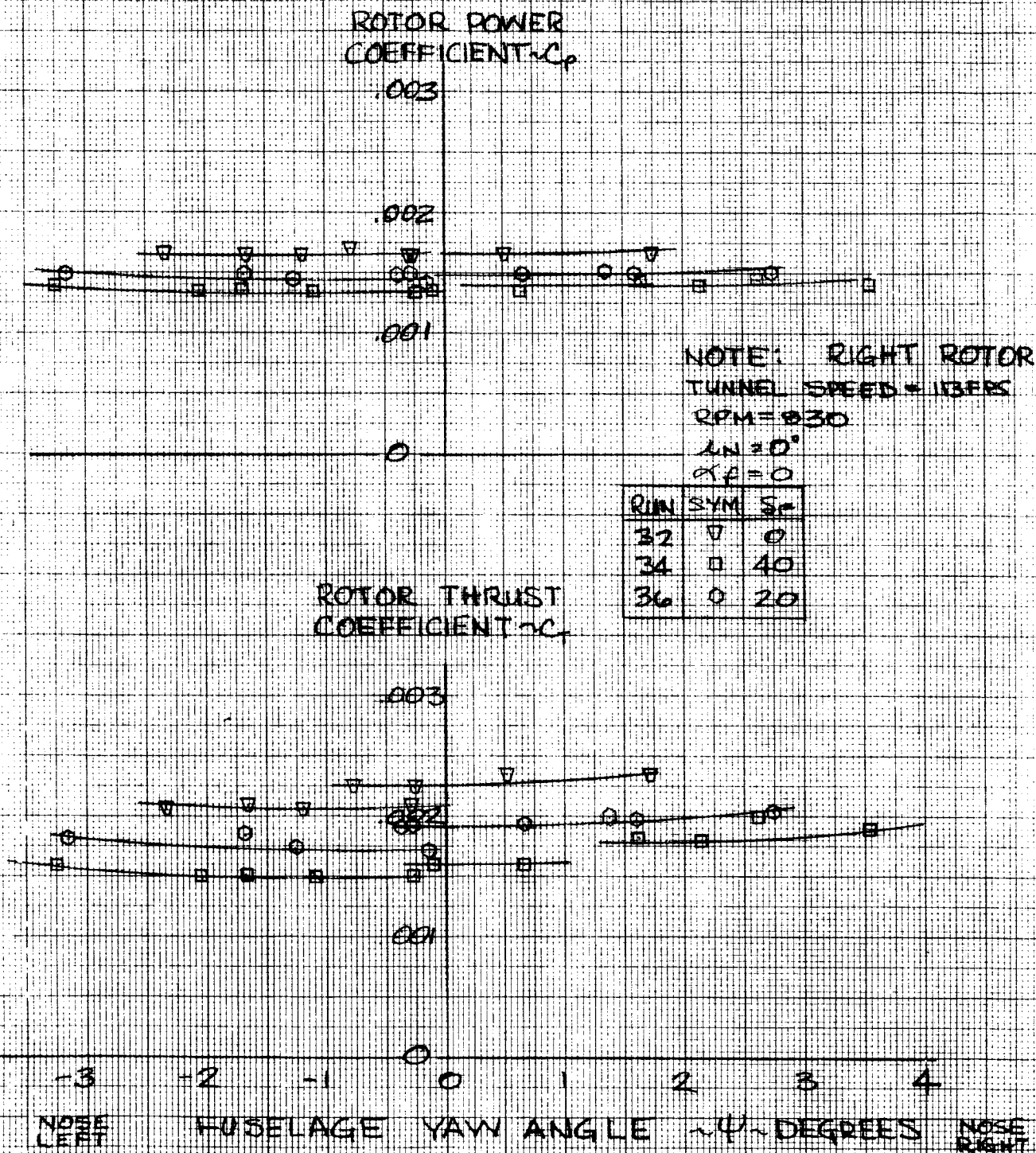


FIGURE 46

COLLECTIVE & LATERAL AND LONGITUDINAL CYCLIC CHANGES DURING YAW ANGLE INVESTIGATION IN CRUISE

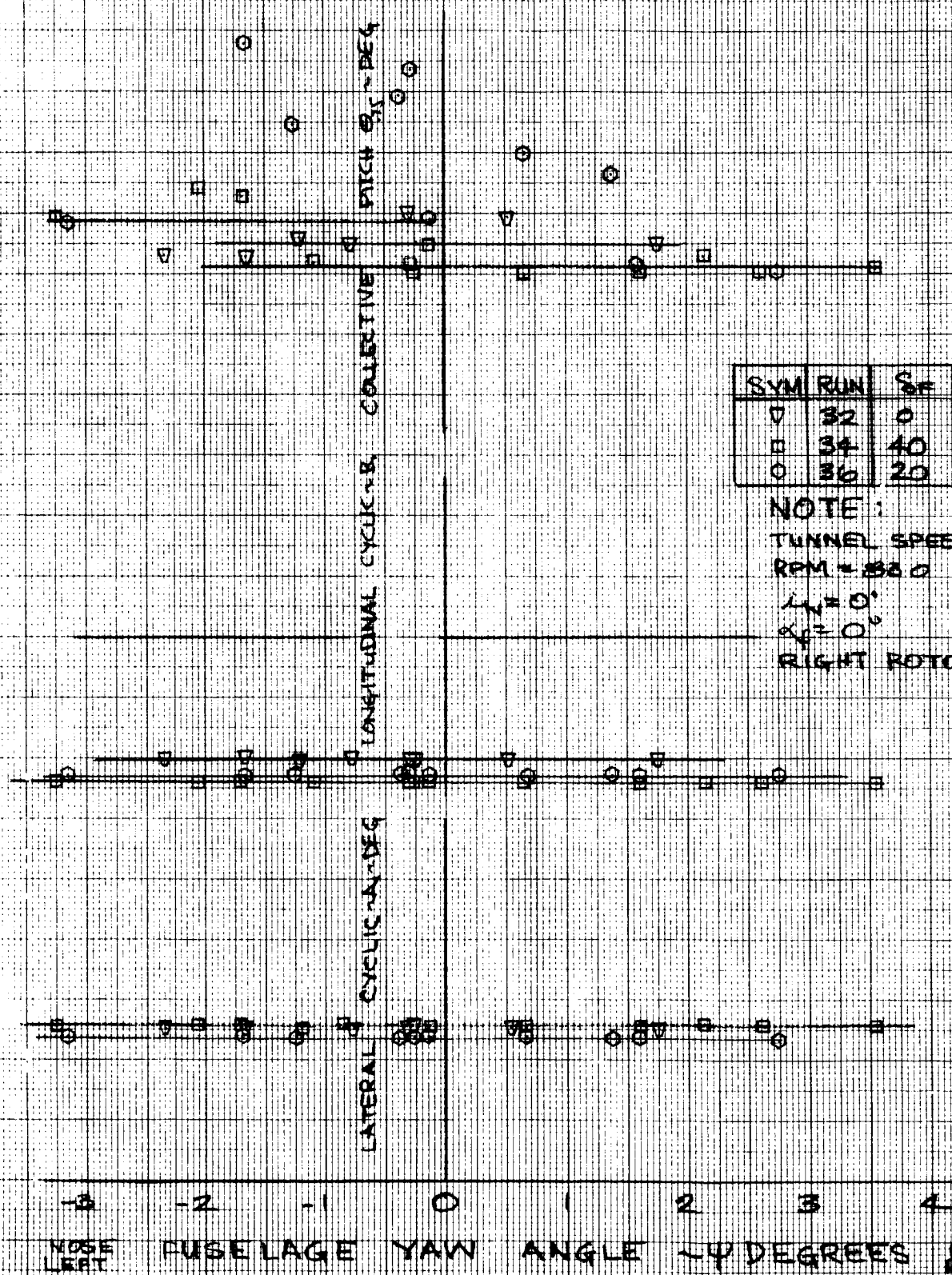
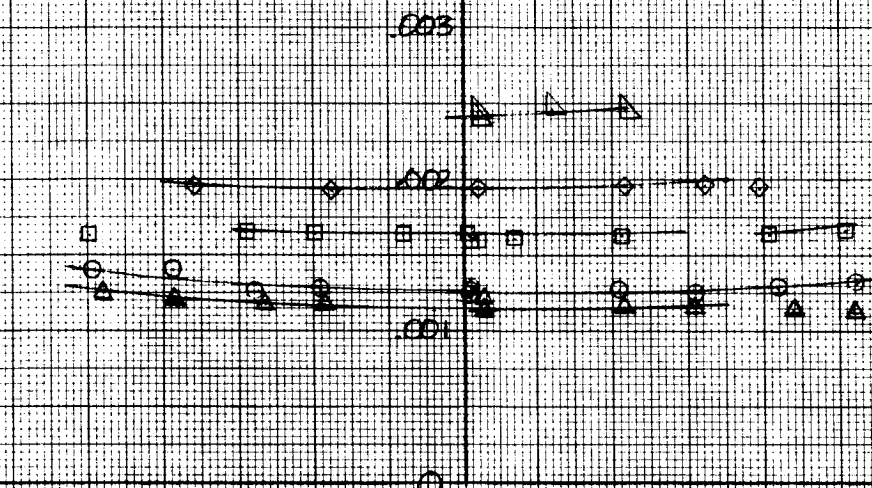


FIGURE 47

EFFECT OF FUSELAGE YAW ANGLE & FORWARD SPEED ON ROTOR THRUST & POWER CHARACTERISTICS IN CRUISE

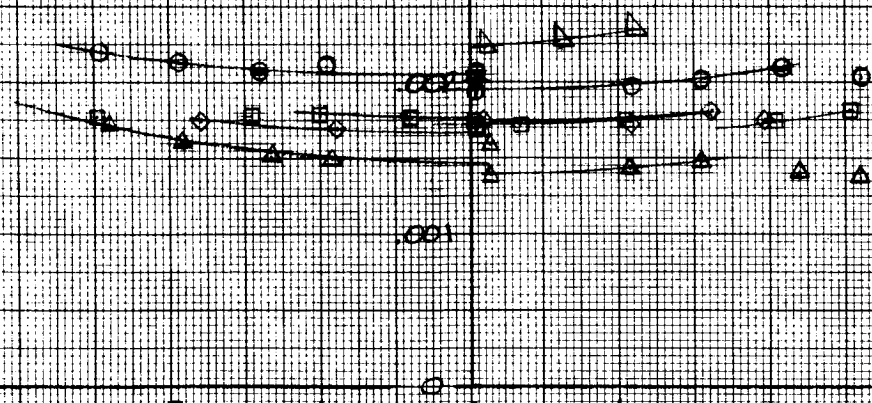
ROTOR POWER
COEFFICIENT $\sim C_p$



NOTE
RPM = 830
 $L_N = 0^\circ$
 $\alpha = 0^\circ$
 $\beta = 0^\circ$

ROTOR THRUST
COEFFICIENT $\sim C_T$

SYM	RUN	TUNNEL SPEED (ft/sec)
○	78	113
△	81	113
□	84	139
◇	90	161
△	98	182



USED FOR DATA FAIRING
FIGS. 164 TO 167

-3 -2 -1 0 1 2 3 4
NOSE FUSELAGE YAW ANGLE $\sim \psi$ - DEGREES NOSE
LEFT RIGHT

FIGURE 48

COLLECTIVE & LATERAL AND LONGITUDINAL CYCLIC CHANGES DURING YAW ANGLE INVESTIGATION IN CRUISE

SYM	RUN	TUNNEL SPEED (FPS)
○	78	113
△	81	113
□	84	139
◇	90	161
▽	98	182

COLLECTIVE PITCH ~ DEG

CYCLIC PITCH ~ DEGREES

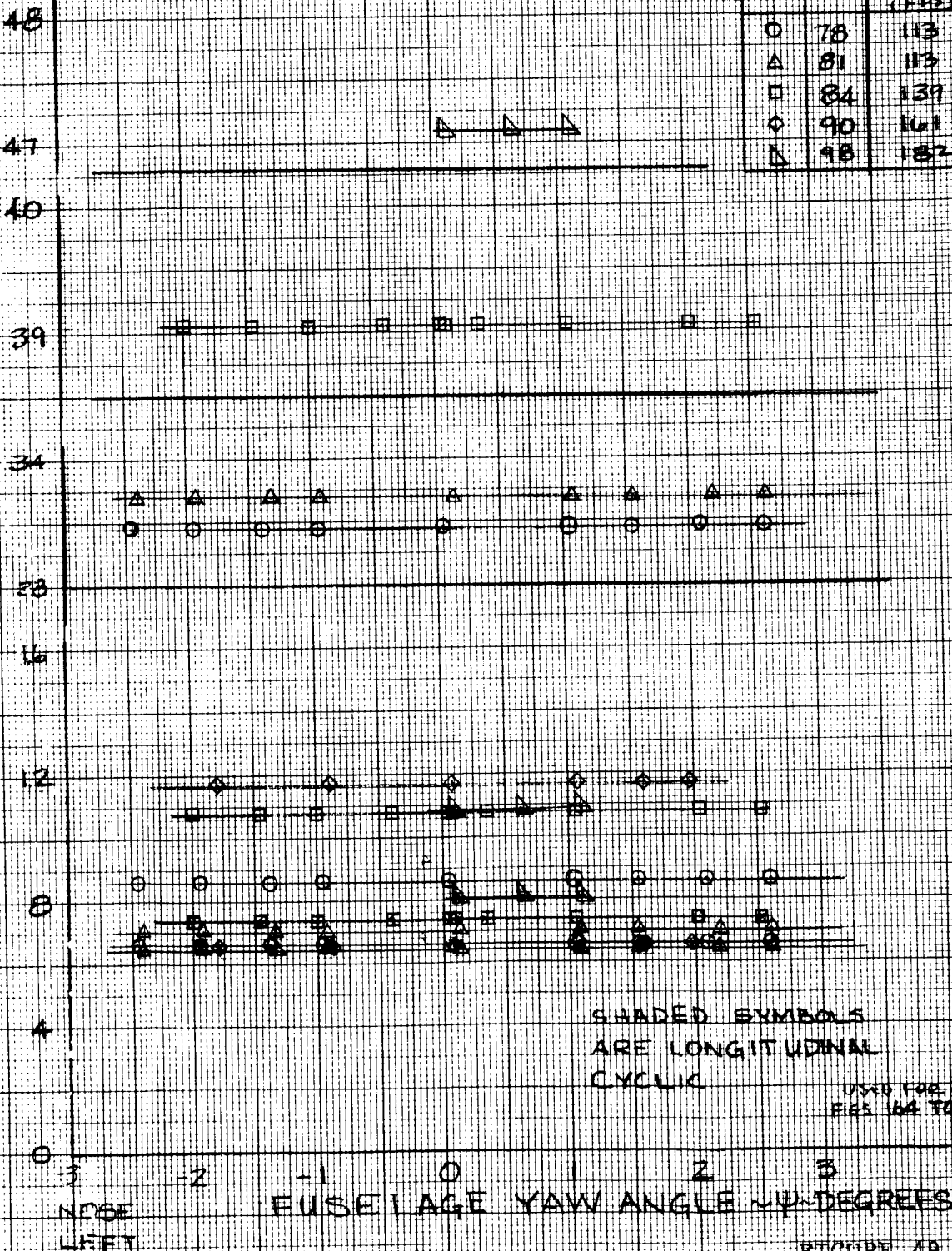


FIGURE 49

COLLECTIVE & LONGITUDINAL CYCLIC CHANGES
DURING LATERAL CYCLIC INVESTIGATION

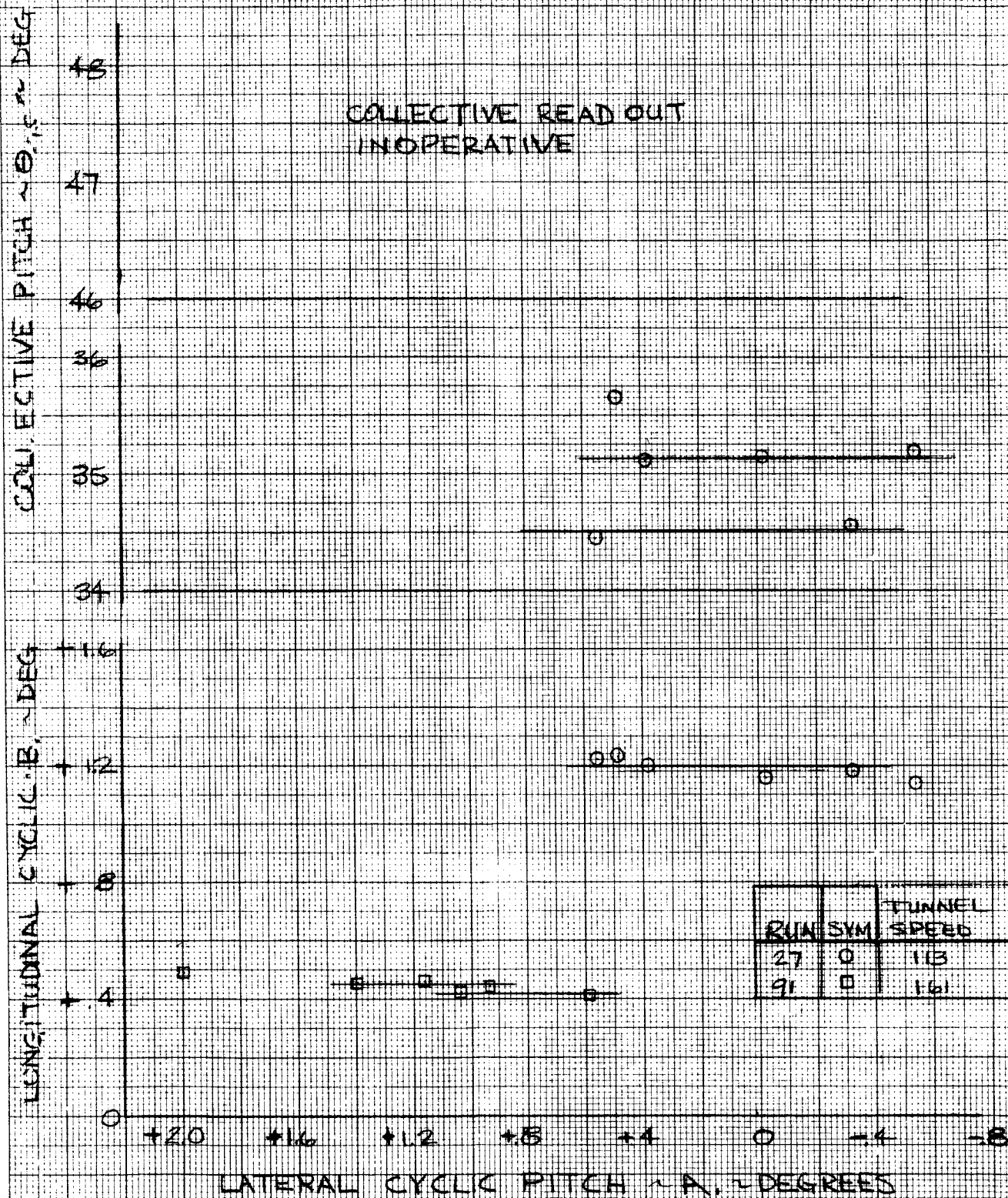


FIGURE 50

EFFECT OF LATERAL CYCLIC & FORWARD SPEED IN CRUISE ON ROTOR POWER & THRUST CHARACTERISTICS

ROTOR POWER
COEFFICIENT C_p

.004

.003

.002

.001

0

ROTOR THRUST
COEFFICIENT C_T

.003

.002

.001

0

+3 +2 +1 0 -1 -2 -3
LATERAL CYCLIC PITCH $\sim A$, \sim DEGREES

RUN	SYM	TUNNEL SPEED
27	0	113 FPS
91	E	161 FPS

FIGURE 51

EFFECT OF LONGITUDINAL CYCLIC & FORWARD SPEED IN CRUISE ON ROTOR POWER & THRUST CHARACTERISTICS

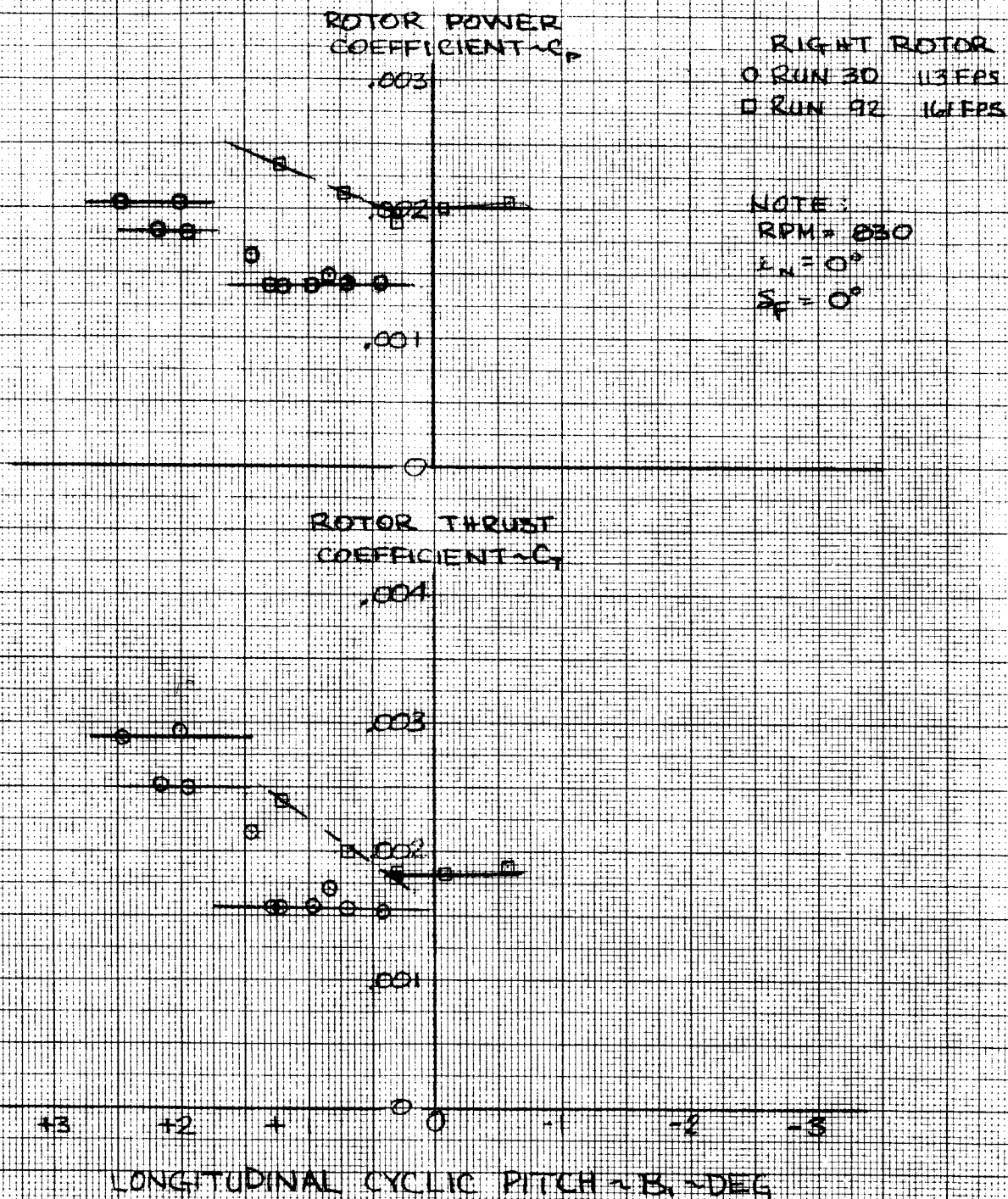


FIGURE 52

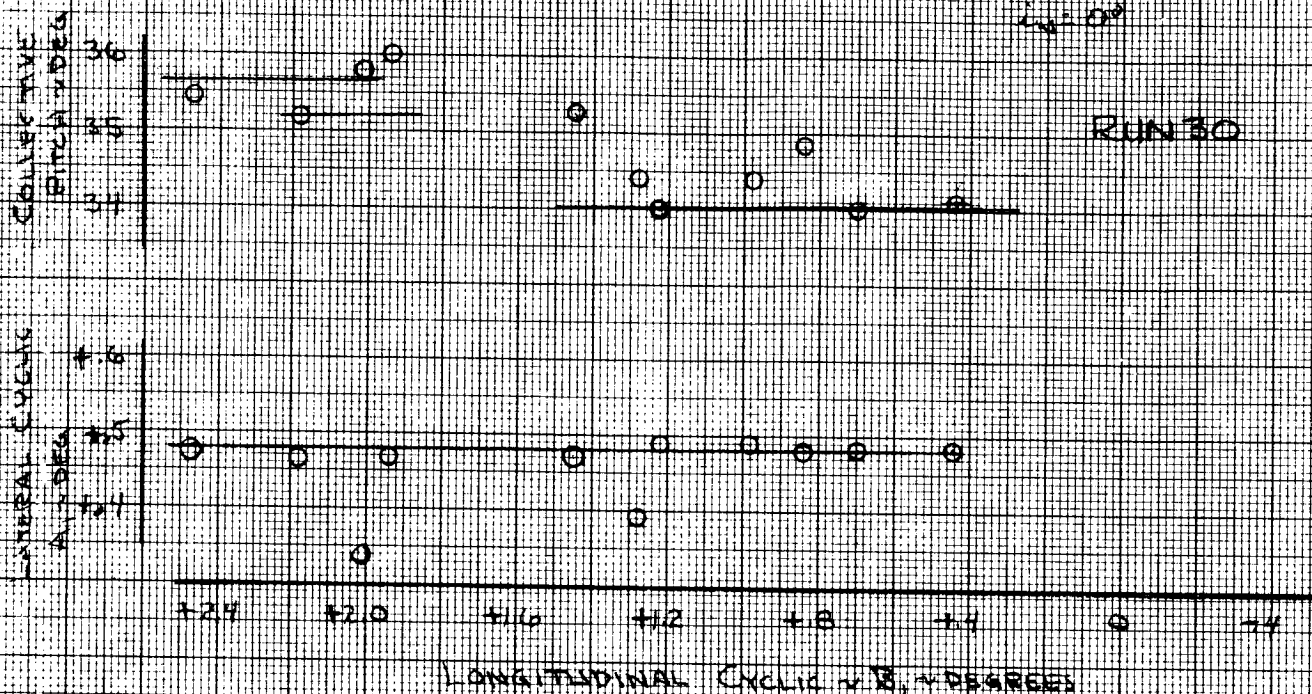
COLLECTIVE & LATERAL CYCLIC CHANGES DURING LONGITUDINAL CYCLIC INVESTIGATION

RIGHT ROTOR

TUNNEL SPEED = 118 KTS

$L_w = 0^\circ$

RUN 30



LONGITUDINAL CYCLIC ~ 8, ~ DEGREES

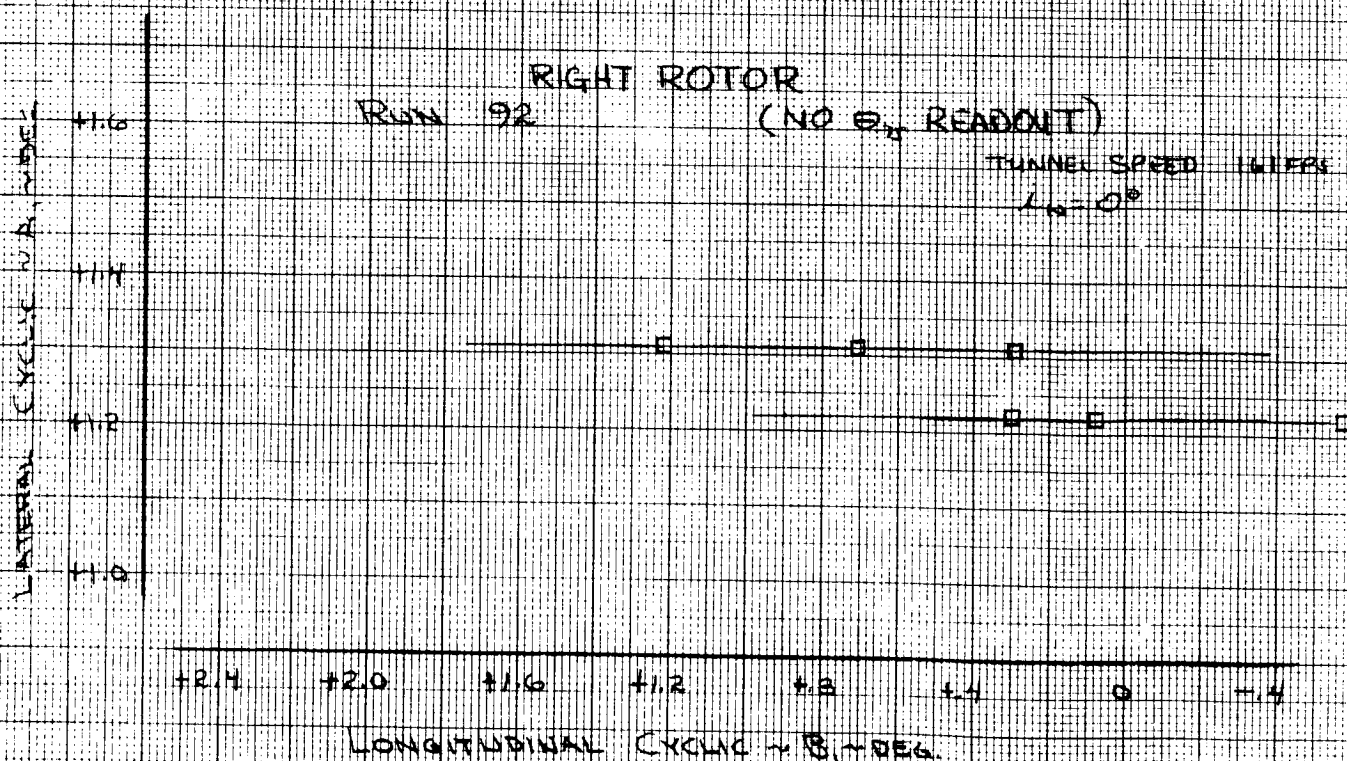
RIGHT ROTOR

RUN 92

(NO θ_r READOUT)

TUNNEL SPEED 116 KTS

$L_w = 0^\circ$



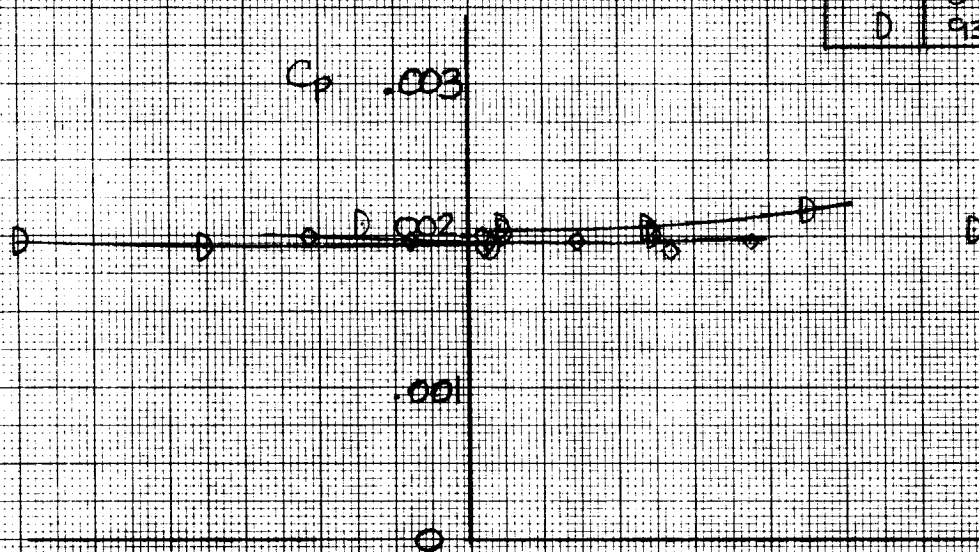
LONGITUDINAL CYCLIC ~ 8, ~ DEG

FIGURE 53

EFFECT OF BLADE LOAD MINIMIZATION ON ROTOR THRUST & POWER IN CRUISE

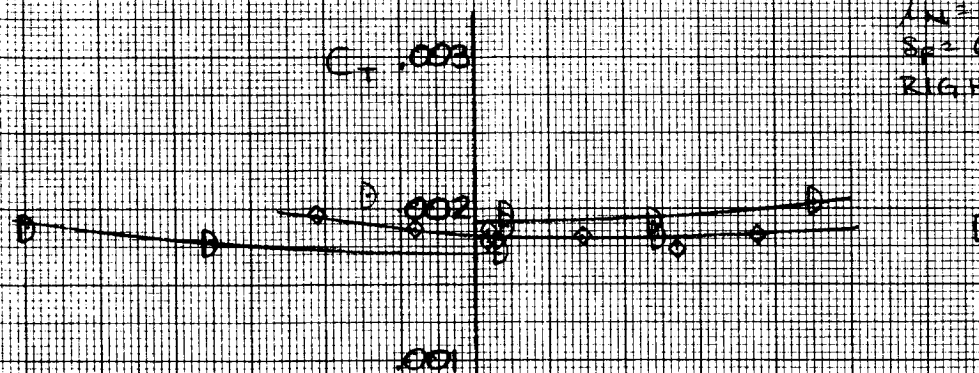
ROTOR POWER COEFFICIENT

SYM	RUN
0	89
D	93



ROTOR THRUST COEFFICIENT

NOTE:
TUNNEL SPEED = 167 FPM
RPM = 830
 $\Lambda = 0^\circ$
 $S_\alpha = 0^\circ$
RIGHT ROTOR



-3 -2 -1 0 1 2 3 4
ROTOR SHAFT ANGLE OF ATTACK α DEG.

FIGURE 54

4.2.2 Aircraft Performance

Aircraft performance in cruise is comprised of the rotor characteristics defined in Section 4.2.1 and the airframe characteristics. Figure 55 presents the variation of airframe lift with angle of attack. Two sets of data are presented for the complete model. The difference between run 40 and 60 is the larger cleaner aerodynamic nacelle and better fitting of the wing fuselage fillets for run 60. Run 75 is a similar test but with the horizontal and vertical tail removed. For this run the airframe has a stall angle of 14 degrees which is for the wing. When adding the tail, as in run 64, the airframe has a stall angle of approximately 19 degrees. To examine the airframe cruise performance requires defining the wing efficiency and the basic airframe profile drag. Figure 56 shows the variation of aircraft drag coefficient with the square of the aircraft lift coefficient (C_L^2) which defines the induced drag increment. At $C_L^2=0$ is the basic profile drag, $C_D=.130$ for run 60, and is compared to the estimate of $C_D=0.030$. This difference is attributed to the poor fit of the skin panels achieved during the test program. The slope of this curve is the relationship of the induced drag to C_L^2 , which is a constant that is a function of wing aspect ratio and efficiency. A value of 0.89 was obtained for the wing efficiency indicating good wing lift carryover across the fuselage, low drag or minimum separation wing root fairing and wing and plating. The wing-fuselage juncture was tested in the wind tunnel prior to fabrication of the final fuselage skins. This testing is summarized in Appendix E and indicates a fairing with no separation in the cruise angle of attack range.

AIRCRAFT LIFT CHARACTERISTICS

ROTORS OFF

○ RUN 14 COMPLETE MODEL
△ RUN 40 COMPLETE MODEL
□ RUN 75 HORIZ & VERT TAIL OFF
TUNNEL SPEED = 113 FPS

$\alpha_w = 0^\circ$

$\delta_F = 0^\circ$

AIRCRAFT LIFT COEFFICIENT C_L

1.6

1.2

0.8

0.4

0

-0.4

-0.8

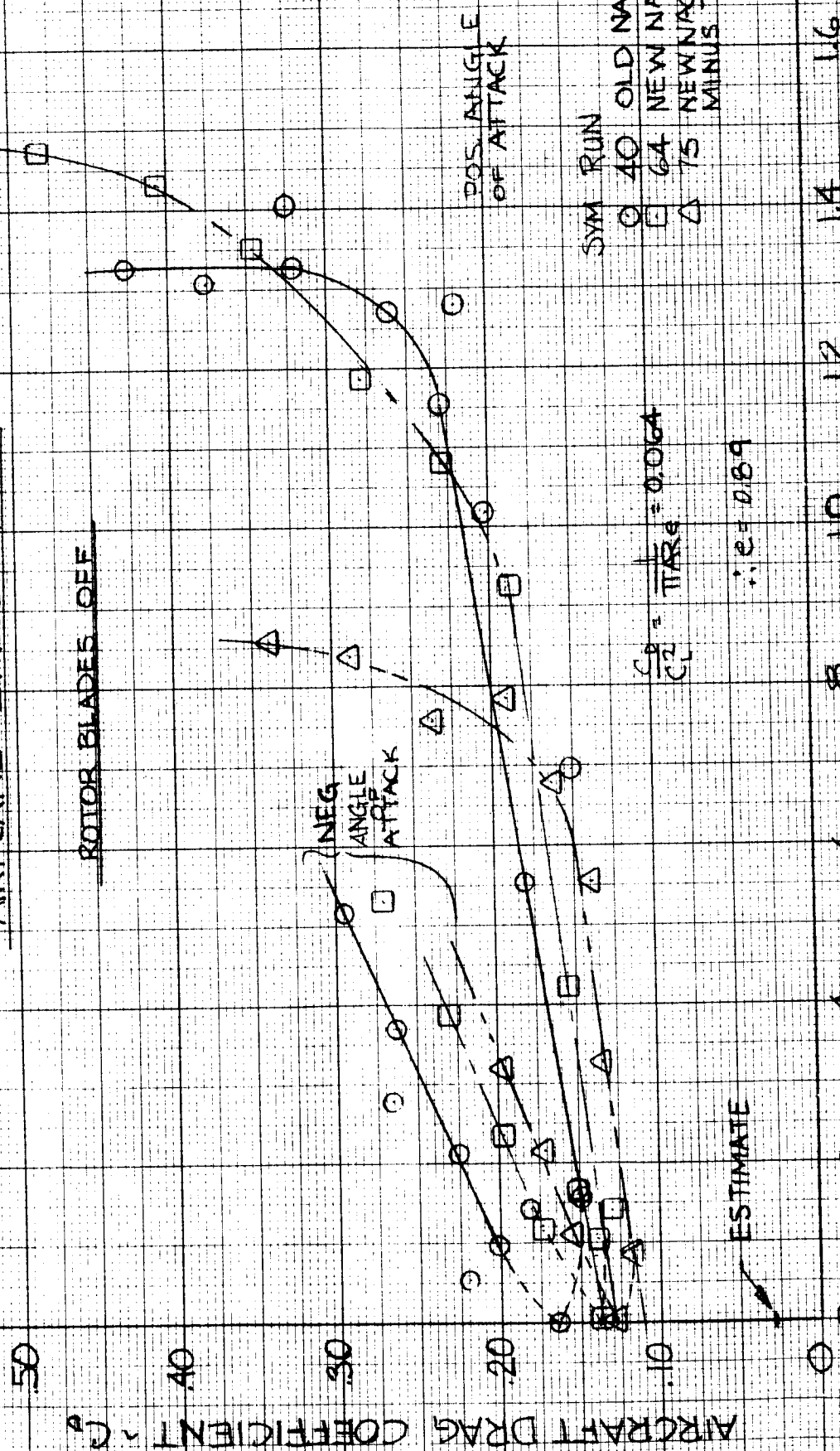
-20 16 -12 -8 -4 0 4 8 12 16 20

FUSELAGE ANGLE OF ATTACK α_f - DEG

FIGURE 55

DEFINITION OF INDUCED DRAG AND AIRPLANE EFFICIENCY

ROTOR BLADES OFF



AIRCRAFT LIFT COEFFICIENT SQUARED ~ C_L^2

Performance data obtained from the model during the flap deflection investigation is presented in Figure 57. The effect of flap deflection on lift curve slope (C_{L_α}) shows an increase from 0.0972 to 0.120 at 20 to 40 degrees. At this speed the lift coefficient equivalent to 13,500 LB is 0.985, which was added to Figure 57 and indicates the "lg" level flight can be achieved with a flap deflection of 40 degrees with a fuselage attitude of minus one degree after correcting for the model drag increment $\Delta C_D = 0.1$. The corresponding yawed flight aircraft performance is presented in Figure 58. This shows there is no change in lift or propulsive force with yaw. Increases in rotor thrust indicated in Section 4.2.1 are apparently just large enough to offset the increase in airframe drag.

Effect of forward speed on aircraft performance are presented in Figures 59 and 60, showing the pitch and yaw influence. This data summarizes all the performance data obtained during this test program.

EFFECT OF FUSELAGE ANGLE OF ATTACK & FLAP DEFLECTION
ON
AIRCRAFT PERFORMANCE
IN CRUISE

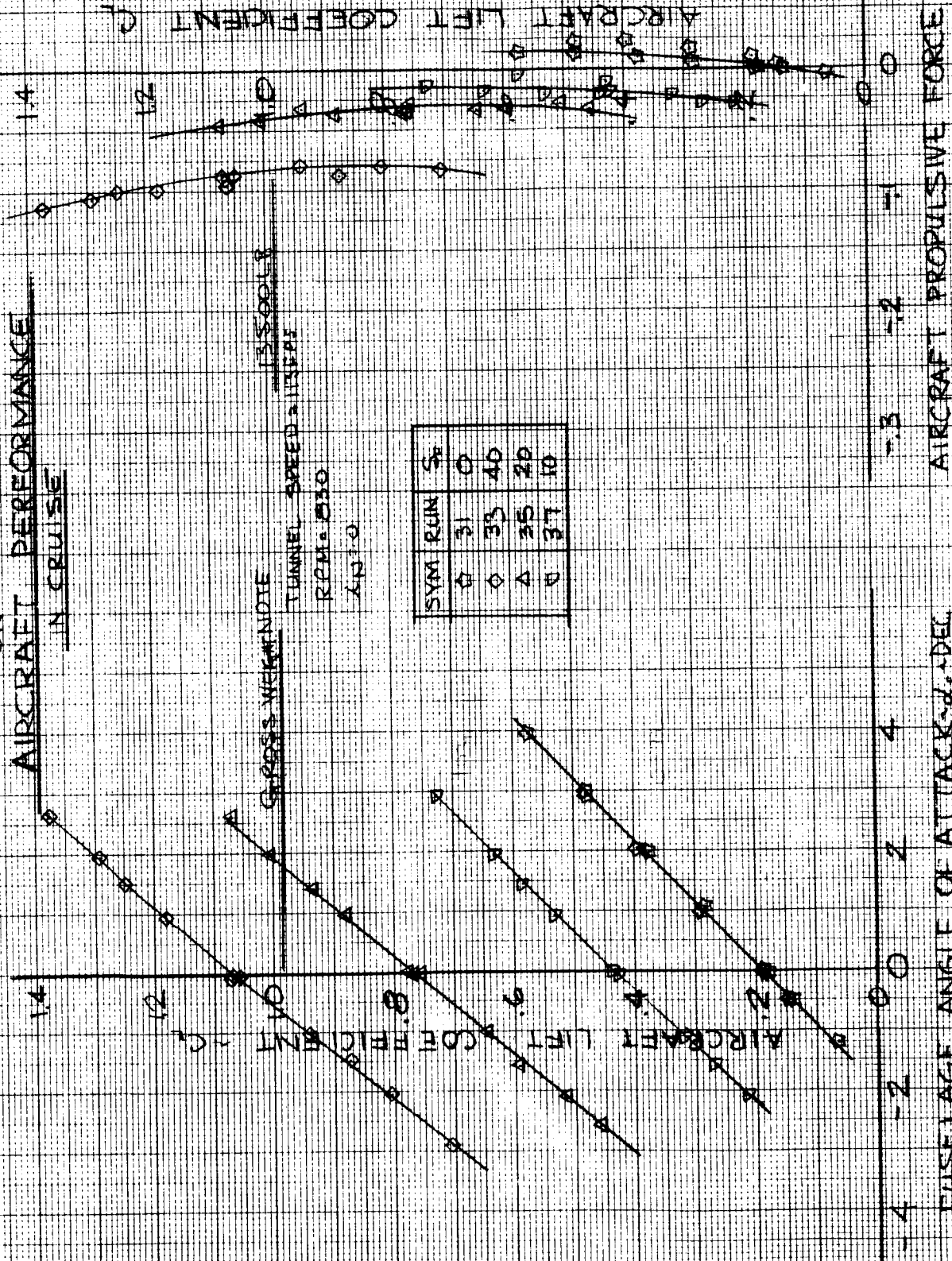


FIGURE 57

EFFECT OF FUSELAGE YAW ANGLE & FLAP DEFLECTION

ON AIRCRAFT PERFORMANCE IN CRUISE

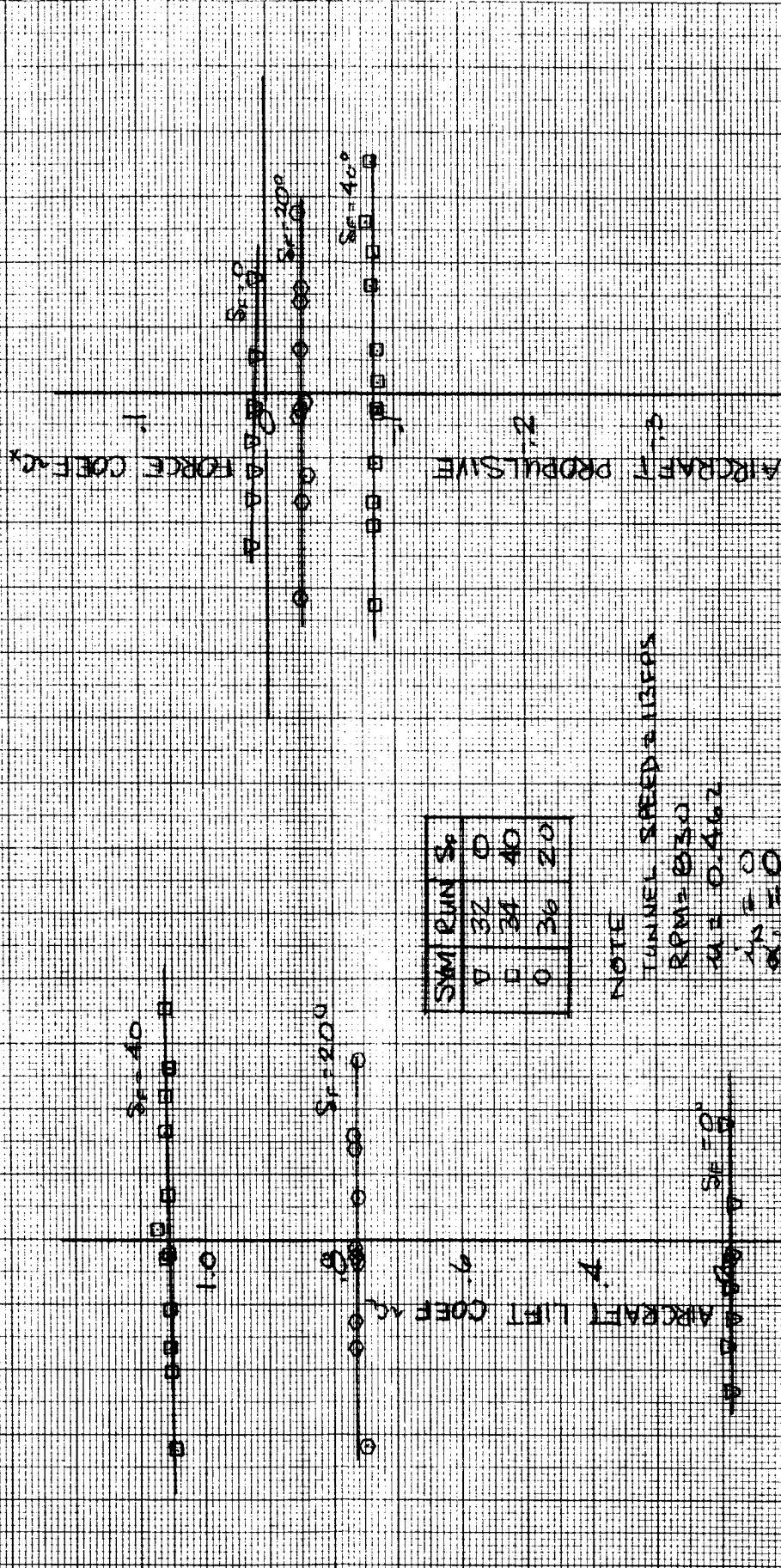
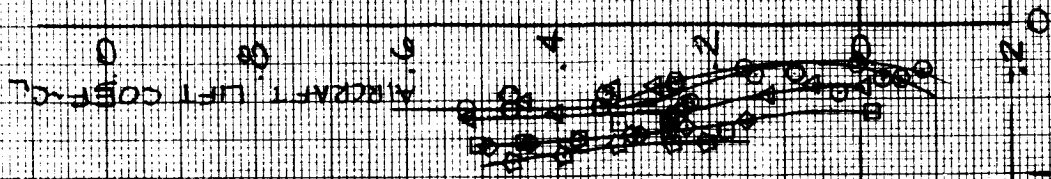
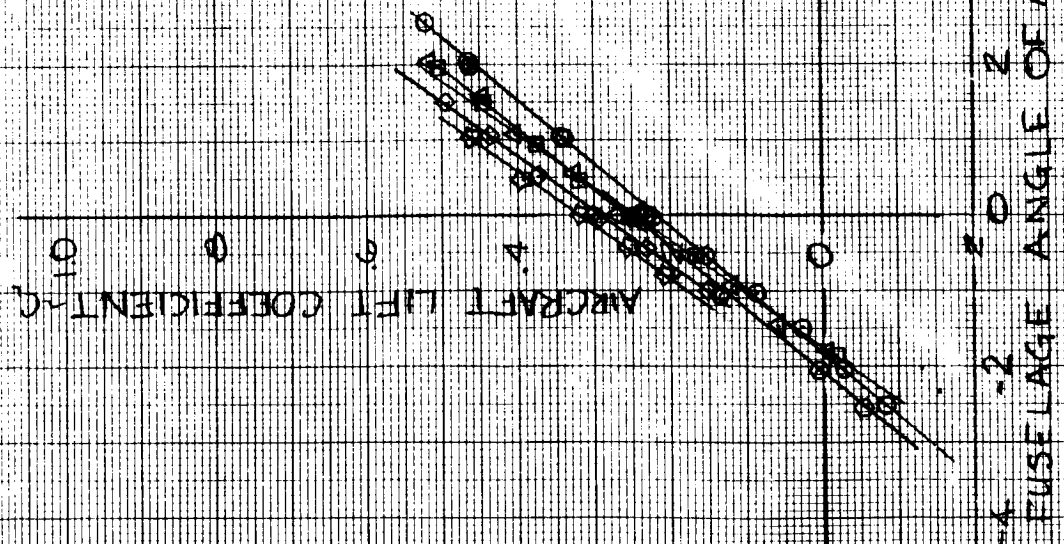


FIGURE 58

EFFECT OF FORWARD SPEED
IN CRUISE
ON AIRCRAFT PERFORMANCE

NOTE
RPM = 830
 $S_c = 0^\circ$
 $\alpha = 0^\circ$



SYM	Q	TURNEL SPEED FPS	ADVANCE RATIO A
○	77	113	0.462
○	80	113	0.462
□	83	139	0.568
△	86	139	0.568
◇	89	162	0.662
☆	97	182	0.750

FIGURE 59

EFFECT OF FUSELAGE YAW ANGLE & FORWARD SPEED

AIRCRAFT PERFORMANCE IN CRUISE

NOTE
RPM# 230
K₁ = 0.0
K₂ = 0.0
S₁ = 0.0

SWM	RPM	TUNNEL SPEED FPS	ADVANCE RATIO	M
0	75	113	0.461	0.461
Δ	81	113	0.461	0.461
□	84	134	0.568	0.568
◇	90	162	0.667	0.667
Δ	95	182	0.750	0.750

AIRCRAFT LIFT COEFFICIENT C_L

FORCE COEFF C_F

AIRCRAFT PROPULSIVE

YAW ANGLE -4 -2 0 2 4
FUSELAGE YAW ANGLE -4 -2 0 2 4
NOSE LEFT NOSE RIGHT

FIGURE 60

4.3 COMPARISON OF TEST AND THEORY

To determine the validity of the methodology being utilized to design and build the tilt rotor, provides an addition objective to this program. Figure 61 shows the variation of rotor thrust with power for transition, presented in Section 4.1.1, corrected for hub tare and Reynolds number and reducing the lateral and longitudinal cyclic to zero. It is compared with the theoretical values obtained from D88 computer program and shows good correlation.

This theory is an aeroelastic analysis for the study of aerodynamic dynamic and structural characteristics of current and advanced rotor and prop/rotor concepts. Airloads are calculated considering the effects of section geometry, compressibility and non-uniform in flow. An iterative process between the airloads and coupled flap-pitch dynamic response establishes blade accelerations which in turn are used to compute hub loads and rotor aerodynamic performance. This program was used to compute the transition rotor performance (thrust, power and collective relationships), static stability (inplane forces and moments) and the cyclic control characteristics. A complete description of this analysis, D-88 computer program is contained in Reference 2.

The comparison of test data and theory in the cruise mode is presented in Figure 62. This prediction is made on VASCOMP II, and aircraft sizing program. The test data is the integration of the data in Section 4.2.1 and 4.2.2 and simulating the cruise thrust required for the full scale aircraft. This data is corrected for Reynolds and the resulting performance comparison appears to be quite good.

COMPARISON OF THEORY AND TEST DATA IN TRANSITION ROTOR PERFORMANCE CHARACTERISTICS

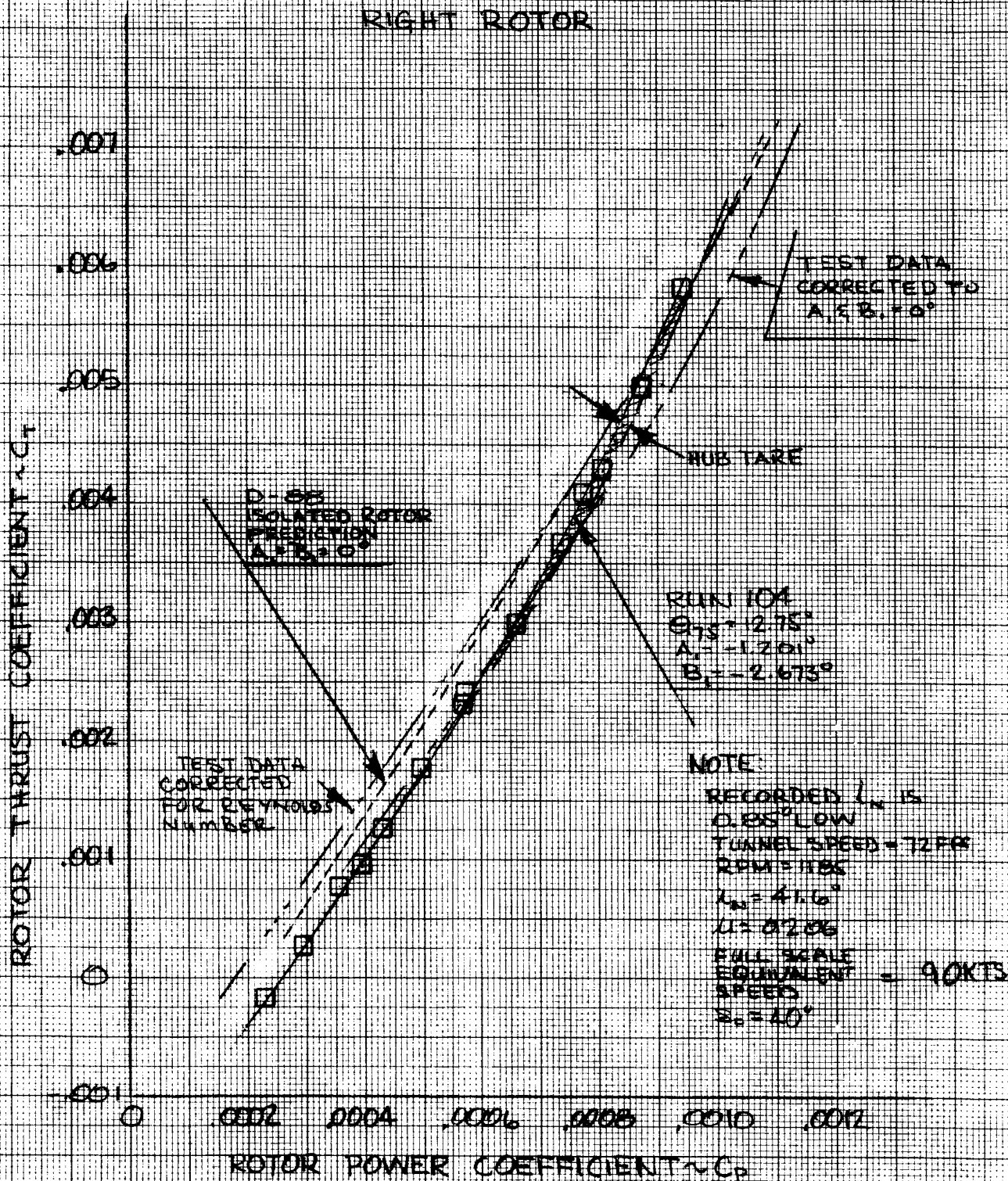


FIGURE 61

COMPARISON OF TEST DATA
AND
PRE TEST PREDICTION
OF
POWER REQUIRED

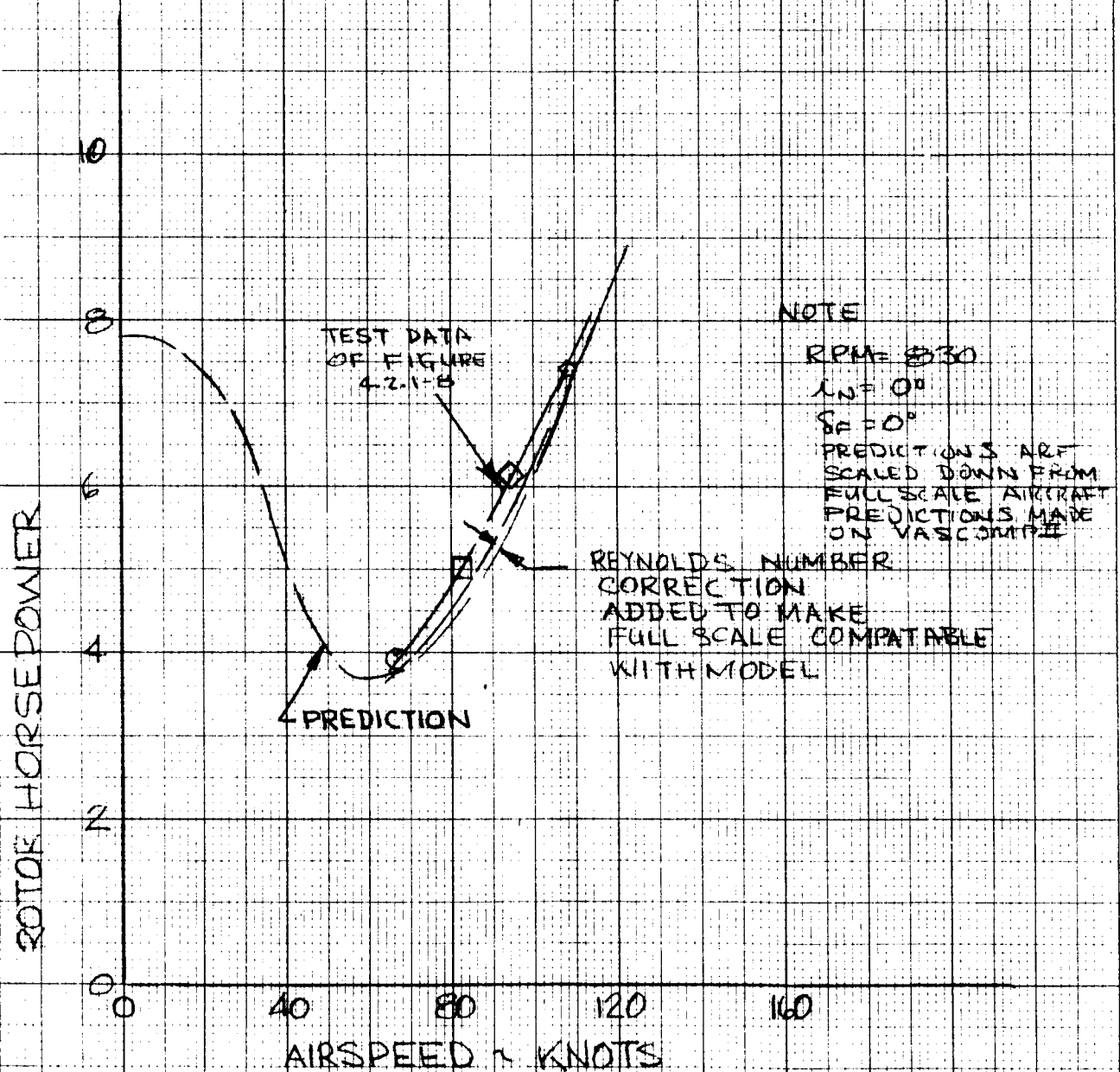


FIGURE 62

5.0 STABILITY AND CONTROL

In evaluating the stability and control data obtained during this test, it must be remembered that because of the Froude scaling used for this dynamic model the test Reynolds numbers were low (0.6×10^6 for transition testing and up to 1.47×10^6 maximum for cruise testing). This results in values of C_{L_α} and $C_{L_{\max}}$ lower than can be expected full scale. The effects of Reynolds number contributes to the difference in neutral point location in transition, rotors off, between test data and the predicted location. Previous model tests indicated that the rotor derivatives and rotor effects on the aircraft characteristics are not significantly affected by Reynolds number. Addition testing at higher Reynolds number is recommended with a larger unpowered model to determine the magnitude of Reynolds number effects.

5.1 Transition Stability and Control

This section addresses the overall aircraft stability and control as well as the individual contributions made by the rotor, the airframe and the controls in the transition flight regime. Transition includes all forward flight conditions for nacelle incidence of 90 degrees to 0 degrees. The following sections will address these items as they were covered in the testing directed at Objectives 2,3, 4 and 8 presented in Section 2.0.

5.1.1 Rotor Stability Derivatives

The rotor stability derivatives obtained from the testing in the transition flight regime is at 72 ft/sec tunnel velocity, which is equivalent to 90 kts full scale. Nacelle incidence of approximately 42 degrees was examined with flap deflections of 40, 30 and 20 degrees and a nacelle incidence of 30 degrees with a flap deflection of 30 degrees was also tested.

Effect of Flap Deflection on Pitch Derivatives

This testing was directed at defining the effect of wing lift on rotor stability characteristics and aircraft performance in transition. Figure 63 presents the variation of aircraft lift with angle of attack for flap deflections of 20, 30 and 40 degrees with the nacelle incidence of 41.6 degrees. The aircraft lift is approximately the same for 20 and 30 degrees but decreases for 40 degrees flap deflection which is opposite to what is expected. Subtracting out the rotor and spinner contribution provides the airframe data presented in Figure 64. Increasing the flap deflection from 20 to 30 degrees results in an increase in lift. Increasing the flap deflection further to 40 degrees shows a decrease in lift of approximately the same magnitude. This is a result of decreased collective producing a lower thrust as shown in Figure 65 and results in a lower downwash and local dynamic pressure on the wing. The rotor characteristics of normal force, pitching moment, side force and yawing moment are presented in Figures 66 through 69, for these flap deflections. Figure 70 shows the variation of collective and cyclic during this series of test runs and was used to define the specific test data points that should be utilized in

the data fairing. The rotor derivatives with angle of attack are summarized in the following table.

TUNNEL SPEED V	ADVANCE RATIO μ	FLAP DEFLECTION δ	$\frac{\partial C}{\partial \alpha}$ NF	$\frac{\partial C}{\partial \alpha}$ PM	$\frac{\partial C}{\partial \alpha}$ SF	$\frac{\partial C}{\partial \alpha}$ YM
72 fps	0.206	20°	0.000033	0.000032	-0.0000305	-0.000005
		30°	0.000028	0.000032	-0.0000122	-0.0000075
		40°	0.000026	0.000034	-0.0000122	-0.000006

This data shows the general impact of wing lift decreasing the normal force and yawing moment derivatives while increasing the side force and pitching moment derivatives. The amount of change in the derivatives is slight and the overall change in level associated with the flap deflection cannot be readily extracted from the data. Since the corrections required to remove the cyclic is large and the variation in lift is small, any slight deviation in the correction would significantly affect the resulting trend with lift. To accomplish this objective will require further testing.

Rotor Directional Stability at 41.6° Nacelle Incidence

At the nacelle incidence of 41.6 degrees and 40 degrees flap deflection, a yaw sweep was made to define the directional stability characteristics. For this investigation the wing lift did not vary and is shown in Figure 71. The rotor characteristics obtained from this run are presented in Figures 72 through 75. Similar data was obtained for a nacelle incidence of 30 degrees with its corresponding flap deflection of 30°. These rotor normal force,

pitching moment, side force and yawing moment characteristics are presented in Figures 76 through 79. A comparison of the rotor derivatives for these two test conditions are shown below.

TUNNEL SPEED V	ADVANCE RATIO μ	NACELLE INCI- DENCE i_N	FLAP DEFLEC- TION δ	$\frac{\partial C}{\partial \psi}$ NF	$\frac{\partial C}{\partial \psi}$ PM	$\frac{\partial C}{\partial \psi}$ SF	$\frac{\partial C}{\partial \psi}$ YM
72 fps	0.206	41.6°	40°	0.0000027	-0.000020	0.000026	0.0000276
72 fps	0.206	30°	30°	0.000008	-0.000029	0.0000254	0.000037

There is a significant increase in normal force and yawing moment derivatives as nacelle incidence is decreased while the side force remains unchanged and the pitching moment decreases.

Effect of Nacelle Incidence on Rotor Longitudinal Stability

While at a nacelle incidence of 30°, a pitch attitude sweep was made and the rotor characteristics were obtained. This data is presented in Figures 80 to 83. A summary of these derivatives is shown below compared to the data obtained at 41.6° nacelle incidence discussed earlier.

TUNNEL SPEED V	ADVANCE RATIO μ	NACELLE INCI- DENCE i_N	FLAP DEFLEC- TION δ_F	$\frac{\partial C}{\partial \alpha}$ NF	$\frac{\partial C}{\partial \alpha}$ PM	$\frac{\partial C}{\partial \alpha}$ SF	$\frac{\partial C}{\partial \alpha}$ YM
72 fps	0.206	41.6°	40°	0.000026	0.000032	-0.0000122	-0.000006
72 fps	0.206	30°	30°	0.000045	0.000041	-0.000034	0.0000075

As the nacelle incidence is decreased the rotor derivatives are increasing and producing a more unstable contribution to the aircraft stability. To provide an understanding of the nacelle incidence effect, a run was made at a fixed fuselage attitude and rotor thrust coefficient while varying the nacelle incidence. The cyclic was varied to provide minimum blade loads at each incidence. The effect on aircraft lift, presented in Figure 84, indicates that the lift is increasing as a result of the increase in vertical component of thrust. The associated impact on rotor characteristics indicates that the normal force is decreasing and the pitching moment is increasing with decreasing nacelle incidence. There is approximately no change in the rotor contribution to the aircraft longitudinal stability since the moment produced by the normal force trades off in magnitude with the rotor hub moment as indicated in Figure 85 and 86.

EFFECT OF FLAP DEFLECTION IN TRANSITION ON AIRCRAFT LIFT COEFFICIENT

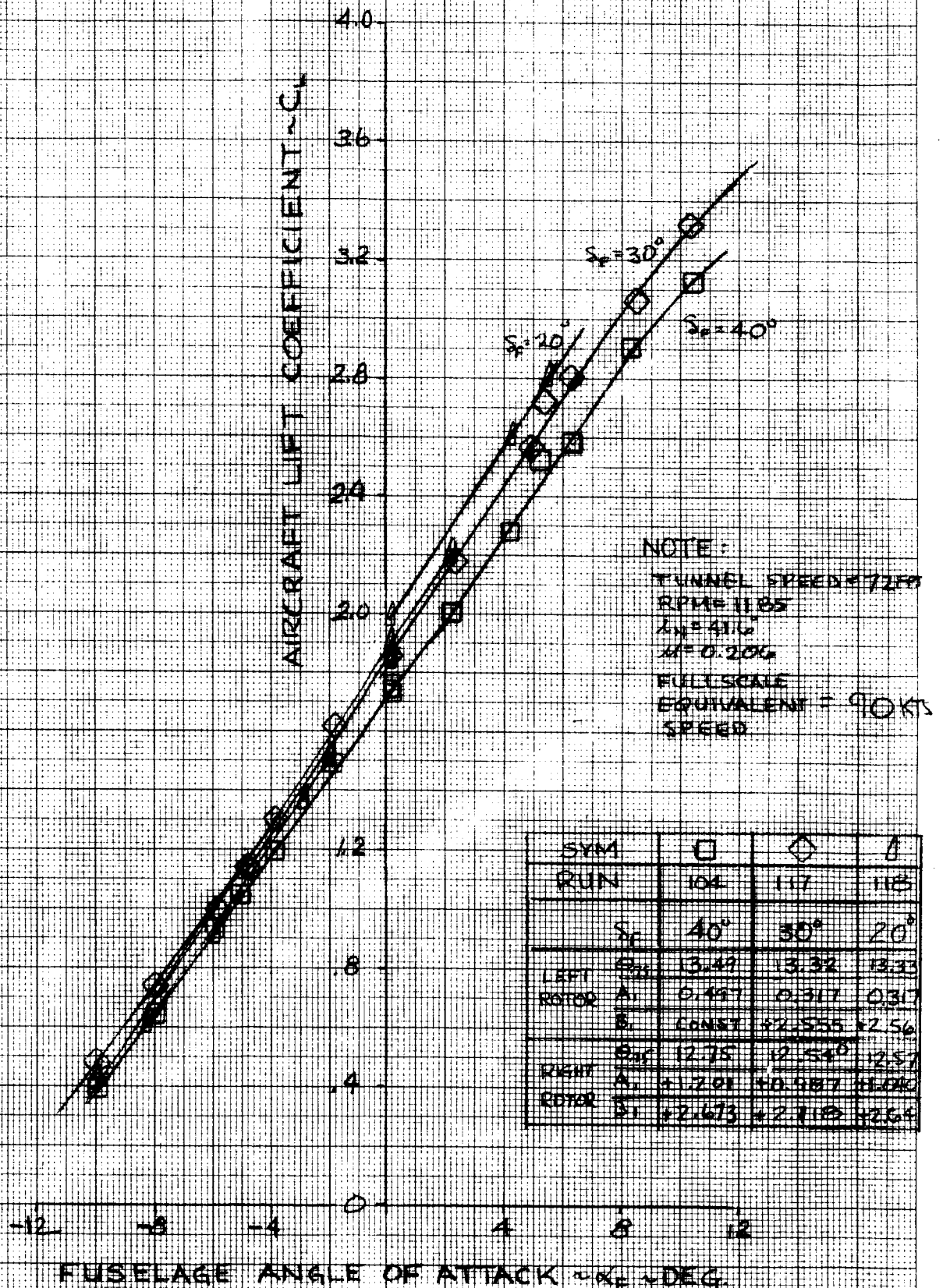


FIGURE 63

EFFECT OF FLAP DEFLECTION IN TRANSITION ON AIRFRAME LIFT COEFFICIENT

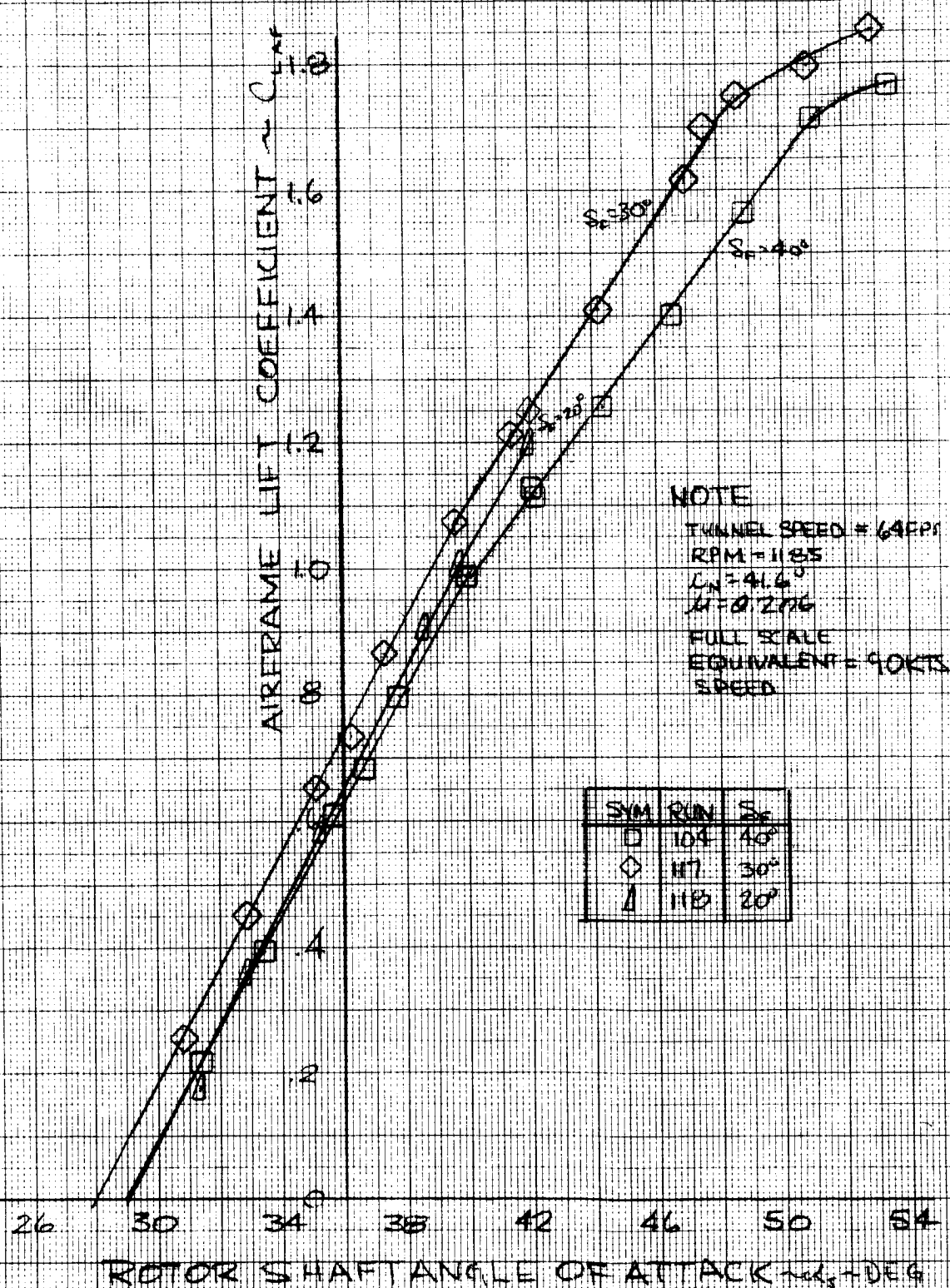


FIGURE 64

EFFECT OF FLAP DEFLECTION IN TRANSITION ON ROTOR THRUST CHARACTERISTICS

RIGHT ROTOR

NOTE

TUNNEL SPEED = 77 FPS
RPM = 1186
 $\alpha_0 = 41.6^\circ$
 $\mu = 0.206$

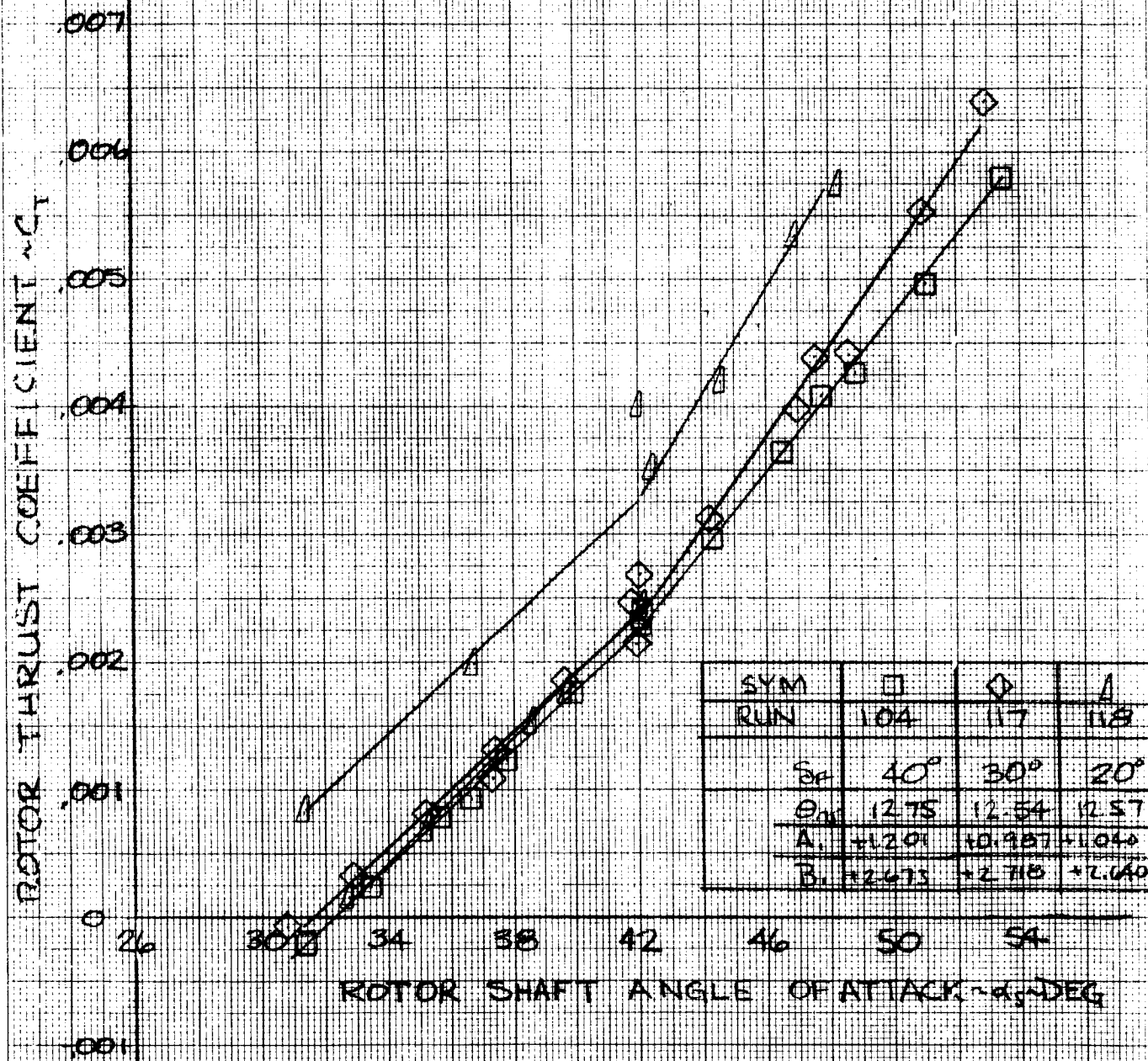


FIGURE 65

EFFECT OF FLAP DEFLECTION IN TRANSITION ON ROTOR NORMAL FORCE COEFFICIENT

RIGHT ROTOR

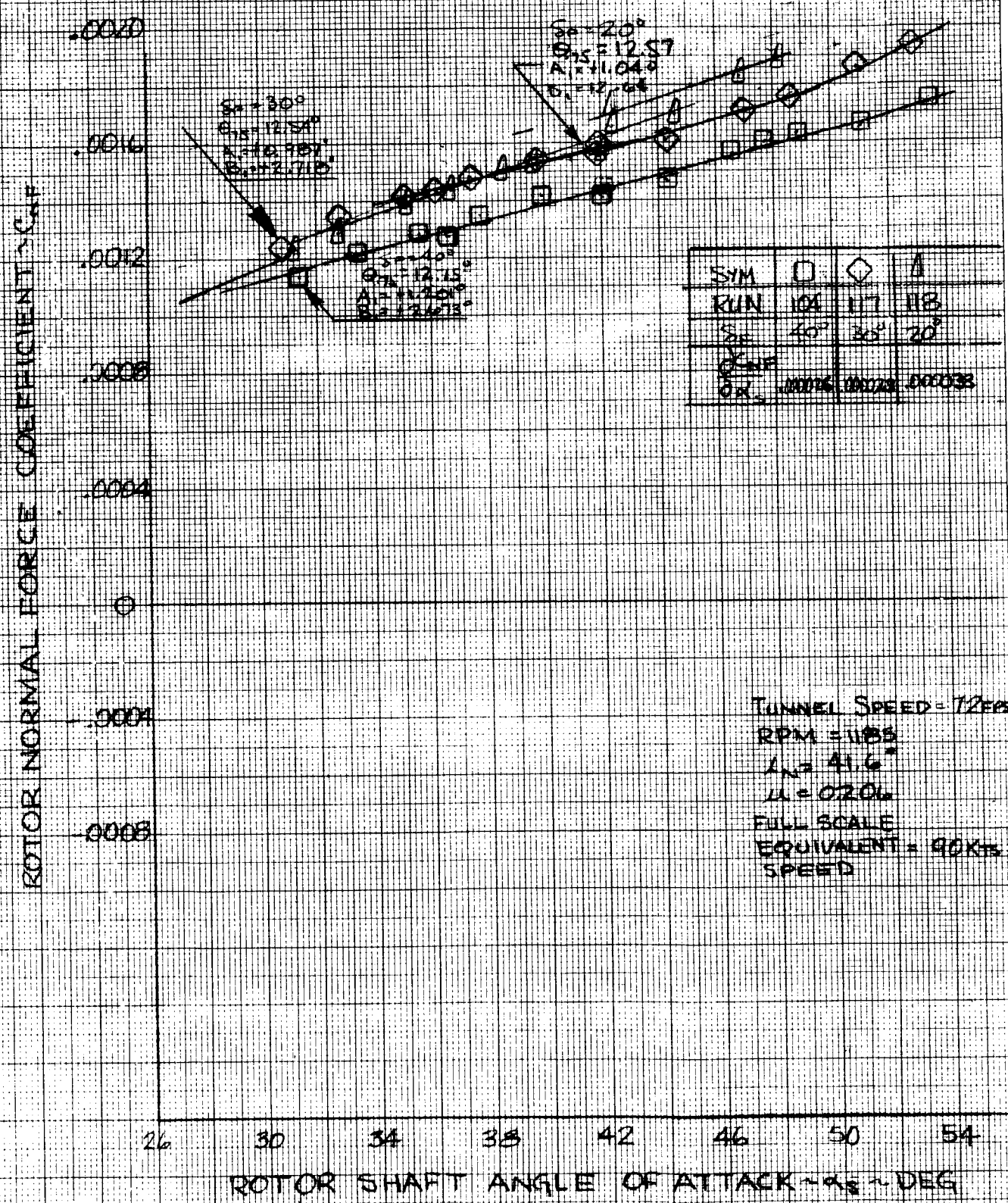


FIGURE 66

EFFECT OF FLAP DEFLECTION IN TRANSITION ON ROTOR PITCHING MOMENT COEFFICIENT

SYM	D	◇	△
RUN	104	117	118
S_F	40	30	20
$\frac{\partial C_{PM}}{\partial \alpha_s}$	0.00014	0.00032	0.00032

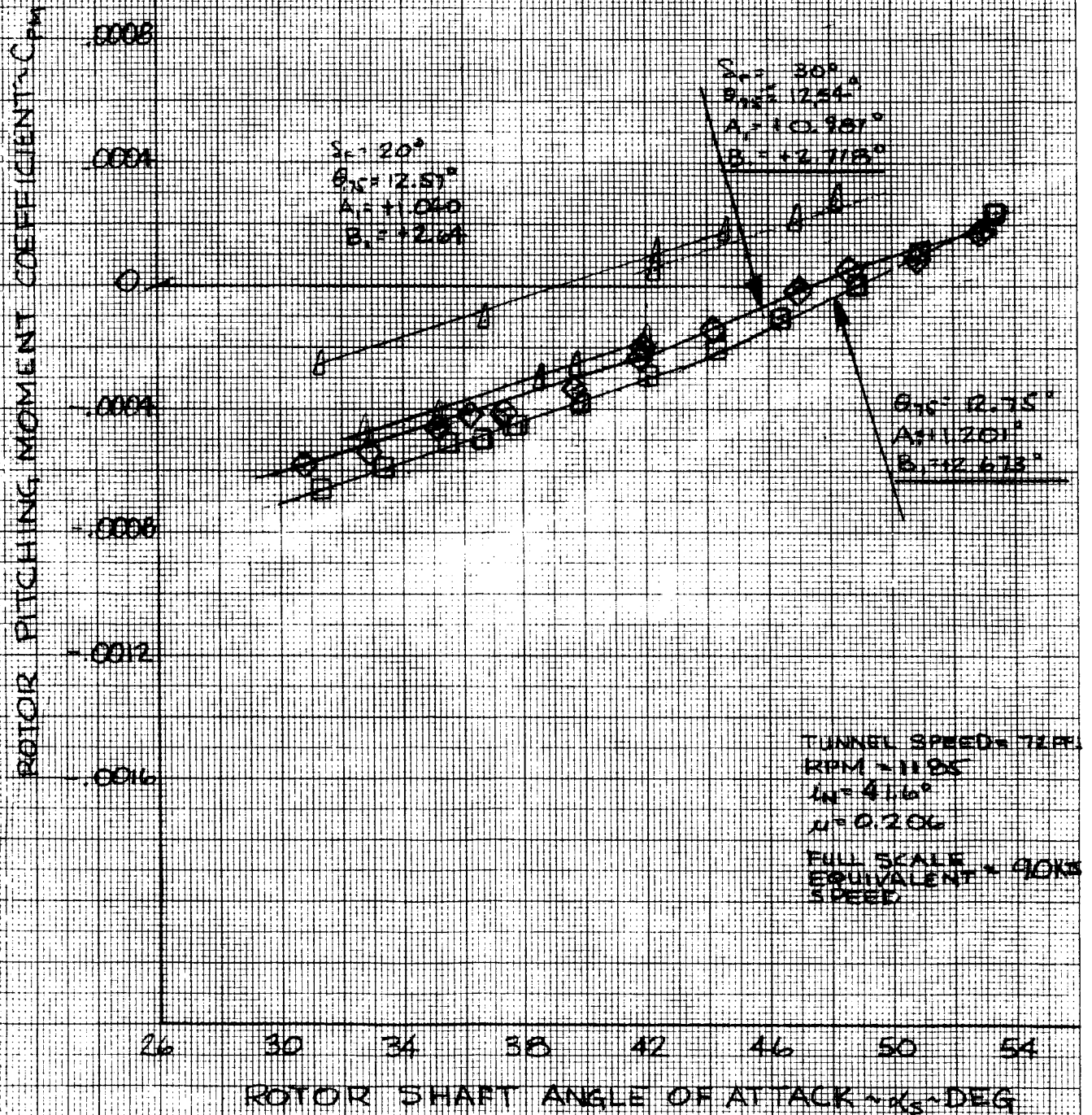


FIGURE 67

EFFECT OF FLAP DEFLECTION IN TRANSITION ON ROTOR SIDE FORCE COEFFICIENT

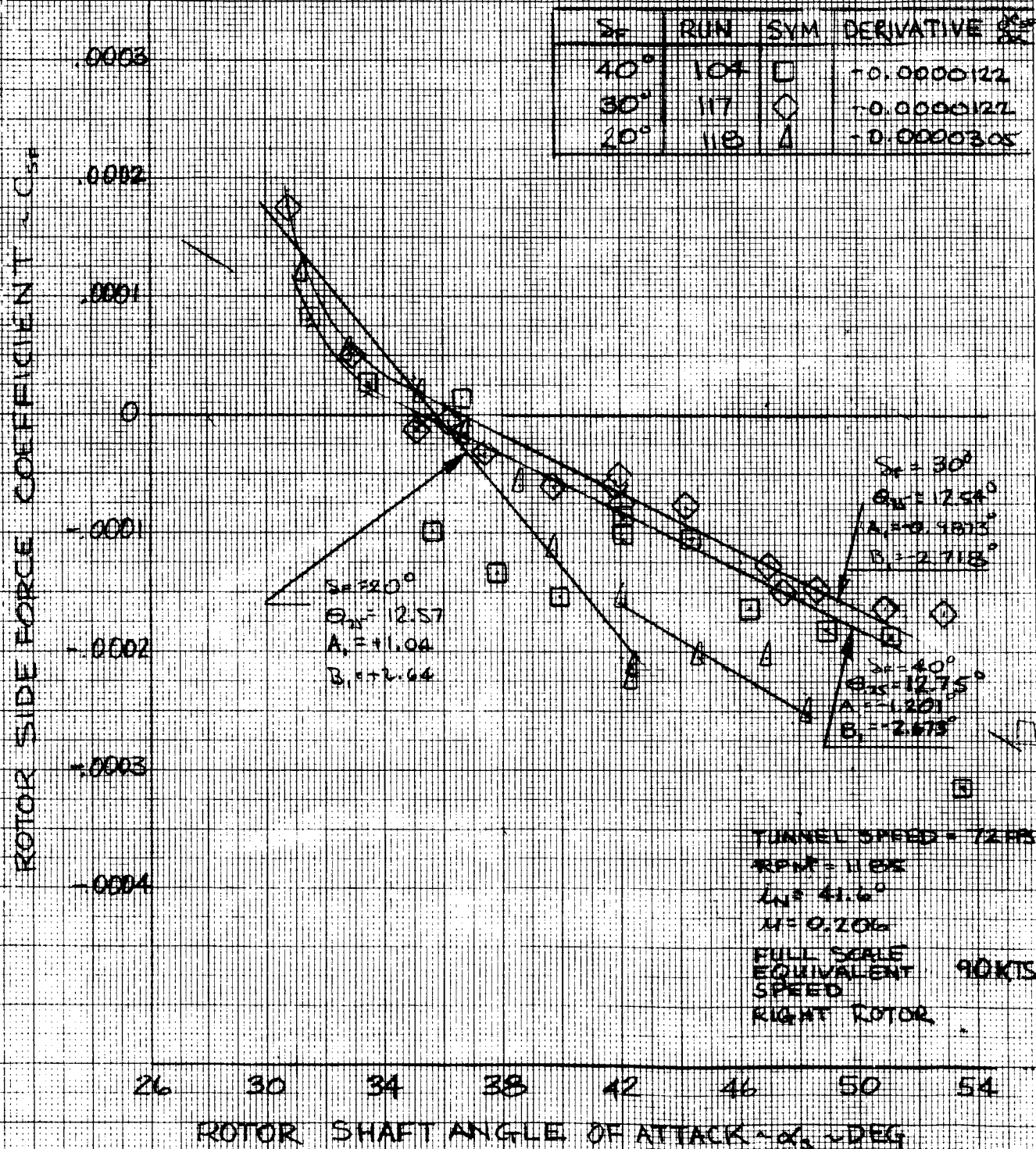


FIGURE 68

EFFECT OF FLAP DEFLECTION IN TRANSITION
ON
ROTOR YAWING MOMENT COEFFICIENT

S _{FL}	RUN	SYM	DERIVATIVE
40°	104	□	-0.000006
30°	117	◇	0.0000075
20°	118	△	-0.000005

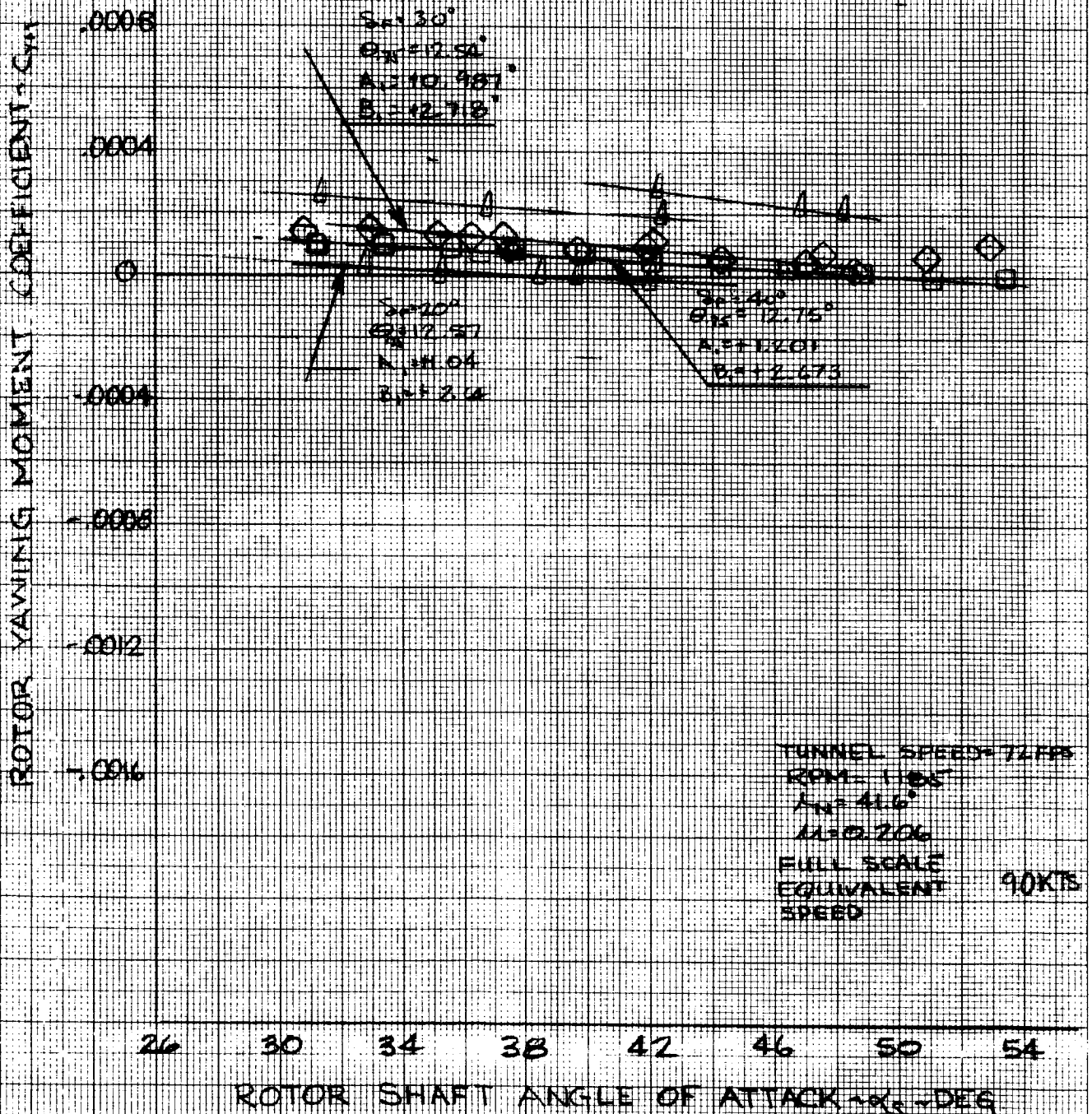


FIGURE 69

BLADE COLLECTIVE LONGITUDINAL & LATERAL CYCLIC VARIATION DURING FLAP DEFLECTION INVESTIGATION

TRANSITION

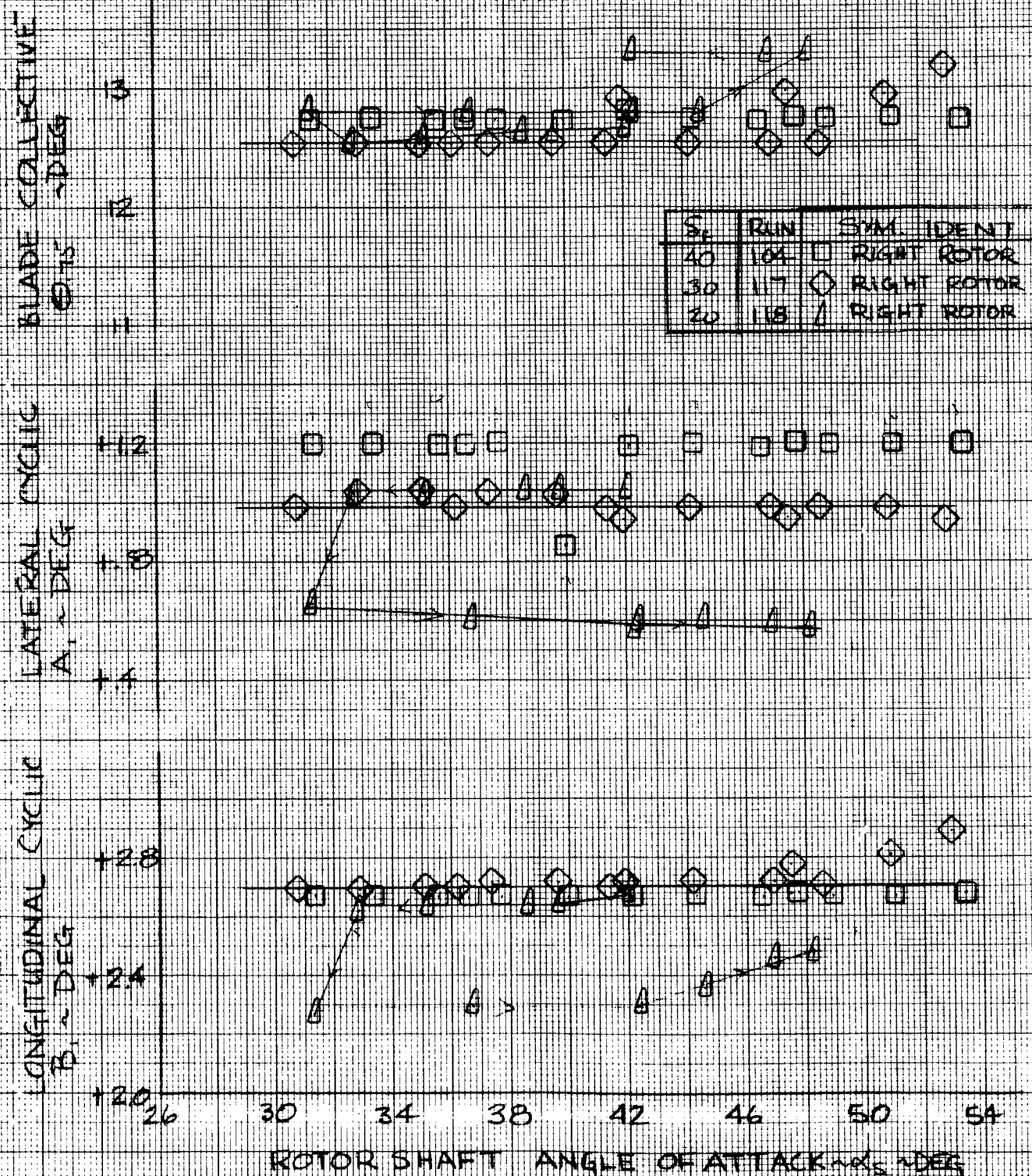


FIGURE 70

EFFECT OF FUSELAGE YAW ANGLE ON AIRCRAFT LIFT COEFFICIENT TRANSITION

NOTE:

TUNNEL SPEED = 72 FPS

RPM = 1185

$\alpha = 41.6^\circ$

$M = 0.205$

FULL SCALE

EQUIVALENT ~ 90 KTS

SPEED

$\alpha = 0^\circ$

RUN 105

AIRCRAFT LIFT
COEFFICIENT C_L

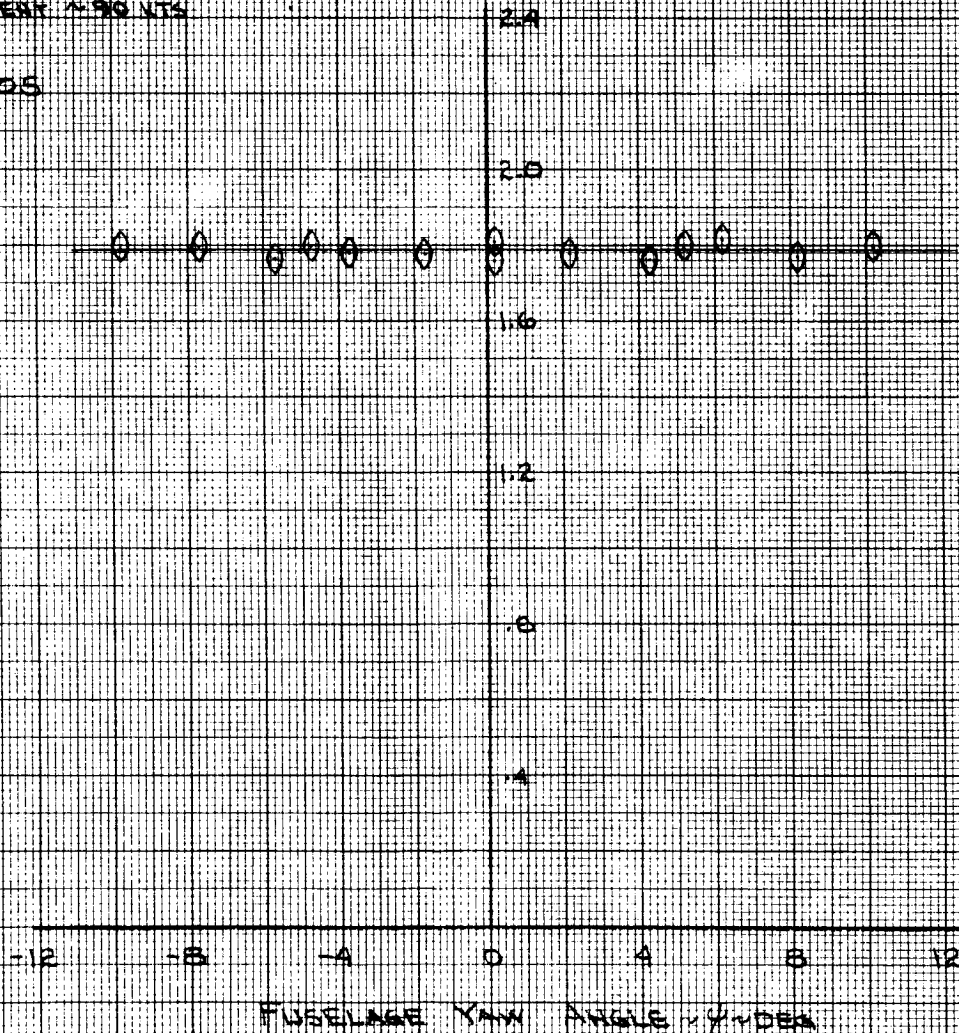


FIGURE 71

EFFECT OF FUSELAGE YAW ANGLE ON ROTOR NORMAL FORCE

TRANSITION

NOTES:

TUNNEL SPEED = 72 FPS
RPM = 1185
 $\beta = 41.6^\circ$
 $\mu = 0.205$
FULL SCALE
EQUIVALENT SPEED = 90 KTS
 $\alpha = 0^\circ$

RUN 105 $V = 72$ FPS

ROTOR NORMAL FORCE COEFFICIENT C_{NF}

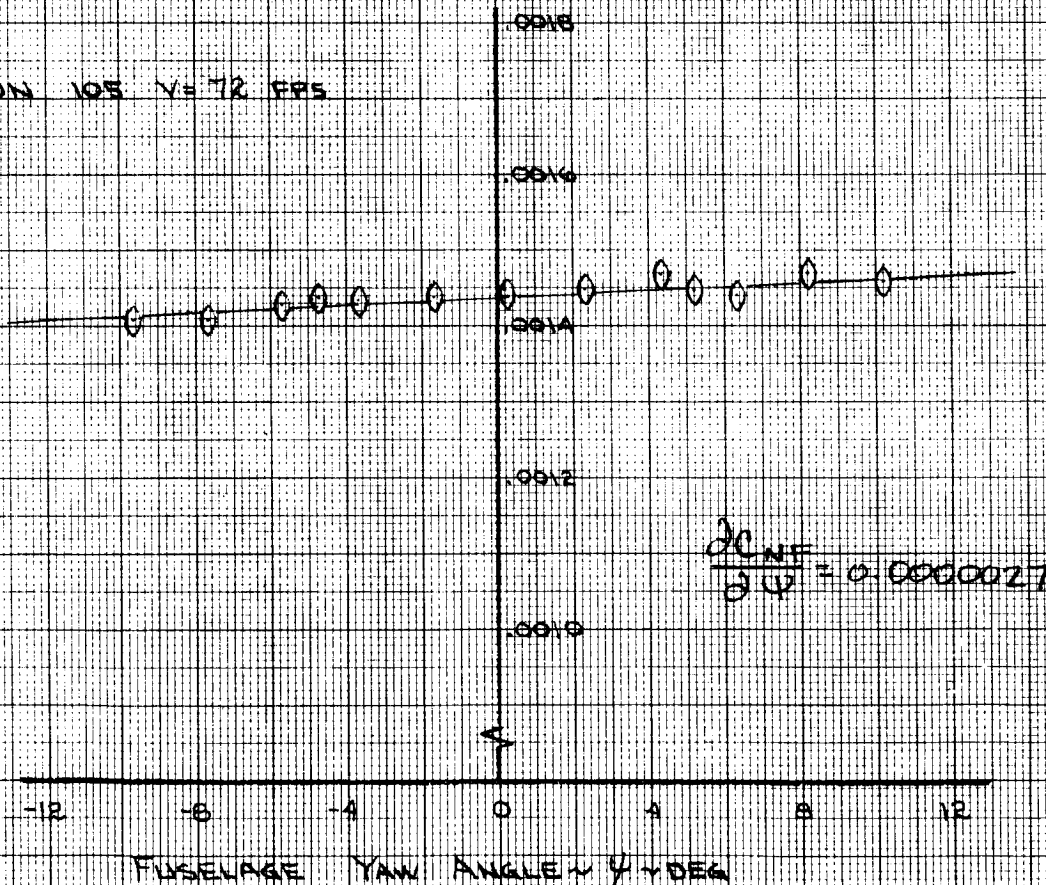


FIGURE 72

EFFECT OF FUSELAGE YAW ANGLE
ON
ROTOR PITCHING MOMENT
TRANSITION

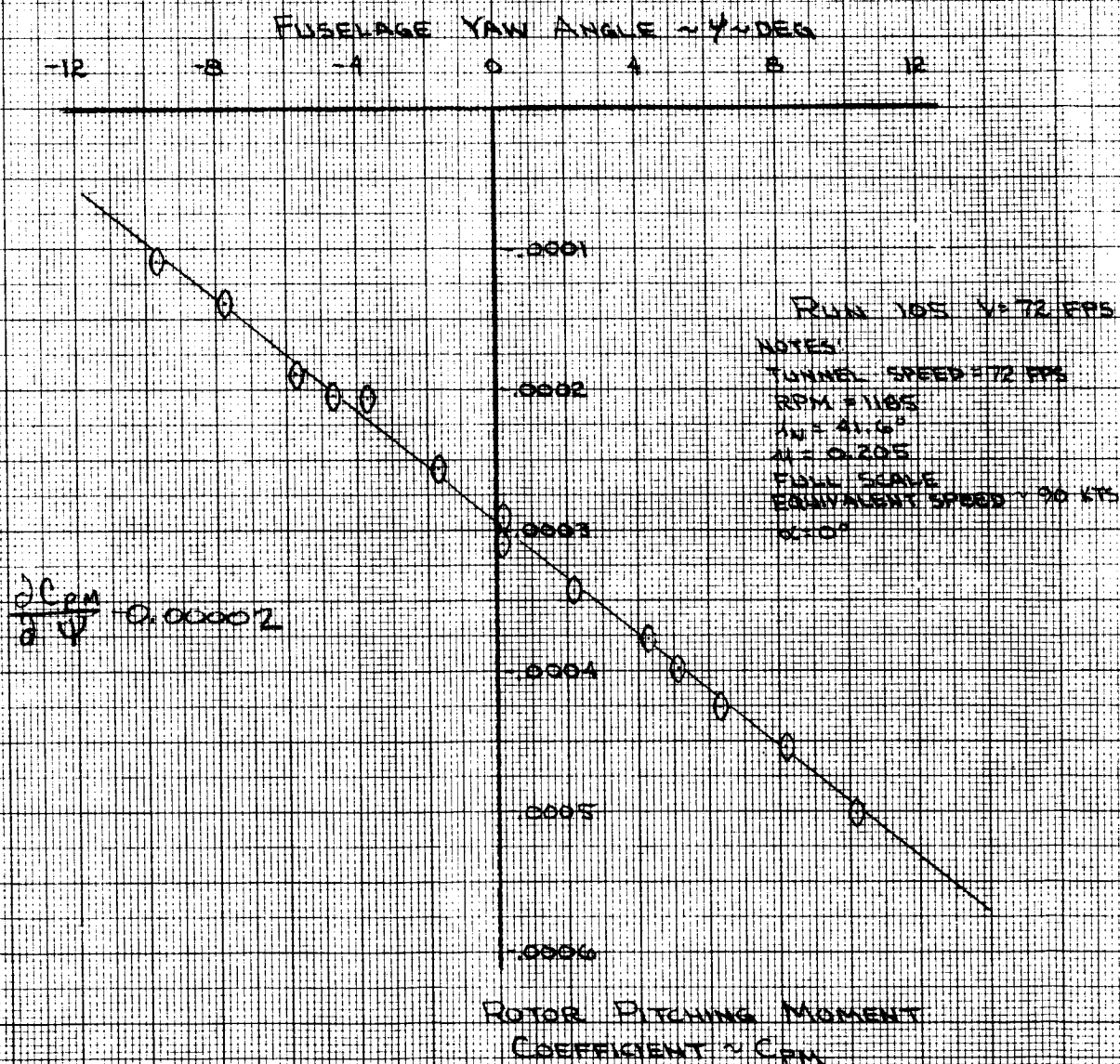


FIGURE 73

EFFECT OF FUSELAGE YAW ANGLE ON ROTOR SIDE FORCE TRANSITION

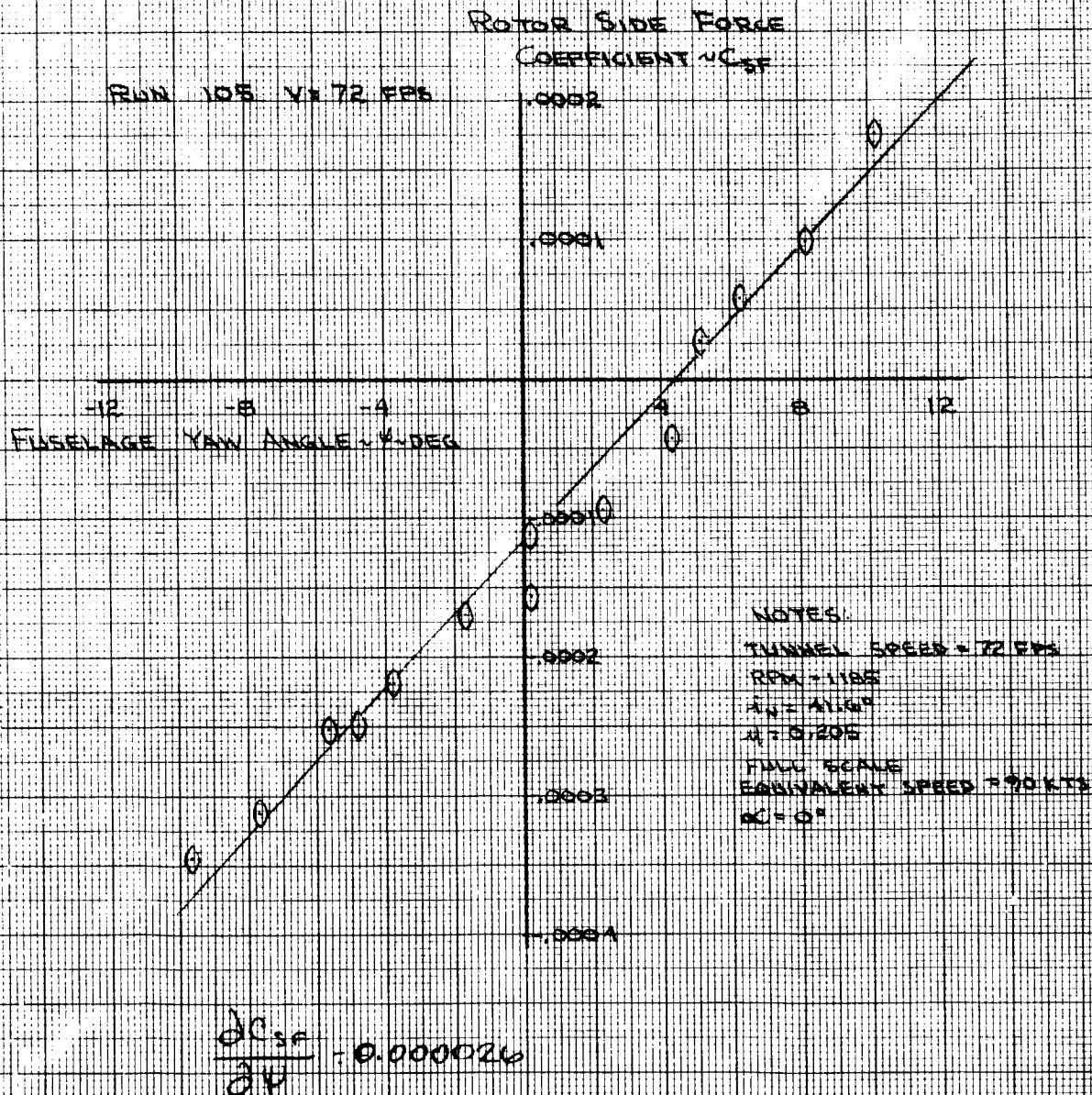
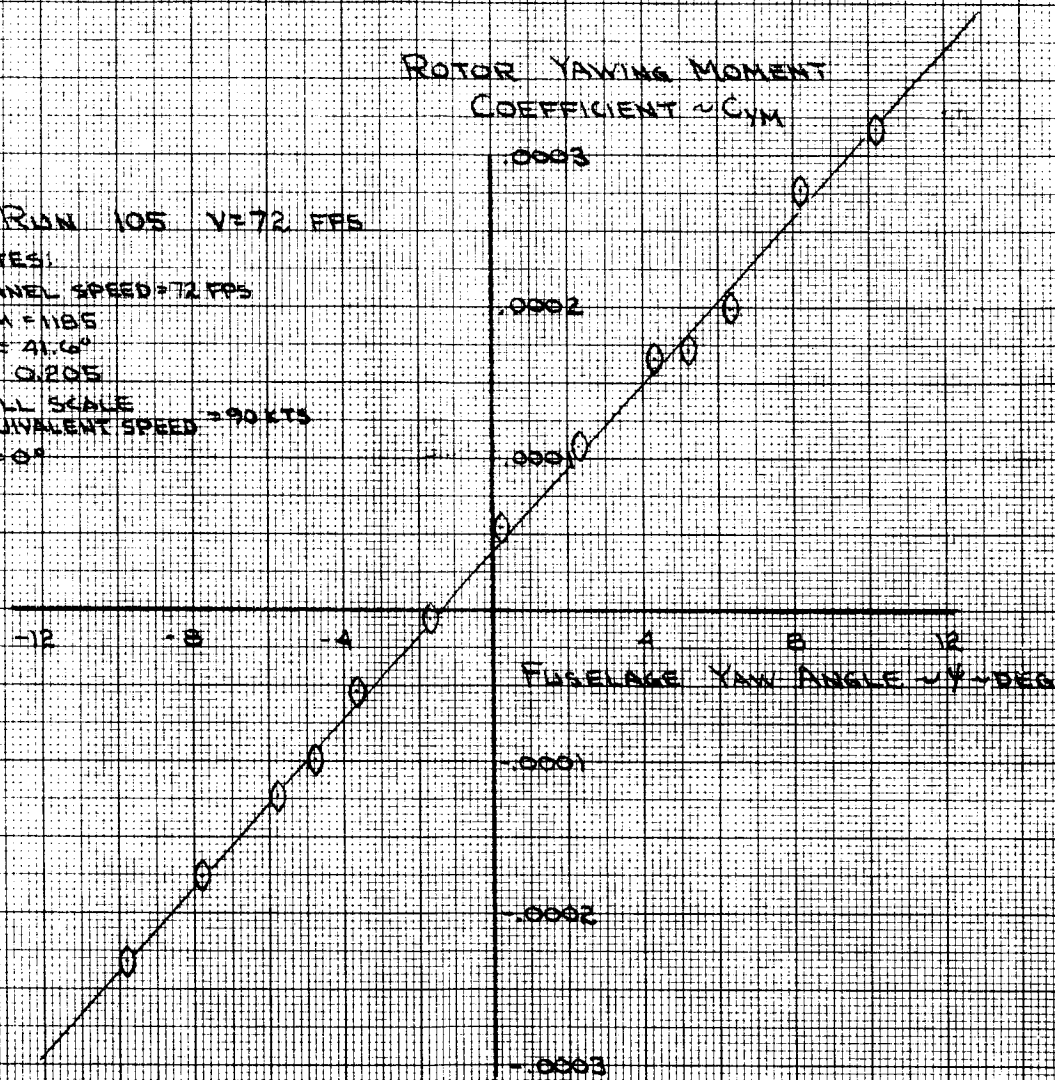


FIGURE 74

EFFECT OF FUSELAGE YAW ANGLE
ON
ROTOR YAWING MOMENT
TRANSITION

RUN 105 $V=72$ FPS
NOTES:
TUNNEL SPEED = 72 FPS
RPM = 1185
 $\gamma_{in} = 41.6^\circ$
 $\lambda = 0.0205$
FULL SCALE
EQUIVALENT SPEED = 90 KTS
 $\alpha = 0^\circ$



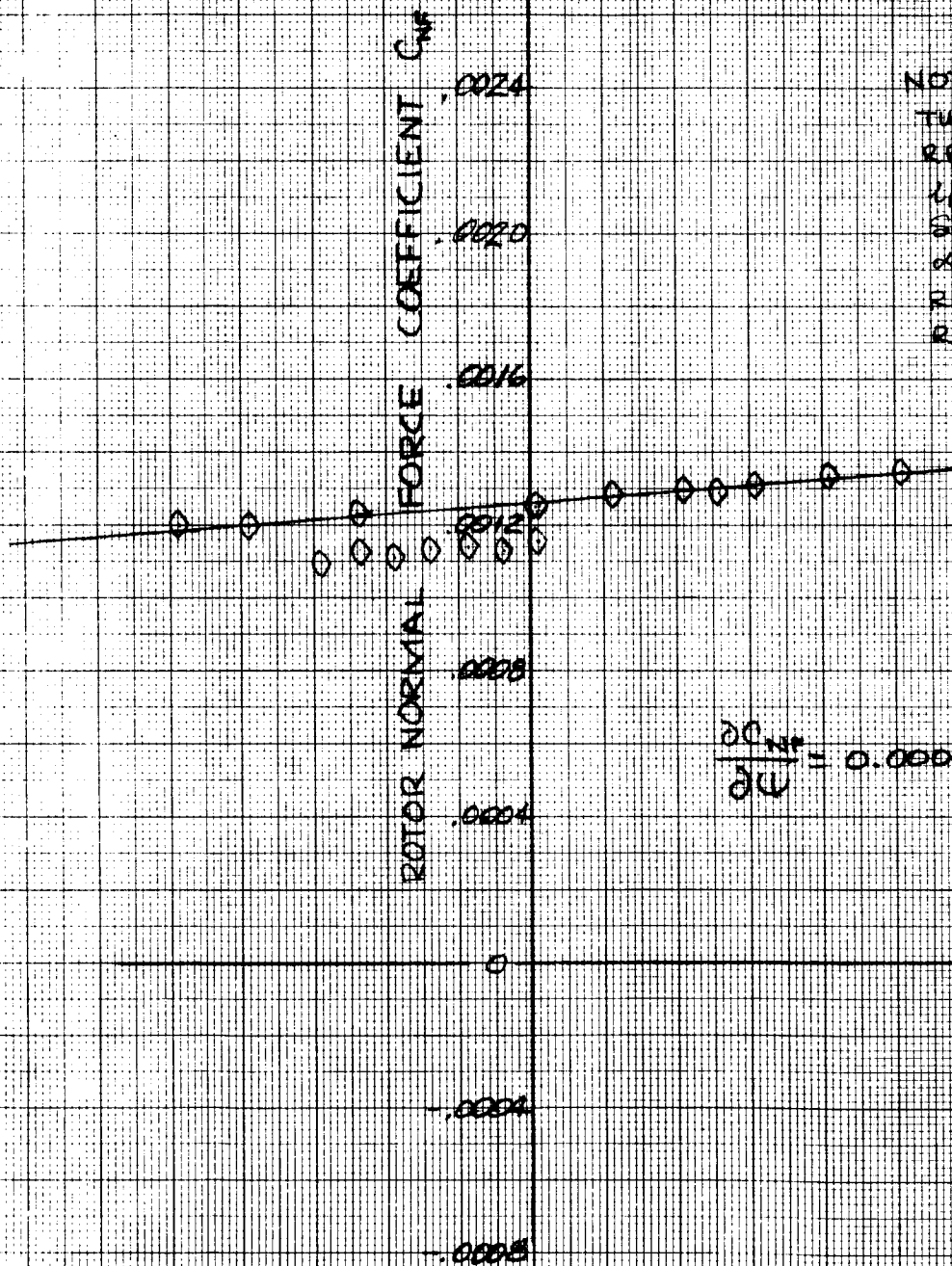
$$\frac{\partial C_{YM}}{\partial \psi} = 0.0000276$$

FIGURE 75

ROTOR NORMAL FORCE CHARACTERISTICS IN YAW ANGLE INVESTIGATION

TRANSITION

NOTE
TUNNEL SPEED = 73 FTS
RPM = 1187
 $\alpha = 30^\circ$
 $\delta = 30^\circ$
 $\alpha = 12^\circ$
RIGHT ROTOR
RUN 102



$$\frac{\partial C_{NF}}{\partial \psi} = 0.000008$$

FIGURE 76

ROTOR PITCHING MOMENT CHARACTERISTICS IN YAW ANGLE INVESTIGATION

TRANSITION

ROTOR PITCHING MOMENT COEFF. C_{pm}

NOTE

TUNNEL SPEED = 73 FPS

RPM = 1187

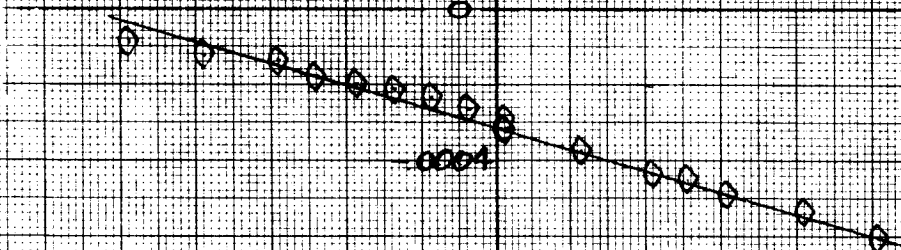
$\alpha_n = 30^\circ$

$S_F = 30^\circ$

$\alpha = 12^\circ$

RIGHT ROTOR

RUN 107



$$\frac{\partial C_{pm}}{\partial \psi} = -0.000029$$

-12 -8 -4 0 4 8 12 16

NOSE
LEFT

FUSELAGE YAW ANGLE ψ - DEG

NOSE
RIGHT

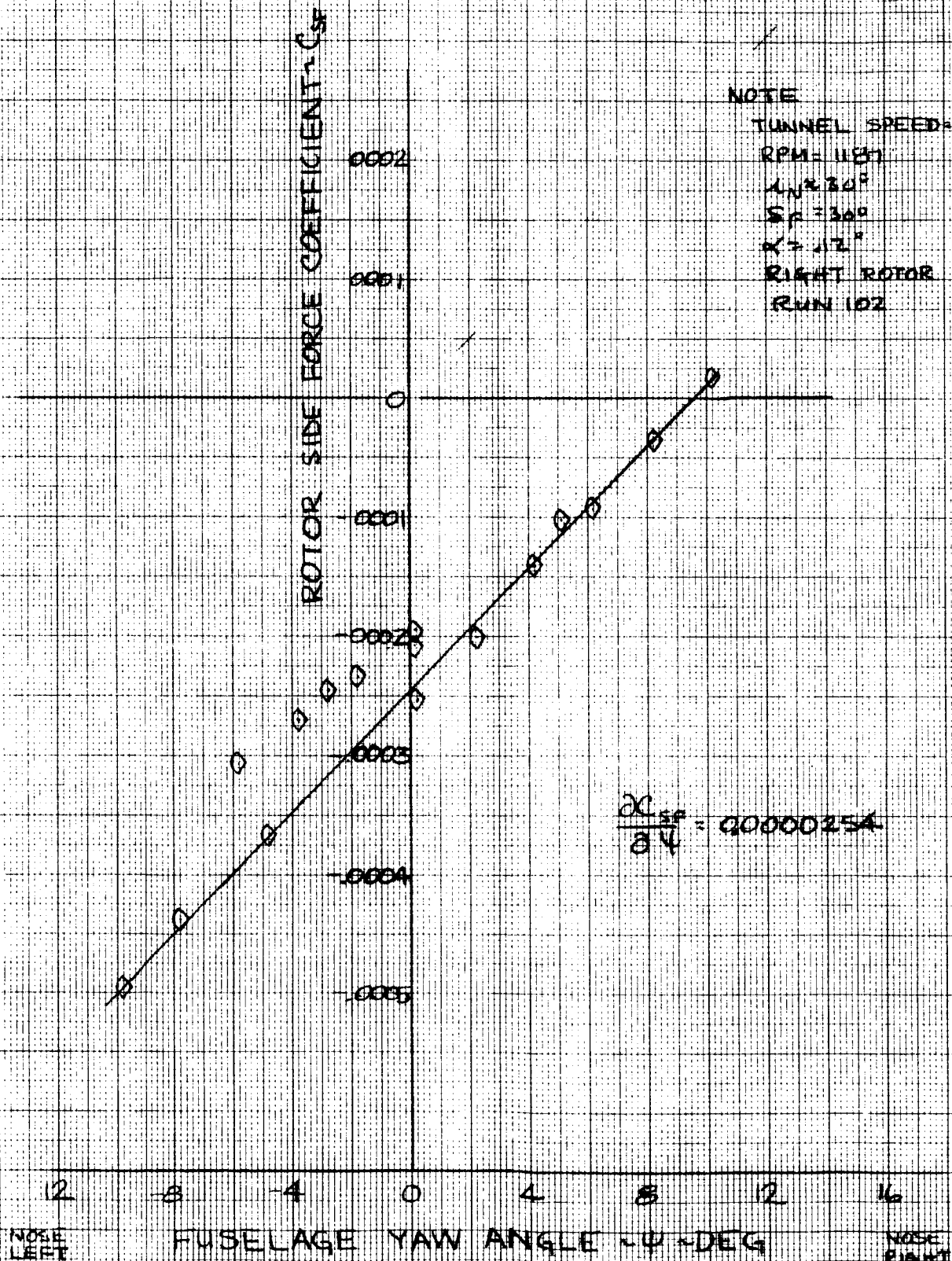
FIGURE 77

ROTOR SIDE FORCE CHARACTERISTICS IN YAW ANGLE INVESTIGATION

TRANSITION

NOTE

TUNNEL SPEED = 73 FPS
RPM = 1187
 $\Lambda_N \approx 30^\circ$
 $S_F = 300$
 $\alpha = 12^\circ$
RIGHT ROTOR
RUN 102



$$\frac{\partial C_{SF}}{\partial \psi} = 0.0000254$$

ROTOR YAWING MOMENT CHARACTERISTICS IN YAW ANGLE INVESTIGATION

TRANSITION

NOTE

TUNNEL SPEED = 13 ft/s
RPM = 1187
 $\Lambda_N = 30^\circ$
 $S_F = 30^\circ$
 $\alpha = 12^\circ$
RIGHT ROTOR
RUN 102

$$\frac{\partial C_{YH}}{\partial \psi} = 0.0000037$$

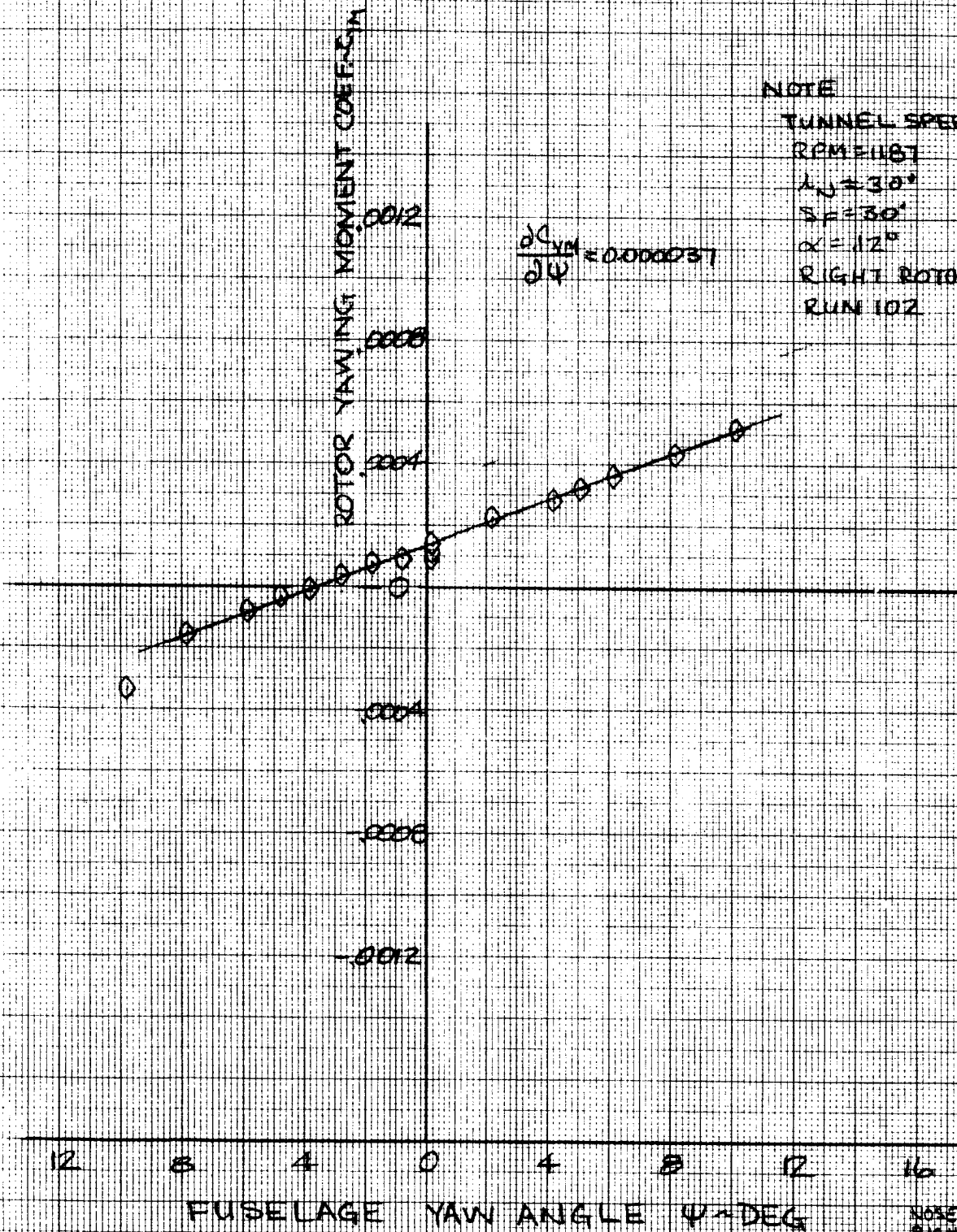


FIGURE 79

ROTOR NORMAL FORCE CHARACTERISTICS
IN ANGLE OF ATTACK INVESTIGATIONTRANSITION

NOTE:

TUNNEL SPEED = 73 FPS

RPM = 1186

 $\lambda_{IN} = 30^\circ$ $S_F = 30^\circ$

RIGHT ROTOR

RUN 101

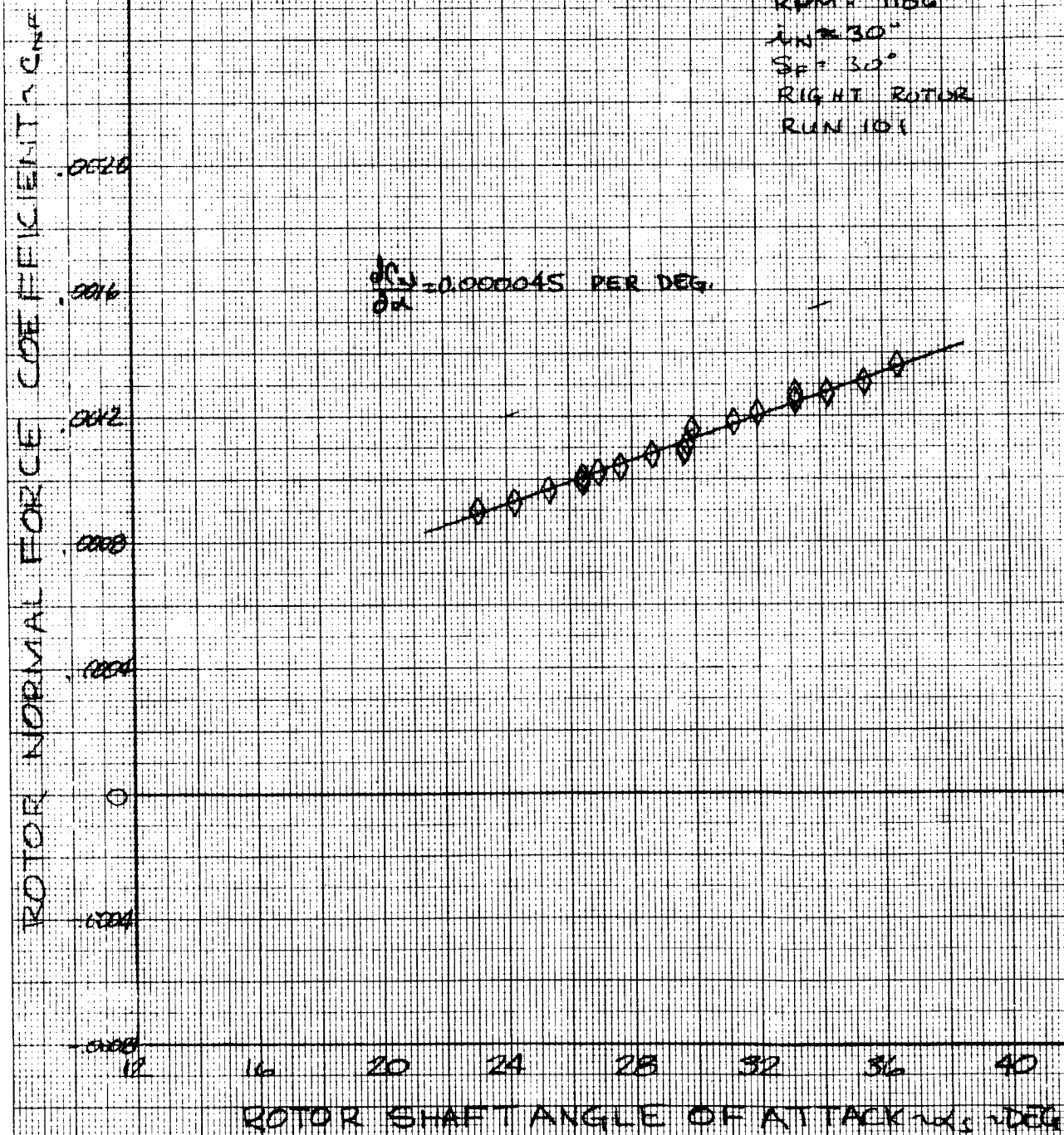


FIGURE 80

ROTOR PITCHING MOMENT CHARACTERISTICS IN ANGLE OF ATTACK INVESTIGATION

TRANSITION

NOTE

TUNNEL SPEED = 73 FPS

RPM = 1186

$L/D = 30$

$S/P = 30$

RIGHT ROTOR

RUN 101

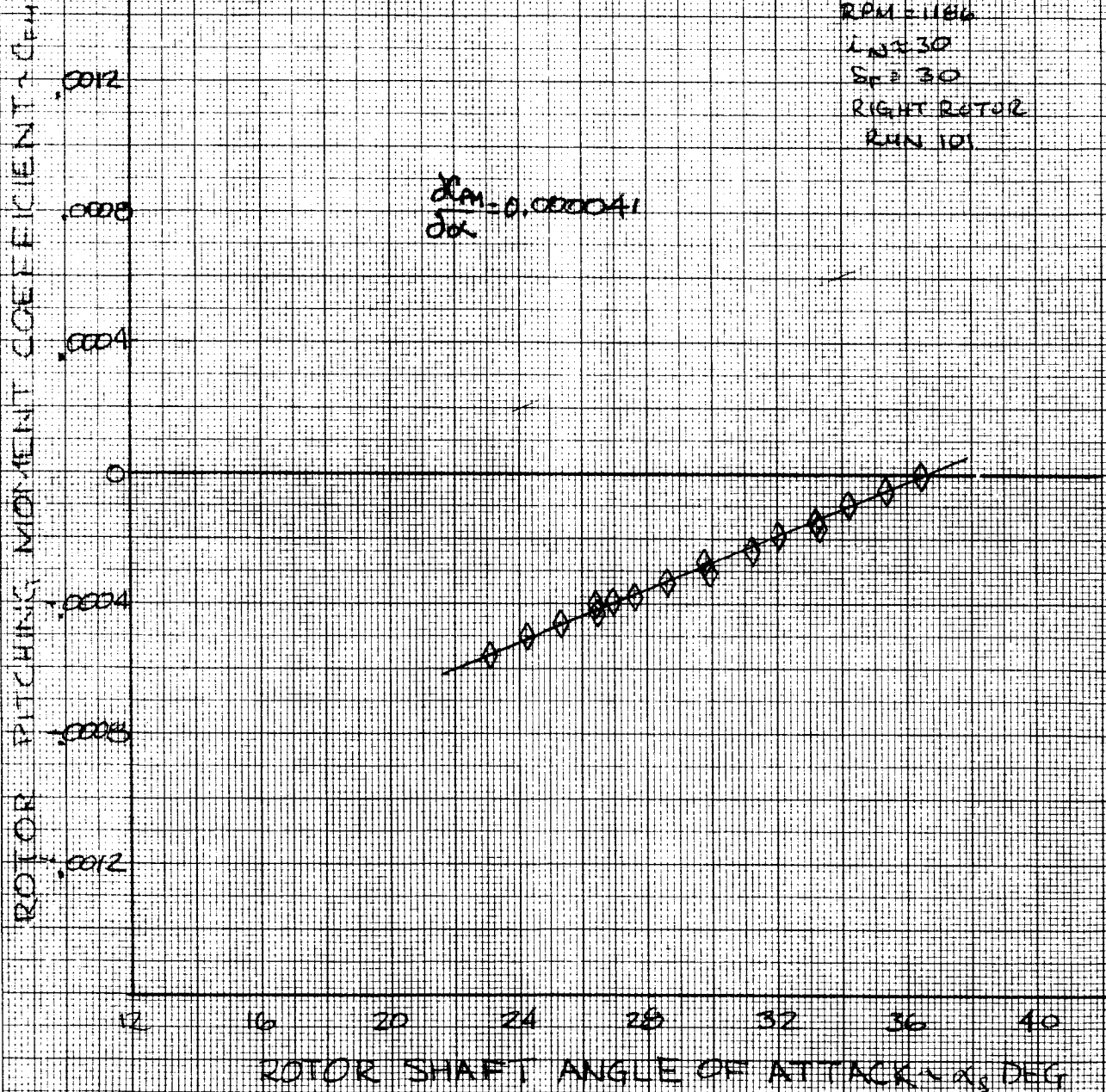


FIGURE 81

ROTOR SIDE FORCE CHARACTERISTICS IN ANGLE OF ATTACK INVESTIGATION

TRANSITION

NOTE

TUNNEL SPEED = 73 FPS

RPM = 1186

$L/D = 3.0$

$S_p = 30^\circ$

RIGHT ROTOR

RUN 101

$\frac{dC_{sf}}{d\alpha} = 0.000034 \text{ PER DEG}$

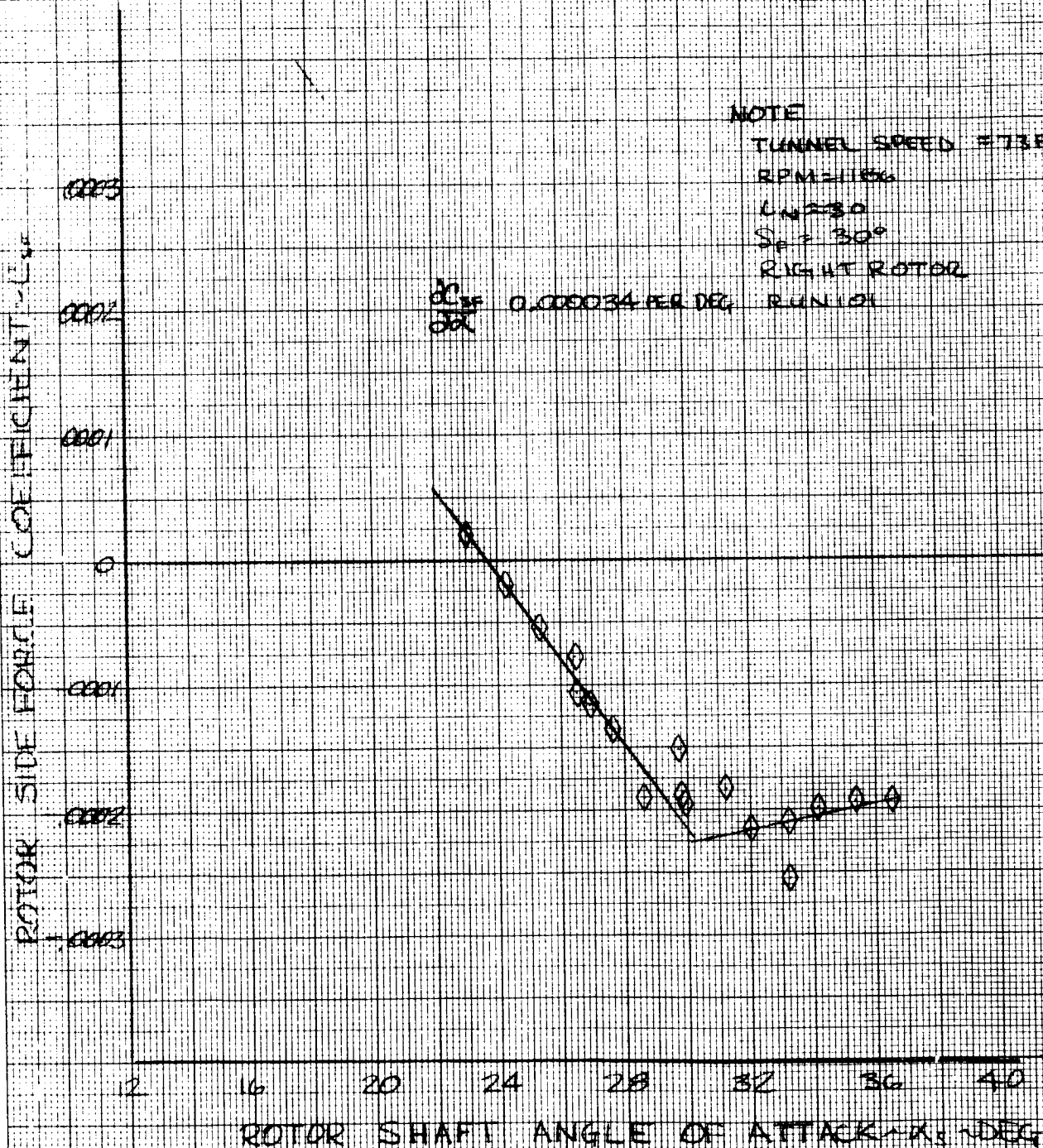


FIGURE 82

ROTOR YAWING MOMENT CHARACTERISTICS IN ANGLE OF ATTACK INVESTIGATION

TRANSITION

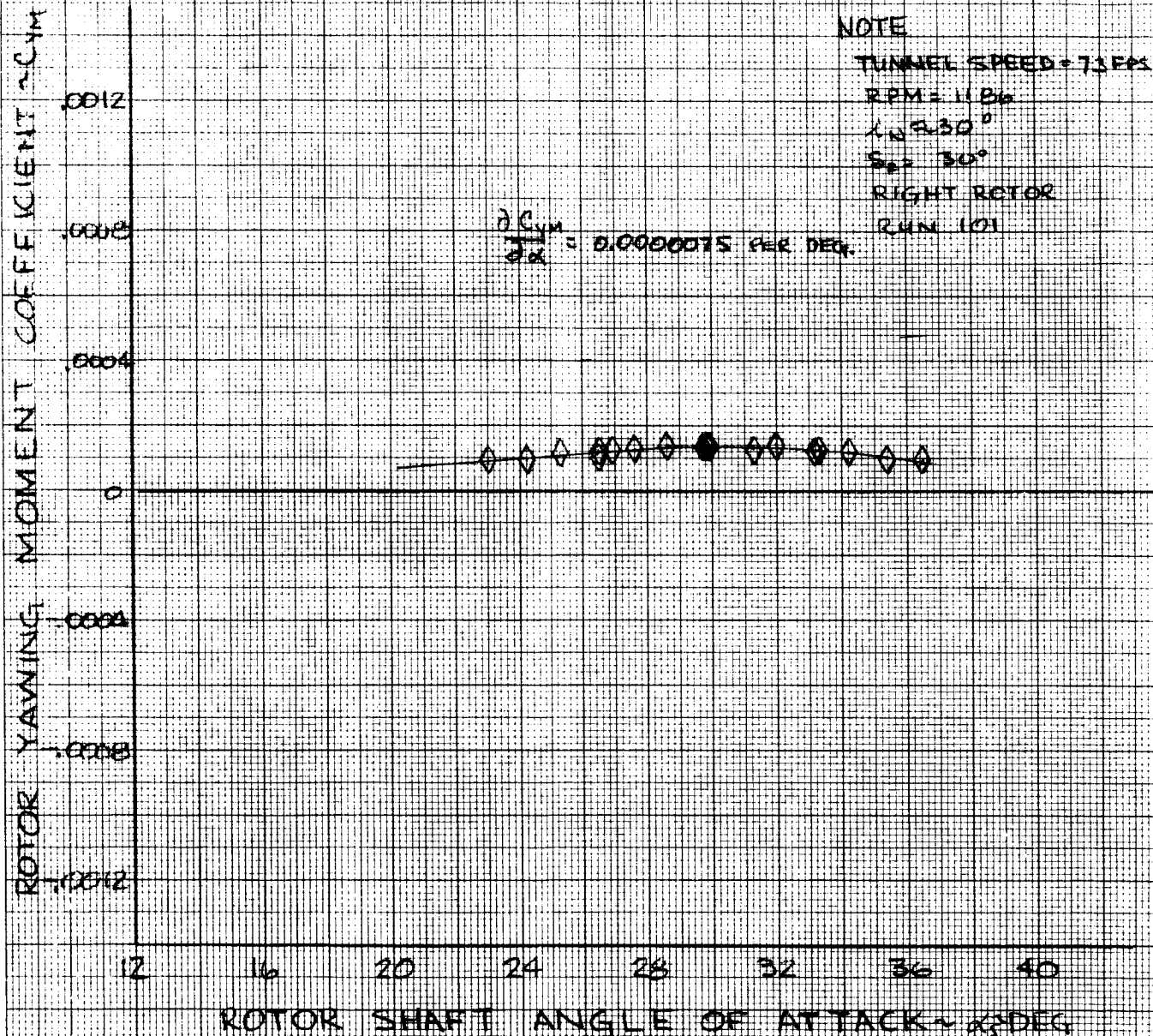


FIGURE 83

EFFECT OF NACELLE INCIDENCE ON AIRCRAFT LIFT COEFFICIENT MID TRANSITION SPEED

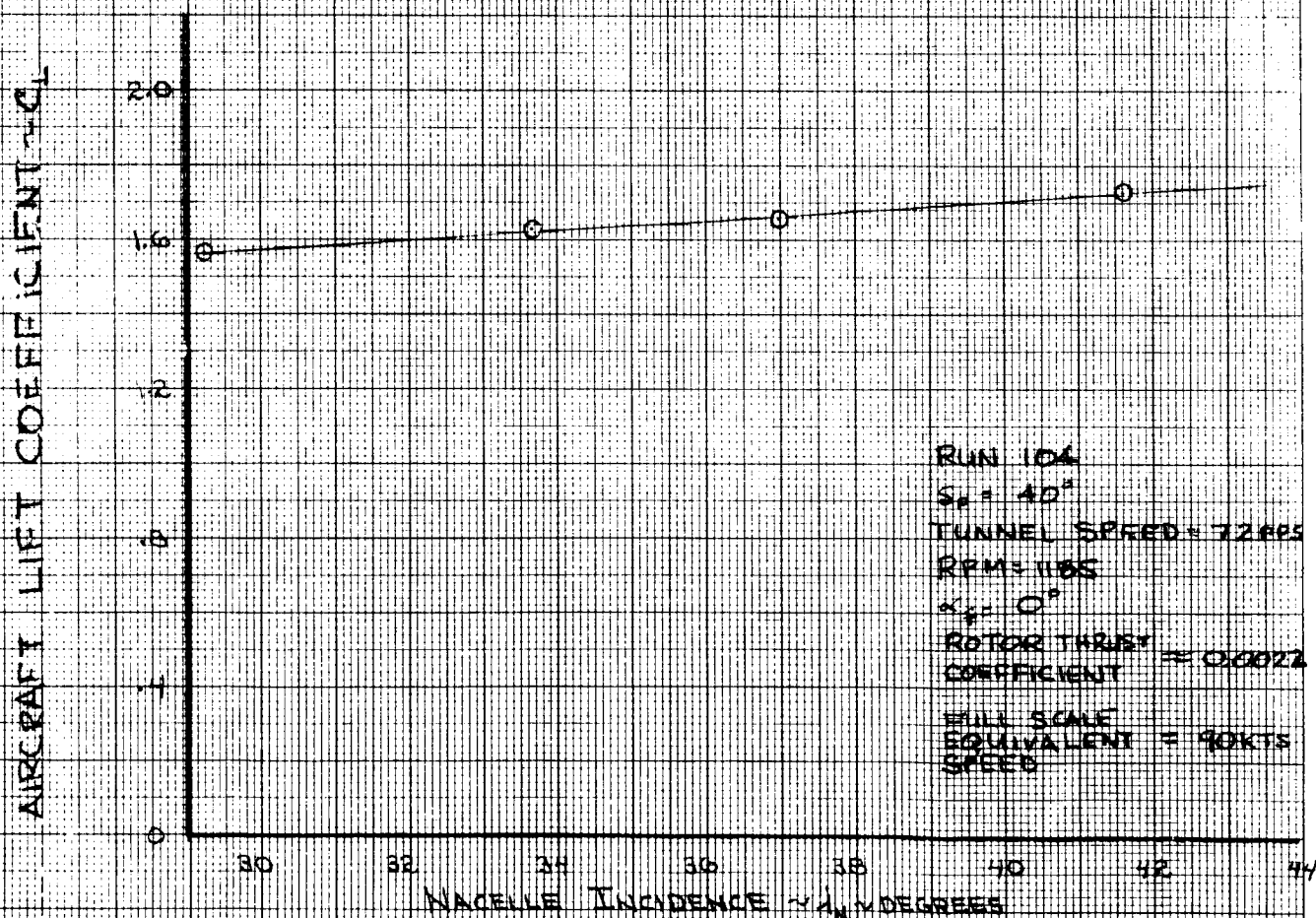


FIGURE 84

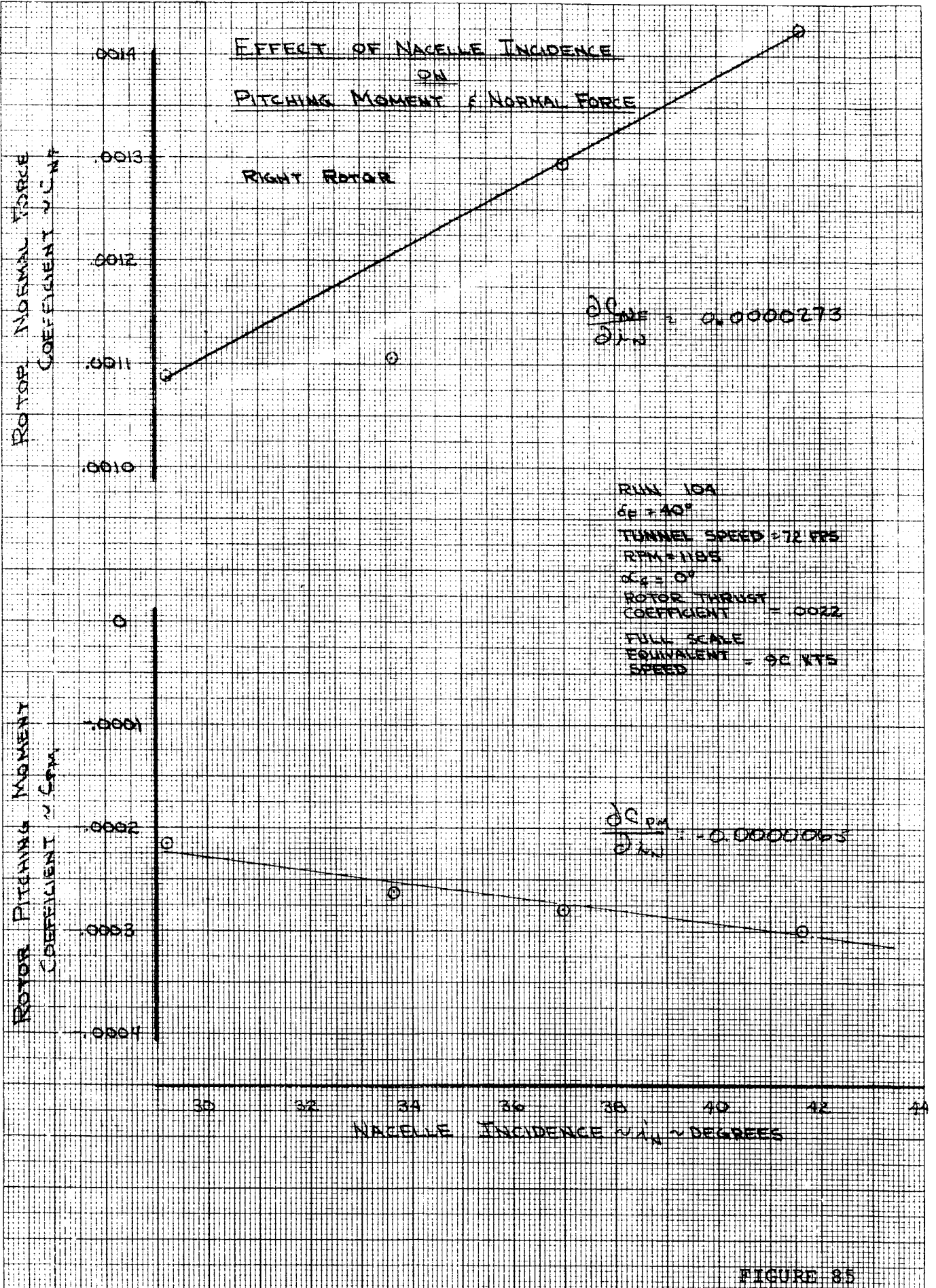


FIGURE 85

EFFECT OF NACELLE INCIDENCE ON SIDE FORCE & YAWING MOMENT

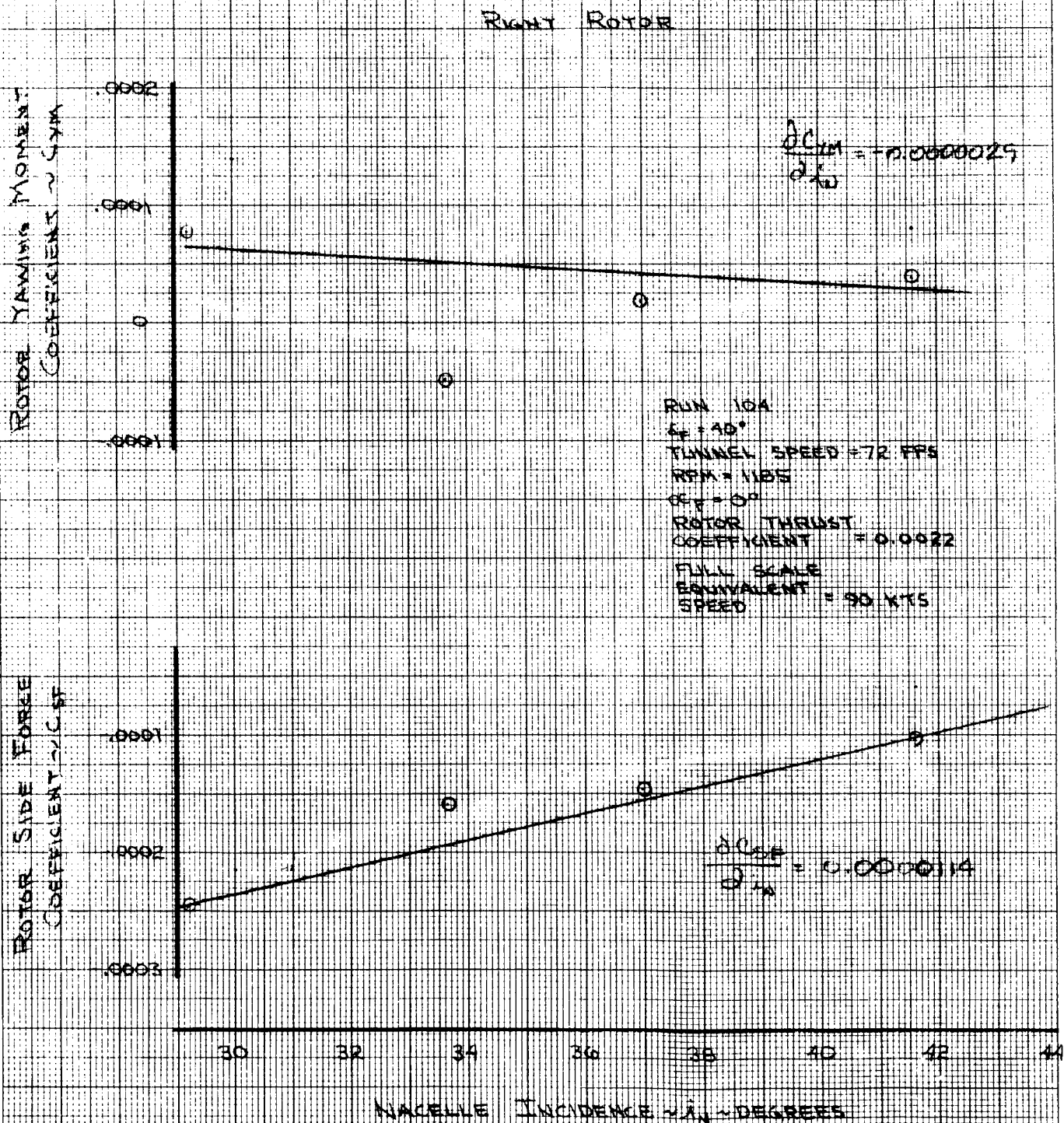


FIGURE 86

5.1.2 AIRCRAFT STABILITY DERIVATIVES

Longitudinal Stability

Test runs to obtain representative aircraft stability derivative data in transition were performed at a tunnel velocity of 72 fps, tunnel q of 6 psf, which represents an equivalent full scale aircraft velocity of 90 knots. Runs were performed with rotors and tail surfaces on and off with 40, 30 and 20 degrees flap settings at nacelle incidence settings of approximately 42 degrees and with flap deflection of 30 degrees at nacelle incidence of 30 degrees.

Figures 87, 88, and 89 illustrate the lift coefficient and pitching moment coefficient variation with angle of attack and longitudinal stability, variation of pitching moment coefficient with lift coefficient, $\frac{dC_m}{dC_L}$, respectively for the conditions of tails on and off with rotors off and on. Figures 90 through 95 indicate the effects of flap deflection on aircraft and airframe lift coefficient and pitching moment coefficient variation with angle of attack and on longitudinal stability, $\frac{dC_m}{dC_L}$. The results are summarized in Table 5. The curves of Figure 87 and those of 90 and 93 indicate that, as expected, the aircraft with rotors on maintains a linear lift curve slope to considerably higher angle of attack than with rotors off. In addition, the airframe coefficients, aircraft with the direct rotor effects subtracted, indicate substantially higher lift coefficient slope than for the aircraft without rotors. Two factors may contribute to this.

RUN	i_N	δ_F	TAILS	ROTORS	NOMINAL C_T	$C_{L\alpha}$	$C_{m\alpha}$	$\frac{dC_m}{dC_L}$	DERIVATIVE REFERENCE	REMARKS
69	44.0°	40°	ON	OFF	-	.086	-.062	-.72	AIRCRAFT	$\delta S_{PL}=45^\circ \delta A_R=20^\circ$
71	43.7	40°	ON	OFF	-	.080	-.057	-.72	AIRCRAFT	
73	43.7	40°	ON	OFF	-	.068	+.0082	+.12	AIRCRAFT	
104	41.6	40°	ON	ON	.0022	.134	-.0233	-.174	AIRCRAFT	
104	41.6	40°				.093	-.053	-.60	AIRFRAME	
101	29.6	30°				.138	-.0015	-.015	AIRCRAFT	
117	41.6	30°				.142	-.0355	-.25	AIRCRAFT	
118	41.6	20°				.158	-.0158	-.10	AIRCRAFT	
101	29.6	30°				.105	-.023	-.23	AIRFRAME	
117	41.6	30°				.100	-.051	-.51	AIRFRAME	
118	41.6	20°				.100	-.048	-.48	AIRFRAME	

TABLE 5 - LONGITUDINAL STABILITY DERIVATIVES IN TRANSITION

One is the variation of rotor contribution to slipstream angle of attack and dynamic pressure. The other is the direct increase of Reynolds number of the wing and the influence of the turbulence caused by the rotor slipstream in increasing the "apparent" Reynolds number effects. The destabilizing influence of the rotor is indicated by comparison of runs 71 and 104 on Figure 89 which indicate a forward shift in neutral point of 54.6 percent \bar{c} rotors on compared to rotors off. The data of run 104, however, indicate a neutral point location at 42.4% \bar{c} which will result in a minimum static margin of approx. 11% with the center of gravity at the aft limit and nacelle incidence of 41.6 degrees. The data indicate a neutral point location of 50% \bar{c} with flaps deflected 30 degrees and 35% \bar{c} for flaps deflected 20 degrees and nacelle incidence of 41.6 degrees. It is noteworthy that the neutral points quoted represent most forward locations, minimum stability, over the angle of attack ranges tested for each condition and for each condition, rotors on, encompasses the lift coefficient required for 1-g flight at the typical flight weights of 12,000-13,000 pounds for the full scale aircraft. The "nominal" value of thrust coefficient, C_T , indicated in the table and on the figures represents merely the nominal value of thrust coefficient of the rotors at zero angle of attack of the fuselage for the reference nacelle incidence, rotor collective pitch and rpm. The test runs were conducted with constant collective pitch settings and constant rpm with power varied as necessary. This results in a relatively large variation in thrust coefficient as a function of angle of attack as illustrated in Figures 22 and 30 of Section 4.1.1, Rotor Perform-

ance. The impact of the changing thrust and power on longitudinal stability for the nominal nacelle incidence settings of 45 degrees is almost zero. This results because the product of the incremental changes in thrust with angle of attack times the moment arm between the thrust line and moment reference location, quarter chord of the wing on the wing chord line, very nearly balances the change in upsetting moment caused by the changes in thrust and manifested by changes in the hub moment and normal force times its moment arm to the moment reference point. The impact of the thrust variation for the condition of 30 degrees nacelle incidence is not zero because of the smaller distance between the thrust and moment reference. Run 101, nacelle incidence zero, indicates approximately neutral stability relative to the wing quarter chord reference. Correction of the pitching moment versus angle of attack for the estimated changes in thrust, normal force, and hub moment variations with changes in power as compared to those resulting with angle of attack variation at constant power setting indicates a resultant C_{m_α} at constant power, as illustrated on Figures 91, of .0113. The corrected lift curve slope is illustrated on Figure 90 and $C_{L_\alpha} = .131$. Thus, the resulting corrected longitudinal stability parameter, $\frac{dC_m}{dC_L}$, would be approximately $-.086$ yielding a neutral point location at $33.6\% \bar{c}$ and static margin with the aircraft center of gravity at the aft limit of approximately $4.4\% \bar{c}$. Longitudinal stability of the full scale aircraft at this condition will be higher than this value indicates. This will result from the stabilizing contribution due to

incremental changes in thrust with angle of attack at constant power causing larger stabilizing moments to result with the center of gravity below the wing chord plane as is the case for all loading conditions of the Model 222.

The effect of the horizontal tail on aircraft longitudinal characteristics is indicated by runs 71 and 73 for the rotors off condition. These runs indicate an increase in aircraft lift coefficient of 0.012 and an aft shift in neutral point of 84 percent MAC caused by adding the tails. These differences, particularly the neutral point shift are much greater than anticipated and will be discussed further in Section 5.1.4, comparison of test and theory.

Figure 96 indicates the effect of changing nacelle incidence on aircraft and airframe lift and pitching moment coefficients in transition. The test points were run at constant thrust coefficient and with fuselage angle of attack of zero degrees. The rotor contribution to pitching moment at constant thrust is illustrated to be nearly invariant with nacelle incidence and the rate of change of lift coefficient attributable to the rotor as a function of nacelle incidence is small, only approximately .009 per degree nacelle incidence change. Changes in lift and pitching moment coefficients for the airframe at this condition results from rotor-airframe interference and from the direct incremental coefficient changes attributable to the nacelles and spinners at angle of incidence. Nacelle incidence was not varied with the

rotors removed, however, so these increments were not measured. The lift coefficient change of +.17 for the incidence range tested, can be compensated, as indicated by the lift curves of Figure 90, by a change in angle of attack of approximately 1.3 degrees. The pitching moment coefficient increment of .058 will be additive to the pitching moment coefficient of approximately .03 resulting from the angle of attack change, Figure 91 but can be trimmed by a small change in longitudinal control as will as be discussed in Section 5.1.3.

Lateral/Directional Stability

Lateral/directional characteristics for the 40 degree flap deflection, near 42 degrees nacelle incidence conditions are illustrated in Figures 97, 98 and 99 and tabulated in Table 6. Data indicate the aircraft to have relatively high positive directional stability with rotors on or rotors off with C_{n_p} levels of .0028 and .0070 respectively. Tail off, rotors off C_{n_p} is indicated to be negative, -.0009. Thus, the tail contribution to directional stability is indicated to be +.0079. The directional stability of the airframe, aircraft with rotors on with the direct aerodynamic contributions of the rotors determined from the nacelle balances subtracted is +.0040. A direct destabilizing contribution of the rotors of $C_{n_p} = -.0012$ is indicated when the C_{n_p} of the airframe of run 105, .0040, is subtracted from the value of .0028 for the total aircraft of run 105. An indirect contribution of the rotors of $C_{n_p} = -.0030$ is indicated by the difference between C_{n_p} of the

RUN	i_N	δ_F	TAILS	ROTORS	C_T	C_{Y_β}	C_{n_β}	C_{l_β}	DERIVATIVE REFERENCE	REMARKS
72	43.8	40	ON	OFF	-	-.0355	.0070	-.0041	AIRCRAFT	
74	43.7		OFF	OFF	-	-.0168	-.0009	-.0028	AIRCRAFT	
105	41.9		ON	ON	.0022	-.0305	.0028	-.00293	AIRCRAFT	
105	41.9		ON	ON	.0022	-.0253	.0040	-.00256	AIRFRAME	

TABLE 6 - LATERAL/DIRECTIONAL STABILITY DERIVATIVES IN TRANSITION

airframe of run 105 and the $C_{n\beta}$ of run 72. Thus, a larger indirect contribution that the direct contribution of the rotor hub moments and inplane forces is indicated. The sideforce coefficient data indicate that the rotors reduce the change in sideforce of the aircraft with sideslip angle. This is indicated by the value of $C_{y\beta}$ of $-.0305$ from run 105 for the aircraft with rotors on as compared to the value of $C_{y\beta}$ of $-.0355$ from run 72 for the aircraft with rotors off. However, the direct contribution of the rotors as indicated by the difference between aircraft and airframe of run 105 is an increase in slope $C_{y\beta}$ from $-.0253$ to $-.0305$ for $\Delta C_{y\beta}$ of $-.0052$. The tail contribution to sideforce coefficient is $-.0187$ calculated from the difference between the $C_{y\beta}$ of run 72 and that of run 74. Dividing the $\Delta C_{y\beta}$ of the tail mentioned earlier, $.0079$ by the $\Delta C_{y\beta}$ of the tail and multiplying by the wing span indicates an "effective" moment arm of the vertical tail of 3.06 feet as compared to the distance of 4.09 feet calculated distance from the quarter chord on the MAC of the vertical tail to the quarter chord of the wing. The variation of rolling moment coefficient with sideslip angle, $C_{l\beta}$, "dihedral effect", for the aircraft with rotors off is indicated to be $-.0041$ per degree from the data of run 72. The tail contribution to $C_{l\beta}$, as determined by the difference between the value for run 72, tail on, and that for run 74, tail off, is $-.0013$. The direct rotor contribution, from the values shown for aircraft and airframe of run 105, is $C_{l\beta} = -.00037$. The difference attributable to "indirect effects" of the rotors, the difference between the $C_{l\beta}$ of the airframe, run 105, and the $C_{l\beta}$ of run 72, is $\Delta C_{l\beta} = +.00154$. Thus, the direct

effect of the rotors is apparently to increase the dihedral effect and the indirect effect is indicated to decrease dihedral effect.

VARIATION OF LIFT COEFFICIENT WITH ANGLE OF ATTACK IN TRANSITION

NOTES:

RUN TAIL ROTORS IN

○	69	ON	OFF	44.0	$\delta_{1/2} = 45^\circ$ $\delta_{1/4} = 20^\circ$
△	71	ON	OFF	43.7	
□	73	OFF	OFF	43.7	
◇	104	ON	ON	41.6	$Q = 0.022$ $M = 0.205$

TUNNEL SPEED = 72 FPS

$R = 6$ PSF

EQUIV FULL SCALE V-SLOTS

$\delta_F = 40^\circ$

PREDICTED
AIRCRAFT /

AIRCRAFT

PREDICTED
AIRFRAME
ROTORS ON

AIRFRAME

$CL_{\alpha} = 1.34$

$CL_{\alpha} = 0.95$

$CL_{\alpha} = 0.98$

$CL_{\alpha} = 0.89$

$CL_{\alpha} = 0.86$

PREDICTED AIRFRAME
ROTORS OFF

$CL_{\alpha} = 0.90$

CL_{α} SHIFTED

LIFT COEFFICIENT - C_L

FUSELAGE ANGLE OF ATTACK - α_{FRL} - DEGREES

FIGURE 87

VARIATION OF PITCHING MOMENT COEFFICIENT
WITH ANGLE OF ATTACK IN TRANSITION

NOTES:

RUN TAILS ROTORS IN

○ 60 ON OFF 440° $\delta_{AR} = 45^\circ$, $\delta_{FR} = 20^\circ$

△ 71 ON OFF 43.7

□ 73 OFF OFF 43.7

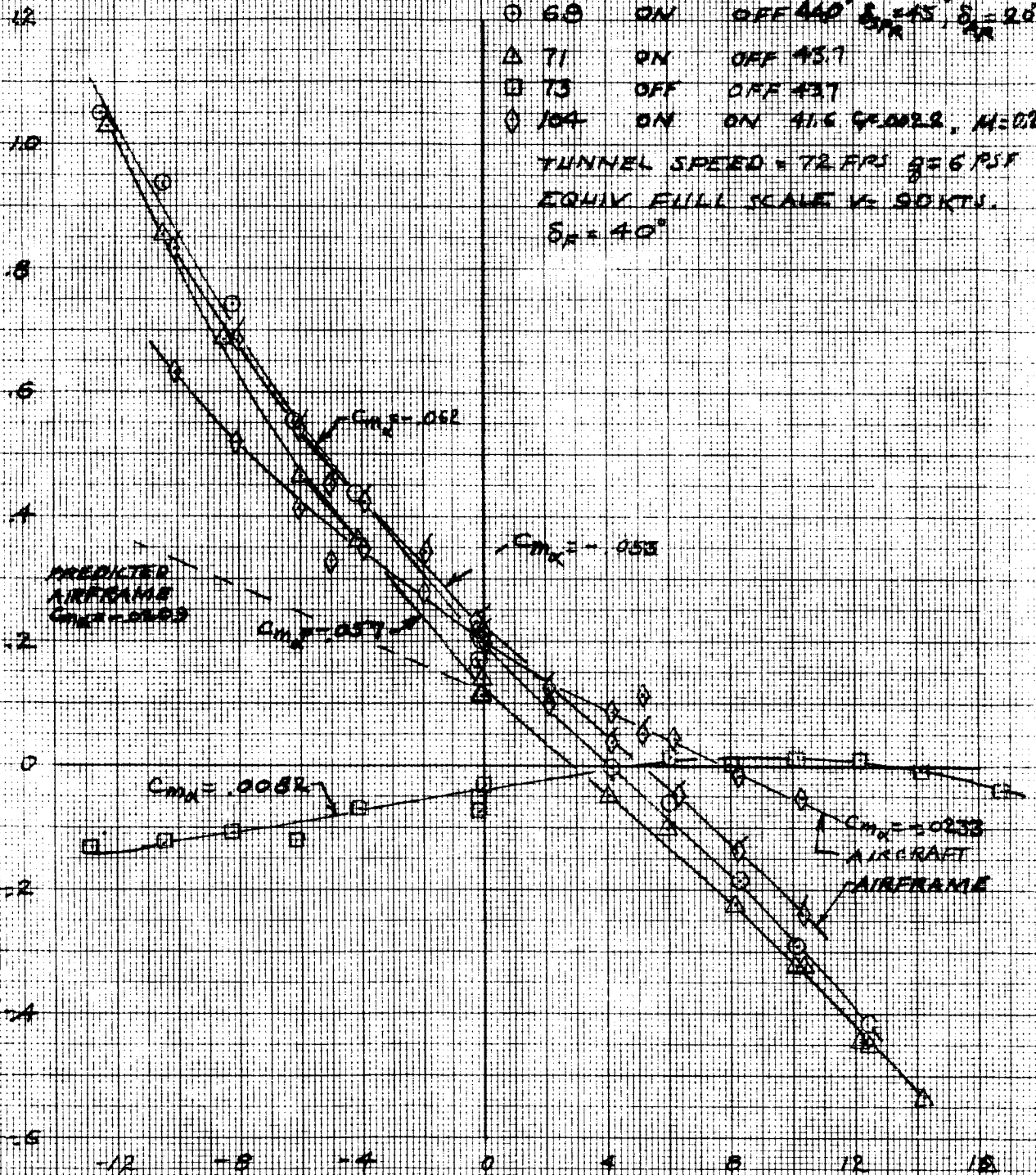
◇ 104 ON ON 41.6 GPM22, $M = 0.205$

TUNNEL SPEED = 72 FPS @ 6 PSF

EQUIV FULL SCALE $V = 90$ KTS.

$\delta_R = 40^\circ$

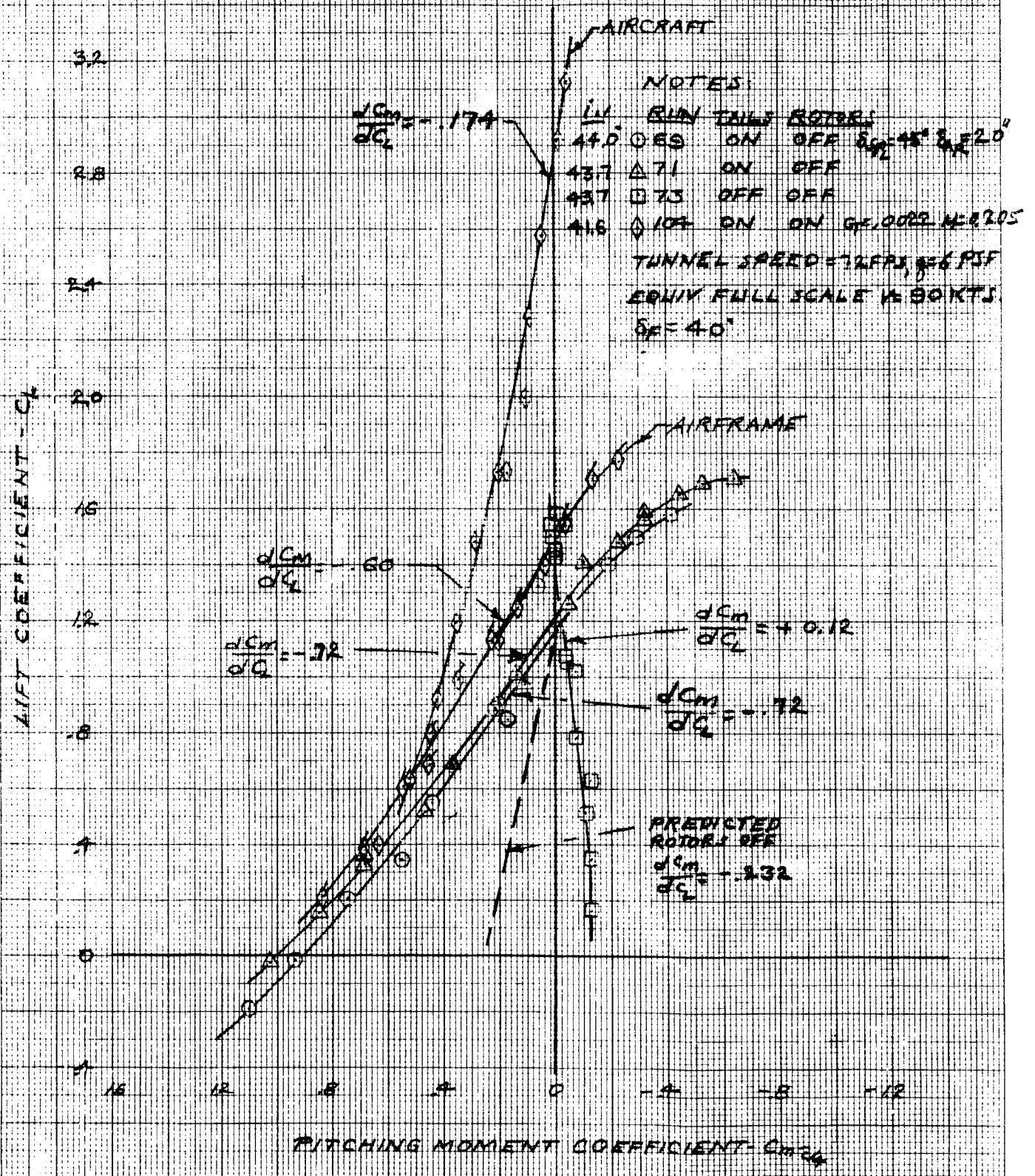
PITCHING MOMENT COEFFICIENT - $C_{M_{XX}}$



FUSELAGE ANGLE OF ATTACK - α_{PR} - DEGREES

FIGURE 88

LONGITUDINAL STABILITY VARIATION OF PITCHING MOMENT WITH LIFT COEFFICIENT IN TRANSITION



LIFT
VARIATION OF LIFT COEFFICIENT WITH ANGLE
OF ATTACK IN TRANSITION
AIRCRAFT

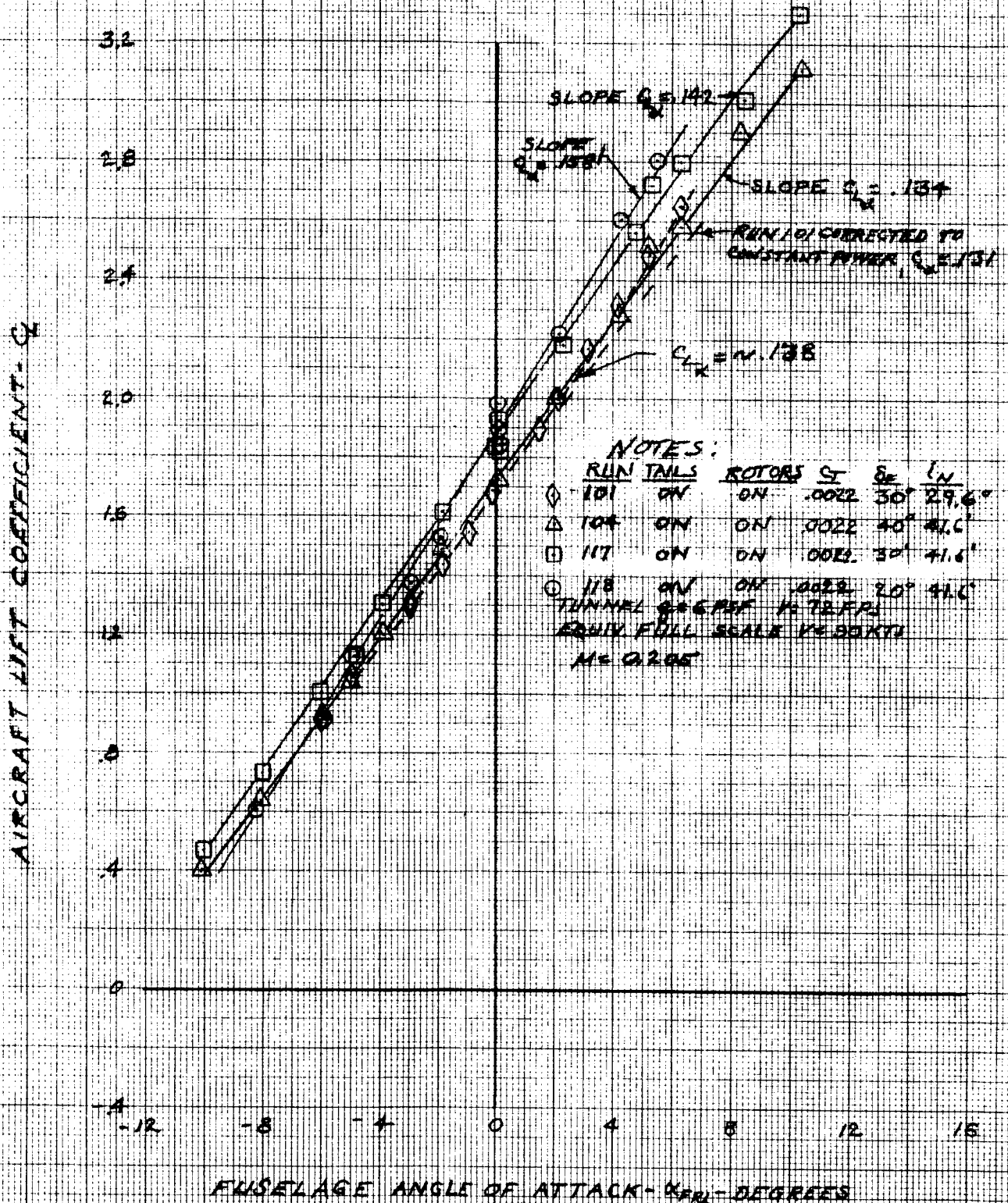


FIGURE 90

PITCHING MOMENT
VARIATION OF PITCHING MOMENT COEFFICIENT
WITH ANGLE OF ATTACK IN TRANSITION
AIRCRAFT

NOTES:

RUN	TAILS	ROTORS	CT	SE	IN
101	ON	ON	.0022	30°	29.6'
104	ON	ON	.0022	40°	41.6'
117	ON	ON	.0022	30°	41.6'
118	ON	ON	.0022	20°	41.6'

TUNNEL 9-6 PSF V=72 FPS
EQUIM FULL SCALE V=142 KTS.
M=0.205

AIRCRAFT PITCHING MOMENT COEFFICIENT - $C_{m\alpha}$

1.0
.8
.6
.4
.2
0
-.2
-.4

-12

-8

-4

0

4

8

12

16

FUSELAGE ANGLE OF ATTACK - α DEGREES

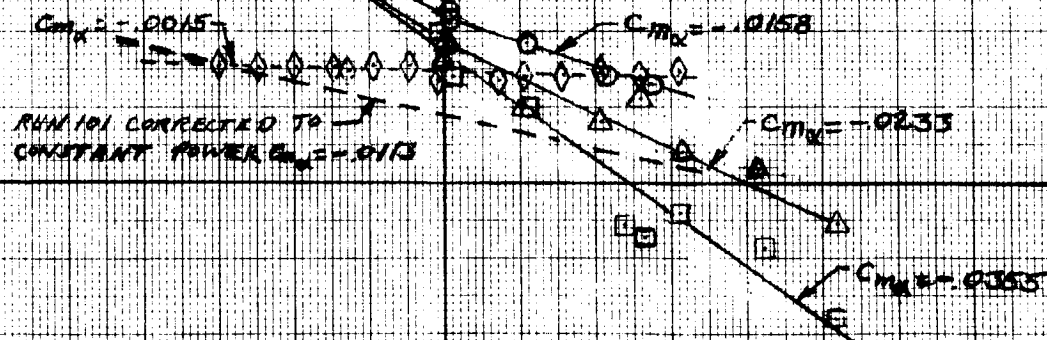


FIGURE 91

LONGITUDINAL STABILITY

VARIATION OF PITCHING MOMENT COEFFICIENT
WITH LIFT COEFFICIENT IN TRANSITION
AIRCRAFT

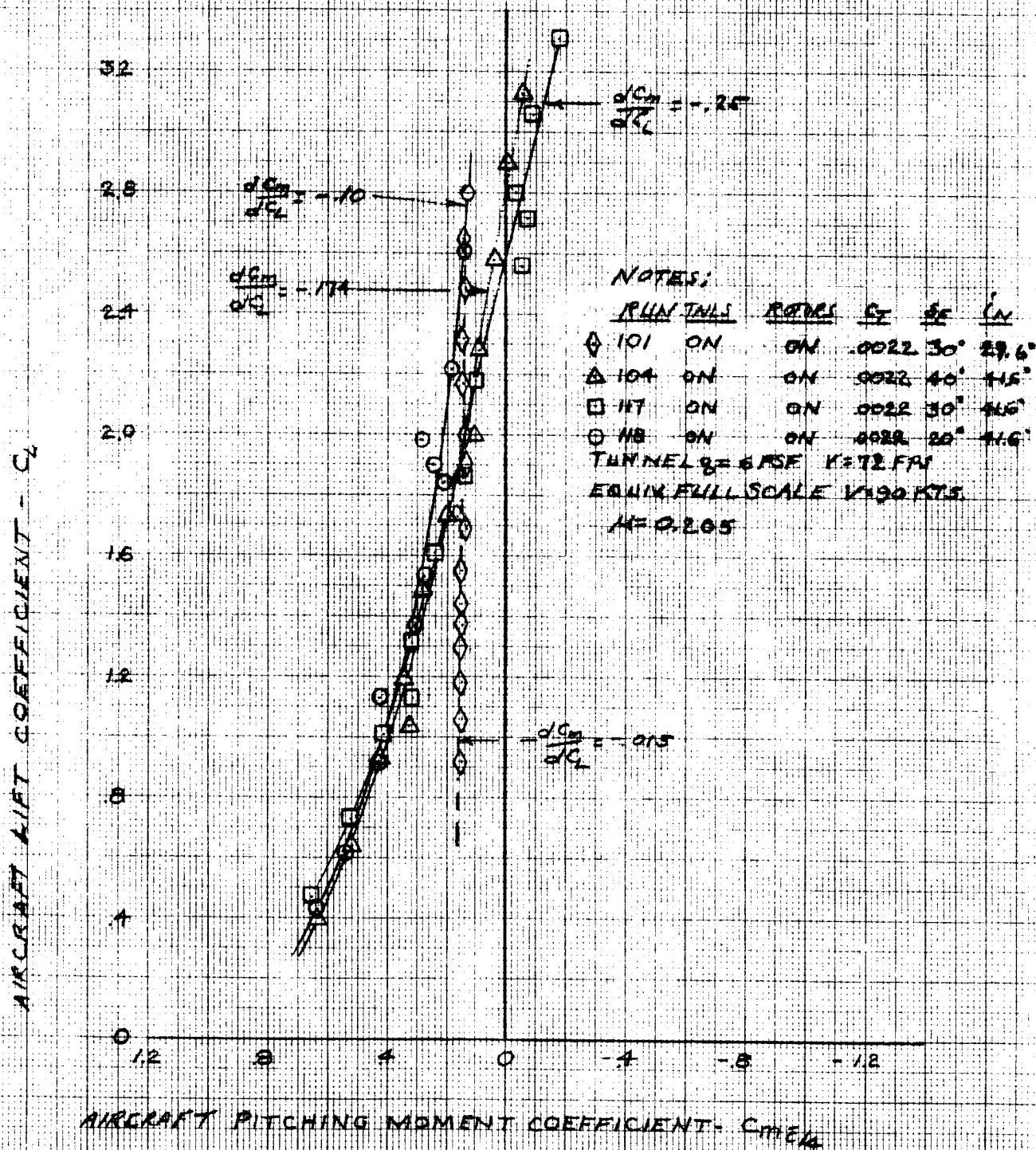


FIGURE 92

LIFT

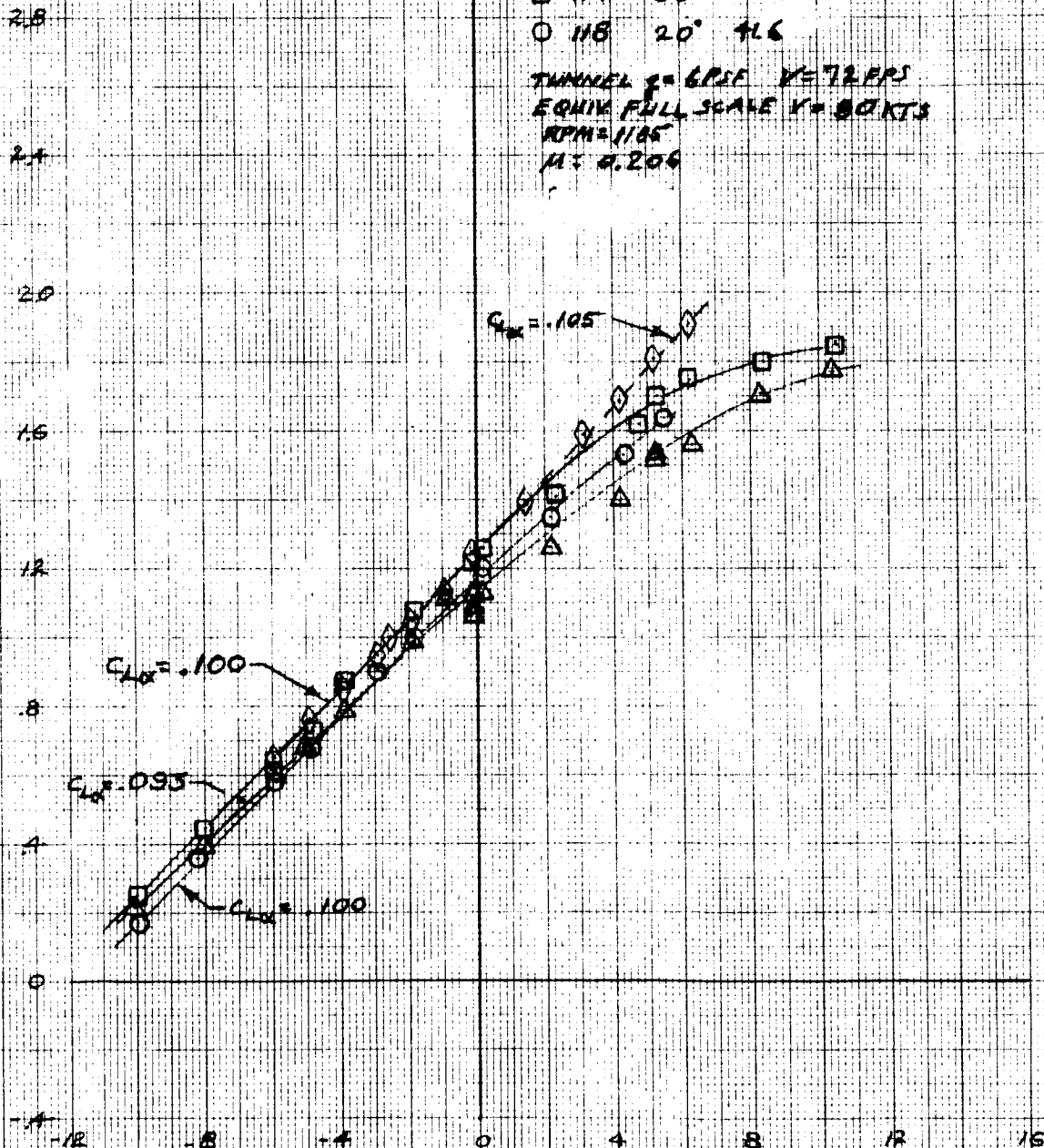
VARIATION OF AIRFRAME LIFT COEFFICIENT WITH ANGLE OF ATTACK IN TRANSITION

NOTES:

RUN	δ	$\frac{1}{N}$
101	30°	2.96
104	40°	4.16
117	30°	4.16
118	20°	4.16

TUNNEL $\rho = 6.25$ $V = 72$ FPS
EQUIV FULL SCALE $V = 80$ KTS
RPM = 1165
 $M = 0.206$

AIRFRAME LIFT COEFFICIENT - C_L



FUSELAGE ANGLE OF ATTACK - α - DEGREES

FIGURE 93

LONGITUDINAL STABILITY
VARIATION OF AIRFRAME PITCHING MOMENT
COEFFICIENT WITH LIFT COEFFICIENT IN
TRANSITION

AIRFRAME PITCHING MOMENT COEFFICIENT

$C_{M_{AC}}$

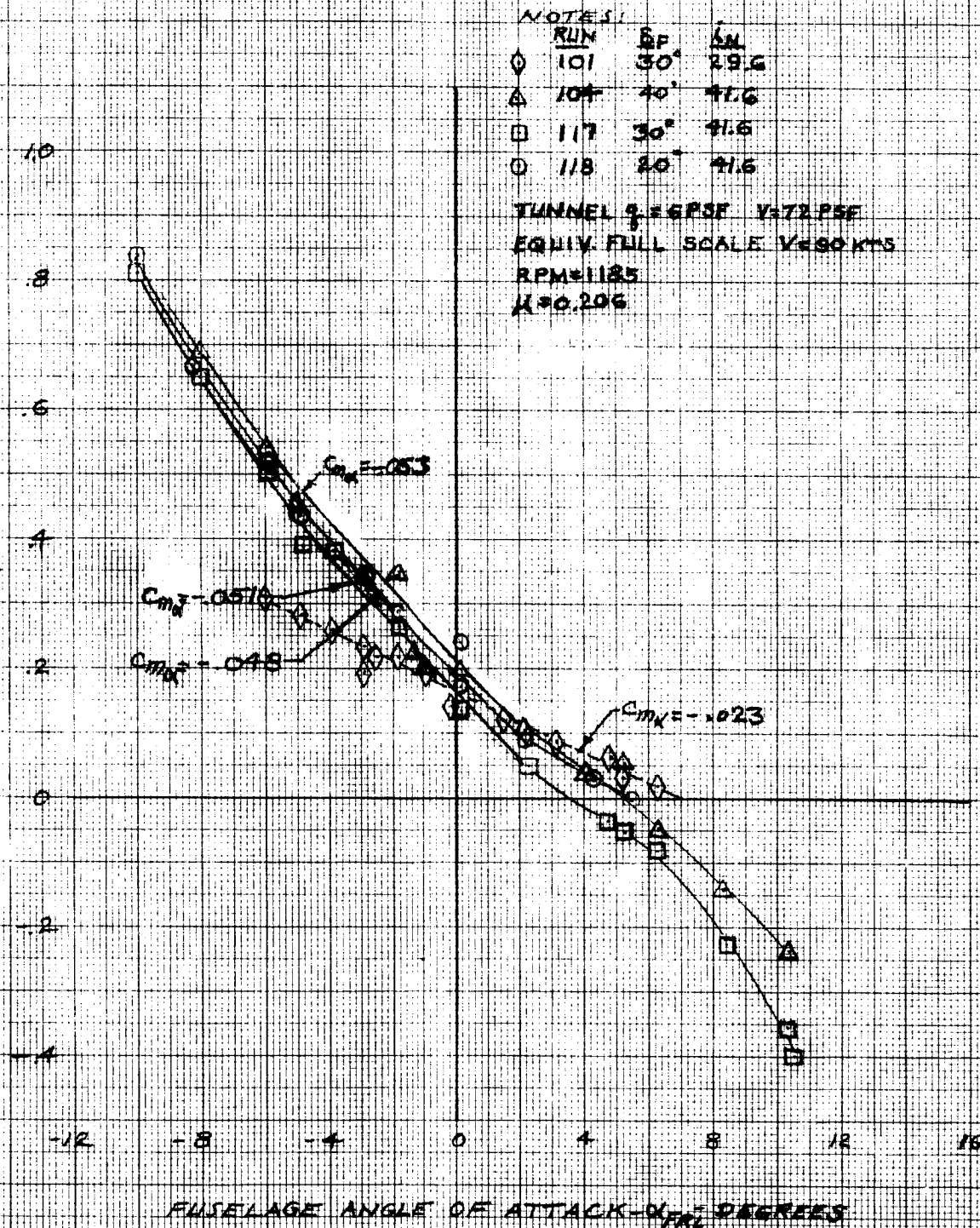


FIGURE 94

PITCH
VARIATION OF AIRFRAME PITCHING MOMENT
COEFFICIENT WITH ANGLE OF ATTACK IN TRANSITION

NOTES:

RUN	SE	LN
101	30°	29.6°
104	40°	41.6°
117	30°	44.6°
118	20°	41.6°

TUNNEL $q = 6.95 \text{ PSF}$ $V = 72 \text{ FPS}$
 EQUIV FULL SCALE $V = 90 \text{ KTS}$
 RPM = 1185
 $M = 0.206$

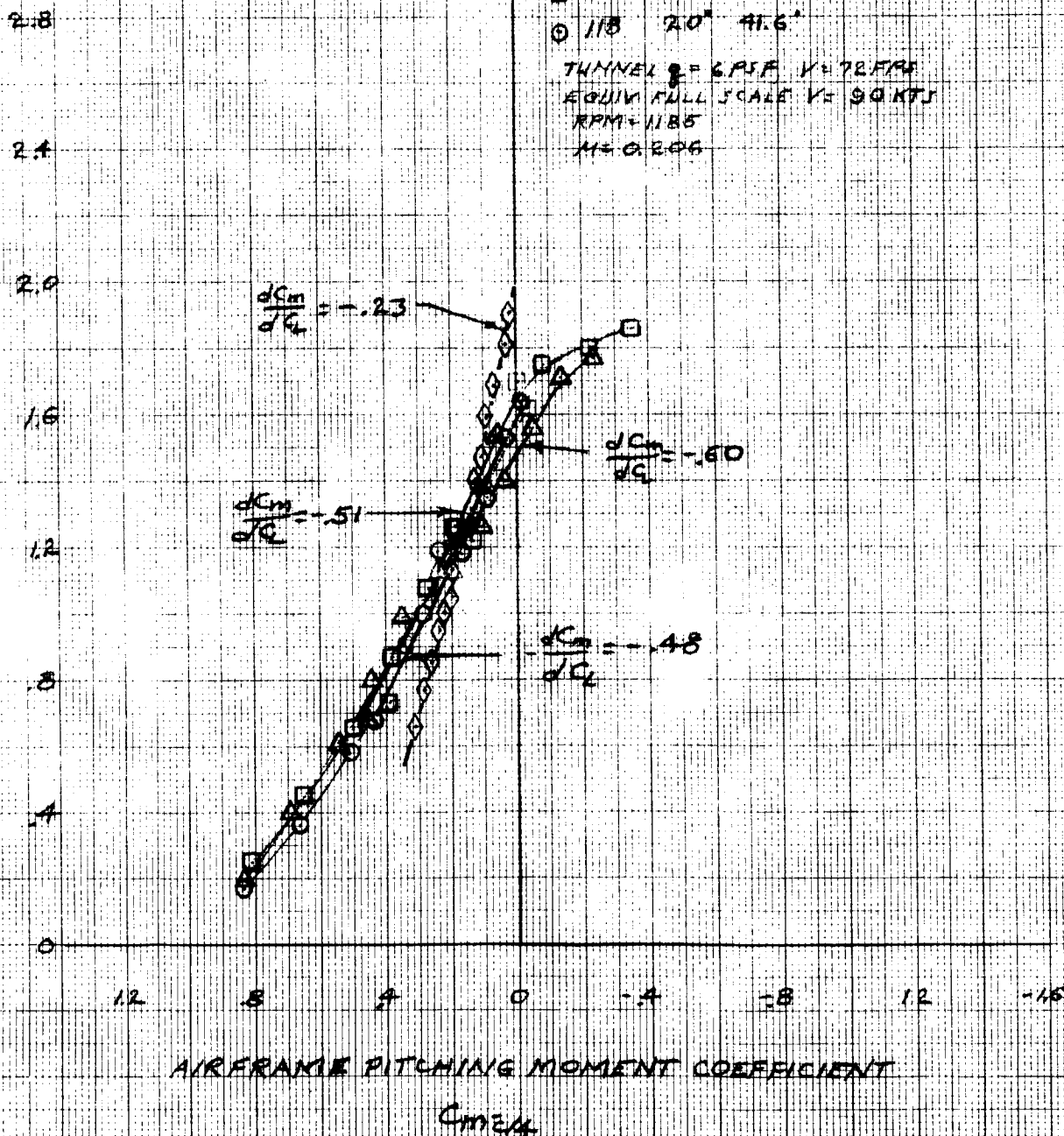
AIRFRAME LIFT COEFFICIENT - C_L 

FIGURE 95

EFFECT OF NACELLE INCIDENCE ON LIFT AND PITCHING MOMENT COEFFICIENTS IN TRANSITION

NOTES

RUN 104

○ AIRCRAFT

△ AIRFRAME

$C_T = 0.0022$ $M = 0.205$

$\delta_F = 40^\circ$ $\alpha_F = 0$

TUNNEL $\beta = 6.5^\circ$ $V = 72 \text{ FPS}$

EQUIV. FULL SCALE $V = 90 \text{ KTS}$

LIFT COEFFICIENT

C_L

PITCHING MOMENT COEFFICIENT

C_{M25}

2.6
2.2
1.8
1.4
1.0
.4
.3
.2
.1
0

20 24 28 32 36 40 44

NACELLE INCIDENCE - δ_N - DEGREES

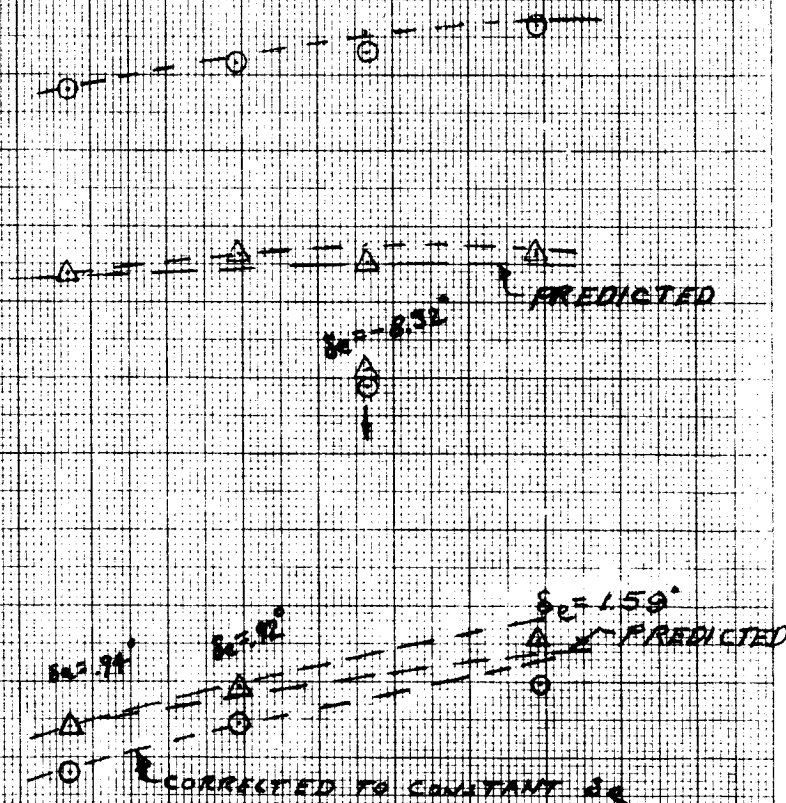


FIGURE 96

DIRECTIONAL STABILITY
VARIATION OF YAWING MOMENT COEFFICIENT
WITH SIDESLIP ANGLE IN TRANSITION

NOTES:

RUN TAILS ROTORS IN

○ 72 ON OFF 438

△ 74 OFF OFF 437

□ 105 ON ON 419 GE.0022 M=2.05

TUNNEL SPEED = 72 FPS

FULL SCALE EQUIV = 90 KTS.

$\delta_F = 40^\circ$

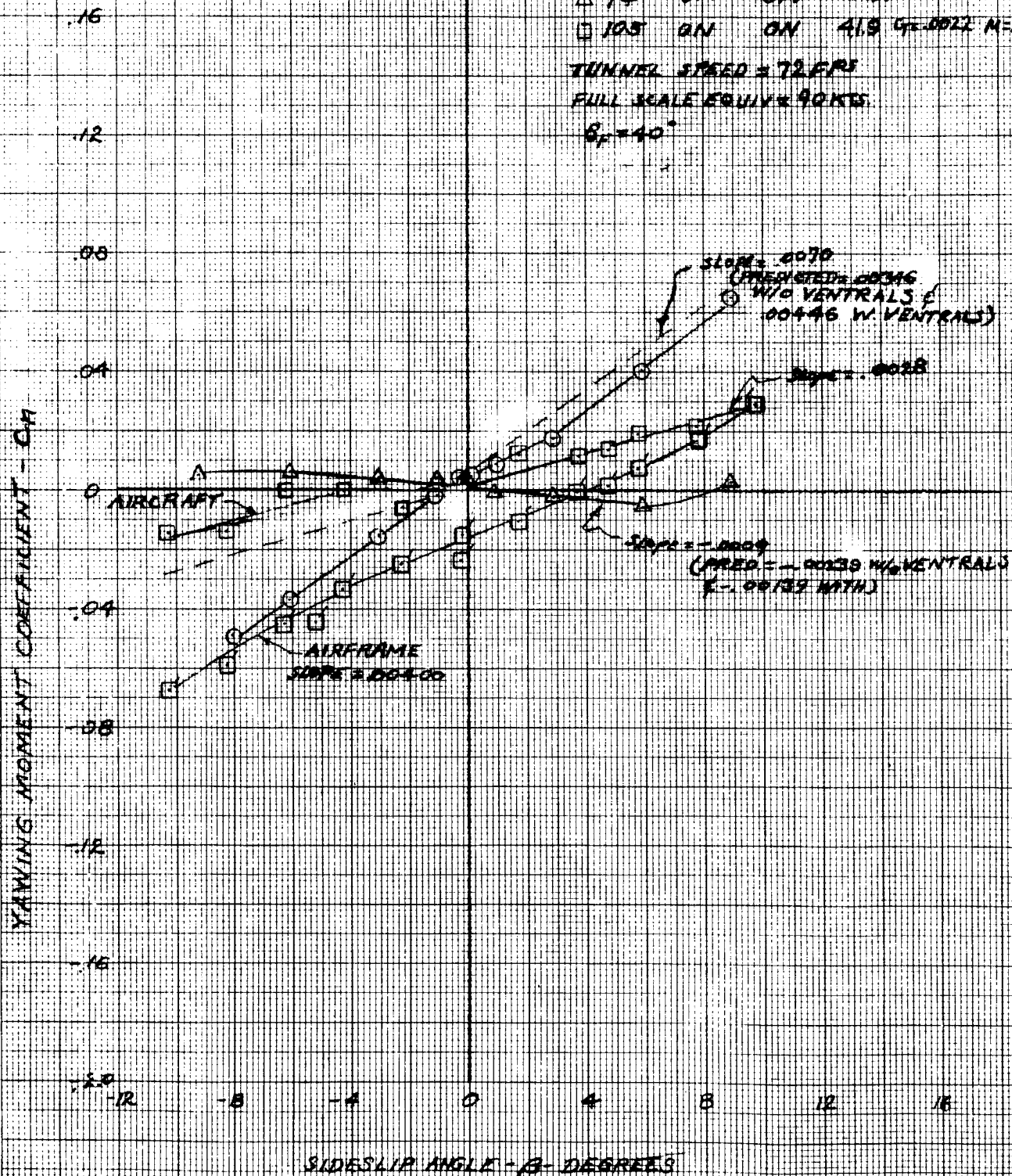


FIGURE 97

DIHEDRAL EFFECT

VARIATION OF ROLLING MOMENT COEFFICIENT WITH SIDESLIP ANGLE IN TRANSITION

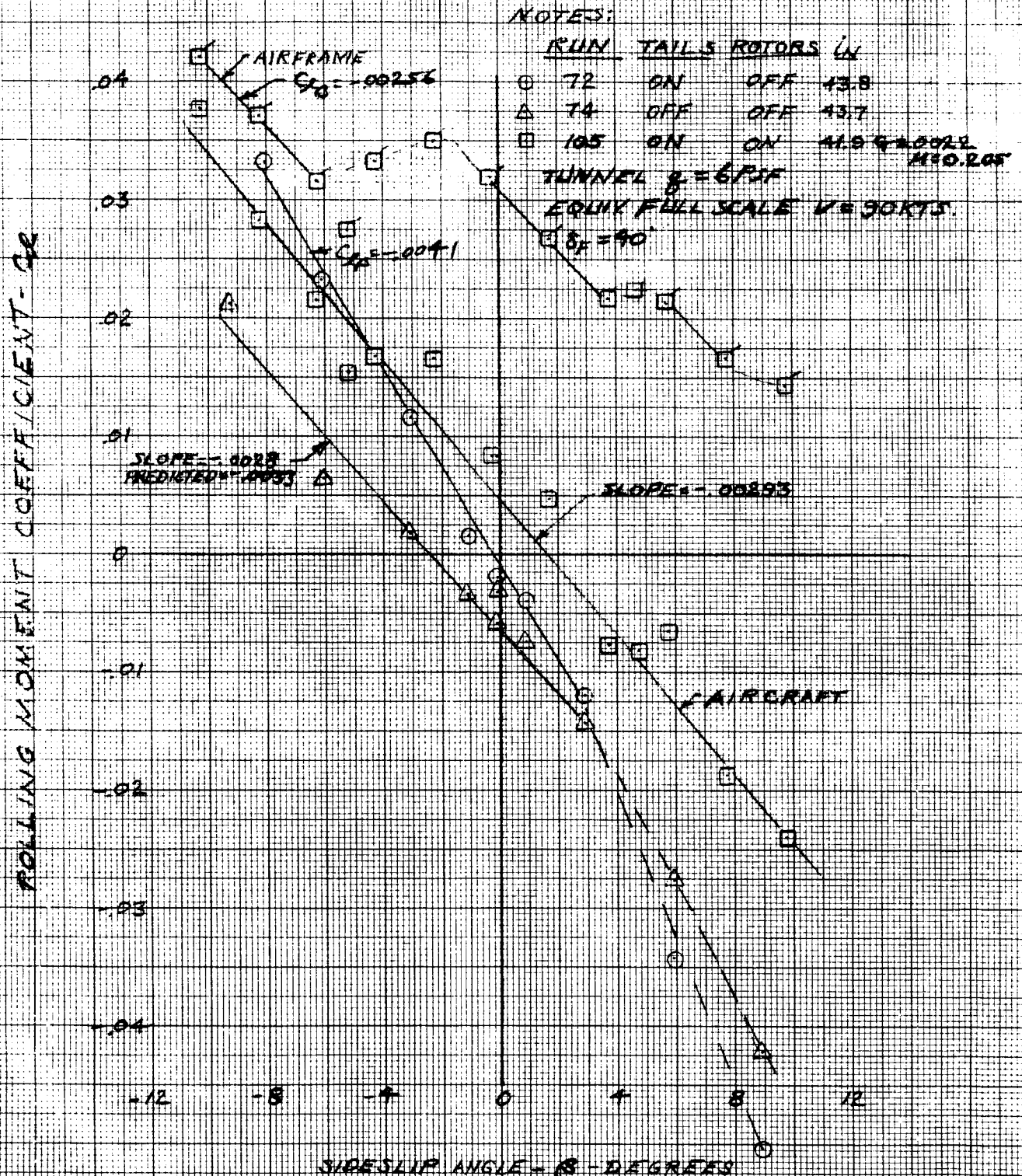


FIGURE 98

SIDEFORCE VARIATION OF SIDEFORCE COEFFICIENT WITH SIDESLIP ANGLE IN TRANSITION

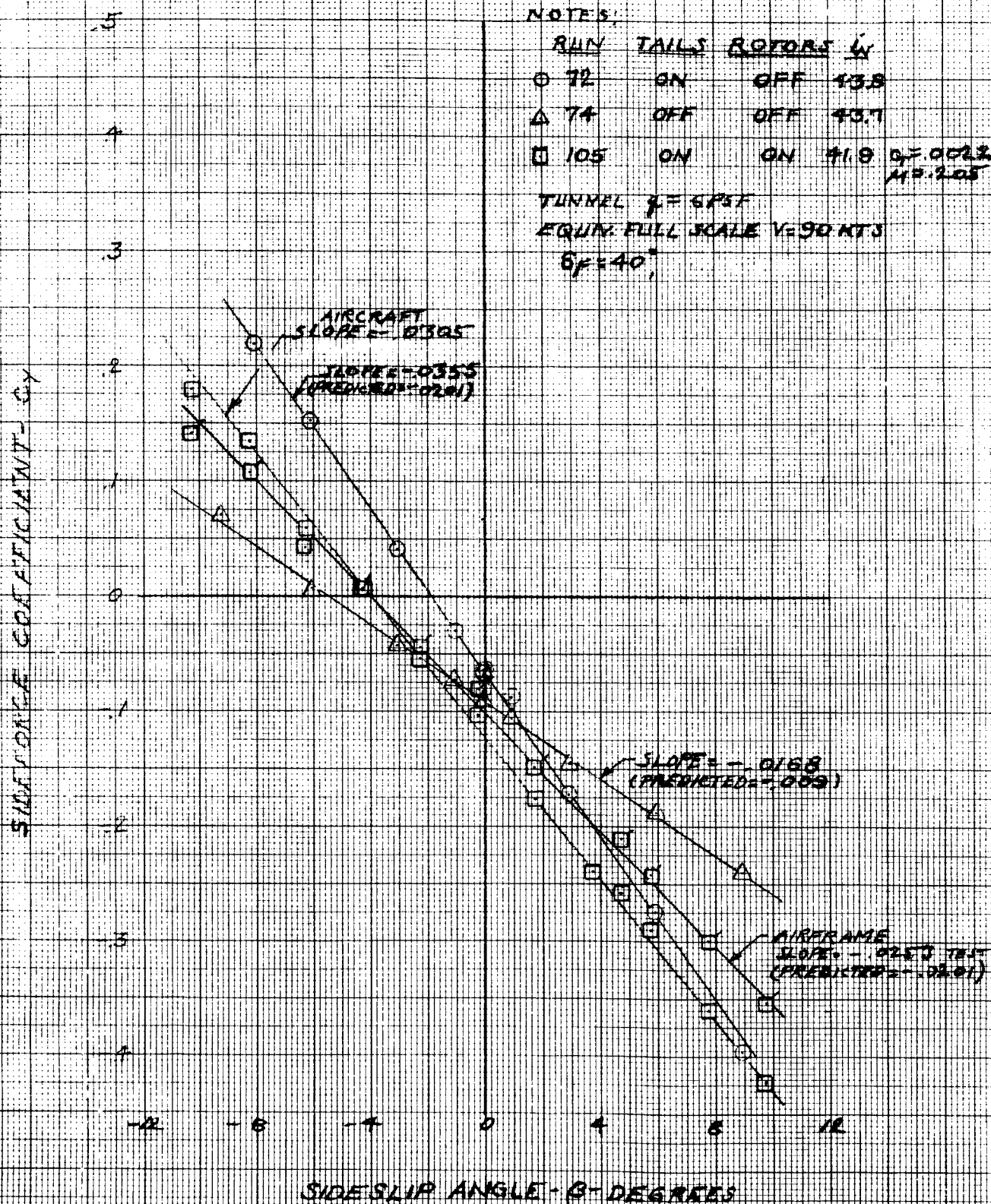


FIGURE 99

5.1.3 Control Power and Mixing

Control in transition is achieved by utilizing both rotor and airframe aerodynamic controls. The amount of control available from each will be examined here.

Rotor Control

During the execution of the transition from hover to cruise the major portion of the control is obtained from rotor cyclic (longitudinal and lateral) and collective pitch. To determine the amount of control available and also provide cyclic effectiveness data that would be integrated into the low rate cyclic feedback system testing was performed at a nacelle incidence of 41.6 degrees and 1185 RPM at a tunnel speed of 72 FPS. This is equivalent to flying at 90 kts at 551 RPM for the full scale vehicle in transition. Longitudinal and lateral cyclic investigations were performed at approximately zero degrees fuselage attitude and Figures 100 to 103 present the rotor normal force, pitching moment, side force and yawing moment data. Figures 104 and 105 show the cyclic and collective variations induced by slop in the control system during the cyclic sweeps. These last two sets of data provide the basis for the data fairings that are shown in these figures. Utilizing these curves and the data to be presented next on the effect of collective, a longitudinal cyclic derivative at a constant value of collective and lateral cyclic ($\theta_{.75}=12.8^\circ$, $A_1=1.17$) was developed. These derivatives are summarized in the following table.

CYCLIC DERIVATIVES

TUNNEL SPEED V	ADVANCE RATIO μ	NACELLE AND FLAP i_N/δ_F	$\frac{\partial C_{NF}}{\partial A_1}$	$\frac{\partial C_{PM}}{\partial A_1}$	$\frac{\partial C_{SF}}{\partial A_1}$	$\frac{\partial C_{YM}}{\partial A_1}$
fps 72	0.206	41.6° 40°	-0.000100	+0.000080	-0.000107	-0.00040
			$\frac{C_{NF}}{B_1}$	$\frac{C_{PM}}{B_1}$	$\frac{C_{SF}}{B_1}$	$\frac{C_{YM}}{B_1}$
fps 72	0.206	41.6° 40°	-0.000057	-0.00063	+0.000164	+0.000040

During this transition testing differential collective was tested to determine the roll-yaw control and the associated coupling. The related impact on the rotor characteristics is shown in Figures 106 through 109. Figures 110 indicates the variation in longitudinal and lateral cyclic induced during this run and is used to define the data fairing achieved. A summary of the collective derivatives is presented below.

TUNNEL SPEED V	ADVANCE RATIO μ	NACELLE AND FLAP i_N/δ_F	$\frac{\partial C_{NF}}{\partial \theta}$	$\frac{\partial C_{PM}}{\partial \theta}$	$\frac{\partial C_{SF}}{\partial \theta}$	$\frac{\partial C_{YM}}{\partial \theta}$
fps 72	0.206	41.6° 40°	-0.000030	0.00013	-0.000017	0.00

Aircraft and Airframe Control Power

The effect on aircraft and rotor parameters of use of the outboard half of the left flap as an aileron is illustrated in Figures 111 through 119. Results indicate that use of the flap as a roll control device at deflections of the surface greater than 40 degrees results in "negative" roll control because of decrease in lift with deflection. Use of the flaps for roll control in the full scale aircraft will be restricted to 35 degrees deflection of the surfaces for combined flap and aileron. Deflection of the aileron with the flaps set at 40 degrees results in essentially no change in yawing moment coefficient for the first 12 degrees, aileron deflection and small adverse yaw up to 20 degrees.

The aircraft experiences a small nose up pitching moment coefficient change with aileron deflection resulting from the forward shift in center of pressure with loss of lift. Figure 117 indicates very small changes in rotor thrust and power coefficient at constant rpm and collective settings resulting from the induced circulation effects of aileron deflection. Figures 117 and 119 indicate substantially no effects of aileron deflection on the right rotor in-plane forces and hub moments. Valid data were not obtained for these coefficients for the left rotor because of instrumentation problems.

Spoiler effects on aircraft and rotor parameters are illustrated in Figures 120 through 129 for deflection of the spoiler on

the outboard semispan of the right wing. Figure 120 indicates incremental rolling moment coefficient of .0535 for 45 degrees spoiler deflection. The yawing moment coefficient data of Figure 121 indicate small favorable yawing moment due to spoiler deflection. The loss in lift coefficient with spoiler deflection is illustrated in Figure 122 indicating the characteristic non-linearity with deflection. Pitching moment coefficient, Figure 123 is observed to change in the "nose up" direction, positive C_m , with spoiler deflection resulting from forward shift in center of pressure on the wing. Aircraft lift coefficient variation with rolling moment coefficient is illustrated in Figure 124. The variation of rolling moment coefficient with lift coefficient indicates an average lateral center of pressure of the lift producing rolling moment to be at approximately 59.5% of the wing semispan. Figure 126 indicates some increase in power coefficient and resulting thrust coefficient of the right rotor compared to the left rotor necessary to maintain rpm constant at constant collective setting and small increase in power required and thrust of the left rotor with increasing deflection of the right spoiler. Figures 127 and 128 indicate the changes in rotor inplane forces and hub moments resulting from spoiler deflection. Rotor hub pitching moment coefficient is observed to be of negative sign, nose down, and converting to aircraft pitching moment coefficient, produces only about 0.6% of the magnitude of the aircraft nose up pitching moment coefficient resulting from spoiler deflection as indicated in Figure 123.

The schedule of spoiler deflection combined with aileron deflection tested for roll control in transition is illustrated in Figure 129. The effects of the combined control are illustrated in Figures 130 through 137. Note that the parameters are all plotted versus aileron deflection with spoiler deflection per the scheduled values. Aircraft rolling moment coefficient change with combined control is less than that for spoiler deflection alone because of the decrease in lift associated with aileron deflection from the initial flap deflection of 40 degrees. Aircraft yawing moment coefficient variation with combined control is observed to be near zero. Aircraft lift coefficient is decreased 0.3 for maximum combined control. Pitching moment coefficient is nose up, in the direction to result in increased lift coefficient due to angle of attack to offset the direct loss of lift due to control deflection. Figure 135 indicates a small increase in power required on the right rotor to maintain rpm constant with constant collective. The effects on inplane forces and hub moments are relatively small and illustrated on Figures 136 and 137. The effects of combined spoiler and aileron, differential thrust and rudder deflection on aircraft parameters are illustrated in Figures 138 through 140. The effects of 20 degrees aileron combined with 50 degrees spoiler deflection on rolling and yawing moment coefficients are as described previously and the effect on sideforce coefficient is negligible. Rudder effect on rolling moment coefficient, for 19 degrees deflection, is $\Delta C_{\ell} = .004$ at zero sideslip and angle of attack. The change in yawing moment coefficient is $\Delta C_n = .087$ and the change in sideforce coefficient is

$\Delta C_Y = .140$. This change in sideforce coefficient with the small change in rolling moment coefficient mentioned earlier indicates that the center of pressure of the change in sideforce is located on the vertical tail at approximately 27% of the rudder height up from the base of the rudder. The change in yawing moment coefficient with sideforce coefficient indicates that the center of pressure of the change in sideforce is at a distance of approximately 62% of the wing span aft of the wing quarter chord compared to a distance from wing quarter chord to the quarter chord of the vertical tail MAC equivalent to 56.5% span.

Differential thrust coefficient, from the test data, of $\Delta C_T = .000847$ (left rotor thrust higher than right) is indicated to yield a $\Delta C_L = .056$, $\Delta C_n = .0325$ and $\Delta C_Y = .02$ at zero angle of attack and sideslip angle. The effect of differential thrust on airframe coefficients, Figure 141 is indicated to yield ΔC_L of .0145 and ΔC_n of -.0075.

The test data indicate a small difference in nacelle incidence angle between the left and right nacelles for run 105 as compared to the incidence for runs 112, 114 and 115. The nacelle incidences are tabulated in Figures 138 through 141. In addition there is a small difference in the cyclic control settings. The cyclic control deflection for left hand B_1 was not tabulated on the test data due to faulty instrumentation. Thus, complete correction of the data cannot be made for the effects of the differential cyclic. The effect of the change in nacelle incidence does not affect the increments in coefficients for rudder and aileron/spoiler effects.

It does, however, significantly affect the increments for the effects attributable to change in thrust. Therefore, the increments quoted above are only approximate for the effects of differential thrust. Figure 142 illustrates the variation of rolling moment with yawing moment coefficient for variation of collective pitch. The variations in collective pitch are tabulated beside the test points and the variations of thrust coefficient, in terms of differential thrust coefficient between left and right rotor, with variations of collective between left and right rotor are plotted in Figure 143 for run 109. This run was performed with constant cyclic and nacelle incidences. Thus, Figure 142 represents realistically the effect of changing thrust differentially on rolling moment and yawing moment coefficients. If there were absolutely no change in cyclic or nacelle incidence and no change in aerodynamic effects of the airframe, i.e. no wing or rotor interference effects the ratio of rolling moment to yawing moment coefficient would be the ratio of $\sin 41.6$ degrees to $\cos 41.6$ degrees, 0.89. The ratio of rolling moment coefficient to yawing moment coefficient from Figure 143 with the curve shifted to go through zero rolling moment at zero yawing moment is 0.817. This indicates some aerodynamic interference effect.

Figures 144 and 145 illustrate the elevator effectiveness in transition in changing pitching moment coefficient and lift coefficient. The pitch effectiveness, $C_{m_{\delta_e}}$, is indicated to be -0.23 in the linear range. Linearity is indicated to approximately 10 degrees surface deflection. The variation of lift coefficient with elevator deflection, is indicated to be .0065 indicating the

effective tail length to be $3.52 \bar{c}$ compared to the distance from wing quarter chord to quarter chord of the horizontal tail MAC of $3.40 \bar{c}$. Elevator effectiveness of the full scale aircraft is anticipated to be higher than indicated by this test. Reynolds number at this test condition was approximately 0.39×10^6 based on horizontal tail MAC compared to Reynolds number = 3.8×10^6 at the equivalent full scale velocity.

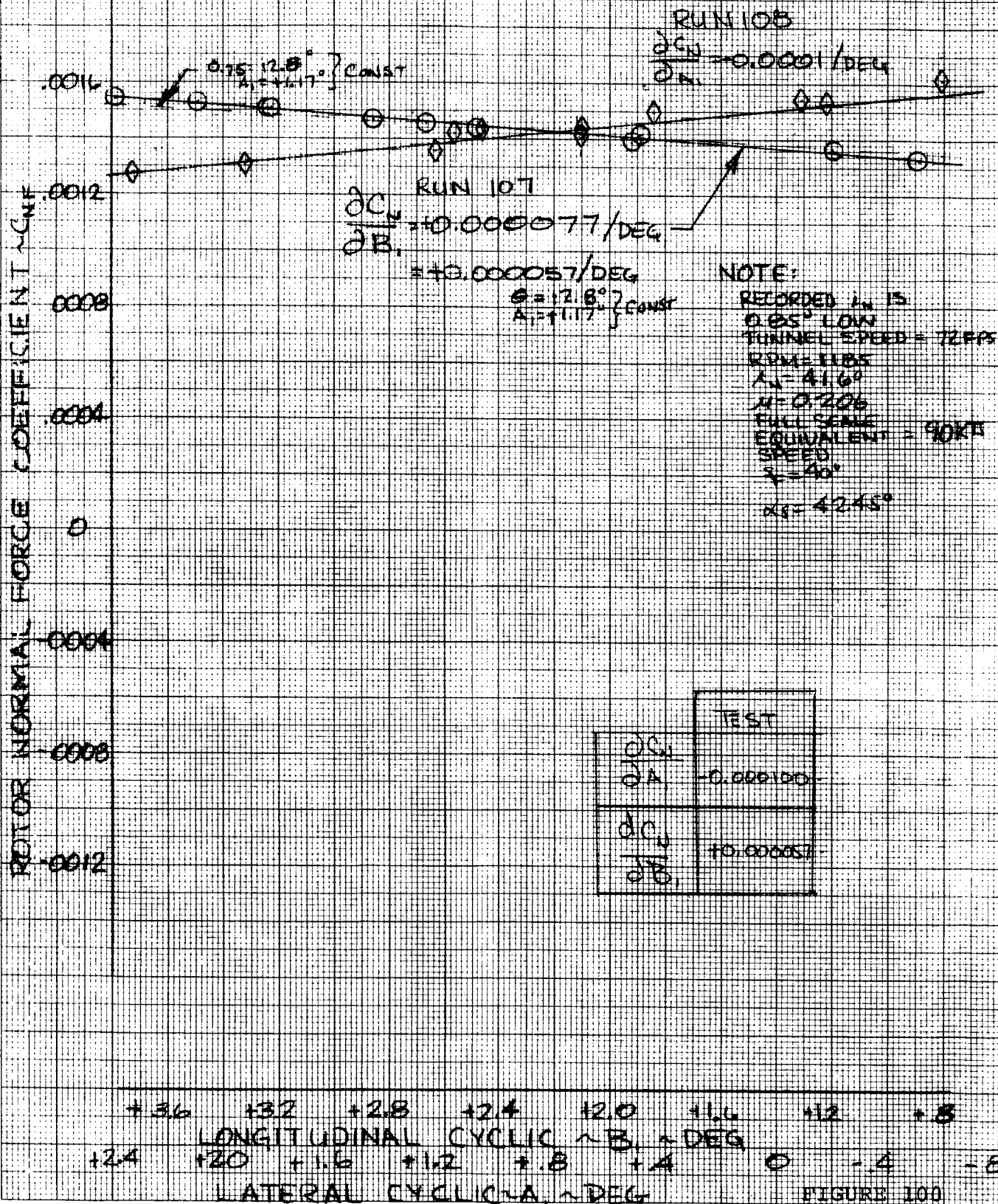
Figures 146 and 147 illustrate the variation of aircraft lift, pitching moment, yawing moment and rolling moment coefficients as a function of longitudinal cyclic deflection, B_1 , of the right rotor. The structure of the nacelle mounts was designed to yield approximately the same deflection of the thrust line per degree cyclic for increased roll and yaw effectiveness, as will result on the full scale aircraft, i.e., approximately 1.5 degrees nacelle tilt plus 0.25 degrees wing torsional deflection per degree cyclic. Thus, the coefficients per degree cyclic are for combined thrust vectoring and cyclic. Power was varied to some extent during the runs and the lines have been faired through the data to represent the slope of the coefficients for constant engine power. The data indicate that C_L per degree $B_1 = -.007$, $C_m/B_1 = -.122$, $C_n/B_1 = .0105$ and $C_{\ell}/B_1 = +.0162$. Pitch control of the Model 222 in transition is accomplished utilizing B_1 cyclic and elevator deflection. At the 41.6 degrees nacelle incidence setting the full scale aircraft will have available ± 20 degrees elevator deflection and ± 1.6 degrees B_1 for full stick deflection of ± 6 inches. Using the $C_{m_{\delta_e}}$ from Figure 144 in the linear region with the B_1

pitching moment effectiveness the total C_m per inch δ_s then is $+.1091$. Roll and yaw control are accomplished in the Model 222 using combined rudder, aileron/spoiler, differential longitudinal cyclic, differential nacelle tilt and differential collective. The incremental effects of rudder, aileron/spoiler, and differential collective are enumerated herein. However, the effects of differential B_1 cyclic were not obtained because of faulty B_1 cyclic instrumentation on the left rotor. In addition, insufficient data were obtained to determine the variation of aircraft rolling and yawing moment coefficients with nacelle tilt as a function of cyclic input. Therefore, control mixing required in transition for uncoupled roll or yaw responses to control inputs cannot be accurately verified.

Figures 148 through 151 illustrate the variation of aircraft yawing moment, rolling moment, lift and pitching moment coefficients with a lateral, A_1 , cyclic inputs. It is not anticipated that lateral cyclic will be a pilot controlled function in the aircraft. It will, however, be programmed as a function of nacelle incidence, angle of attack and sideslip angle to decrease rotor loads and to improve aircraft stability. The data of Figures 148 and 149 have been faired to illustrate the effects of lateral cyclic inputs at constant power and at constant thrust. These figures indicate an aircraft yawing moment coefficient variation with A_1 , C_{nA_1} , at constant thrust of $.027$ for the left rotor and $-.027$ for the right rotor, and at constant power $C_{nA_1} = .024$ for the left rotor and $-.0223$ for the right rotor. Rolling moment coefficient

variation with $A_1, C_{\ell A_1}$, at constant thrust is .020 for the left rotor and -.014 for the right rotor, and at constant power is .0127 for the left rotor and -.0115 for the right rotor. The lift and pitching moment coefficient data of Figures 150 and 151 have been faired for constant power and indicate a variation of lift coefficient with $A_1, C_{L A_1}$, of .0083 for the left rotor and -.012 for the right rotor. Pitching moment coefficient variation with $A_1, C_{m A_1}$, is indicated to be .025 for the left rotor and .012 for the right rotor.

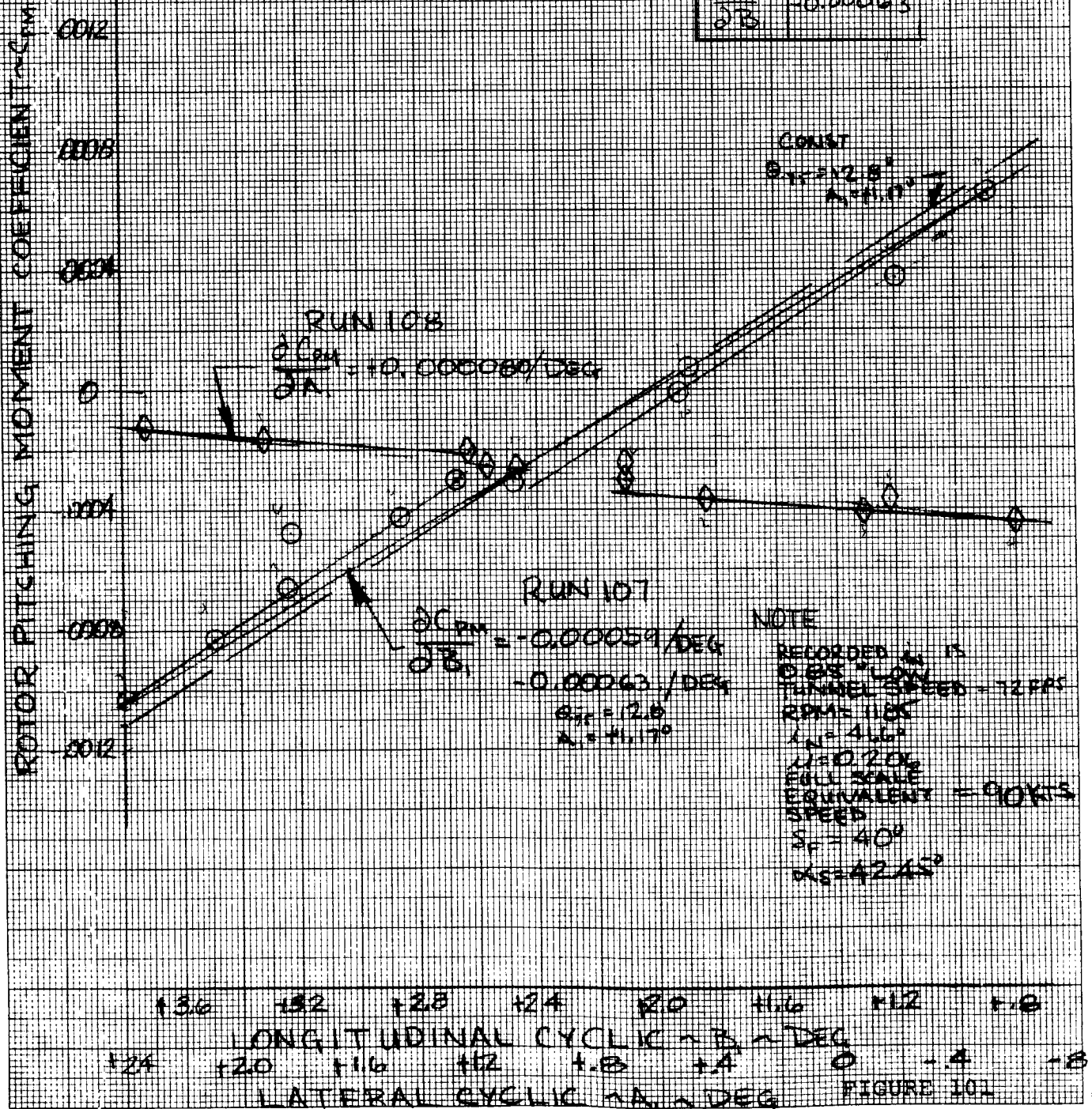
EFFECT OF CYCLIC IN TRANSITION ON ROTOR NORMAL FORCE CHARACTERISTICS RIGHT ROTOR



EFFECT OF CYCLIC IN TRANSITION ON ROTOR PITCHING MOMENT CHARACTERISTICS

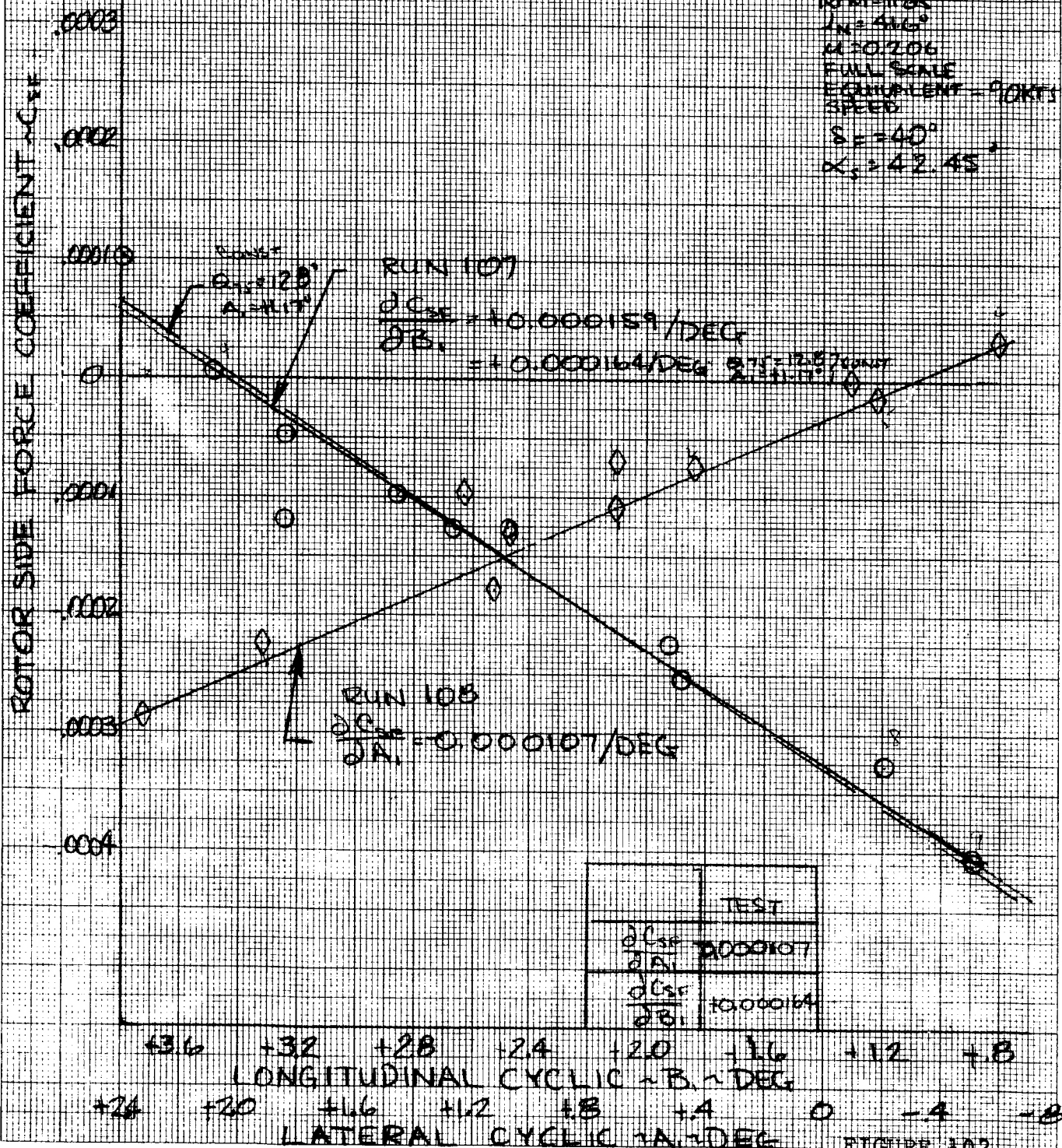
RIGHT ROTOR

TEST	
$\frac{\partial C_m}{\partial \alpha}$	10.000080
$\frac{\partial C_m}{\partial \beta}$	-0.00063



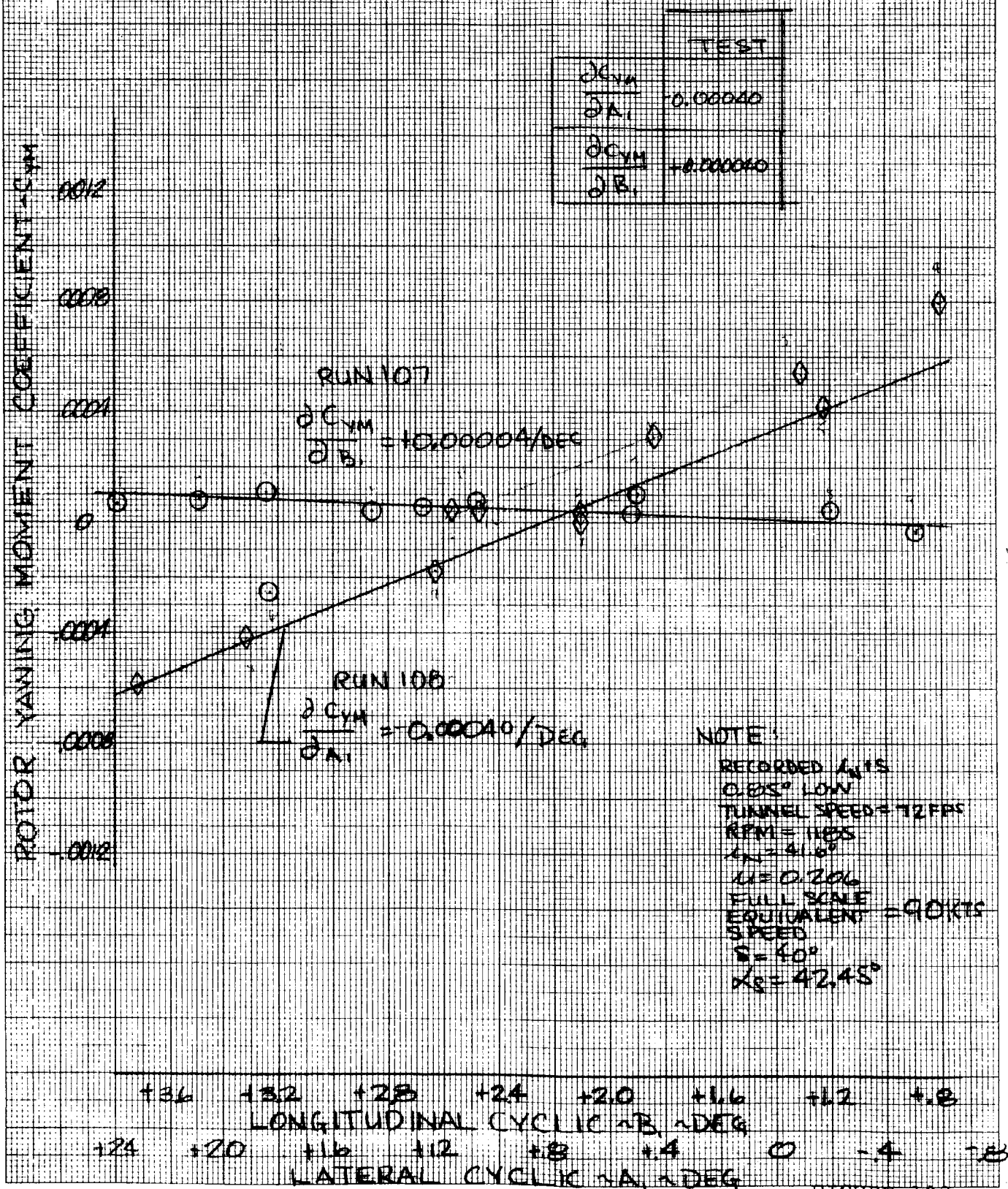
EFFECT OF CYCLIC IN TRANSITION ON ROTOR SIDE FORCE CHARACTERISTICS RIGHT ROTOR

NOTE:
RECORDED $\lambda_{1/3}$
0.85° LOW
TUNNEL SPEED = 7228
RPM = 1185
 $\lambda_{1/3} = 4.6^\circ$
 $\mu = 0.706$
FULL SCALE
EQUIVALENT = 90KTS
SPEED
 $\delta = 40^\circ$
 $\alpha_s = 42.45^\circ$



EFFECT OF CYCLIC IN TRANSITION ON ROTOR YAWING MOMENT CHARACTERISTICS

RIGHT ROTOR

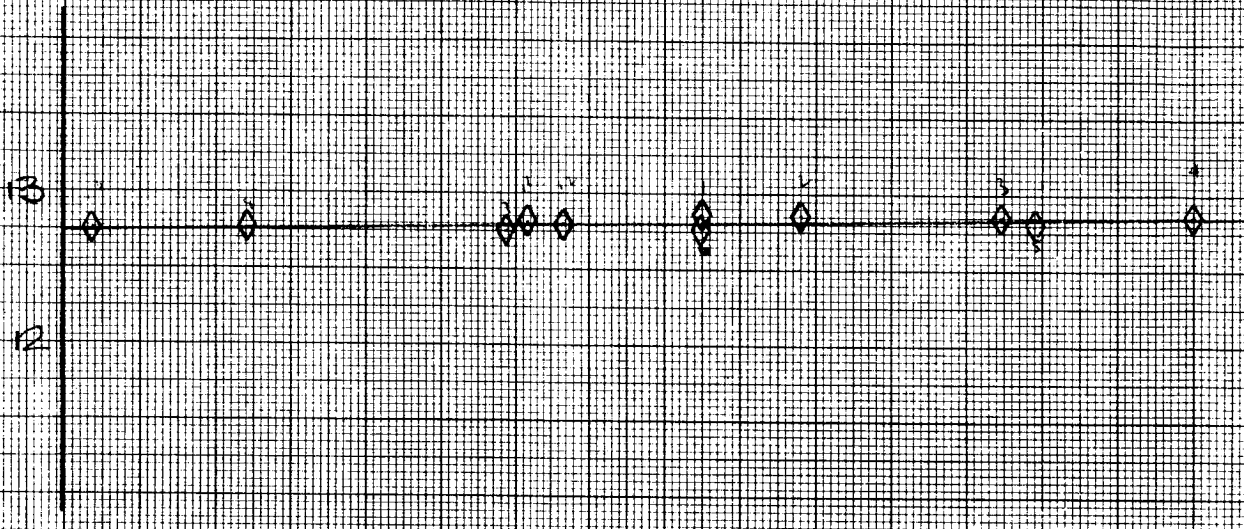


LONGITUDINAL CYCLIC AND BLADE COLLECTIVE
CHANGES DURING LATERAL CYCLIC SWEEP

RIGHT ROTOR

RUN 108

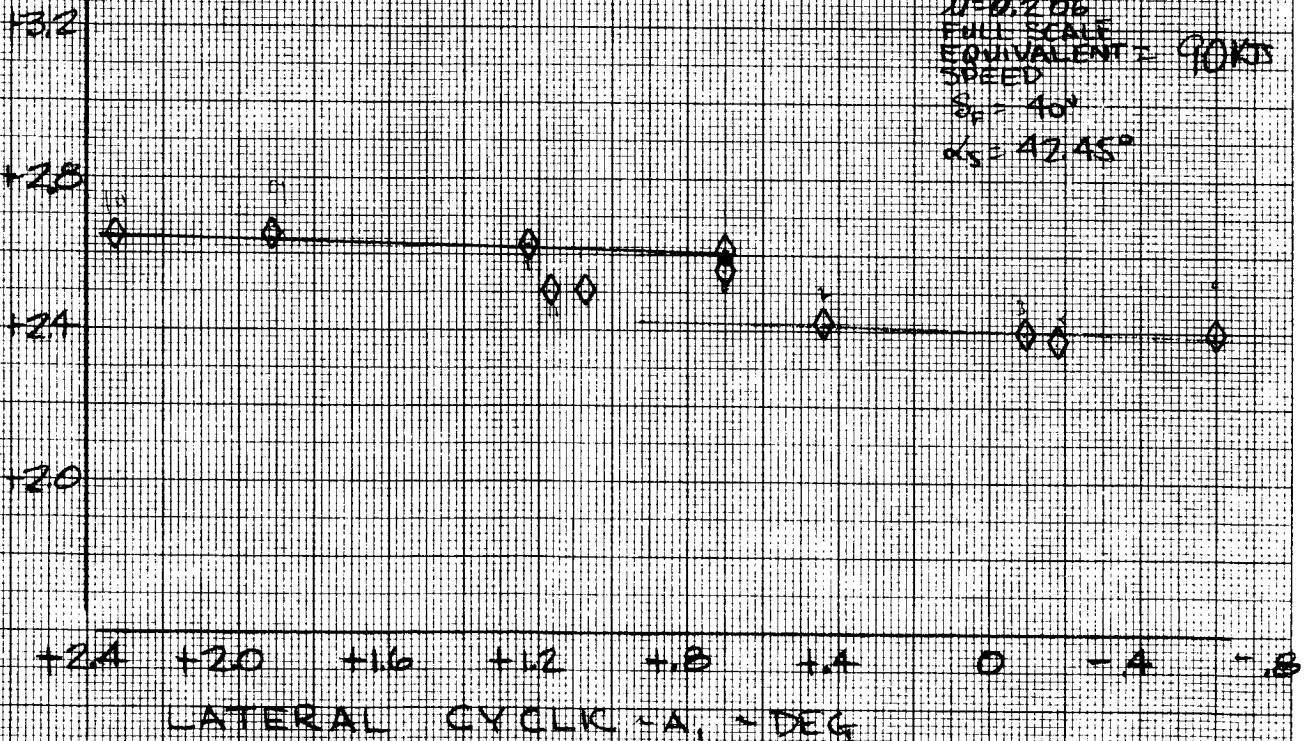
BLADE COLLECTIVE $\sim \delta_{11}$ - DEG



NOTE:

RECORDED $\lambda_{0.15} = 15$
 0.85° LOW
 TUNNEL SPEED = 72 MPH
 RPM = 1185
 $\lambda_{0.15} = 4.6^\circ$
 $\lambda = 0.206$
 FULL SCALE
 EQUIVALENT ~ 90 KTS
 SPEED
 $\delta_0 = 40^\circ$
 $\alpha_s = 42.45^\circ$

LONGITUDINAL CYCLIC $\sim \delta_{11}$ - DEG



LATERAL CYCLIC $\sim A_1$ - DEG

FIGURE 104

LATERAL CYCLIC AND BLADE COLLECTIVE CHANGES DURING LONGITUDINAL CYCLIC SWEEP

BLADE COLLECTIVE ~ δ_1 , DEG

RIGHT ROTOR

RUN 107

NOTE:

RECORDED λ_N IS
0.85° LOW
TUNNEL SPEED = 72 FPS
RPM = 1165
 $\lambda_N = 4.6^\circ$
 $N = 0.206$
FULL SCALE
EQUIVALENT = 90 KTS
SPEED
 $\gamma_P = 40^\circ$

13
12

$$\frac{\partial \delta_1}{\partial \beta} = +0.367$$

$$\lambda_S = 42.45^\circ$$

LATERAL CYCLIC ~ δ_A , DEG

+16
+12
+8
+4
0

+36 +32 +28 +24 +20 +16 +12 +8

LONGITUDINAL CYCLIC ~ β , DEG

FIGURE 105

EFFECT OF COLLECTIVE IN TRANSITION
ON
ROTOR NORMAL FORCE CHARACTERISTICS

Run 109

RIGHT ROTOR

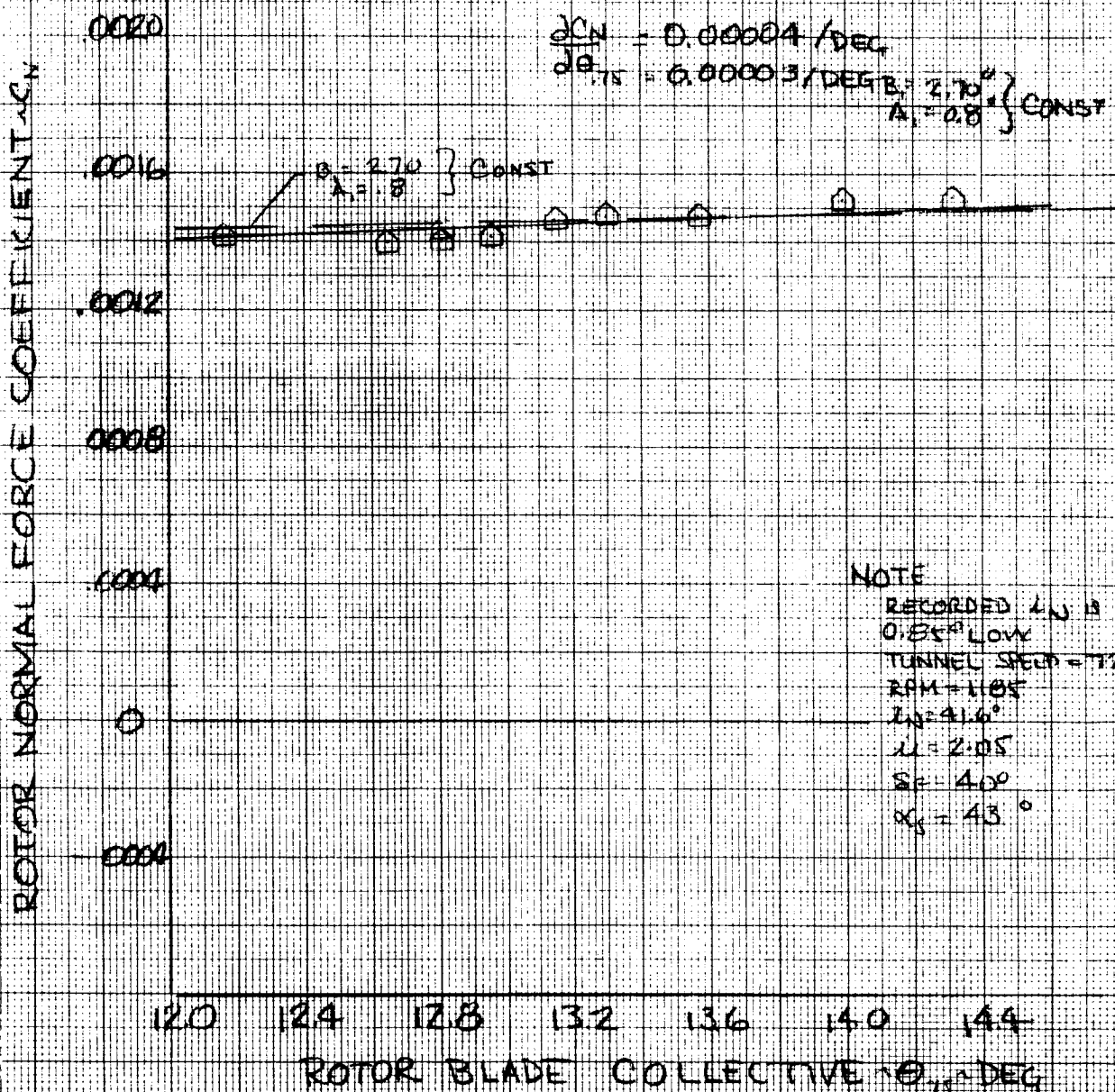


FIGURE 106

EFFECT OF COLLECTIVE IN TRANSITION
ON
ROTOR PITCHING MOMENT CHARACTERISTICS

RUN 109

RIGHT ROTOR

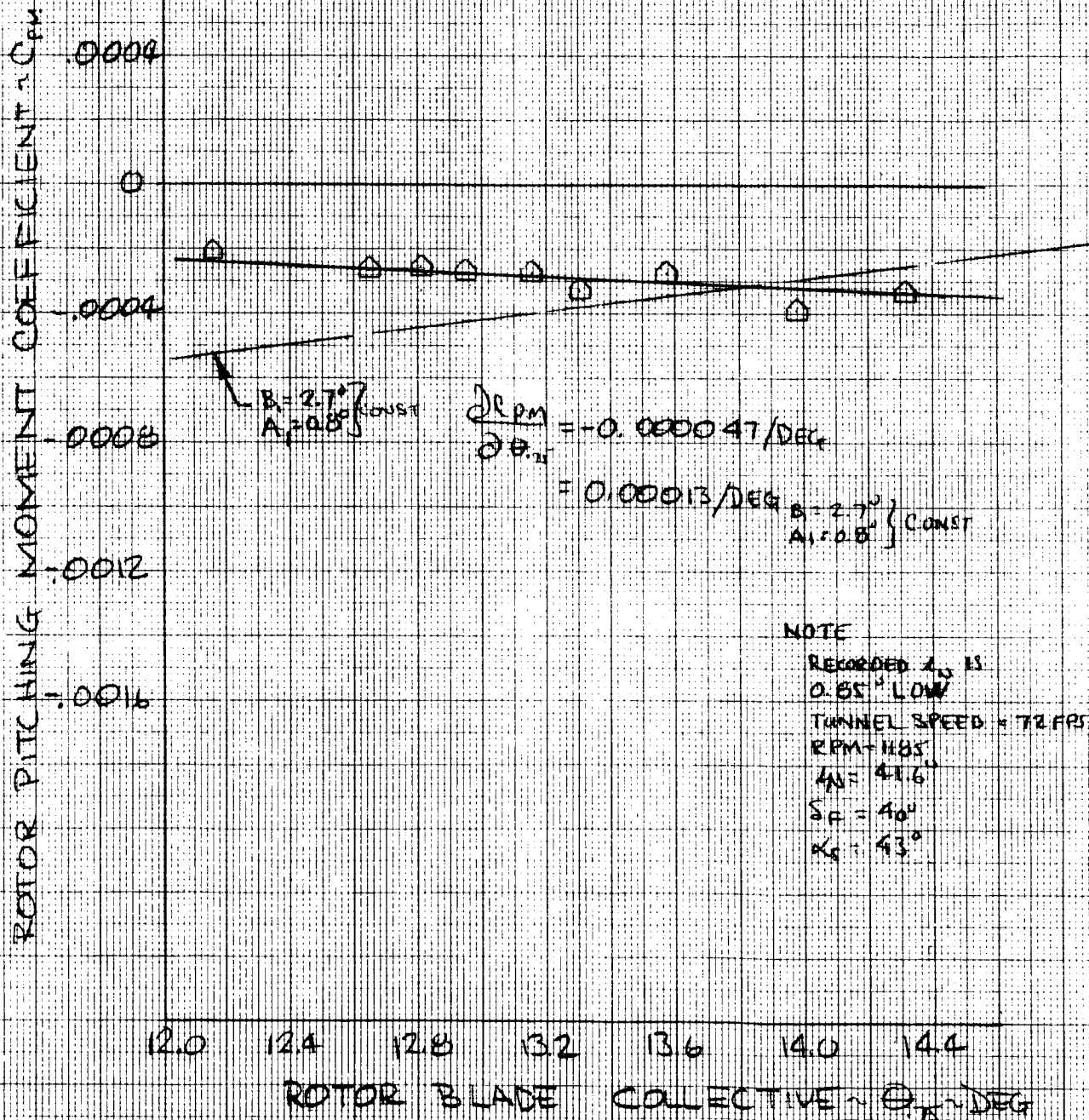


FIGURE 107

EFFECT OF COLLECTIVE IN TRANSITION ON ROTOR SIDE FORCE CHARACTERISTICS

RUN 109

RIGHT ROTOR

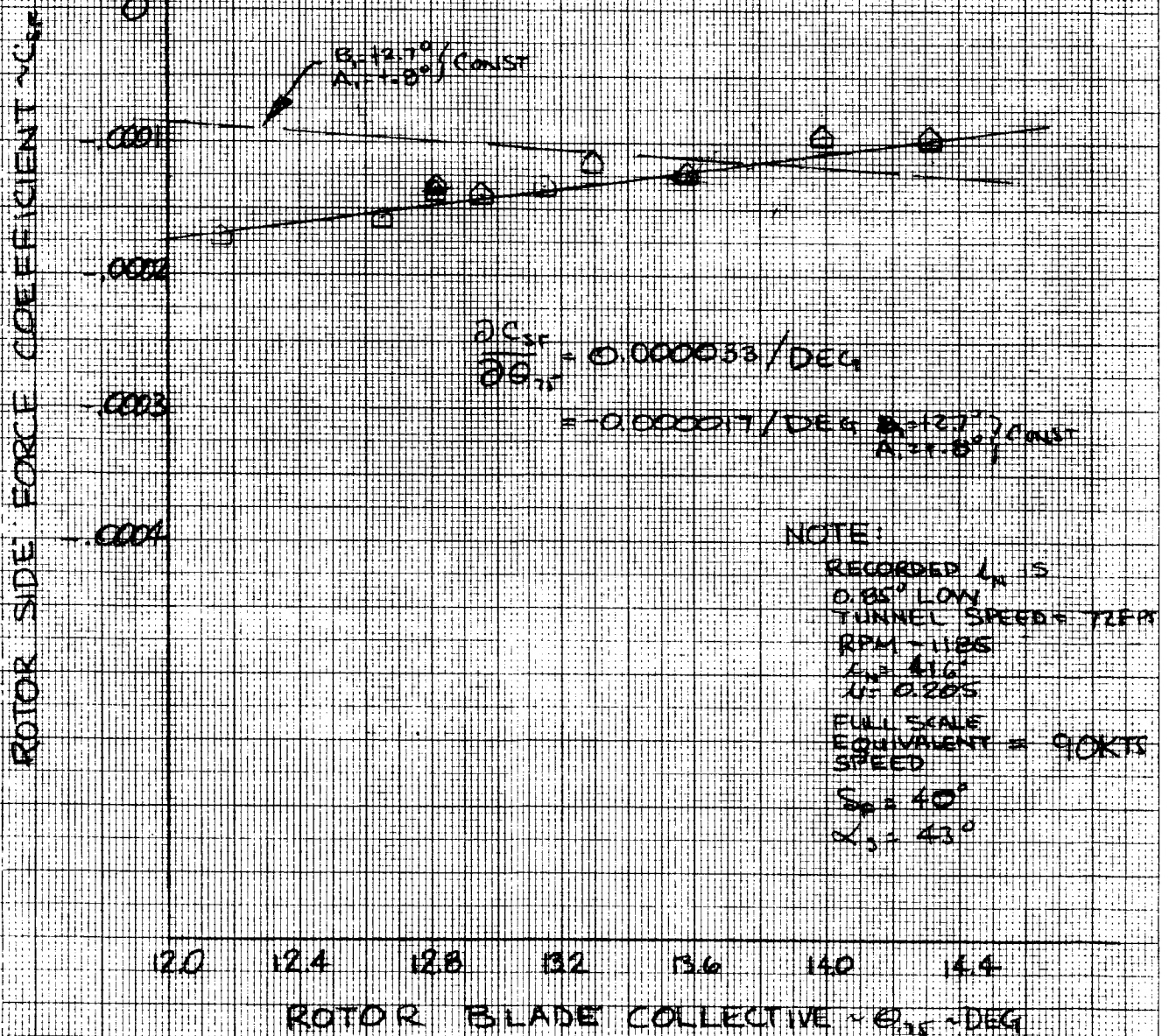
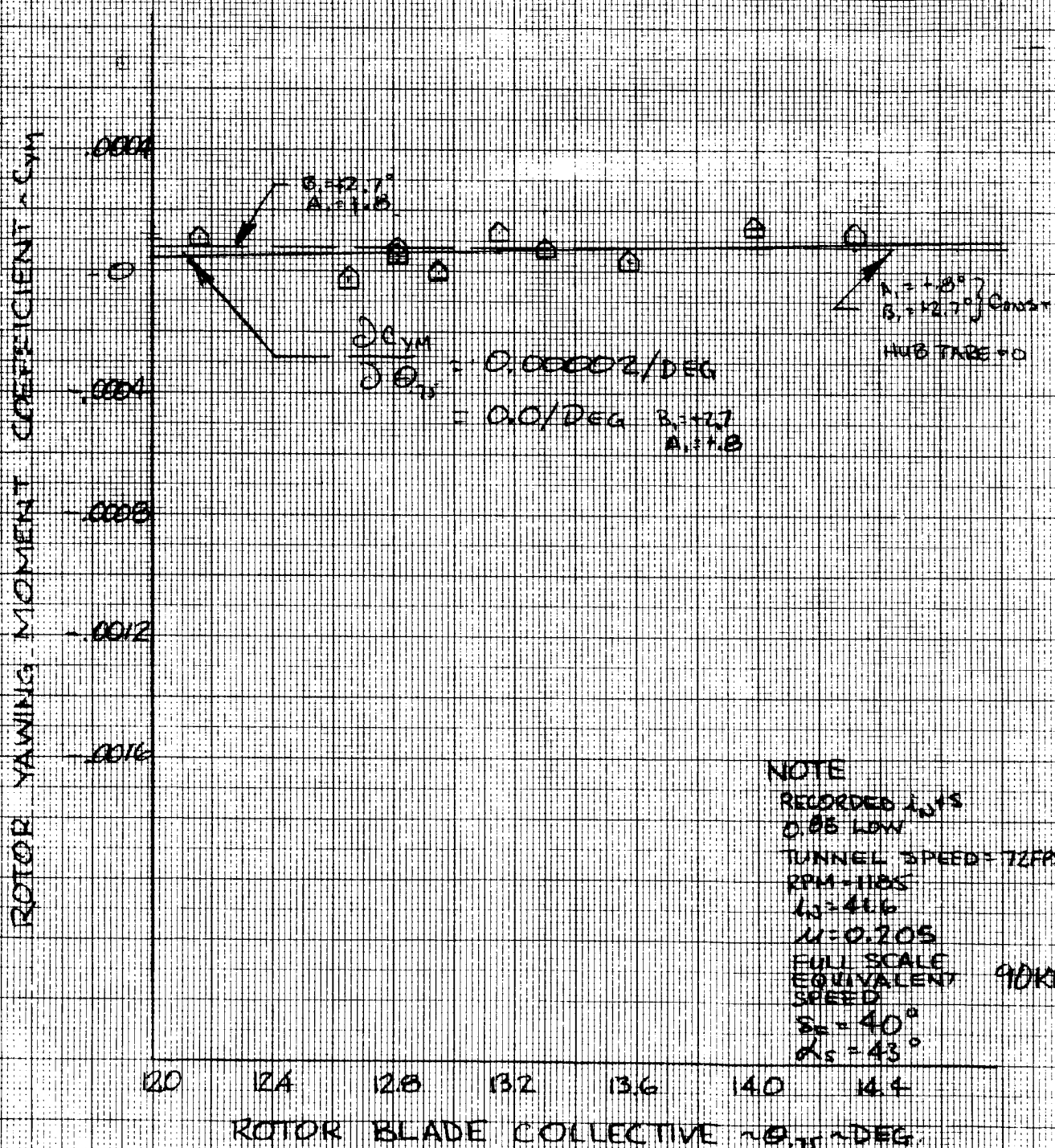


FIGURE 108

EFFECT OF COLLECTIVE IN TRANSITION ON ROTOR YAWING MOMENT CHARACTERISTICS

RUN 109

RIGHT ROTOR



LONGITUDINAL & LATERAL CYCLIC CHANGES DURING DIFFERENTIAL COLLECTIVE

RUN 109

RIGHT ROTOR

NOTE

RECORDED α IS
0.85° LOW
TUNNEL SPEED = 72 FPS
RPM = 485
 $\alpha = 41.6^\circ$
 $\beta = 0.205$
FULL SCALE
EQUIVALENT = 90 KTS
SPEED
 $\beta = 40^\circ$
 $\alpha_s = 43^\circ$

LATERAL CYCLIC
 A_1 - DEG

LONGITUDINAL CYCLIC
 B_1 - DEG

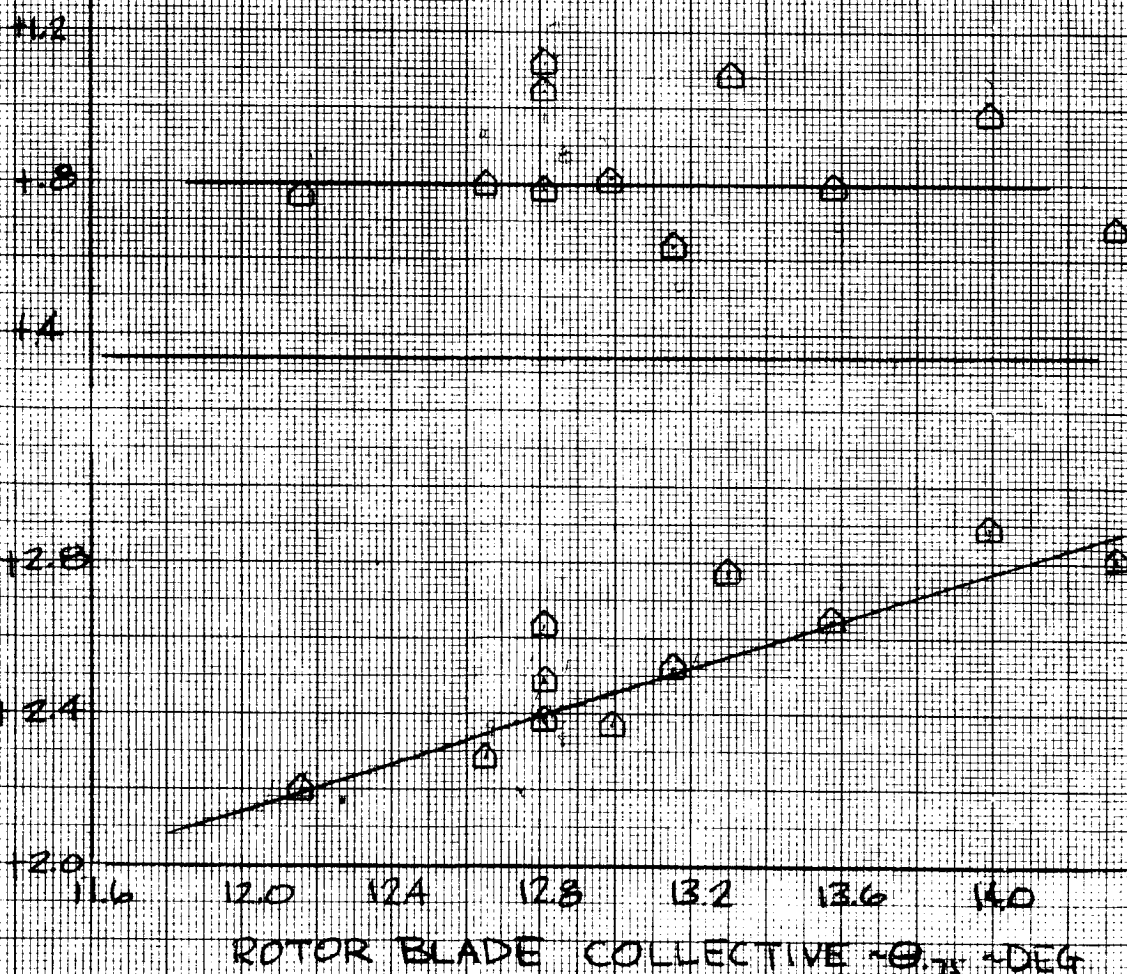


FIGURE 110

EFFECT OF ALERON DEFLECTION ON AIRCRAFT ROLLING MOMENT

TRANSITION

RUN 106
TUNNEL SPEED = 72 FPS
RPM = 1185
 $\mu = 0.205$
 $\delta^* = 40^\circ$
FULL SCALE
EQUIVALENT SPEED = 90 KTS
 $\alpha = 0^\circ$
 $\alpha_0 = 4.16^\circ$

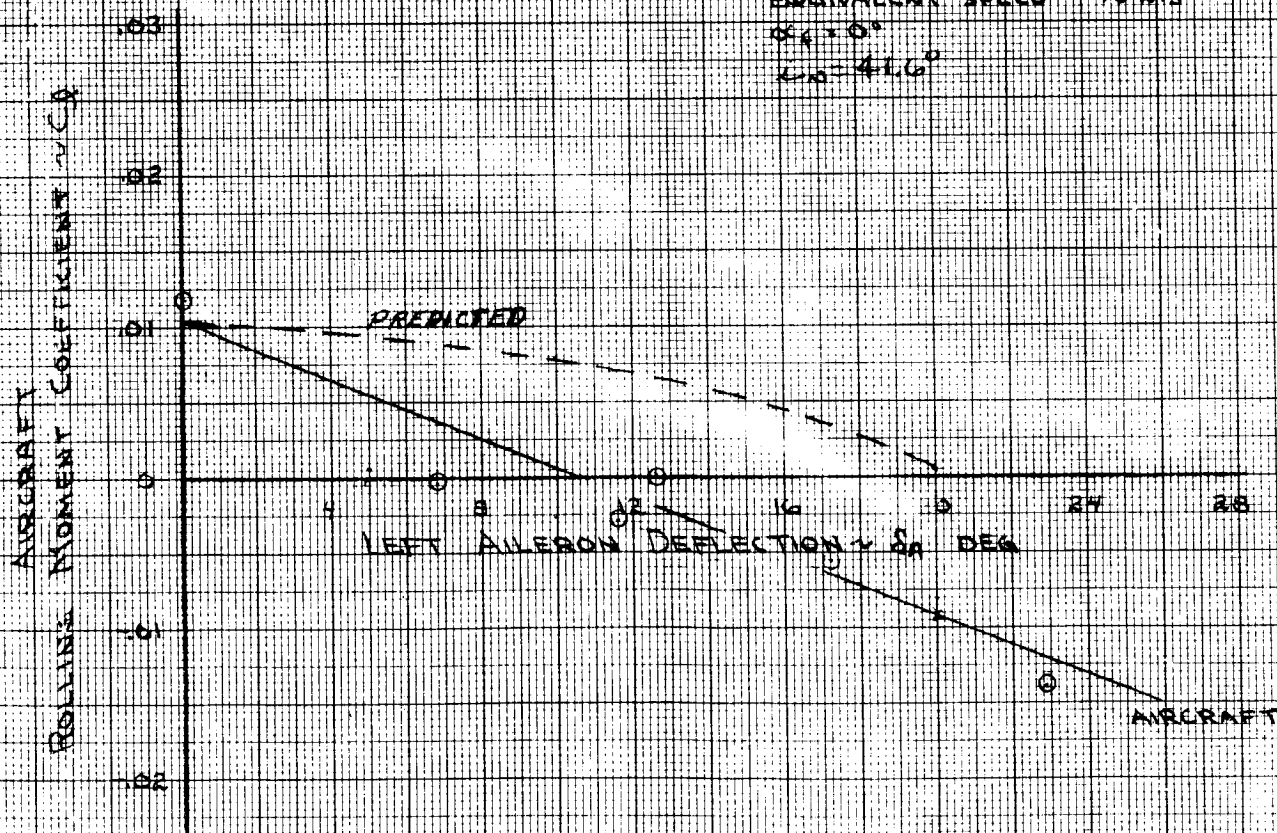


FIGURE 111

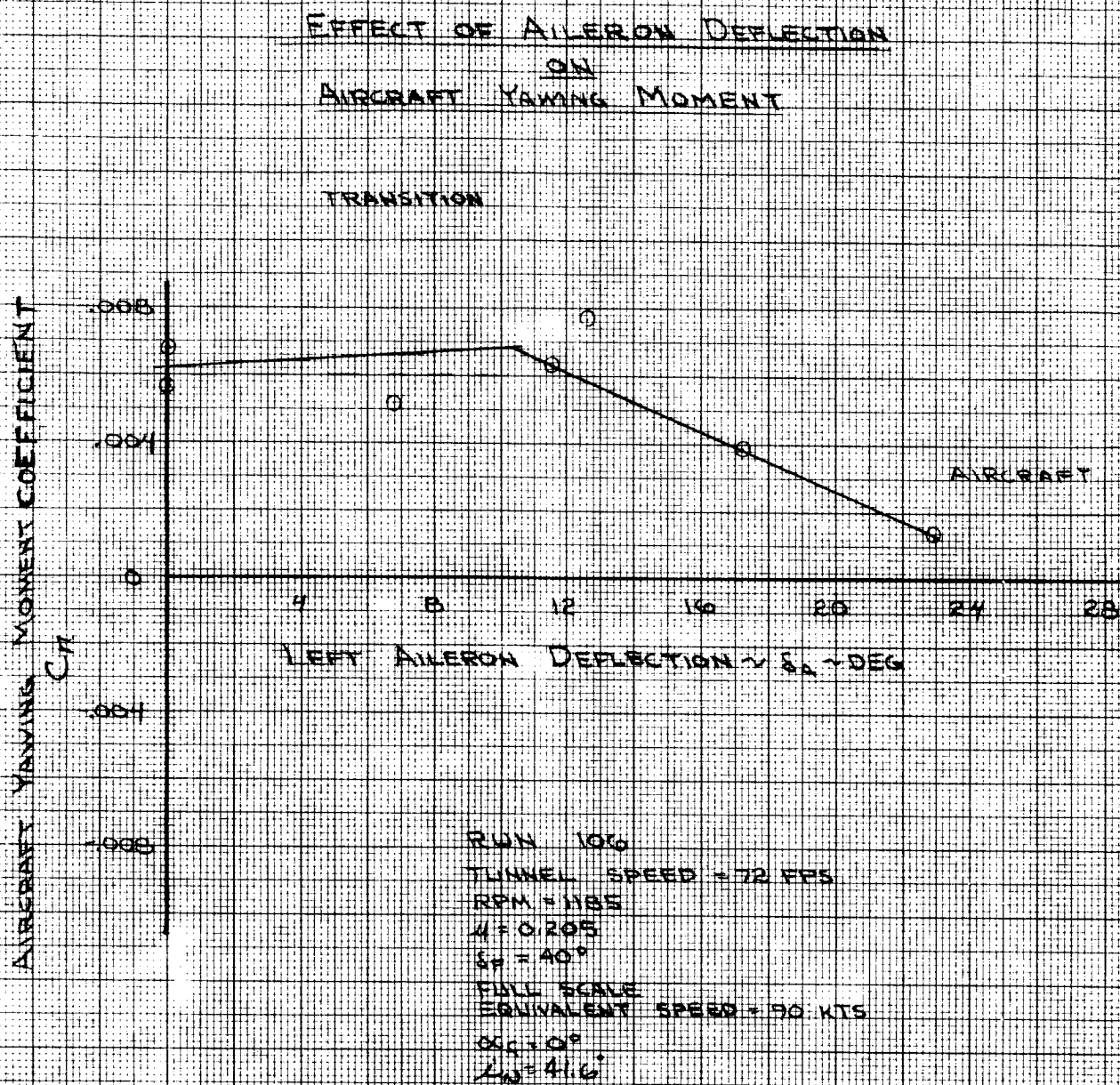


FIGURE 112

EFFECT OF AILERON DEFLECTION ON AIRCRAFT LATERAL STABILITY

TRANSITION

AIRCRAFT
LIFT COEFFICIENT $\sim C_L$

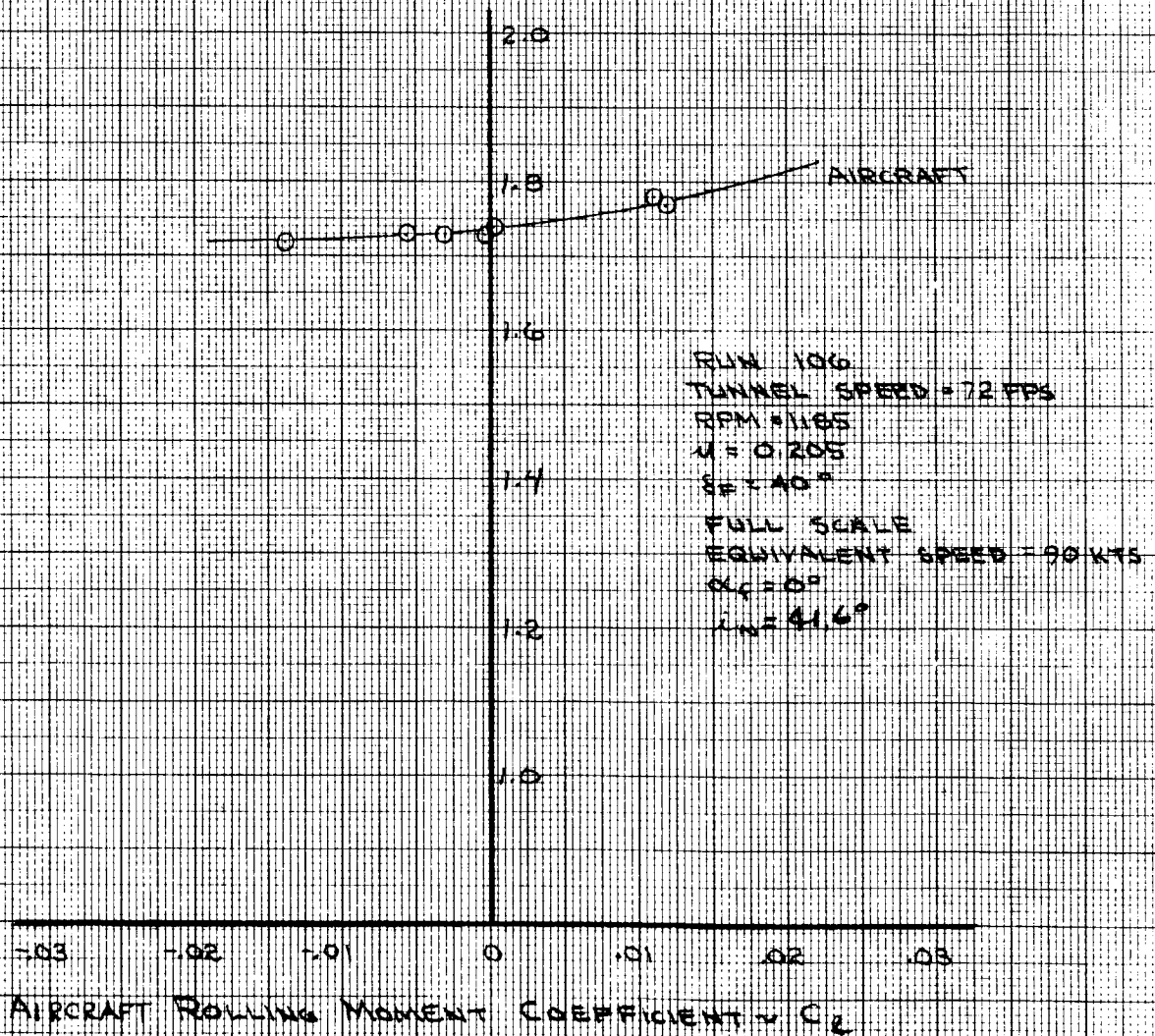


FIGURE 113

EFFECT OF AILERON DEFLECTION ON AIRCRAFT LIFT

TRANSITION

RUN 106
TUNNEL SPEED = 12 FPS
RPM = 1185
 $\mu = 41.6^\circ$
 $\beta = 6.0$ PSF
 $\delta_c = 40^\circ$
 $\delta_E = 16^\circ$
 $M = 0.205$
 $\alpha = 0^\circ$
FULL SCALE
EQUIVALENT - 90 KTS
SPEED

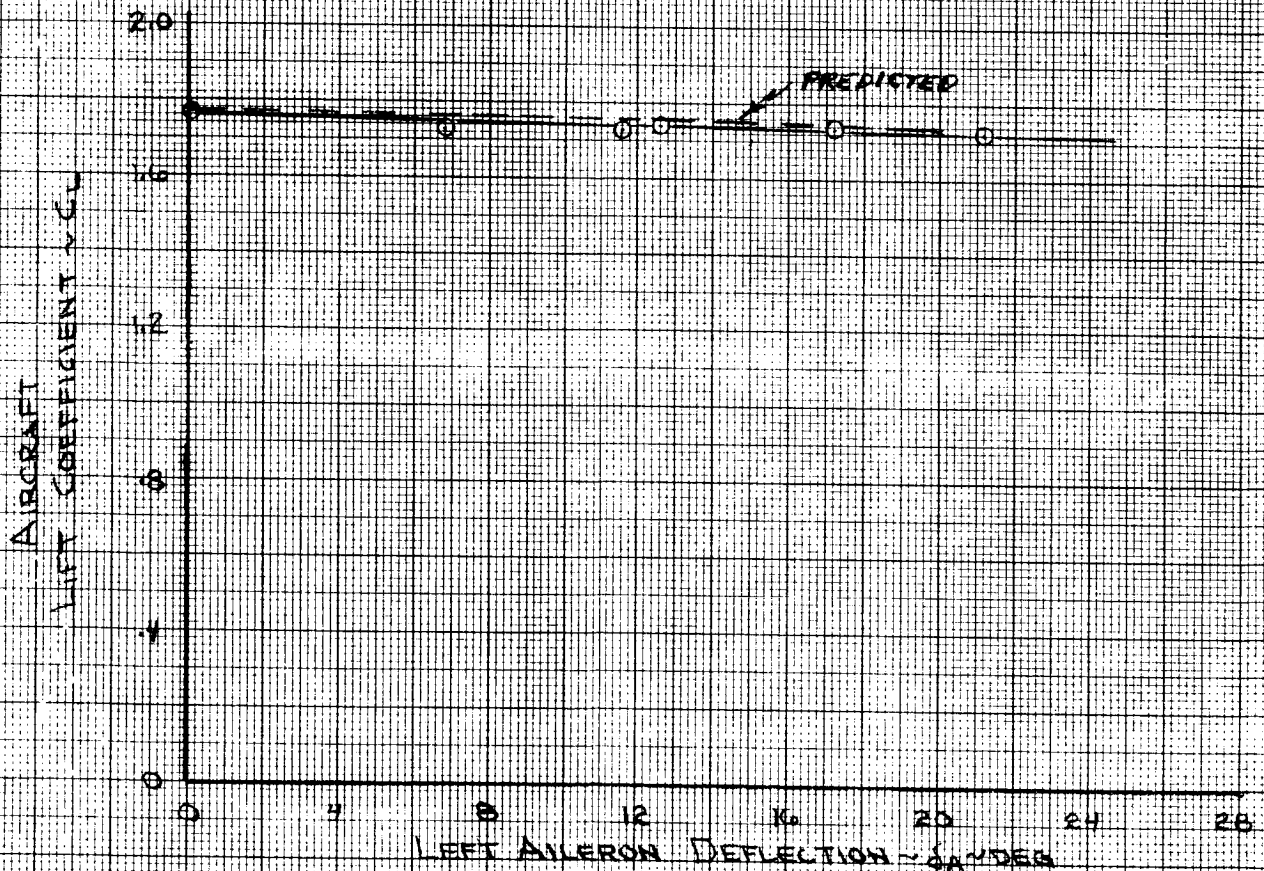


FIGURE 114

EFFECT OF AILERON DEFLECTION ON AIRCRAFT PITCHING MOMENT

TRANSITION

RUN 106
TUNNEL SPEED = 72 FPS
RPM = 1185
 $M = 0.205$
 $\delta_a = 40^\circ$
FULL SCALE
EQUIVALENT SPEED = 90 KTS
 $\alpha = 0^\circ$
 $\lambda = 41.6^\circ$

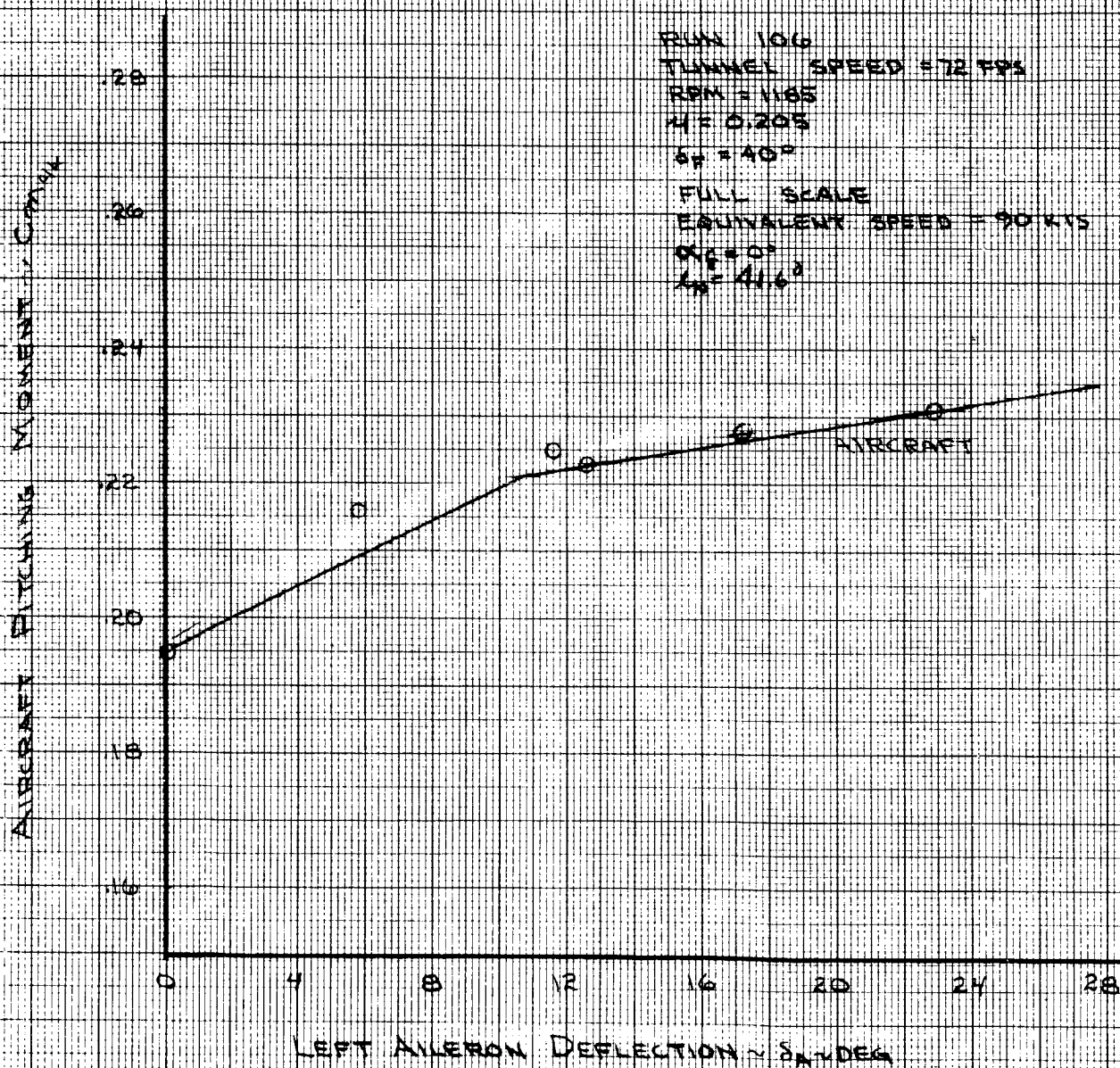


FIGURE 115

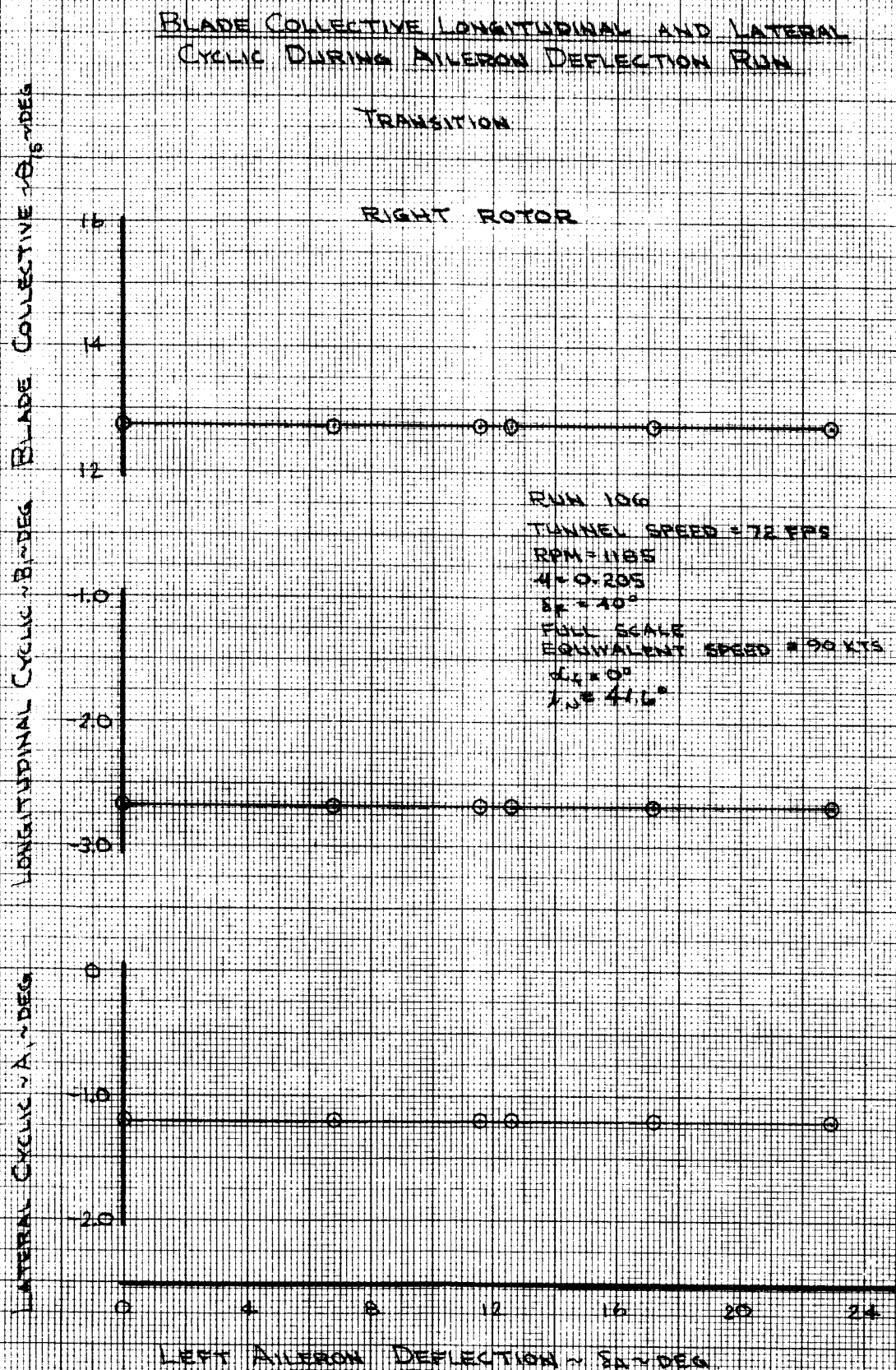


FIGURE 116

EFFECT OF AILERON DEFLECTION ON ROTOR THRUST & POWER

+ LEFT ROTOR
O RIGHT ROTOR

TRANSITION

ROTOR POWER COEFFICIENT
NCP

0.00064
0.00060
0.00056

RUN 106
TUNNEL SPEED = 72 FPS
RPM = 1185
 $\mu = 0.805$
 $\delta = 40^\circ$
FULL SCALE
EQUIVALENT SPEED = 90 KTS
 $C_{\delta} = 0^\circ$
 $\mu = 41.6^\circ$

ROTOR THRUST COEFFICIENT
NCT

0.028
0.024
0.020

0 4 8 12 16 20 24

LEFT AILERON DEFLECTION - δ_A - DEG

FIGURE 117

EFFECT OF AILERON DEFLECTION
ON
ROTOR NORMAL FORCE & PITCHING MOMENT ○ RIGHT ROTOR
TRANSITION

ROTOR PITCHING MOMENT
COEFFICIENT ~ CPM

ROTOR NORMAL FORCE
COEFFICIENT ~ CN

0.00028
0.00024
0.00020
0.00016

0.0020
0.0016
0.0012

0 4 8 12 16 20 24

LEFT AILERON DEFLECTION ~ δ_A ~ DEG

RUN 106

TUNNEL SPEED = 72 FPS

RPM = 1185

$\mu = 0.208$

$\delta_F = 40^\circ$

FULL SCALE

EQUIVALENT SPEED = 90 KTS

$\alpha_F = 0^\circ$

$\lambda_N = 4.6^\circ$

FIGURE 118

EFFECT OF AILERON DEFLECTION
ON
ROTOR SIDE FORCE AND YAWING MOMENT

○ RIGHT ROTOR

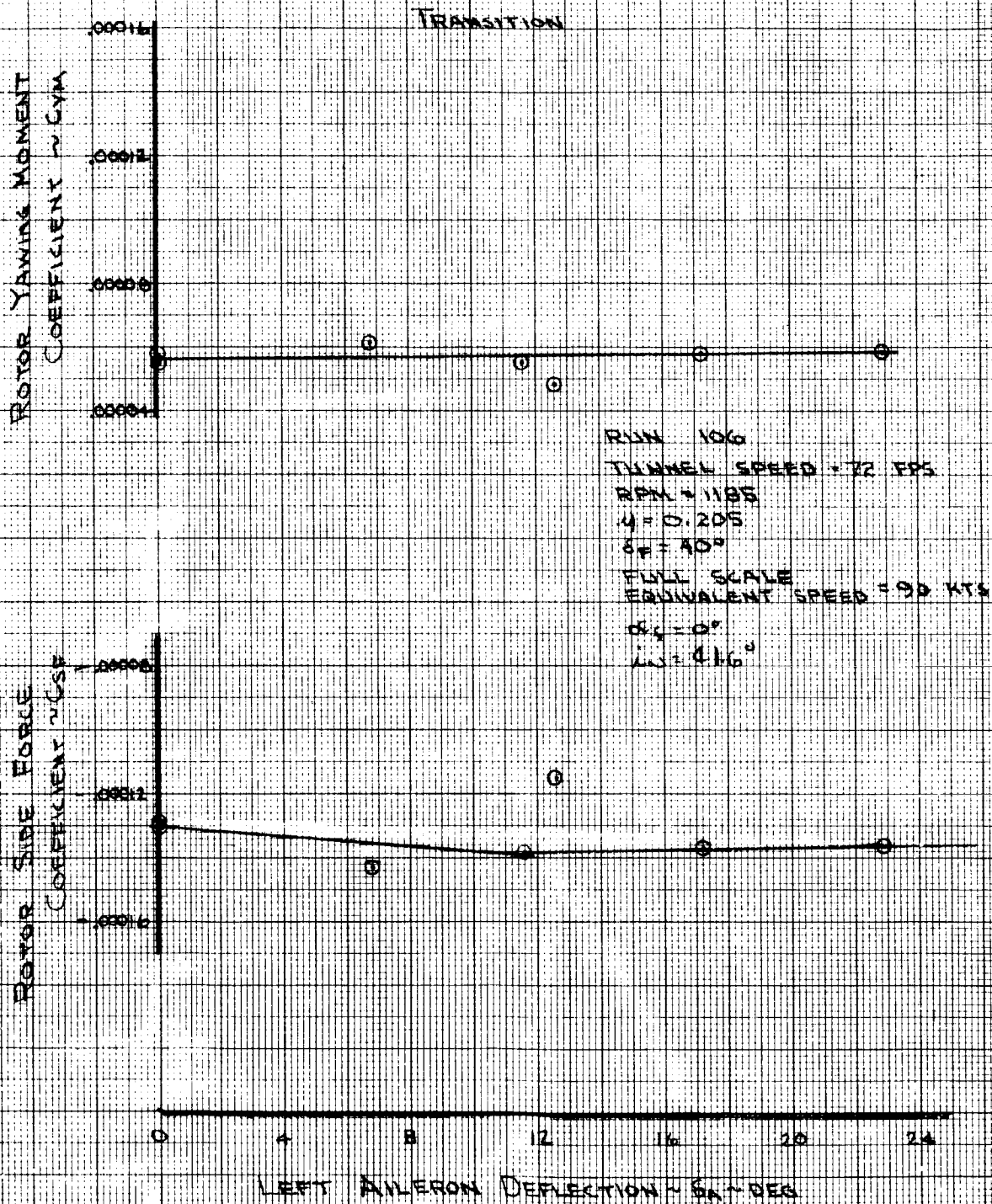


FIGURE 119

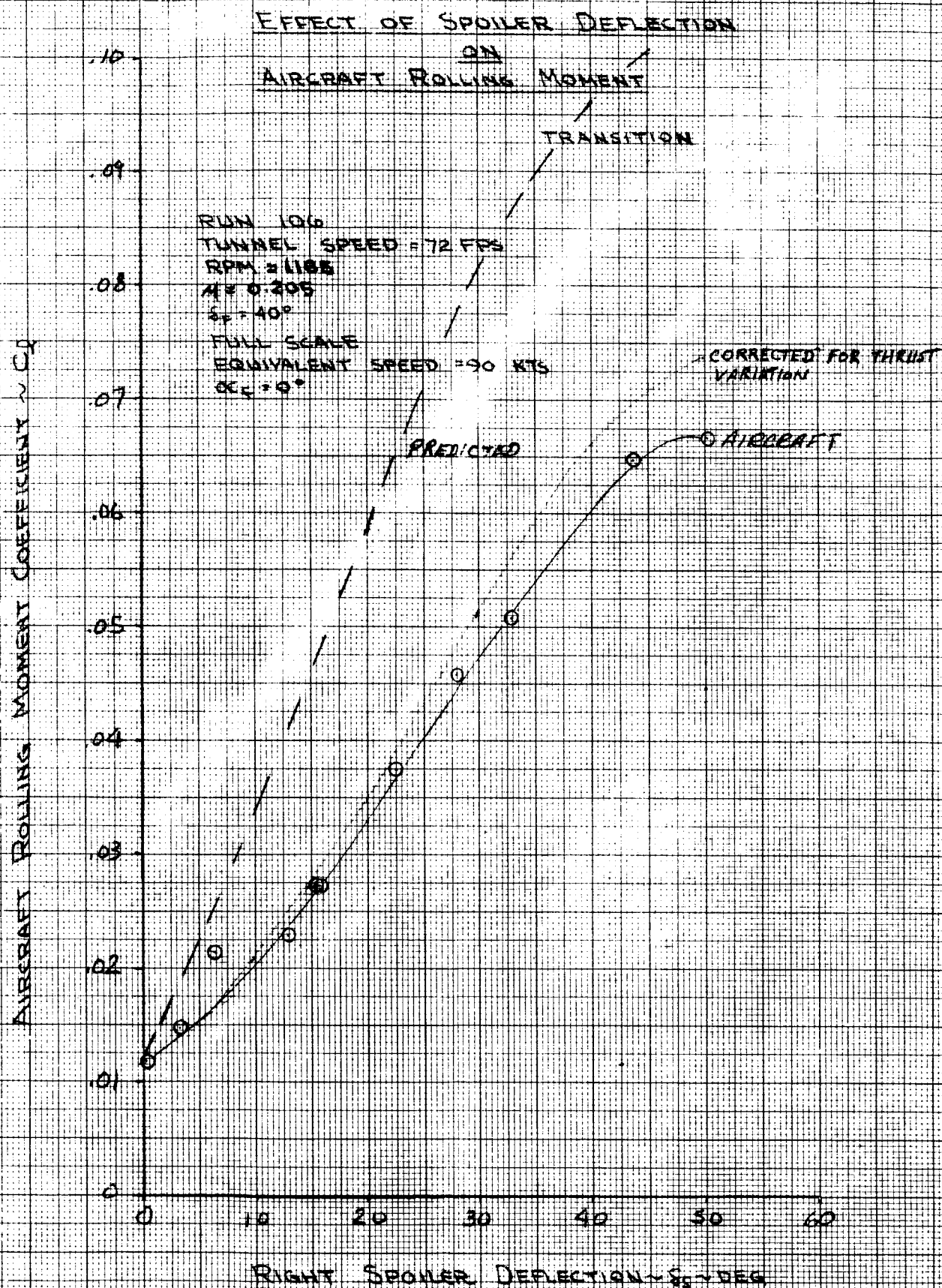


FIGURE 120

EFFECT OF SPOILER DEFLECTION ON AIRCRAFT YAWING MOMENT

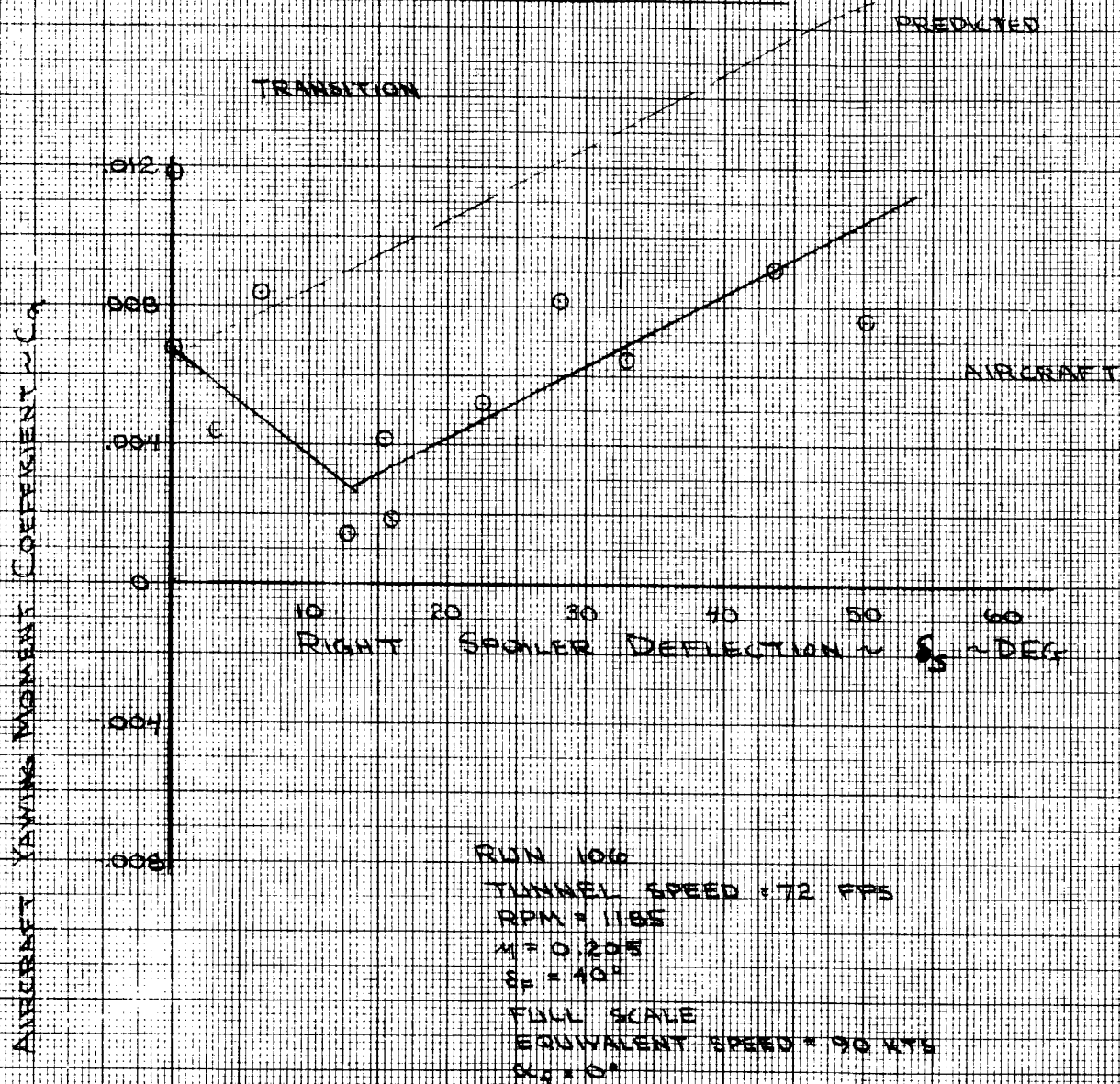


FIGURE 121

EFFECT OF SPOILER DEFLECTION ON AIRCRAFT LIFT

TRANSITION

RUN 106

TUNNEL SPEED = 72 FPS

RPM = 1185

 $\mu = 0.205$ $\delta_p = 10^\circ$

FULL SCALE

EQUIVALENT SPEED = 90 KTS

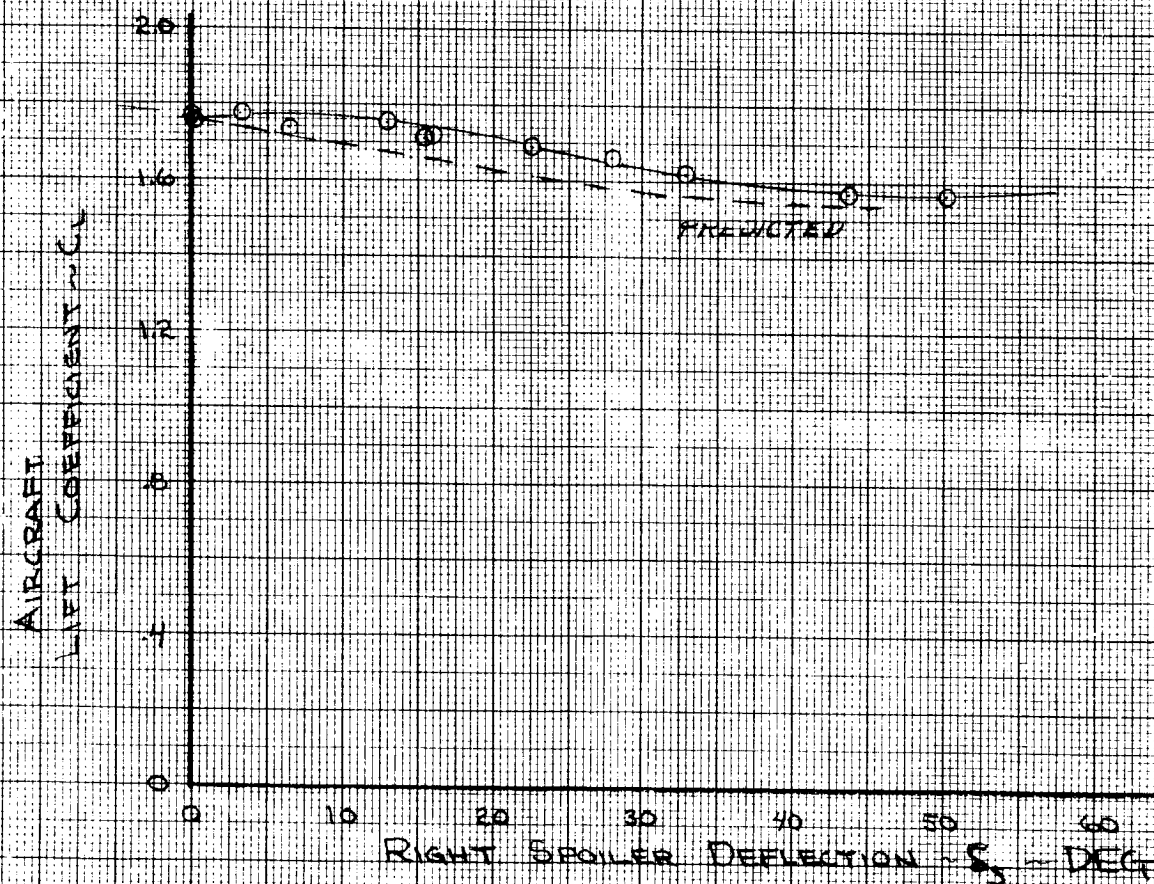
 $\alpha_c = 0^\circ$ 

FIGURE 122

EFFECT OF SPOILER DEFLECTION ON AIRCRAFT PITCHING MOMENT

TRANSITION

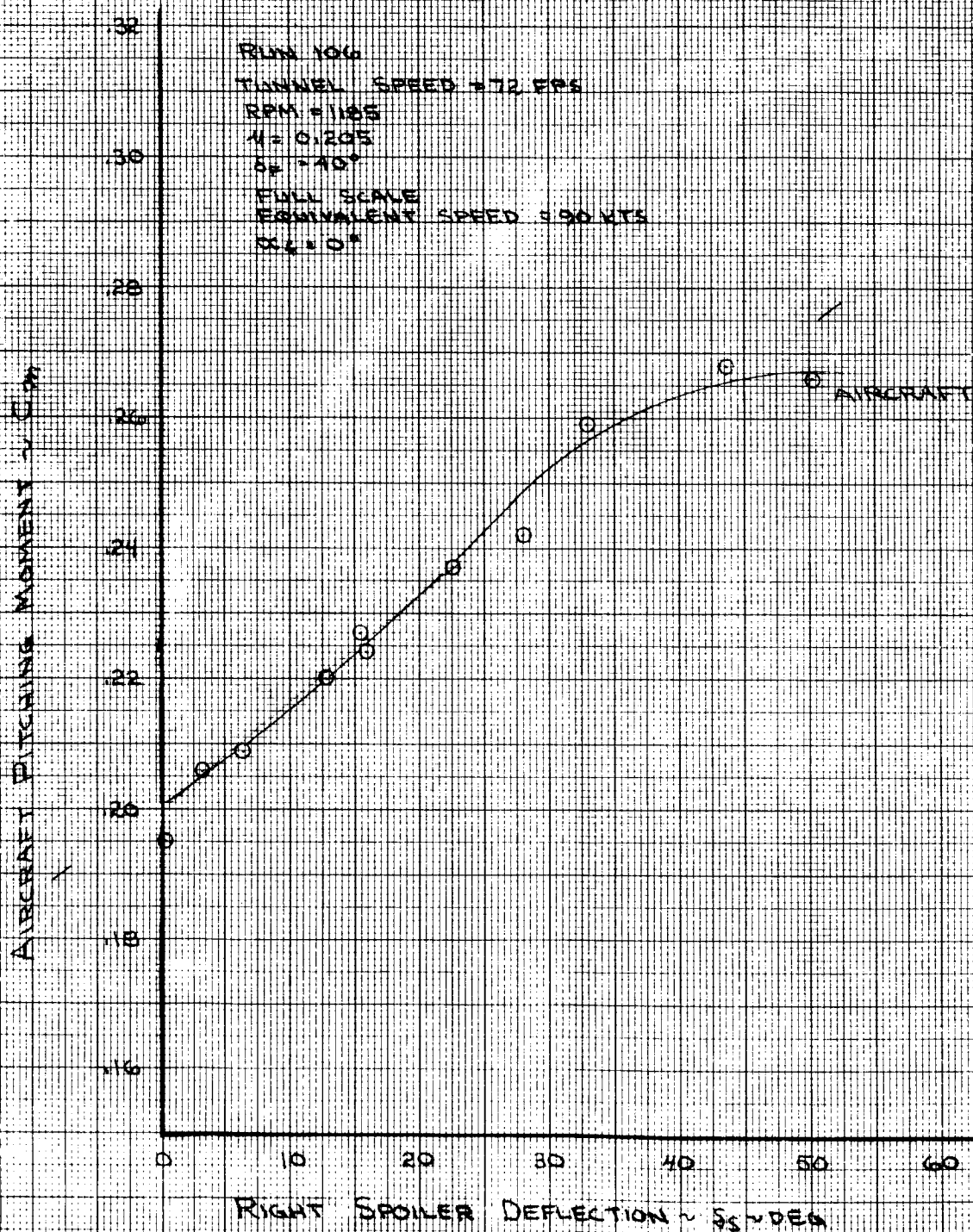


FIGURE 123

EFFECT OF SPOILER DEFLECTION
ON
AIRCRAFT LATERAL STABILITY

TRANSITION

PREDICTED

AIRCRAFT

RUN 106
TUNNEL SPEED = 72 FPS
RPM = 1185
 $\mu = 0.205$
 $\delta = 40^\circ$
FULL SCALE
EQUIVALENT SPEED = 90 KTS
 $\alpha = 0^\circ$

AIRCRAFT ROLLING MOMENT COEFFICIENT C_{Lr}

FIGURE 124

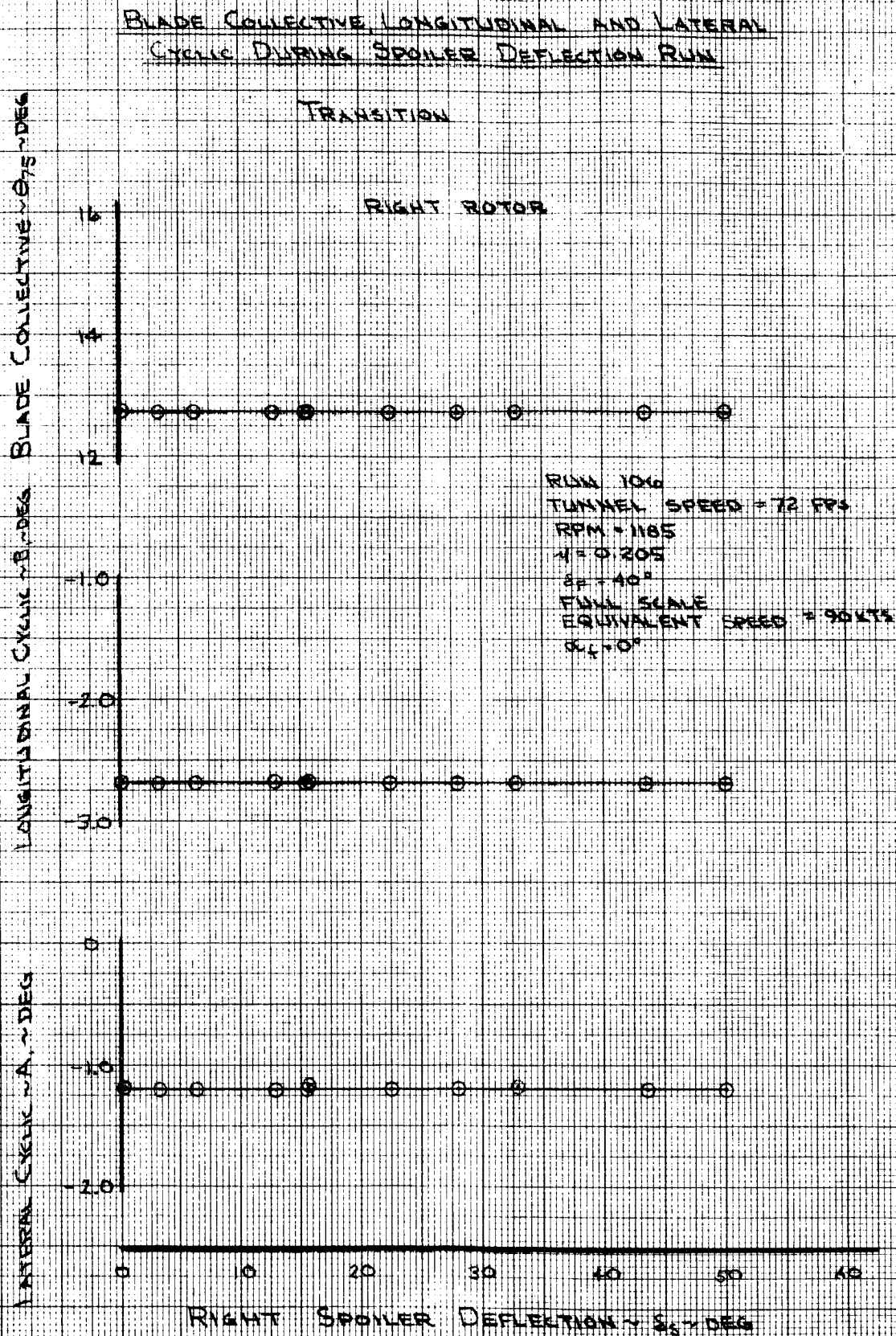
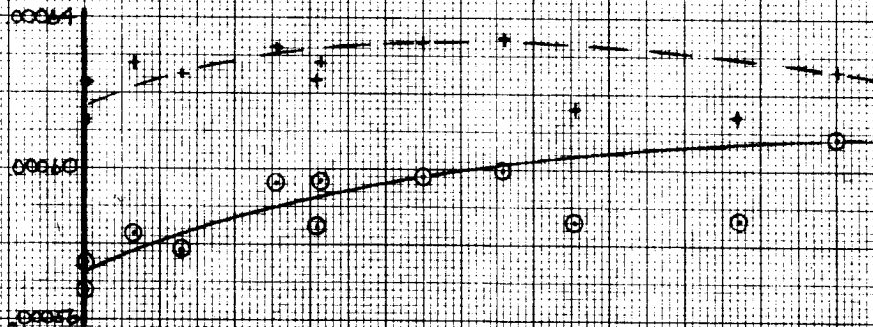


FIGURE 125

EFFECT OF SPOILER DEFLECTION ON ROTOR THRUST AND POWER TRANSITION

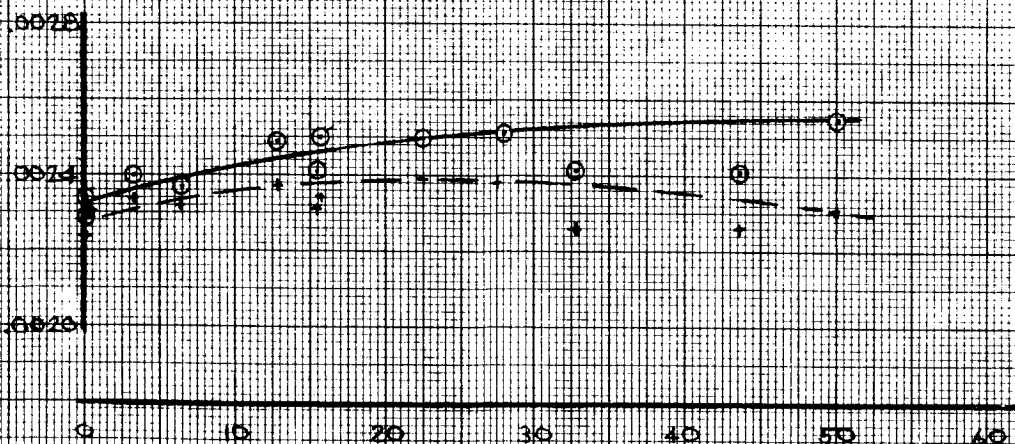
+ LEFT ROTOR
O RIGHT ROTOR

ROTOR POWER
COEFFICIENT $\sim C_P$



RUN 106
TUNNEL SPEED = 72 FPS
RPM = 1185
 $M = 0.205$
 $\delta_f = 40^\circ$
FULL SCALE
EQUIVALENT SPEED = 96 KTS
 $\alpha_f = 0^\circ$

ROTOR THRUST
COEFFICIENT $\sim C_T$



RIGHT SPOILER DEFLECTION $\sim \delta_s$ - DEG

FIGURE 126

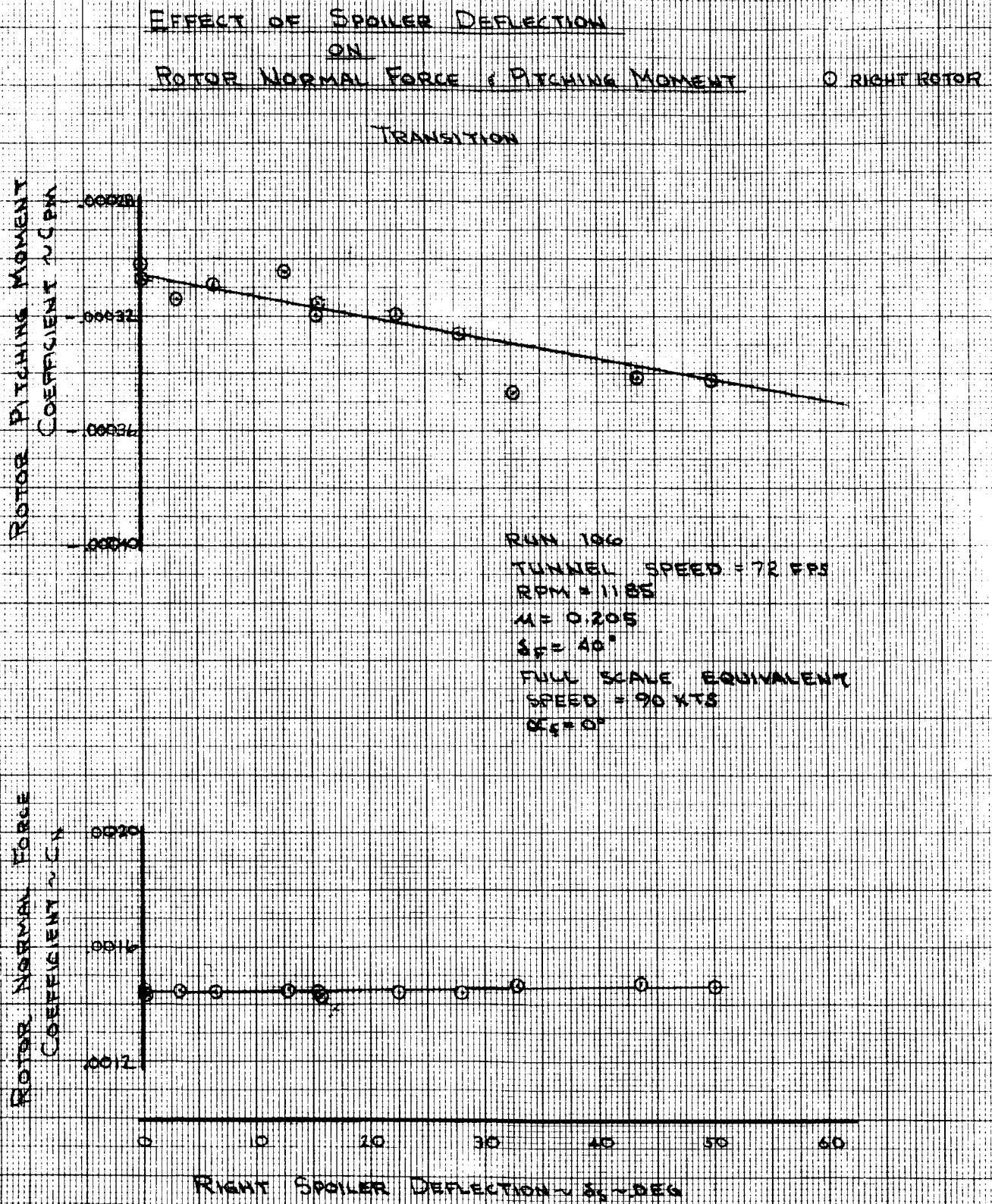


FIGURE 127

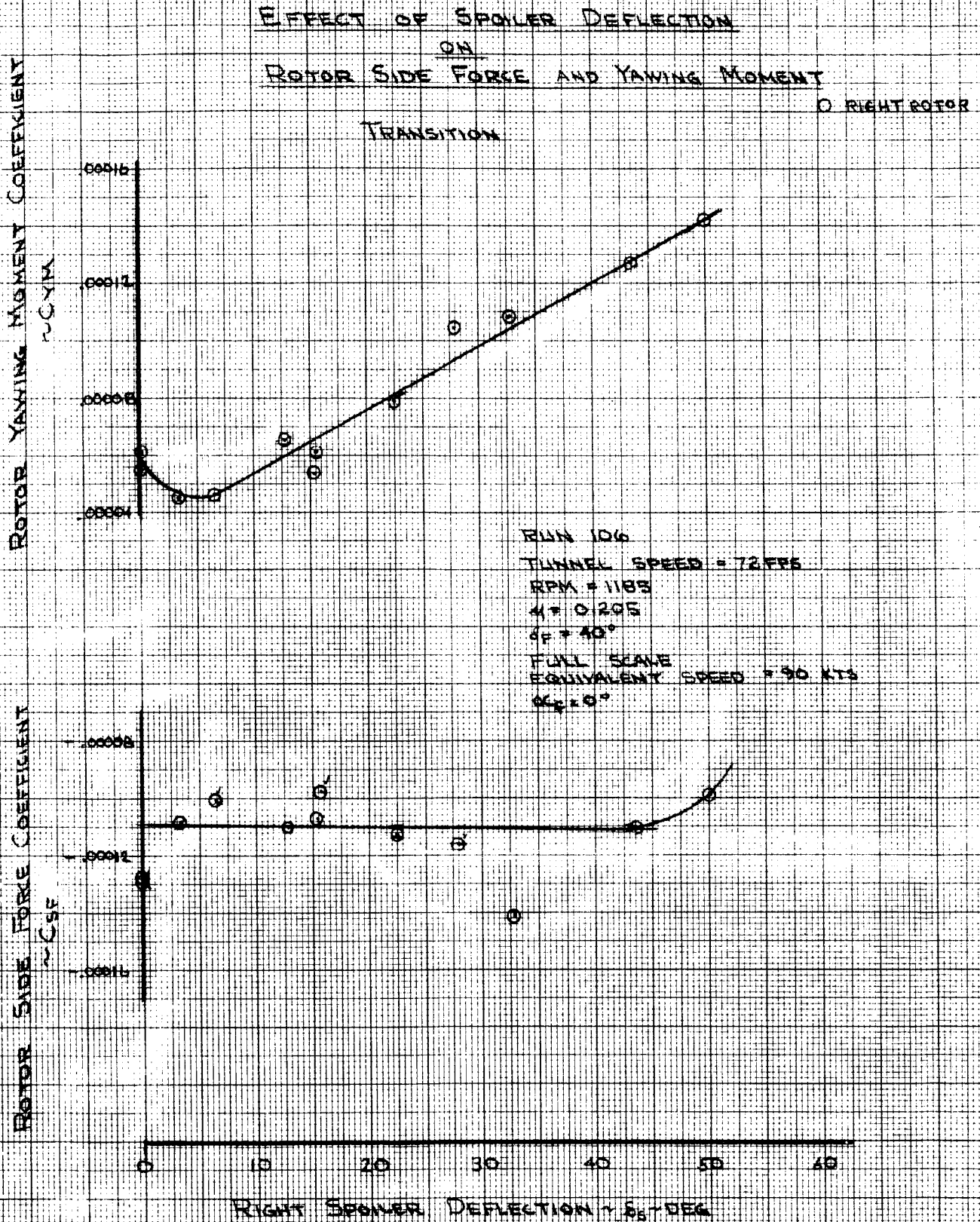


FIGURE 128

SCHEDULE OF AILERON DEFLECTION
VERSUS
SPOILER DEFLECTION
TRANSITION

Run 1016
TUNNEL SPEED = 72 FPS
RPM = 1185
 $\mu = 0.205$
 $\phi = 40^\circ$
FULL SCALE
EQUIVALENT SPEED = 90 KTS
 $\alpha = 0^\circ$
 $\lambda_1 = 41.6^\circ$

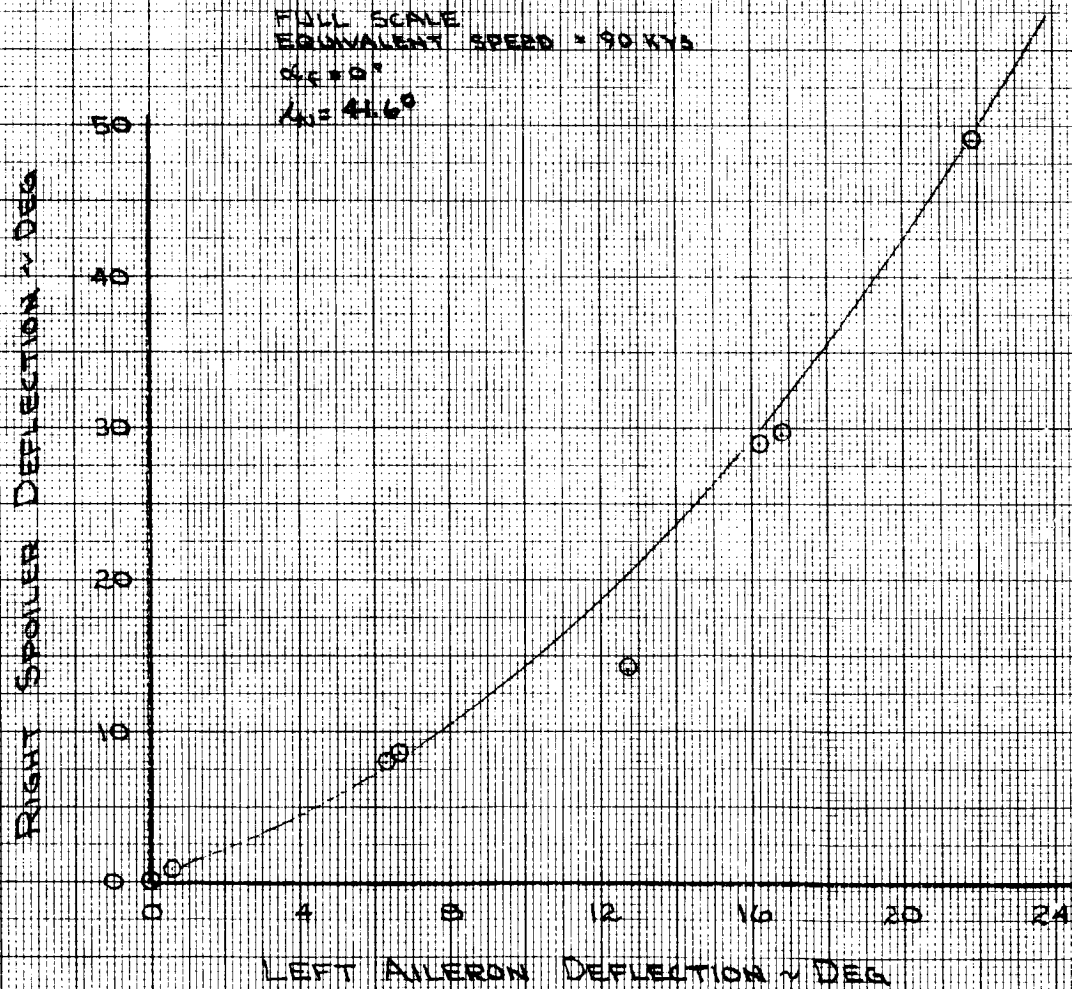
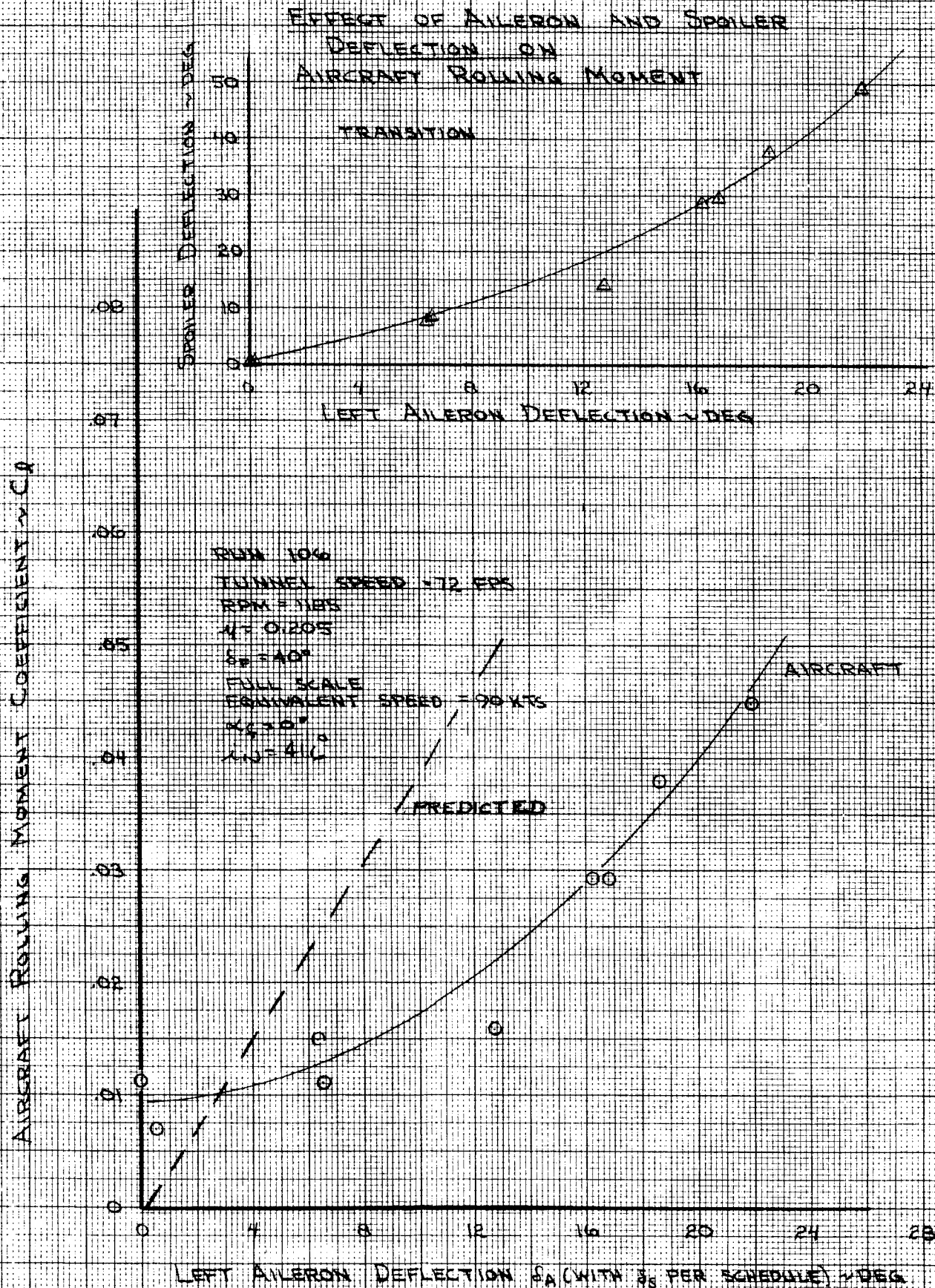


FIGURE 129

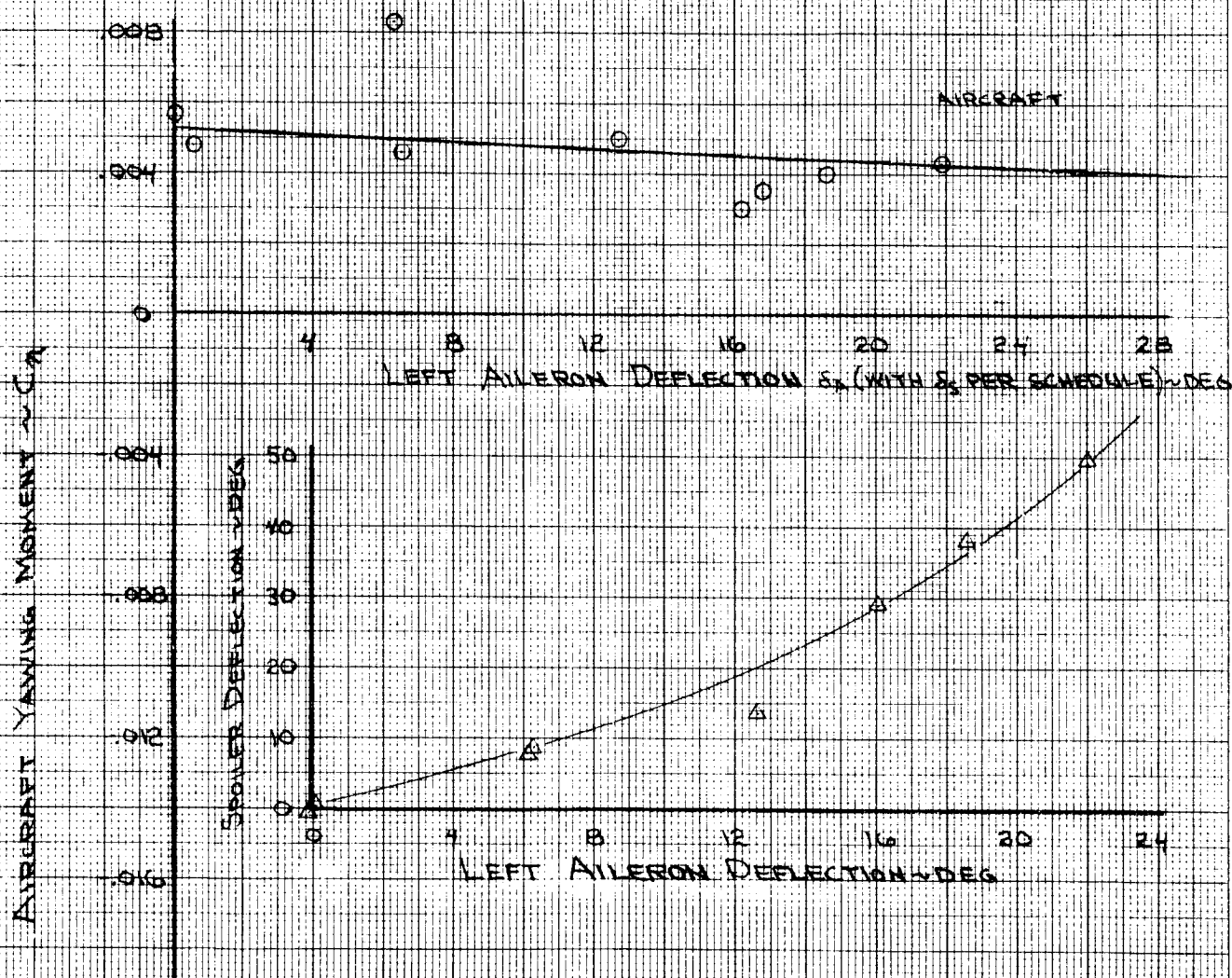


EFFECT OF AILERON AND SPOILER DEFLECTION

ON

AIRCRAFT YAWING MOMENT

TRANSITION



RUN 1016
TUNNEL SPEED = 72 FPS
RPM = 1185
 $M = 0.205$
 $\beta = 40^\circ$
FULL SCALE
EQUIVALENT SPEED = 90 KTS
 $\alpha_g = 0^\circ$
 $\alpha = 4.6^\circ$

FIGURE 131

EFFECT OF AILERON AND SPOILER DEFLECTION ON AIRCRAFT LIFT

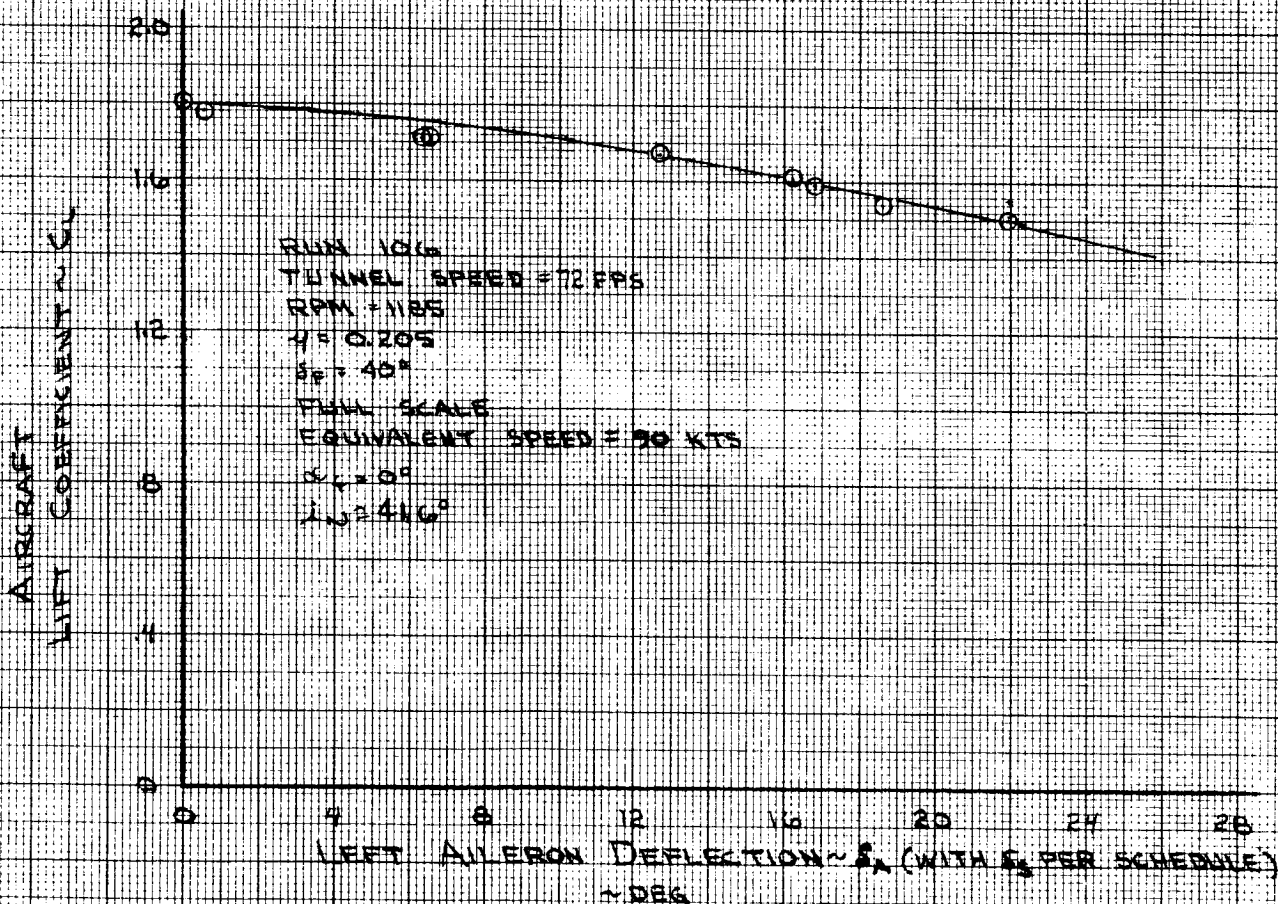
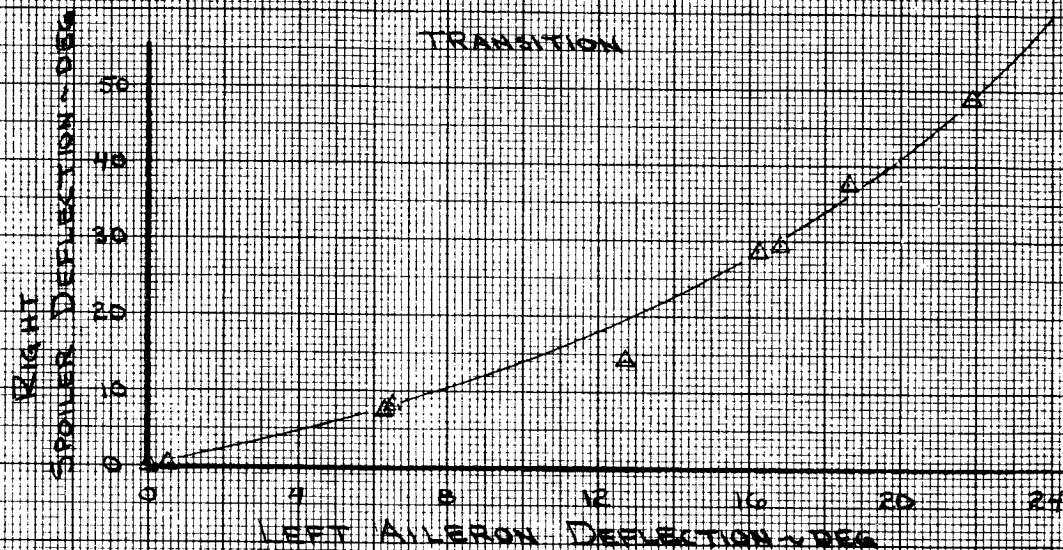


FIGURE 132

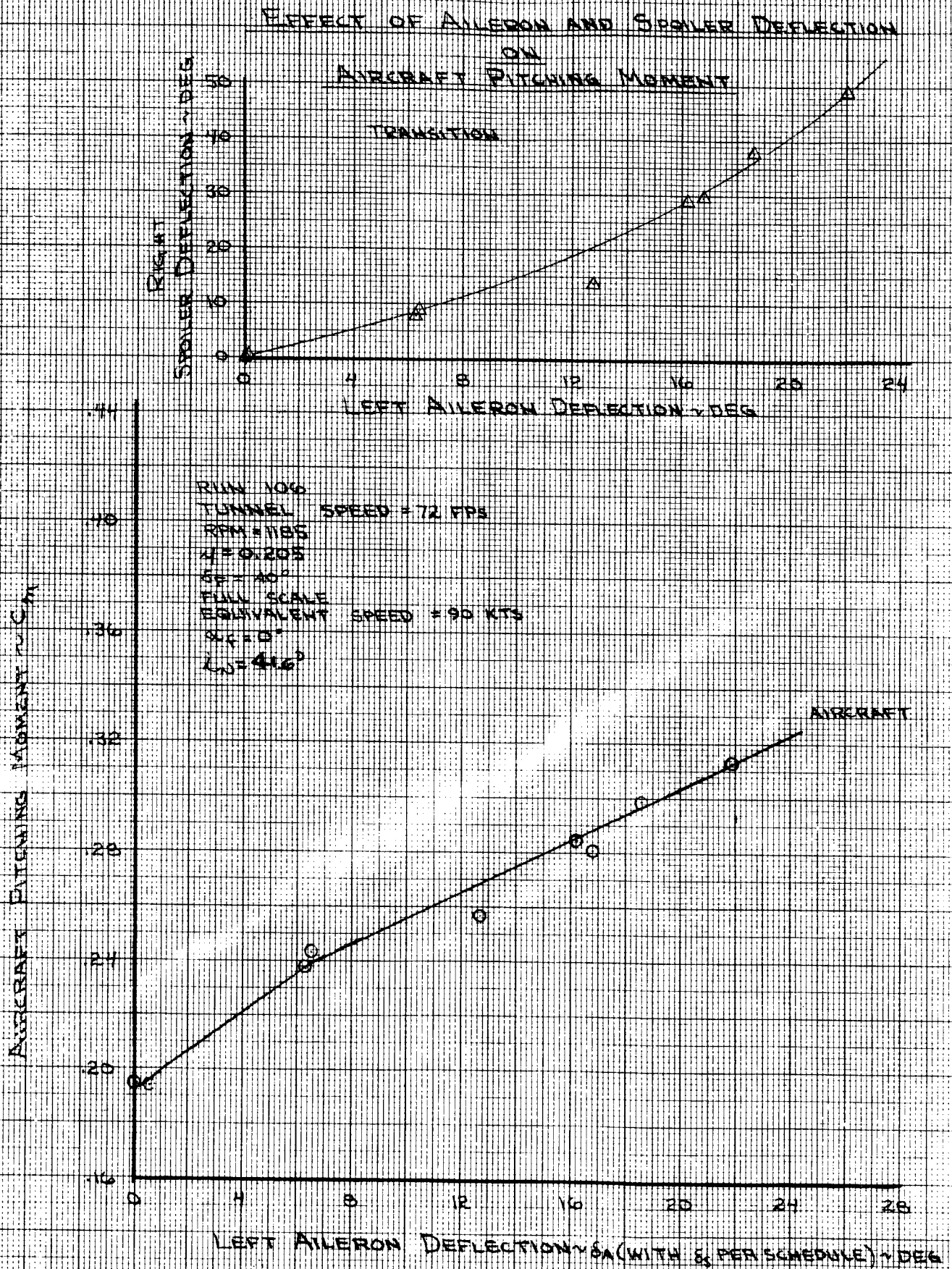


FIGURE 133

BLADE COLLECTIVE, LONGITUDINAL AND LATERAL
CYCLIC DURING COMBINED AILERON AND
SPOILER RUN

TRANSITION
RIGHT ROTOR

BLADE COLLECTIVE $\sim \delta_{cs} \sim \text{DEG}$

LONGITUDINAL CYCLIC $\sim \delta_{ls} \sim \text{DEG}$

LATERAL CYCLIC $\sim \delta_{ls} \sim \text{DEG}$

LEFT AILERON DEFLECTION $\sim \delta_a$ (WITH δ_s PER SCHEDULE) $\sim \text{DEG}$

RUN 106
TUNNEL SPEED = 72 FPS
RPM = 1185
 $\mu = 0.205$
 $\beta = 40^\circ$
FULL SCALE
EQUIVALENT SPEED = 96 KTS
 $\alpha_g = 0^\circ$
 $\lambda = 41.6^\circ$

FIGURE 134

EFFECT OF AILERON AND SPOILER DEFLECTION ON ROTOR THRUST AND POWER

+ LEFT ROTOR
O RIGHT ROTOR

TRANSITION

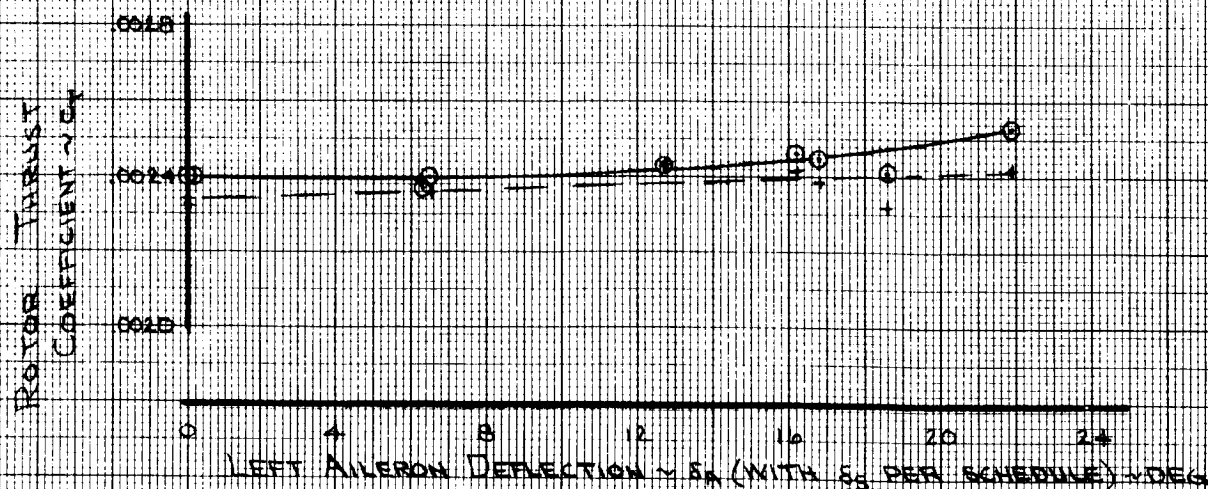
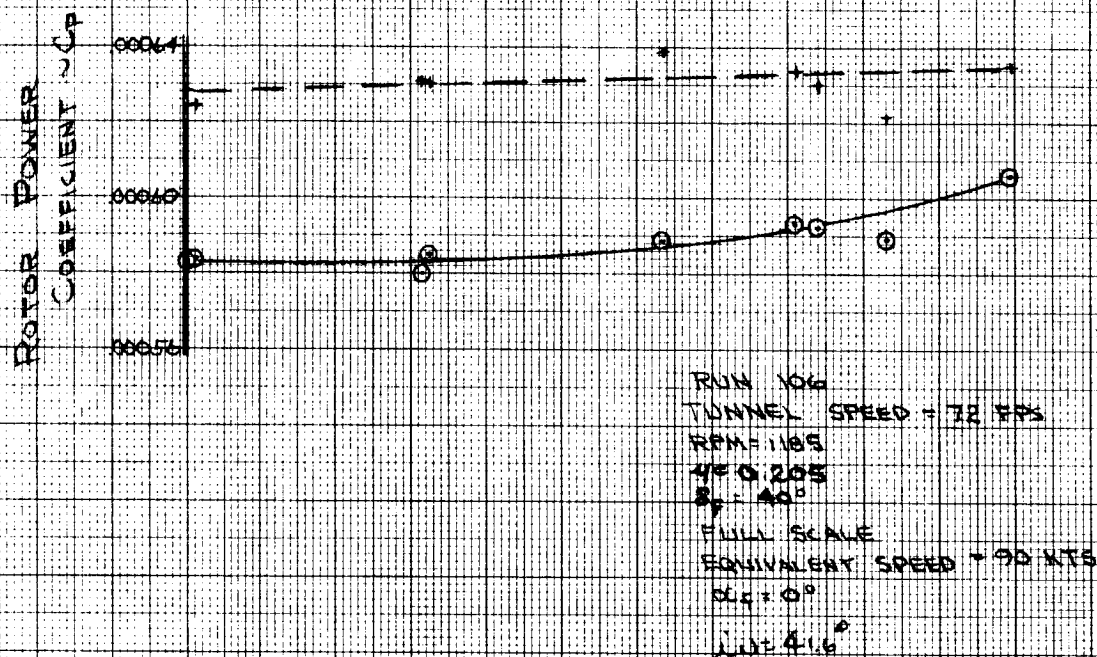


FIGURE 135

EFFECT OF AILERON AND SPOILER
DEFLECTION ON
ROTOR NORMAL FORCE AND PITCHING MOMENT

○ RIGHT ROTOR

TRANSITION

ROTOR PITCHING MOMENT
COEFFICIENT $\sim CPM$

.00012
.00008
.00004
0
-.00004
-.00008

RUN 106
TUNNEL SPEED = 72 FPS
RPM = 1185
 $M = 0.205$
 $\delta = 40^\circ$
FULL SCALE
EQUIVALENT SPEED = 90 KTS
 $\alpha = 0^\circ$
 $\lambda = 4.6^\circ$

ROTOR NORMAL FORCE
COEFFICIENT $\sim CNF$

.0020
.0016
.0012
0
-.0012
-.0016
-.0020

0 4 8 12 16 20 24
LEFT AILERON DEFLECTION $\sim \delta_A$ (WITH δ_S PER SCHEDULE) \sim DEG

FIGURE 136

EFFECT OF AILERON AND SPOILER
DEFLECTION ON
ROTOR SIDE FORCE & YAWING MOMENT

⊙ RIGHT ROTOR

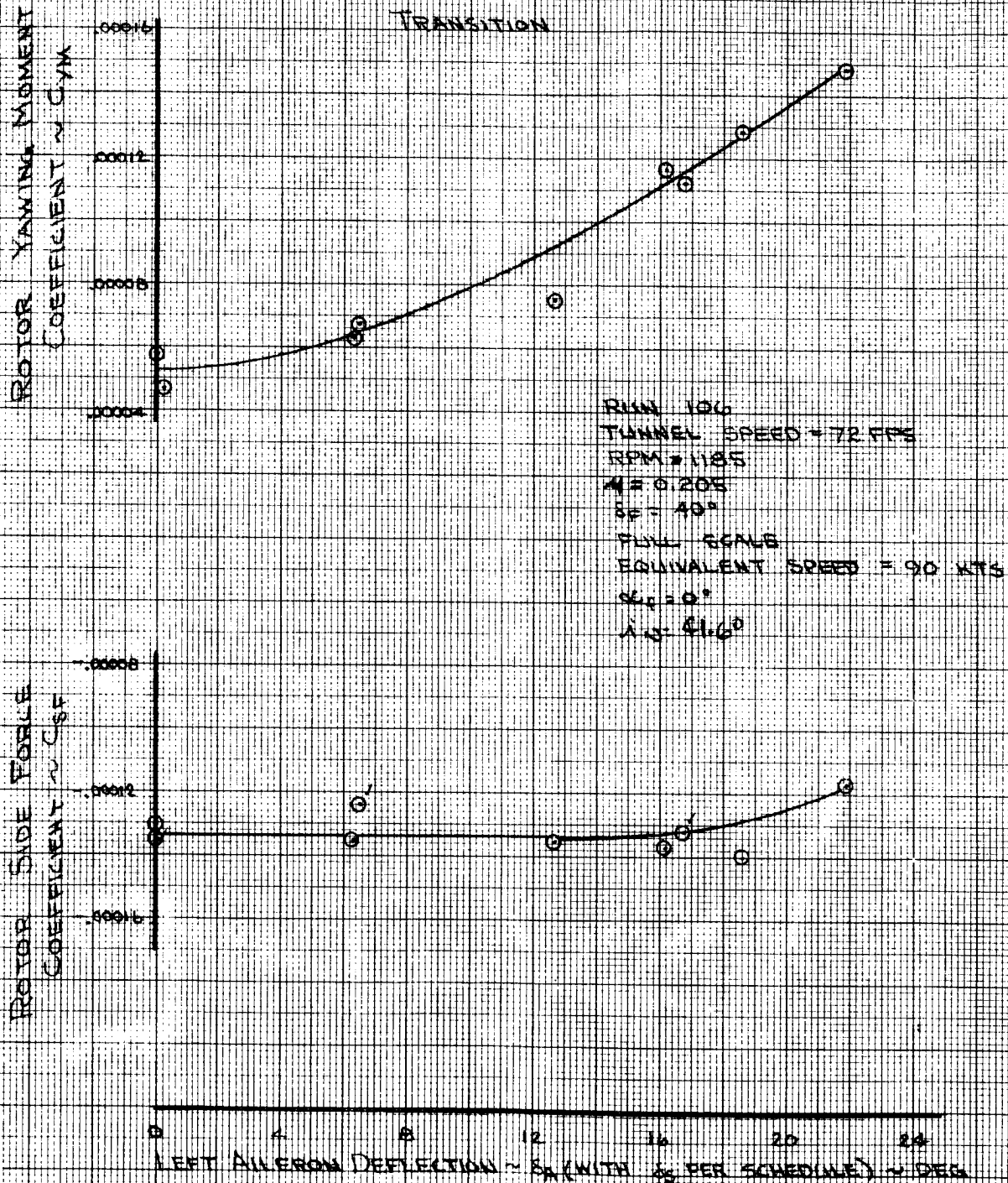


FIGURE 137

EFFECT OF DIFFERENTIAL THRUST, SPOILER & AILERON DEFLECTION AND RUDDER DEFLECTION ON ROLLING MOMENT COEFFICIENT IN TRANSITION

C_{LR} C_{NR}
○ 41.5° 42.3°
△ 43.1° 41.3°
□ 43.1° 41.8°
◇ 43.1° 41.8°

NOTES

RUN	C_{LR}	C_{NR}	δ_{SPL}	δ_{SPL}	δ_{FL}	δ_{FL}	δ_{R}	M
○ 105	0.002	0.002	0	0	40	40	0	0.205
△ 112	0.002	0.010	0	0	40	40	0	0.205
□ 114	0.002	0.010	0	50	60	40	0	0.205
◇ 115	0.002	0.010	0	50	60	40	10	0.205

$C_N = 42^\circ$ $\delta_{FL} = 40^\circ$ $\delta_{RFL} = 0$

TUNNEL $q = 6100$

EQUIV FULLSCALE $V = 90$ KTS

ROLLING MOMENT COEFFICIENT - C_L

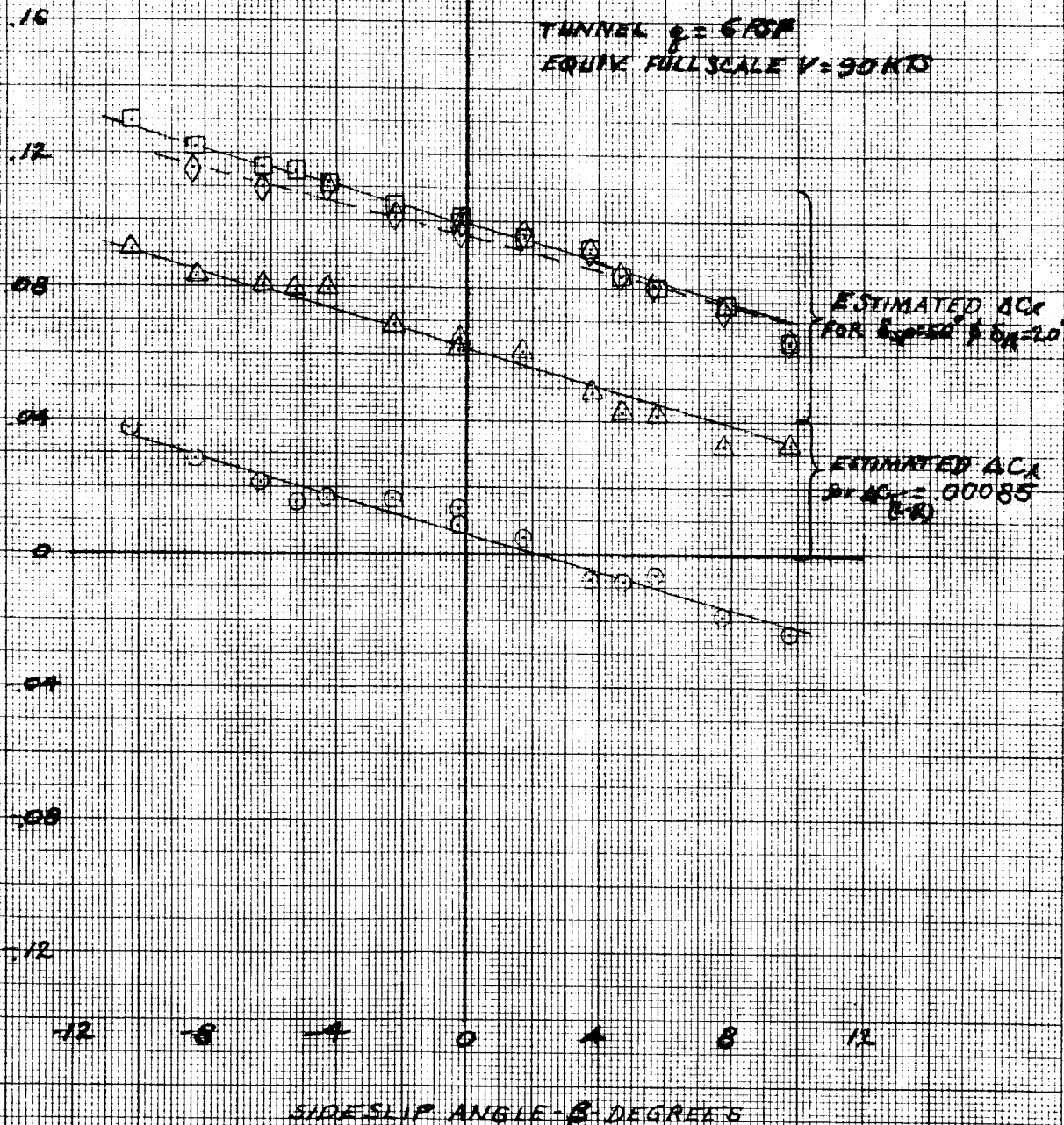


FIGURE 138

EFFECT OF DIFFERENTIAL THRUST, SPOILER & AILERON DEFLECTION AND RUDDER DEFLECTION ON YAWING MOMENT COEFFICIENT IN TRANSITION

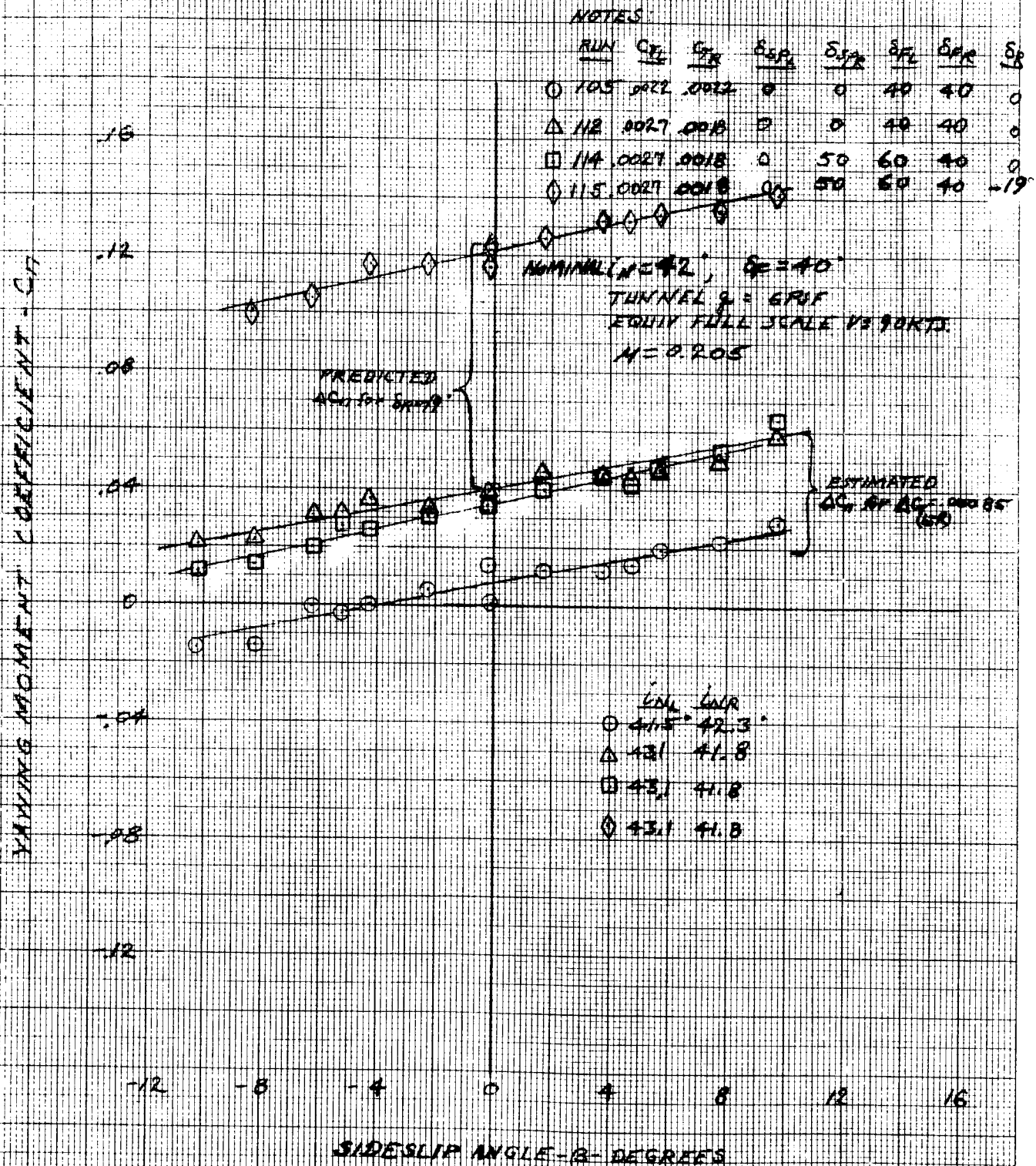
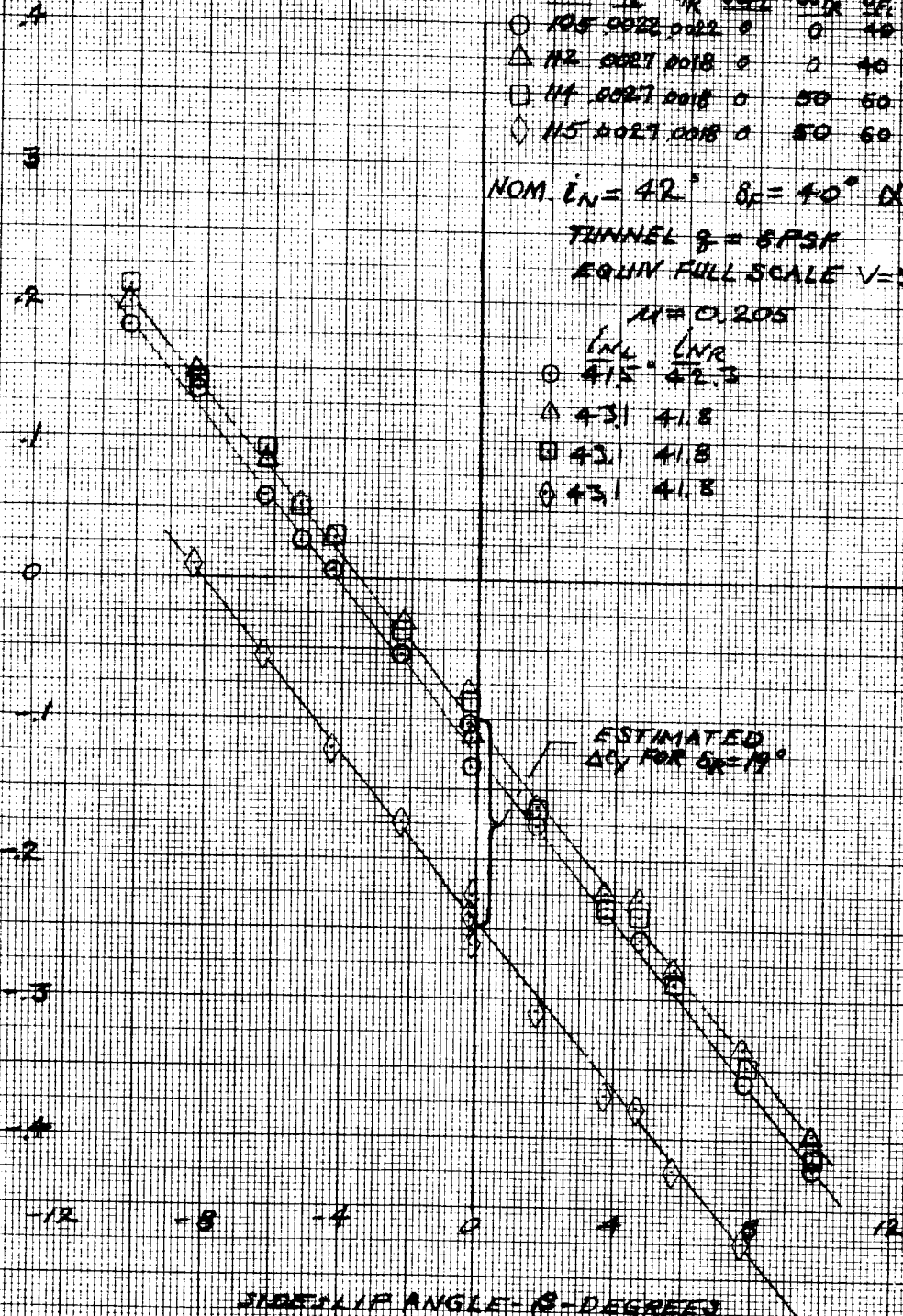


FIGURE 139

EFFECT OF DIFFERENTIAL THRUST, SPOILER &
AILERON DEFLECTION AND RUDDER DEFLECTION
ON SIDEFORCE COEFFICIENT IN TRANSITION

SIDEFORCE COEFFICIENT - C_Y



NOTES:

RUN	SR	CP	SPCL	SR	SP	SR	SR
○ 105	0022	0022	0	0	40	40	0
△ 112	0027	0018	0	0	40	40	0
□ 114	0027	0018	0	50	50	40	0
◇ 115	0029	0018	0	50	50	40	19

NOM. $i_N = 42^\circ$ $\delta_F = 40^\circ$ $\alpha_{PAL} = 0$

TUNNEL $\beta = 8$ PSF

EQUIN FULL SCALE $V = 90$ KTS

$M = 0.205$

i_{NL}	i_{NR}
○ 41.5	42.3
△ 43.1	41.8
□ 42.1	41.8
◇ 43.1	41.8

ESTIMATED
 C_Y FOR $SR = 19^\circ$

FIGURE 140

EFFECT OF DIFFERENTIAL THRUST ON ROLLING
AND YAWING MOMENT COEFFICIENTS IN TRANSITION
AIRFRAME COEFF

NOTES:

RUN	$C_{L\beta}$	$C_{L\dot{\beta}}$	$\delta C_{L\beta}$	$\delta C_{L\dot{\beta}}$	$\delta C_{Y\beta}$	$\delta C_{Y\dot{\beta}}$	$\delta C_{N\beta}$	$\delta C_{N\dot{\beta}}$
105	.0022	.0022	0	0	40	40	0	0
112	.0027	.0018	0	0	40	40	0	0

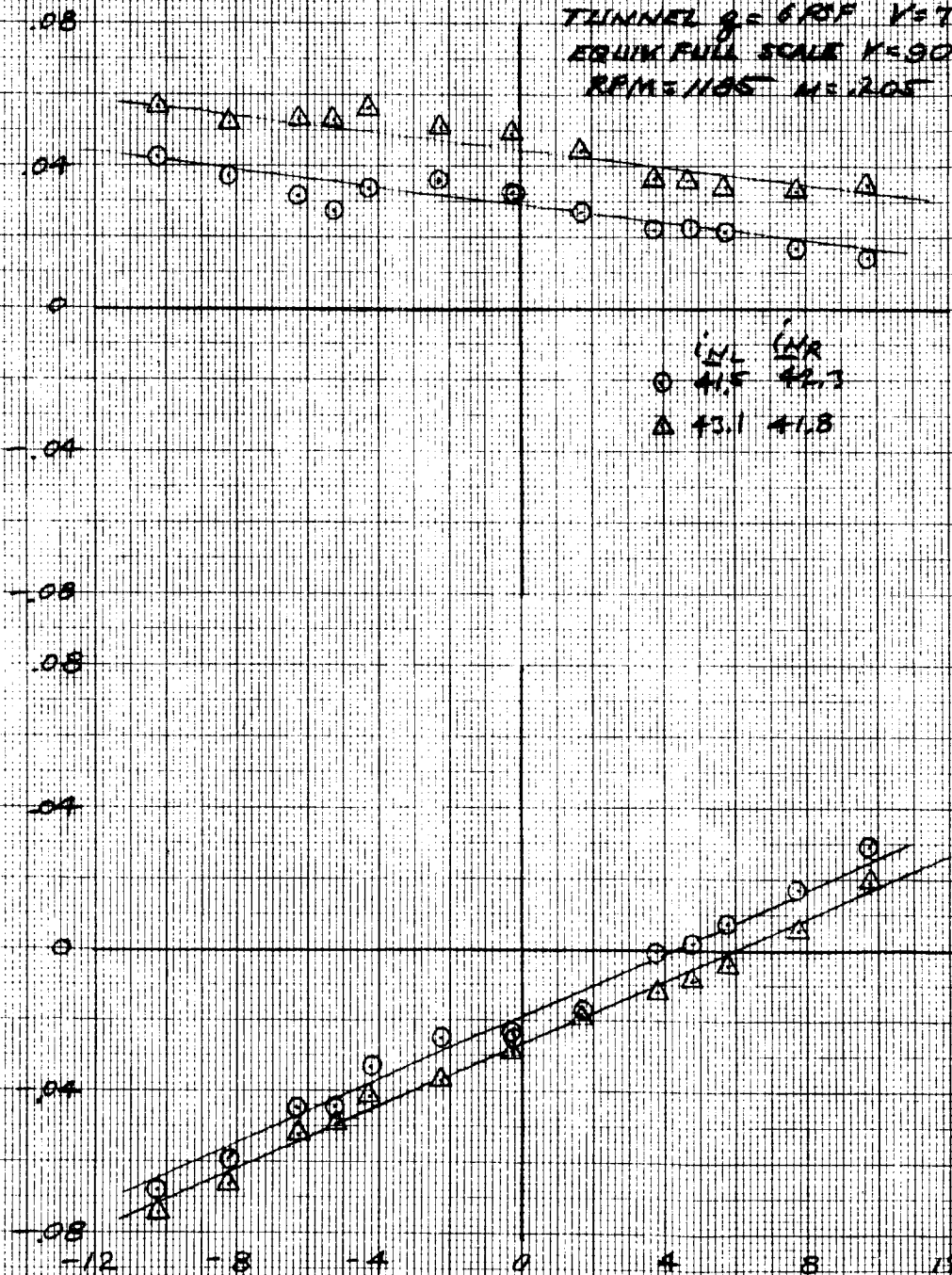
NOM $C_N = 42^\circ$ $\alpha_{FRL} = 0$

TUNNEL $Q = 6.0 \text{ PSF}$ $V = 72 \text{ FPS}$

EQUIV FULL SCALE $V = 90 \text{ KTS}$

REF $M = 1.05$ $M = 2.05$

ROLLING MOMENT COEFFICIENT
 $C_{L\beta}$
YAWING MOMENT COEFFICIENT
 $C_{Y\beta}$



SIDESLIP ANGLE - β - DEGREES

FIGURE 141

EFFECT OF DIFFERENTIAL COLLECTIVE
AIRCRAFT ROLLING MOMENT COEFFICIENT
VERSUS YAWING MOMENT COEFFICIENT

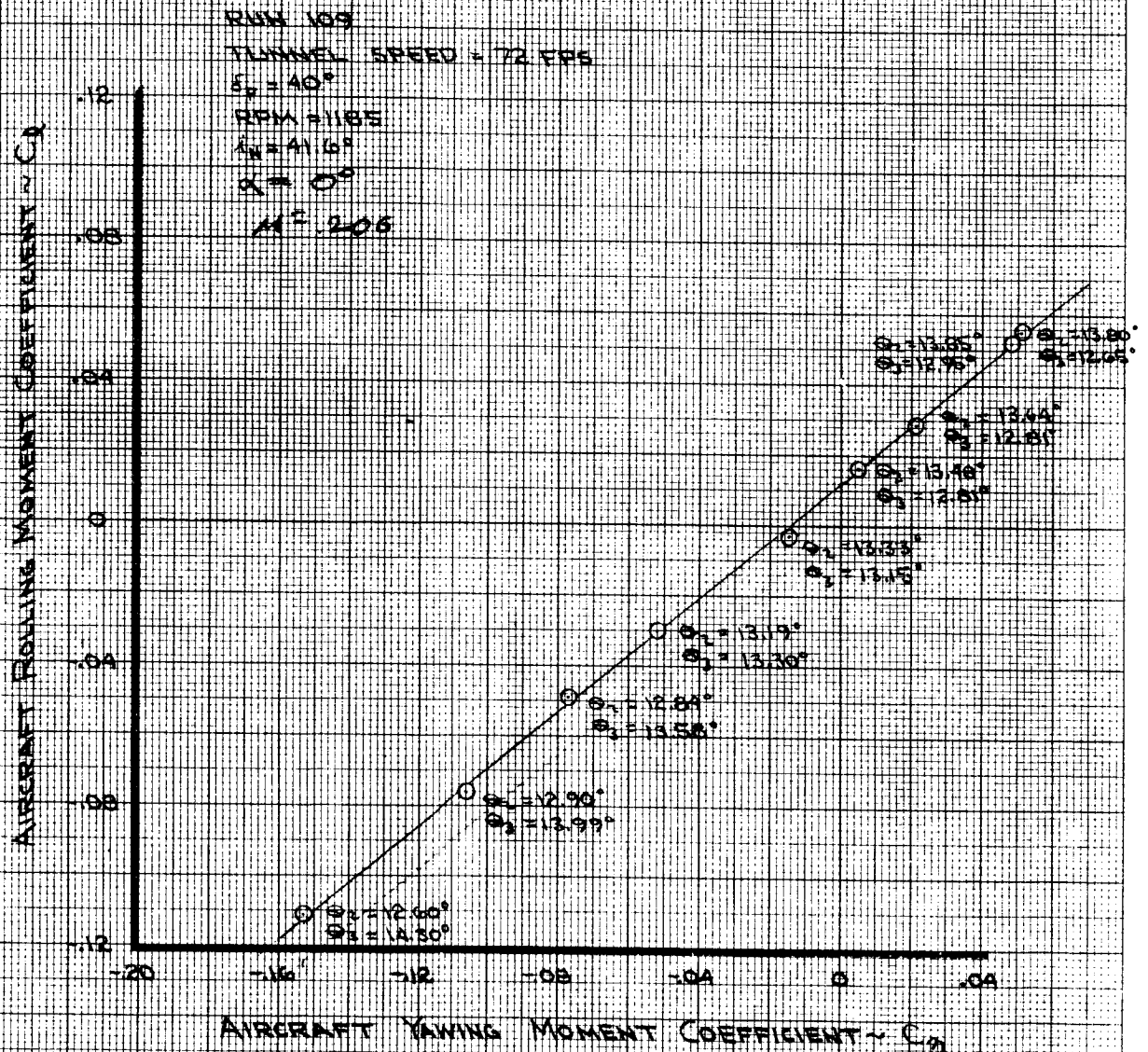


FIGURE 142

CHANGE IN THRUST COEFFICIENT WITH COLLECTIVE PITCH

RUN 109

TUNNEL SPEED = 72 FPS

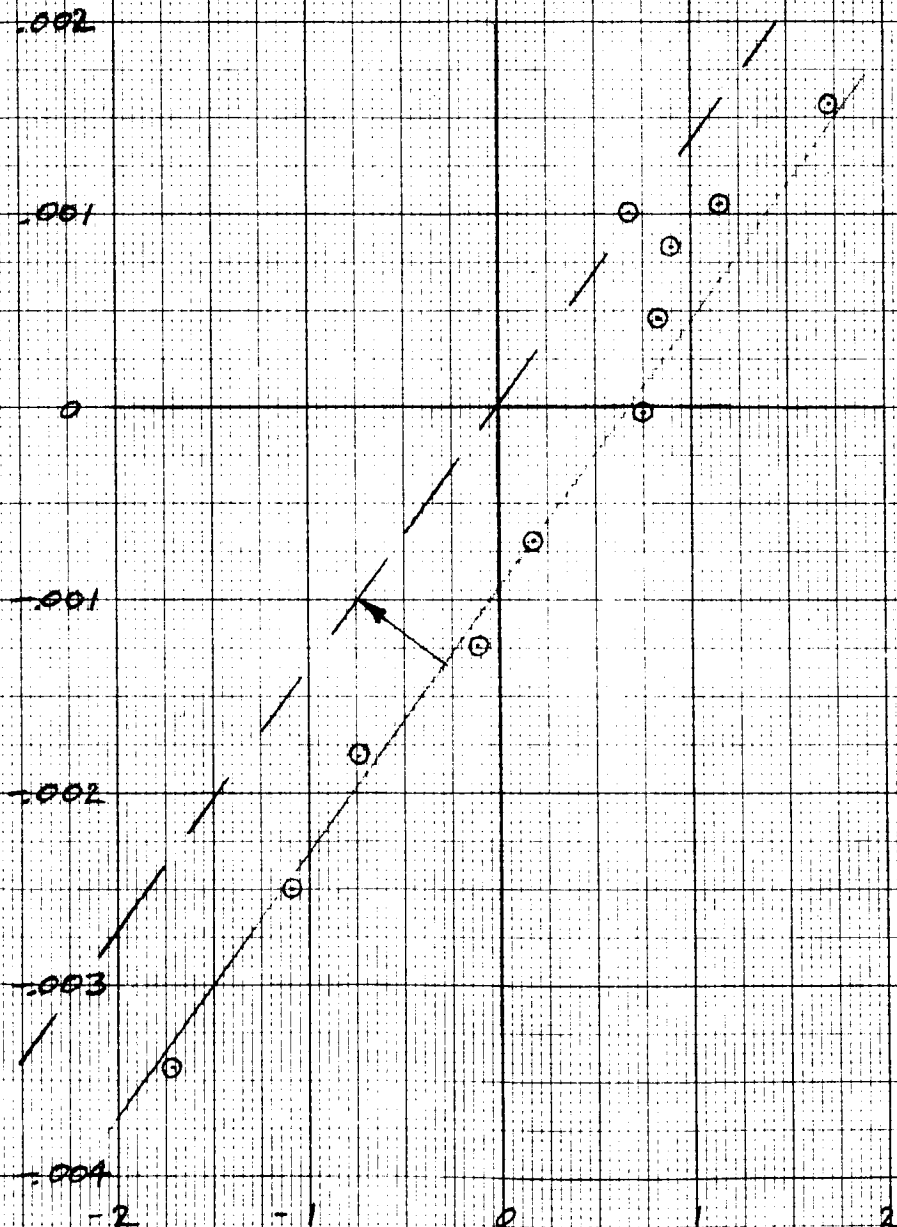
$\delta = 40^\circ$

RPM = 1185 $M = 0.06$

$IN = 4.6$

$\alpha = 0$

DELTA THRUST COEFFICIENT - ΔC_T
(LEFT ROTOR - RIGHT ROTOR)



DELTA COLLECTIVE - $\Delta \theta$
(LEFT ROTOR - RIGHT ROTOR)

FIGURE 143

ELEVATOR EFFECTIVENESS IN TRANSITION

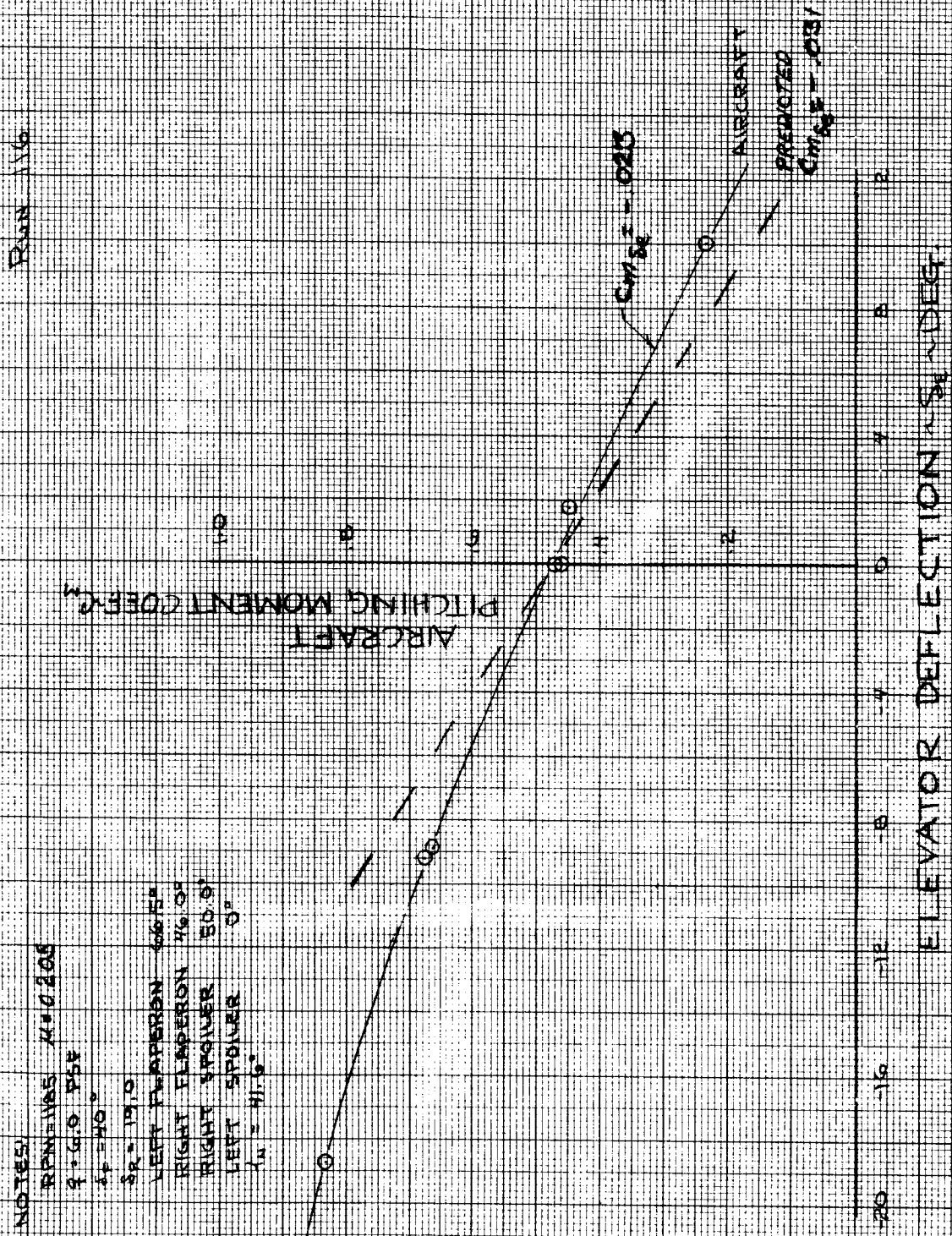
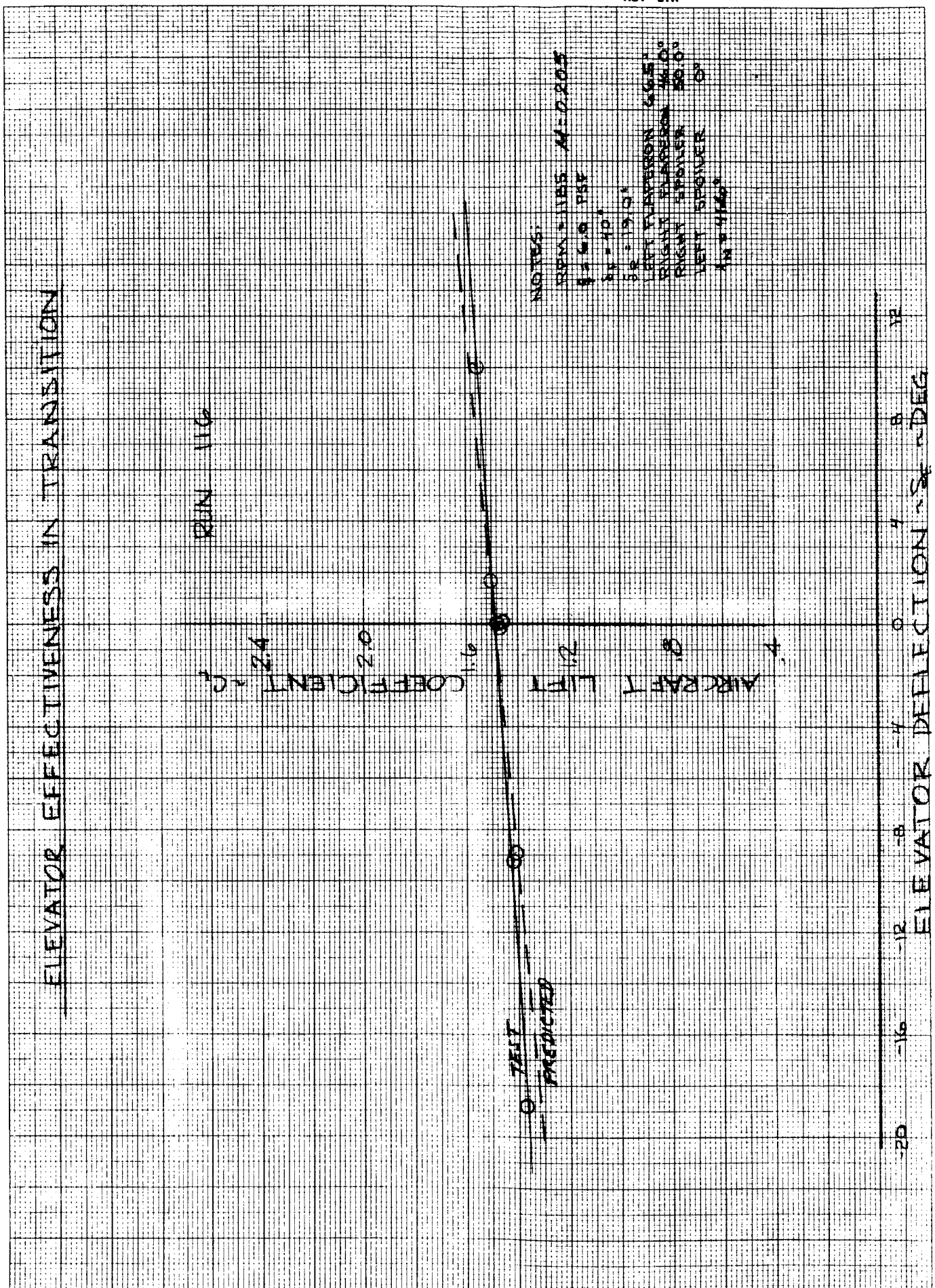


FIGURE 144



LONGITUDINAL CYCLIC EFFECTIVENESS
VARIATION OF LIFT AND PITCHING MOMENT
COEFFICIENTS WITH LONGITUDINAL CYCLIC IN
TRANSITION

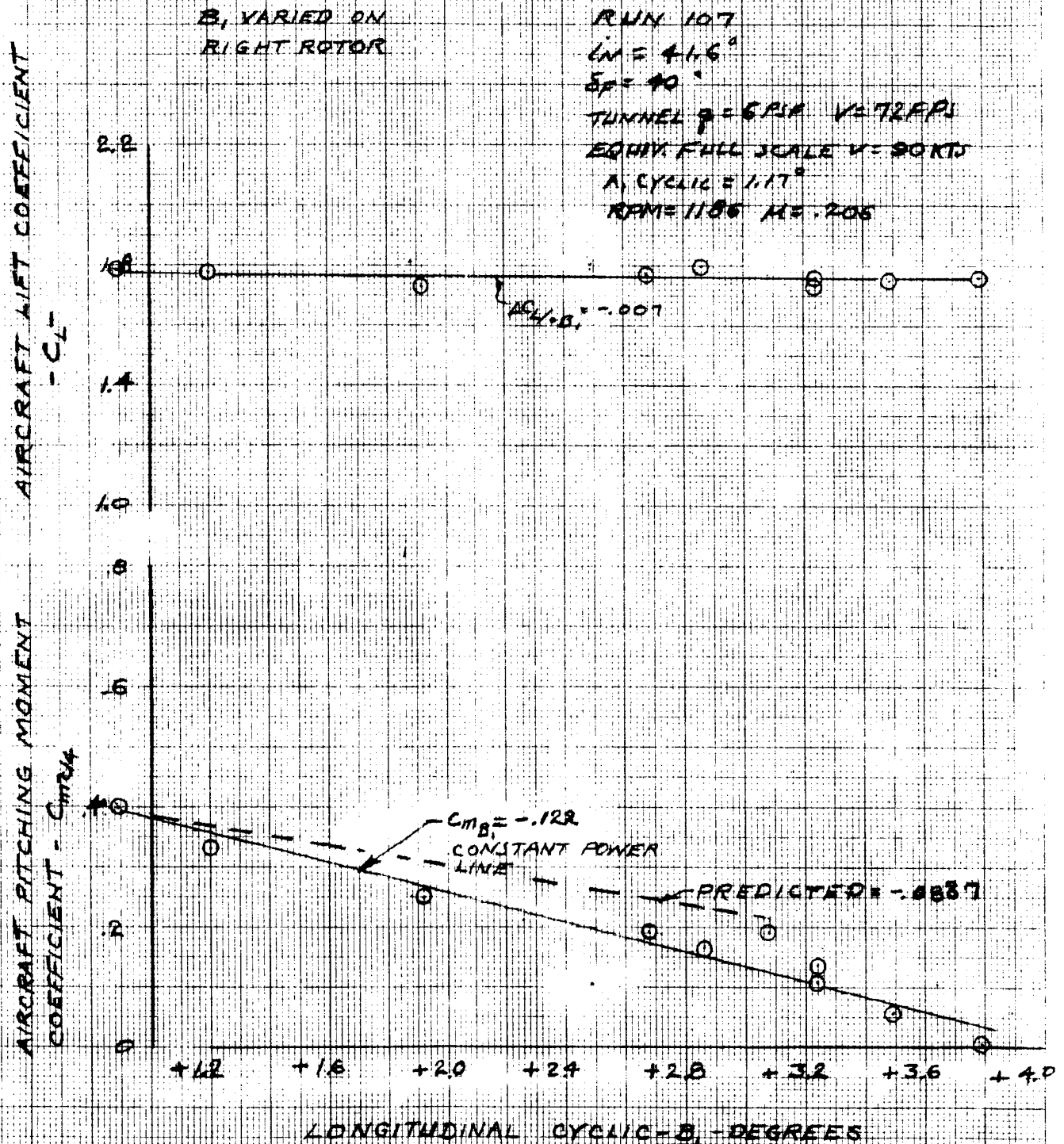


FIGURE 146

LONGITUDINAL CYCLIC EFFECTIVENESS VARIATION OF ROLLING AND YAWING MOMENT COEFFICIENTS WITH LONGITUDINAL CYCLIC RY TRANSITION

B₁ VARIED ON
RIGHT ROTOR

NOTES:

RUN 197

$\alpha = 4.6^\circ$ $\delta = 40^\circ$

TUNNEL 8-6 FWT $V = 72$ KTS

EQUIV. FULL SCALE $V = 90$ KTS

RPM = 1196 $M = .206$

AIRCRAFT YAWING MOMENT
COEFFICIENT - C_Y

.08

.04

0

-.04

CONSTANT
POWER LINE
 $C_{H_1} = +0.0105$

AIRCRAFT ROLLING MOMENT
COEFFICIENT - C_L

.08

.06

.04

.02

CONSTANT
POWER LINE
 $C_{H_1} = +0.0162$

0

+5

+4

+3

+2

+1

0

-1

-2

LONGITUDINAL CYCLIC - δ_1 - DEGREES

FIGURE 147

LATERAL CYCLIC EFFECTIVENESS VARIATION OF ROLLING AND YAWING MOMENT COEFFICIENTS WITH LATERAL CYCLIC IN TRANSITION

A_1 VARIED ON
LEFT ROTOR

NOTES:
RUN 108
 $\alpha = 42.2^\circ$ $\delta_F = 43.7^\circ$
 $C_T = 0.023$
RPM 1185 $M = 2.06$
TUNNEL 8' x 6' 0.3PIF V = 125 FPS
EQIV. FULL SCALE V = 90 KTS.

AIRCRAFT YAWING MOMENT
COEFFICIENT - C_Y

AIRCRAFT ROLLING MOMENT
COEFFICIENT - C_L

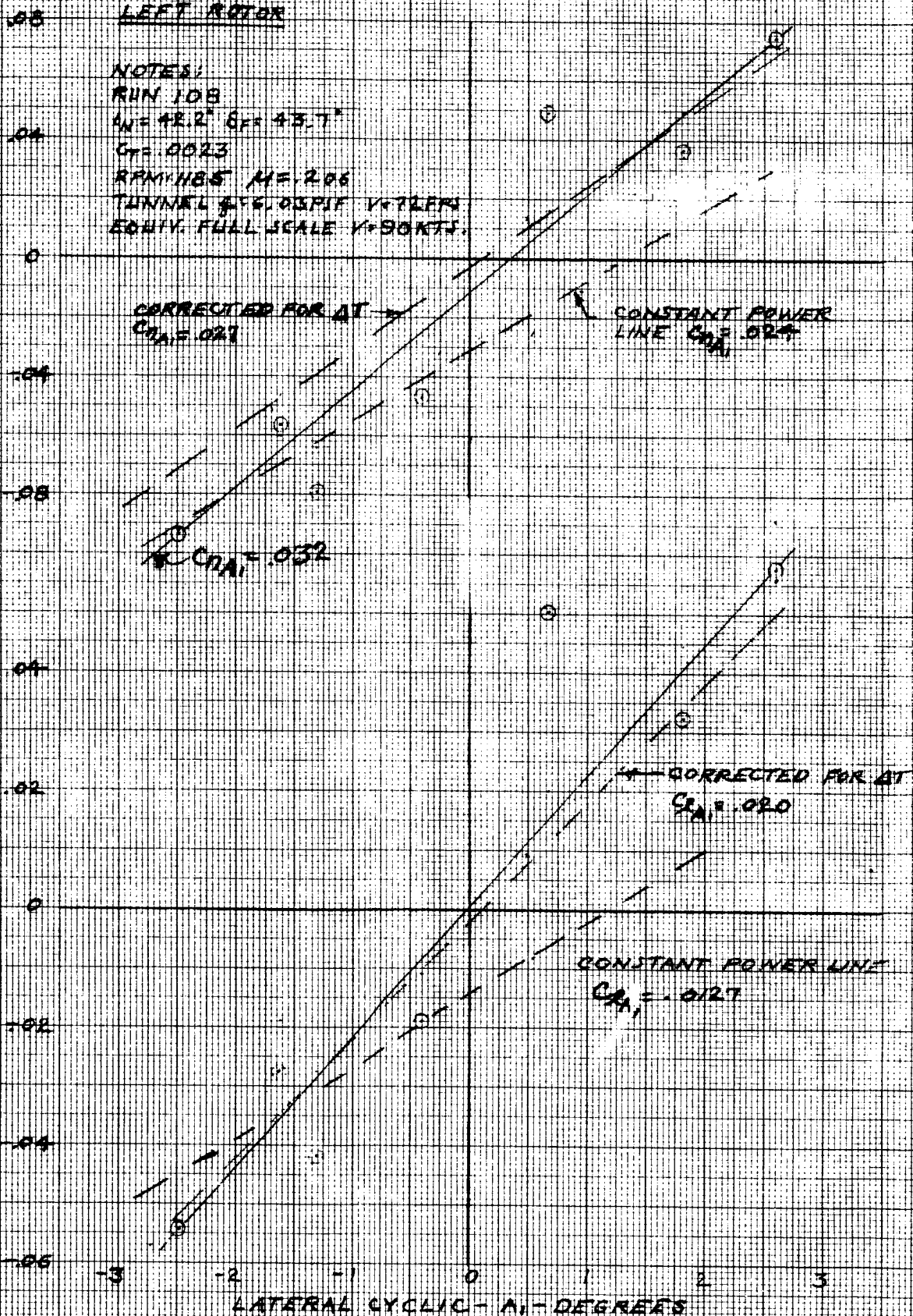


FIGURE 148

LATERAL CYCLIC EFFECTIVENESS VARIATION OF ROLLING AND YAWING MOMENT COEFFICIENTS WITH LATERAL CYCLIC IN TRANSITION

A_1 VARIED ON
RIGHT ROTOR

NOTES:

RUN 108

$i_N = 42.2^\circ$ $\delta_R = 43.7^\circ$

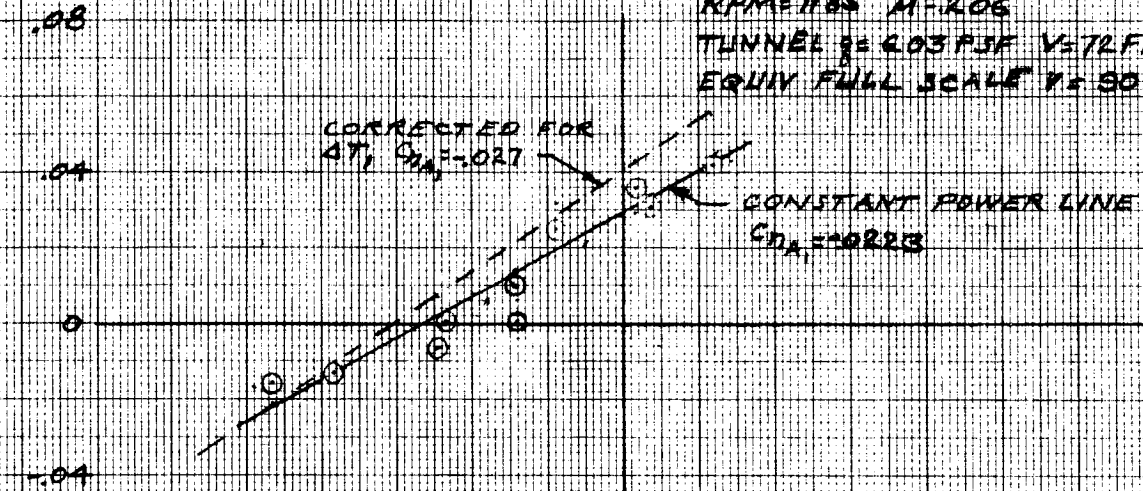
$C_T = .0023$

RPM = 1185 M = 2.06

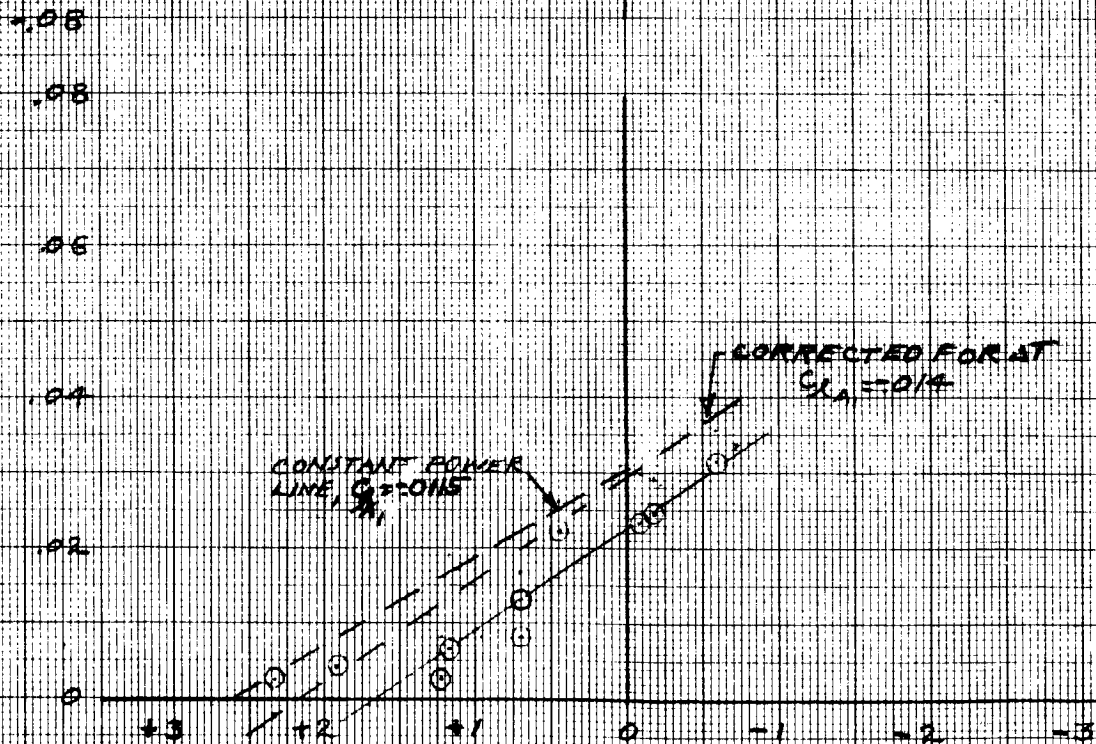
TUNNEL $q = 603$ PSF $V = 72$ FPS

EQUIV FULL SCALE $V = 90$ KTS

AIRCRAFT YAWING MOMENT
COEFFICIENT - C_Y



AIRCRAFT ROLLING MOMENT
COEFFICIENT - C_R



LATERAL CYCLIC - A_1 - DEGREES

FIGURE 149

LATERAL CYCLIC EFFECTIVENESS
VARIATION OF LIFT AND PITCHING MOMENT
COEFFICIENTS WITH LATERAL CYCLIC IN
TRANSITION

A, VARIED ON
LEFT ROTOR

NOTES

RUN 108

$\lambda = 42.2$

$\delta p = 13.7$

$C_T = 0.023$

RPM = 1185

$M = 2.06$

TUNNEL $q = 603 \text{ PKF}$ $V = 72 \text{ FPS}$

EQUIV FULL SCALE $V = 30 \text{ KTS}$

AIRCRAFT LIFT COEFFICIENT
 C_L

AIRCRAFT PITCHING MOMENT
COEFFICIENT - C_{MA}

2.6

2.2

1.8

1.4

1.0

.8

.6

.4

.2

0

-3

-2

-1

0

+1

+2

+3

LATERAL CYCLIC - A_1 - DEGREES

CONSTANT POWER LINE

$C_{LA_1} = +0.0033$

CONSTANT POWER LINE

$C_{MA_1} = .025$

FIGURE 150

LATERAL CYCLIC EFFECTIVENESS VARIATION OF LIFT AND PITCHING MOMENT COEFFICIENTS WITH LATERAL CYCLIC IN TRANSITION

A₁ VARIED ON
RIGHT ROTOR

NOTES:

RUN 108

$i_n = 42.2$

$\delta p = 43.7$

$C_{\delta} = .0023$

RPM = 1185

$M = .206$

TUNNEL $\rho = 6.03 \text{ ASL}$ $V = 72 \text{ FPS}$

EQUIV FULL SCALE $V = 90 \text{ KTS}$

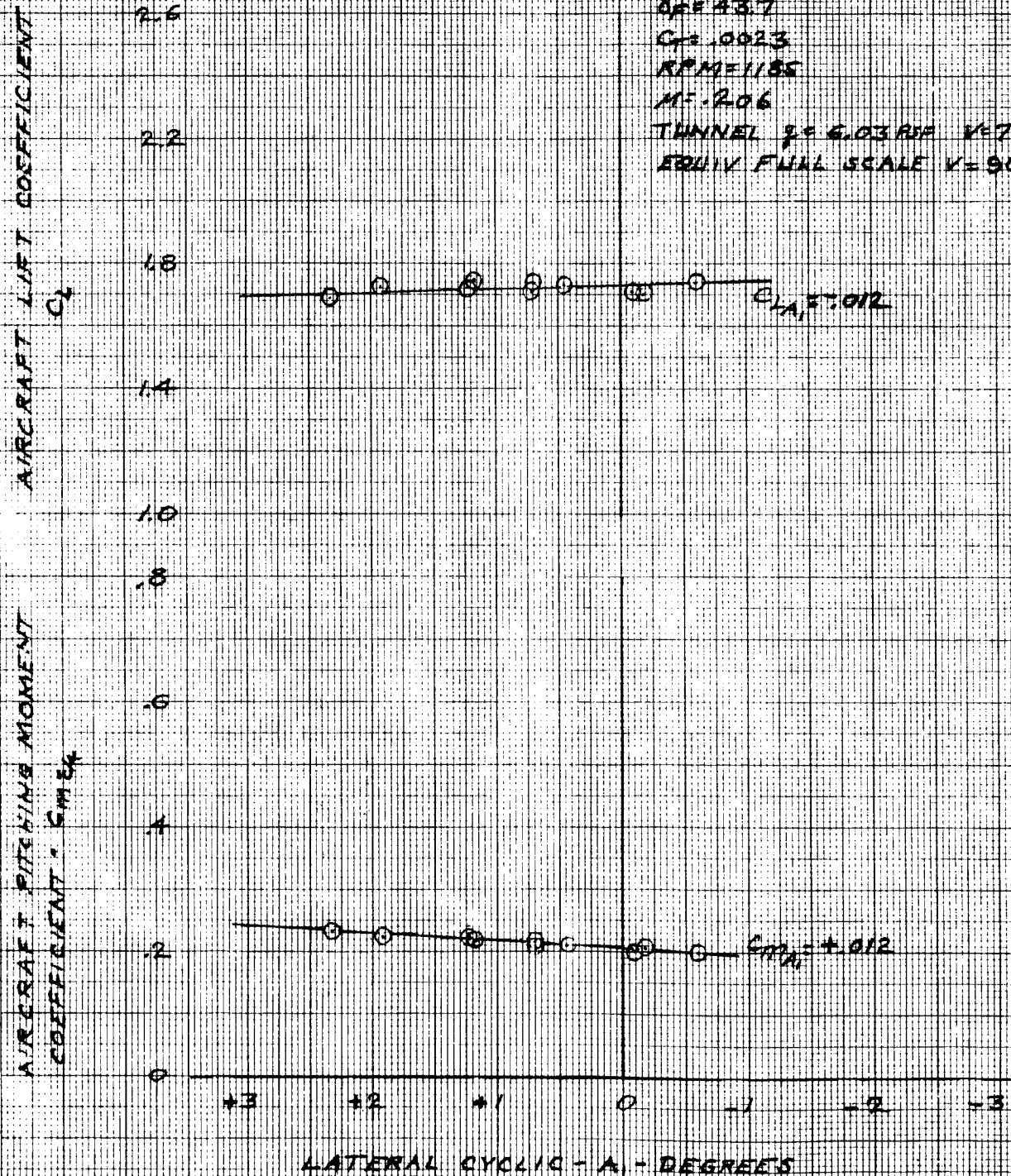


FIGURE 151

5.1.4 Comparison of Test and Theory in Transition

Rotor Forces and Moments

To define the adequacy of the prediction techniques utilized in the design and development of the tilt rotor aircraft, a comparison of this theory is presented to validate it with test data.

The theory utilized is an aeroelastic analysis for the study of aerodynamic, dynamic and structural characteristics of current and advanced rotor and prop/rotor concepts. Airloads are calculated considering the effects of section geometry, compressibility and non-uniform inflow. An iterative process between the airloads and coupled flap-pitch dynamic response establishes blade accelerations which in turn are used to compute hub loads and rotor aerodynamic performance. This program was used to compute the transition rotor performance (thrust, power and collective relationships), static stability (inplane forces and moments) and the cyclic control characteristics. A complete description of this analysis, D-88 computer program, is contained in Reference 2.

The rotor attitude and control derivatives presented in Sections 5.1.1 and 5.1.3 summarize the rotor data obtained in the transition flight regime of this test program. To make a direct comparison with theory, this test data was adjusted to remove the longitudinal and lateral cyclic effects and to remove the hub tares, since the theory accounts for only the blades. The hub tares are summarized in Appendix D.

Figures 152 and 153 present the variation of rotor normal force and pitching moment with rotor shaft angle of attack at a flight condition equivalent to 90 knots and a rotor speed of 551 RPM for

the full scale research aircraft.

Correcting the normal force test data indicates there is a large contribution of the hub to the level of in-plane force but the impact of cyclic is small. This results in an almost exact agreement in level and slope, or derivative. The pitching moment hub tares are small but removing the cyclic has a large level shift associated with it which is a result of the longitudinal cyclic contribution. Figure 153 indicates a significant difference between theory and test in the pitching moment level but there is a small difference in the slope or derivative.

A comparison of the rotor force and moment derivatives with respect to cyclic is also included here to provide the validation of the rotor control effectiveness. Figure 154 presents the lateral cyclic derivatives for the in-plane forces and the hub moments. The predicted in-plane force derivatives with lateral cyclic are approximately the same as the test data. Pitching and yawing moment derivatives have more of a deviation from the test data. The difference in the net moment produced per degree of cyclic is only ten percent but the phase angle at which it occurs is approximately 20 degrees ahead of the test data. Figure 155 presents the rotor force and moment derivatives with longitudinal cyclic. There is a larger deviation between the theory and test in-plane force derivatives with longitudinal cyclic than with lateral cyclic. This could be a result of wing circulation producing an equivalent angle of attack effect that would be additive to the longitudinal cyclic effect, whereas the lateral cyclic input is 90 degrees out

of phase with the angle of attack effect and is not influenced by it. The theory utilized here does not include circulation effects and therefore would tend to reinforce the reason that the longitudinal cyclic derivatives do not agree as well with test data. Comparing the moment derivatives indicates that the resulting phase angle predicted leads the test data by approximately 30-degrees and the net moment is 45-percent less than the test data. This large difference is the result of the net moment derivative with longitudinal cyclic from test being 35-percent greater than that obtained with lateral cyclic which also indicates that the wing circulation reinforces the longitudinal cyclic derivatives. The effectiveness of longitudinal cyclic is greater than predicted and provides a margin for control in transition where most of the aircraft control comes from the rotor and not the aerodynamic surfaces.

Longitudinal Stability

Test results indicate the basic aircraft, rotors off, to have a lower than predicted C_{L_α} , .080 per degree compared to .090 predicted at the test Reynolds number. Stability of the model dC_m/dC_L , was much greater than predicted for the airframe with rotors off. Test data indicate the neutral point to be at 97-percent of the MAC (Figure 89) compared to 46.5-percent predicted. This is a result of greater than estimated horizontal tail lift curve slope and lower aircraft C_{L_α} . The neutral point of the model with rotors on, Figure 89, is indicated to be at 42.4-percent MAC. This compares with an estimated neutral point location for the full scale aircraft at approximately 44-percent MAC. The estimate for the full

scale aircraft is based on a vertical location of the center of gravity some 15 inches full scale below that used for test data reference. The incremental change in airframe lift curve slope attributable to the horizontal tail is $\Delta C_{L_\alpha} = .012$, from Figure 87. This compares with a predicted $\Delta C_{L_\alpha} = .0091$ based on an estimated value of $d\epsilon/d\alpha = 0.49$ for the 40-degree flap deflection condition. The change in slope of pitching moment coefficient with angle of attack caused by the horizontal tail is indicated to be $\Delta C_{m_\alpha} = -.0652$ compared to a predicted value of $-.0308$. The estimated aircraft and airframe lift coefficients versus angle of attack for the rotors on configuration are illustrated on Figure 87 for comparison with test data. These estimates are based on the normal force and thrust coefficients measured from test combined with estimated slipstream effects and airframe lift coefficients. The predictions are again higher than test values of lift coefficient slopes.

The effects of nacelle incidence, at constant fuselage angle of attack, on lift and pitching moment coefficients are illustrated on Figure 96 and compared with the predicted effects on airframe coefficients. The test data indicate a larger effect on both lift and pitching moment coefficients than estimated. The nacelles used on the model were, however, somewhat larger than the scaled nacelles for the aircraft to house the model gearboxes and balances which are larger than the scaled aircraft motors. The predictions are for the full scale aircraft nacelles. As indicated, the increments for the nacelles are relatively small. Thus, the predictions for the full scale nacelle effects are adequate.

Lateral-Directional Stability

Directional stability coefficient slope with sideslip for the aircraft with rotors and tails off is indicated to be $-.0009$ from Figure 97 compared with a predicted value of C_{n_β} of $-.00139$ including the effects of the ventral fins. Initial estimates for the Model 222 did not include the effects of the ventrals, or strakes, and C_{n_β} tails off was estimated to be $-.00239$. The effect of the strakes is, thus, significant increasing C_{n_β} by $+.0010$. Tails on and rotors off C_{n_β} is indicated from test data to be $.0070$ compared to a predicted value of $.00346$. The change in sideforce coefficient caused by the tails, from test data, is indicated in Figure 99 to be, $\Delta C_{Y_\beta} = -.0187$ compared to a predicted value of $-.0111$ indicating considerably higher vertical tail lift curve slope than estimated. This could result from higher lift carry-over on the fuselage than predicted. The test values of ΔC_{Y_β} and ΔC_{n_β} for the tails indicates an effective tail length of $.422b$ compared to a calculated value of $.562b$ from the quarter chord of the wing to the quarter chord of the vertical tail MAC, indicating that the effective CP of the tail is forward of the tail. This supports a recommendation to obtain data at higher Reynolds number. Rotors on and tails on directional stability is good, $.0028$.

Control Effectiveness

Aileron rolling moment effectiveness in transition with the flap-eron deflected for roll control from an initial deflection of 40-degrees is indicated to yield a negative C_l as anticipated.

The rolling moment coefficient versus aileron deflection from test is compared with the predicted value on Figure 111. This is of academic interest as it is not anticipated that the flaperons will be used for roll control on the aircraft at deflections greater than 35-degrees for combined aileron and flap deflection. The effect of flap deflection as aileron on lift coefficient is observed in Figure 114 to decrease lift coefficient slightly more than predicted. This is believed to result from detached flow on the upper surface at the higher deflections resulting from low Reynolds number flow or non-optimum flap gap. The effect of spoiler deflection on rolling moment coefficient in transition is compared with the predicted values in Figure 120. The test values are indicated to be lower than predicted. This is believed to result, also, from low Reynolds number causing separation of flow from the flap upper surface prior to spoiler deflection. Spoiler effectiveness in roll with flaps deflected 40-degrees initially is indicated to result in C_{ℓ} of .071 at 45-degrees deflection compared to a predicted value of .101. The change in yawing moment coefficient with spoiler deflection in transition is indicated on Figure 121 to be less favorable, proverse, than predicted and for maximum deflection of 45-degrees small enough to be neglected. The change in lift coefficient with spoiler deflection is, as anticipated from the rolling moment coefficient, smaller than predicted as indicated by Figure 122. Figure 138 indicates that the change in rolling moment coefficient resulting from differential thrust coefficient, $C_{T_L} = .0027$ and $C_{T_R} = .0018$, with spoiler and flaperon deflection zero is approximately 1.37 times the predicted

value. The resulting change in yawing moment coefficient, Figure 139 is indicated to be .805 times the predicted value. These figures indicate that the change in thrust coefficient coupled with 50-degrees spoiler deflection and 20-degrees aileron deflection results in a rolling moment coefficient of .093 and yawing moment coefficient of .028 compared to predicted values of .110 and .031 respectively. The rolling and yawing moment coefficients for rudder deflection of -19-degrees are -.0035 and .087 compared to predicted values of -.0104 and .084 respectively at zero sideslip angle. The yawing moment coefficient agrees well with prediction, but the rolling moment coefficient indicates that the vertical center of pressure of the sideforce due to rudder deflection is much lower on the vertical tail than estimated since the sideforce coefficient due to rudder deflection, indicated on Figure 140, agrees well with prediction and the rolling moment coefficient is low. This and the higher-than-predicted sideforce coefficient due to the sideslip of the vertical tail indicate considerable carry-over of sideforce from the rudder and vertical tail on the aft end of the fuselage.

Elevator effectiveness in transition is indicated to be lower than predicted in Figure 144. The test value of $C_{m_{\delta_e}}$ is -.0242 compared to a predicted value of -.031. Figure 145 indicates a change in lift coefficient per degree elevator of .0065 compared to a predicted value of .0092. The test values of $C_{L_{\delta_e}}$ and $C_{m_{\delta_e}}$ indicate an effective tail length of $3.52 \bar{c}$ compared to a predicted value of $3.40 \bar{c}$ from the quarter chord of the wing to the quarter

chord of the horizontal tail MAC.

The longitudinal cyclic effectiveness in changing total aircraft pitching moment coefficient is indicated in Figure 146 to be $C_{m_{B_1}}$ = $-.122$ compared to a predicted value of $-.0837$ based on the assumption that cyclic application results in no rotor-on-wing interference effect. Using the normal force and pitching moment coefficients per degree B_1 from test data measured at the rotor hub, Figure 100 and Figure 101 to calculate the pitching moment about the wing quarter chord results in $C_{m_{B_1}}$ of $-.155$. The yawing moment coefficient resulting from lateral cyclic is indicated to be approximately $.032$ per degree A_1 from raw test data of Figure 148. Correcting to constant thrust yields a slope, $C_{n_{A_1}}$, of $.027$ and correcting to constant power yields $.024$ for the left rotor and $.0223$ for the right rotor. The predicted value of $C_{n_{A_1}}$ about the wing quarter chord using estimated rotor characteristics or the test data for rotor sideforce and yawing moment at the hub per degree A_1 yield $C_{n_{A_1}} = .0208$. Thus, there is reasonable agreement between predicted and test values of aircraft pitching moment coefficient per degree B_1 and yawing moment coefficient per degree A_1 .

COMPARISON OF THEORY AND TEST DATA
IN TRANSITION
ROTOR NORMAL FORCE CHARACTERISTICS

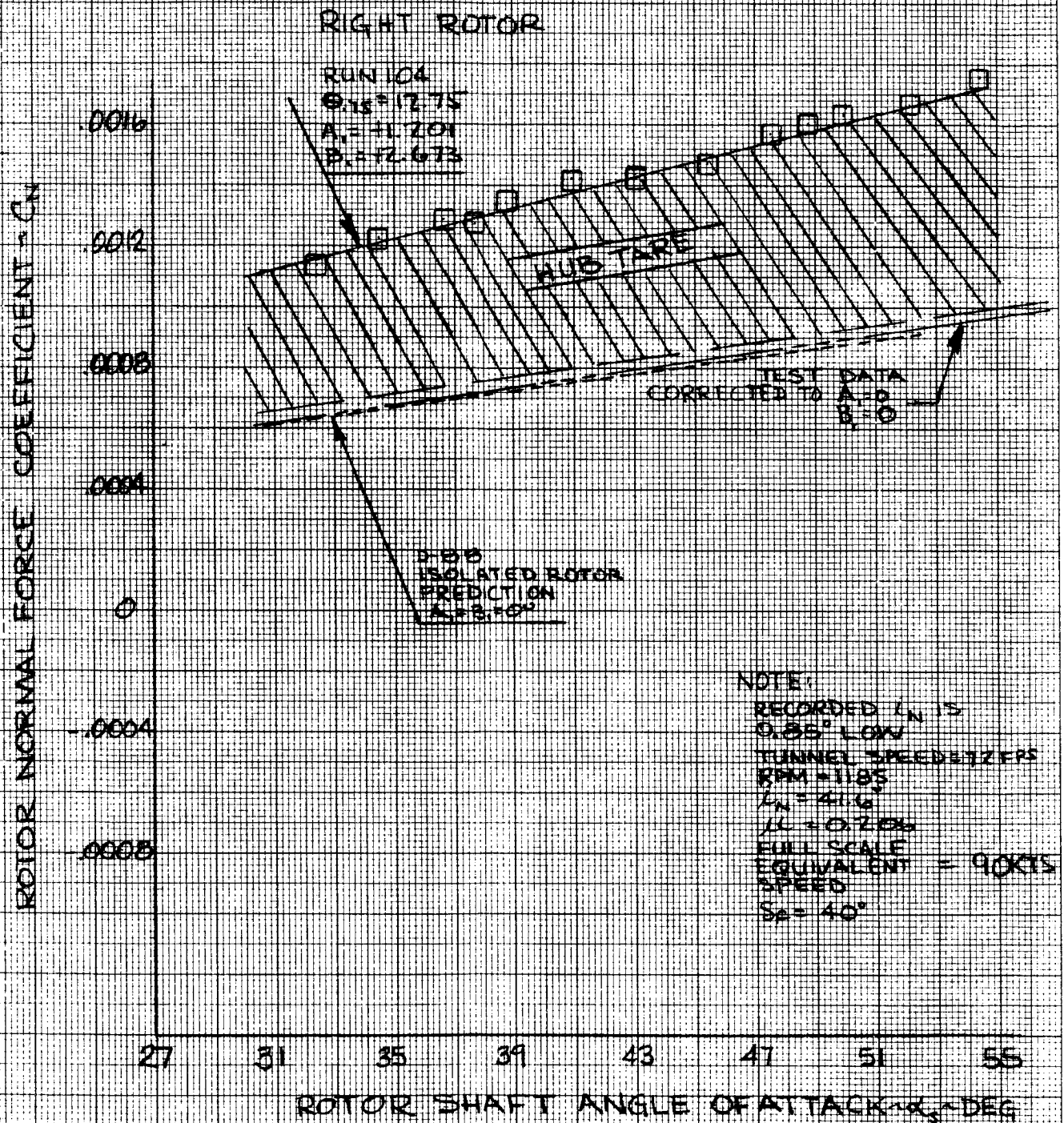


FIGURE 152

COMPARISON OF THEORY AND TEST DATA IN TRANSITION ROTOR PITCHING MOMENT CHARACTERISTICS

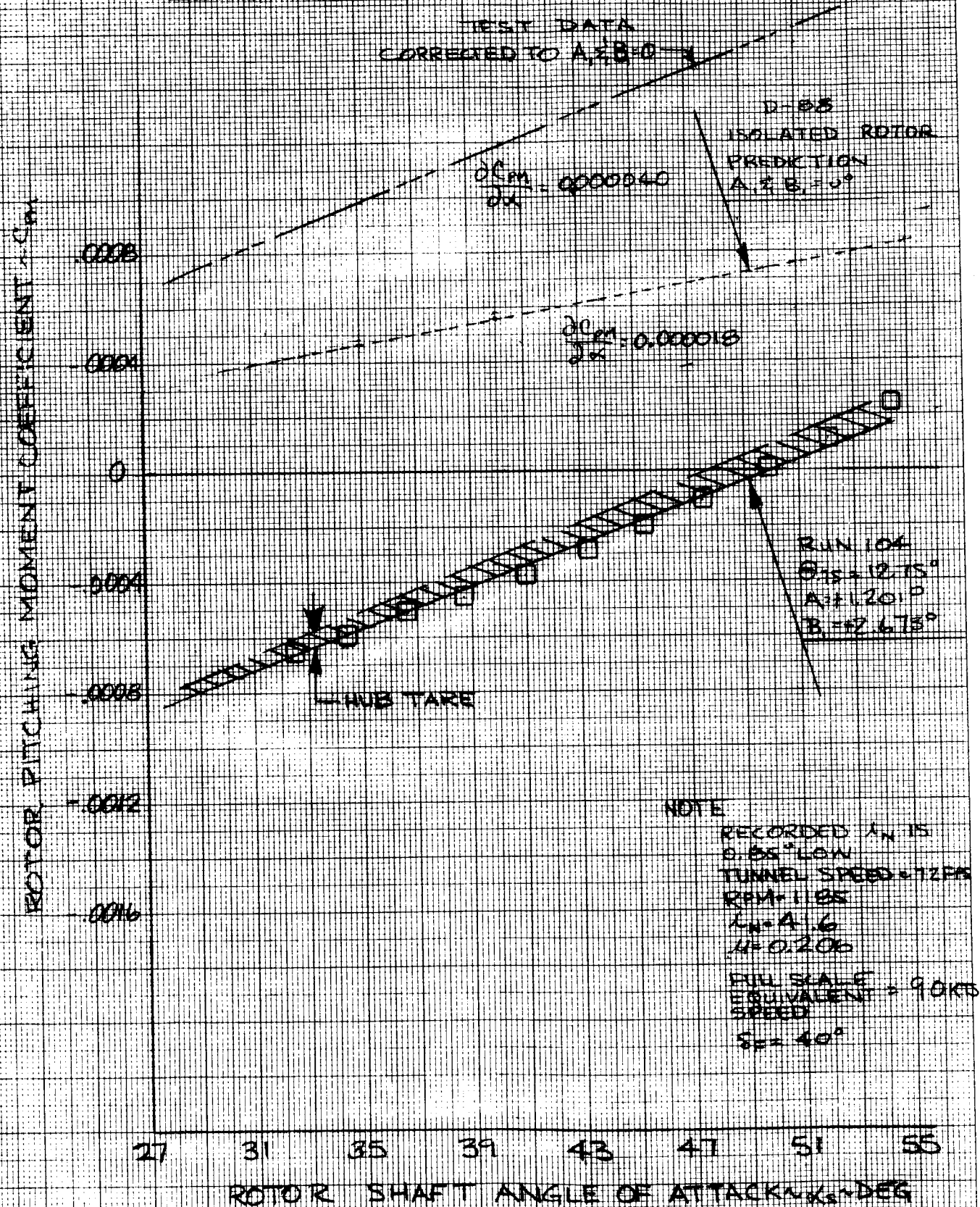


FIGURE 153

COMPARISON OF TEST AND THEORY
FOR
LATERAL CYCLIC ROTOR DERIVATIVES
IN TRANSITION

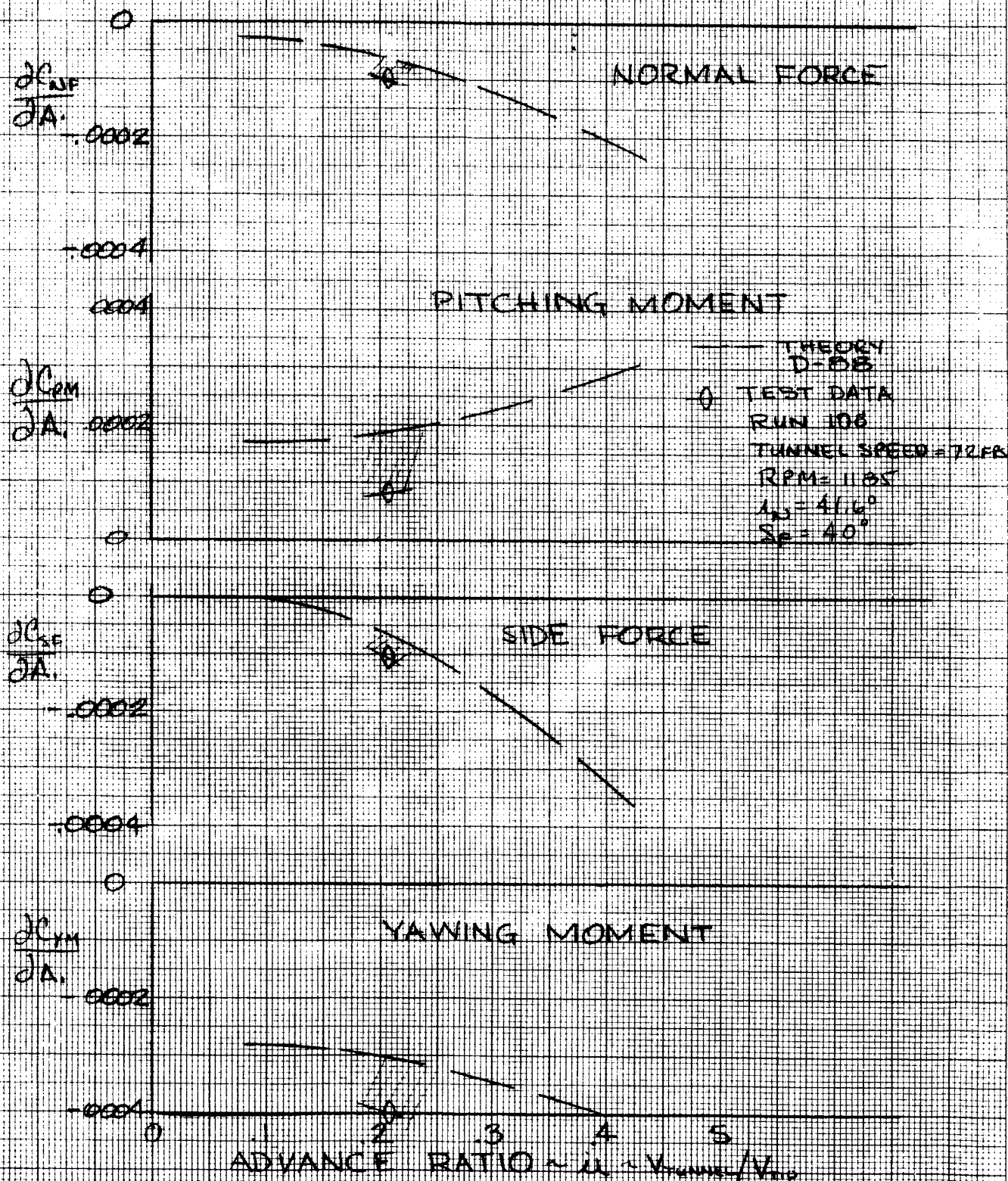


FIGURE 154

COMPARISON OF TEST AND THEORY
FOR
LONGITUDINAL CYCLIC ROTOR DERIVATIVES
IN TRANSITION

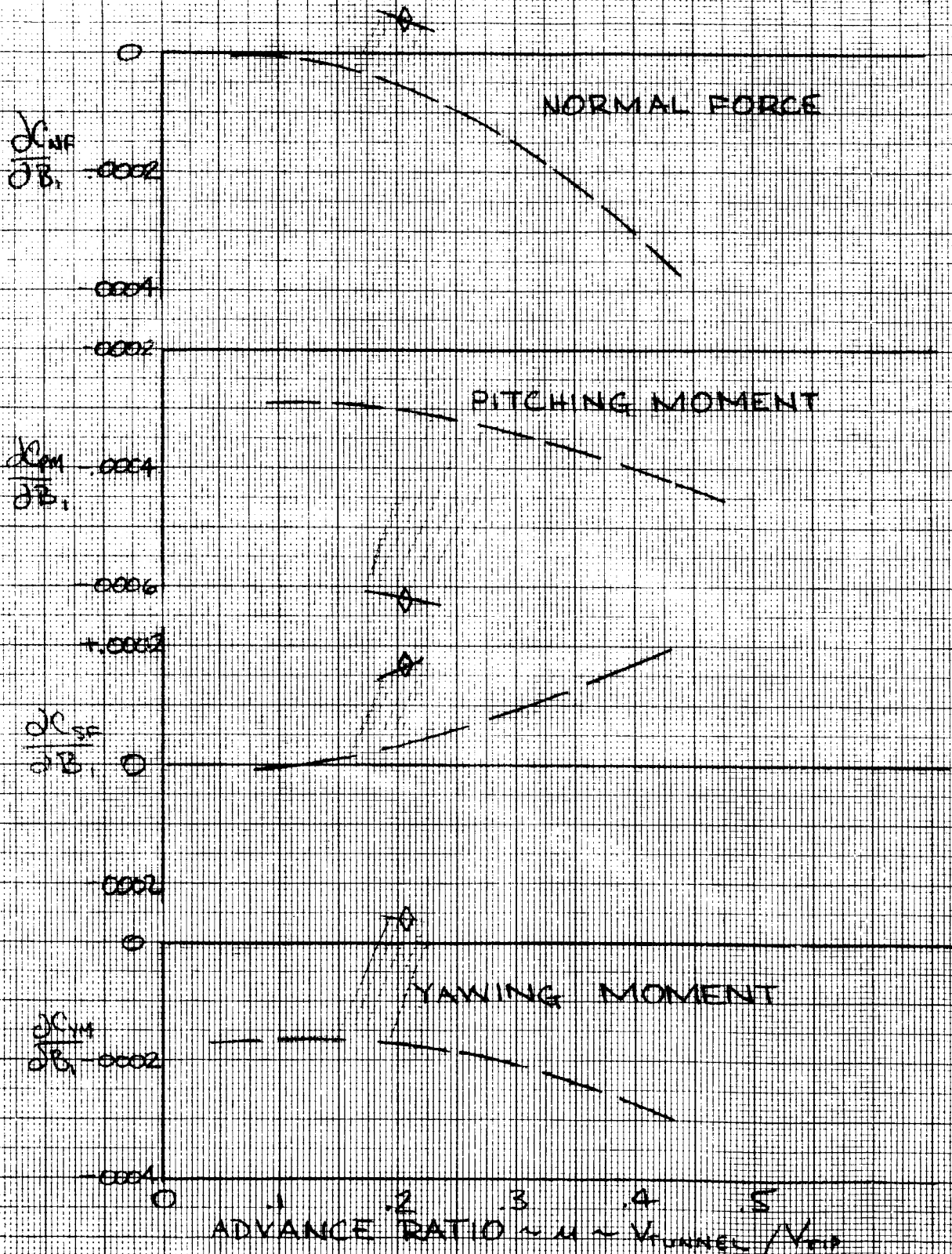


FIGURE 155

5.2 Cruise Stability and Control

The aircraft stability and control and the rotor and airframe contributions for all forward speed in the cruise regime, nacelle incidence of zero degrees, will be presented here. The data analysis includes all the testing accomplished during this test program that addressed Objectives 2, 3, 4, and 8 defined in Section 2.0.

5.2.1 Rotor Stability Derivatives

The rotor stability obtained during this test program include the following test conditions: pitch and yaw investigations at tunnel speeds of 113 ft/sec to 182 ft/sec (full scale equivalent speeds of 142 kts to 225 kts). Pitch and yaw sweeps were also made with various flap settings to establish the rotor contribution to directional stability and to define the effect of wing lift at 113 ft/sec.

Effect of Flap Deflection on Yaw Derivatives

As indicated in Reference 3 the utilization of yaw sweeps in the cruise mode provides a representation of an isolated rotor since the wing circulation or lift is constant and therefore the only variable is the rotor attitude. Yaw sweeps were made at 113 ft/sec, equivalent to 142 kts for the full scale aircraft, which is representative of the end of transition. Figure 156 presents the airframe lift for this testing with flap settings of 0, 20 and 40 degrees deflection. This data shows no variation with yaw angle and represents the lift of the aircraft with the rotor and spinner characteristics removed. As indicated previously there was some slop in the rotor control and this results in steps and shifts in

the data trends. It is therefore necessary to examine the cyclic and collective variation during each run as well as the rotor thrust (C_T) and power (C_P) coefficients to ensure proper data fairing is achieved. Figures 157 and 158 show these variations and provide the basis for the data fairing in the subsequent curves. The trends in C_T and C_P appear to reflect the impact of airframe lift, indicating that as the lift increases the thrust and power decrease by proportional amounts. Normal force characteristics presented in Figure 159 also reflect the direct influence of wing lift with respect to level but the slope, derivatives, are the same for each of the flap deflections. The rotor pitching moment, Figure 160, shows an increase in moment with increasing flap deflection from 0-degree to 20-degrees. When increasing the flap deflection from 20-degrees to 40-degrees there is no increase in the rotor pitching characteristics. This is more representative of the trends reflected in the longitudinal cyclic data of Figure 157. The level of side force, Figure 161, decreases with increasing flap deflection but the derivatives show no change with flap deflection. Yawing moment presented here, Figure 162, appear to increase in magnitude with flap deflection but this trend follows the change in longitudinal cyclic and indicates that flap deflection has no effect on yawing moment derivative. These derivatives, summarized in the following table, show the impact on directional stability made by the rotor and also represent the isolated rotor characteristics.

DIRECTIONAL STABILITY DERIVATIVES

TUNNEL SPEED V	ADVANCE RATIO μ	FLAP DEFLECTION δ_F	$\frac{\partial C_{NF}}{\partial \Psi}$	$\frac{\partial C_{PM}}{\partial \Psi}$	$\frac{\partial C_{SF}}{\partial \Psi}$	$\frac{\partial C_{YM}}{\partial \Psi}$
113 fps	0.462	0°	0.000003	-0.000215	0.000280	-0.000006
		20°	0.000003	-0.000215	0.000280	-0.000006
		40°	0.000003	-0.000215	0.000280	-0.000006

Effect of Forward Speed on Yaw Derivatives

Directional stability testing was extended from 113 ft/sec to speeds up to 182 ft/sec, with a flap deflection of zero, which is equivalent to 225 kts for the full scale aircraft. The rotor characteristics are presented in Figures 163 to 167 showing normal force, pitching moment, side force and yawing moment characteristics as influenced by yaw angle and speed. This data is faired to achieve a constant level of collective and cyclic so that the resulting derivatives reflect only the yaw angle influence. These derivatives are summarized in the table below.

DIRECTIONAL STABILITY DERIVATIVES

TUNNEL SPEED V	ADVANCE RATIO μ	FLAP DEFLECTION δ_F	$\frac{\partial C_{CN}}{\partial \Psi}$	$\frac{\partial C_{PM}}{\partial \Psi}$	$\frac{\partial C_{SF}}{\partial \Psi}$	$\frac{\partial C_{YM}}{\partial \Psi}$
fps						
113	0.462	0°	0.000044	-0.000230	0.000320	-0.000011
113	0.462	0°	0.000044	-0.000230	0.000360	---
139	0.568	0°	-0.000018	-0.000330	0.000540	-0.000149
161	0.662	0°	-0.000142	-0.000400	---	---
182	0.750	0°	-0.000300	-0.000465	---	---

There is a slight difference in the normal force and side force derivatives obtained from the flap variation and the speed variation at 113 ft/sec. This appears to be the result of modifying the nacelle fairing between the two sets of runs. The speed variation occurred later in the test program and has a nacelle more representative of the full scale aircraft. This difference does not compromise the fact that the variation of wing lift obtained with flap deflection does not affect the derivatives but only the level.

Effect of Flap Deflection on Pitch Derivatives

Longitudinal stability testing was conducted at a speed of 113 ft/sec with flap deflections of 0, 10, 20 and 40 degrees. From the data obtained during Runs 31, 33, 35, and 37, shown in Figure 168 there is a slight increase in the airframe lift curve slope (C_{L_α}) from 0.065 per degree at zero degrees to $C_{L_\alpha}=0.08$ per degree at 20 degrees flap deflection. Pitch sweeps performed later in the test program, Runs 77 and 80, show a higher lift curve slope ($C_{L_\alpha} = 0.085$ per degree) at zero degrees flap deflection indicating improved wing fuselage lift characteristics. This is a result of improved nacelle fairings and careful fitting of fuselage and wing skins. The changes in lift and lift curve slope are evident in the rotor normal force, pitching moment, side force and yawing moment characteristics presented in Figures 169 through 172 respectively. These variations with rotor shaft angle summarize the effects of flap deflection on rotor longitudinal stability derivatives and are presented in the following table.

LONGITUDINAL STABILITY DERIVATIVES

TUNNEL SPEED V	ADVANCE RATIO μ	δ_F FLAP DEFLECTION	$\frac{\partial C_{NF}}{\partial \alpha}$	$\frac{\partial C_{PM}}{\partial \alpha}$	$\frac{\partial C_{SF}}{\partial \alpha}$	$\frac{\partial C_{YM}}{\partial \alpha}$
113 fps	0.462	0°	0.000500	0.000010	-0.000076	0.000254
		0°	0.000430	0.000065	-0.000060	0.000252
		0°	0.000430	0.000080	-0.000060	0.000515
		10°	0.000500	0.000038	-0.000081	0.000254
		20°	0.000500	0.000054	-0.000125	0.000262
		40°	0.000520	0.000053	-0.000124	0.000270

The effect of lift on rotor characteristics in cruise can be extracted by correcting the data to zero yaw cyclic and examining the variation with lift. Figure 173 presents the variation for normal force and pitching moment at zero degrees rotor shaft angle defining a slope of $\frac{\partial C_{NF}}{\partial C_L} = 0.00090$ and $\frac{\partial C_{PM}}{\partial C_L} = 0.0058$ at 113 ft/sec.

Rotor side force and yawing moment are presented in Figure 174 defining a slope of $\frac{\partial C_{SF}}{\partial C_L} = -0.00042$ and $\frac{\partial C_{YM}}{\partial C_L} = 0.00020$. There is

an apparent zero data shift in runs 35 and 37 that results in an offset in level in the side force trend.

Effect of Forward Speed on Pitch Derivatives

Longitudinal stability testing was expanded from 113 ft/sec to 182 ft/sec and the variation of the rotor characteristics with rotor shaft angle of attack are presented in Figures 175 to 178. A summary of these rotor derivatives are presented the following table.

LONGITUDINAL STABILITY DERIVATIVES

TUNNEL SPEED V	ADVANCE RATIO μ	FLAP DEFLECTION δ_F	$\frac{\partial C_{CN}}{\partial \alpha}$	$\frac{\partial C_{PM}}{\partial \alpha}$	$\frac{\partial C_{SF}}{\partial \alpha}$	$\frac{\partial C_{YM}}{\partial \alpha}$
113	0.462	0°	0.000430	0.000065	-0.000060	0.000250
113	0.462	0°	0.000430	0.000080	-0.000060	--
139	0.568	0°	0.000740	0.000060	-0.000032	-0.000013
139	0.568	0°	0.000740	0.000048	-0.000032	0.00045
161	0.662	0°	0.001160	-0.000017	--	--
182	0.750	0°	0.001470	-0.000070	--	--

Wing Lift Effects on Rotor Derivatives

A definition of the impact of wing lift on the rotor derivatives at other speeds can be achieved by comparing the pitch and yaw derivatives. To eliminate any asymmetric flow influence of the aircraft and/or the hub (spinner) the hub tares presented in Appendix D must be removed. The comparison can then be accomplished by reorienting the rotor forces and moments by 90 degrees azimuth as follows:

$$\frac{\partial C_{NF}}{\partial \psi} = -\frac{\partial C_{SF}}{\partial \alpha}$$

$$\frac{\partial C_{PM}}{\partial \psi} = -\frac{\partial C_{YM}}{\partial \alpha}$$

$$\frac{\partial C_{SF}}{\partial \psi} = \frac{\partial C_{NF}}{\partial \alpha}$$

$$\frac{\partial C_{YM}}{\partial \psi} = \frac{\partial C_{PM}}{\partial \alpha}$$

Figure 179 presents this comparison and the area between the

trends obtained from yaw sweeps and pitch sweeps is a result of the wing lift influence and is indicated by the shaded area. The lift influence on the force derivatives appears to be an advance ratio squared effect (μ^2) and the influence on the moment derivatives appears to be a μ^4 effect. As seen in the normal force and pitching moment trend, the wing lift effect on the rotor produces a destabilizing contribution to the aircraft stability and must be accounted for in analyzing the aircraft.

Cyclic Effectiveness in Cruise

Testing was accomplished with zero nacelle incidence to determine the cyclic effectiveness in the cruise regime as part of Objective 8 in Section 2.0. This is directed at the reduction of blade loads with the use of low rate cyclic feedback. To determine the azimuth phasing or distribution of lateral (A_1) and longitudinal (B_1) cyclic input for the feedback system requires defining the trend of rotor force and hub moment produced by cyclic. Figures 180 to 183 present the variation of rotor normal force, pitching moment, side force and yawing moment coefficients with lateral cyclic at 113 ft/sec and 161 ft/sec tunnel speed. As a point of clarification, positive lateral cyclic is decreasing blade angle at $\psi=0$ and positive longitudinal cyclic is decreasing blade angle at $\psi=90^\circ$ azimuth. The following table summarizes these derivatives.

LATERAL CYCLIC DERIVATIVES

TUNNEL SPEED V	ADVANCE RATIO μ	FLAP DEFLECTION δ_F	$\frac{\partial C_{NF}}{\partial A_1}$	$\frac{\partial C_{PM}}{\partial A_1}$	$\frac{\partial C_{SF}}{\partial A_1}$	$\frac{\partial C_{YM}}{\partial A_1}$
fps						
113	0.462	0	-0.00021	0.00039	-0.00041	-0.00017
161	0.662	0	-0.00041	0.00066	--	--

The variation of the rotor forces and moments with longitudinal cyclic are shown in Figures 184 to 187 for tunnel speeds of 113 ft/sec and 161 ft/sec. These derivatives are summarized below.

TUNNEL SPEED V	ADVANCE RATIO μ	FLAP DEFLECTION δ_F	$\frac{\partial C_{NF}}{\partial B_1}$	$\frac{\partial C_{PM}}{\partial B_1}$	$\frac{\partial C_{SF}}{\partial B_1}$	$\frac{\partial C_{YM}}{\partial B_1}$
fps						
113	0.462	0	-0.00096	-0.00030	0.00033	-0.00069
161	0.662	0	-0.00154	-0.00028	--	--

The application of this cyclic for blade load minimization at 161 ft/sec is presented in Section 6.3.2 and the associated impact on rotor forces and moment is presented here. This condition is representative of 200 kts for the full scale aircraft. The impact of this load minimization on rotor normal force and pitching moment is presented in Figures 188 and 189 respectively. Reducing the blade loads reduces the normal force and pitching moment derivatives with angle of attack which is stabilizing for the total aircraft and will be quantified in Section 5.2.2.

EFFECT OF FUSELAGE YAW ANGLE & FLAP DEFLECTION ON AIRFRAME LIFT CHARACTERISTICS IN CRUISE

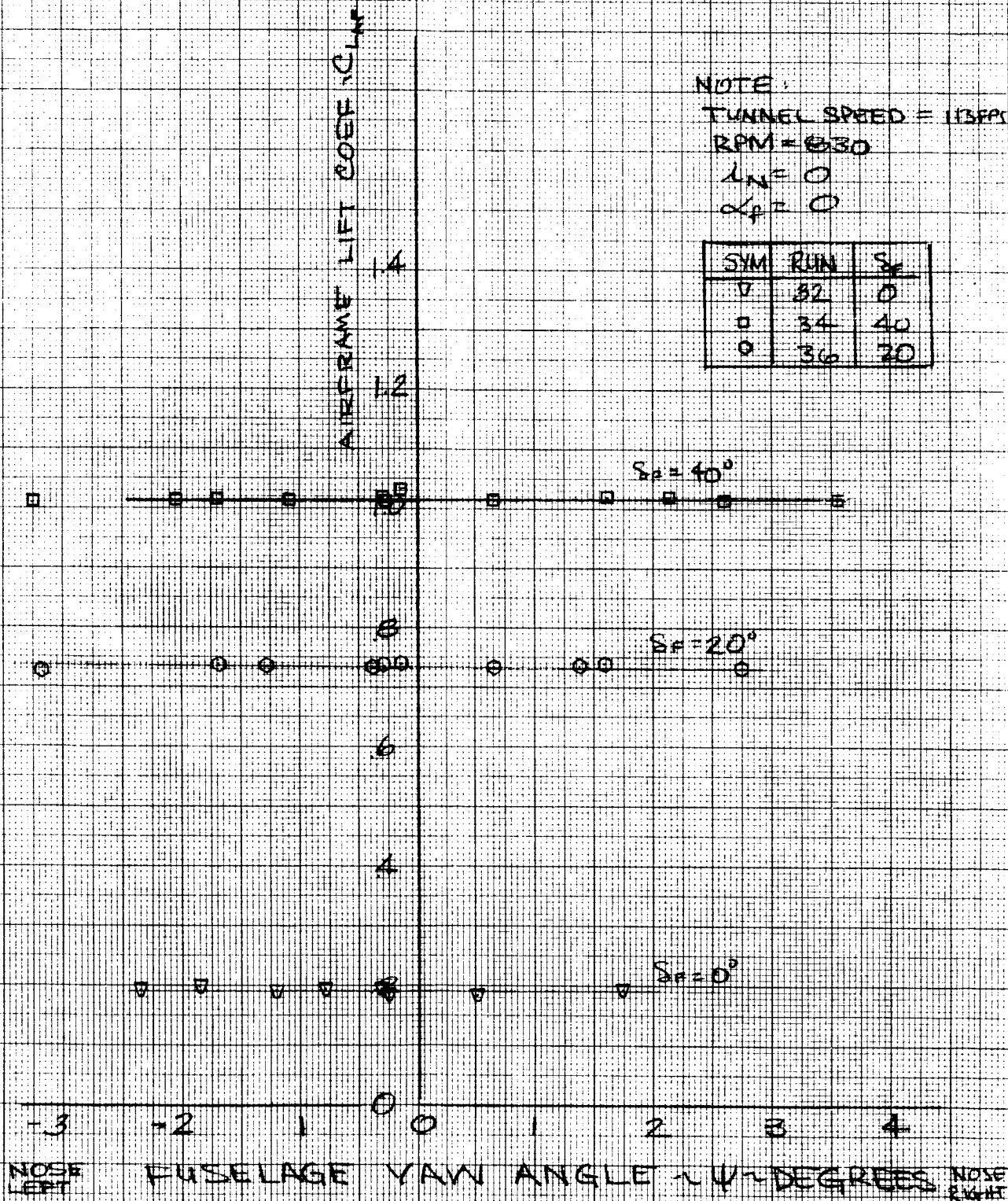


Figure 156

COLLECTIVE & LATERAL AND LONGITUDINAL CYCLIC CHANGES
DURING YAW ANGLE INVESTIGATION
IN CRUISE

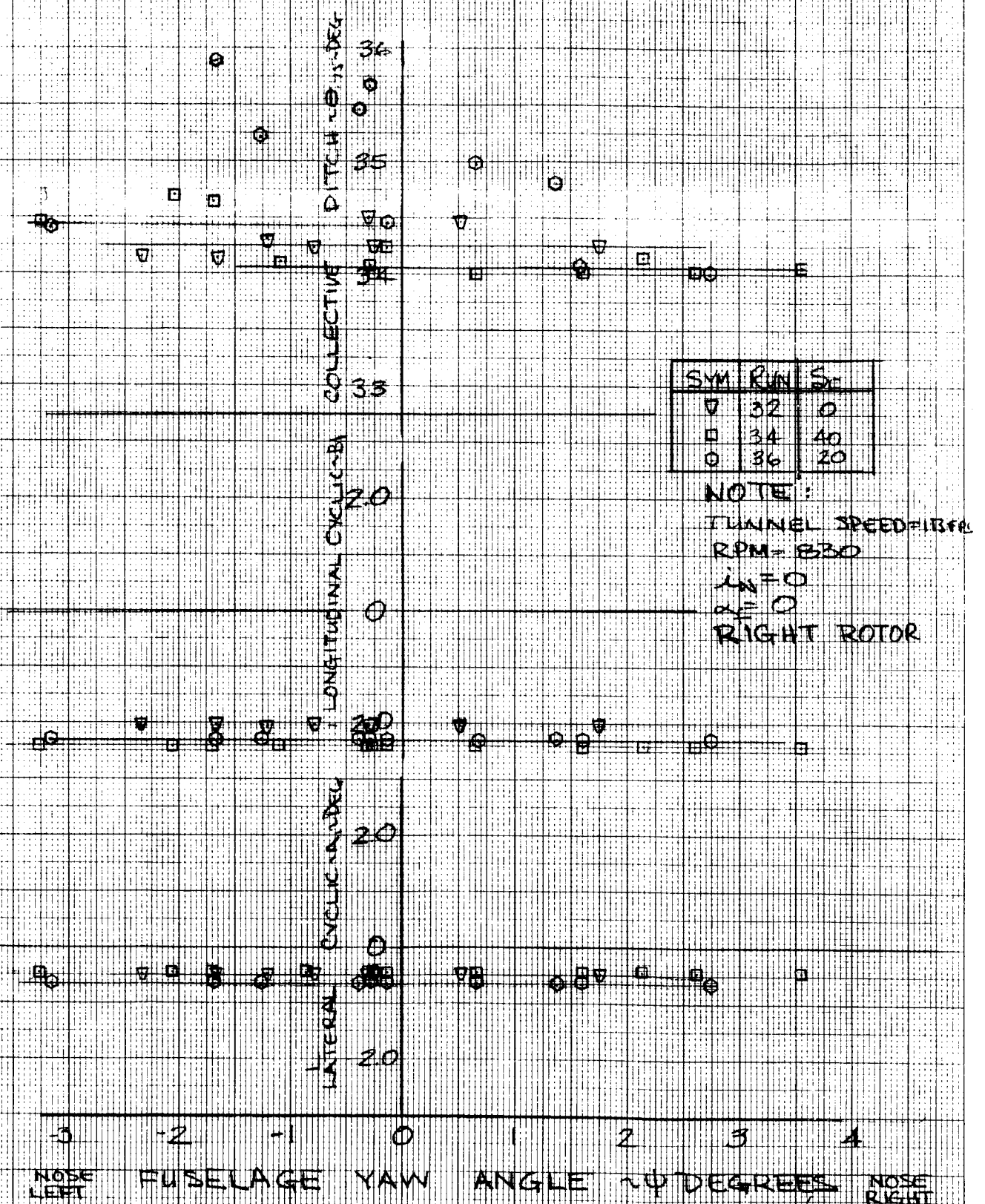


Figure 157

EFFECT OF FUSELAGE YAW ANGLE & FLAP DEFLECTION ON ROTOR THRUST & POWER CHARACTERISTICS IN CRUISE

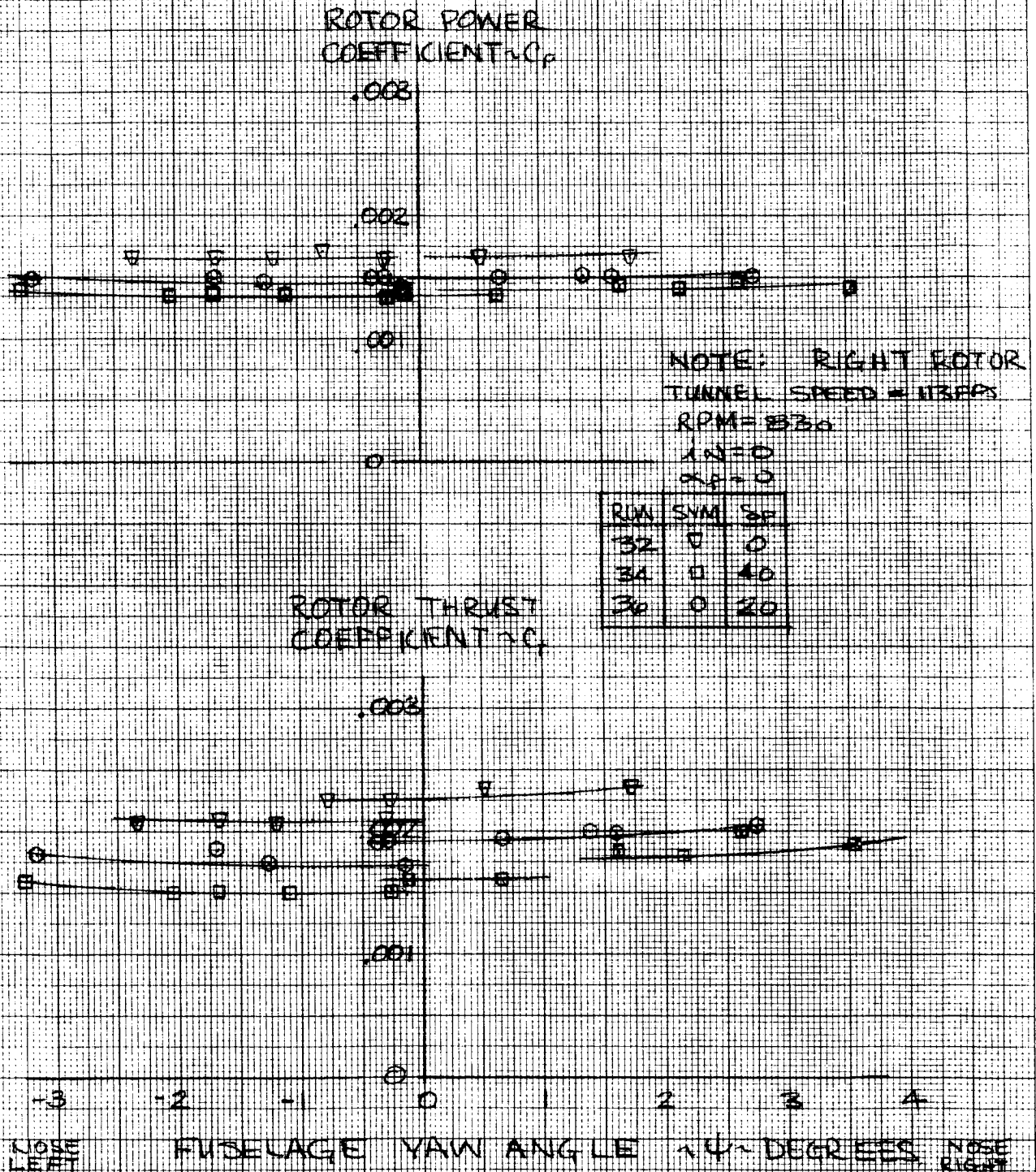


Figure 158

EFFECT OF FUSELAGE YAW ANGLE & FLAP DEFLECTION ON ROTOR NORMAL FORCE IN CRUISE

RUN	SYM	δ	$\frac{\partial C_N}{\partial \psi}$
32	▽	0	0.000003
34	□	40	0.000003
36	○	20	0.000003

NOTE:
TUNNEL SPEED - 113 FPS
RPM - 830
 $\lambda = 0^\circ$
 $\alpha = 0^\circ$
RIGHT ROTOR

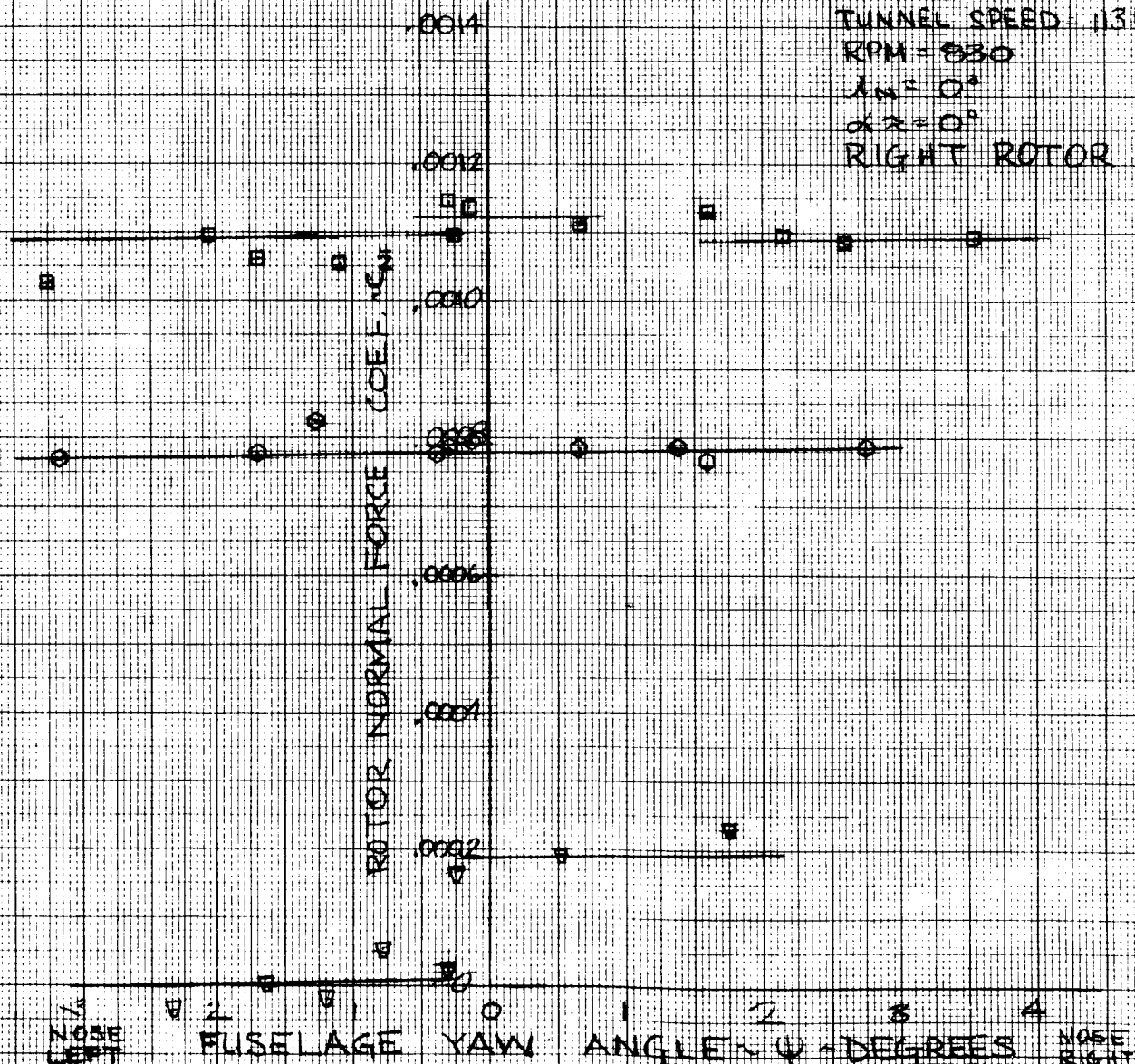


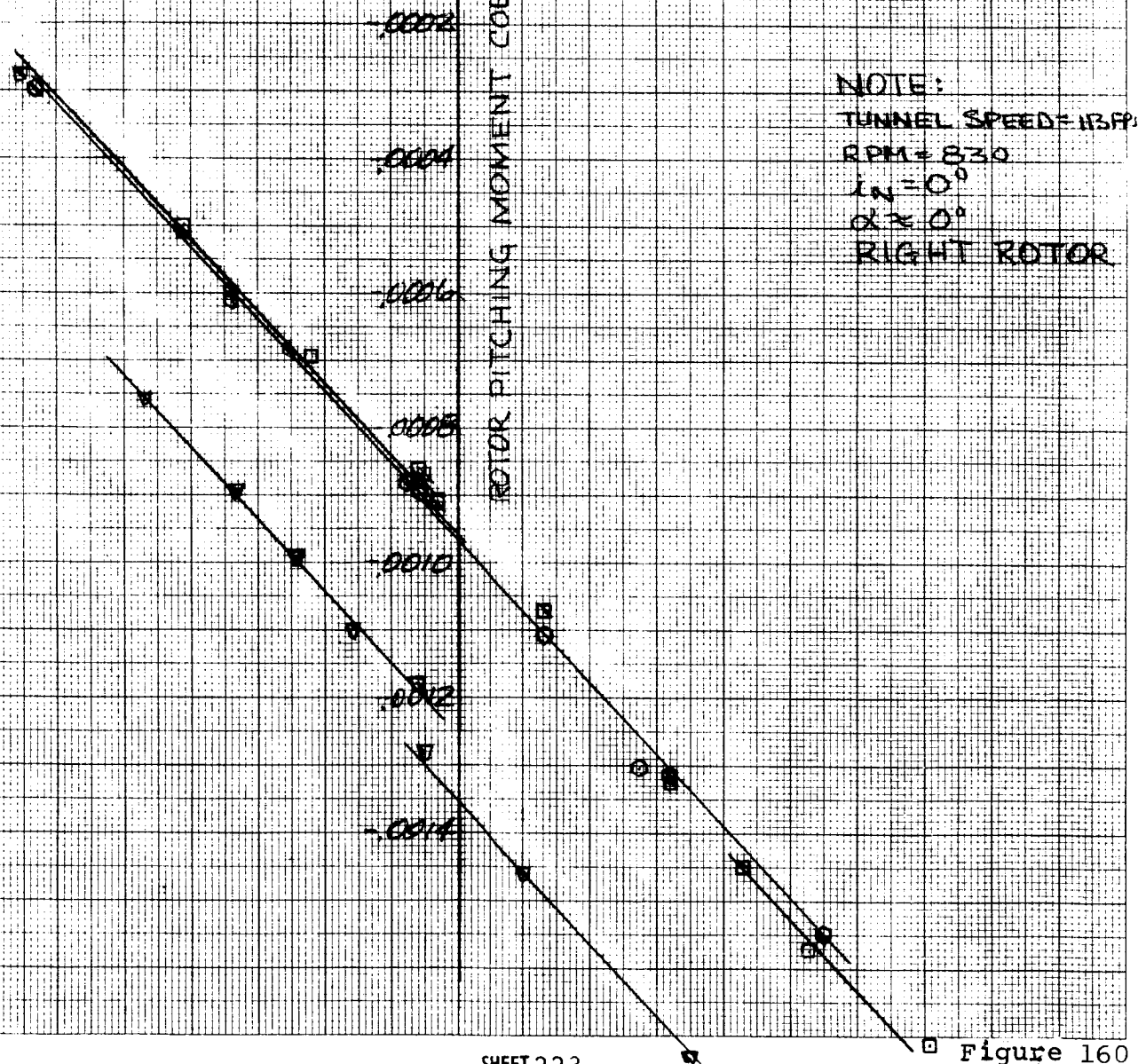
Figure 159

EFFECT OF FUSELAGE YAW ANGLE & FLAP DEFLECTION
ON
ROTOR PITCHING MOMENTS
IN CRUISE

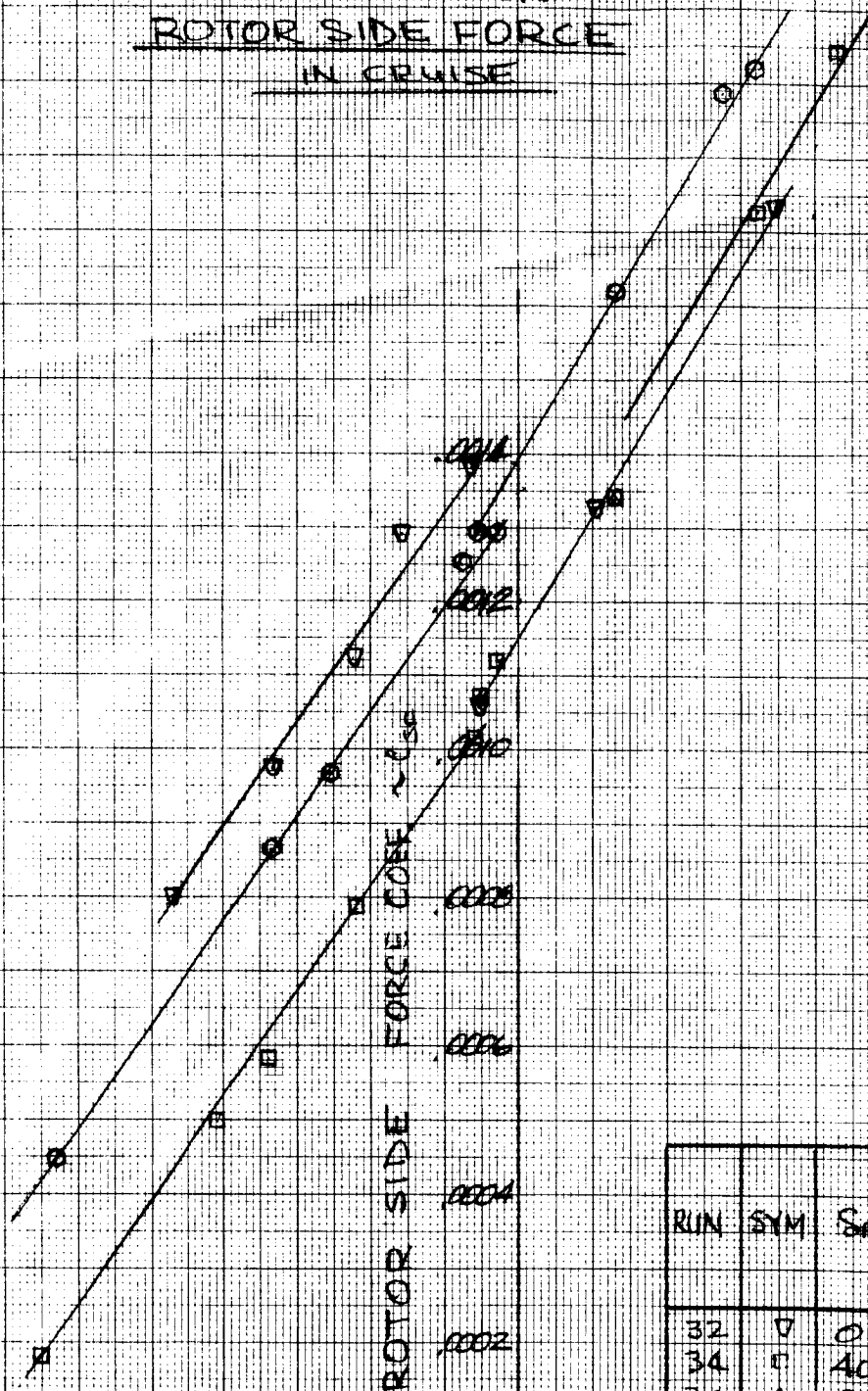
RUN	SYM	S _P	$\frac{\delta C_{PM}}{\delta \psi}$
32	▽	0	-0.000215
34	□	40	-0.000215
36	○	20	-0.000215

NOSE LEFT FUSELAGE YAW ANGLE ψ - DEGREES NOSE RIGHT

-3 -2 -1 0 0 1 2 3 4



EFFECT OF FUSELAGE YAW ANGLE & FLAP DEFLECTION ON ROTOR SIDE FORCE IN CRUISE



NOTE:
TUNNEL SPEED = 113 ft/s
RPM = 630
 $\alpha = 0$
 $\alpha = 2.0$
RIGHT ROTOR

RUN	SYM	δ	$\frac{\partial C_{sf}}{\partial \psi}$
32	○	0	0.000250
34	△	40	0.000260
36	□	20	0.000260

-3 NOSE LEFT
-2
-1
0
1
2
3 NOSE RIGHT
FUSELAGE YAW ANGLE ~ ψ ~ DEGREES

Figure 161

EFFECT OF FUSELAGE YAW ANGLE & FLAP DEFLECTION
ON
ROTOR YAWING MOMENT
IN CRUISE

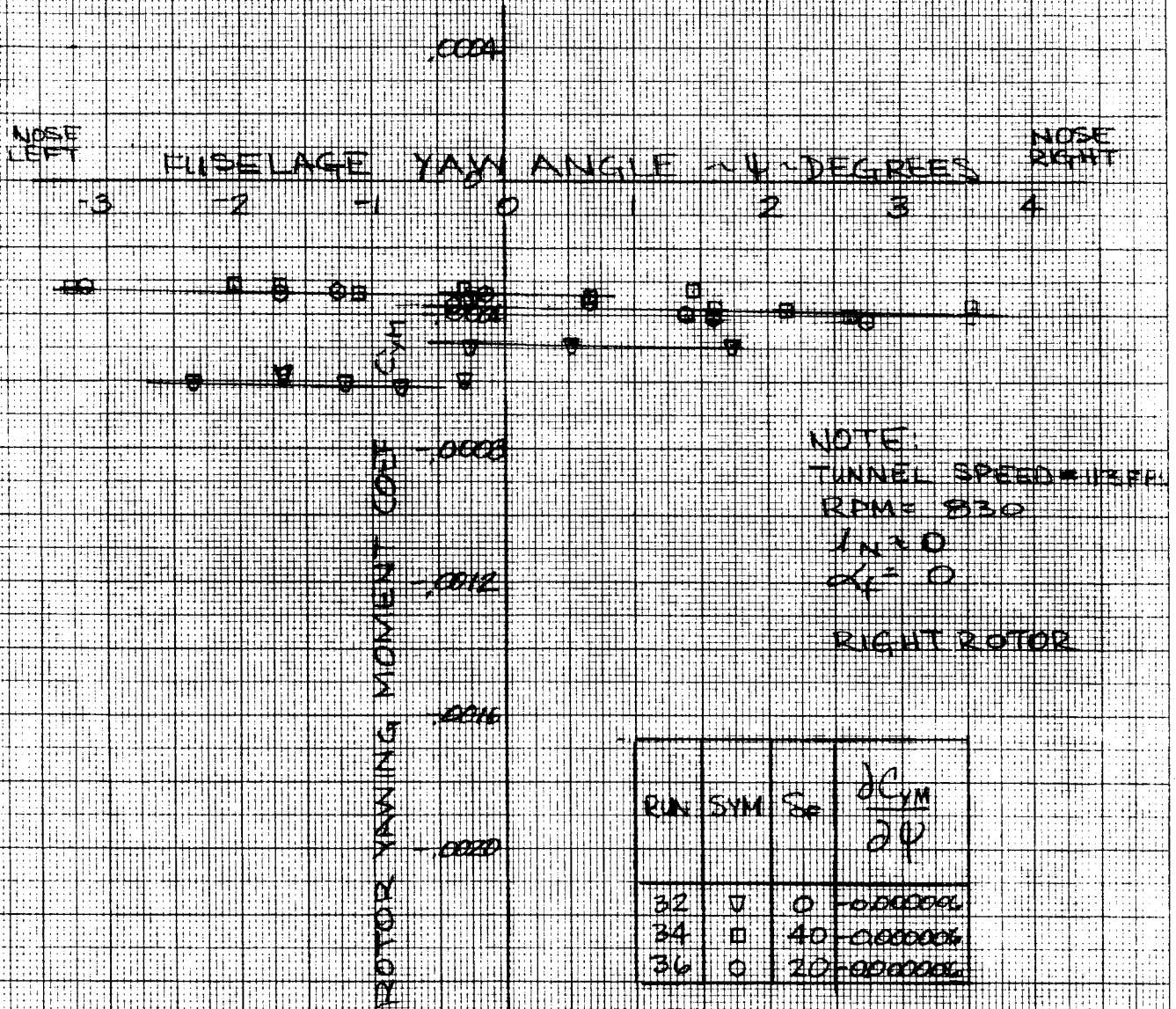


Figure 162

EFFECT OF FUSELAGE YAW ANGLE & SPEED ON ROTOR NORMAL FORCE

CRUISE

SYM	RUN	TUNNEL SPEED (FPS)	$\frac{\partial C_N}{\partial \psi}$
O	78	113	+0.000044
Δ	81	113	+0.000044
□	84	139	-0.000018
◇	90	161	-0.000142
△	98	182	-0.000300

ROTOR NORMAL FORCE
COEFFICIENT $\sim C_{NF}$

NOTES:
RPM = 839
 $\alpha = 0^\circ$
 $\alpha_r = 0^\circ$
 $\delta_F = 0^\circ$
RIGHT ROTOR

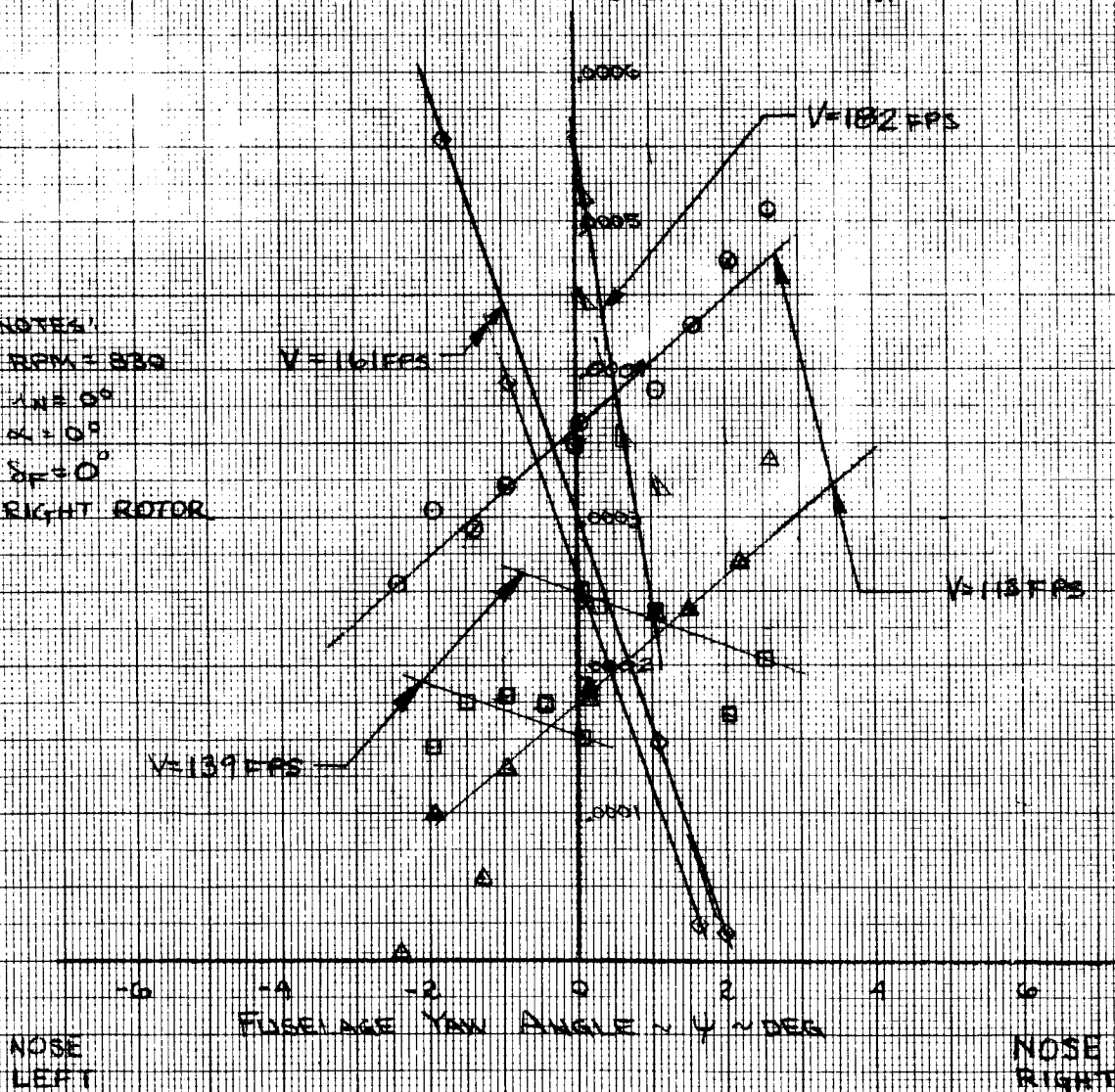


Figure 163

EFFECT OF FUSELAGE YAW ANGLE & SPEED
ON
ROTOR PITCHING MOMENT

CRUISE

ROTOR PITCHING MOMENT
COEFFICIENT $\times C_{PM}$

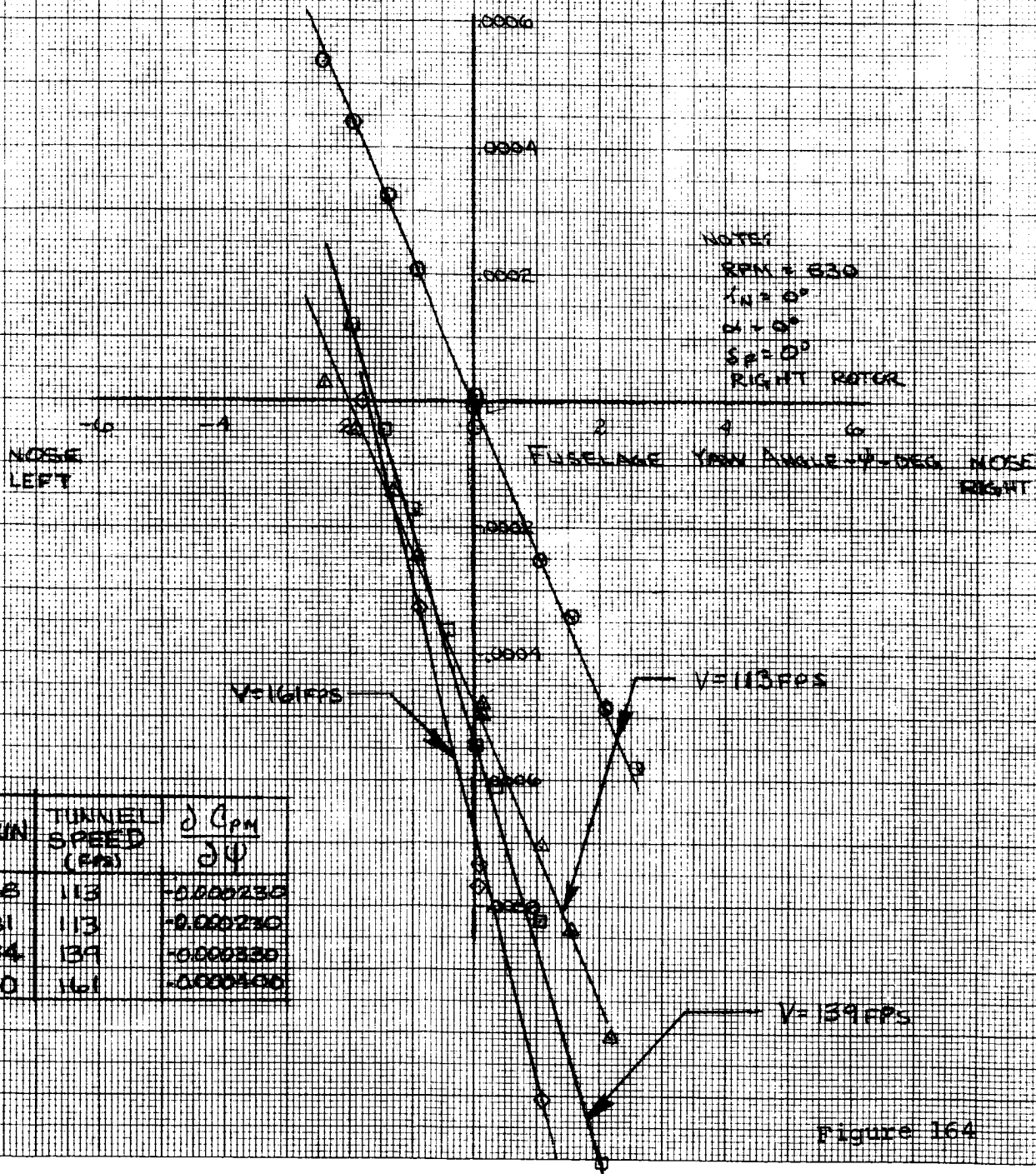


Figure 164

EFFECT OF FUSELAGE YAW ANGLE
ON
ROTOR PITCHING MOMENT

CRUISE

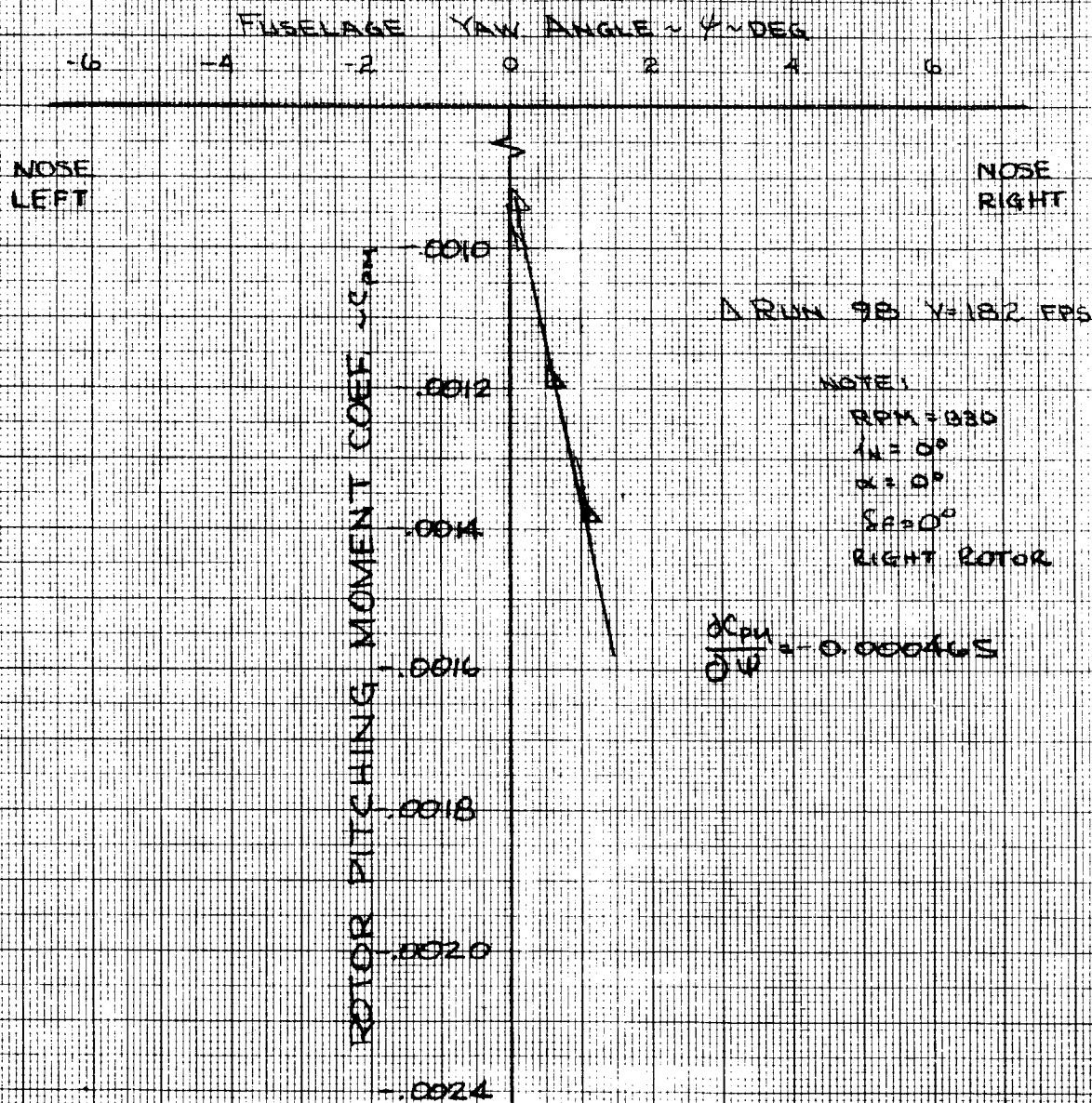


Figure 165

EFFECT OF FUSELAGE YAW ANGLE & SPEED

ON
ROTOR SIDE FORCE

CRUISE

ROTOR SIDE FORCE
COEFFICIENT C_{YR} .0012

SYM	RUN	TUNNEL SPEED (FPS)	$\frac{\partial C_{YR}}{\partial \Psi}$
O	78	113	0.000320
Δ	81	113	0.000360
□	84	139	0.000540

NOTE:

RPM = 830

$\gamma = 0^\circ$

$\alpha = 0^\circ$

$S_p = 0^\circ$

RIGHT ROTOR

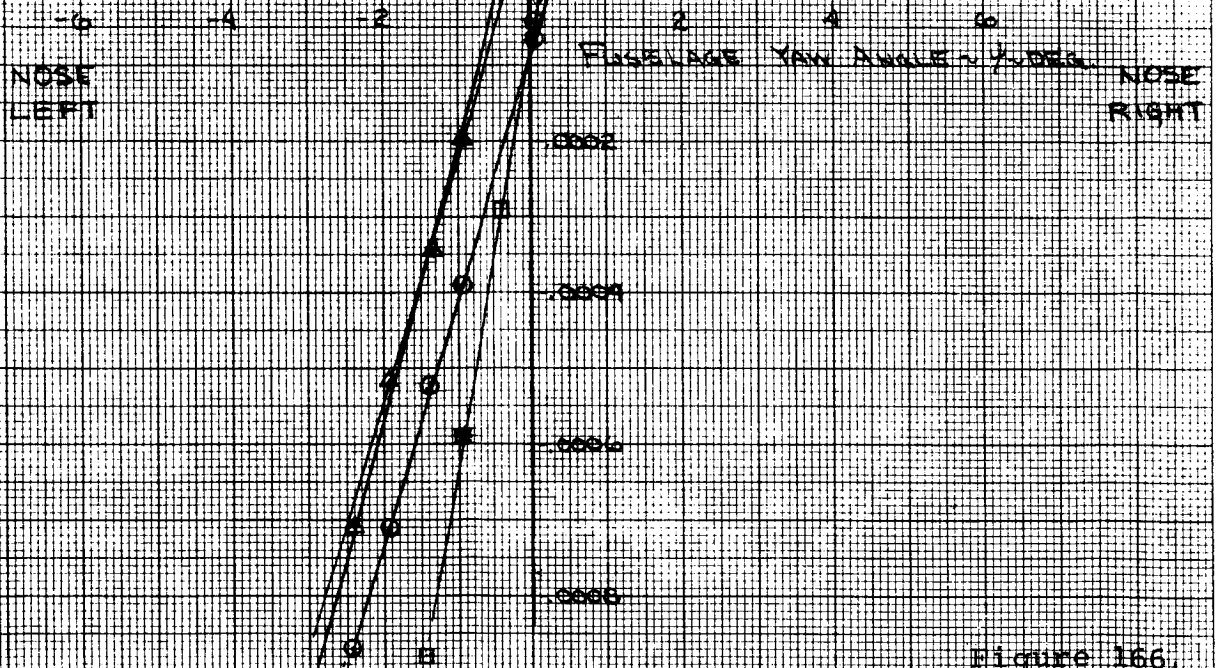


Figure 166

EFFECT OF FUSELAGE YAW ANGLE & SPEED
ON
ROTOR YAWING MOMENT

CRUISE

ROTOR YAWING MOMENT
COEFFICIENT $\sim C_{Ym}$

SYM	RUN	TUNNEL SPEED (FAS)	$\frac{\partial C_{Ym}}{\partial \psi}$
○	78	113	-0.000011
□	84	139	-0.000149

NOTE:

RPW=830

$\psi = 0^\circ$

$\alpha = 0^\circ$

$S_2 = 0^\circ$

RIGHT ROTOR

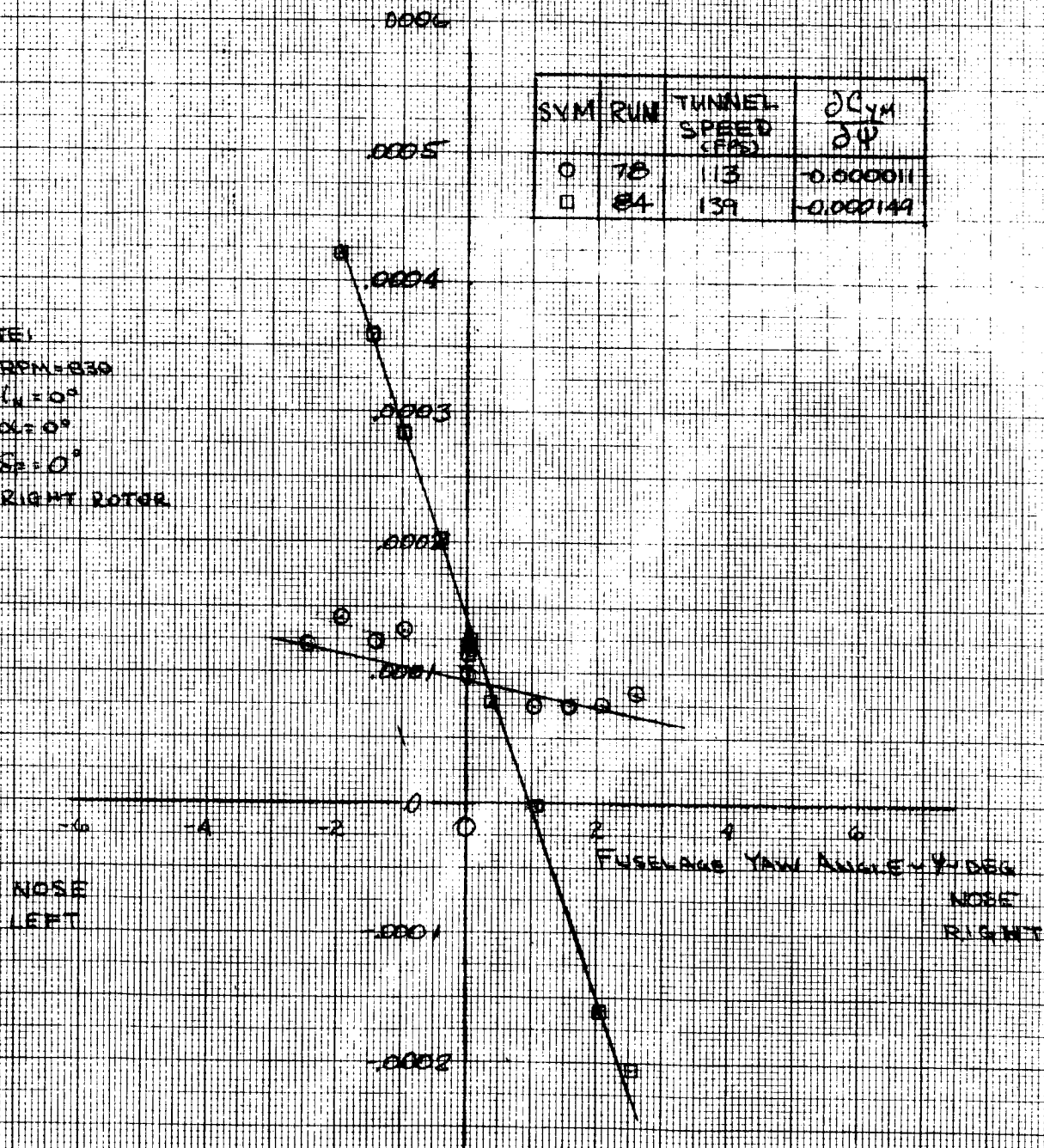


Figure 167

EFFECT OF ROTOR SHAFT ANGLE & FLAP DEFLECTION ON AIRFRAME LIFT COEFFICIENT IN CRUISE

SYM	RUN	δ_F
\diamond	31	0°
\circ	33	40
Δ	35	20
∇	37	10
\square	77	0
\circ	80	0

NOTE
TUNNEL SPEED=113FPM
 $\alpha_0 = 0^\circ$
830 RPM

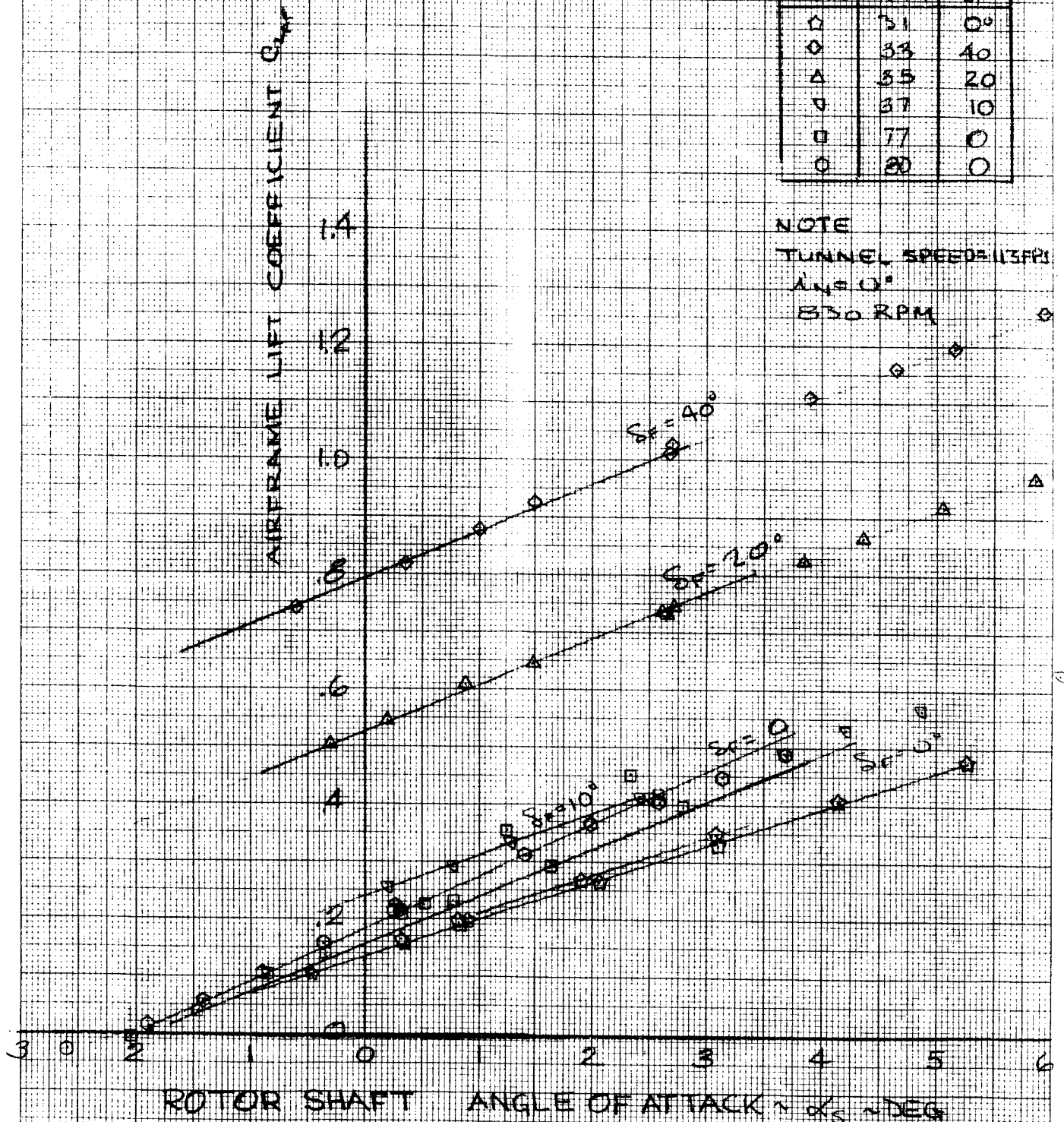
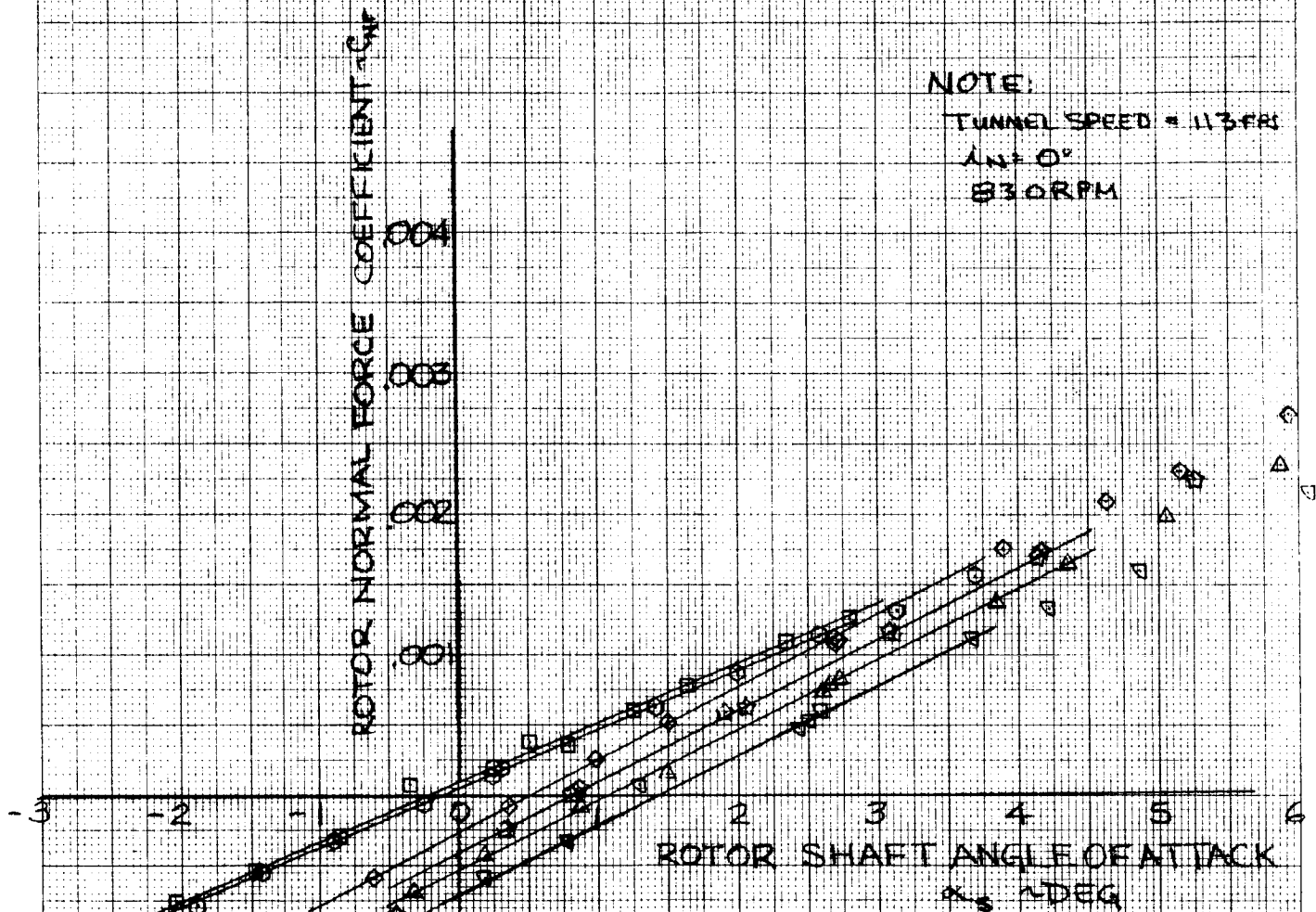


Figure 168

EFFECT OF ROTOR SHAFT ANGLE & FLAP DEFLECTION
ON
ROTOR NORMAL FORCE
IN CRUISE



SYM	RUN	δ
○	31	0°
○	23	40°
△	35	20°
□	37	10°
□	77	0
○	80	0

Figure 169

EFFECT OF ROTOR SHAFT ANGLE & FLAP DEFLECTION
ON
ROTOR PITCHING MOMENT
IN CRUISE

ROTOR PITCHING MOMENT
COEFFICIENT $\sim C_{PM}$

SYM	RUN	δ_c
○	31	0°
○	33	40
△	35	20
□	37	10
□	77	0
□	80	0

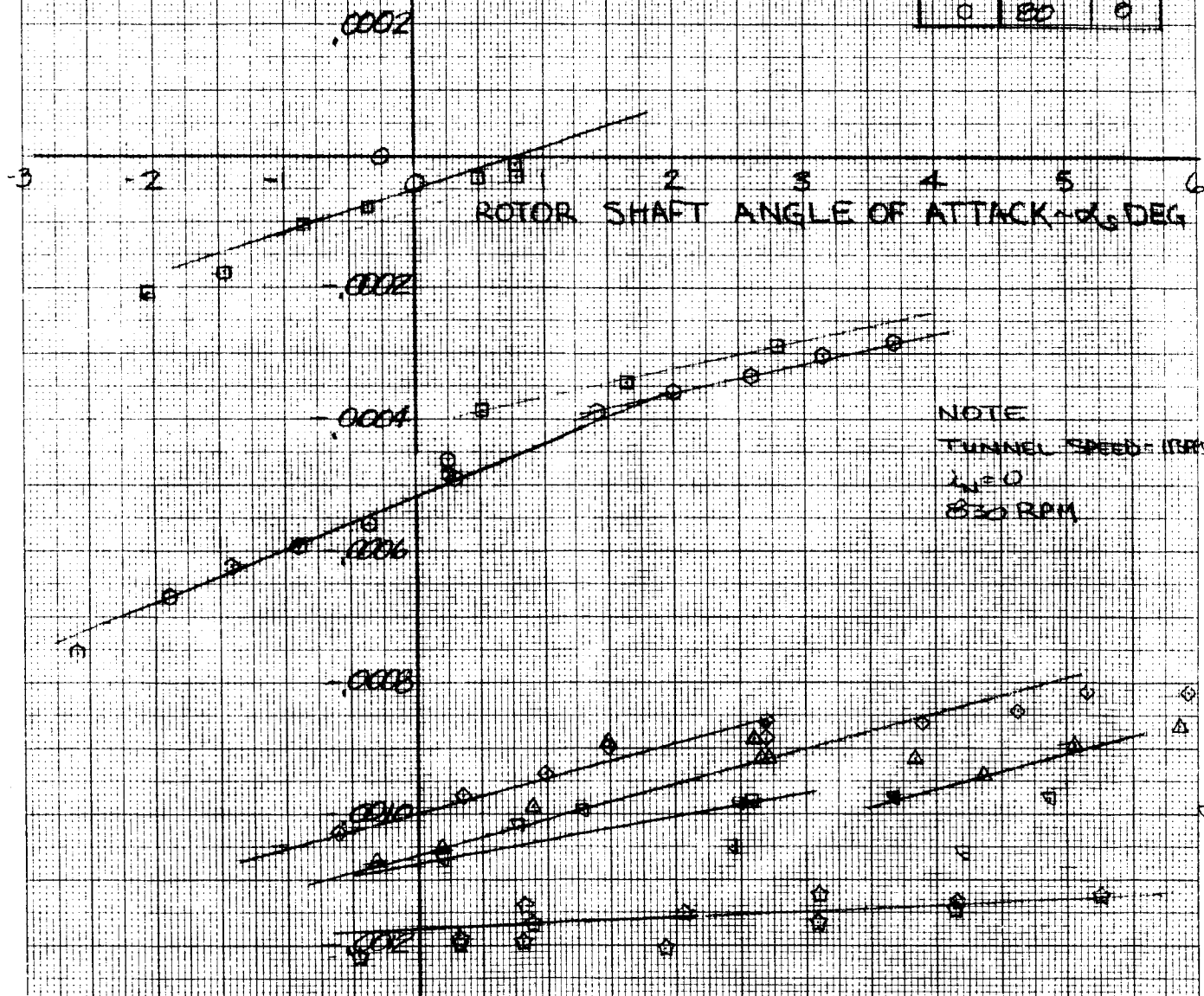


Figure 170

EFFECT OF ROTOR SHAFT ANGLE & FLAP DEFLECTION ON ROTOR SIDE FORCE IN CRUISE

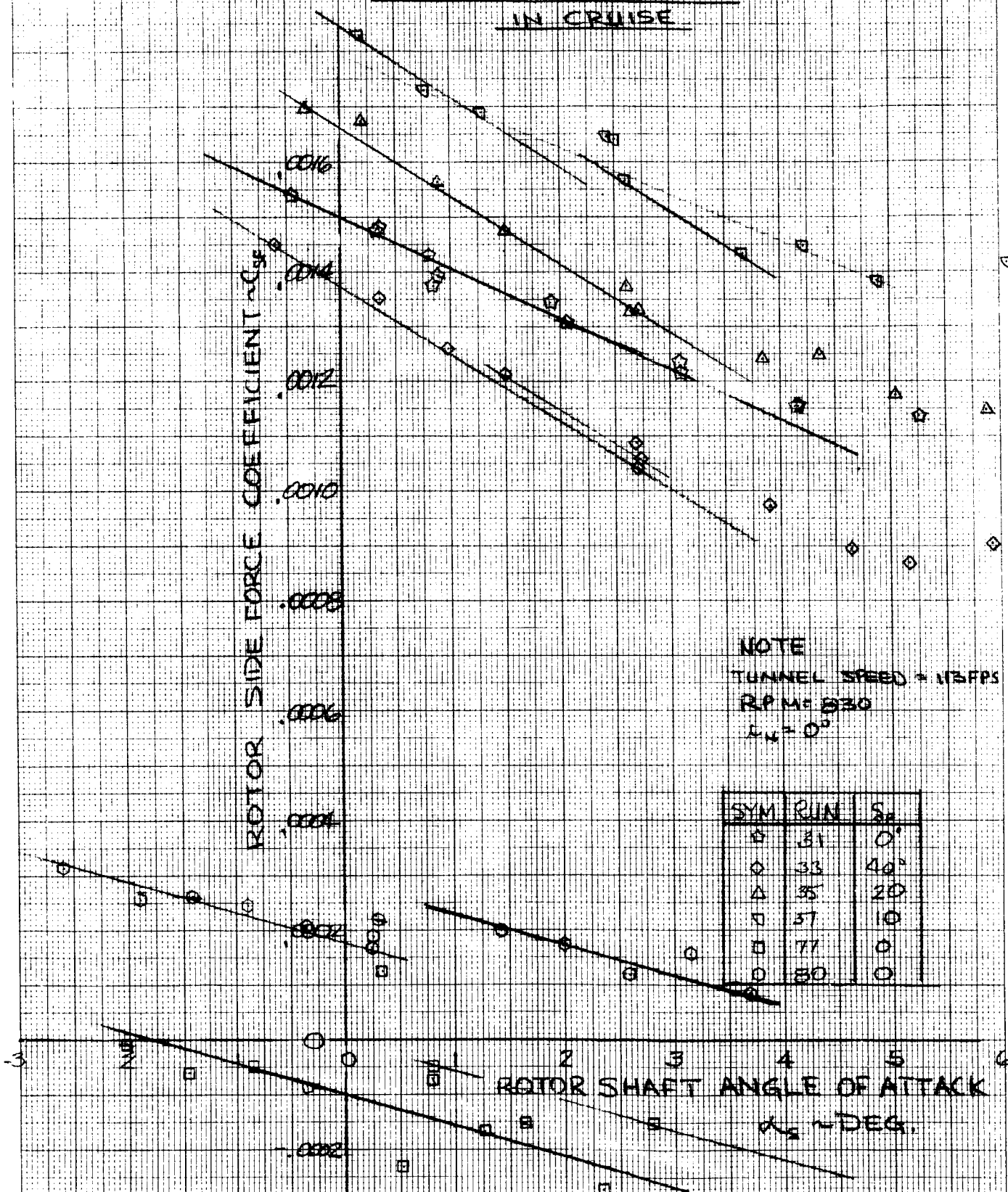


Figure 171

EFFECT OF ROTOR SHAFT ANGLE α & FLAP DEFLECTION ON ROTOR YAWING MOMENT IN CRUISE

NOTE
TUNNEL SPEED = 113 FPM
RPM = 550
 $\alpha = 0^\circ$

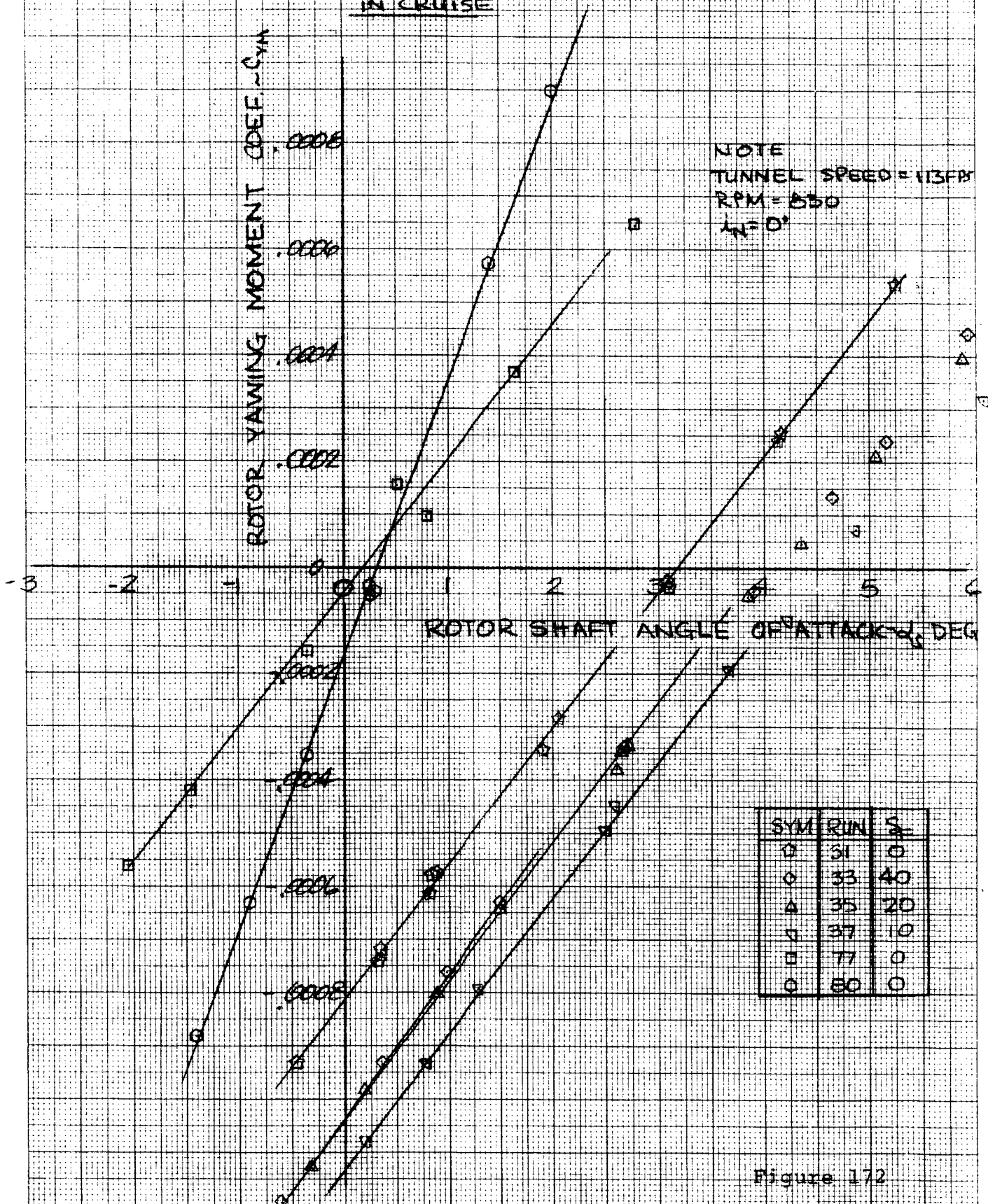


Figure 172

EFFECT OF WING LIFT IN CRUISE ON ROTOR NORMAL FORCE AND PITCHING MOMENT

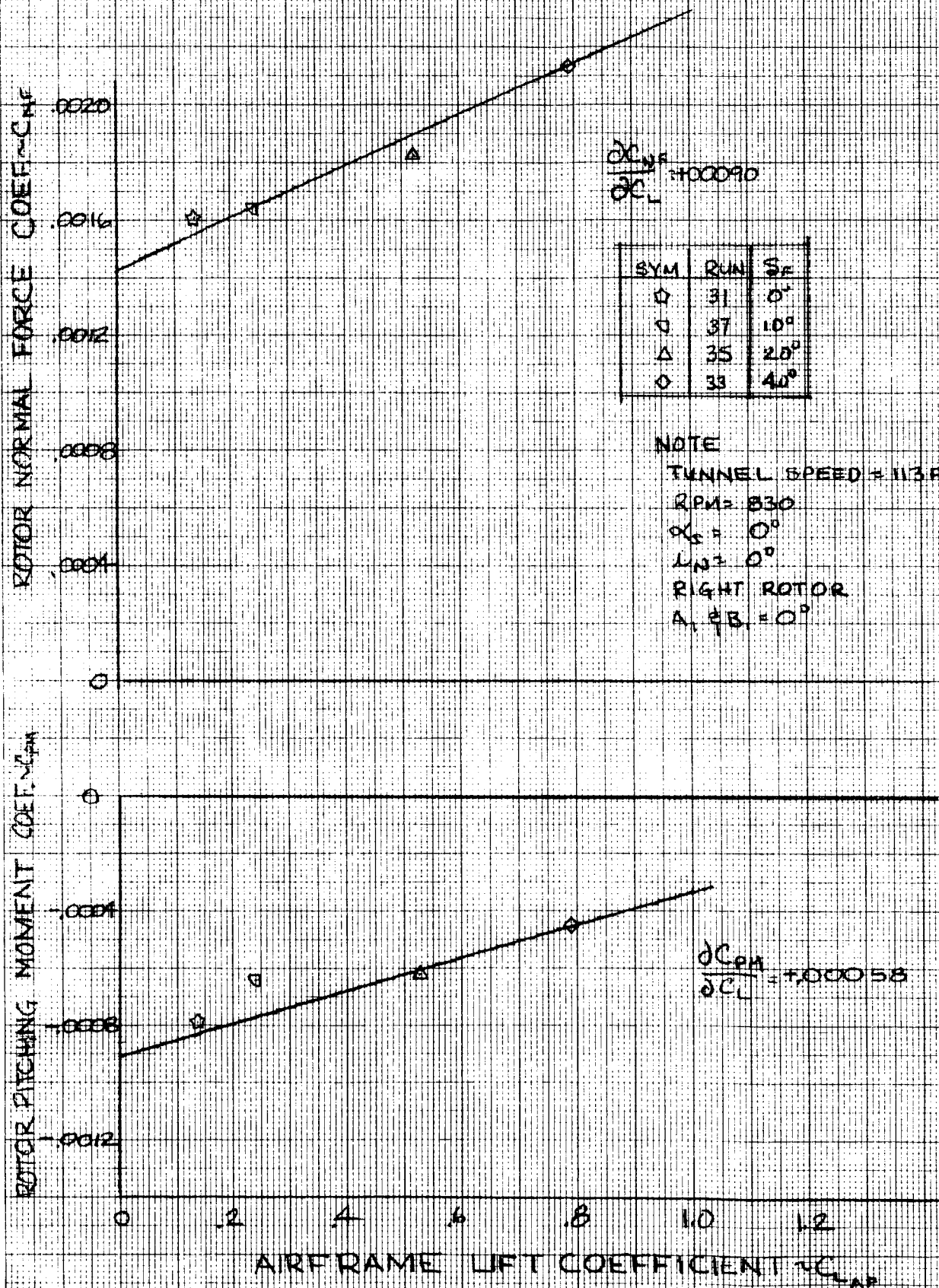


Figure 173

EFFECT OF WING LIFT IN CRUISE ON ROTOR SIDE FORCE AND YAWING MOMENT

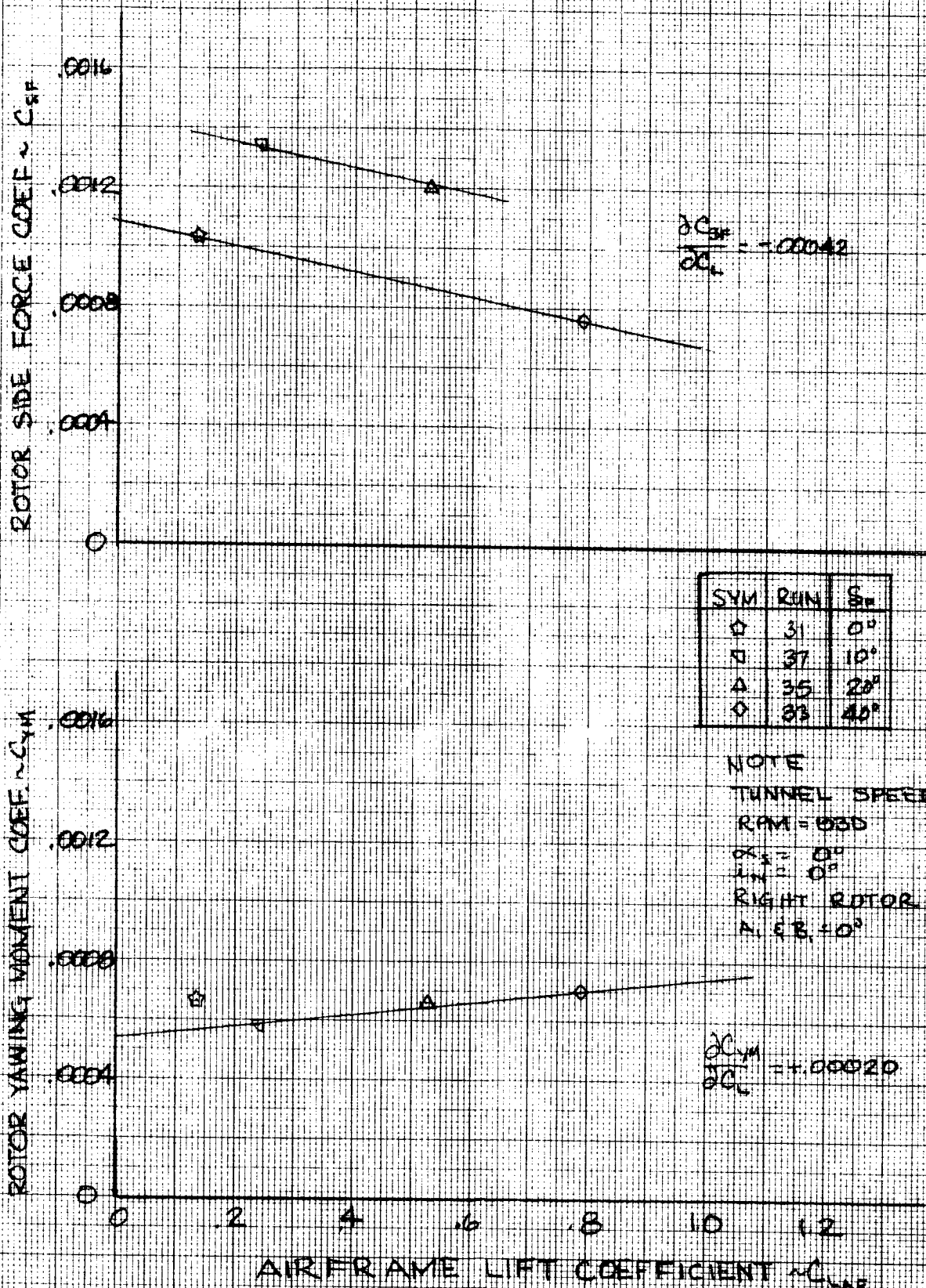
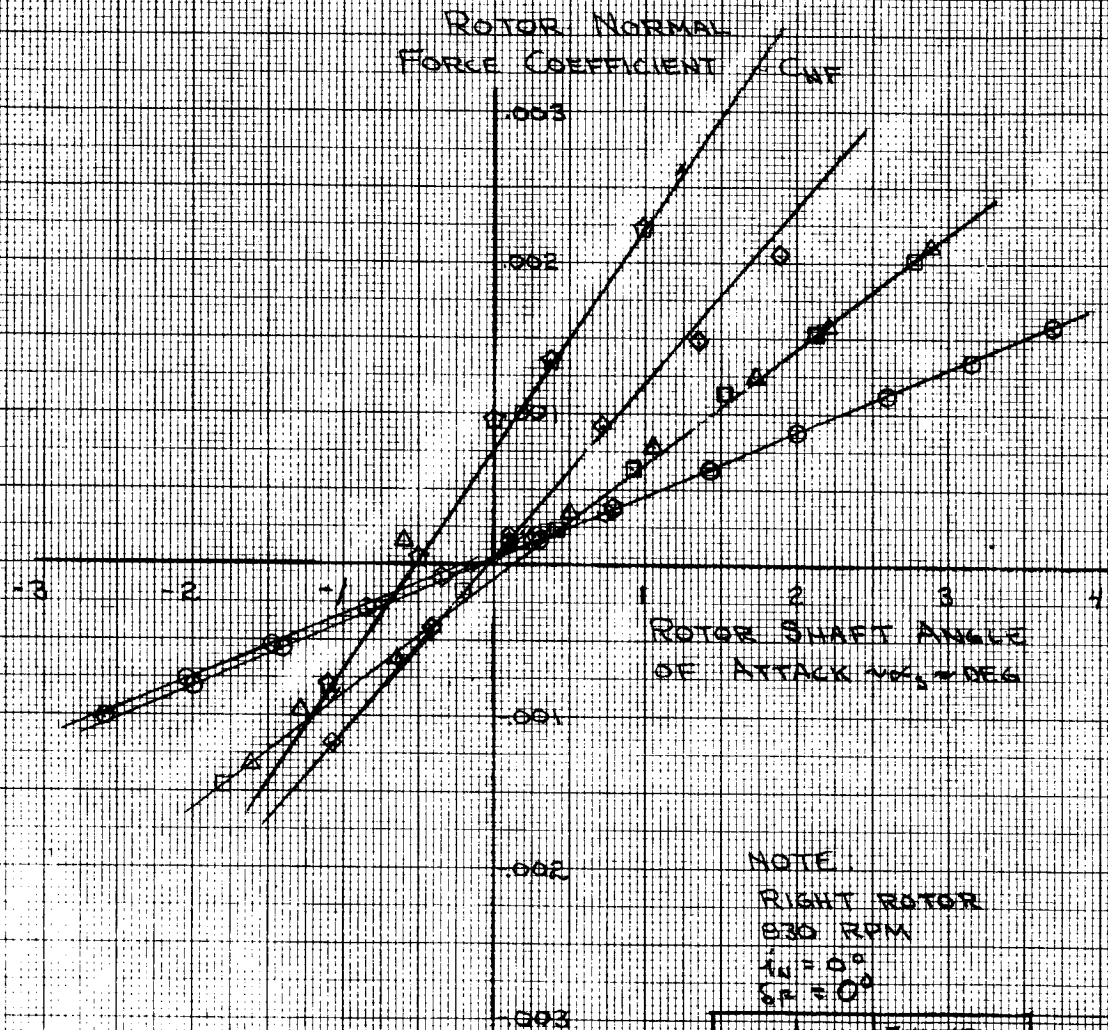


Figure 174

EFFECT OF FORWARD SPEED IN CRUISE ON ROTOR NORMAL FORCE CHARACTERISTICS



SYM	RUN	TUNNEL SPEED (FPS)	ΔCWF
O	77	113	+0.00041
O	80	113	+0.00042
□	83	139	+0.000740
△	86	139	+0.000740
◇	89	162	+0.00160
☆	97	182	+0.00170

Figure 175

EFFECT OF FORWARD SPEED IN CRUISE ON ROTOR PITCHING MOMENT CHARACTERISTICS

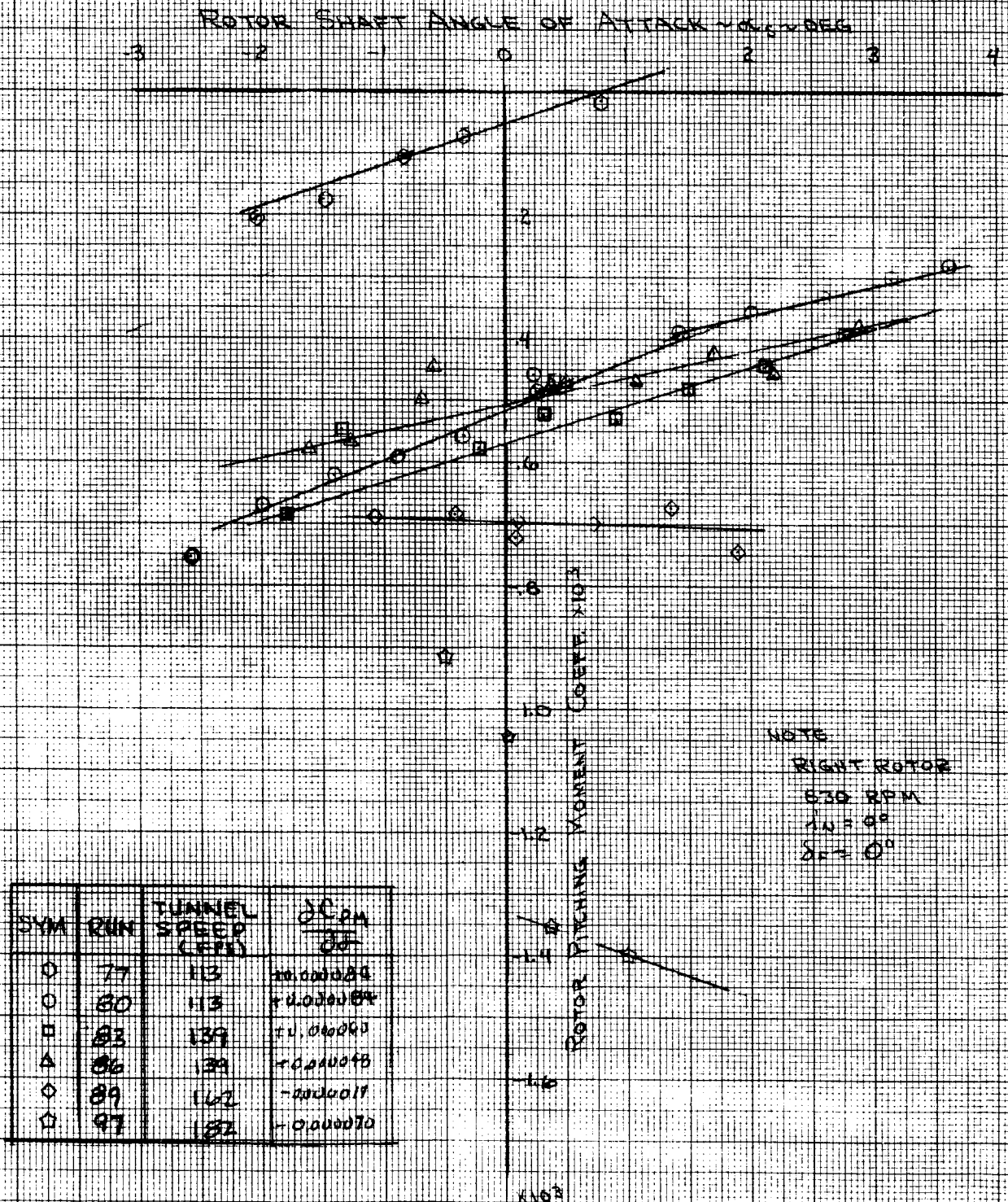
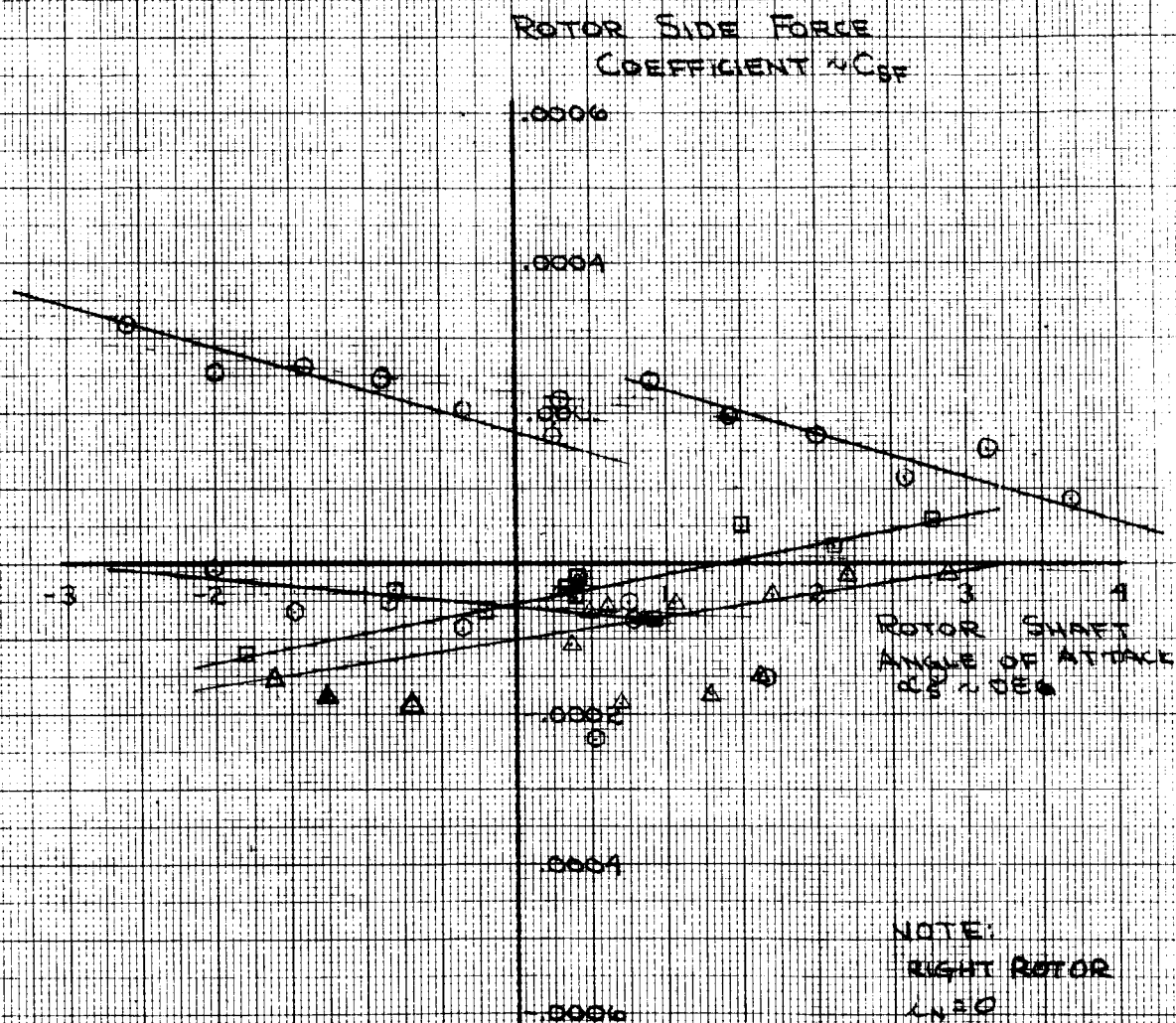


Figure 176

EFFECT OF FORWARD SPEED IN CRUISE ON ROTOR SIDE FORCE CHARACTERISTICS



NOTE:
RIGHT ROTOR
 $C_N = 0$
830 RPM
 $S_0 = 100$

SYM	RUN	TUNNEL SPEED (FPS)	$\frac{\partial C_{SF}}{\partial \alpha}$
O	77	113	-0.000024
O	80	113	-0.000025
□	83	139	-0.000032
Δ	86	139	-0.000032

Figure 177

EFFECT OF FORWARD SPEED IN CRUISE
ON
ROTOR YAWING MOMENT

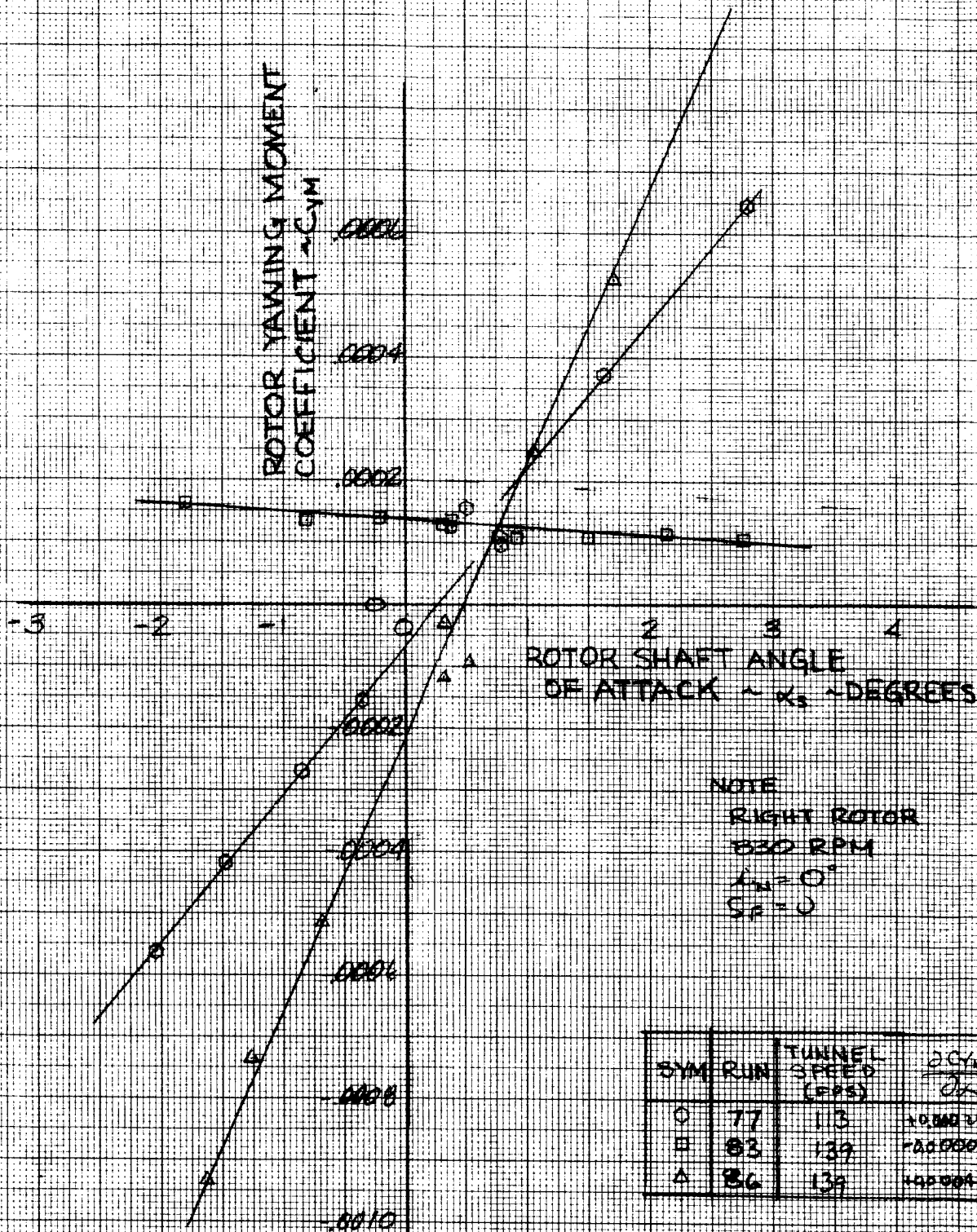


Figure 178

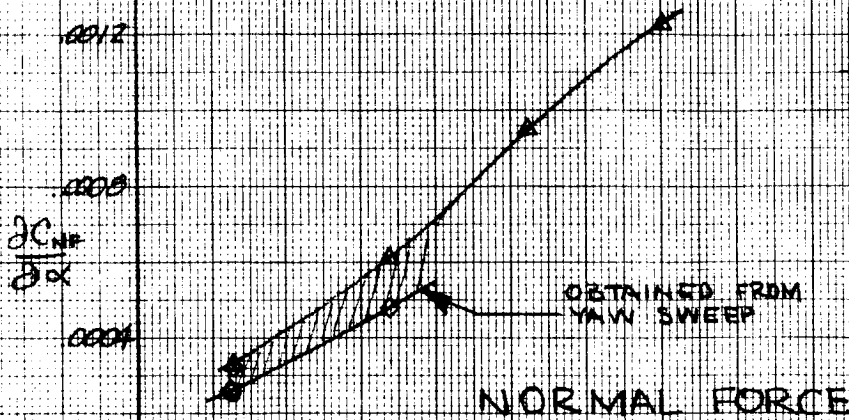
COMPARISON OF ROTOR DERIVATIVES OBTAINED FROM PITCH AND YAW SWEEPS

SYM	RUNS	TYPE OF SWEEP
○	32, 34, 36	ψ
◇	75, 81, 84, 90, 98	ψ
□	31, 33, 35, 37, 77, 80	α
△	77, 80, 83, 86, 89, 97	α

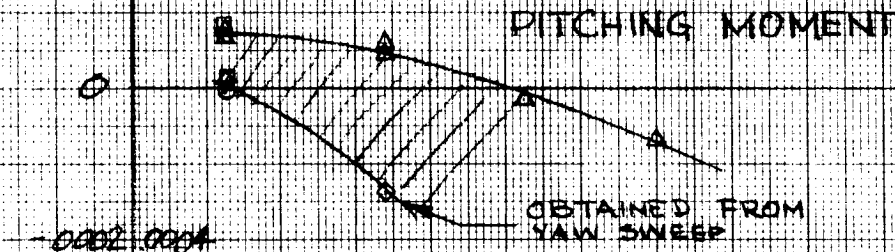
$$\frac{\partial C_{NF}}{\partial \psi} = \frac{\partial C_{NF}}{\partial \alpha}$$



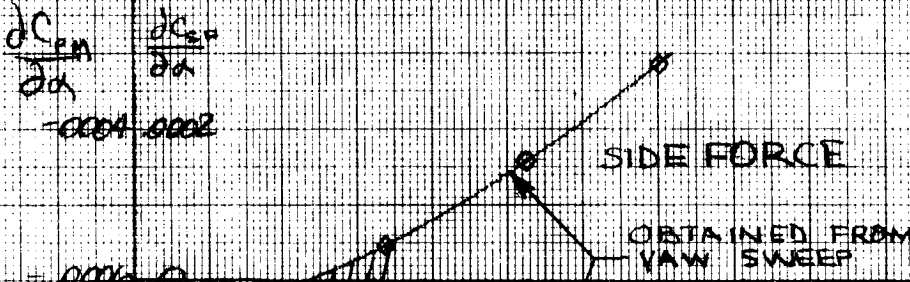
WING LIFT
EFFECT



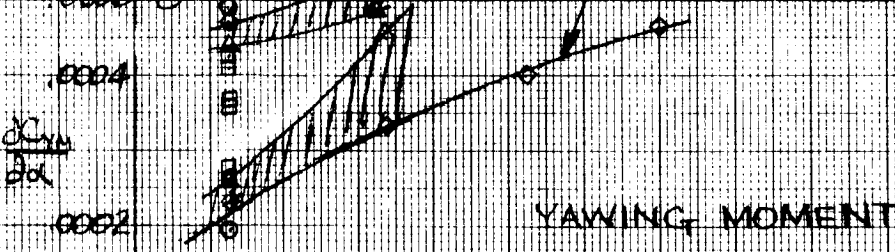
$$\frac{\partial C_{PM}}{\partial \psi} = \frac{\partial C_{PM}}{\partial \alpha}$$



$$\frac{\partial C_{SF}}{\partial \psi} = -\frac{\partial C_{SF}}{\partial \alpha}$$



$$\frac{\partial C_{YM}}{\partial \psi} = \frac{\partial C_{YM}}{\partial \alpha}$$



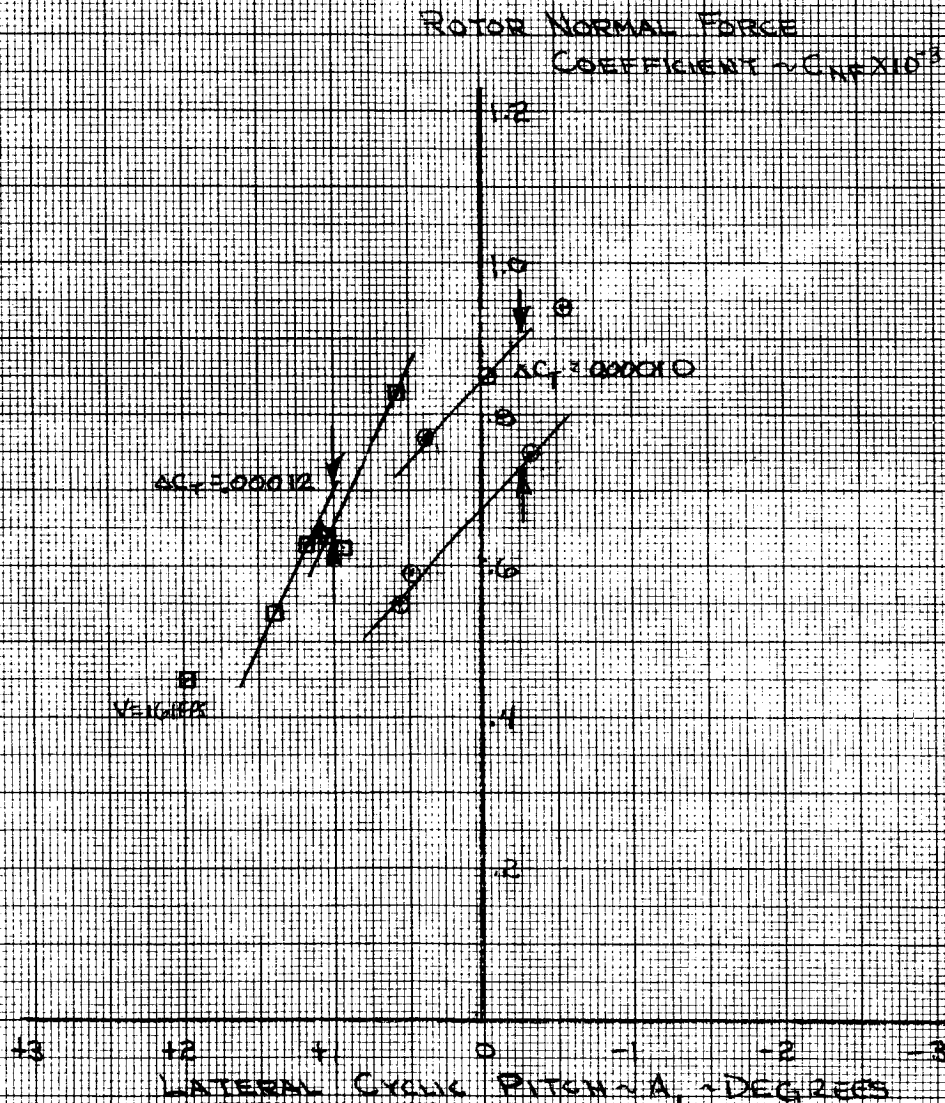
NOTE
RIGHT ROTOR
RPM = 1320
λ = 0°

ADVANCE RATIO ~ μ = V_{TUNNEL} / V_{TIP}

Figure 179

EFFECT OF LATERAL CYCLIC FORWARD SPEED IN CRUISE
ON
ROTOR NORMAL FORCE CHARACTERISTICS

RUN	SYM	LA	TUNNEL SPEED (FPS)	DCU DA
27	○	0.00012	113	-0.00021
91	□	0.00012	141	-0.00041



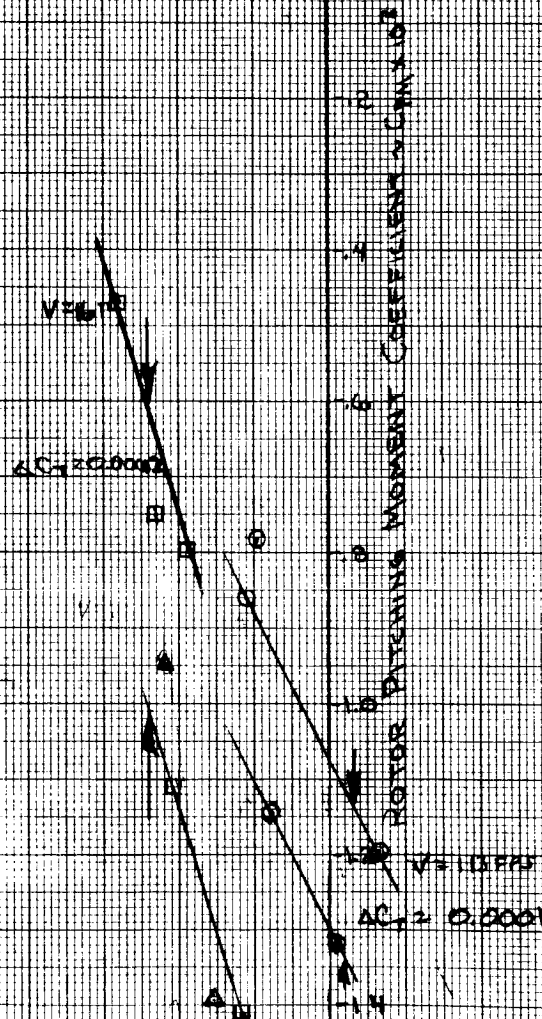
NOTE
RPM = 530
 $S = 0^\circ$
 $\Lambda = 0^\circ$
RIGHT ROTOR

Figure 180

EFFECT OF LATERAL CYCLIC & FORWARD SPEED IN CRUISE ON ROTOR PITCHING MOMENT CHARACTERISTICS

LATERAL CYCLIC PITCH δA_1 - DEGREES

+3 +2 +1 0 -1 -2 -3

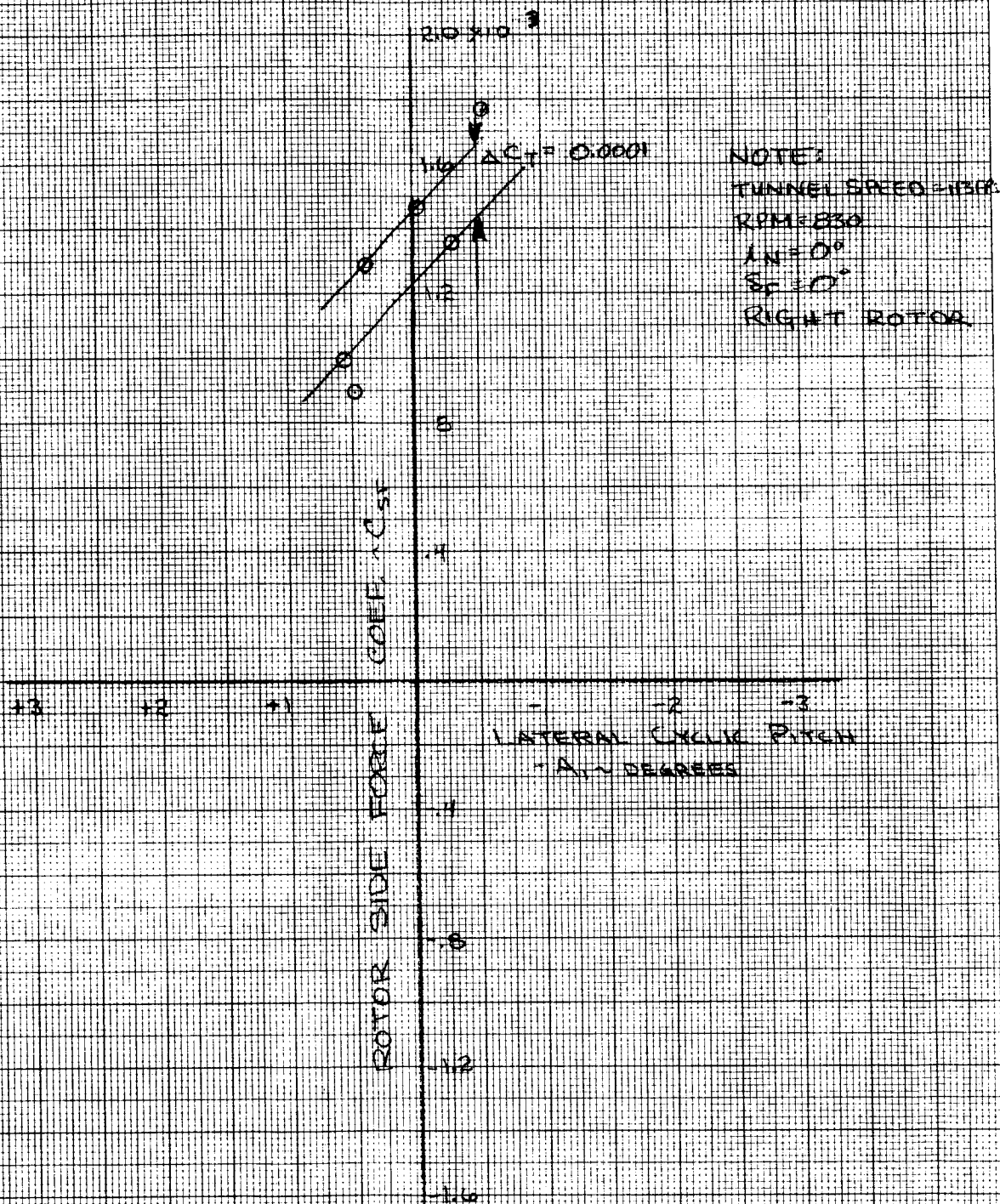


NOTE
RPM=830
 $\Lambda_N = 0^\circ$
 $S_p = 0^\circ$
RIGHT ROTOR

RUN	SYM	M	TUNNEL SPEED FPS	$\frac{\partial C_{PM}}{\partial A_1}$
27	0	0.464	113	0.00039
91	□	0.662	161	0.00066

Figure 181

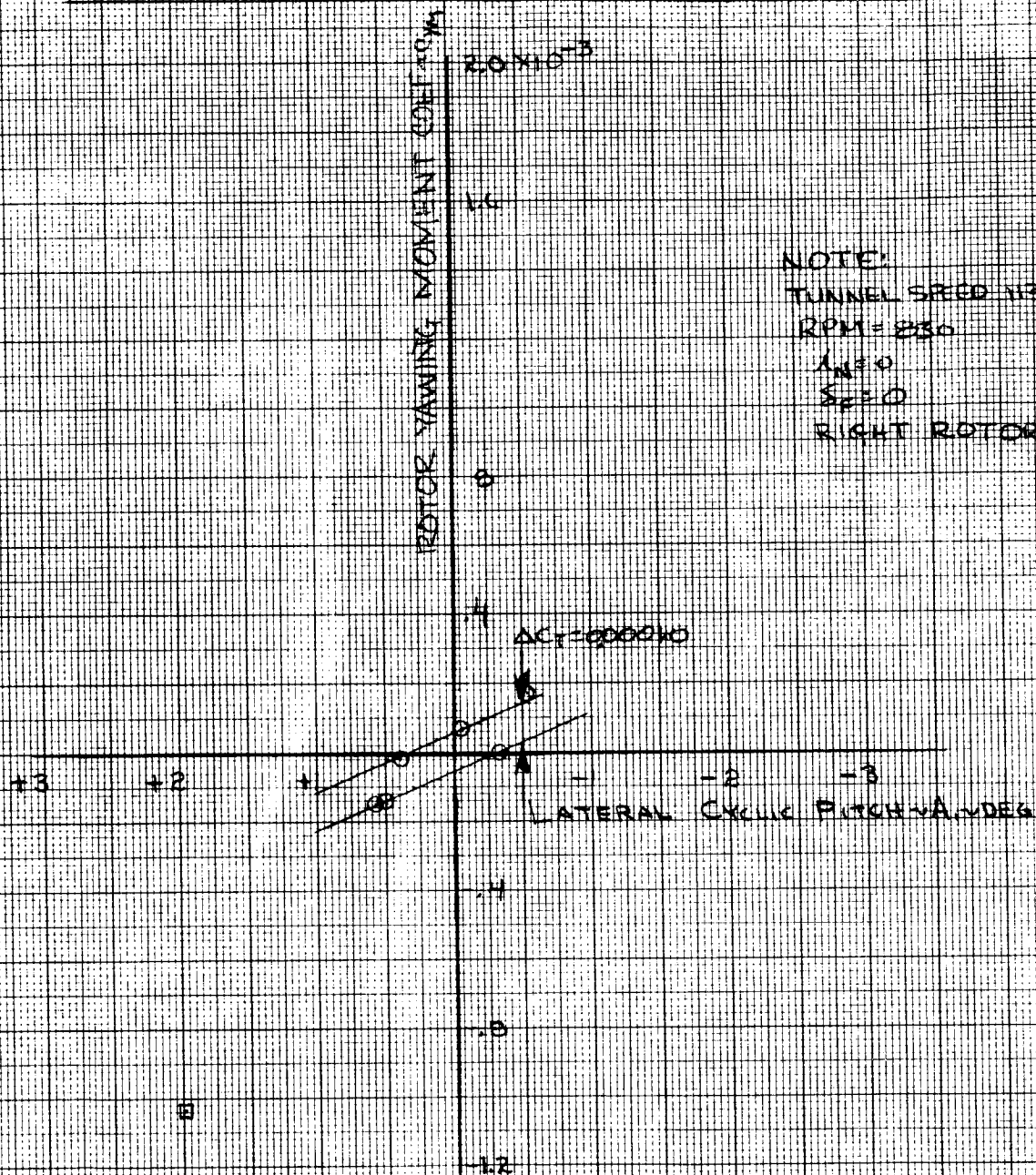
EFFECT OF LATERAL CYCLIC IN CRUISE ON ROTOR SIDE FORCE CHARACTERISTICS



RUN	SYM	U	TUNNEL SPEED (FPS)	ΔC_{sf} $\Delta \Lambda$
27	Q	0.004	113	0.0001

Figure 182

EFFECT OF LATERAL CYCLIC INCREASE ON ROTOR YAWING MOMENT CHARACTERISTICS



RUN	SYM	M	TUNNEL SPEED (FPM)	$\frac{\partial C_{YH}}{\partial A_1}$
27	0	0.464	113	-0.000170

Figure 183

EFFECT OF LONGITUDINAL CYCLIC & FORWARD SPEED IN CRUISE ON ROTOR NORMAL FORCE CHARACTERISTICS

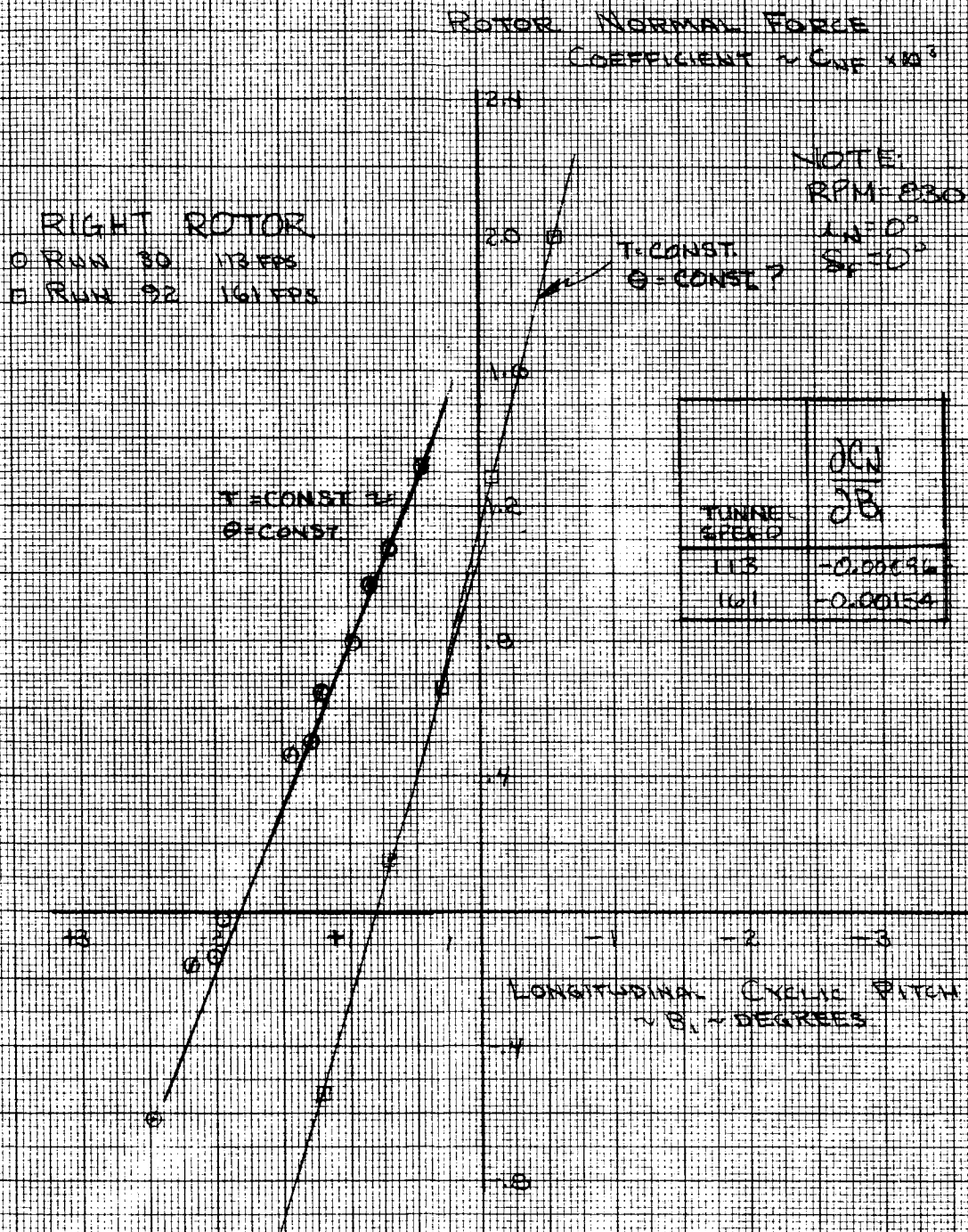


Figure 184

EFFECT OF LONGITUDINAL CYCLIC & FORWARD SPEED IN CRUISE ON ROTOR PITCHING MOMENT CHARACTERISTICS

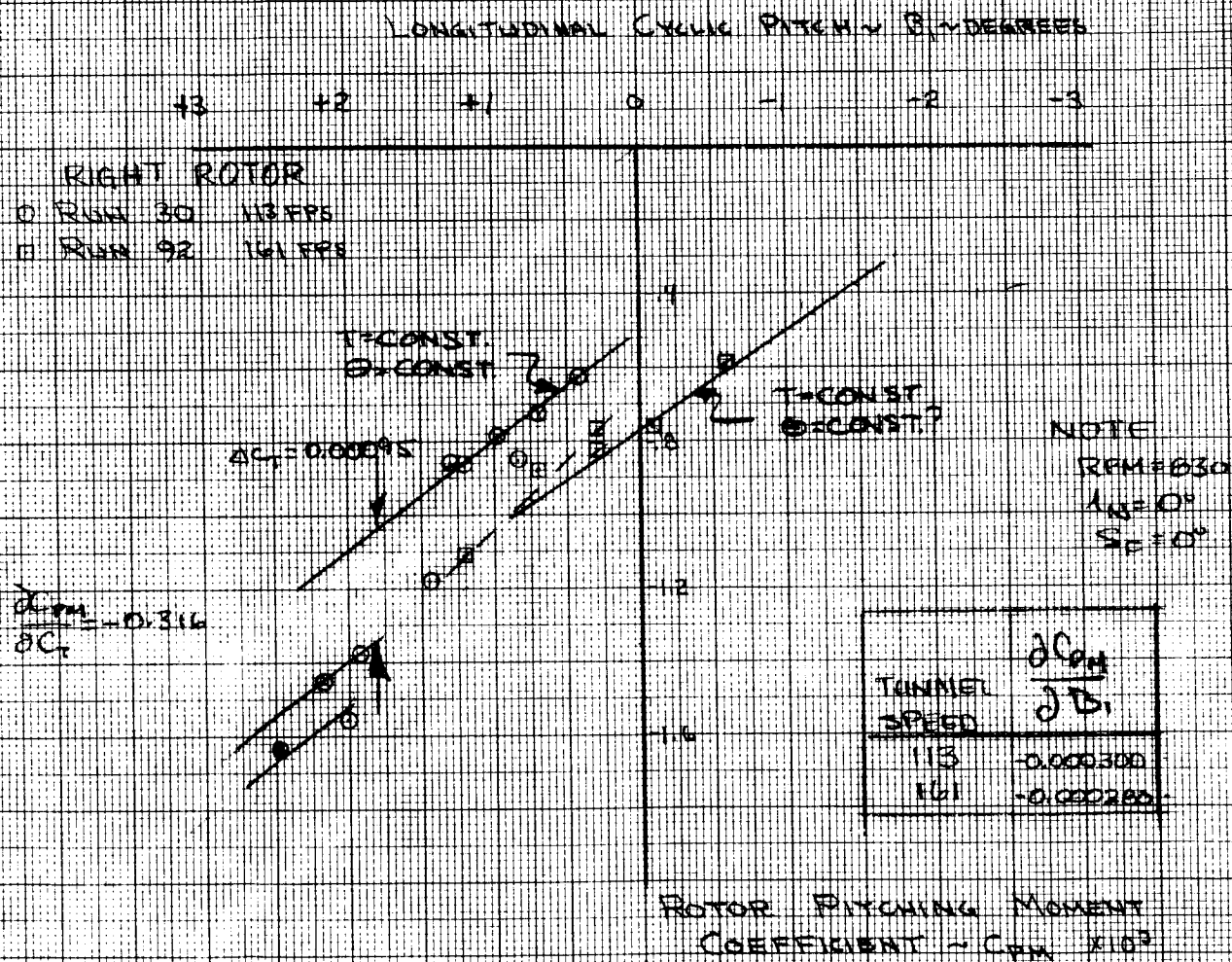


Figure 185

EFFECT OF LONGITUDINAL CYCLIC IN CRUISE ON ROTOR SIDE FORCE CHARACTERISTICS

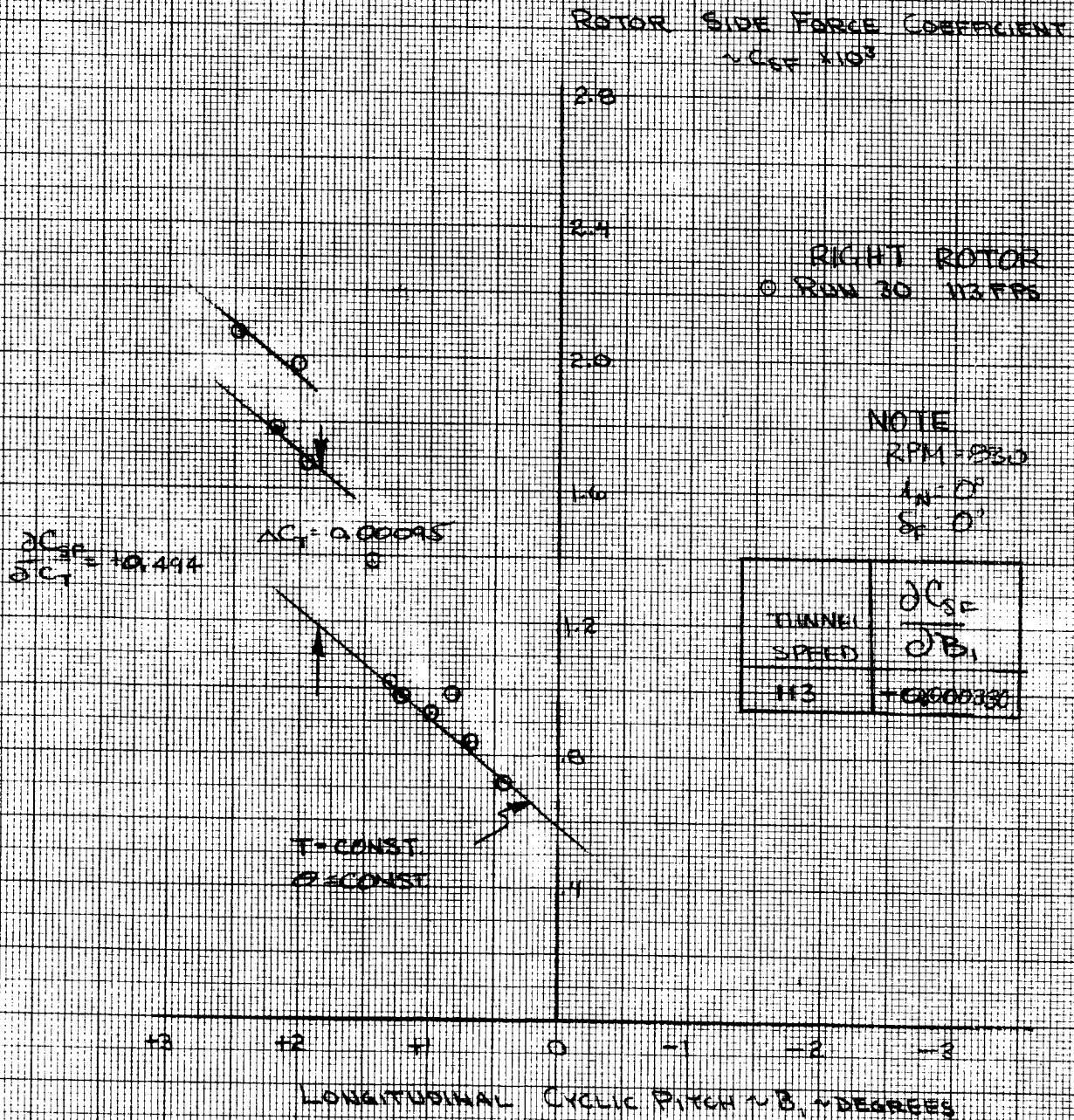


Figure 186

EFFECT OF LONGITUDINAL CYCLIC FORWARD SPEED IN CRUISE ON ROTOR YAWING MOMENT CHARACTERISTICS

RIGHT ROTOR
O RUN 30 113 FPS

NOTE:
RPM = 830
 $L_H = 0^\circ$
 $S_R = 0^\circ$

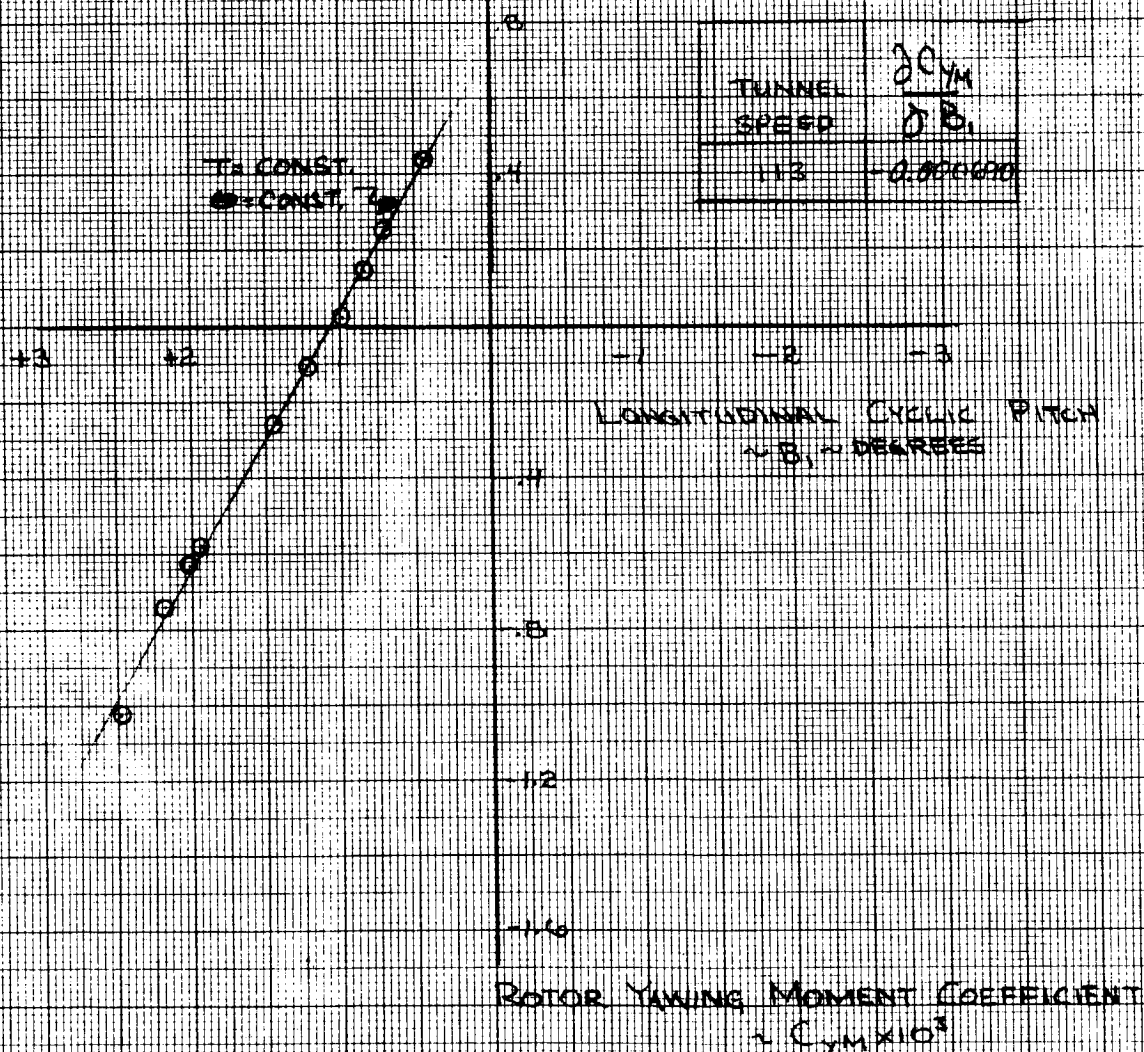
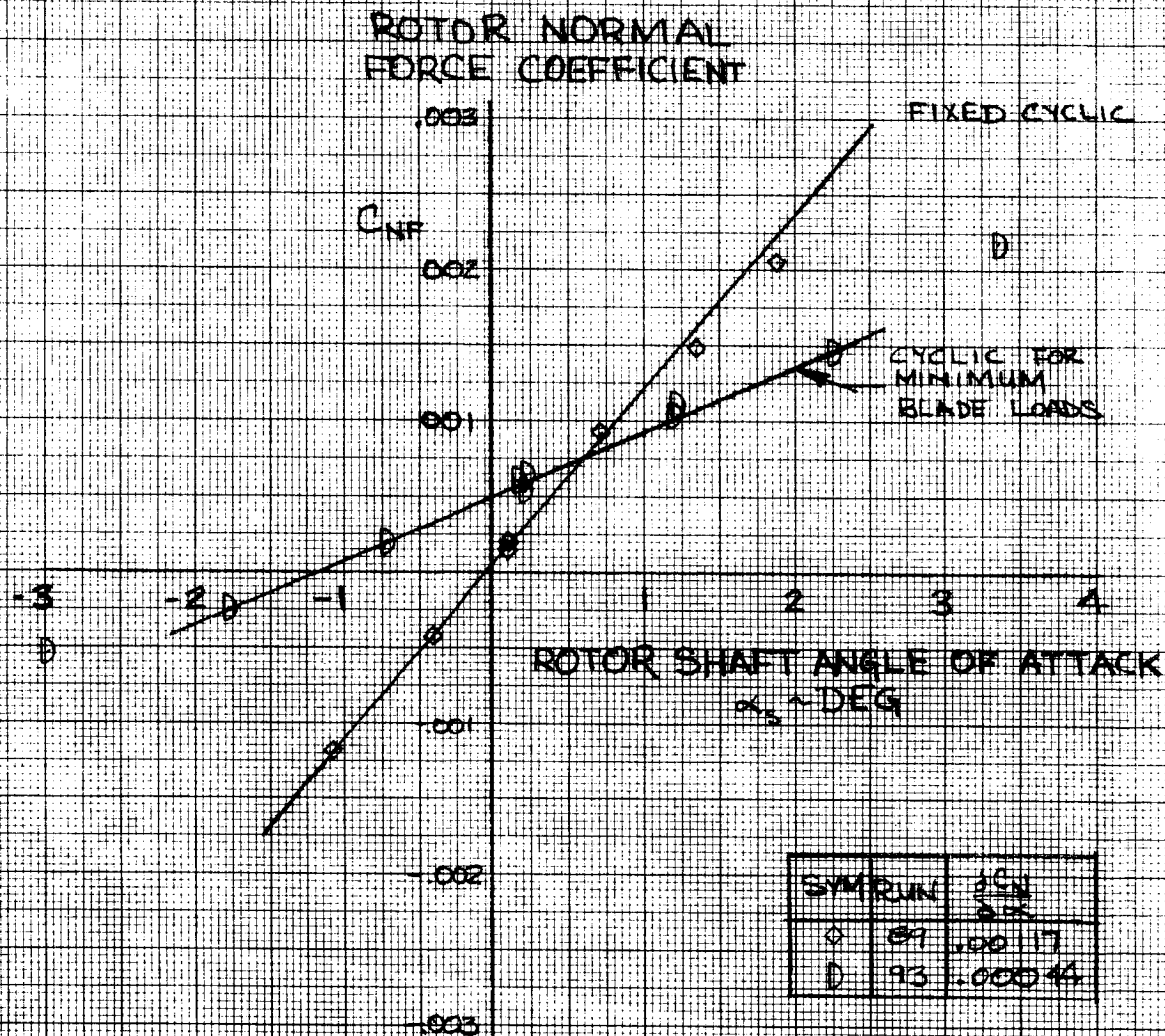


Figure 187

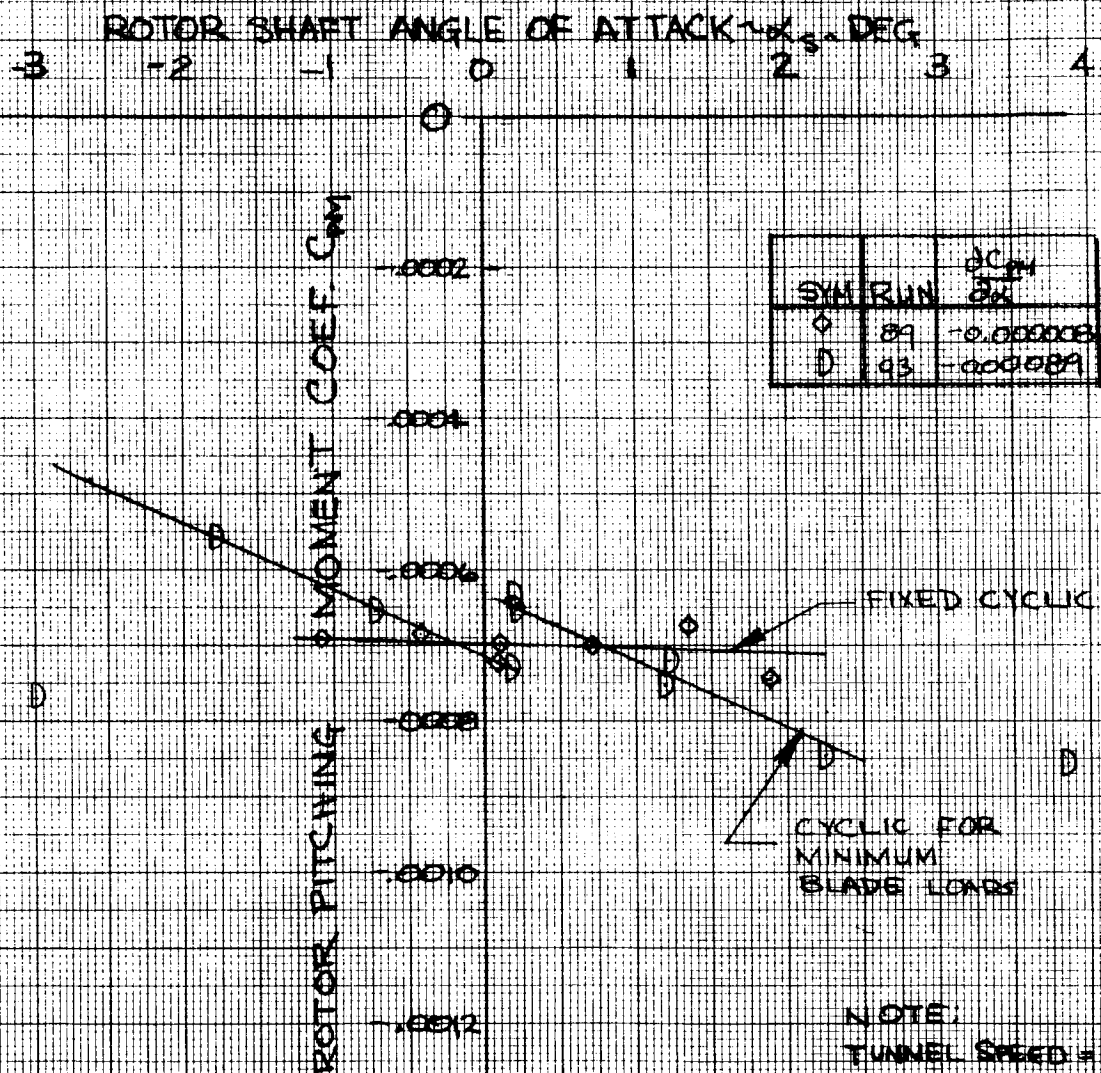
EFFECT OF BLADE LOAD MINIMIZATION ON ROTOR NORMAL FORCE CHARACTERISTICS IN CRUISE



NOTE
RPM = 520
TUNNEL SPEED = 162 KPS
 $\alpha_n = 0^\circ$
 $S_F = 0^\circ$
RIGHT ROTOR

Figure 188

EFFECT OF BLADE LOAD MINIMIZATION ON ROTOR PITCHING MOMENT CHARACTERISTICS IN CRUISE



NOTE:
TUNNEL SPEED = 162 m
RPM = 830
 $\alpha_N = 0^\circ$
 $\alpha_F = 0^\circ$
RIGHT ROTOR

Figure 189

5.2.2 AIRCRAFT STABILITY DERIVATIVES

Longitudinal Stability

Figures 190 through 195 indicate the variation of lift and pitching moment coefficients with angle of attack, pitching moment coefficient variation with lift coefficient and the effect of the horizontal tail on these characteristics. The longitudinal stability derivatives, for the linear ranges of the derivatives, are summarized in Table 7.

The data for the aircraft with rotors off, Figure 190, indicate that the lift curve slope begins to become non-linear between approximately 6 and 8 degrees angle of attack, and maximum lift coefficient is reached at approximately 15 to 16 degrees angle of attack. It is characteristic for thick airfoils, such as the 21 percent thick 634221 modified section used on the Model 222, to exhibit non-linearity of the lift curve slope in this angle of attack range. The maximum value of C_L for the complete aircraft of approximately 1.21 rotors off was obtained at a tunnel test Reynold's number, R_N , of approximately 0.91×10^6 as compared to the full scale aircraft R_N of 9 million at the equivalent full scale velocity. Thus, an incremental C_L of 0.2 to 0.3 higher may be anticipated for the aircraft, rotors off as predicted by Reference 4 (DATCOM) and shown in Figure 190. In addition, the lift curve slope will be higher because of R_N effects and also because of smoothness. Because of the construction of the model as a dynamically similar configuration it was not finished to the degree of smoothness and fit representative of the full scale aircraft. Note, for example, the difference in lift

TABLE 7. LONGITUDINAL STABILITY DERIVATIVES IN CRUISE

Run	i_N	δ_F	Tunnel q-psf	Equivalent Full Scale V-Kts	Tails	Rotors	Nominal C_T	$C_{L\alpha}$	$C_{m\alpha}$	$\frac{dC_m}{dC_L}$	Derivative Reference	Remarks
40	0	0	15	142	on	off	-	.086	-.0253	-.295	Airframe	
64			15	142	on	off	-	.080	-.0235	-.295	Airframe	
75			15	142	off	off	-	.075	+.0137	+.185	Airframe	
80			15	142	on	on	.0017	.120	-.0130	-.108	Aircraft	$\delta_e = .13^\circ$
83			22.4	175	on	on	.0017	.134	-.0144	-.107	Aircraft	$\delta_e = .12^\circ$
89			29.4	200	on	on	.0019	.141	-.0174	-.123	Aircraft	$\delta_e = 2.98^\circ$
97			37.6	225	on	on	.0019	.146	-.0172	-.118	Aircraft	$\delta_e = 8.12^\circ$
120			15	142	off	on	.0017	.102	+.0270	+.270	Aircraft	
120			15	142	off	on	.0017	.077	+.0068	+.088	Airframe	
80			15	142	on	on	.0017	.097	-.0368	-.380	Airframe	$\delta_e = .13^\circ$
83			22.4	175	on	on	.0017	.105	-.0400	-.381	Airframe	$\delta_e = .12^\circ$
89			29.4	200	on	on	.0019	.107	-.0375	-.350	Airframe	$\delta_e = 2.98^\circ$
97			37.6	225	on	on	.0019	.104	-.0360	-.345	Airframe	$\delta_e = 8.12^\circ$

curve slope between runs 40 and 64, $C_{L_\alpha} = .086$ and $.080$. This difference was caused by a difference in nacelle fairings. The curves of pitching moment coefficient versus angle of attack for the rotors off condition, Figure 191, indicate a break in the stable sense at an angle of attack of approximately 5 degrees. This stable break in C_{m_α} is not reflected as an abrupt break in stability in the lift coefficient versus pitching moment curves of Figure 192, but, because of the non-linearity of the lift curves, is manifested as a "smoothly increasing stability" as lift coefficient is increased. The minimum slope $\frac{dC_m}{dC_L}$, referenced to the wing quarter cord, is $-.295$ indicating a most forward location of the neutral point of 54.5 percent chord for the rotors off condition. It may be noted also from Figures 191 through 193 that the contribution of the horizontal tail to aircraft lift and pitching moment is continuously increasing up to the maximum angle of attack tested indicating no tail stall up to maximum lift coefficient. The incremental change in lift curve slope, ΔC_{L_α} , contributed by the horizontal tail, is indicated to be $.011$ and the increment in pitching moment coefficient slope, ΔC_{m_α} , is $.0390$. The change in stability, $\frac{\Delta dC_m}{dC_L}$, is indicated to be $-.480$ or a 48 percent aft shift in neutral point.

The influence of the rotors on aircraft stability characteristics of the model are illustrated in Figures 194 and 195. The lift curve slope, rotors on, at a tunnel q of 15 psf, is illustrated to be $.120$ as compared to the value of $.086$ with rotors off. Slope of the pitching moment coefficient curve at this condition is $-.0130$ compared to $-.0253$ rotors off and longitudinal stability, $\frac{dC_m}{dC_L}$, is

-.108 compared to -.295 rotors off. Thus, the effect of the rotors is to increase the aircraft lift curve slope and to decrease aircraft stability. The effect of q is indicated to result in increasing lift curve slope with increasing q accompanied by a small increase in stability. Comparison with the curves of airframe characteristics, rotor effects subtracted, Figures 196 and 197 indicates that the effects on lift curve slopes are attributable to the variation of the rotor contributions with q , i.e., the increasing rotor normal force slope primarily. The change in stability with q is of the same order of magnitude for the airframe as for the aircraft and, in fact, just slightly larger, but in the opposite direction, less stable, while the lift curve slope variation of the airframe is significantly less than for the aircraft. It is noteworthy to observe that the lift curve slope of the airframe for the rotors on condition is significantly increased in comparison to the slope of the airframe without rotors. This is probably due to the substantially higher effective Reynolds number caused by the turbulence in the rotor slipstream. The shifts in levels of the pitching moment data between runs illustrated on Figures 194 through 197 are a result of constant elevator deflection differences between runs. Runs 80 and 83 had approximately 0.12 degrees positive elevator deflection, run 89 was indicated to have 2.98 degrees, and run 97 had 8.12 degrees indicated.

The data of run 97 are consistent with an elevator deflection of 8.1 degrees but the shift of pitching moment coefficient of run 89 is too large for 2.98 degrees deflection. Therefore, the elevator deflection indicated for run 89 is believed erroneous.

Figures 198 and 199 illustrate the effect of the horizontal tail on the longitudinal stability characteristics for the rotors on condition for the aircraft and for the airframe. These data indicate that adding the horizontal tail to the aircraft with rotors on increases the lift curve slope by $\Delta C_{L_\alpha} = .018$ compared to an increment for "airframe" from the same runs of .020. These figures compare with ΔC_{L_α} of .011 for the airframe with rotors off determined from runs 40 and 75, Figure 190. The effect on pitching moment coefficient slope of adding the horizontal tail is $\Delta C_{m_\alpha} = -.0400$ for the aircraft and $\Delta C_{m_\alpha} = -.0436$ for the airframe with rotors on as compared to $-.0390$ for the airframe with rotors off. The effect on longitudinal stability for the aircraft is $\frac{\Delta dC_m}{dC_L} = -.378$ for the airframe, rotors on, $-.466$ compared to $-.480$ for the airframe without rotors. Thus, the data indicate that the horizontal tail provides a larger change in lift curve slope, ΔC_{L_α} , and pitching moment coefficient slope, ΔC_{m_α} , for the aircraft or airframe with rotors as compared to airframe with rotors off but a considerably smaller shift in neutral point for the aircraft with rotors on as compared to the airframe rotors off. This is to be expected as the tail contribution to stability, neutral point shift, is smaller for the aircraft having higher lift curve slope. The shift in neutral point for the airframe with rotors on compares well with that indicated for the airframe with rotors off.

Figures 200 and 201 present summaries of the lift curve slopes, pitching moment coefficient slopes and neutral points as a function of velocity, for the conditions tested, extrapolated to aircraft velocities. Adequate longitudinal stability is indicated, rotors on.

throughout the cruise speed range.

Lateral/Directional Stability

Lateral and directional characteristics of the model in the cruise configuration with rotors off and tails on and off are presented in Figures 202 through 205. The effects of dynamic pressure on the model lateral and directional characteristics with rotors on are illustrated on Figures 205 and 206. The effects of vertical tail on and off with rotors on are illustrated on Figure 207 and 208. The results in terms of derivatives, coefficient variation with sideslip angle, are summarized in Table 8 and are presented as a function of velocity extrapolated to full scale aircraft velocity in Figures 209, 210 and 211.

It may be observed from the figures that the variations of the coefficients with sideslip angle through the ranges of sideslip tested are relatively linear. Figure 193 indicates that the directional stability of the aircraft with rotors off increases at sideslip angles larger than approximately 12 degrees.

The data of Table 8 indicate good directional stability, tail on for all conditions tested rotors on and off. The "base" level of C_{n_β} at the 142 knot condition with rotors off and tail on is indicated to be .0057 from run 45. Addition of the rotors reduces C_{n_β} to .00349 (average of runs 78 and 81). The slopes of directional stability have been adjusted to correct for the change in thrust due to power changes during the runs as indicated by the dashed line on Figure 205. The tail contribution to C_{n_β} , rotors off, is indicated to be

.0070. Unfortunately the side force instrumentation was inoperative during run 45. Thus, the incremental C_{y_β} for the rotors off cannot be obtained, so the effective tail arm for the rotors off condition cannot be calculated directly. The base level of dihedral effect, rotors off, of $C_{l_1} = -.00213$ for a ratio of $C_{n_\beta}/C_{l_\beta} = -2.68$. Addition of the rotors is indicated to reduce C_{l_β} to $-.00083$ (average of runs 78 and 81) at the $q=15$ psf condition for a C_{n_β}/C_{l_β} ratio, rotors on, of 4.2. The effect of increase in dynamic pressure is indicated to result in substantial increase in both C_{n_β} and C_{l_β} because of the reduced destabilizing effects of the rotors at the higher speeds. For example at the tunnel q of 29.4 psf, equivalent full scale aircraft velocity of 200 knots, C_{n_β} is .00466 and C_{l_β} is $-.00332$ for the relatively favorable ratio of $C_{n_\beta}/C_{l_\beta} = 1.4$. The effect of adding the vertical tail to the aircraft with rotors on is to increase C_{y_β} by $-.0114$, C_{n_β} by .00656, and C_{l_β} is not affected enough to measure with any accuracy. The apparent tail length parameter $\frac{l}{b} \left(1 + \frac{d\sigma}{d\beta} \right) \frac{qt}{q_0}$ obtained by dividing ΔC_{n_β} by ΔC_{y_β} is .575. If $\left(1 + \frac{d\sigma}{d\beta} \right) \frac{qt}{q_0}$ is assumed to be 1.0 the effective tail length is 50", model scale, compared to 49" calculated as the distance from the wing quarter chord to the vertical tail quarter chord on the MAC.

The airframe, rotors on and tail on, C_{n_β} is .0064 compared to .0057 rotors off and the tail increment for the airframe rotors on is $\Delta C_{n_\beta} = .0070$, the same as the value rotors off.

TABLE 8. LATERAL/DIRECTIONAL STABILITY DERIVATIVES IN CRUISE

Run	i_N	δ_F	Tunnel q	Equivalent Full Scale V-Knots	Tails	Rotors	Nominal C_T	$C_{Y\beta}$	$C_{n\beta}$	$C_{z\beta}$	Derivative Reference	Remarks
45	0	0	15	142	on	off	--	--	.0057	-.00213	Airframe	
76			15	142	off	off	--	-.0125	.0013	-.00215	Airframe	
81			15	142	on	on	.0017	-.0410	.00346	-.00104	Aircraft	
78			15	142	on	on	.0017	-.0410	.00352	-.00062	Aircraft	
84			22.4	175	on	on	.0017	-.0436	.00386	-.00218	Aircraft	
90			29.4	200	on	on	.0019	-.0472	.00466	-.00332	Aircraft	
121			15	142	off	on	.0017	-.0296	.00310	-.00104	Aircraft	
81			15	142	on	on	.0017	-.0259	.0064	-.00200	Airframe	
121			15	142	off	on	.0017	-.0130	.0006	-.00264	Airframe	

LIFT CURVE SLOPE
EFFECT OF VERTICAL AND
HORIZONTAL TAILS

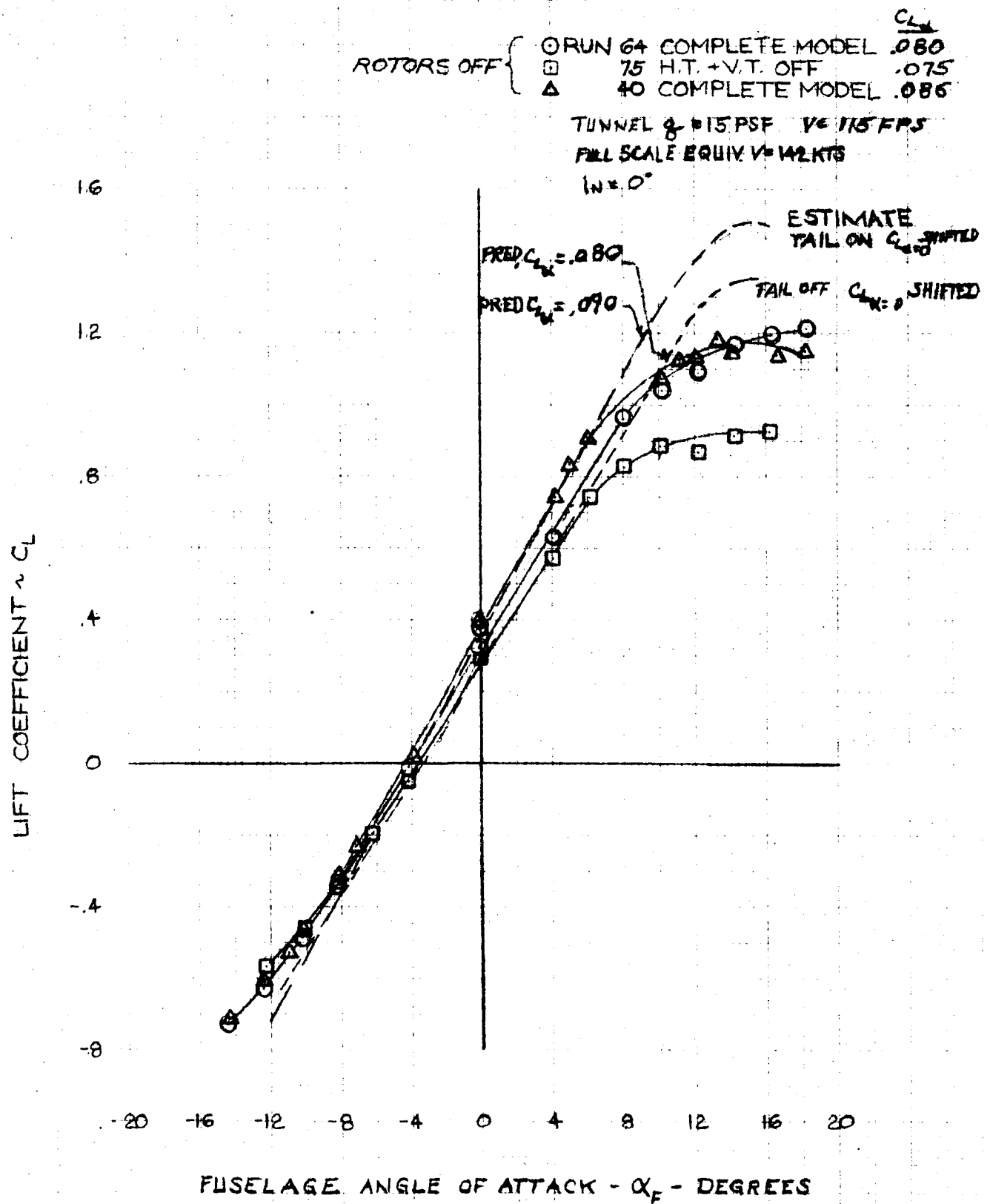


Figure 190

PITCHING MOMENT COEFFICIENT
EFFECT OF VERTICAL AND
HORIZONTAL TAILS
 ROTORS OFF

○ RUN 64 COMPLETE MODEL
 □ 75 H.T. + V.T. OFF
 △ 40 COMPLETE MODEL

TUNNEL $q = 15 \text{ PSF}$

FULL SCALE EQUIV. $V = 142 \text{ KTS}$

$L_N = 0^\circ$

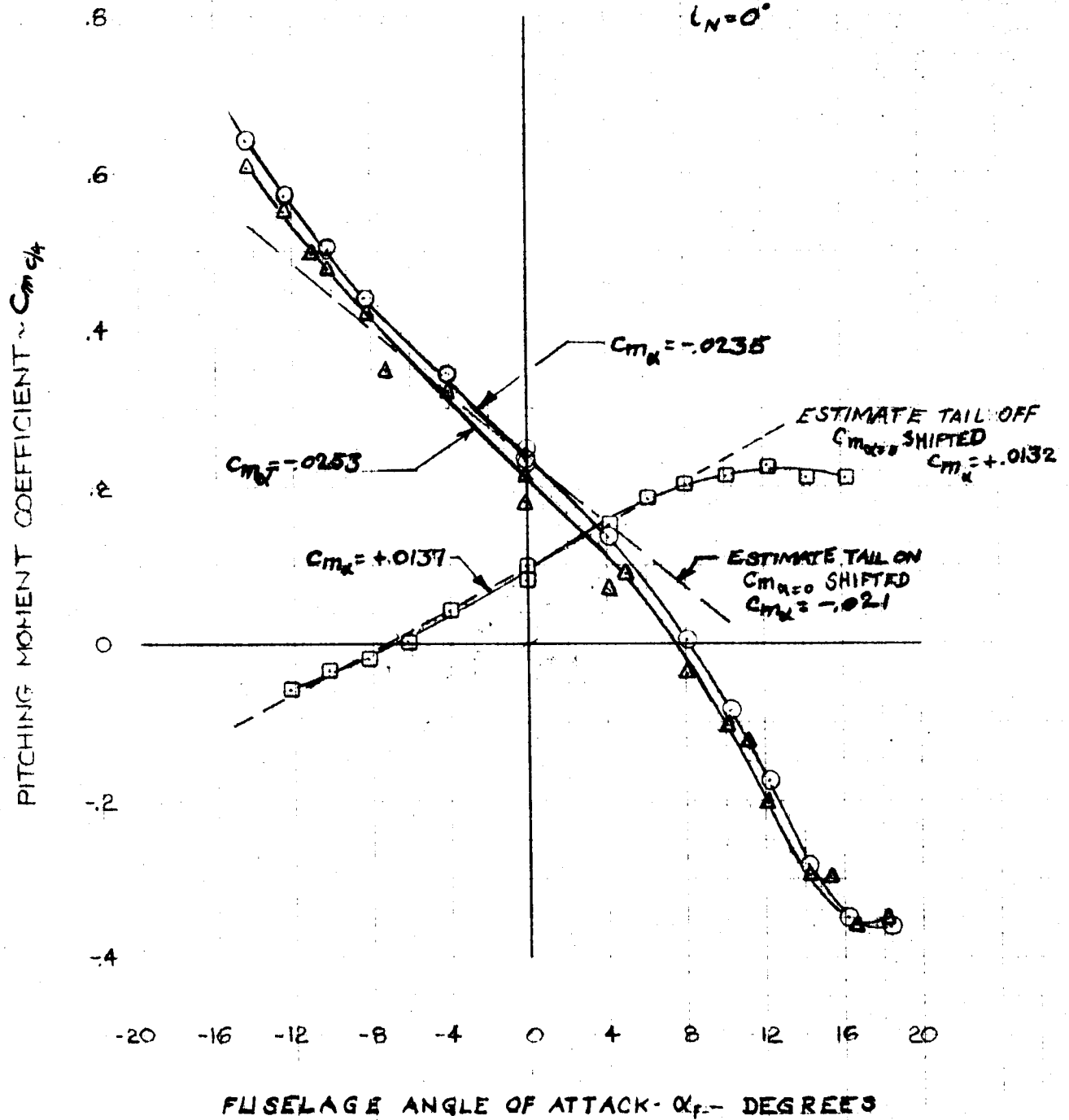


Figure 191

LONGITUDINAL STABILITY
EFFECT OF VERTICAL AND
HORIZONTAL TAILS
 ROTORS OFF

- RUN 64 COMPLETE MODEL
 □ 75 H.T. + V.T. OFF
 △ 40 COMPLETE MODEL

TUNNEL $q = 15 \text{ PSF}$
 FULL SCALE EQUIV. $V = 142 \text{ KTS.}$
 $i_w = 0^\circ$

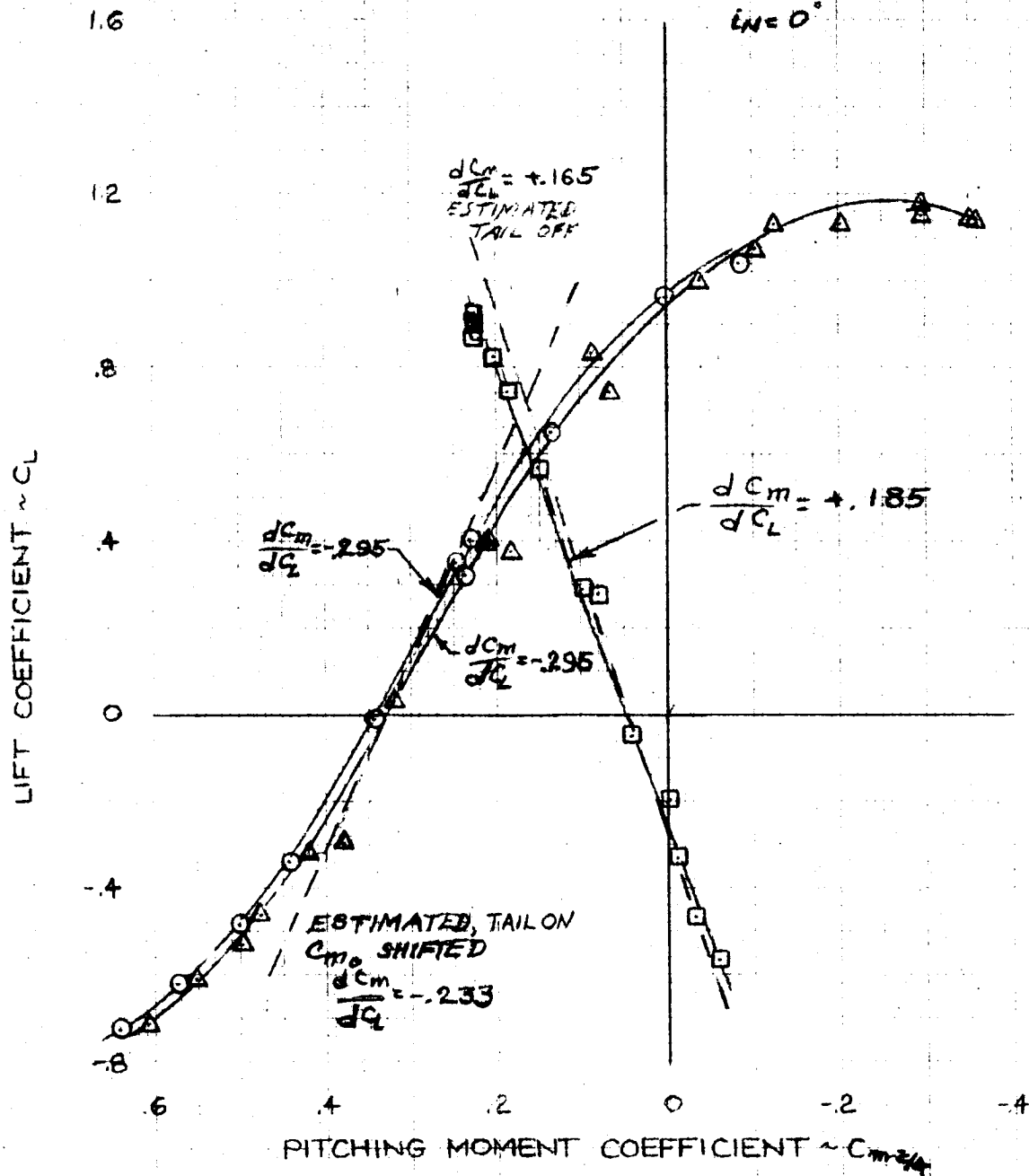


Figure 192

MODEL 222
 HORIZONTAL TAIL EFFECTIVENESS
 ROTORS OFF

TUNNEL $\beta = 15^\circ$ F
 FULL SCALE EQUIV. $V = 90$ KTS
 $i_N = 0$
 DATA FROM RUNS 40 & 75

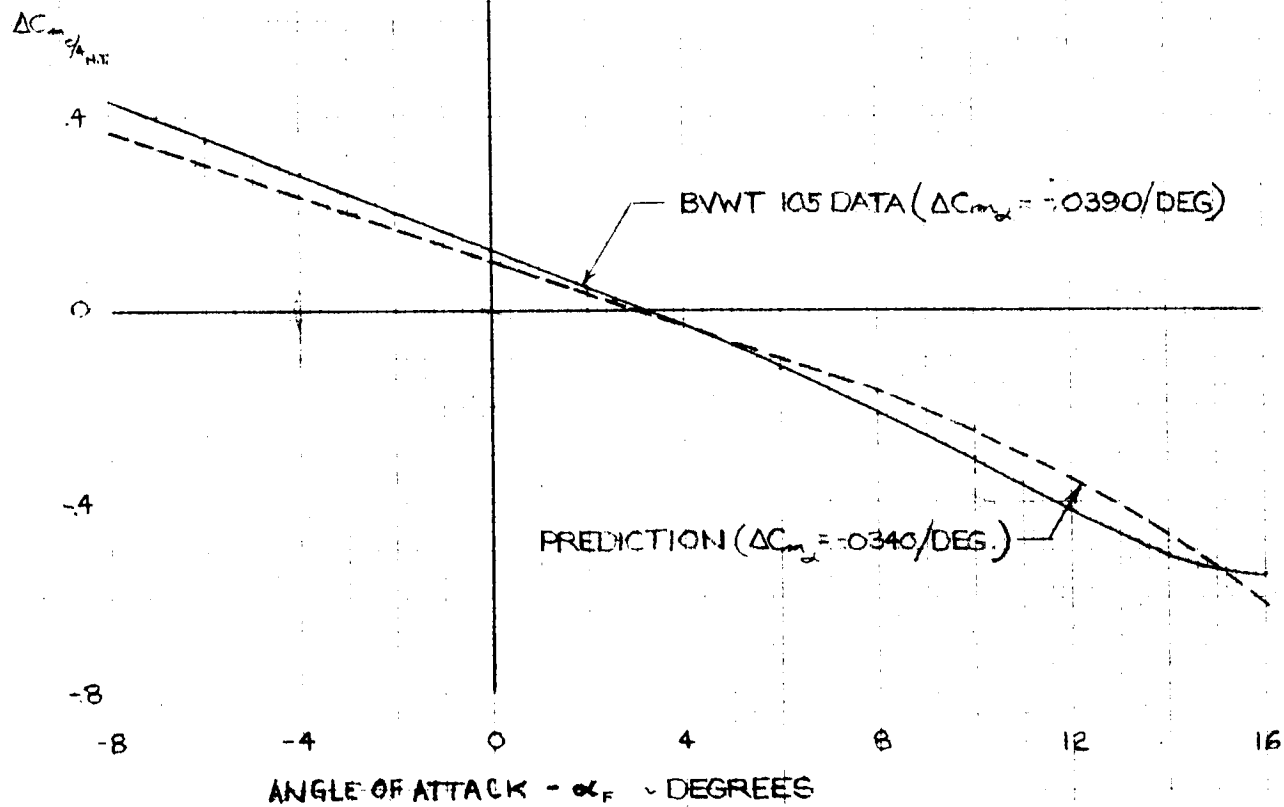
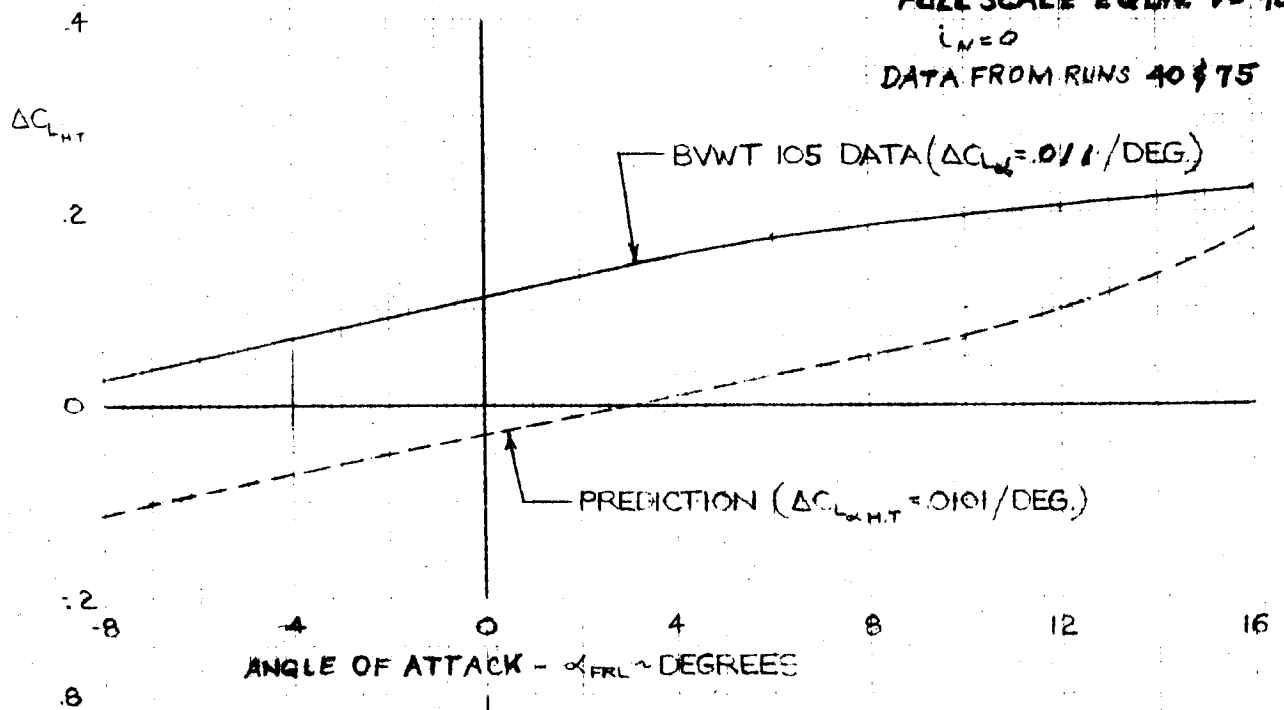


Figure 193

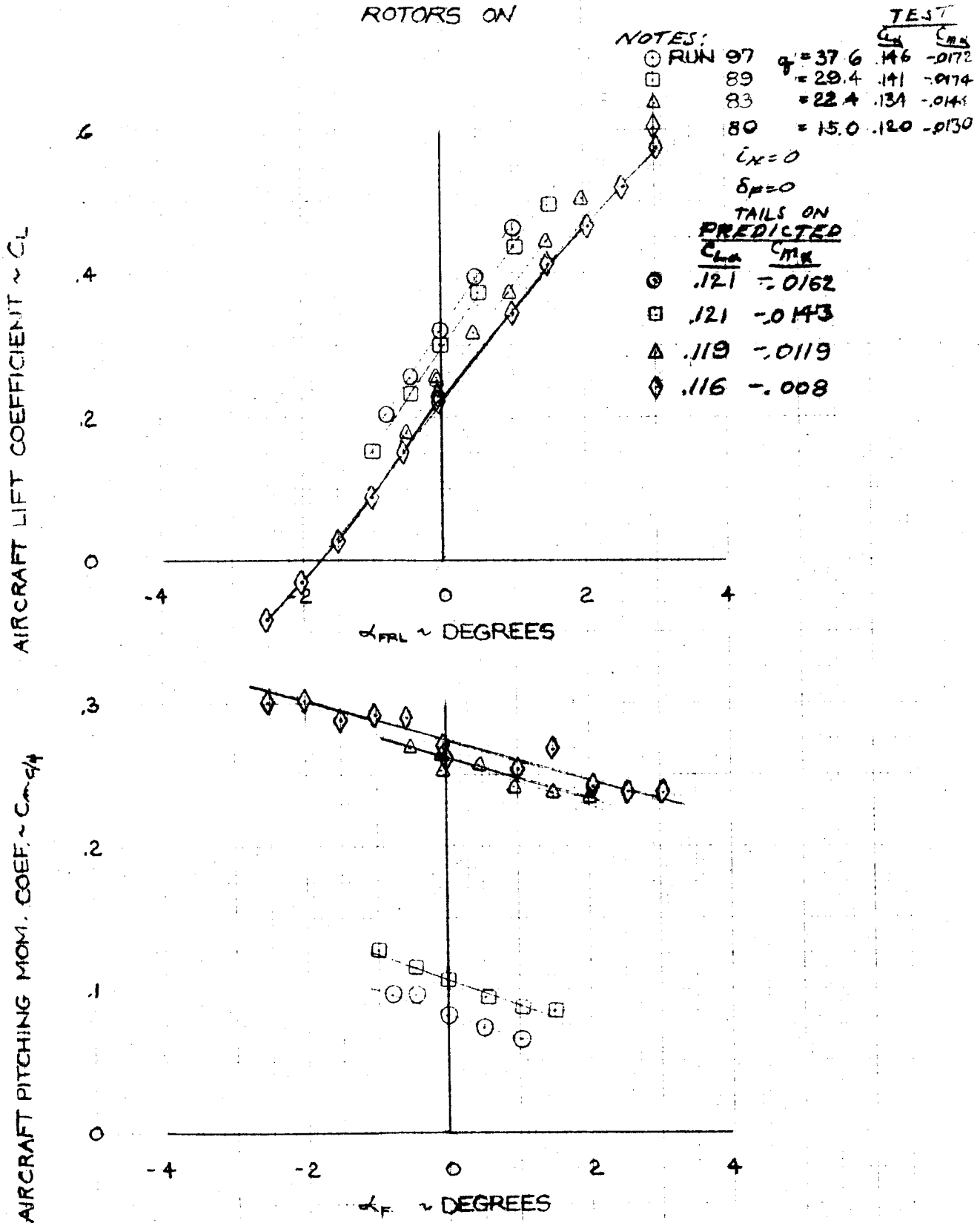
MODEL 222EFFECT OF q ON LONGITUDINAL CHARACTERISTICS
ROTORS ON

Figure 194

B/NIT 102 LAT

MODEL 222

EFFECT OF q ON LONGITUDINAL STABILITY

NOTES:	TEST	PREL
○ RUN 97	$q = 37.6$	$\frac{dC_m}{dC_L} = -.138$
□ 99	$= 29.4$	$= -.112$
△ 83	$= 22.4$	$= -.089$
◇ 80	$= 15.0$	$= -.071$
$i_N = 0$ $\delta_F = 0$		
TAILS ON		

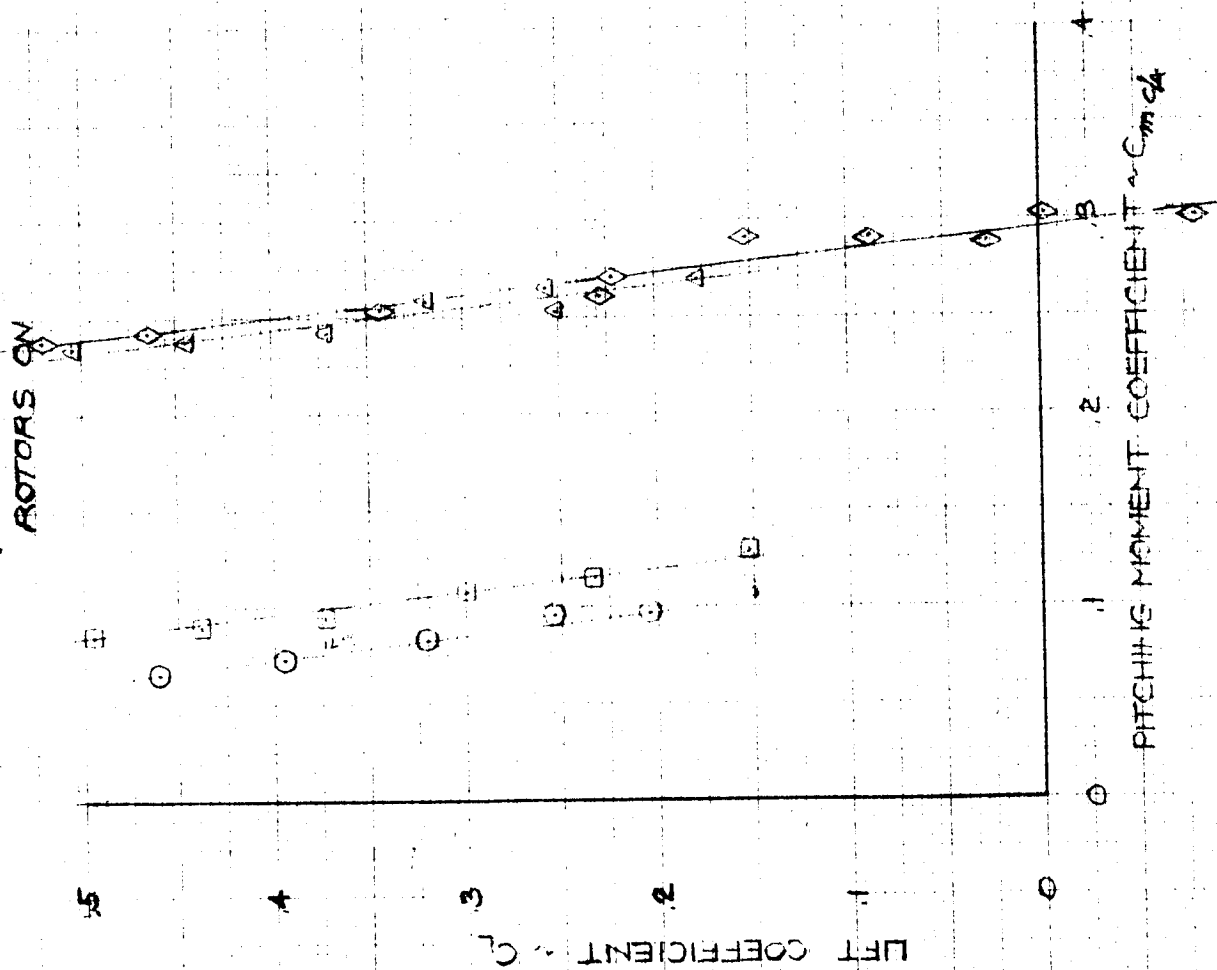


Figure 195

EFFECT OF β ON LONGITUDINAL CHARACTERISTICS
AIRFRAME-ROTORS ON

NOTES:

RUN	β	$C_{L\alpha}$	$C_{m\alpha}$
97	37.6	.104	-.0360
89	29.4	.101	-.0375
83	22.4	.105	-.0400
80	15.0	.097	-.0368

(NEO)
(FFO)

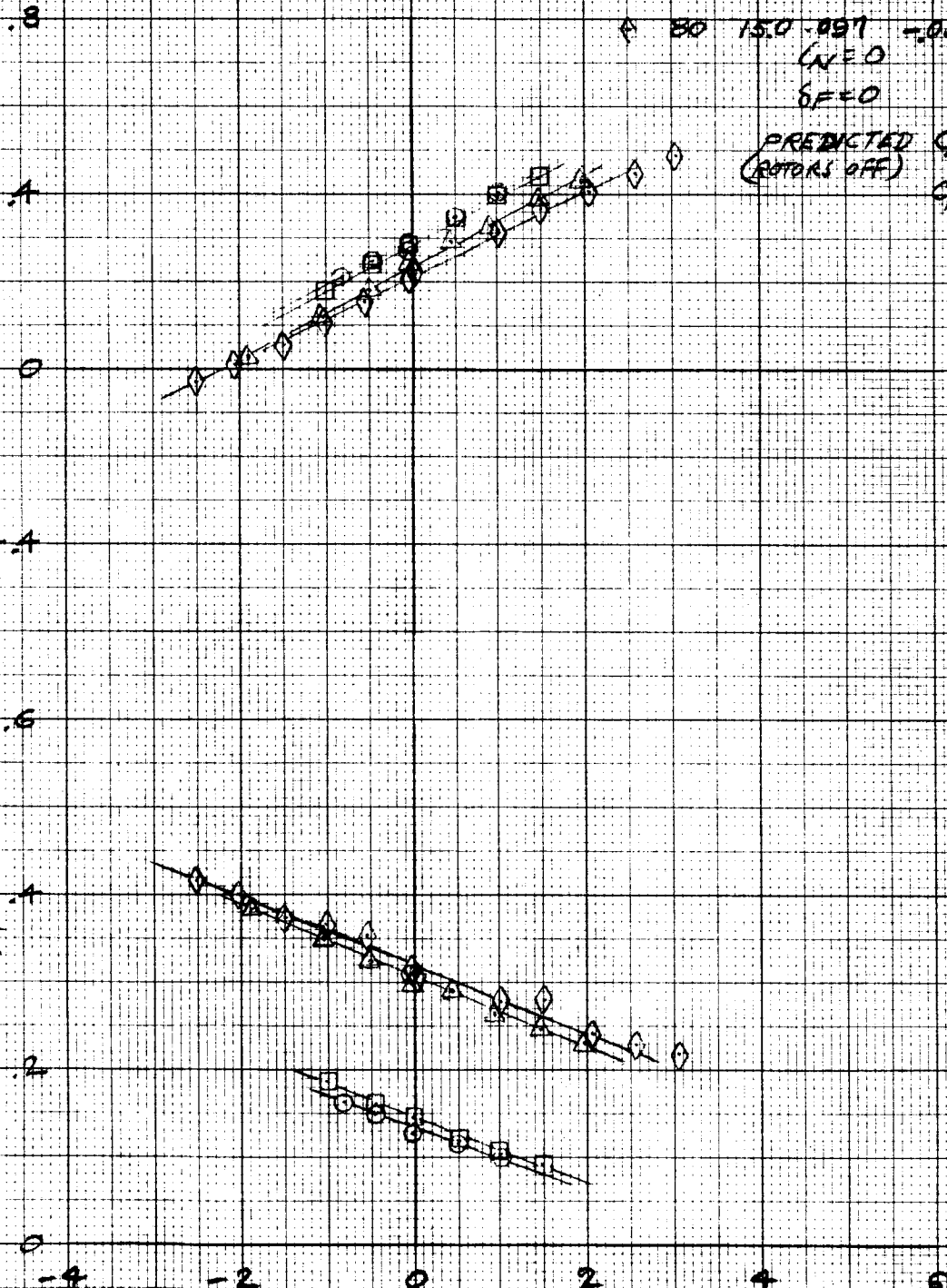
PREDICTED C_{Lj} .0972
(ROTORS OFF)
 $C_{m\alpha}$ -.0209

LIFT COEFFICIENT

C_L

PITCHING MOMENT COEFFICIENT

$C_{m\alpha}$



FUSELAGE ANGLE OF ATTACK - α_f - DEGREES

Figure 196

EFFECT OF δ ON LONGITUDINAL STABILITY AIRFRAME-ROTORS ON

NOTES:

	RUN	δ	$\frac{dC_m}{dC_L}$
○	97	37.6	-.345
□	89	29.4	-.350
△	83	22.4	-.381
◇	80	15.0	-.380

$$i_N = 0$$

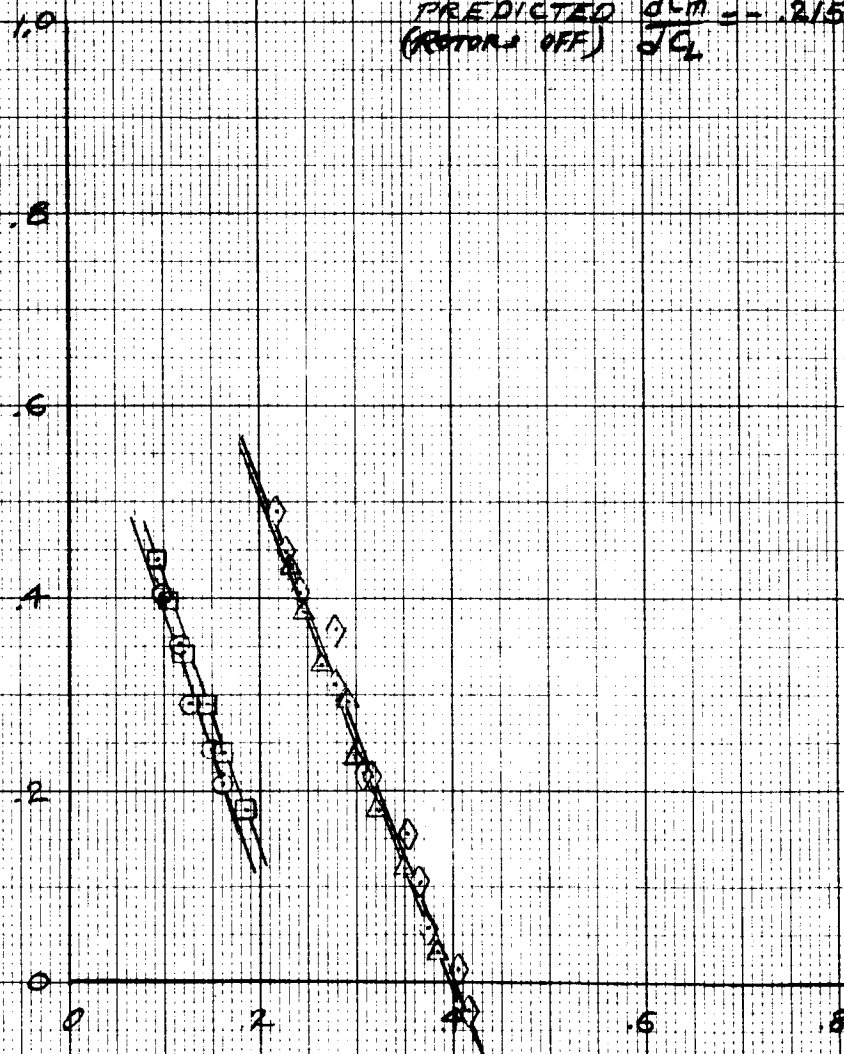
$$\delta_F = 0$$

$$\text{PREDICTED } \frac{dC_m}{dC_L} = -.215$$

(ROTORS OFF)

LIFT COEFFICIENT

C_L



PITCHING MOMENT COEFFICIENT

$C_{m\delta}$

Figure 197

EFFECT OF HORIZONTAL TAIL ON LONGITUDINAL CHARACTERISTICS IN CRUISE ROTORS ON

NOTES:

RUN TAILS

○ BO ON

△ 120 OFF

$W=0$ $\delta F=0$ $q=0.0017$

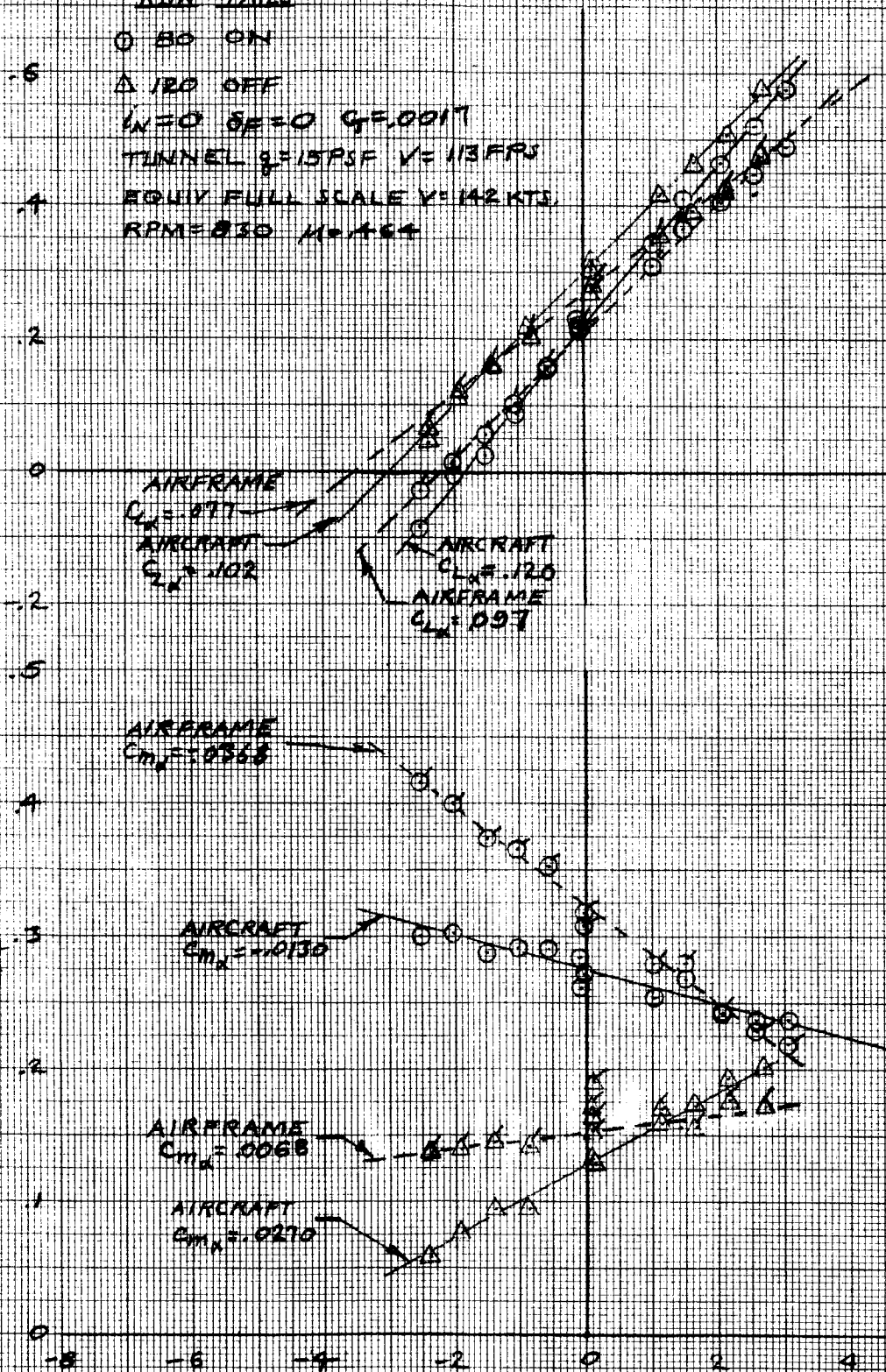
TUNNEL $q=15$ PSF $V=113$ FPS

EQUIV FULL SCALE $V=142$ KTS

RPM=830 $M=0.64$

LIFT COEFFICIENT
- C_L -

PITCHING MOMENT COEFFICIENT
- $C_{m\alpha/4}$ -



FUSELAGE ANGLE OF ATTACK - α_f - DEGREES

Figure 198

EFFECT OF HORIZONTAL TAIL ON LONGITUDINAL STABILITY ROTORS ON

NOTES:

RUN TAILS

O 80 ON

Δ 120 OFF

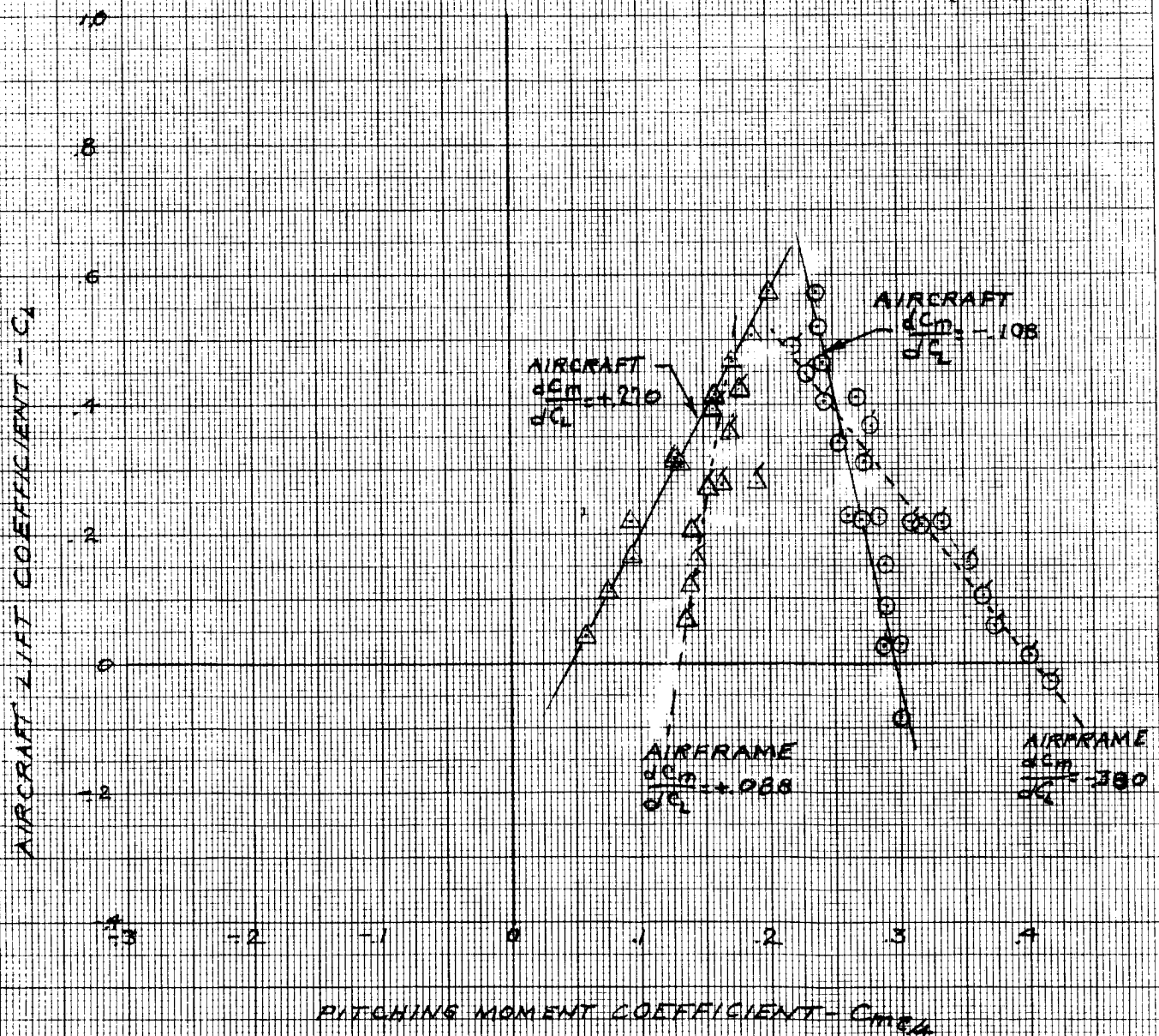
 $\mu = 0$ SPEED $C_T = 0.017$ TUNNEL $\beta = 15.0$ EQUIV FULL SCALE $V = 142$ KTSRPM = 830 $\mu = 4.64$ 

Figure 199

SUMMARY LIFT CURVE SLOPE VARIATION WITH VELOCITY-ROTORS ON AND OFF

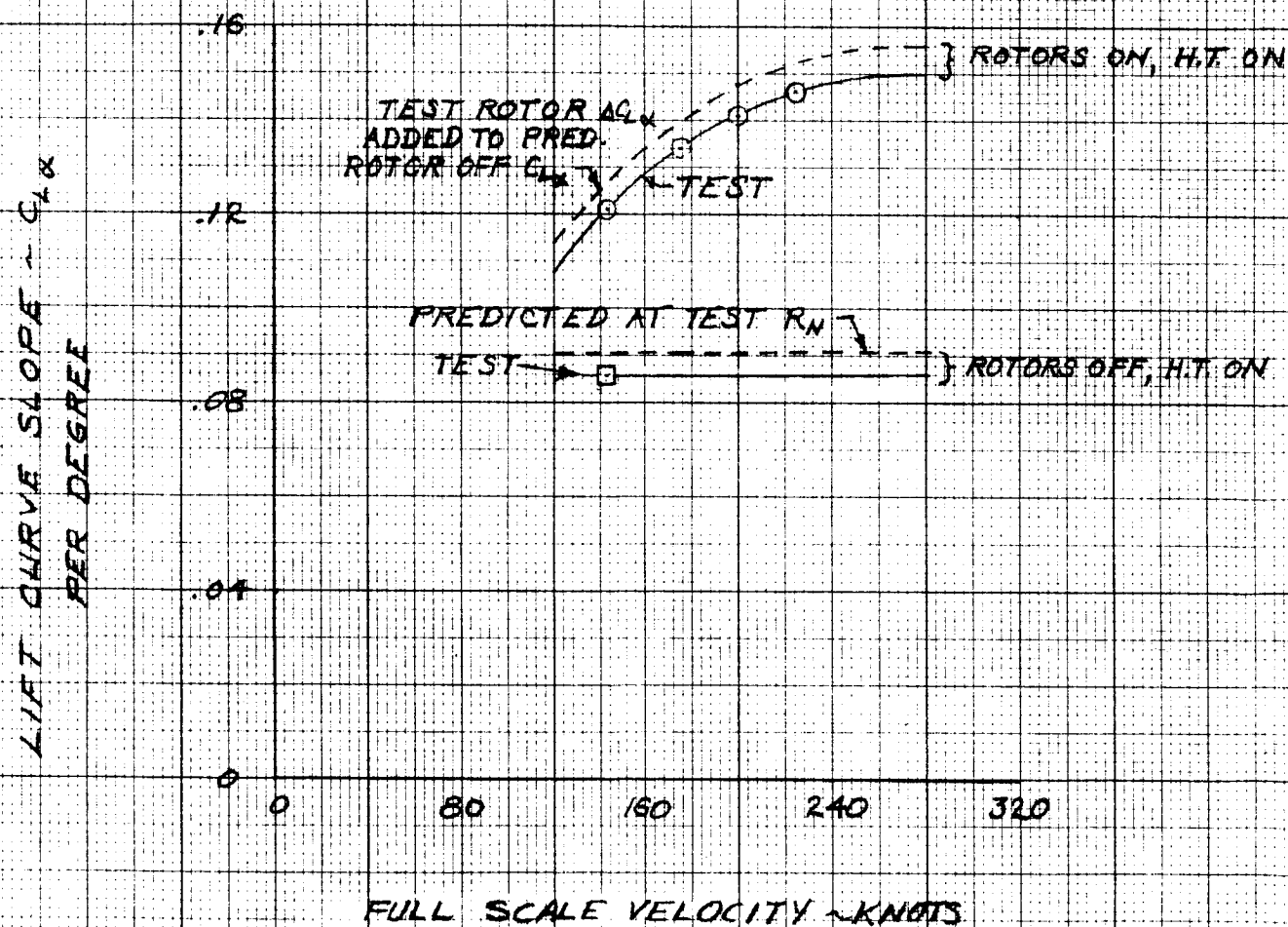


Figure 200

MODEL 222
STATIC LONGITUDINAL STABILITY SUMMARY

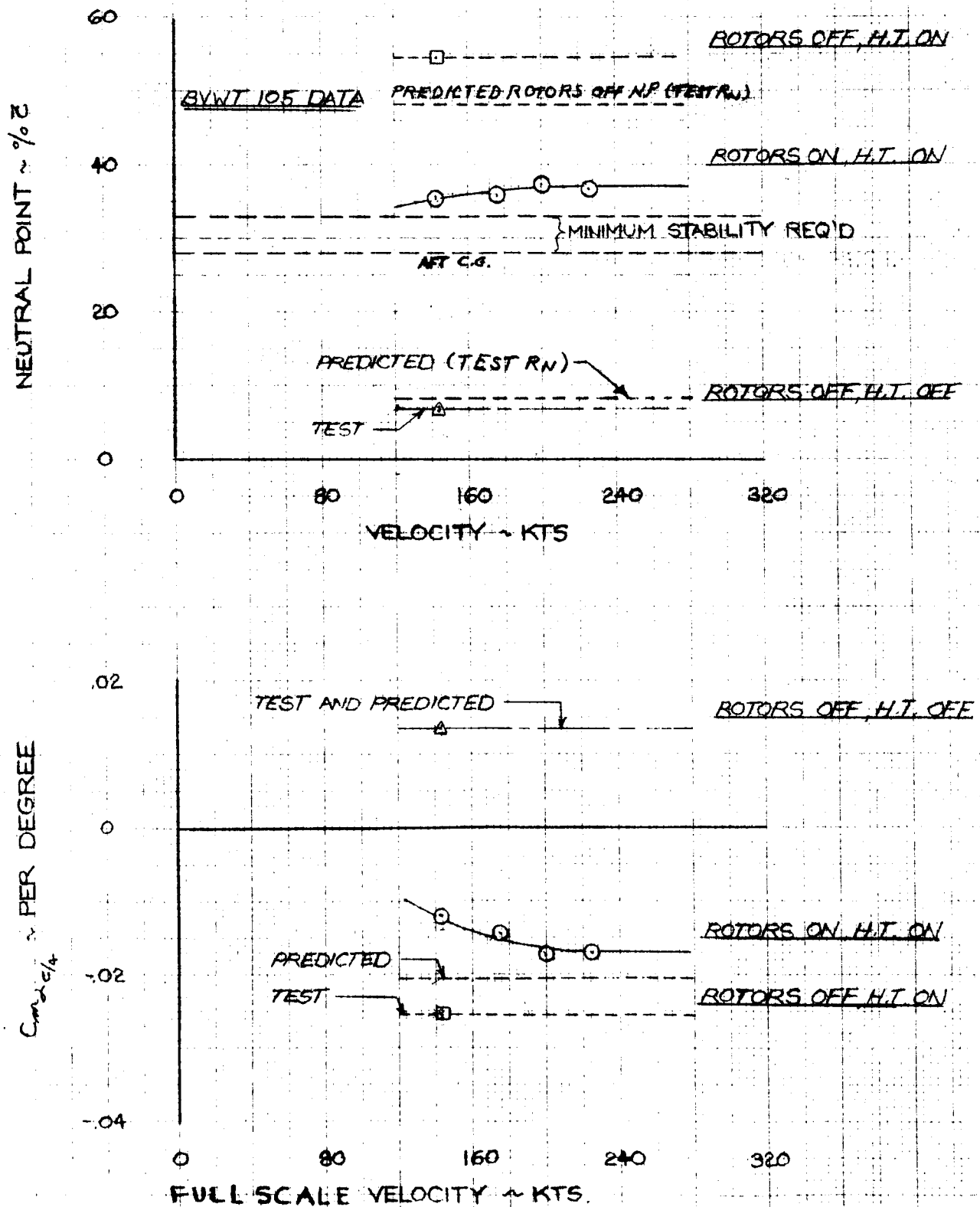


Figure 201

SIDEFORCE VARIATION OF SIDEFORCE COEFFICIENT WITH SIDESLIP ANGLE IN CRUISE

ROTORS OFF

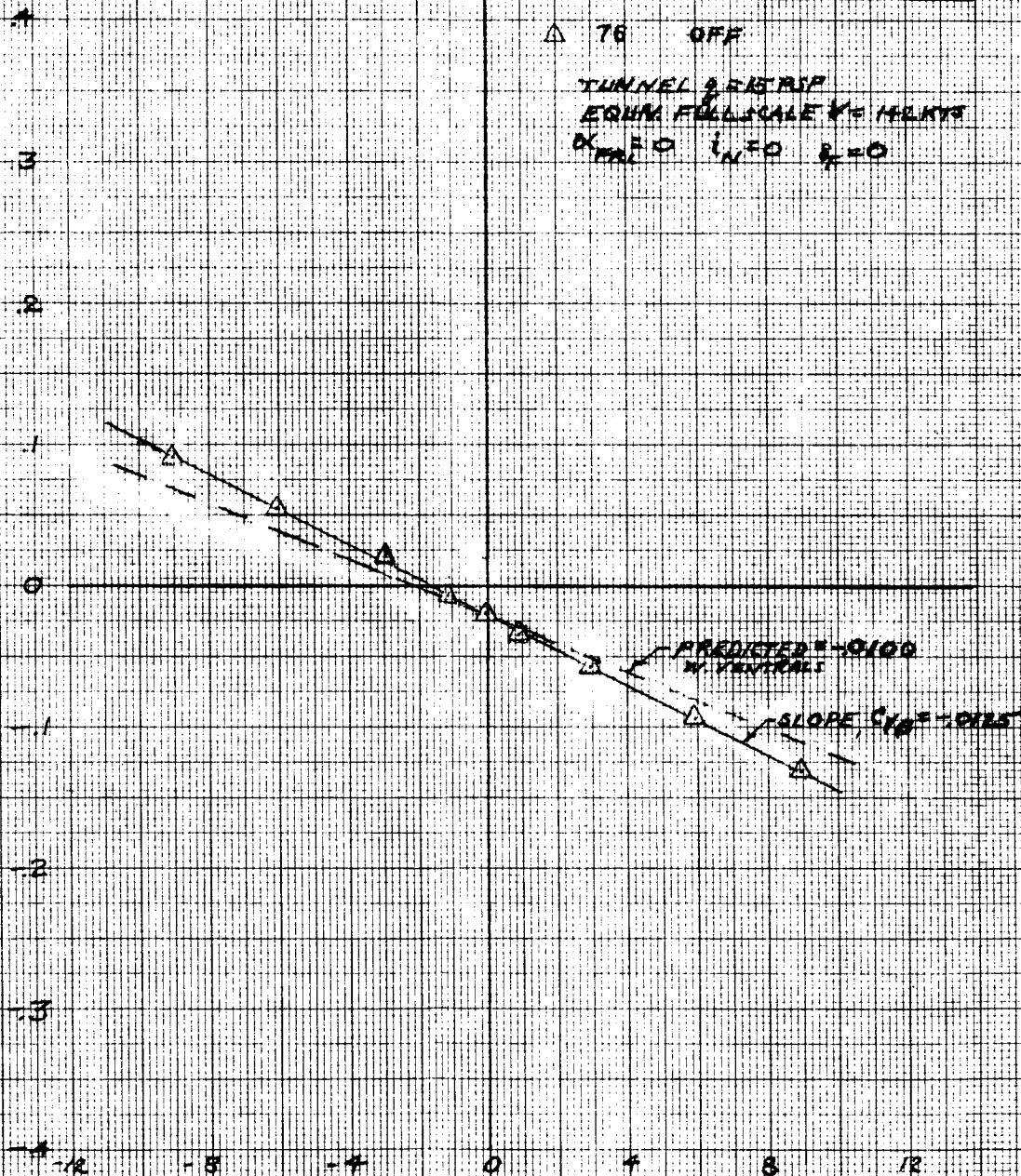
NOTES

RUN TAKE

- 45 ON DATA NOT AVAIL
- △ 76 OFF

TUNNEL 2.25 MSP
EQUIM FULL SCALE $V = 14.4$ KTS
 $\alpha_{REL} = 0$ $i_N = 0$ $\beta = 0$

SIDEFORCE COEFFICIENT - C_Y



SIDESLIP ANGLE - β - DEGREES

Figure 202

DIRECTIONAL STABILITY

VARIATION OF YAWING MOMENT COEFFICIENT WITH SIDESLIP ANGLE IN CRUISE ROTORS OFF

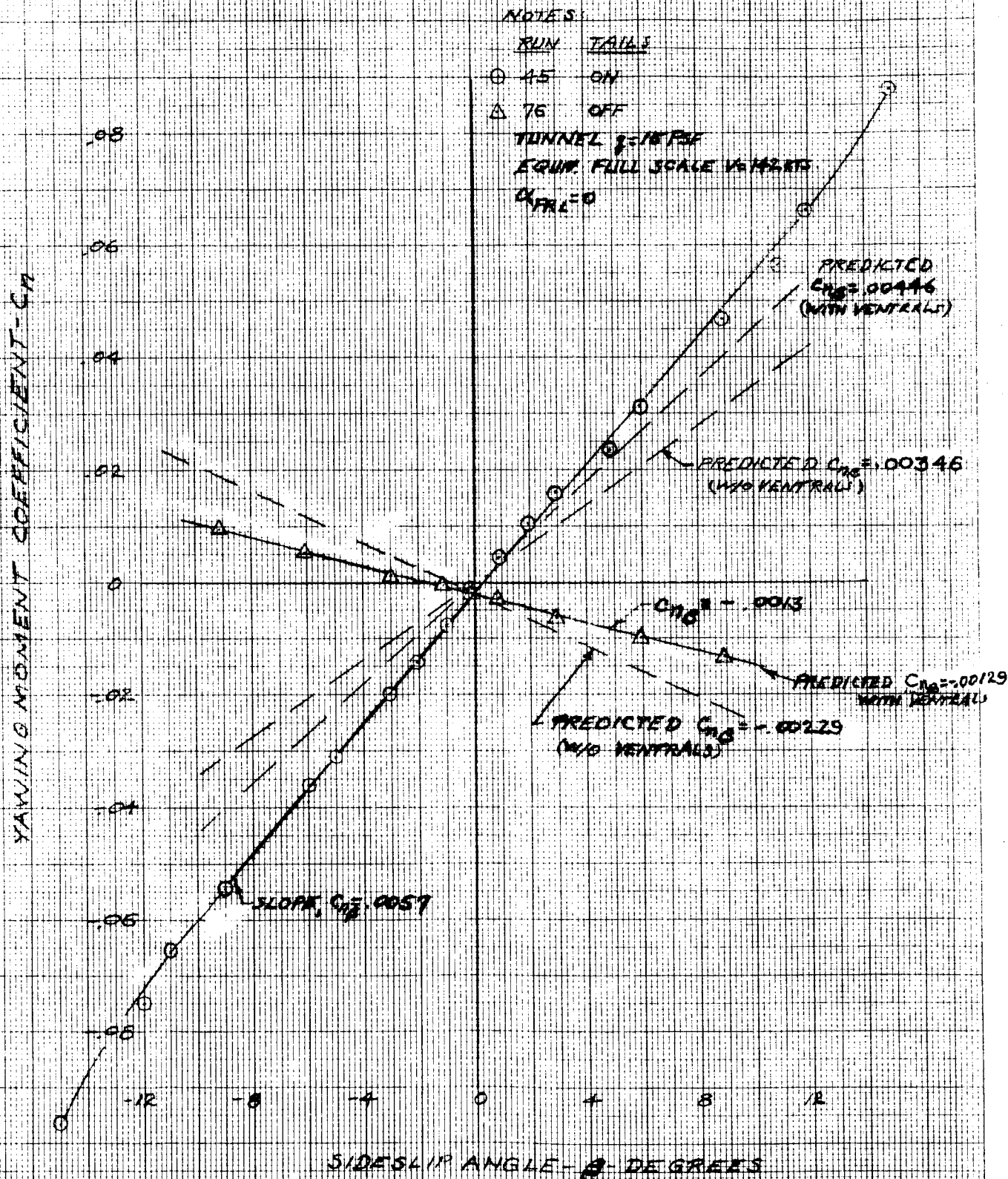


Figure 203

DIHEDRAL EFFECT

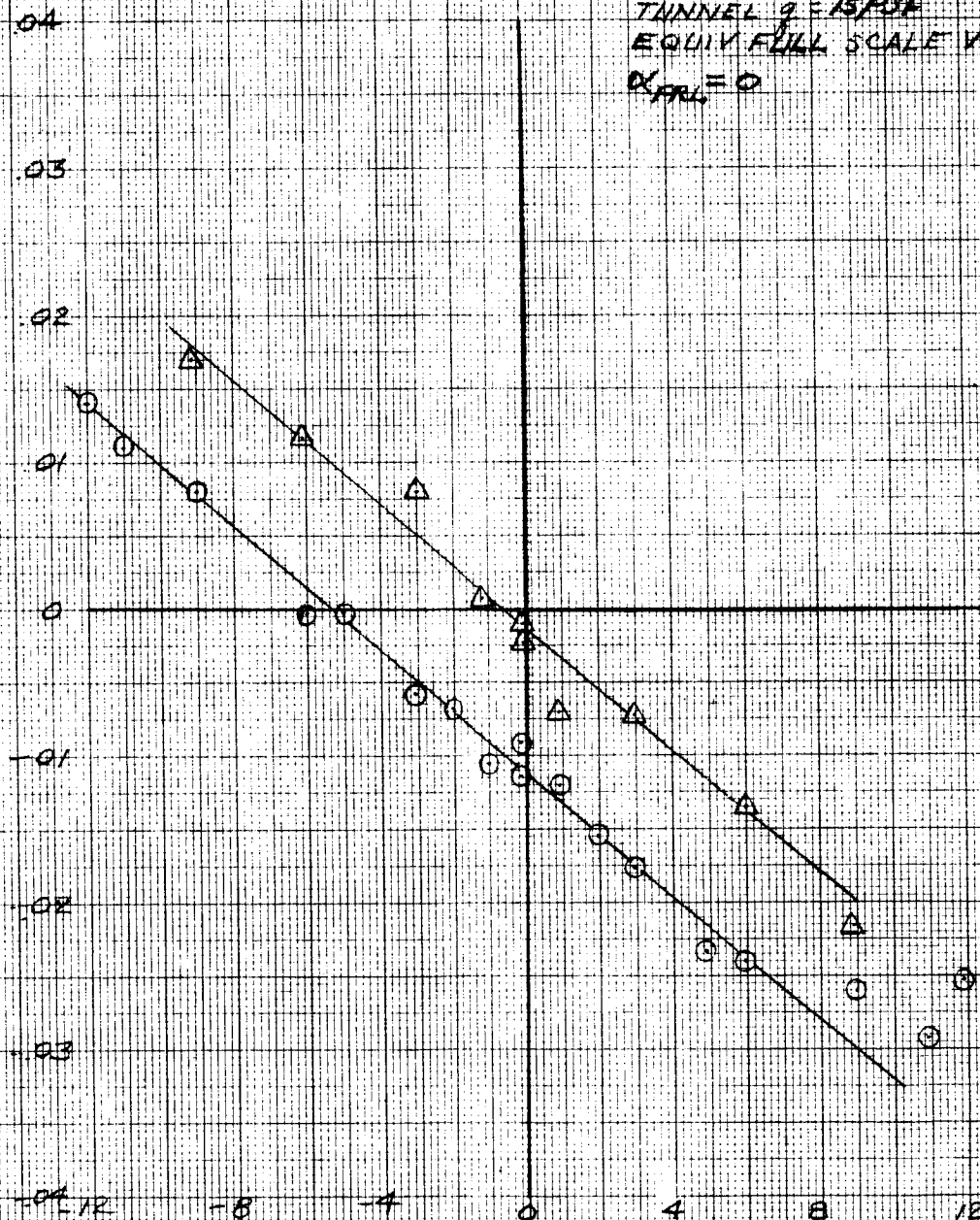
VARIATION OF ROLLING MOMENT COEFFICIENT
WITH SIDESLIP ANGLE TAILS ON AND TAILS OFF
ROTORS OFF

NOTES:

TAILS	$C_{R\text{TEST}}$	$C_{R\text{PREDICTED}}$
ON	-0.00213	-0.00230
OFF	-0.00215	-0.00199

TUNNEL $\alpha = 15^\circ$ SE
EQUIV FULL SCALE $V = 142$ KNOTS
 $\alpha_{PRL} = 0$

ROLLING MOMENT COEFFICIENT, C_R



SIDESLIP ANGLE - β - DEGREES

Figure 204

EFFECT OF TUNNEL 2 ON YAWING & ROLLING MOMENT
COEFFICIENTS VERSUS SIDESLIP ANGLE, ROTORS ON

YAWING MOMENT COEFFICIENT
 C_{Y1}

ROLLING MOMENT COEFFICIENT
 C_{R1}

NOTES:

RUN	β	C_T	ENGINE	C_{Y1}	C_{R1}
61	15	.0017	142	-.00346	-.00104
78	15	.0017	142	-.00352	-.00062
84	22.4	.0017	175	-.00385	-.00218
90	29.4	.0019	200	-.00466	-.00332

PREDICTED

C_{Y1}	C_{R1}
-.00284	-.00259
-.00224	-.00259
-.00267	-.00377
-.00305	-.00460

$\alpha = 0$ $\beta = 0$
RPM = 830

CORRECTED FOR
DIFFERENCE IN
POWER

SIDESLIP ANGLE - β - DEGREES

Figure 205

EFFECT OF TUNNEL β ON SIDEFORCE COEFFICIENT VERSUS SIDESLIP ANGLE

NOTES:

	RUN	β	C_T	EQUIV. F.S. V	$C_{Y\beta}$ TEST	$C_{Y\beta}$ CORR.
\diamond	81	15	.0017	142	-.0410	-.0416
\circ	78	15	.0017	142 KTS	-.0410	-.0416
\triangle	84	22.4	.0017	175	-.0436	-.0429
\square	90	29.4	.0019	200	-.0472	-.0423

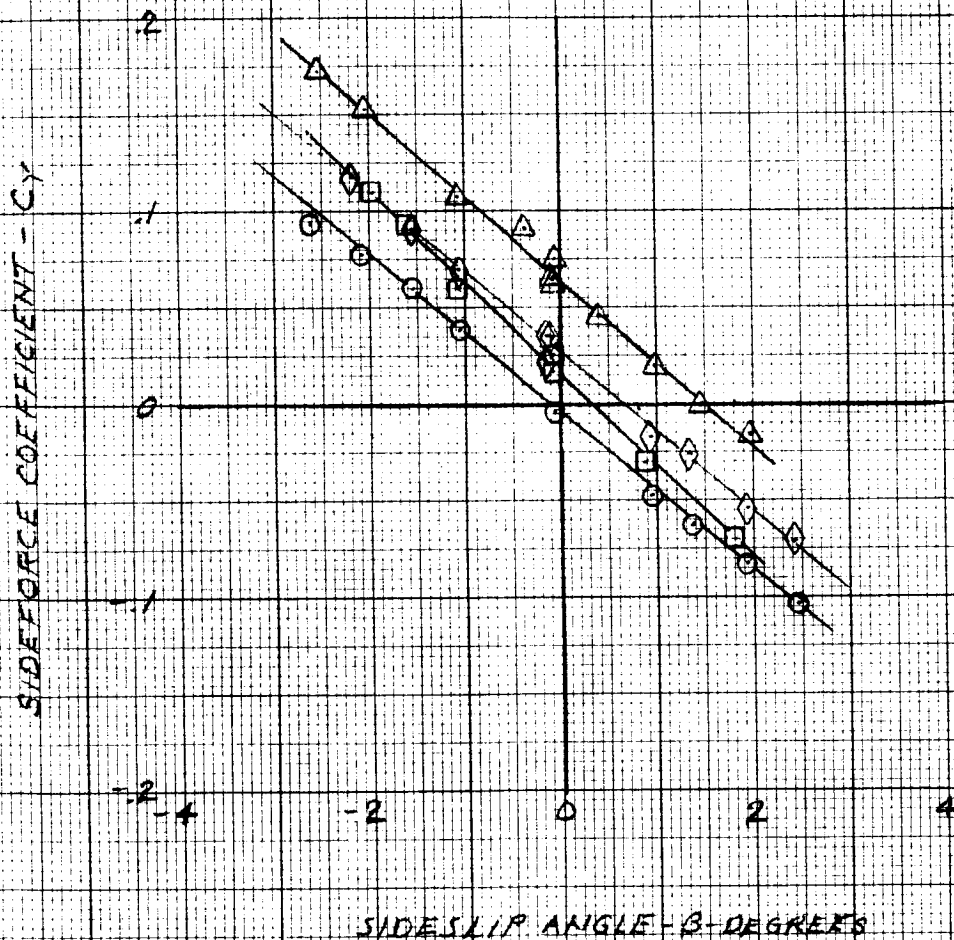


Figure 206

VARIATION OF YAWING AND ROLLING MOMENT COEFFICIENTS WITH SIDESLIP ANGLE TAILS ON AND TAILS OFF WITH ROTORS ON

YAWING MOMENT COEFFICIENT
 $C_{m\dot{\alpha}}$

ROLLING MOMENT COEFFICIENT
 $C_{l\dot{\alpha}}$

NOTES:

RUN TAILS

	$C_{m\dot{\alpha}}$	$C_{l\dot{\alpha}}$	$C_{m\dot{\alpha}}$	$C_{l\dot{\alpha}}$
O 51 ON	.00300	-.00104	.00224	-.00259
A 121 OFF	-.00310	-.00104	-.00350	-.00228

TUNNEL $\beta = 15^\circ$ P.F.

2000 FT FULL SCALE $V = 142$ KTS

$C_T = .0017$

AIRCRAFT

TEST PREDICTED

	$C_{m\dot{\alpha}}$	$C_{l\dot{\alpha}}$	$C_{m\dot{\alpha}}$	$C_{l\dot{\alpha}}$
--	---------------------	---------------------	---------------------	---------------------

O 51 ON	.00300	-.00104	.00224	-.00259
---------	--------	---------	--------	---------

A 121 OFF	-.00310	-.00104	-.00350	-.00228
-----------	---------	---------	---------	---------

AIRFRAME

TEST PRED

	$C_{m\dot{\alpha}}$	$C_{l\dot{\alpha}}$	$C_{m\dot{\alpha}}$	$C_{l\dot{\alpha}}$
--	---------------------	---------------------	---------------------	---------------------

O 51 ON	.0064	-.00200	.0046	-.00230
---------	-------	---------	-------	---------

A 121 OFF	-.0006	-.00264	-.0028	-.00189
-----------	--------	---------	--------	---------

.016

.008

0

-.008

-.016

-.016

-.008

0

-.008

-4

-2

0

2

4

Figure 207

VARIATION OF SIDEFORCE COEFFICIENT WITH SIDESLIP ANGLE TAILS ON AND TAILS OFF ROTORS ON

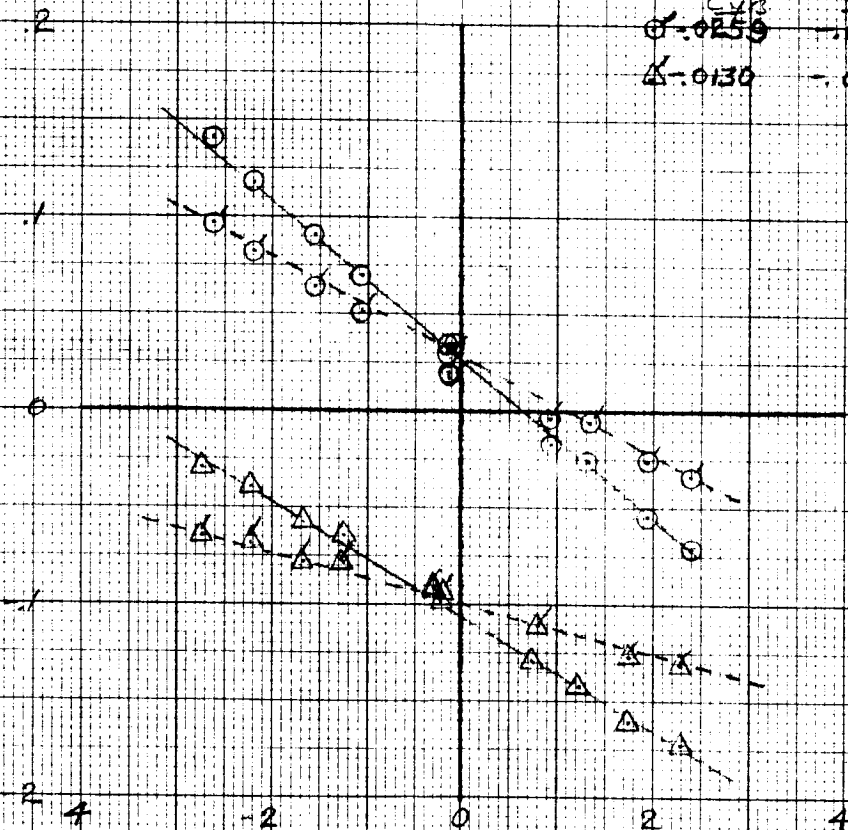
NOTES:

RUN	TAILS	AIRCRAFT	
		CY _{TEST}	CY _{PRED.}
81	ON	-0.0410	-0.0416
121	OFF	-0.0296	-0.0314

FUNNEL $\frac{2}{3}$ = 1570 SF
EQUIV FULL SCALE V = 142 KNOTS
C_T = .0017

TEST	AIRFRAME	
	CY _B	CY _B
ϕ	-0.0259	-0.0262
δ	-0.0130	-0.0100

SIDEFORCE COEFFICIENT - C_Y



SIDESLIP ANGLE - β - DEGREES

Figure 208

DIRECTIONAL STABILITY SUMMARY DIRECTIONAL STABILITY DERIVATIVE VERSUS VELOCITY

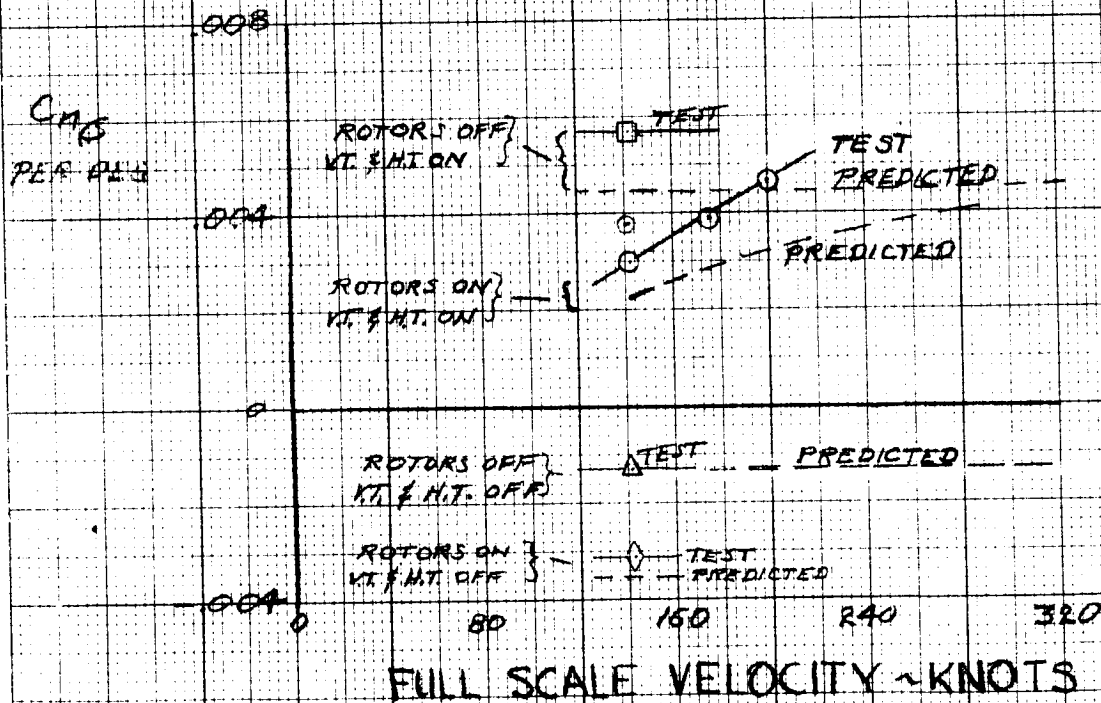


Figure 209

DIHEDRAL EFFECT SUMMARY LATERAL STABILITY DERIVATIVE VS VELOCITY

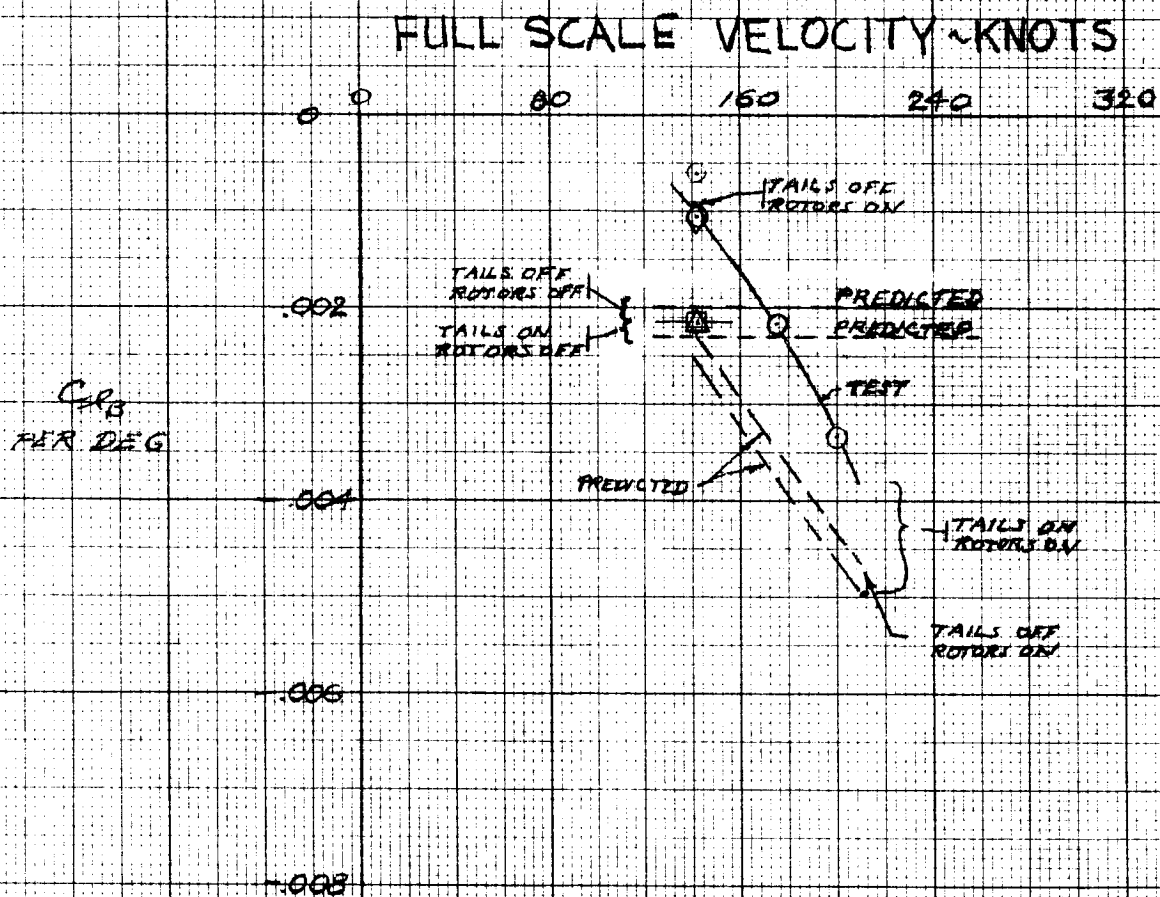


Figure 210

SIDEFORCE SUMMARY
SIDEFORCE DERIVATIVE VS VELOCITY

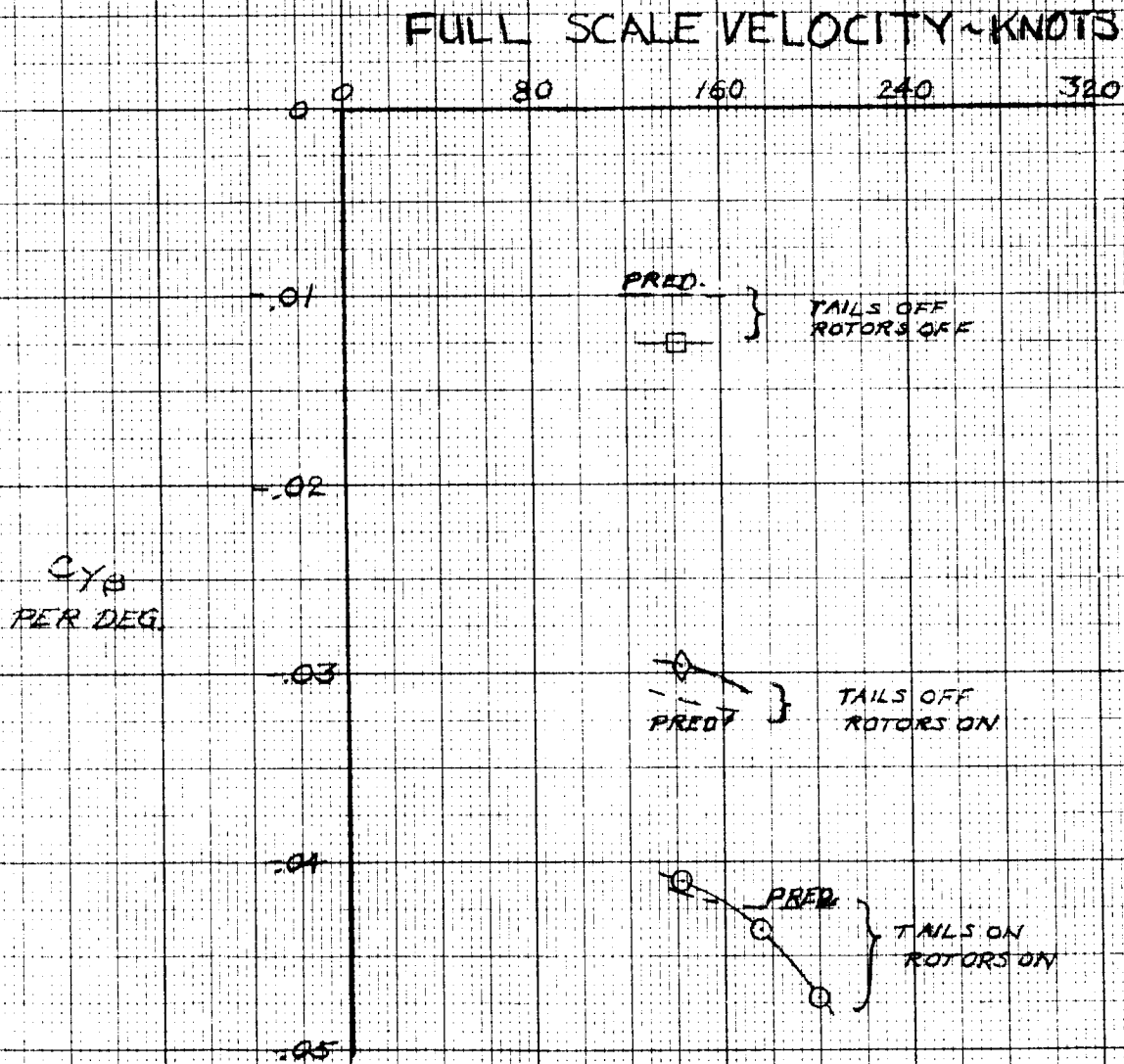


Figure 211

5.2.3 Control Effectiveness

Control effectiveness tests were performed to determine the effectiveness of lateral and longitudinal cyclic, elevator, aileron (flaperon), spoilers, rudder, and flaps. Cyclic control is not presently planned to be used as a primary control in cruise in the Model 222 aircraft. It will, however, be used to improve aircraft stability and reduce rotor blade loads in cruise as part of the load alleviation system.

Cyclic Effects

Lateral cyclic effectiveness in varying total aircraft stability coefficients is illustrated in Figures 212 and 213. Effectiveness is illustrated for conditions representing full scale aircraft velocities of 142 and 200 knots at zero fuselage angle of attack, flap deflection and nacelle incidence. The variations of aircraft stability parameters with cyclic deflection are summarized in Table 9. Note that the variation of parameters is for cyclic deflection of right rotor only, i.e., it represents the contribution of only one rotor. Lateral cyclic application results in only a small aircraft change in lift coefficient in the positive direction per degree cyclic, but considerably larger change in the negative direction in sideforce coefficient. Aircraft pitching moment coefficient change per degree A_1 is also observed to be larger than the change in yawing moment coefficient. For example, data from run 27 indicates the change in pitching moment coefficient to be 5.97 times the change in yawing moment coefficient. The change in lift coefficient relative to sideforce coefficient indicates the order of magnitude of force on the aircraft as both coefficients are nondimensionalized on q_s . However, pitching moment coefficient is nondimensionalized

Run	Tunnel q - PSF	Full Scale Air- Craft V-Knots	$\frac{\Delta C_L}{A_1}$	$\frac{\Delta C_m}{A_1}$	$\frac{\Delta C_Y}{A_1}$	$\frac{\Delta C_n}{A_1}$
27	15	142	.0012	.0175	-----	-.00293
91	29.3	200	.0033	.0190	-.018	-.0036

Table 9 Effect of Lateral Cyclic on Aircraft Stability
Parameters (Right Rotor)

on $q\bar{s}$, and yawing moment coefficient is nondimensionalized on qsb . Thus, the magnitude of pitching moment and yawing moment change is similar b is 5.6 times \bar{c} .

Longitudinal cyclic effectiveness is illustrated on Figure 214, 215 and 216 and derivatives for the right rotor are tabulated in Table 10. Application of longitudinal cyclic results in much larger negative change in lift than in positive sideforce coefficient for the right rotor while lateral cyclic resulted in larger sideforce coefficient change than lift coefficient as expected. Note, however, as in the case of lateral cyclic, longitudinal cyclic results in considerably larger pitching moment coefficient change than yawing moment coefficient. Again, the ratio of the coefficients is 5.75 very nearly the same as the ratio of wing span to wing chord, so that pitching and yawing moments are nearly equal.

Elevator Effectiveness

Elevator effectiveness is illustrated in Figure 217 and 218 for the rotors on condition. Data with rotors removed are presented in Figures 219 through Figure 223. Figure 217 and 218 indicate that the variation of lift and pitching moment coefficients with elevator deflection are linear to approximately 12 degrees deflection. Variation of pitching moment coefficient with elevator deflection, $C_{m_{\delta_e}}$, is indicated to be $-.0242$ in the linear range. Lift coefficient variation with elevator deflection, $C_{L_{\delta_e}}$, is $.0061$. Figure 219 rotors off, indicates that the elevator effectiveness is not substantially affected by the rotors, at least within the accuracy of the slope of the line faired through the data points. Figure 220 through 223 indicate that angle of attack and

Run	Tunnel q - PSF	Full Scale Air- craft V-Knots	$\frac{\Delta C_L}{B_1}$	$\frac{\Delta C_m}{B_1}$	$\frac{\Delta C_y}{B_1}$	$\frac{\Delta C_n}{B_1}$
30	15	142	-.0267	-.0303	-----	-.00527
92	29.4	200	-.0363	-.0195	.0041	-.00537

Table 10 Effect of Longitudinal Cyclic on Aircraft Stability
Parameters (Right Rotor)

sideslip angle have negligible effect on elevator effectiveness.

Roll Control Effectiveness

The schedule of spoiler deflection versus aileron deflection which has been established for the Model 222, estimated to provide near-linear rolling moment with stick deflection, is illustrated on Figure 224. The recorded variation of spoiler deflection versus aileron deflection for test run 65 is also illustrated on this figure. Roll control effectiveness is illustrated on Figures 225 through 231 for test conditions representing an equivalent aircraft velocity of 142 knots. Figure 225 illustrates the variation of rolling and yawing moment coefficients for combined spoiler and aileron deflection plotted versus deflection of the left aileron. The rolling moment coefficient indicates some nonlinearity with increasing roll effectiveness as deflection is increased. The maximum C_{ℓ} is .0617 at 17 degrees deflection. This value was attained deflecting only the outboard half of the left flap span and right spoiler span for roll control. The Model 222 will use the full span of the flap on one wing coupled with the full span of the spoiler on the other for roll control. The yawing moment coefficient at the test condition of zero fuselage angle of attack is favorable, or proverse, with a value of .0073 at the maximum deflection tested, and with the ratio of $C_{\ell}/C_n = 8.5$. Figure 226, run 65, indicates the rolling moment and yawing moment coefficient variations with left spoiler deflection and with right aileron deflection, individually, compared on the same plot. The rolling moment plot illustrates an abrupt change in level at an aileron deflection of 6.5 degrees. This is believed to have

been caused by an instrumentation problem. The spoiler rolling moment coefficient was $-.034$ at 45.7 degrees deflection. The characteristic favorable yaw due to spoiler deflection is indicated with $C_n = -.008$ at maximum deflection. Figure 227 , run 66 , again illustrates the individual contributions of the spoilers and ailerons to roll and yaw moment coefficients but with the inboard flaps on the wings set to 20 degrees. Variation of rolling and yawing moment coefficients are illustrated on Figure 228 as a function of angle of attack with the left spoiler set at 50.3 degrees and right aileron 26.4 degrees. The maximum rolling moment coefficient during this run is indicated to be $-.085$ at a fuselage angle of attack of zero degrees and diminishing to $-.060$ at -12.4 degrees and $-.054$ at $+12.2$ degrees angle of attack. Yawing moment coefficient due to roll control is near zero at angles of attack greater than 3 degrees and reaches a maximum of $.024$ at -12.4 degrees angle of attack. This compares with a value of $C_{n\beta}$ of $.0030$ from test with rotors on indicating a response of approximately 8 degrees sideslip for full roll control input at the large negative angle of attack condition. The effects of roll control input on lift and pitching moment coefficient variation with angle of attack are illustrated in Figure 229 and 230. The effects on longitudinal stability are illustrated in Figure 231 , lift coefficient versus pitching moment coefficient. These figures indicate that with the roll controls deflected lift curve slope is increased, pitching moment coefficient variation with angle of attack, $C_{m\alpha}$, is more negative, and longitudinal stability is increased.

Rudder Effectiveness

The variation of yawing moment coefficient with rudder deflection, rudder effectiveness, is illustrated in Figure 232 for the rotors off condition. This figure indicates linear rudder effectiveness to near 15 degrees deflection and a C_n of $-.084$ at 20 degrees. Figure 233 indicates practically no variation in yawing moment due to rudder deflection as a function of sideslip to ± 12 degrees sideslip. Figure 234 indicates that the rolling moment coefficient variation with sideslip does not vary appreciably between ± 8 degrees sideslip. The variation of rolling moment coefficient with rudder deflection is illustrated in Figure 235. The rate of change of rolling moment coefficient with rudder deflection is indicated to be $.00045$ at zero sideslip and angle of attack.

Flap Effectiveness

The effects of various flap deflections on lift and pitching moment coefficient variation with angle of attack and on longitudinal stability for the airframe with rotors off are illustrated in Figures 236, 237, and 238 respectively. Lift curve slope and pitching moment curve slope with angle of attack are both increased as flaps are deflected. Longitudinal stability is relatively unaffected at lift coefficients between $\pm .4$ and flap deflection of 20 degrees or less. Linearity of lift versus pitching moment coefficient is maintained to a lift coefficient of approximately 1.3 with flaps deflected 21 and 44 degrees and then the pitching moment breaks sharply stable. This break should occur

at considerably higher C_L at full scale aircraft Reynolds number as these test runs were conducted at the low Reynolds number of approximately $.91 \times 10^6$. The effects of flap deflection on the longitudinal characteristics with rotors on are illustrated in Figures 239, 240 and 241 for a limited range of angles of attack. Again, the trend with flap deflection is to increase lift curve slope and increase pitching moment curve slope negatively. However, the rate of change of pitching moment coefficient with angle of attack as a function of flap deflection is decreased and the net result is to make $\frac{dC_m}{dC_L}$ less negative. Near neutral stability is indicated for the aft center of gravity limit of 27.8 percent chord for the Model 222 with flaps deflected 20 degrees, neutral point at 28.0 percent chord for the test vertical reference location. As discussed earlier, in Section 5.2.2, the results are slightly conservative, however, for the test vertical reference is on the wing chord line and the full scale aircraft center of gravity will be at least 19 inches below the chord plane for all loading conditions anticipated. The thrust changes which occur with change in angle of attack, will, therefore, be more stabilizing because of the larger moment arm.

Figure 242 illustrates the effect of flap deflection on yawing and rolling moment coefficient variation with sideslip angle. The fairing of the lines through the data points has been adjusted to represent constant engine power settings for each run as opposed to constant collective and constant rpm. The 20 degree flap deflection line indicates some decrease in directional stability as compared to zero flap deflection and the 40 degree flap deflection line

indicates increased directional stability. The rolling moment coefficient variation indicates an increase in dihedral effect with flaps deflected as compared to zero deflection with a larger increase for 20 degrees deflection than for 40 degrees. Summaries of the effects of flap deflection on lift coefficient and pitching moment coefficient as a function of flap deflection are presented for the rotors off and rotors on conditions in Figures 243 and 244. The dropoff of flap lift effectiveness indicated at flap deflections greater than 40 degrees is not anticipated to be as rapid for the full scale aircraft operating at the associated much higher Reynolds number. It is believed that this decrease in lift was at least partially due to separation of flow over the flaps and higher Reynolds number should delay this separation. The pitching moment coefficient variations illustrated on Figure 244 indicate that for constant angle of attack or for constant lift coefficient increasing flap deflection results in increasing nose down pitching moment coefficient. The constant C_L curve indicates a change in C_m of $-.045$ between zero and 20 degrees flap deflection which would require a change of elevator for trim of only -1.86 degree per the effectiveness illustrated in Figure 217. The rotors off data of Figure 243 indicate that deflecting the flaps from zero to 20 degrees at constant C_L would require a change in elevator for trim of $+6.0$ degrees, nose down, to offset the ΔC_m of $+.145$.

LATERAL CYCLIC EFFECTIVENESS VARIATION OF AIRCRAFT LIFT AND PITCHING MOMENT COEFFICIENTS WITH LATERAL CYCLIC-RIGHT ROTOR

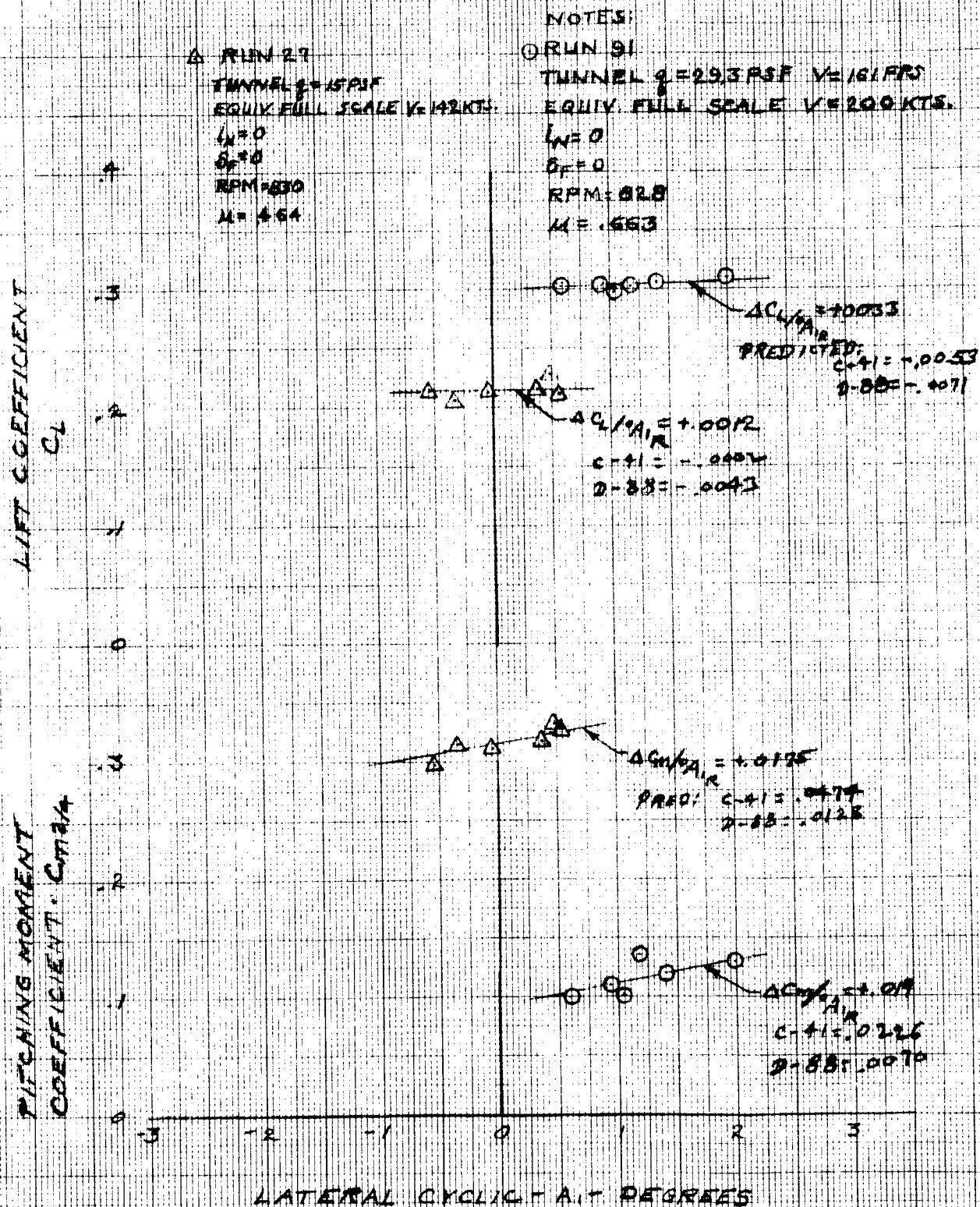


Figure 212

LATERAL CYCLIC EFFECTIVENESS VARIATION OF AIRCRAFT SIDEFORCE AND YAWING MOMENT COEFFICIENTS WITH LATERAL CYCLIC - RIGHT ROTOR

△ RUN 27
TUNNEL $q = 15 \text{ PSF}$
EQUIV. FULL SCALE $V = 142 \text{ KTS}$
 $i_N = 0$
 $\delta_F = 0$
RPM = 836
 $H = .664$

○ RUN 91
TUNNEL $q = 29.3$ $V = 161 \text{ FPS}$
EQUIV. FULL SCALE $V = 200 \text{ KTS}$
 $i_N = 0$
 $\delta_F = 0$
RPM = 828
 $H = .663$

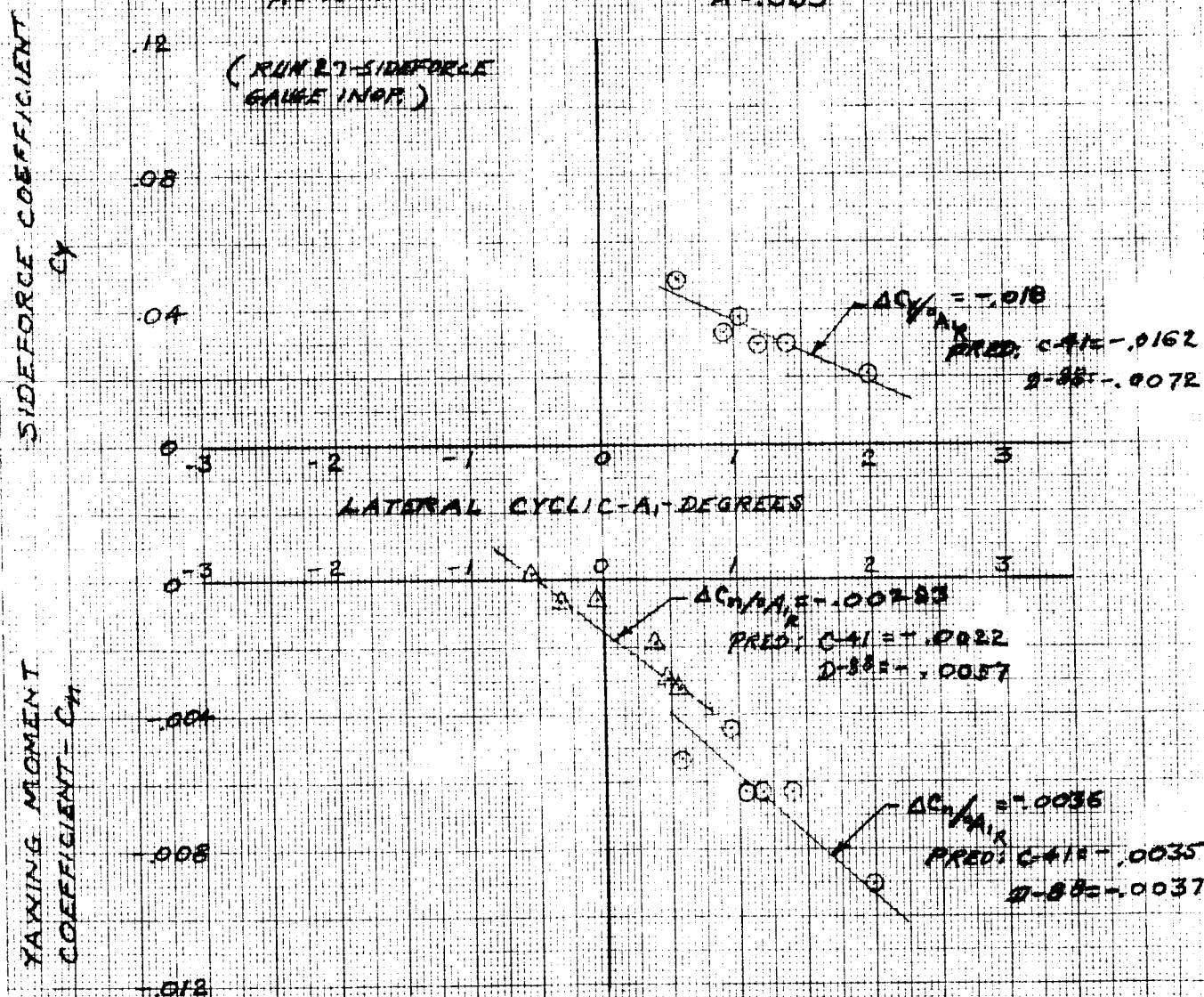


Figure 213

LONGITUDINAL CYCLIC EFFECTIVENESS VARIATION OF LIFT AND PITCHING MOMENT COEFFICIENTS WITH LONGITUDINAL CYCLIC

LIFT COEFFICIENT
 C_L

PITCHING MOMENT
COEFFICIENT - $C_{m\delta}$

RUN 30

△ RIGHT ROTOR

△ LEFT ROTOR

TUNNEL $\beta = 15^\circ$

EQUIV FULL SCALE $V = 142$ KTS

$C_N = 0$ $C_F = 0$

RPM = 830

$\mu = 7.64$

NOTES:

RUN 92

○ RIGHT ROTOR

△ LEFT ROTOR

TUNNEL $\beta = 28^\circ$ $V = 162$ FPS

EQUIV FULL SCALE $V = 200$ KTS

$C_N = 0$ $C_F = 0$

RPM = 830 $\mu = 6.60$

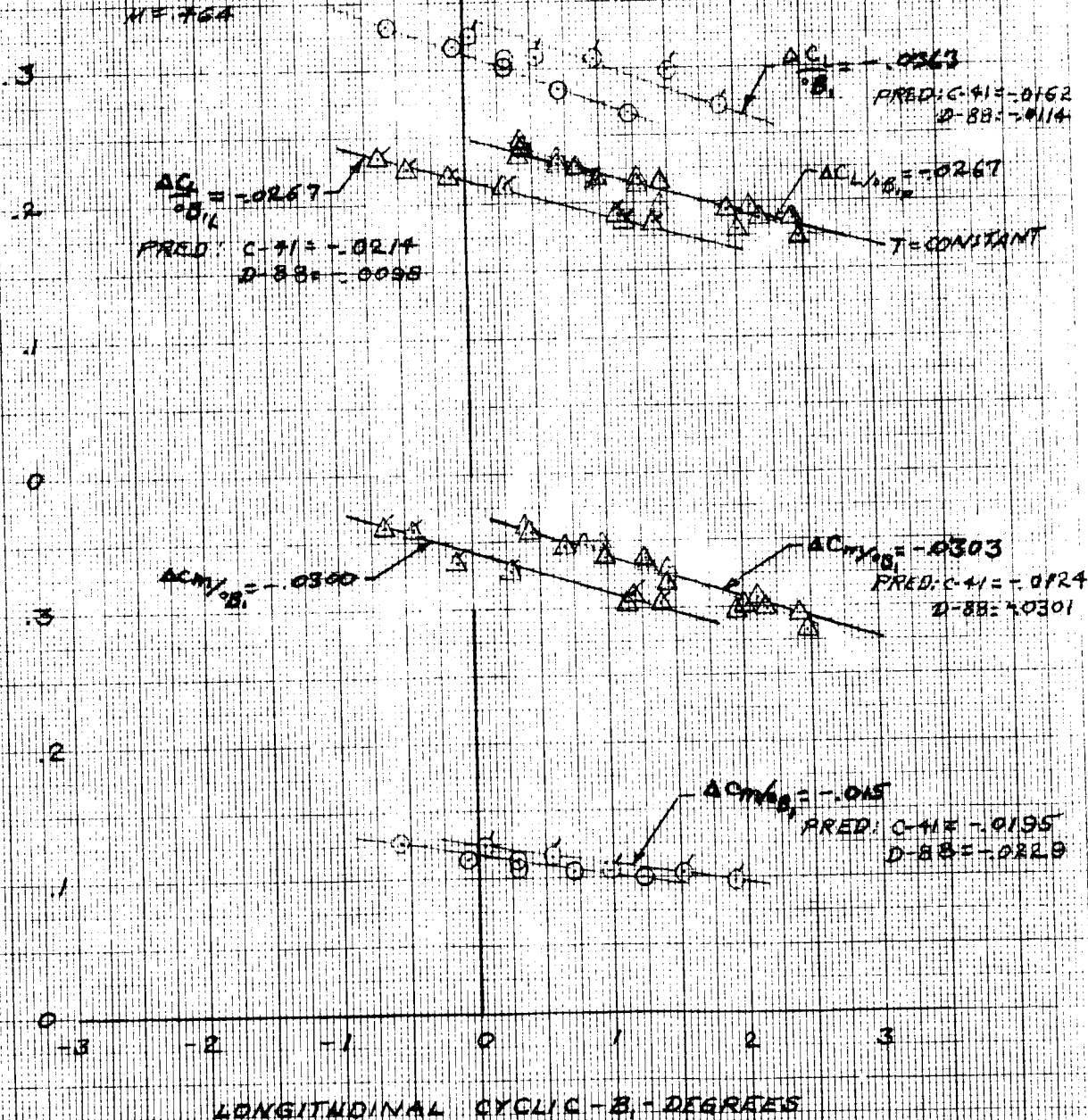


Figure 214

LONGITUDINAL CYCLIC EFFECTIVENESS VARIATION OF AIRCRAFT SIDEFORCE AND YAWING MOMENT COEFFICIENTS WITH LONGITUDINAL CYCLIC

NOTES:

RUN 92

⊙ RIGHT ROTOR

⊙ LEFT ROTOR

TUNNEL $q = 29.4$ $V = 162$ FPS

EQUIV FULL SCALE $V = 200$ KTS

$I_N = 0$

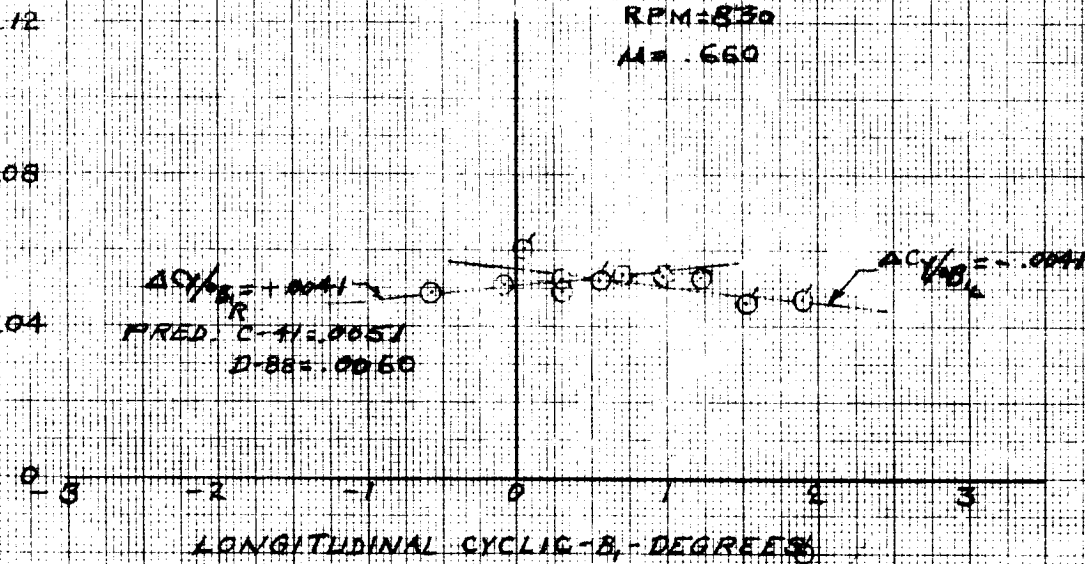
$\delta_F = 0$

RPM = 830

$M = .660$

SIDEFORCE COEFFICIENT

C_Y



YAWING MOMENT COEFFICIENT - C_N

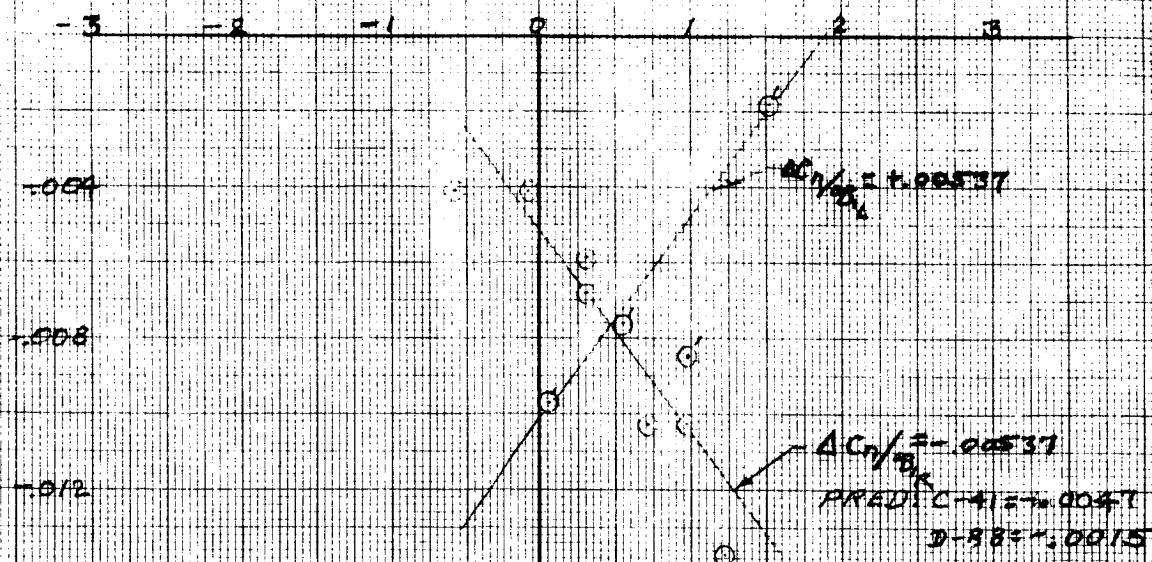


Figure 215

LONGITUDINAL CYCLIC EFFECTIVENESS VARIATION OF YAWING MOMENT COEFFICIENT WITH LONGITUDINAL CYCLIC

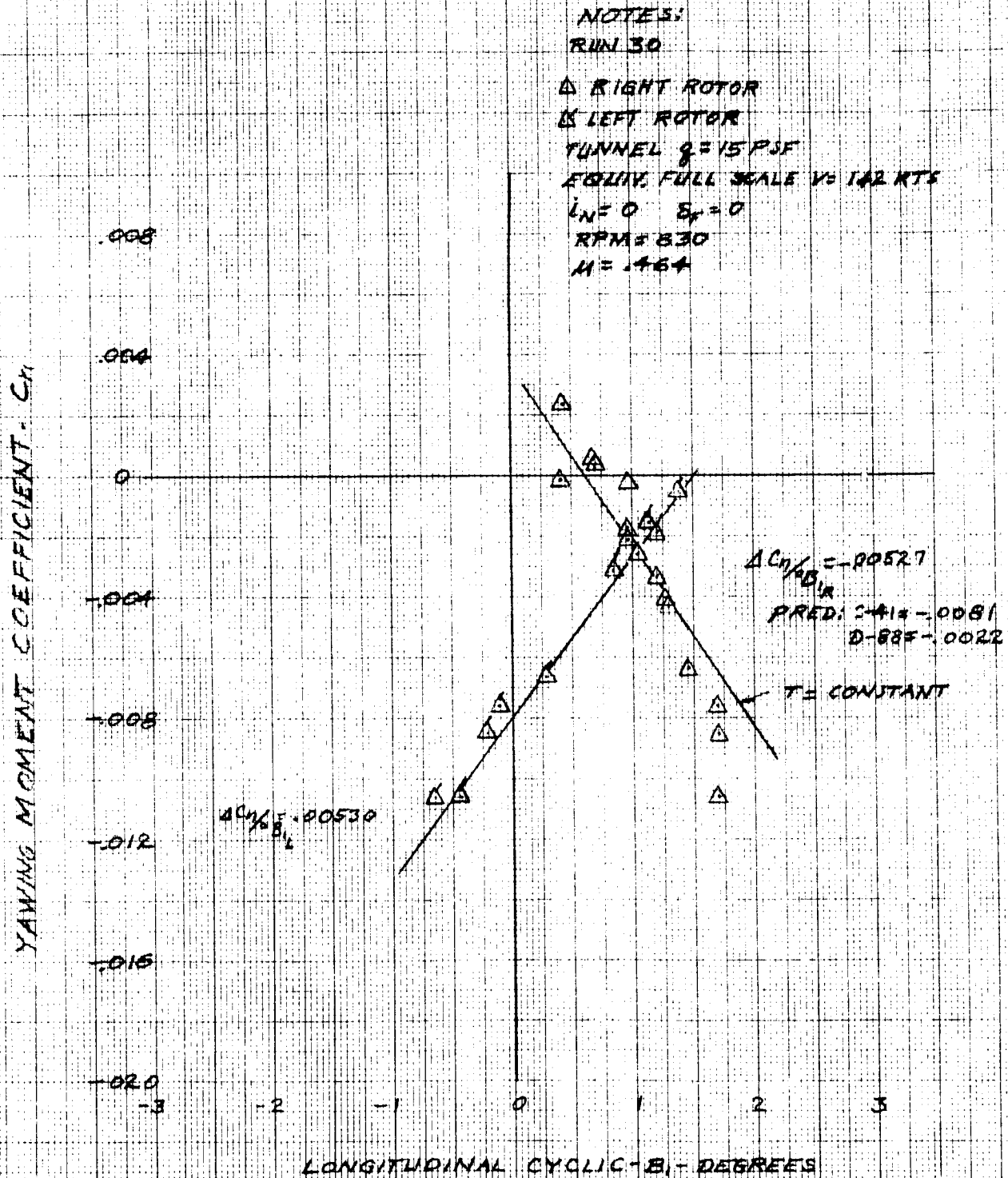


Figure 216

ELEVATOR EFFECTIVENESS IN CRUISE - ROTORS ON

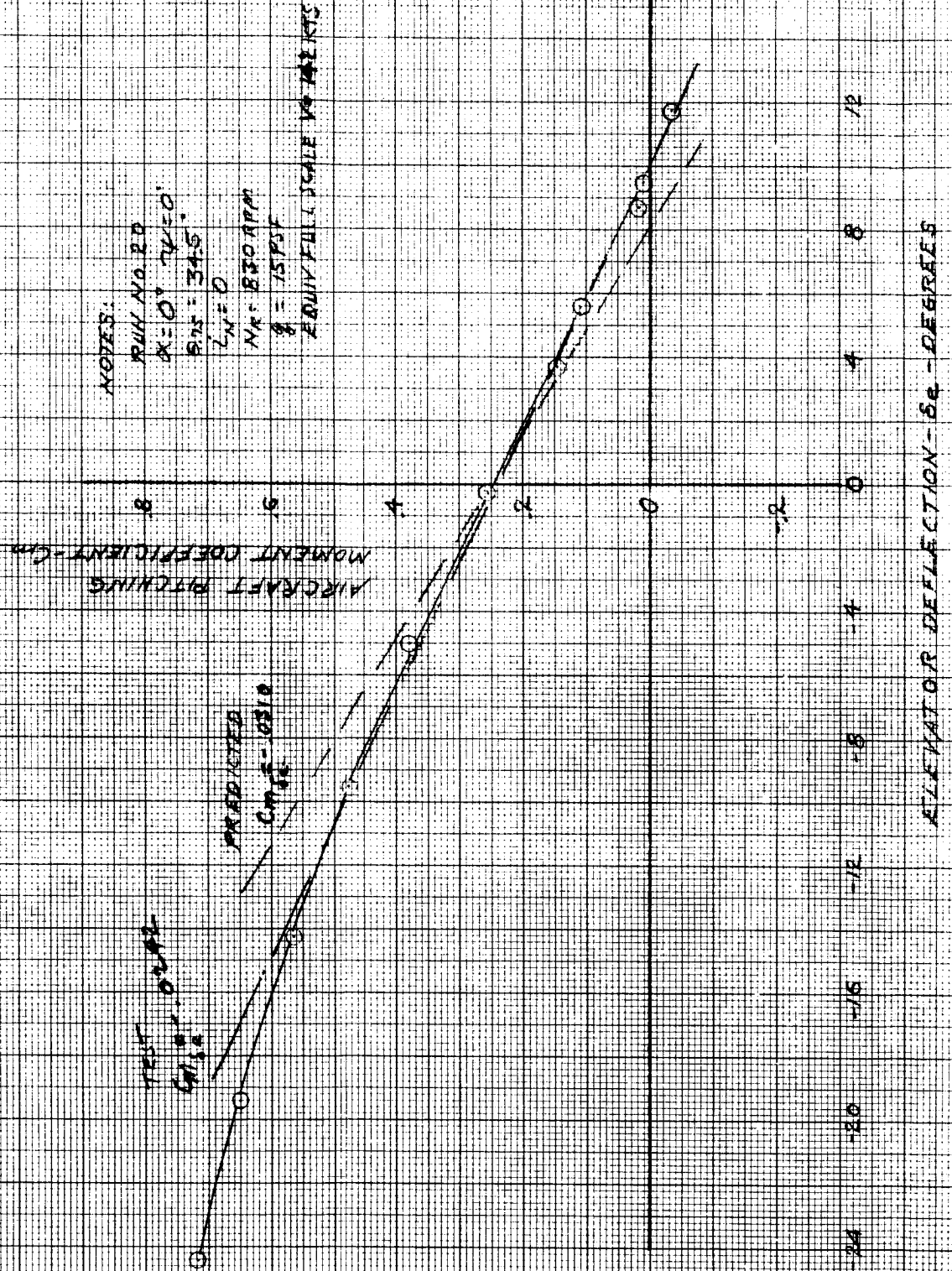


Figure 217

VARIATION OF LIFT COEFFICIENT WITH ELEVATOR DEFLECTION

CRUISE - ROTORS ON

NOTES:
RUN AUG. 20
ASD: 7420
BPF: 34.5
NR: 830 RPM
2-15 PJF
EQUIV FULL SCALE VS. 142 KG.

AIRBORNE
COEFFICIENT

PREDICTED
 $C_L = 0.092$
 $C_L = 0.092$

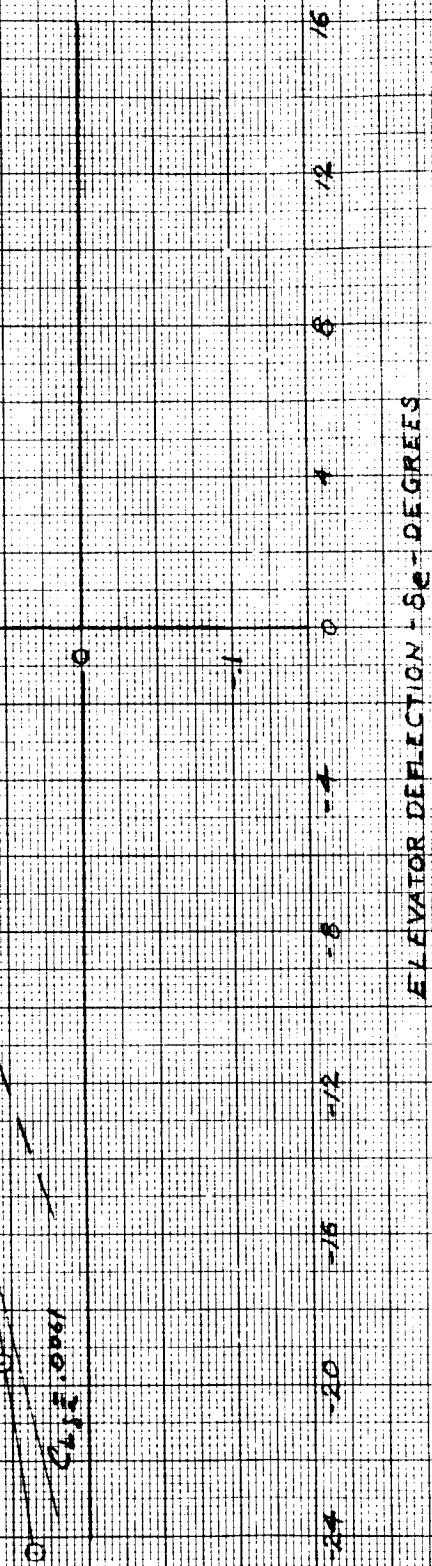
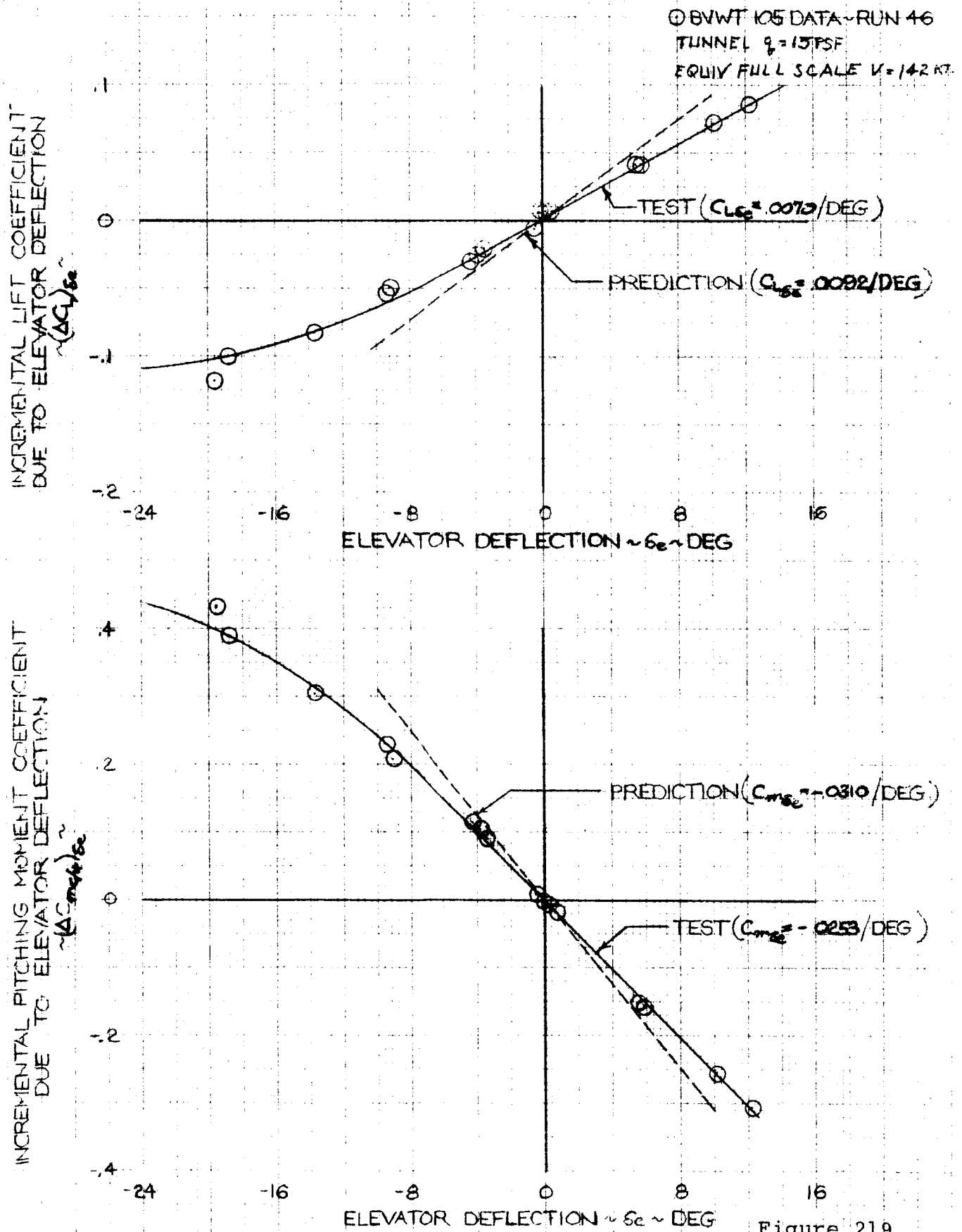


Figure 218

MODEL 222
 ELEVATOR EFFECTIVENESS
 ROTORS OFF
 $\alpha = 0^\circ$



MODEL 222
 ELEVATOR EFFECTIVENESS
 ROTORS OFF
 $\alpha = 0$

Δ RUN 40 $\delta e \approx 0.1^\circ$
 \square 47 $\approx 10.4^\circ$

TUNNEL 23 MPF
 EQUIV. FULL SCALE $V = 142$ KTS.

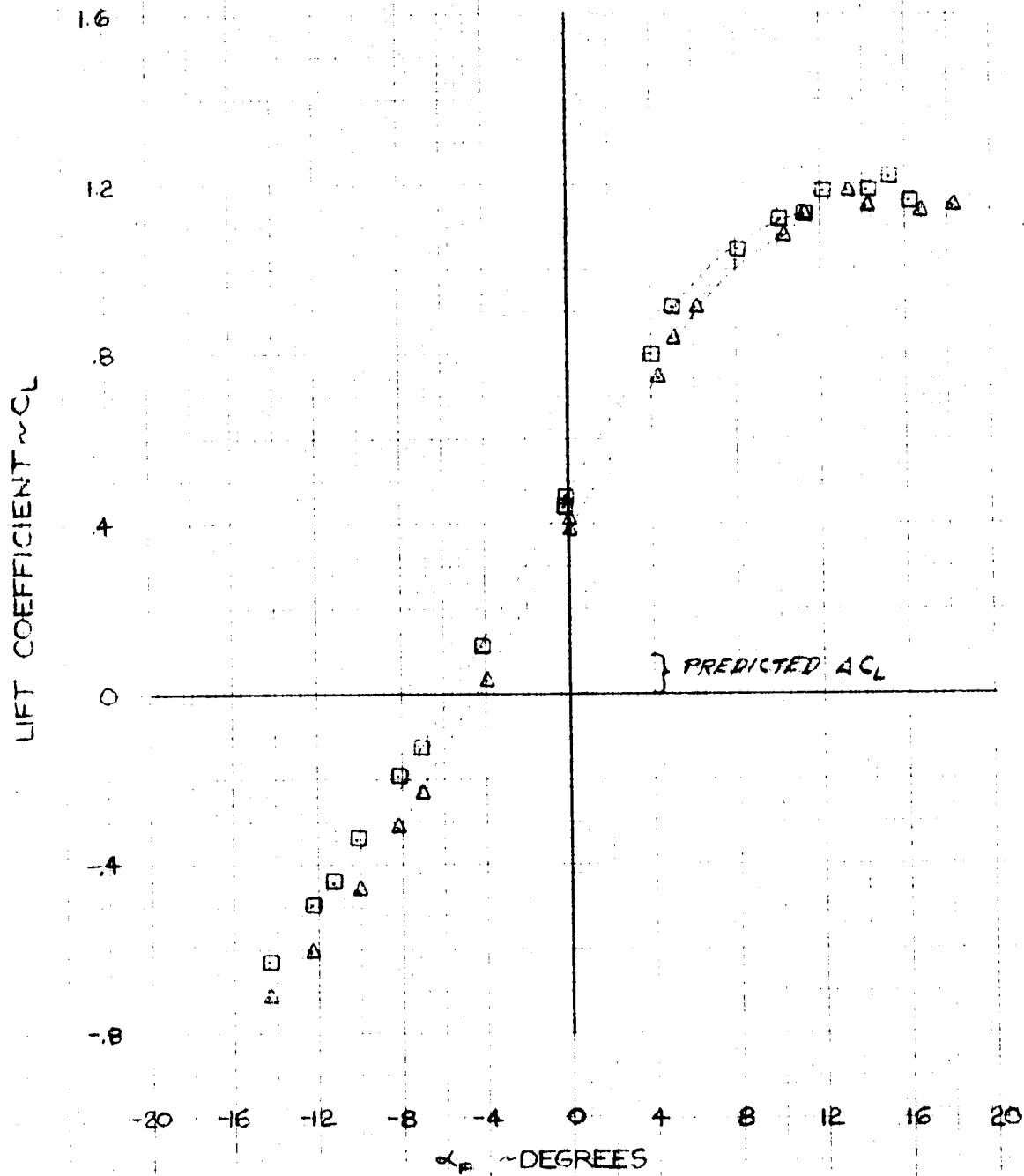


Figure 220

MODEL 222
 ELEVATOR EFFECTIVENESS
 ROTORS OFF
 $\alpha = 0$

Δ RUN 40 $\delta_e = 0.1^\circ$
 \square 47 $\delta_e = 10.4^\circ$

TUNNEL $q_\infty = 15 \text{ PSF}$
 EQUIV FULL SCALE $V = 142 \text{ KNOTS}$

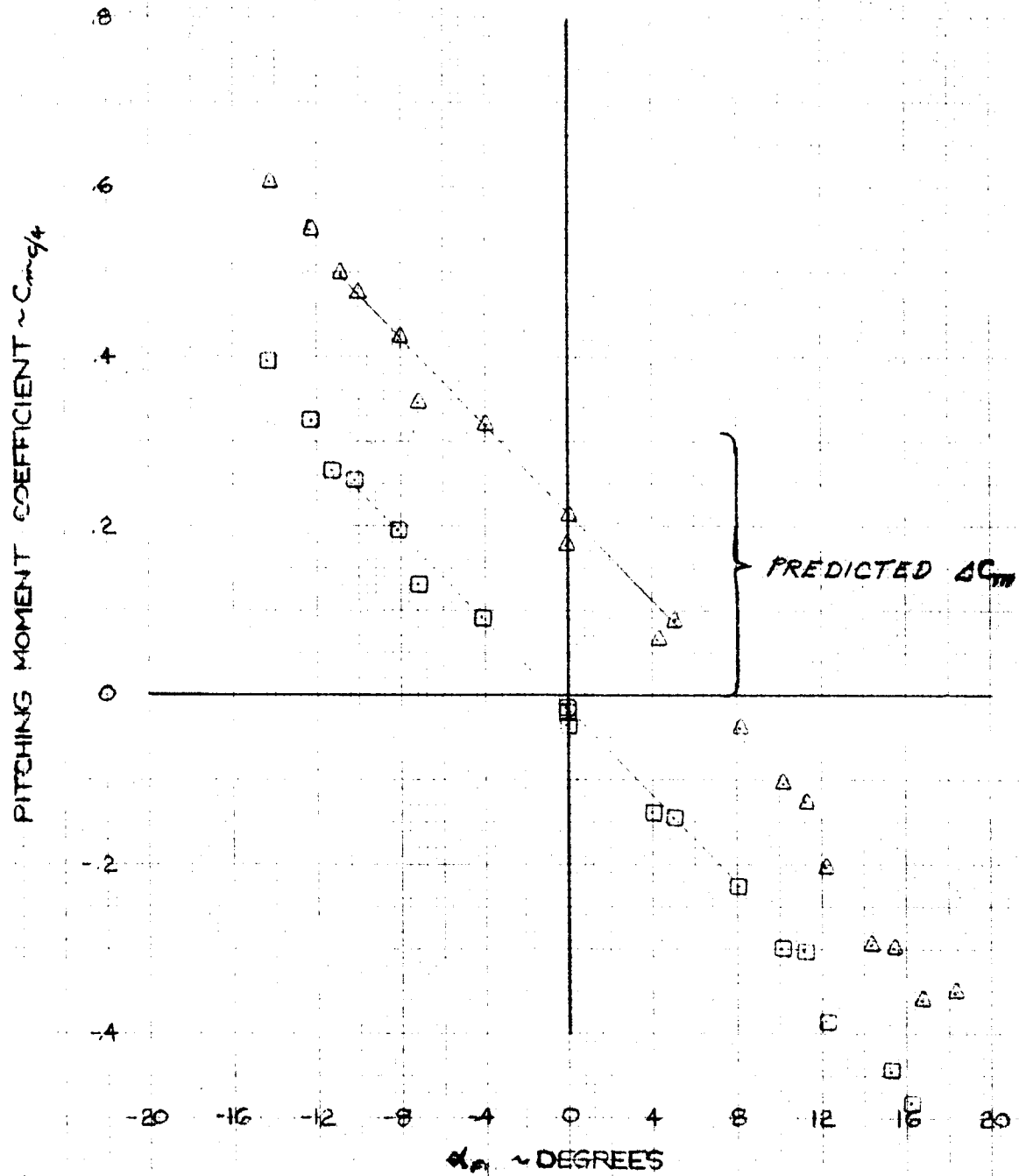


Figure 221

MODEL 222
 ELEVATOR EFFECTIVENESS
 ROTORS OFF
 $\alpha = 0$

Δ RUN 40 $\delta_e \approx 0.1^\circ$
 \square 47 $\delta_e \approx 10.4^\circ$
 TUNNEL $\rho = 15 \text{ PSF}$
 EQUIV FULL SCALE $V = 142 \text{ KTS}$

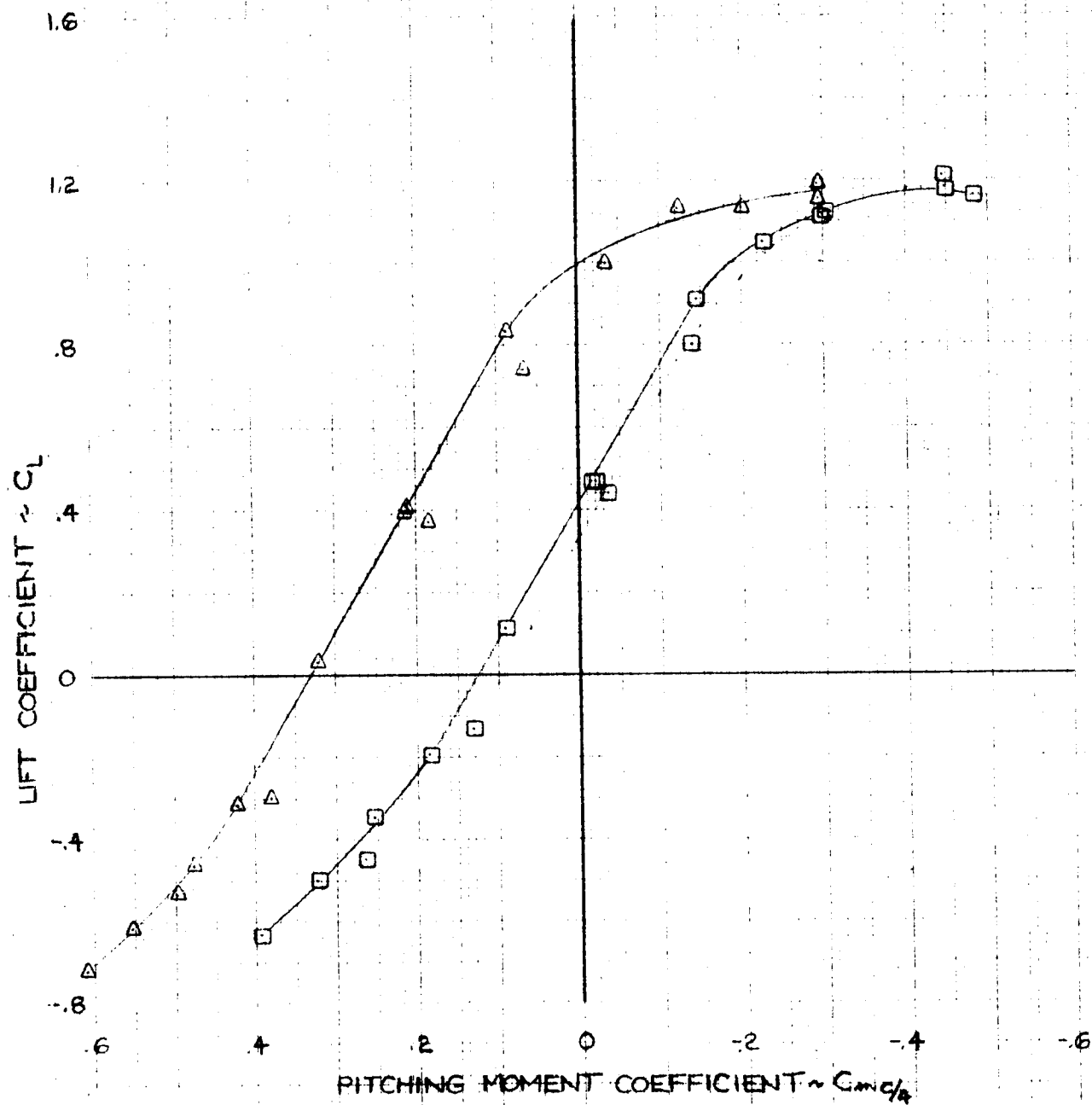


Figure 222

MODEL 222
 ELEVATOR EFFECTIVENESS IN YAW
 ROTORS OFF
 $\alpha = 0^\circ$

BVWT 105 DATA

○ RUN 45 $\delta_c = 0$
 □ 48 $\delta_c = +10^\circ$

WIND AXIS DATA
 TUNNEL $q = 15 \text{ PSF}$
 EQUIV. FULL SCALE $V = 142 \text{ KTS}$

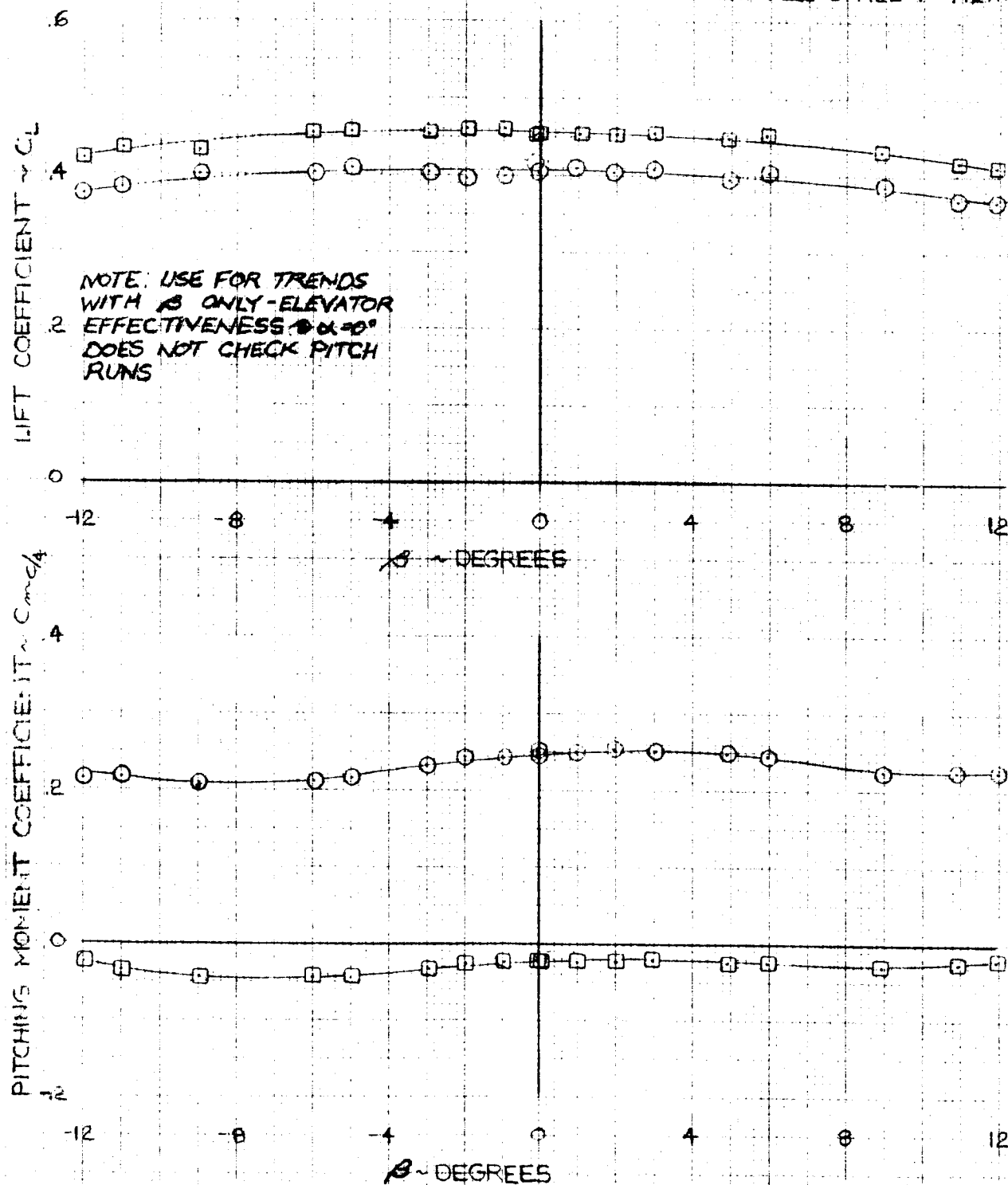


Figure 223

SCHEDULE OF SPOILER DEFLECTION
VERSUS AILERON DEFLECTION

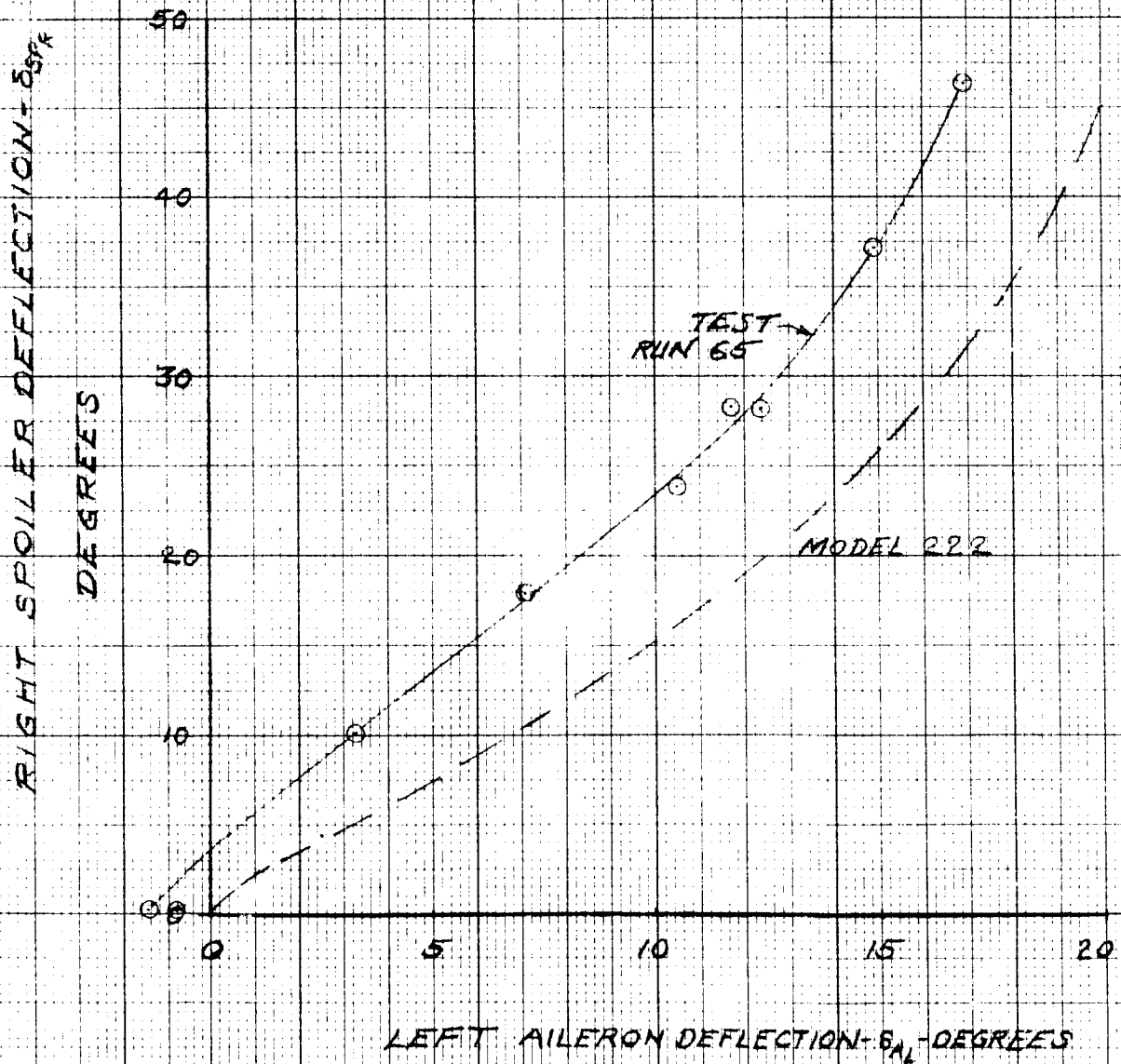


Figure 224

ROLL CONTROL EFFECTIVENESS IN CRUISE VARIATION OF ROLLING AND YAWING MOMENT COEFFICIENTS WITH COMBINED AILERON AND SPOILER DEFLECTIONS - ROTORS OFF

NOTES:

RUN 65

INLET, $\delta_{A} = 0$ $\delta_{S} = 0$

TUNNEL $q = 15 \text{ PSF}$

EQUIV FULL SCALE $V = 192 \text{ KTS}$

SPOILER DEFLECTION SCHEDULED
WITH AILERON DEFLECTION

ROLLING MOMENT COEFFICIENT

C_{Lr}

.06

.01

.02

.02

.01

.01

TEST

PREDICTED

YAWING MOMENT
COEFFICIENT - C_{Y1}

TEST

PREDICTED

0

5

10

15

20

LEFT AILERON DEFLECTION - δ_{AL} DEGREES

ROLL CONTROL EFFECTIVENESS IN CRUISE

VARIATION OF ROLLING AND YAWING MOMENT COEFFICIENTS WITH SPOILER AND AILERON DEFLECTION - ROTORS OFF

NOTES:

RUN 65

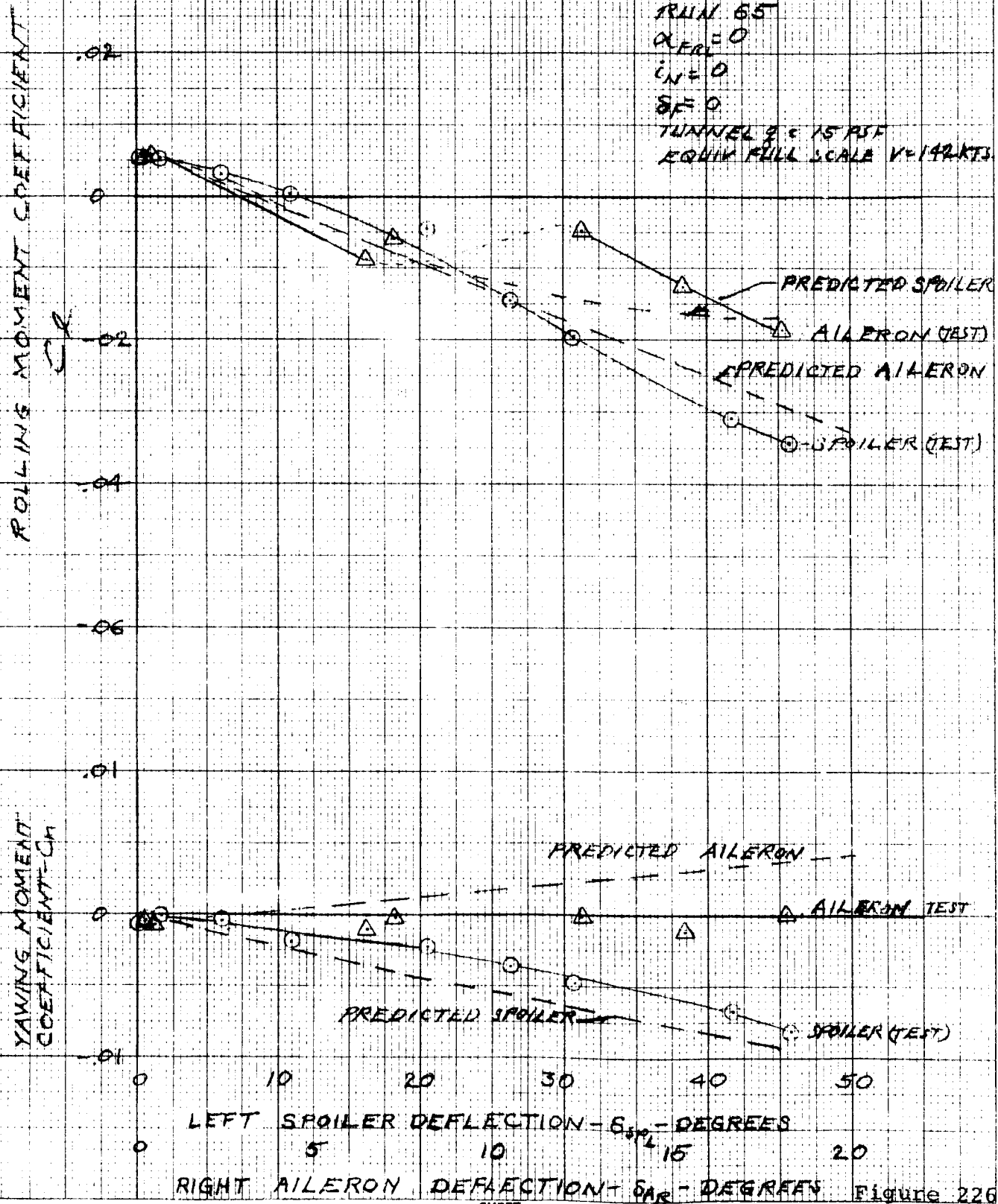
$\alpha_{REL} = 0$

$i_{NL} = 0$

$\delta F = 0$

TUNNEL 2: 15 PSF

EQUIV FULL SCALE $V = 142$ KTS.



ROLL CONTROL EFFECTIVENESS IN CRUISE
VARIATION OF ROLLING AND YAWING MOMENT
COEFFICIENTS WITH SPOILER ANDAILERON
DEFLECTION- ROTORS OFF

NOTES:
RUN 66
 $\alpha = 0^\circ$
INBOARD FLAPS SET AT 2.0
TUNNEL 92/15 P.S.F.
EQUIV FULL SCALE V_∞ 148 KTS

ROLLING MOMENT COEFFICIENT

C_{ℓ}

.02

.02

.04

.06

.01

YAWING MOMENT COEFFICIENT - C_{η}

.01

LEFT SPOILER DEFLECTION - δ_{sL} - DEGREES

RIGHT AILERON DEFLECTION - δ_{aR} - DEGREES

TEST AILERON
PREDICTED SPOILER
PREDICTED AILERON
TEST SPOILER

PREDICTED AILERON
TEST AILERON
TEST SPOILER
PREDICTED SPOILER

Figure 227

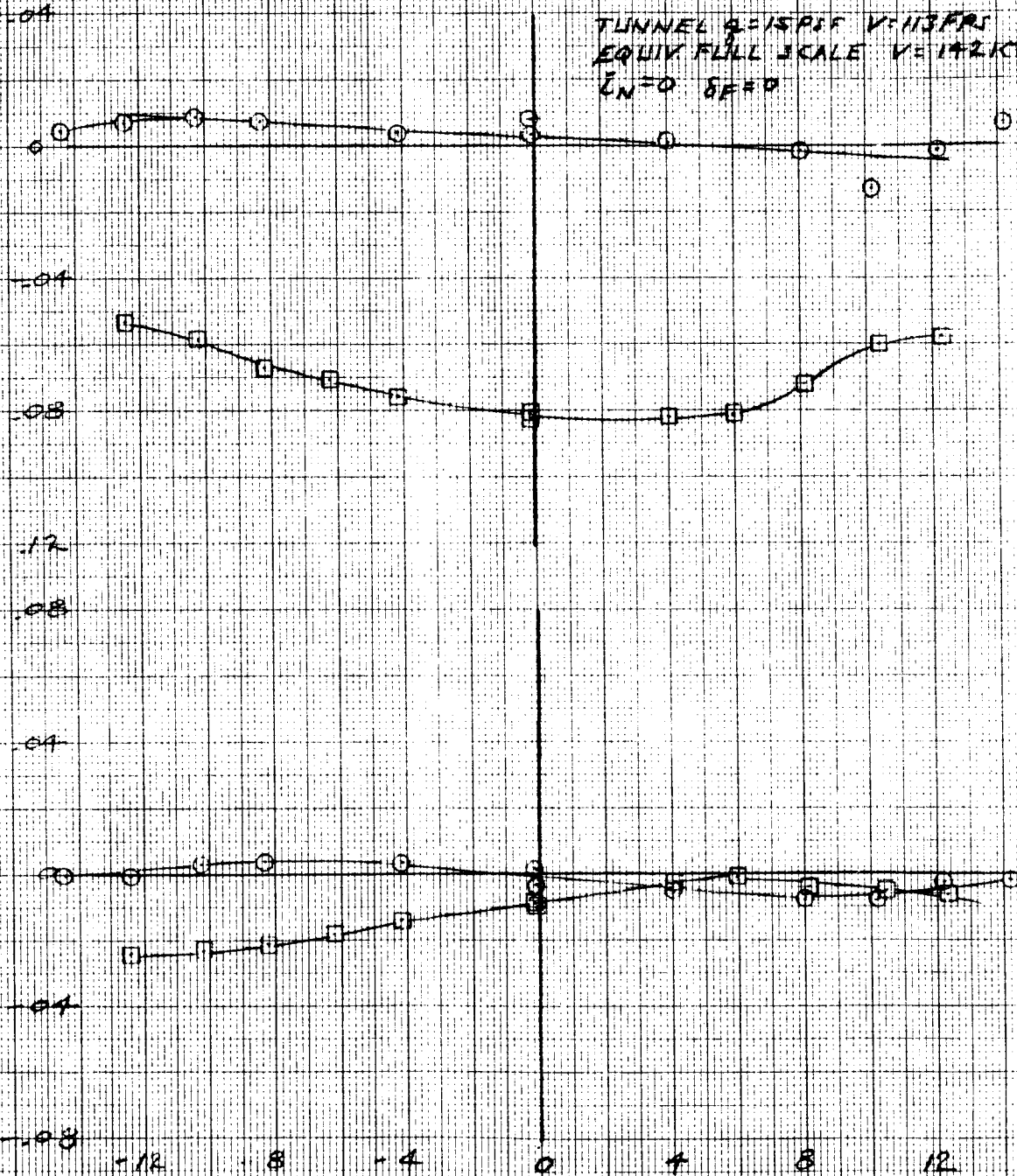
ROLL CONTROL EFFECTIVENESS VARIATION OF ROLLING AND YAWING MOMENT COEFFICIENTS WITH ANGLE OF ATTACK IN CRUISE - ROTORS OFF

NOTES:

RUN	δ_{SP}	δ_{AR}
64	0	0
67	50.3	26.4

TUNNEL $Q=15 \text{ PSI}$ $V=113 \text{ FPS}$
EQUIV FULL SCALE $V=142 \text{ KTS}$
 $\bar{C}_N=0$ $\delta_F=0$

ROLLING MOMENT COEFFICIENT
 C_{Lr}



YAWING MOMENT COEFFICIENT
 $C_{L\dot{y}}$

FUSELAGE ANGLE OF ATTACK - α - DEGREES

Figure 228

EFFECT OF ROLL CONTROL ON LIFT

VARIATION OF LIFT COEFFICIENT WITH ANGLE OF ATTACK

ROTORS OFF

NOTES:

REIN	δ_{PL}	δ_{RR}
64	0	0
67	50.3	26.4

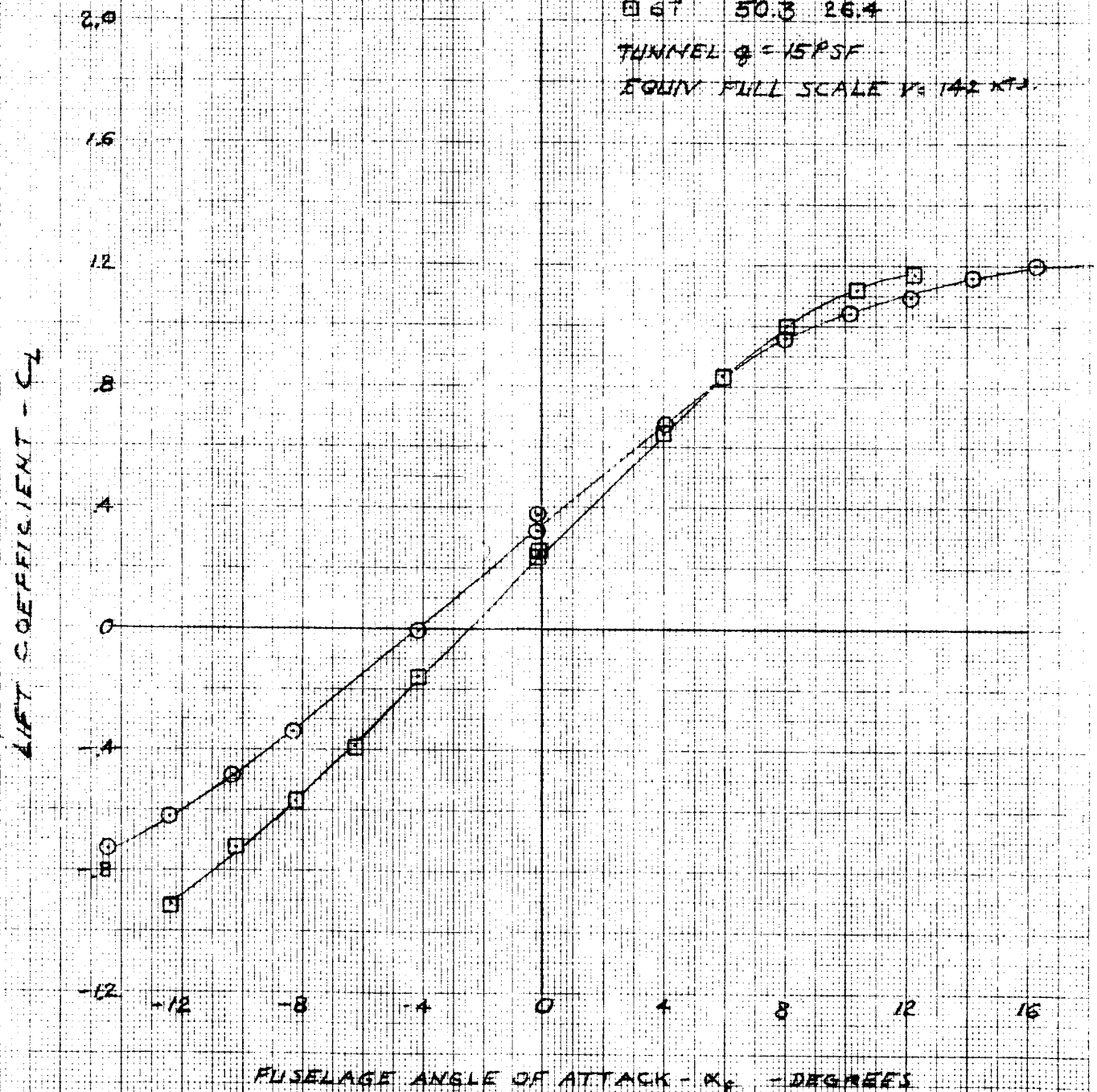
TUNNEL $q = 15 \text{ PSF}$ EQUIV FULL SCALE $V = 142 \text{ KTS}$ 

Figure 229

EFFECT OF ROLL CONTROL ON PITCHING MOMENT COEFFICIENT VARIATION WITH ANGLE OF ATTACK

ROTORS OFF

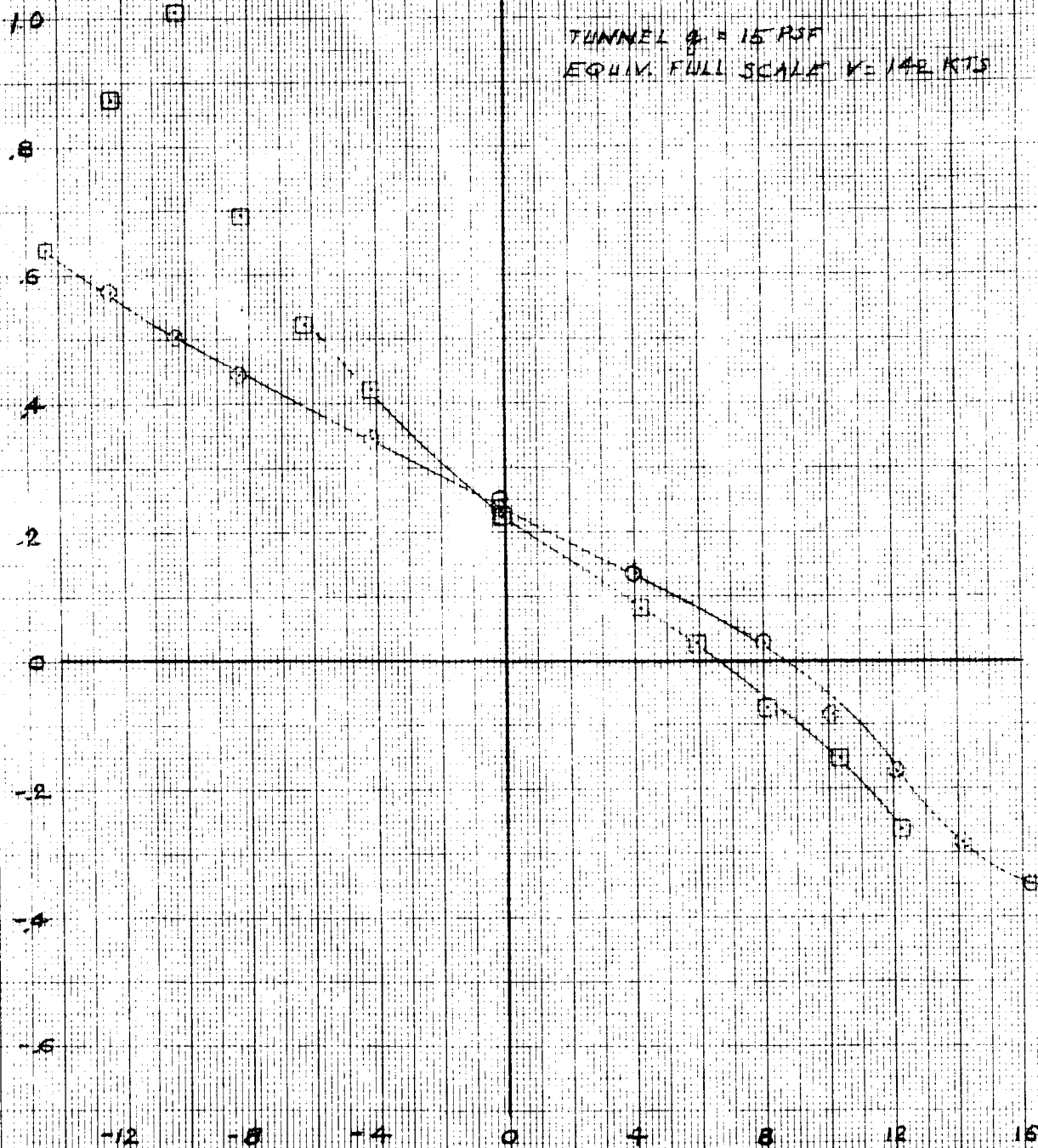
NOTES:

	RUN	δ_{JPL}	δ_{RR}
①	64	0	0
②	57	50.3	26.4

TUNNEL $q = 15$ PSF

EQUIV. FULL SCALE $V = 142$ KTS

PITCHING MOMENT COEFFICIENT - $C_{m\alpha}$



FUSELAGE ANGLE OF ATTACK - α DEGREES

Figure 230

EFFECT OF ROLL CONTROL ON LONGITUDINAL STABILITY

NOTES:

RUN	δ_{FL}	δ_{FR}
64	0	0
67	503	264

TUNNEL $Q = 15 \text{ PSF}$
EQUIV FULL SCALE $V = 142 \text{ KNOTS}$

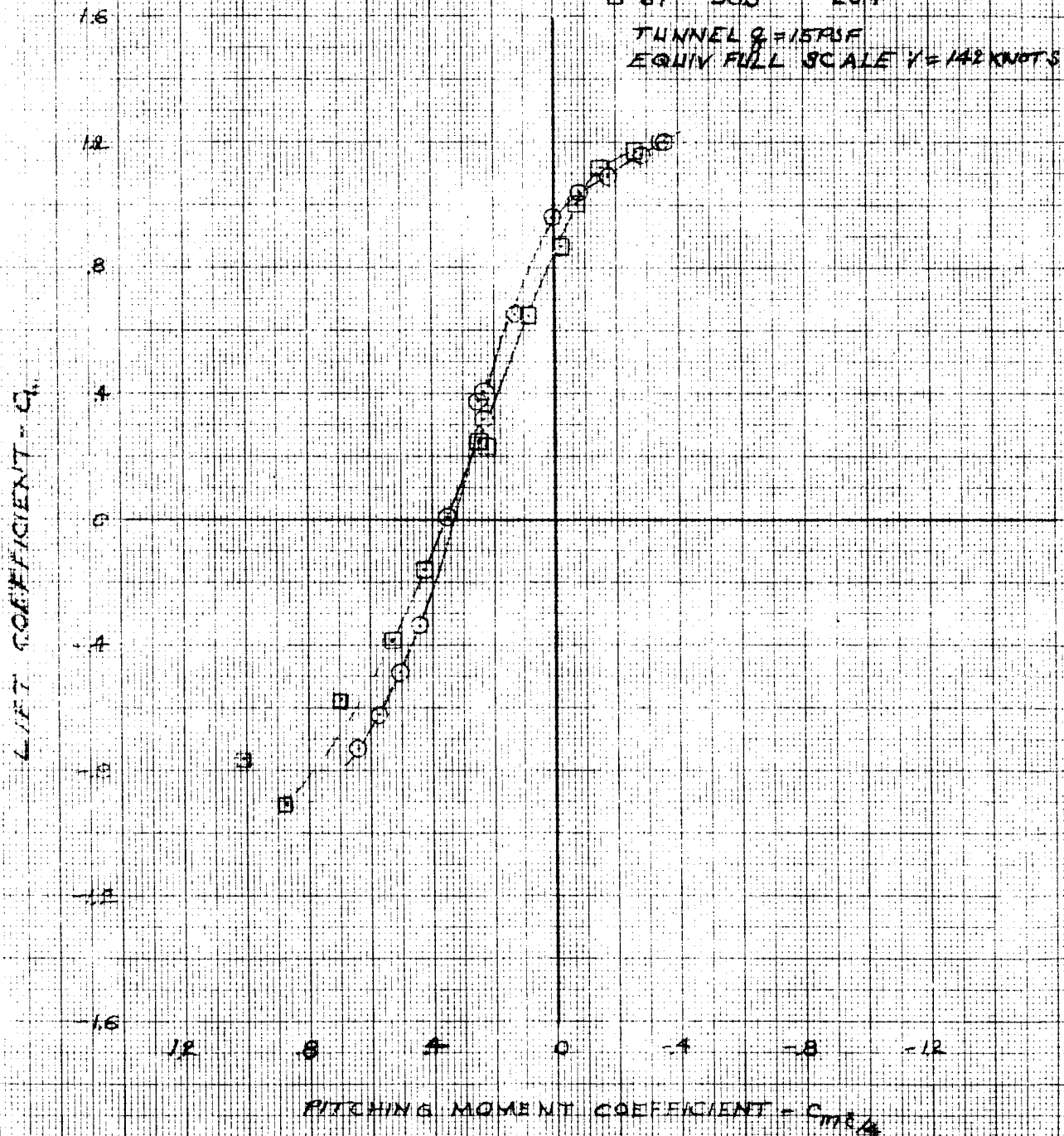


Figure 231

RUDDER EFFECTIVENESS
VARIATION OF YAWING MOMENT COEFFICIENT
WITH RUDDER DEFLECTION

ROTORS OFF

OBVWT 105 DATA - RUN 49

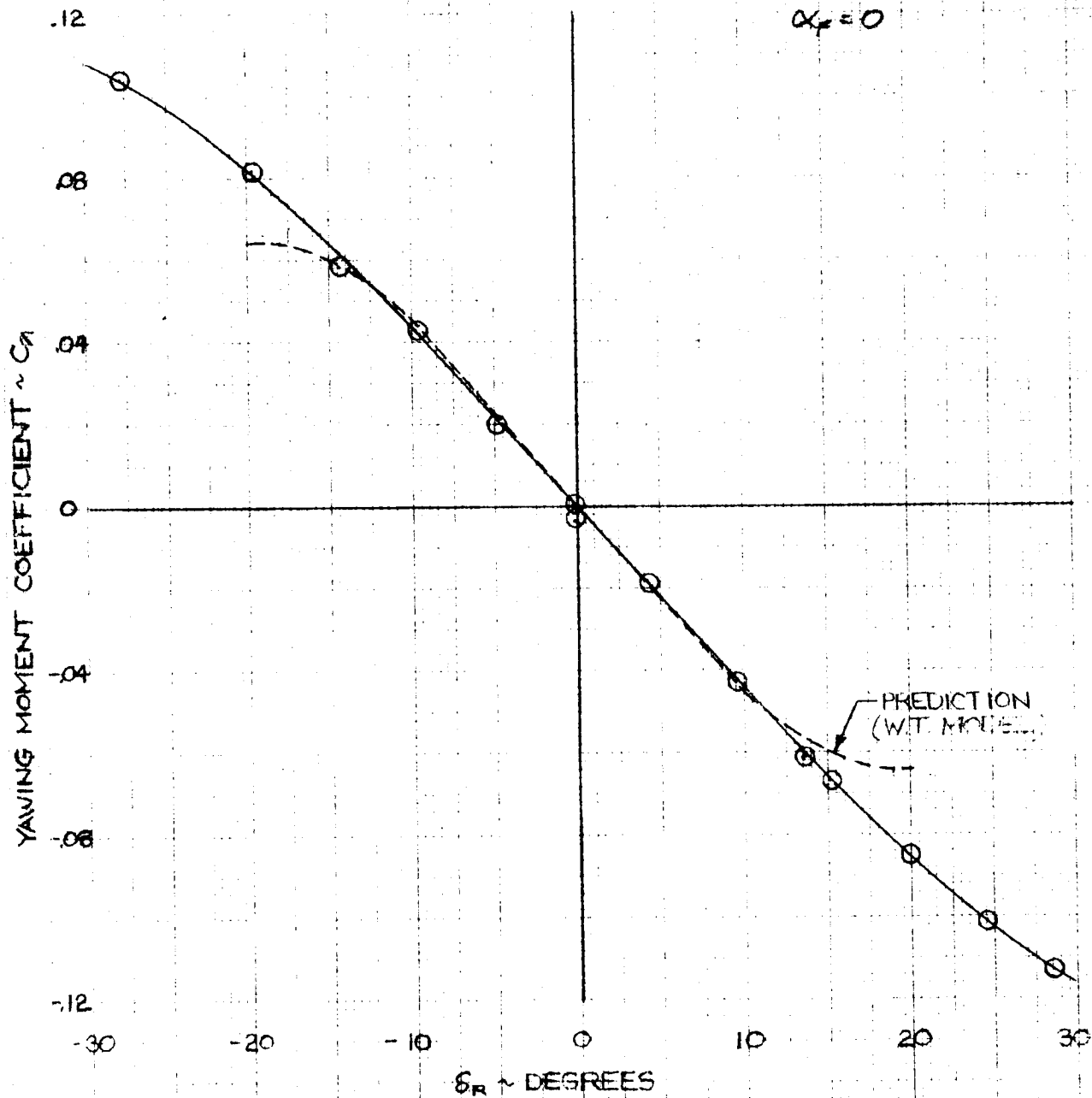
 $\dot{\alpha}_N = 0$ $\delta_F = 0$ TUNNEL $q = 15$ PSFEQUIV FULL SCALE $V = 192$ KTS $\alpha_F = 0$ 

Figure 232

MODEL 222
RUDDER EFFECTIVENESS IN YAW
EFFECT OF SIDESLIP ANGLE ON YAWING MOMENT
COEFFICIENT DUE TO RUDDER DEFLECTION

○ RUN 45 - $\delta_R = 0^\circ$

ROTORS OFF

□ 51 $\delta_R = 20^\circ$

TUNNEL $Q = 15$ PSF
 EQUIV. FULL SCALE $V = 142$ KNOTS

$\alpha_{FRL} = 0$

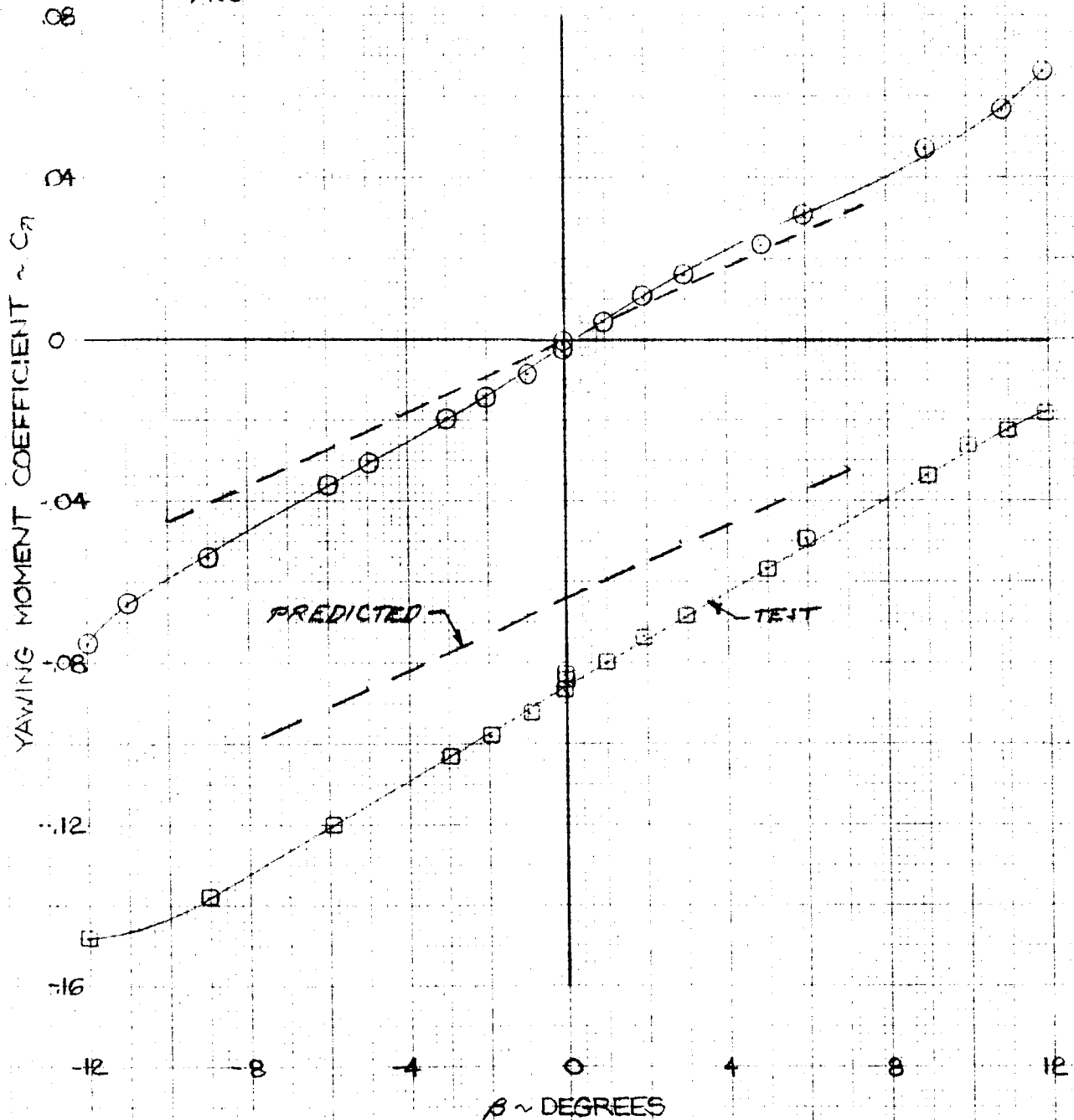


figure 233

EFFECT OF RUDDER ON ROLLING MOMENT
COEFFICIENT VS SIDESLIP ANGLE

ROTORS OFF

NOTES:

RUN	$\delta\alpha$
○ 45	0
□ 51	20°

TUNNEL 7 F 15R5F
EQUIV FULL SCALE $V = 142$ KTS

$\alpha_F = 0$

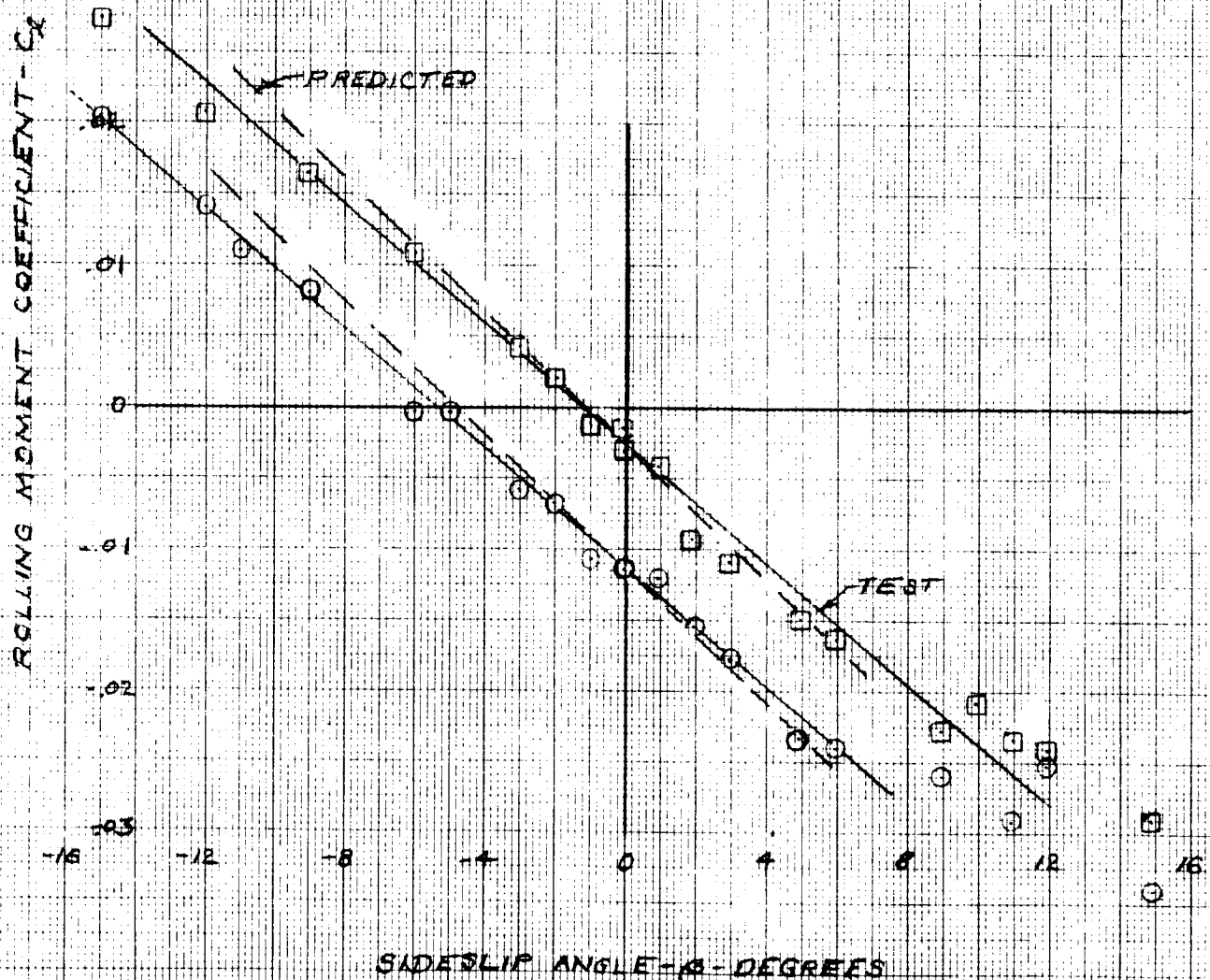


Figure 234

VARIATION OF ROLLING MOMENT COEFFICIENT
WITH RUDDER DEFLECTION
ROTORS OFF

RUN 49
TUNNEL 2 F 15 PSE
AQUA FULL SCALE $V = 192 \text{ KTS}$
 $\alpha = 0$
 $\beta = 0$

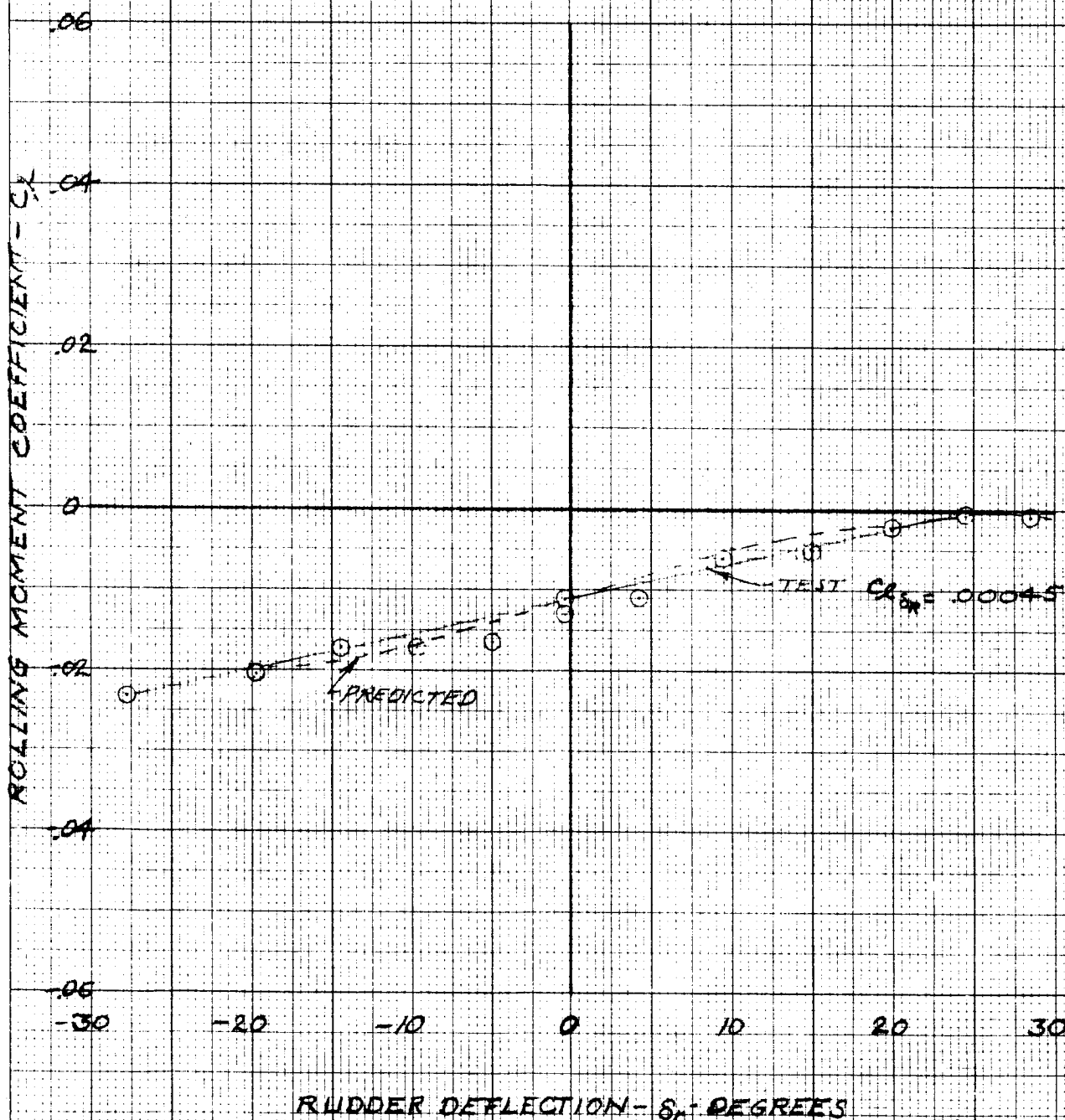


Figure 235

EFFECT OF FLAP DEFLECTION ON VARIATION OF LIFT COEFFICIENT WITH ANGLE OF ATTACK

ROTORS OFF

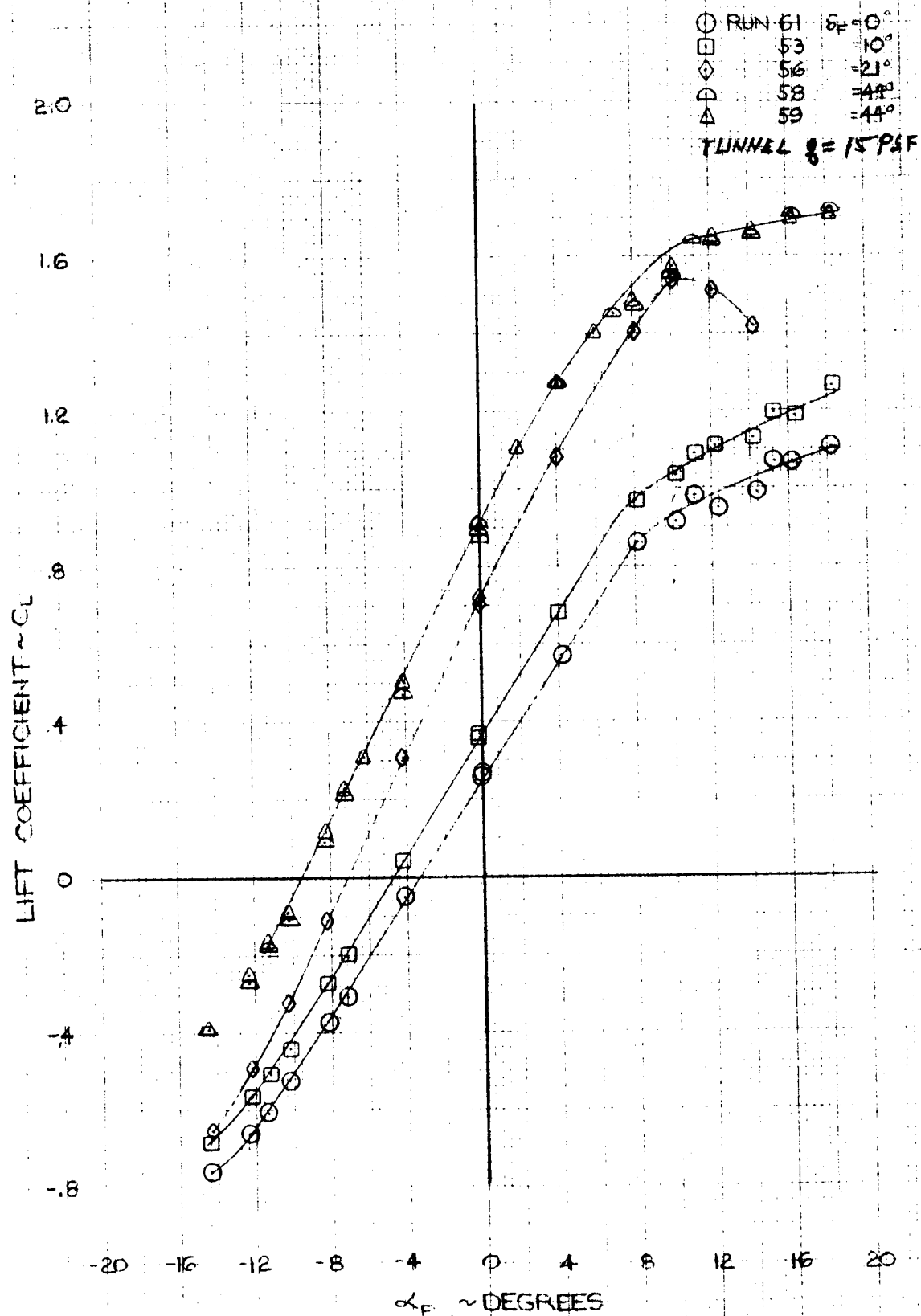


Figure 236

EFFECT OF FLAP DEFLECTION ON VARIATION OF
PITCHING MOMENT WITH ANGLE OF ATTACK
 ROTORS OFF

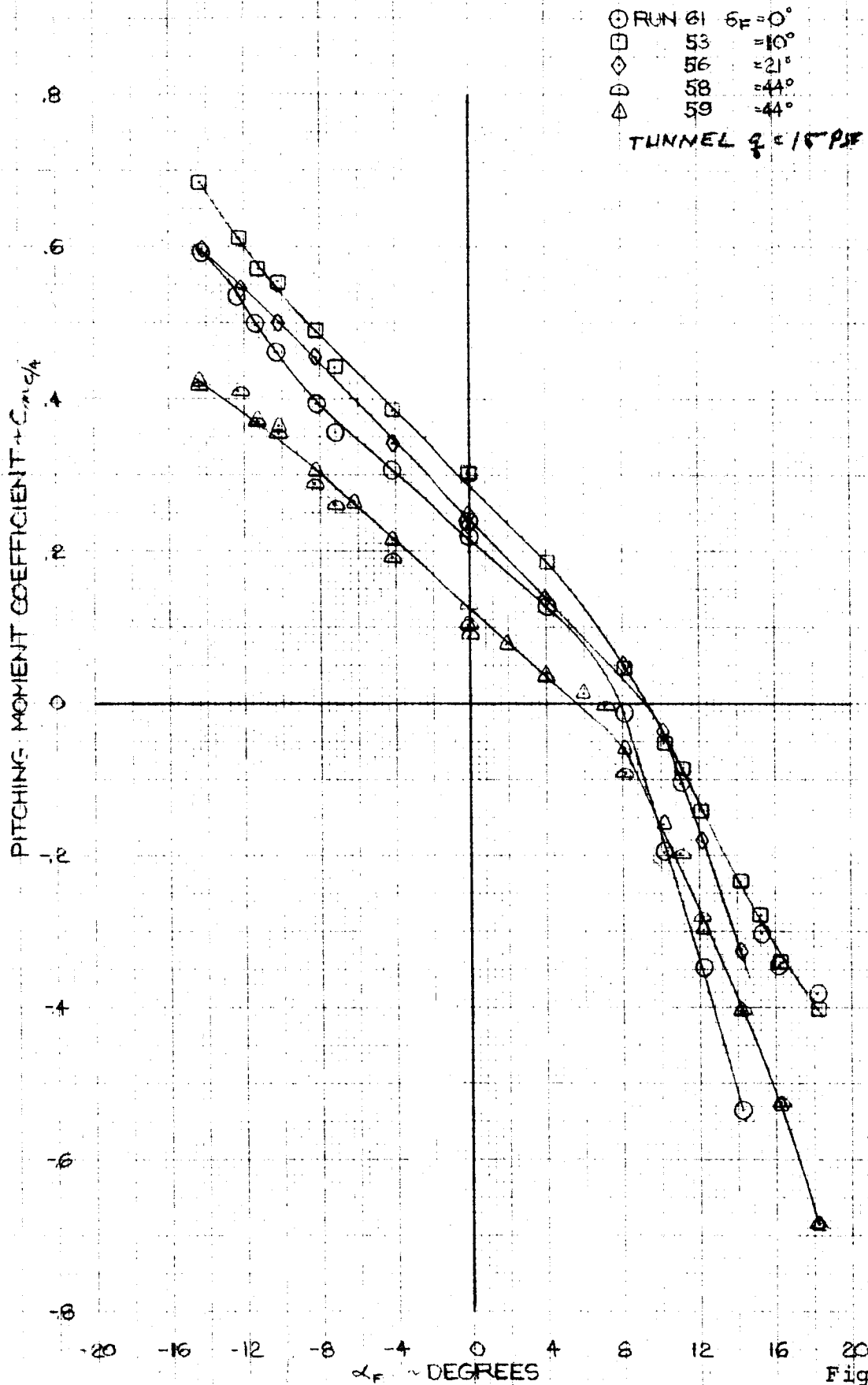


Figure 237

EFFECT OF FLAP DEFLECTION ON STATIC LONGITUDINAL STABILITY ROTORS OFF

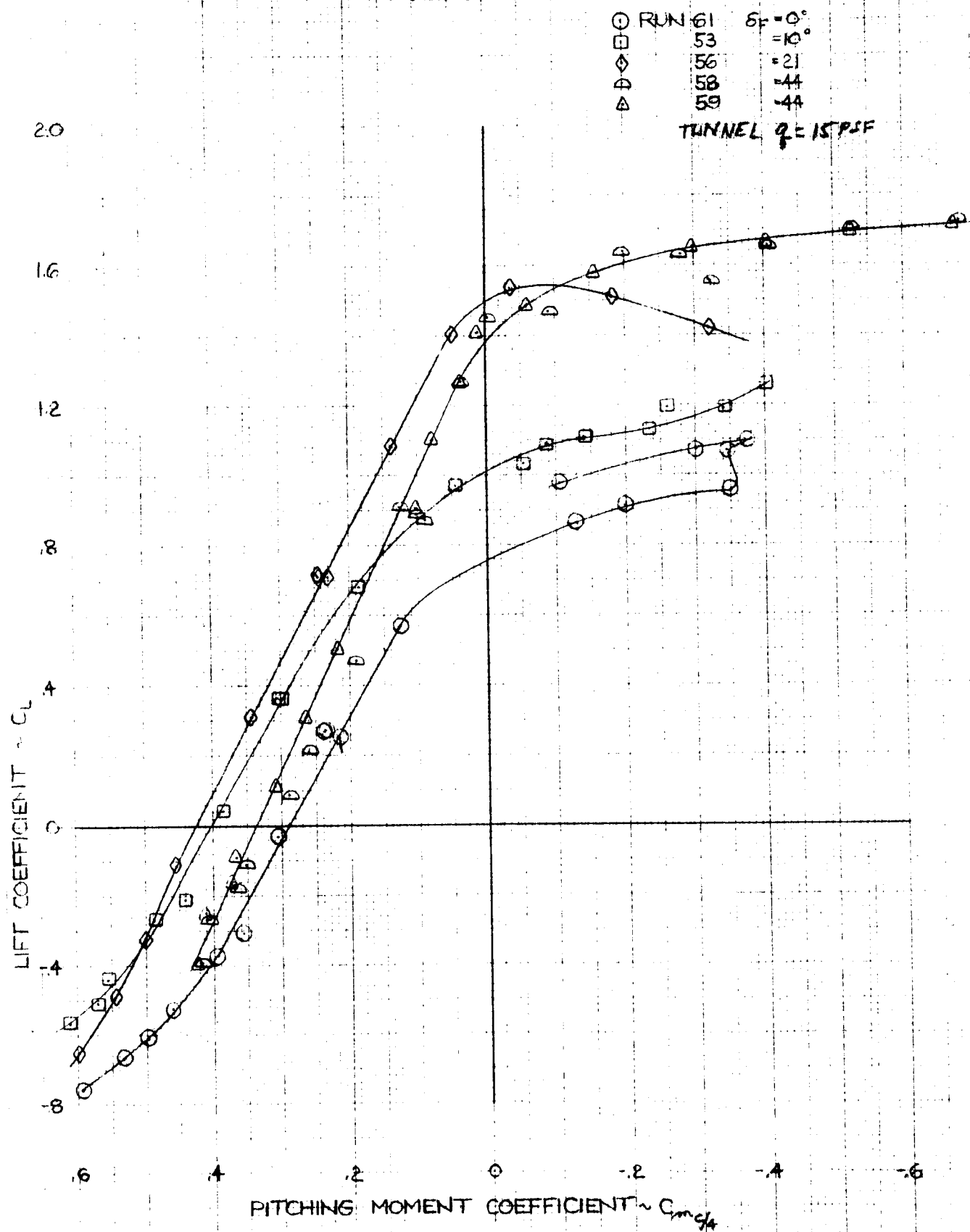


Figure 238

EFFECT OF FLAP DEFLECTION ON LIFT COEFFICIENT
VARIATION WITH ANGLE OF ATTACK
ROTORS ON

NOTES:

RUN	δF	α	C_L
33	40°	1.8°	.0016
35	20°	1.5°	.0019
37	10°	1.6°	.0019
38	0°	8.0°	.0021

TUNNEL $\beta = 15^\circ$ $V = 113$ FPS
EQUIV FULL SCALE $V = 142$ KTS.
RPM = 830
 $\mu = .464$

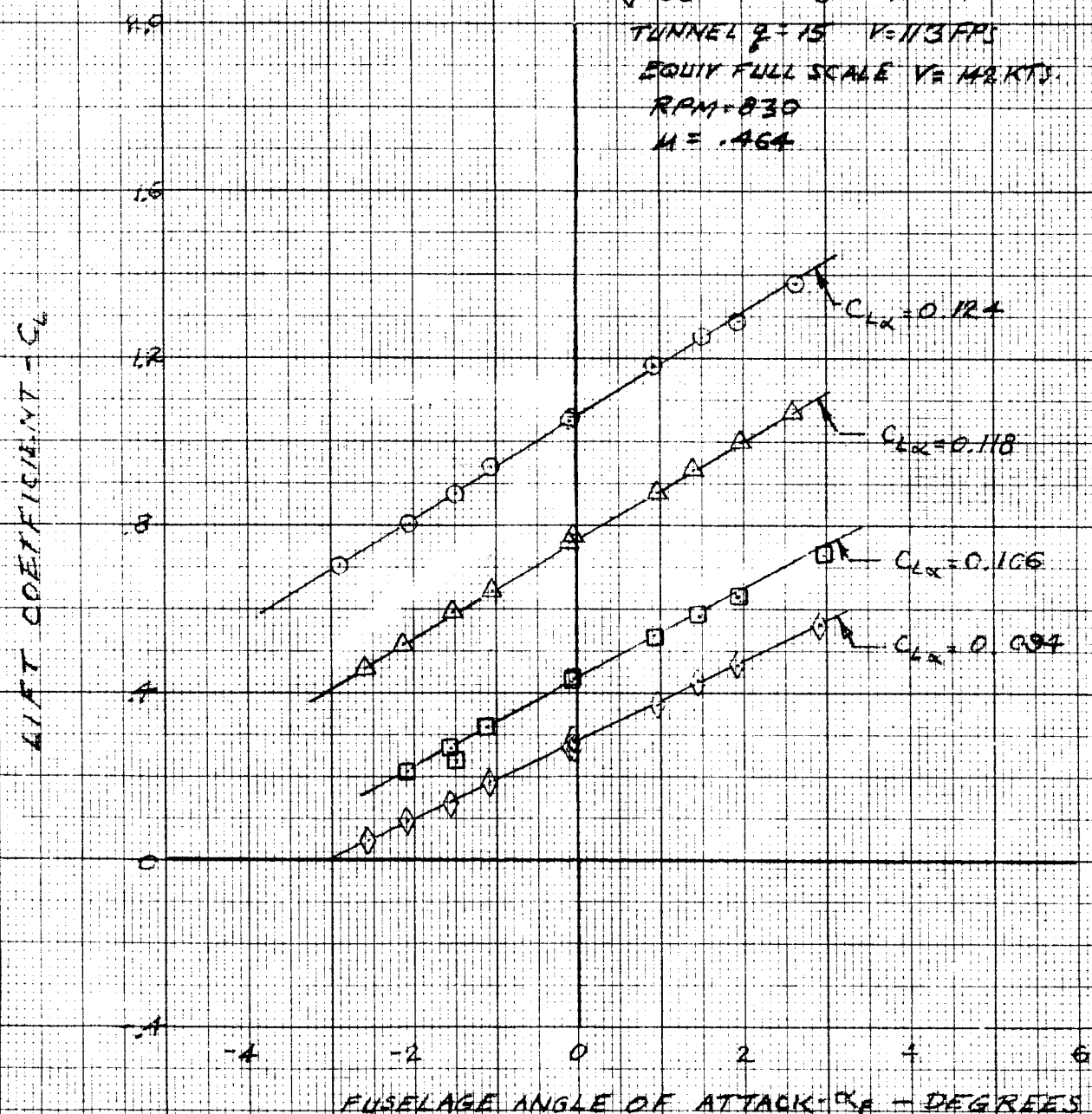


Figure 239

EFFECT OF FLAP DECTION ON PITCHING
MOMENT COEFFICIENT VARIATION WITH
ANGLE OF ATTACK
ROTORS ON

NOTES:

	RUN	BE	IN	CT	$C_{m\alpha}$
○	33	40°	18"	.0016	-.0074
△	35	20°	15"	.0019	-.0035
□	37	10°	16"	.0019	-.0048
◇	38	0°	8.0"	.0021	-.0094

TUNNEL $q = 15 \text{ PSF}$ $V = 113 \text{ FPS}$
EQUIV FULL SCALE $V = 142 \text{ KTS.}$
RPM = 830
 $M = 4.64$

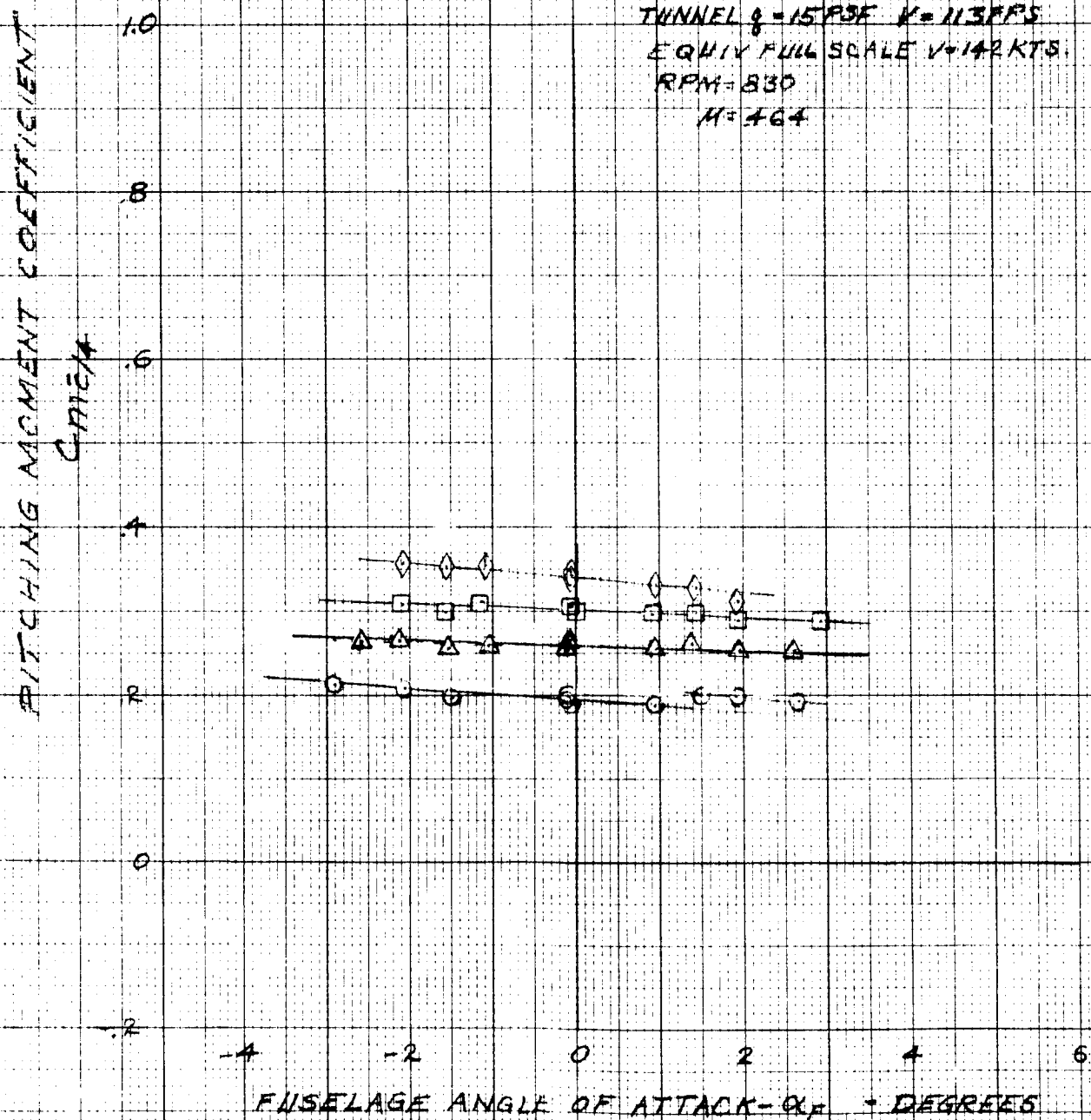


Figure 240

EFFECT OF FLAP DEFLECTION ON LONGITUDINAL STABILITY ROTORS ON

NOTES:

$\frac{L}{b}$	δ_F	$\frac{L}{b}$	C_T
0.33	40°	1.8	.0016
0.35	20°	1.5	.0019
0.37	10°	1.6	.0019
0.38	0	8.0	.0021

TUNNEL $q = 15 \text{ PSF}$ $V = 113 \text{ FPS}$
EQUIV. FULL SCALE $V = 142 \text{ KTS.}$
RPM = 330
 $H = .464$

AIRCRAFT LIFT COEFFICIENT

C_L

2.0

1.6

1.2

.8

.4

0

-.4

$$\frac{dC_m}{dC_L} = -0.06$$

$$\frac{dC_m}{dC_L} = -0.030$$

$$\frac{dC_m}{dC_L} = -0.045$$

$$\frac{dC_m}{dC_L} = -0.10$$

4

2

0

-.2

-.4

-.6

AIRCRAFT PITCHING MOMENT COEFFICIENT

$C_{m/a}$

Figure 241

EFFECT OF FLAP DEFLECTION ON YAWING AND ROLLING MOMENT COEFFICIENT VARIATION WITH SIDESLIP ROTORS ON

YAWING MOMENT COEFFICIENT

$C_{Y\beta}$

ROLLING MOMENT COEFFICIENT

$C_{l\beta}$

NOTES:

RUN	δ
○ 32	0°
△ 34	40°
□ 36	20°

TUNNEL 2-15 P.S.F. $V = 113$ FPS
EQUIV. FULL SCALE $V = 142$ KTS
 $C_N = 0$
RPM: 830
 $H = 464$

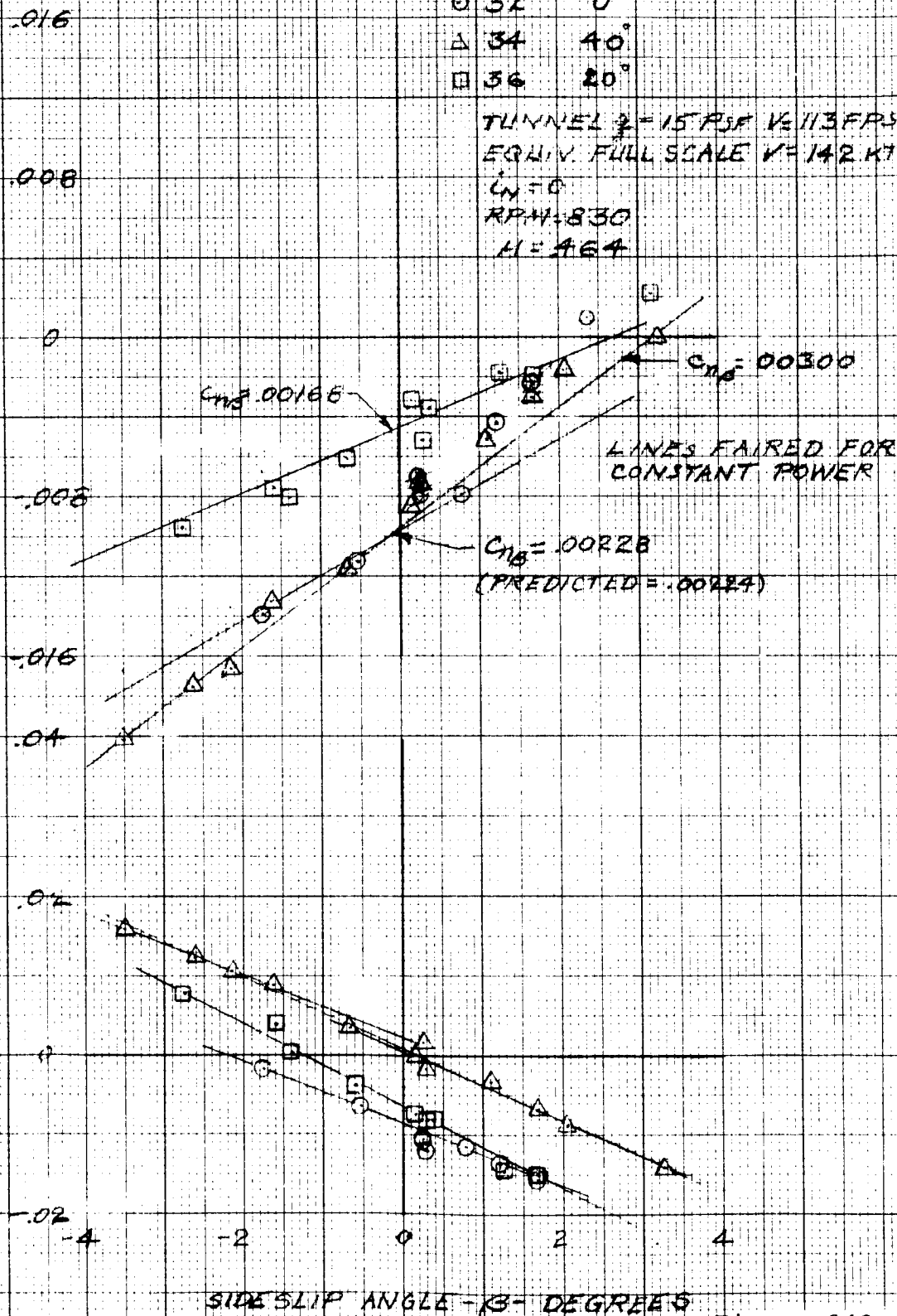


Figure 242

FLAP EFFECTIVENESS

TAILS ON - ROTORS OFF

$$\alpha_{FRL} = 0$$

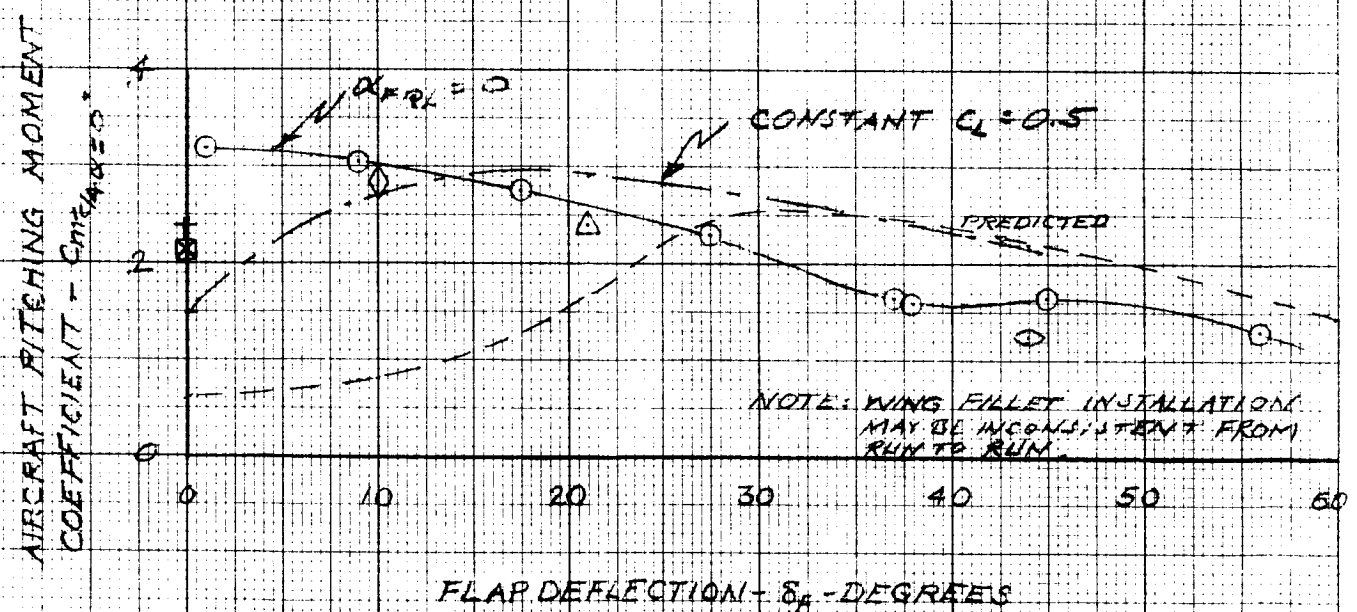
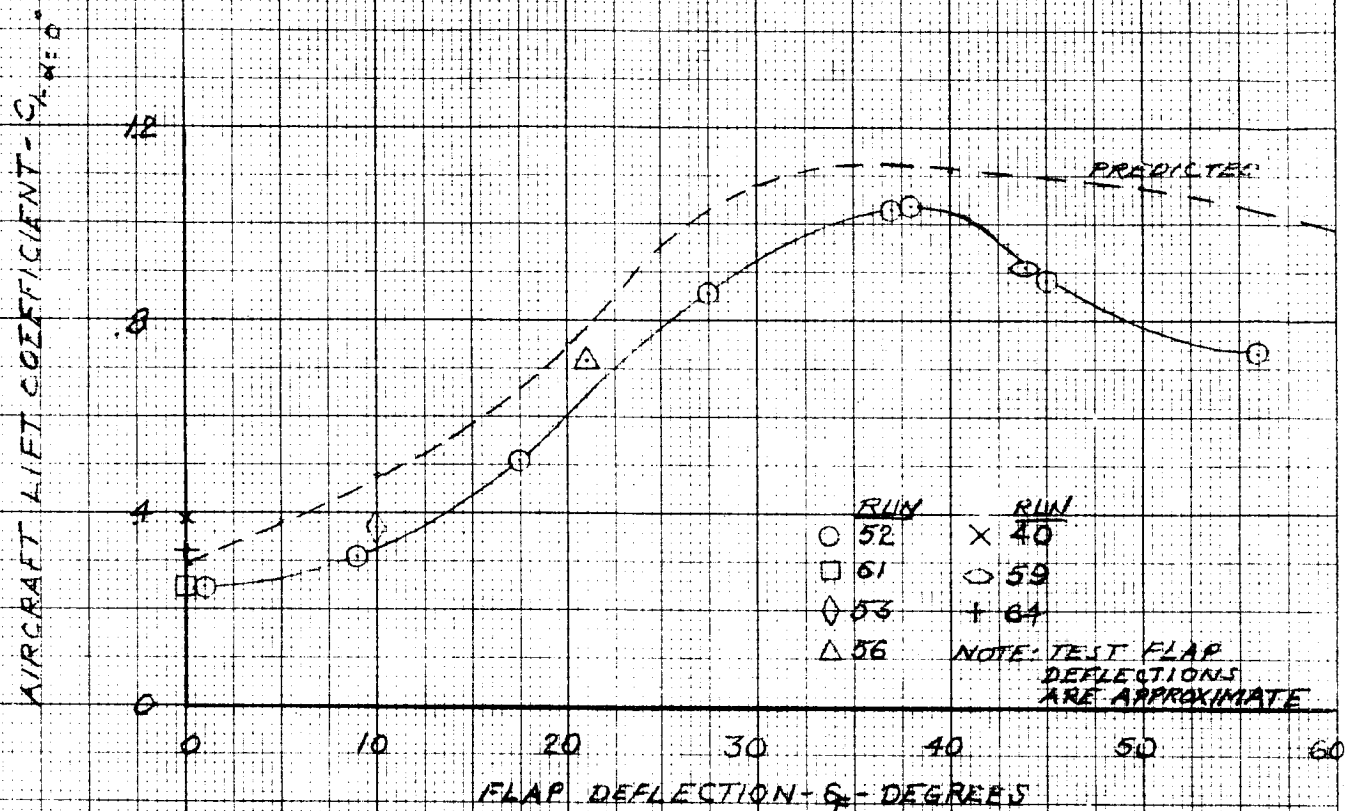


Figure 243

FLAP EFFECTIVENESS

TAILS ON - ROTORS ON
 $\alpha_{FRL} = 0$

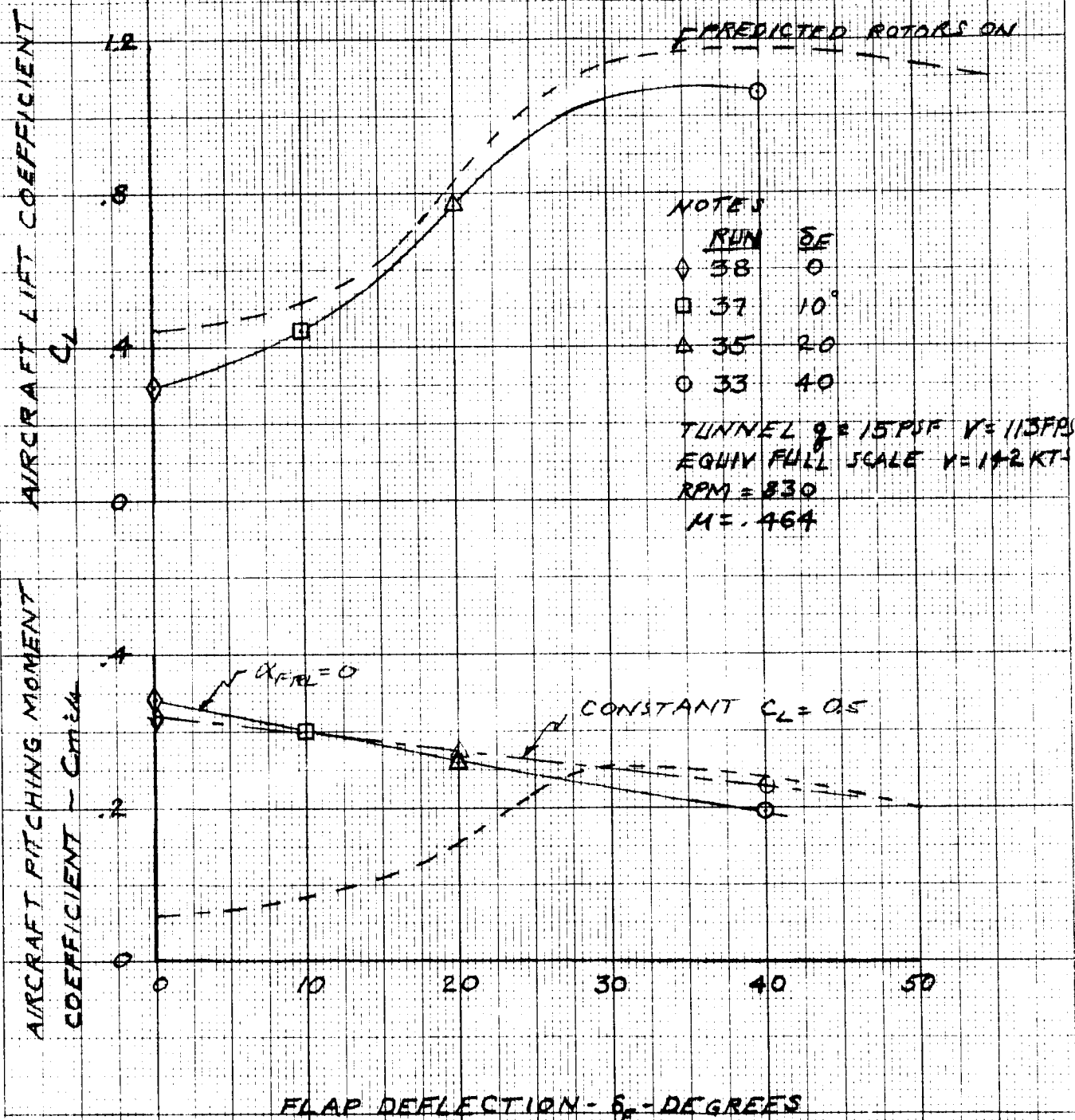


Figure 244

THIS PAGE INTENTIONALLY LEFT BLANK

5.2.4 Comparison of Test and Theory in Cruise

Rotor Characteristics

The comparison of theory with test data in cruise will provide a validation theory as well as verify the adequacy of the airframe stability. Test data presented in Section 5.2.1 summarizes the cruise rotor stability derivatives and are presented in Figure 245 with the hub tares removed. The cruise hub tares are presented in Appendix D.

The theory presented here is a dynamic stability rotor analysis that also provides the static stability derivatives. It defines dynamic and static derivatives for a rotor system taking account of the modal behavior of the blades in two general flap-lag modes. These derivatives are given as matrix arrays of the partial derivatives of rotor forces with respect to unit amounts of elementary linear and angular motions of the hub and unit displacements in the blade modes. These effects are separated into inertial, damping and gyroscopic and stiffness effects. A more detailed explanation of program methodology and instructions for the use of the program are discussed in Reference 5.

An additional comparison is provided in rotor normal force with the prediction technique utilized for transition. Both of these predictions are for an isolated rotor and do not include the circulation effects induced by the wing.

Rotor characteristics obtained from the model in a yaw sweep in the cruise mode define the rotor responses with a fixed amount of circulation and the resulting derivatives are representative of an

C-5

isolated rotor. For an isolated rotor, a yaw derivative can be related to a pitch derivative, by rotating the forces and moments 90 degrees and modifying the signs to be consistent with the sign convention, as follows:

$$\frac{\partial C_{NF}}{\partial \alpha} = \frac{\partial C_{SF}}{\partial \psi}$$

$$\frac{\partial C_{PM}}{\partial \alpha} = \frac{\partial C_{YM}}{\partial \psi}$$

$$\frac{\partial C_{SF}}{\partial \alpha} = -\frac{\partial C_{NF}}{\partial \psi}$$

$$\frac{\partial C_{YM}}{\partial \alpha} = \frac{\partial C_{PM}}{\partial \psi}$$

Comparing the derivatives obtained from the yaw sweeps in Figure 245 show close agreement with the predictions obtained from C-41 across the cruise speed range tested. The normal force comparison with D-88 shows exact agreement between test and theory. The derivatives obtained from the pitch sweeps shows a distinct change in level as well as a change in trend with forward speed. This is a result of wing circulation and appears as an angle of attack effect which is more destabilizing to the aircraft in cruise. From the data presented in this figure this circulation effect appears to be a speed squared (μ^2) effect on all the force derivatives and μ^4 on all moment derivatives.

Cyclic variations were done in cruise to supplement the load alleviation or low rate feedback system. These derivatives are compared to theory in Figures 246 and 247 for lateral cyclic.

The inplane force derivatives agree well with D-88 and only fair with C-41. Predicted moment derivatives obtained from D-88 and C-41 bracket the test data and provide a fair correlation. Longitudinal cyclic derivatives in cruise are presented in Figures 248 and 249. These derivatives show approximately the same trend as the test data with D-88 predicting inplane force derivatives well and C-41 and D-88 bracketing the moment derivative test data.

The capability of the theory to predict the static rotor stability is good but an accountability for wing circulation must be made. The prediction for the cyclic derivatives is fair but the deviation results in the aircraft having more cyclic effectiveness on the major contributions to aircraft longitudinal stability than was predicted; therefore, the aircraft would achieve a greater stabilizing contribution from the low rate feedback than was predicted.

Longitudinal Stability

Lift coefficient variation with angle of attack is compared with prediction in Figure 190. This figure indicates closer agreement between predicted and test values of C_{L_α} in cruise and in transition. Tails and rotors off C_{L_α} from test is .075 compared to .080 predicted. Tails on and rotors off data from run 64 indicated C_{L_α} to be .080 and from run 40 $C_{L_\alpha} = .086$ compared to a predicted value of .090. The airframe neutral point from test data for tails and rotors off, as indicated by the values of $\frac{dC_m}{dC_L}$ on Figure 193 is at 6.5% \bar{c} compared to a predicted location of 8.5% \bar{c} . Tails on and rotors off neutral point is indicated to be at 54.5% \bar{c} compared to 48.3% \bar{c} estimated at the test Reynolds number. Horizontal tail lift effectiveness, $C_{L_{\delta_e}}$, is indicated to be .011 compared to .0101 predicted and pitching moment effectiveness, $C_{m_{\delta_e}}$, is indicated to be -.0390 compared to -.0340 predicted. This indicates an effective tail length of 3.54 \bar{c} compared to 3.36 \bar{c} calculated distance from wing quarter chord to quarter chord of the horizontal tail MAC. Rotors on aircraft C_{L_α} , C_{m_α} , and $\frac{dC_m}{dC_L}$ test data are compared with predictions on Figures 194 and 195 for values of tunnel q corresponding to equivalent full scale velocities of 142, 175, 200 and 255 knots. Note that the values of C_{L_α} are all slightly higher than predicted, C_{m_α} is higher than predicted with relatively good agreement as the maximum test q, and $\frac{dC_m}{dC_L}$ indicates a neutral point aft of predicted at the three lowest values of q and forward of predicted at maximum q (2% \bar{c} forward). Figures 196 and 197 indicate airframe C_{L_α} to agree quite well with prediction at the lowest q and higher than predicted at the higher q's, C_{m_α} to be much higher than predicted, and neutral point approximately 13 to 16% \bar{c} aft of the

predicted location. This indicates the airframe to be more stable than predicted, but with the rotor more destabilizing than predicted. Figure 199 indicates that adding the horizontal tail to the aircraft with rotors on results in an aft shift of neutral point of $37.8\% \bar{c}$. This compares with a predicted aft shift of $32.0\% \bar{c}$ for the rotors on condition. Summaries of test values of C_{L_α} , C_{m_α} and neutral point location are presented versus velocity in Figures 200 and 201 and comparisons with predictions are presented. The test data indicate satisfactory stability for all test conditions for the complete aircraft rotors on.

Lateral-Directional Stability

Directonal stability is indicated by Figure 203 to be better than predicted for the rotors off configuration with $C_{n_\beta} = .0057$ compared to a predicted value of $.00446$. Directional stability with tails off is indicated to agree with the predicted value when the effect of the ventral fins is included. Thus, the tail contribution to directional stability is indicated to be higher than predicted. The dihedral effect is indicated on Figure 204 to be slightly lower than predicted with $C_{l_\beta} = -.00213$ from test compared to $-.00230$ predicted. Figure 205 indicates that addition of the rotors has a smaller destabilizing effect on directional stability than predicted, and that dihedral effect C_{l_β} is lower than predicted. Sideforce coefficient variation with sideslip is indicated to agree well with the predicted values on Figure 206 at the three values of dynamic pressure at which tests were conducted. Figure 207 again illustrates that addition of the vertical tail increases directional stability more than predicted and has an effect on C_{l_β} opposite to that predicted. The

The effect on C_{ℓ_β} cannot be readily explained. The effect of the vertical tail on sideforce coefficient variation with sideslip angle, C_{Y_β} , is indicated on Figure 208 for the aircraft and airframe. The effect on aircraft coefficient agrees well with the predicted value and the change in airframe coefficient indicates a ΔC_{Y_β} of $-.0129$ compared to a predicted value of $-.0102$, or a 26% higher "tail lift curve slope" than predicted. Test and predicted values of C_{n_β} , C_{ℓ_β} , and C_{Y_β} are summarized versus equivalent full scale aircraft velocity in Figures 209, 210 and 211. Directional stability is indicated to be higher than predicted and dihedral effect lower than predicted for the complete aircraft, rotors on.

Control Effectiveness

The effects of lateral cyclic control on aircraft lift, pitching moment, sideforce and yawing moment coefficients are illustrated in Figures 212 and 213 for two values of tunnel dynamic pressure and compared with predictions calculated using predicted rotor coefficients from the C-41 and D-88 digital programs. The change in lift coefficient with lateral cyclic is of opposite sign compared to the predicted values and small in magnitude. Pitching moment coefficient change falls between the C-41 and D-88 estimates, incremental sideforce coefficient agrees closely with C-41 prediction and yawing moment coefficient is in good agreement with both C-41 and D-88 predictions at a tunnel q of 29.3 psf and agrees better with C-41 than D-88 at the 15 psf dynamic pressure condition.

The variations of aircraft C_L , C_m , C_Y , and C_n with longitudinal cyclic, B_1 , are illustrated on Figures 214, 215 and 216 for 15 and

and 29.4 psf tunnel q 's and compared with predicted values computed using rotor coefficient data from the C-41 and D-88 programs. The change in lift coefficient is larger than predicted by either of the digital programs with the largest discrepancy at the higher q . The change in C_m agrees well with the prediction based on D-88 at the higher q , $C_{m_{B_1}} = -.0302$ compared to $-.0301$ predicted, and lower than prediction at $q=15$ psf but in better agreement with C-41 than with D-88 yielding a test value of $C_{m_{B_1}} = -.015$ compared to $-.0195$ predicted from C-41 coefficients. The sideforce data at $q=29.4$ psf agree closer with but less than the C-41 predictions, $C_{y_{B_1}} = .0041$ from test compared to $.0051$ predicted. The change in yawing moment coefficient for $q=29.4$ psf agrees closer with but higher than the C-41 based predictions, $C_{n_{B_1}} = -.00537$ test compared to $-.0047$ predicted for the right rotor. The change in yawing moment coefficient, $C_{n_{B_1}}$, at $q=15$ psf is $-.0053$ compared to $-.0081$ predicted using C-41 coefficients and $-.0022$ predicted using D-88 coefficients.

Elevator effectiveness is indicated to be lower than predicted in cruise, as it was in transition, as illustrated in Figure 218 for the rotors on condition. Pitching moment coefficient due to elevator deflection is indicated to be $-.0242$ compared to a predicted value of $-.0310$. Lift effectiveness, $C_{L_{\delta_e}}$, is indicated to be $.0061$ compared to a predicted value of $.0092$. Test data obtained with rotors off indicates similar results as indicated in Figure 219. Lift effectiveness, $C_{L_{\delta_e}}$, is $.0070$ compared to $.0092$ predicted and $C_{m_{\delta_e}}$ is $-.0253$ compared to $-.0310$ predicted. Figures 220, 221 and 222 indicate that elevator effectiveness is maintained near constant as a function of angle of attack up to angles commensurate with

maximum lift coefficient.

Rolling moment coefficients due to aileron and spoiler deflections, following the schedules of Figure 224, are indicated on Figure 225 to be slightly lower for small deflection and higher for maximum control deflection than predicted. The same is also true of yawing moment coefficient. Figure 226 indicates that for left spoiler deflection alone the maximum rolling moment coefficient, at 45 degrees deflection, is $-.034$ compared to $-.017$ predicted. The yawing moment coefficient is lower than predicted being $-.0078$ compared to $-.0092$ predicted. Aileron effectiveness for right aileron deflection is indicated to be lower than predicted for deflections greater than 7 degrees, but a large discontinuity in the rolling moment coefficient data is indicated at the larger deflections casting doubt on the validity of these data. Aileron yawing moment coefficients are negligible, lower than predicted. Figure 227 indicates similar results for spoiler and aileron effectiveness for tests performed with the inboard flap set at 20 degrees deflection. These data indicate no discontinuity in the aileron rolling moment coefficient data but lower than predicted effectiveness.

The effects of rudder deflection on rolling and yawing moment coefficients are illustrated on Figures 232 through 235. Figure 232 indicates good agreement of $C_{n_{\delta_r}}$ test with prediction for deflections up to 13 degrees and higher than predicted effectiveness at larger deflections, better linearity. Effectiveness at 20 degrees deflection is $C_n = -.086$ compared to $-.064$ predicted. The rolling moment coefficient data indicate smaller than predicted C_{ℓ} for small deflections and the predicted value of ΔC_{ℓ} , $.0090$, at 20

degrees deflection.

Effects of flap deflection on lift and pitching moment coefficients are illustrated for rotors off and rotors on, on Figures 237 through 243, and are summarized and compared with predictions on Figures 243 and 244. The flap effects on lift coefficient with rotors off are observed to be slightly smaller than predicted for deflections less than 40 degrees and with a sharper decrease in effectiveness than predicted at larger deflections. The more rapid decrease at large deflections can be attributed to either the effect non-optimum slot gap or separation of flow on the flap upper surface at large deflections resulting from operation at Reynolds numbers much lower than full scale. The change in lift coefficient with rotors on is indicated to be very close to the predicted values for deflections up to 40 degrees, the largest deflection tested. Pitching moment coefficient change is indicated to be in the nose down direction up to maximum deflections for constant angle of attack, $\alpha_{FRL}=0$ with rotors off and for constant angle of attack on lift coefficient with rotors on. With rotors off, the change in pitching moment coefficient with flap deflection is closer to prediction with a nose up pitching moment coefficient change with deflection to 20 degrees and nose down at larger deflections. The pitching moment coefficient change at constant C_L based on test data, for deflection of 40 degrees would require an up elevator deflection of 3.7 degrees to compensate compared to a predicted change of 5.8 degrees down elevator. Tests of flap effectiveness were not performed with the horizontal tail off. Thus, data are not available from which to determine whether change in downwash or change in

direct flap moment about the wing quarter chord is responsible for the difference between test and predicted pitching moment coefficient change with flap deflection.

COMPARISON OF TEST AND THEORY FOR ANGLE OF ATTACK ROTOR DERIVATIVES IN CRUISE

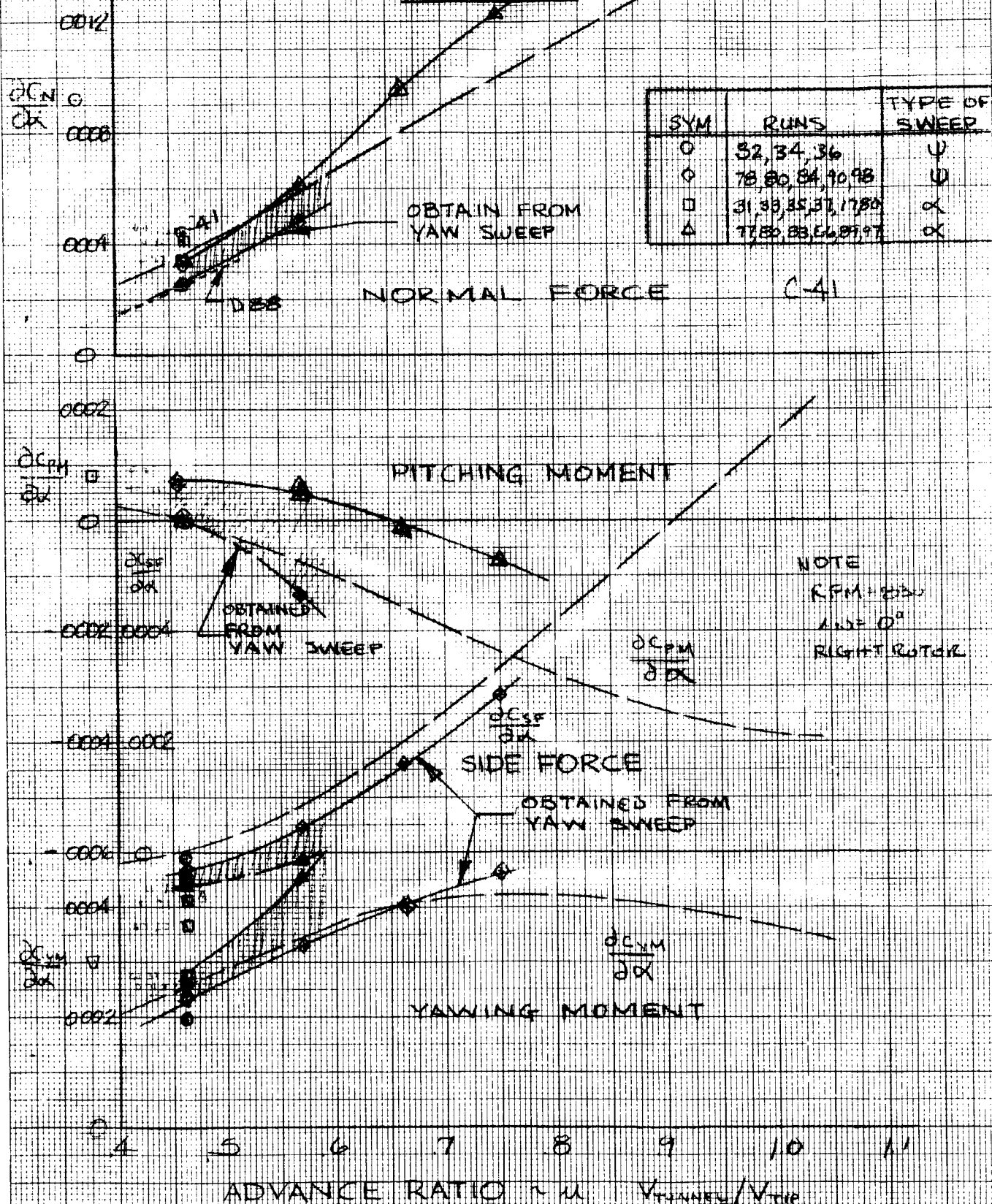


Figure 245

COMPARISON OF TEST AND THEORY FOR LATERAL CYCLIC ROTOR DERIVATIVES IN CRUISE

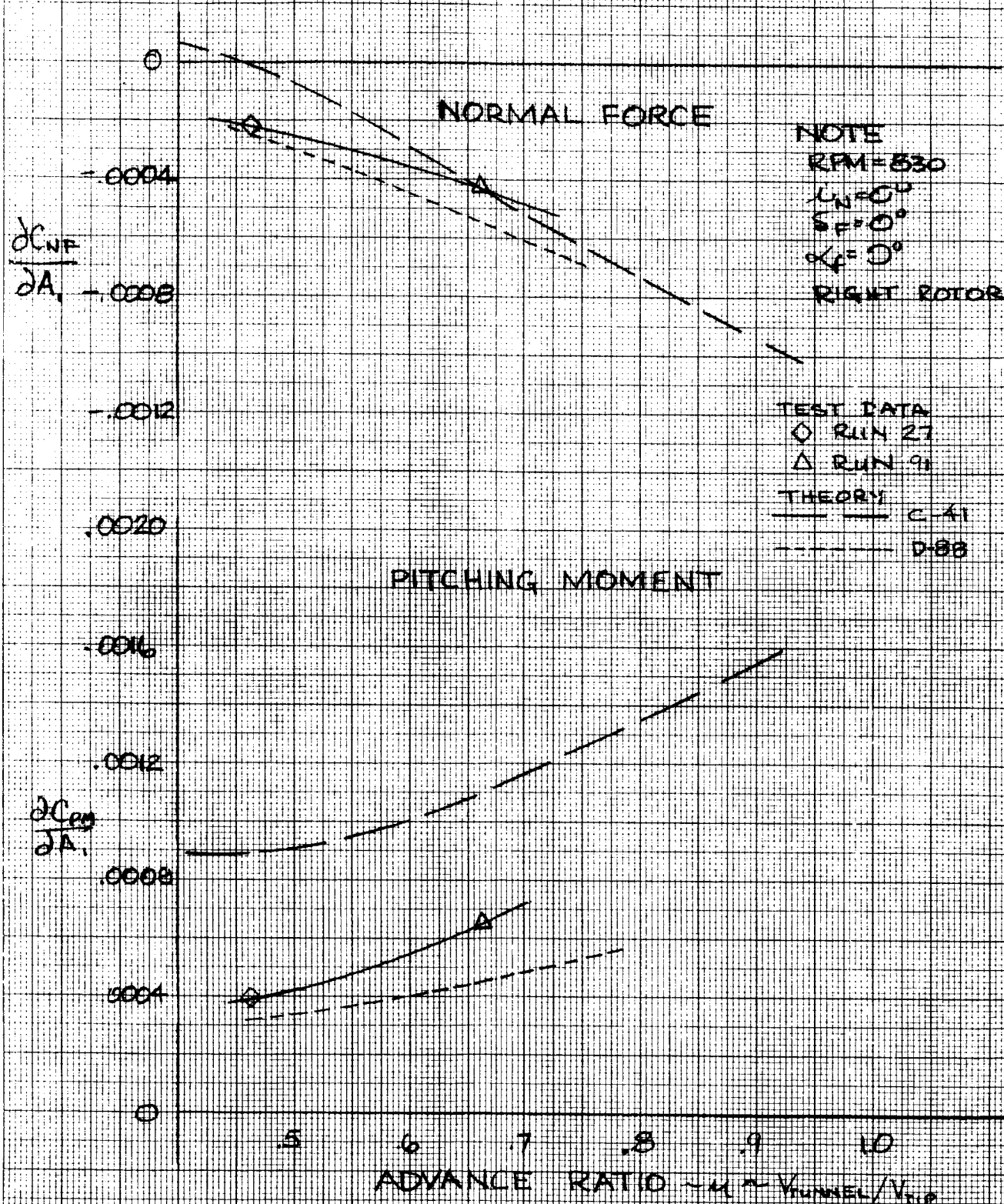


Figure 246

COMPARISON OF TEST AND THEORY
FOR
LATERAL CYCLIC ROTOR DERIVATIVES
IN CRUISE

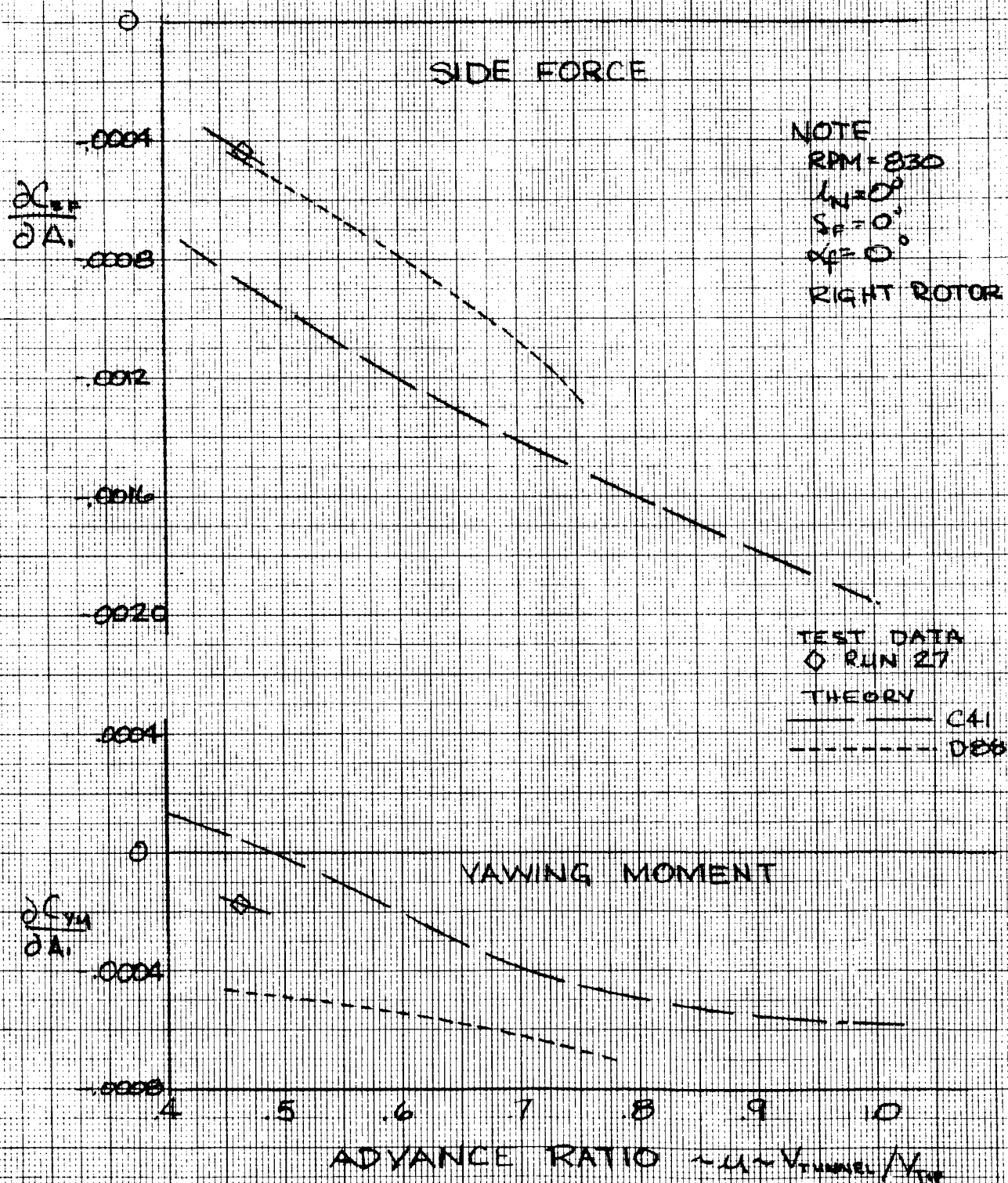


Figure 247

COMPARISON OF TEST AND THEORY FOR LONGITUDINAL CYCLIC ROTOR DERIVATIVES IN CRUISE

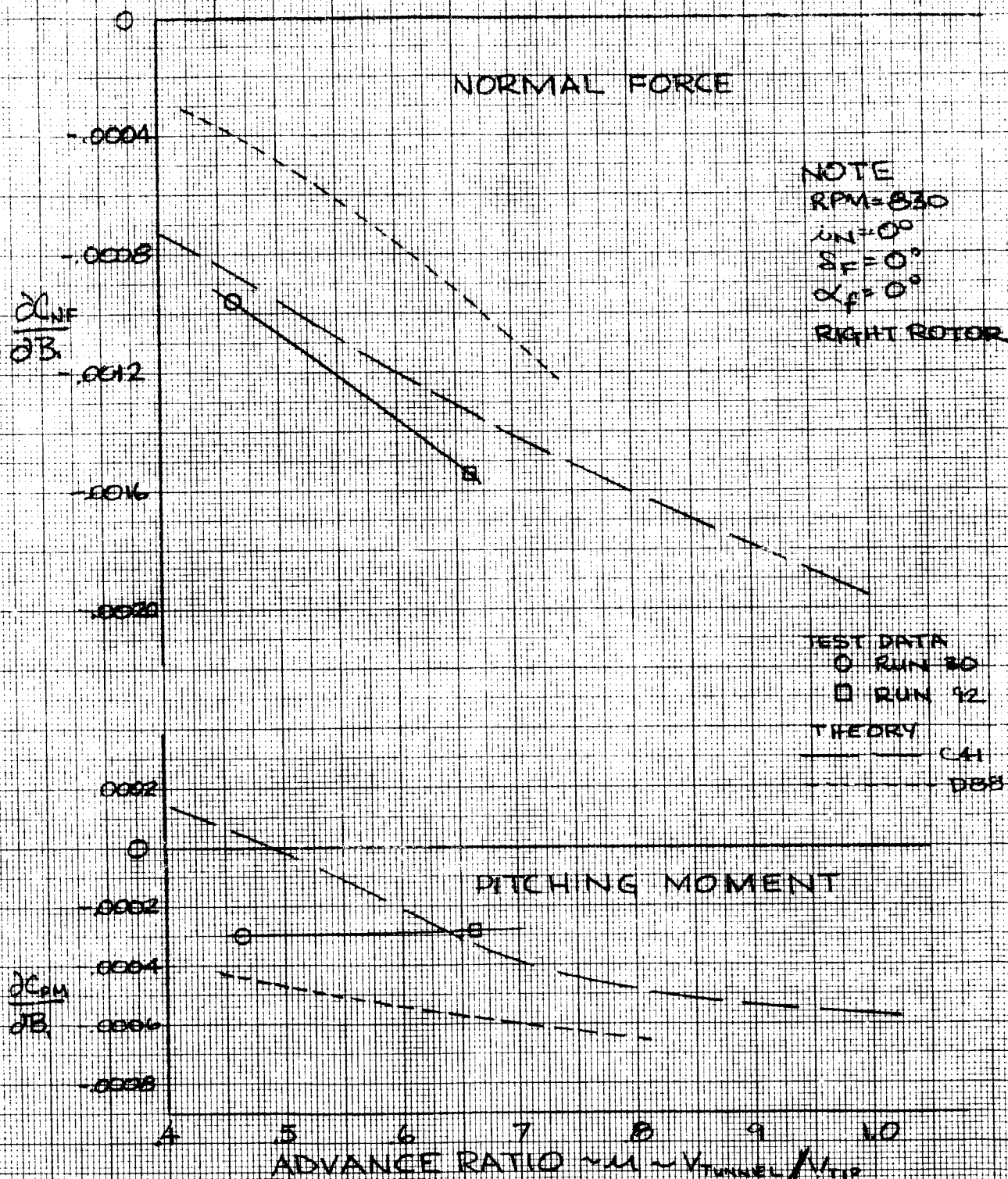


Figure 248

COMPARISON OF TEST AND THEORY
FOR
LONGITUDINAL CYCLIC ROTOR DERIVATIVES
IN CRUISE

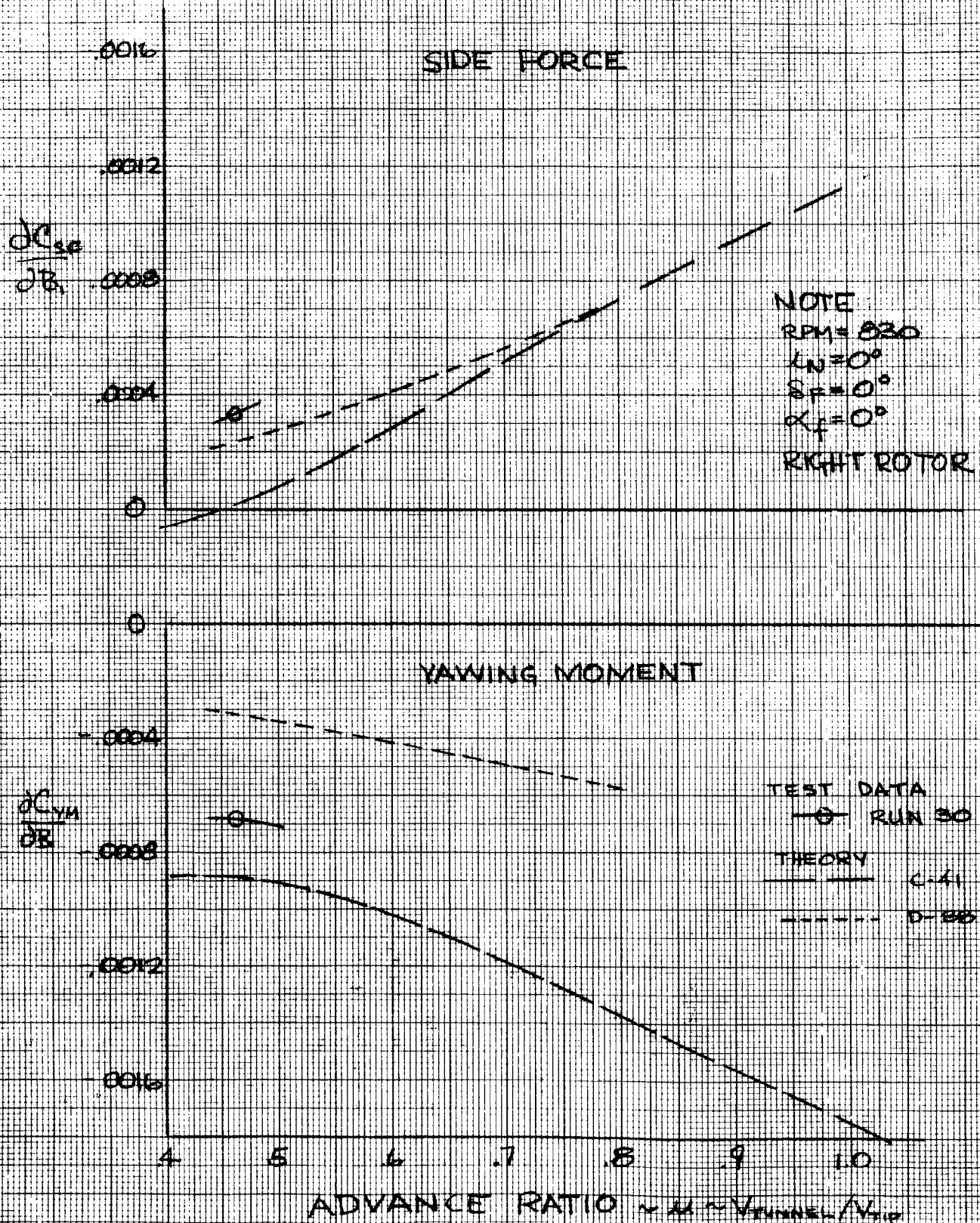


Figure 249

6.0 ROTOR LOADS

Rotor loads characteristics obtained during this test program are summarized in this section. The blade frequencies and alternating blade root bending moment data are discussed for the transition and cruise flight regime. The following sections will address these items as they were covered in the testing directed at Objective 5 in Section 2.0.

6.1 Blade Frequencies

6.1.1 Non-Rotating Frequencies

The blade frequencies were determined by individually "tweaking" the blades in the flapwise, chordwise and torsional directions with the blade roots rigidly clamped. The resulting output from the blade root strain gages was analyzed to determine the blade frequencies. This was done before and after testing, and the results are shown in Table 11. It can be seen that there is little change in frequencies from pre-test to post-test, which indicates that no substantial fatigue damage occurred. The blade frequencies would be expected to drop if blade stiffness had dropped due to fatigue damage.

6.1.2 Rotating Frequencies

The predicted rotating natural frequencies are shown in Figure 250 together with the experimental data. Predictions are given for hover and cruise conditions.

The 1st mode is inplane. Since the 0.75 radius blade angle range of 12° - 33° corresponds to the blade root at 45° - 66° the inplane mode is predominantly a blade flapwise mode. The predictions at 0 rpm fall slightly below the static flap frequency of Table 11. Similarly the 2nd mode which is out-of-plane is predominantly a blade chordwise mode and corresponds closely with the measured static frequency.

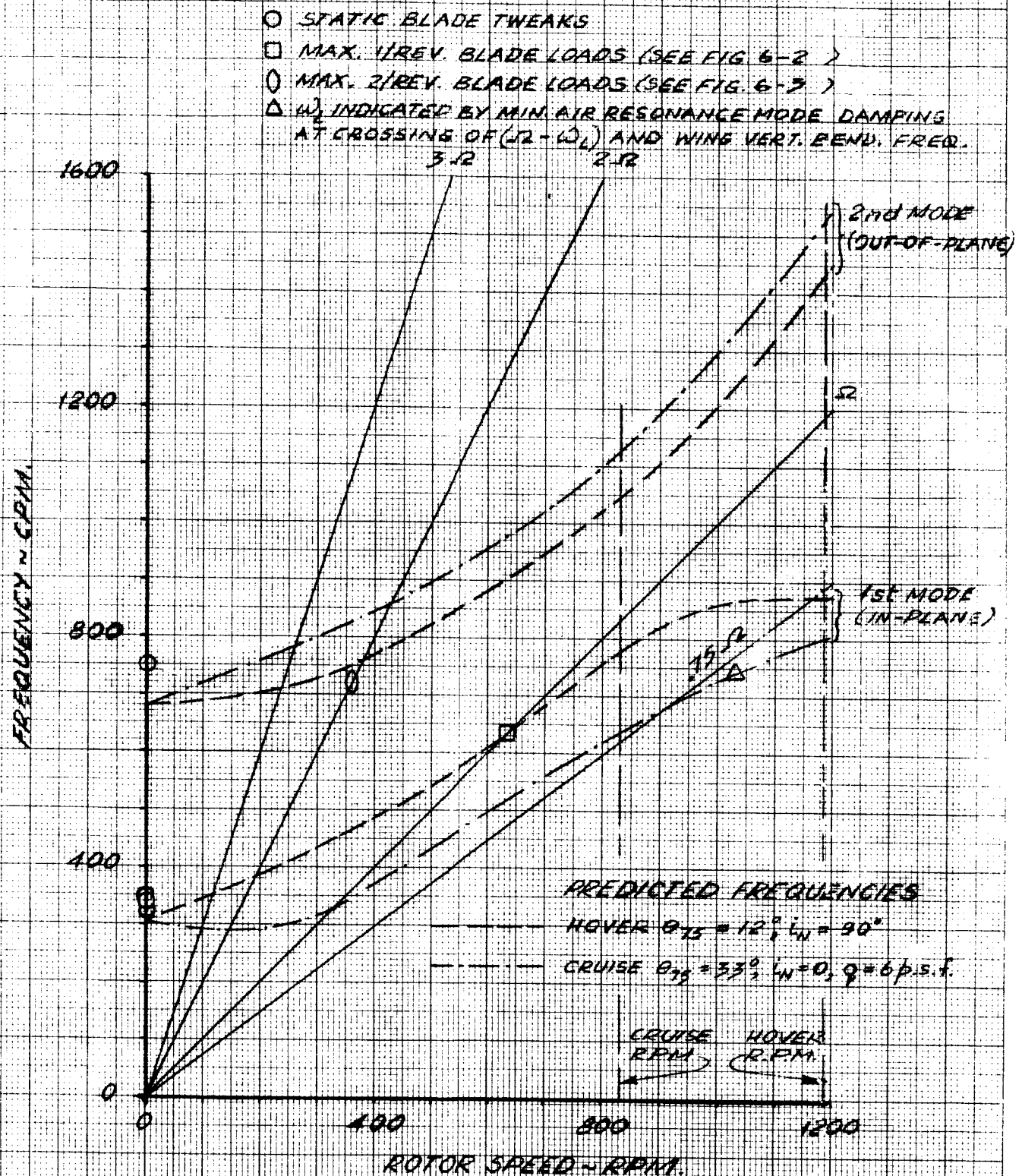
Hover tests were conducted where the blade root alternating flap and chord bending gage outputs were filtered to measure the content in

discreet narrow frequency bands. This was done at several rotor speeds covering the anticipated 1/rev and 2/rev crossings of the blade modes. The results of these tests are given in Figures 251 and 252 which show the 1/rev and 2/rev content of the blade loads respectively. The peak response points from these figures have been superimposed on the Ω and 2Ω lines of Figure 250 and show good agreement with the predicted hover case frequencies.

An additional check on the predicted frequencies has been made using the dynamic data of Figure 271. These data show the minimum damping of the wing vertical bending mode in the cruise configuration occurs at 1030 rpm. This indicates that this is the rpm where the lower blade lag mode ($\Omega - \omega_l$) crosses the wing vertical bending frequency of 4.8 Hz (288cpm), and therefore ω_l at 1030 rpm is 742 cpm. This point shows good agreement with the cruise condition in-plane mode frequency prediction of Figure 250.

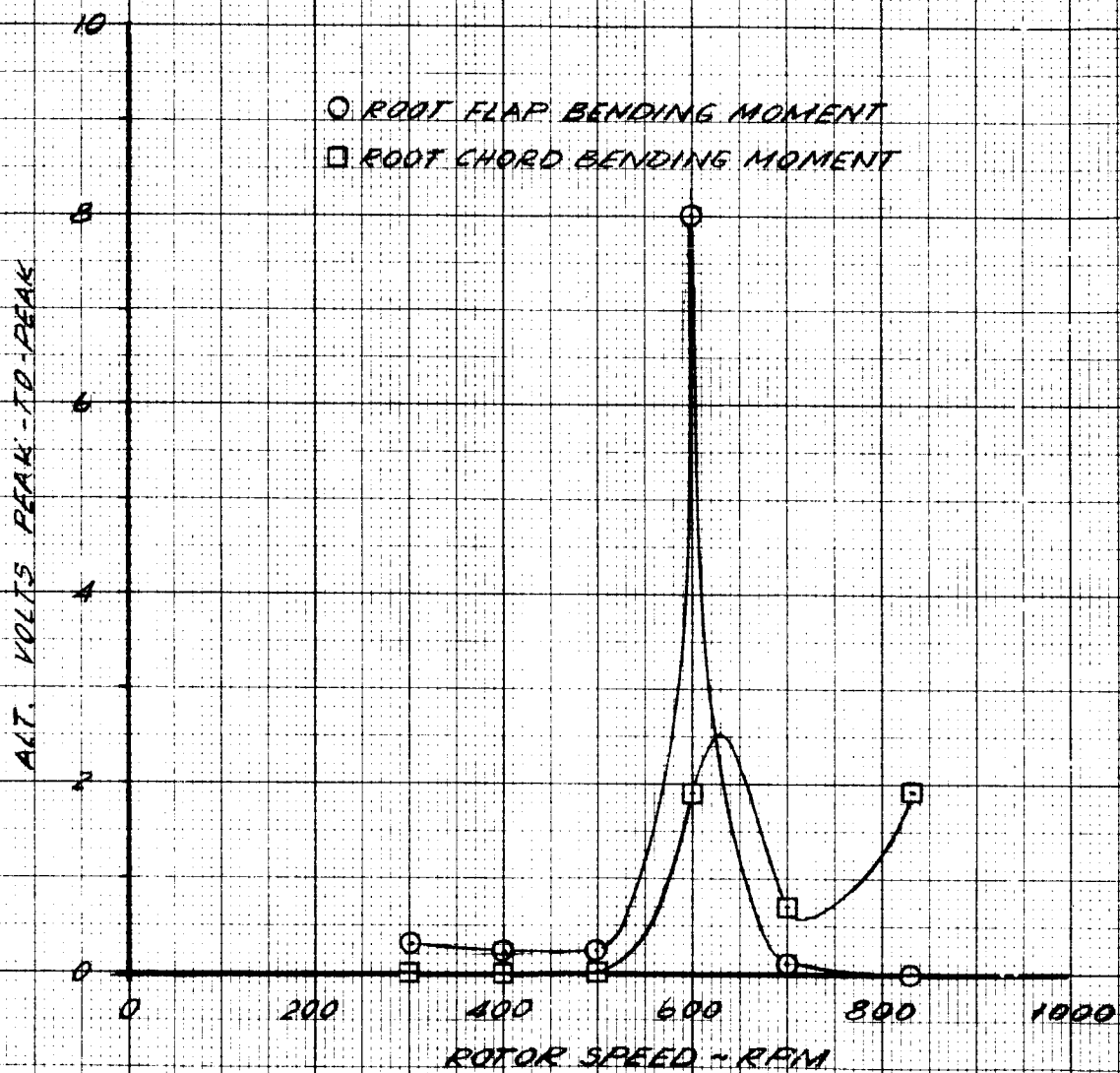
TABLE 11. BLADE FREQUENCIES FROM STATIC TWLEAK TESTS

BLADE #	FLAP FREQUENCIES (CPM)				CHORD FREQUENCY (CPM)		TORSIONAL FREQUENCY (CPM)	
	1ST MODE		2ND MODE		PRETEST	POST TEST	PRETEST	POST TEST
	PRETEST	POST TEST	PRETEST	POST TEST				
271	338	345	2230	2273	745	751	6000	5950
272	340	348	--	2273	750	766	6000	5940
273	332	336	2270	2254	745	756	6000	5932
263	345	354	--	2201	750	761	5900	6132
265	340	346	--	2350	745	766	6100	6015
266	328	-	--	--	745	-	5900	



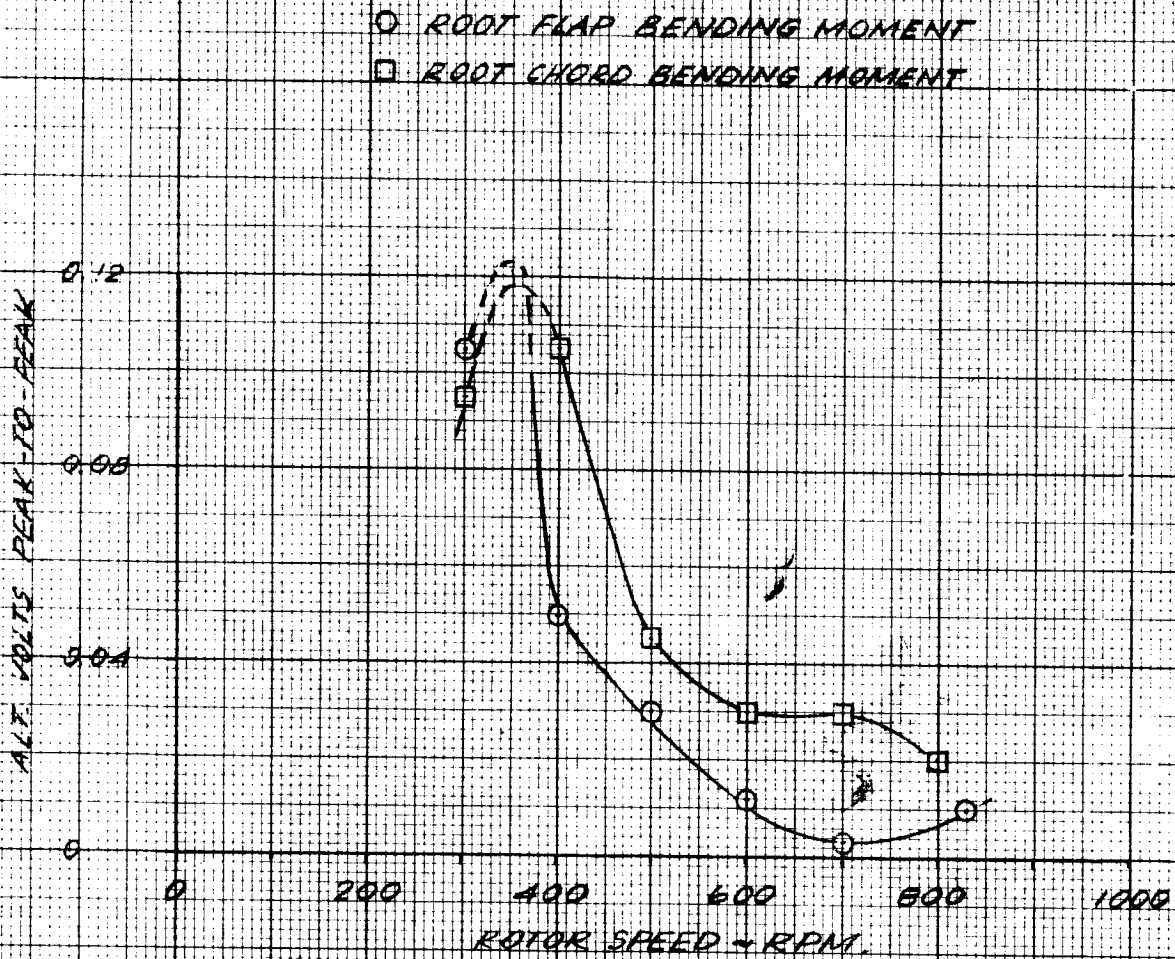
SUMMARY OF BLADE ROTATING NATURAL FREQUENCIES

Figure 250



1/REV CONTENT OF ALTERNATING 12.5% R
BLADE LOADS IN HOVER, $\alpha_N = 90^\circ$, $\theta_{75} = 12^\circ$

Figure 251



2/REV. CONTENT OF ALTERNATING 12.5% R
BLADE LOADS IN HOVER, $i_N = 90^\circ$, $\theta_{75} = 12^\circ$

figure 252

6.2 TRANSITION BLADE LOADS

6.2.1 Attitude Effects

Testing was performed in mid transition at 72 ft/sec with a rotor speed of 1185 RPM which is equivalent to 90 kts and 551 RPM on the full scale aircraft. For this speed the nacelle incidence, specified by the normal transition schedule, was set at 41.6 degrees and the effect of pitch attitude and flap deflection on alternating root bending blade loads were examined. This data is presented in Figure 253 and indicates a significant effect resulting from flap deflection. Increasing the flap deflection from 20 to 30 degrees increases the wing lift coefficient by 0.09 and the associated increase in alternating flap bending load was approximately 5.0 in-lb and there was a 34 in-lb increase in alternating chord bending load. This is equivalent to a 5 degree decrease in angle of attack in addition to an increase in blade loads equivalent to 2 degrees angle of attack. As the angle of attack is increased the lift is also increasing but to get an indication of the rate of increase of blade loads with angle without this changing lift requires an isolated rotor. Figure 254 presents the data obtained from yaw sweep for 40 degrees flap deflection. The change in alternating chord bending load is 3.2 in-lbs/deg for the yaw sweep but is 5.2 in-lbs/deg for the pitch sweep.

As part of the performance and stability testing an additional nacelle incidence ($i_N=30^\circ$) was investigated. This is presented in Figure 255 again as the blade load variation with angle of attack along with 41.6 nacelle incidence. Decreasing the nacelle

incidence by 11.6 degrees results in a 7 percent decrease in the rate of change in blade loads with angle of attack.

6.2.2 Effects of Nacelle Incidence

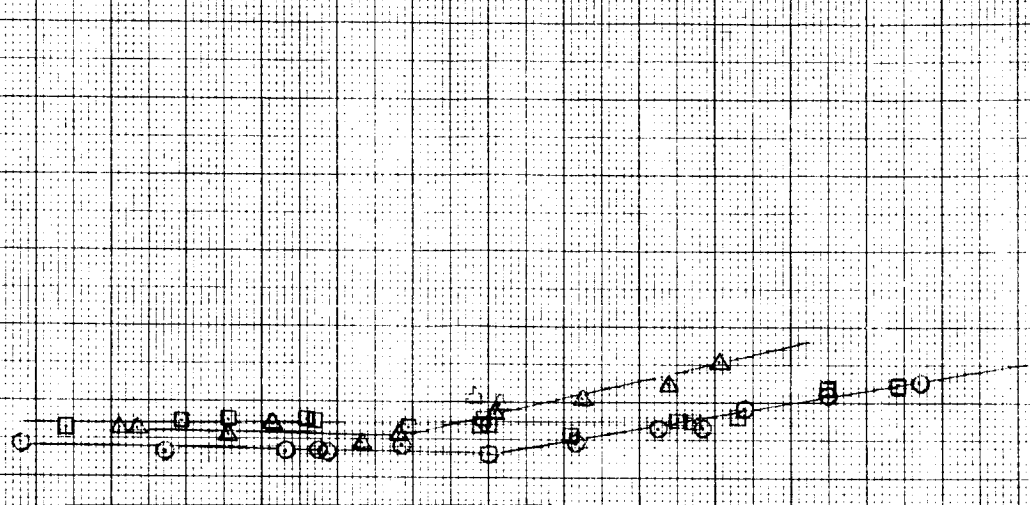
The difference in the minimum blade loads and the variation with angle of attack between 30 and 41.6 degrees nacelle incidence was slight. To insure that the trend was linear a variation in nacelle incidence was tested with the fuselage fixed at zero degrees angle of attack. This data is presented in Figure 256. At each nacelle incidence the thrust coefficient was adjusted to approximately 0.0023 and the cyclic was changed to minimize the blade loads. Figure 257 presents the collective and collective values during this test.

6.2.3 Cyclic Pitch Effects

The variations in blade root alternating bending moments with cyclic pitch are shown in Figures 258 and 259 at an equivalent full scale speed of 90 KTS and 41.6 degrees nacelle tilt. Cyclic effects on the flap bending loads are small. Sensitivity of chord bending loads to longitudinal and lateral cyclics are approximately equal at this condition. Comparing effect of cyclic on blade loads with the angle of attack effects indicates that cyclic is 15 times more effective than yaw angle but only 9 times more effective than pitch angle.

EFFECT OF FLAP DEFLECTION IN TRANSITION ON ALTERNATING BLADE LOADS

ALTERNATING
BLADE FLAP BENDING - IN LBS
12.4% γ/R

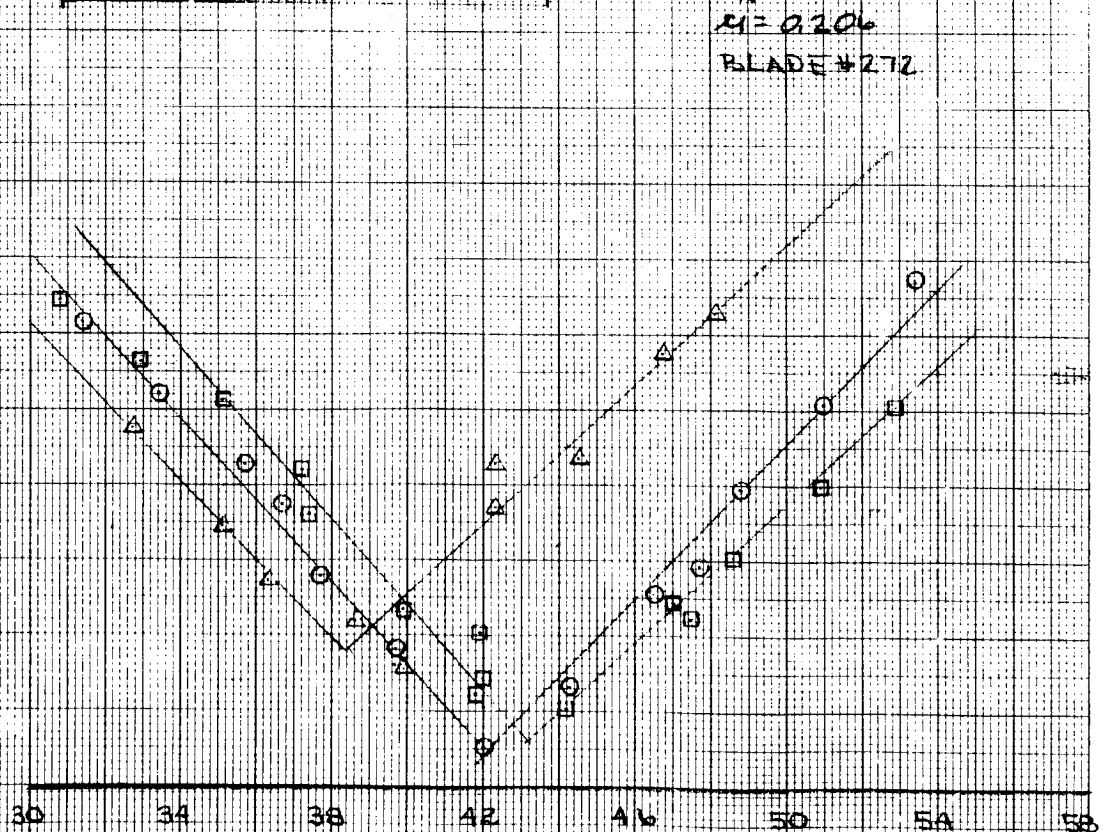


SYM	RUN	SP	Θ	A	B
○	104	40	12.75	1.201	2.673
□	117	30	12.84	0.957	2.718
△	118	20	12.51	1.040	2.640

NOTE

TUNNEL SPEED = 113 FPS
RPM = 1185
 $C_N = 41.6^\circ$
 $M = 0.206$
BLADE #272

ALTERNATING
BLADE CHORD BENDING - IN LBS
12.4% γ/R



ROTOR SHAFT ANGLE OF ATTACK - α_s - DEG
Figure 153

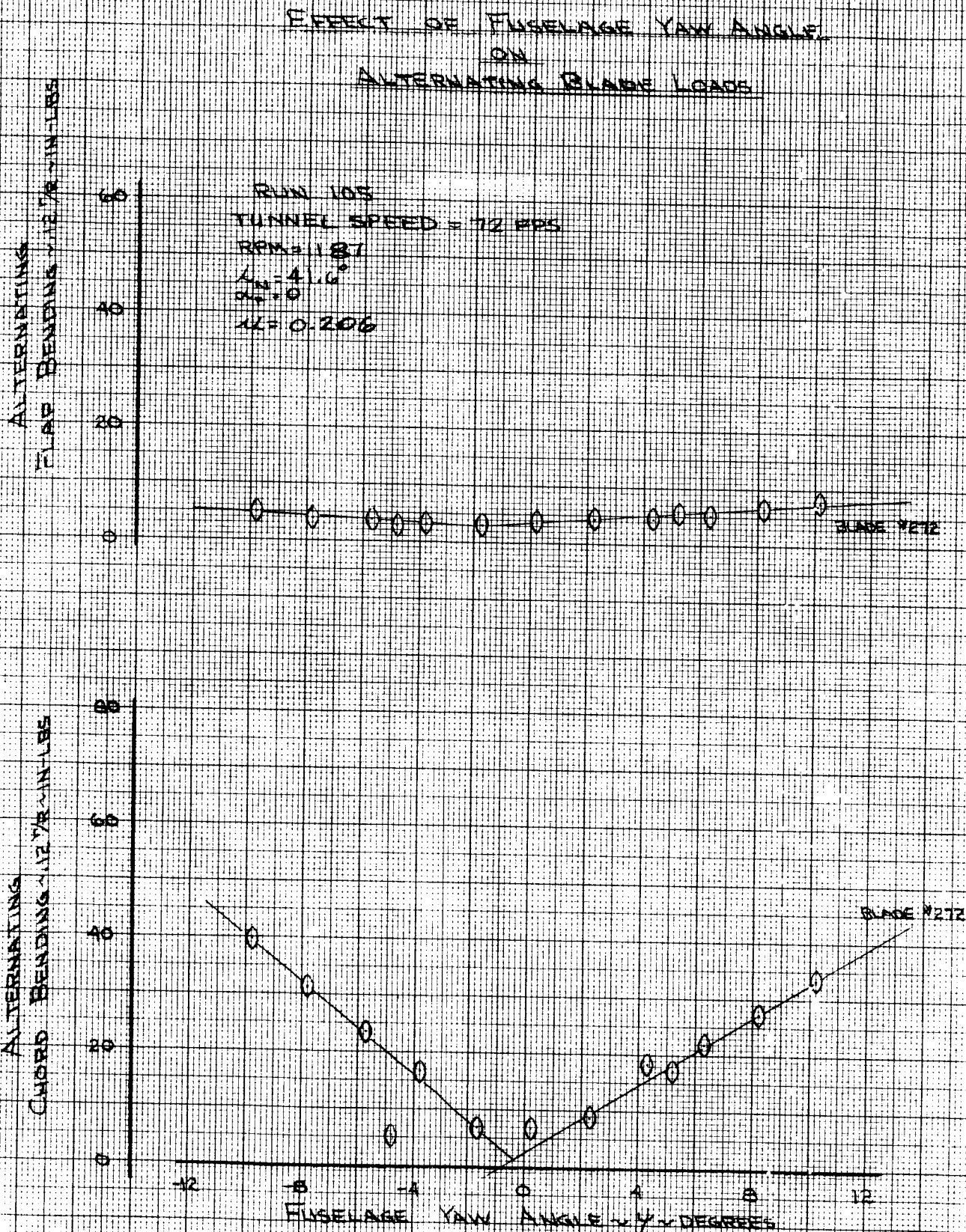


Figure 254

EFFECT OF NACELLE INCIDENCE IN TRANSITION ON ALTERNATING BLADE LOADS

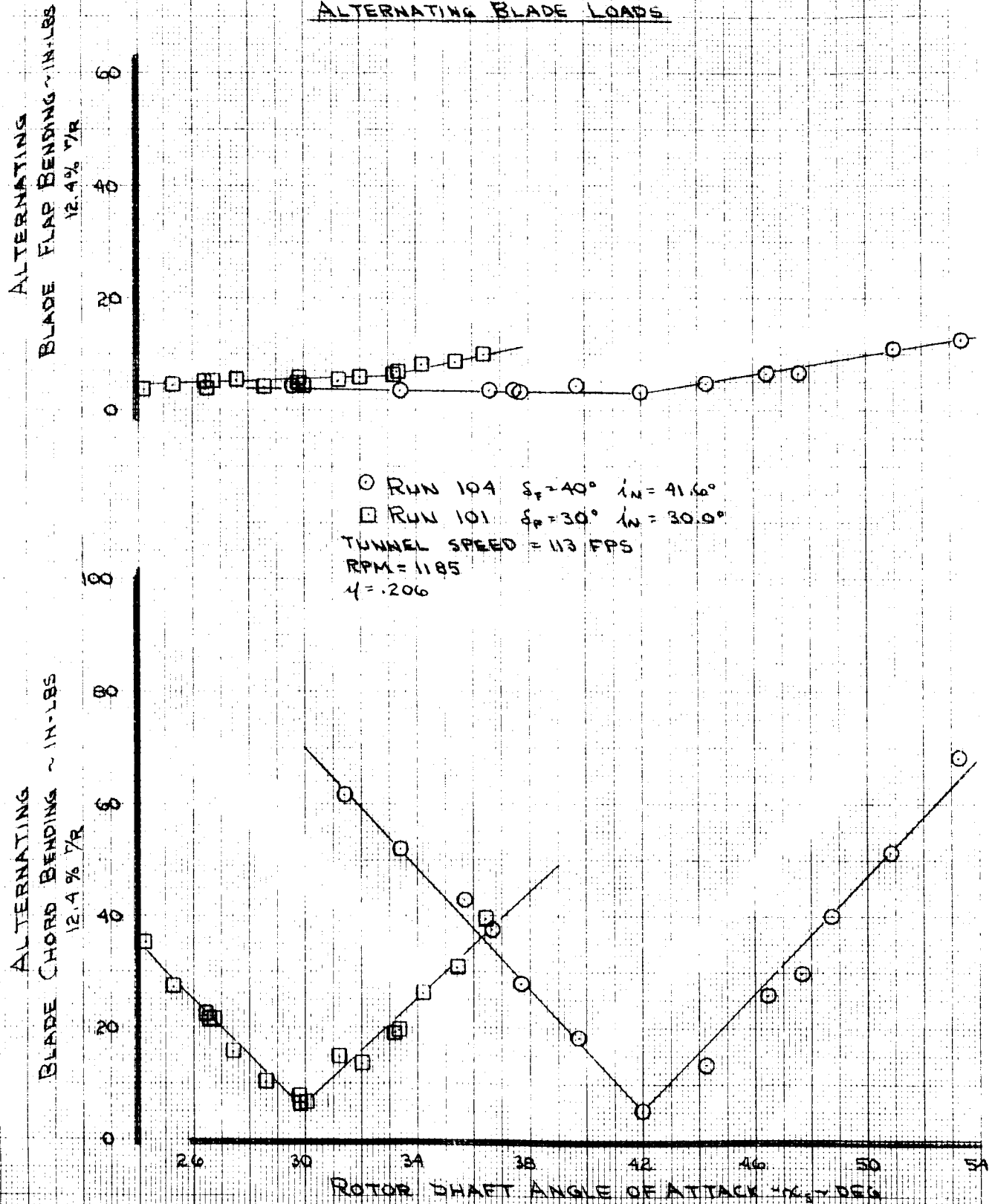


Figure 255

EFFECT OF NACELLE INCIDENCE ON ALTERNATING BLADE LOADS

RUN 104

RFM = 1185

$q = 6.0$ PSF

$\alpha_f = 0^\circ$

TUNNEL SPEED = 72 FPS

ALTERNATING
FLAP BENDING - 1272 IN-LBS

8
6
4
2
0

ALTERNATING
CHORD BENDING - 1272 IN-LBS

8
6
4
2
0

30 32 34 36 38 40 42

NACELLE INCIDENCE - i_n - DEGREES

figure 256

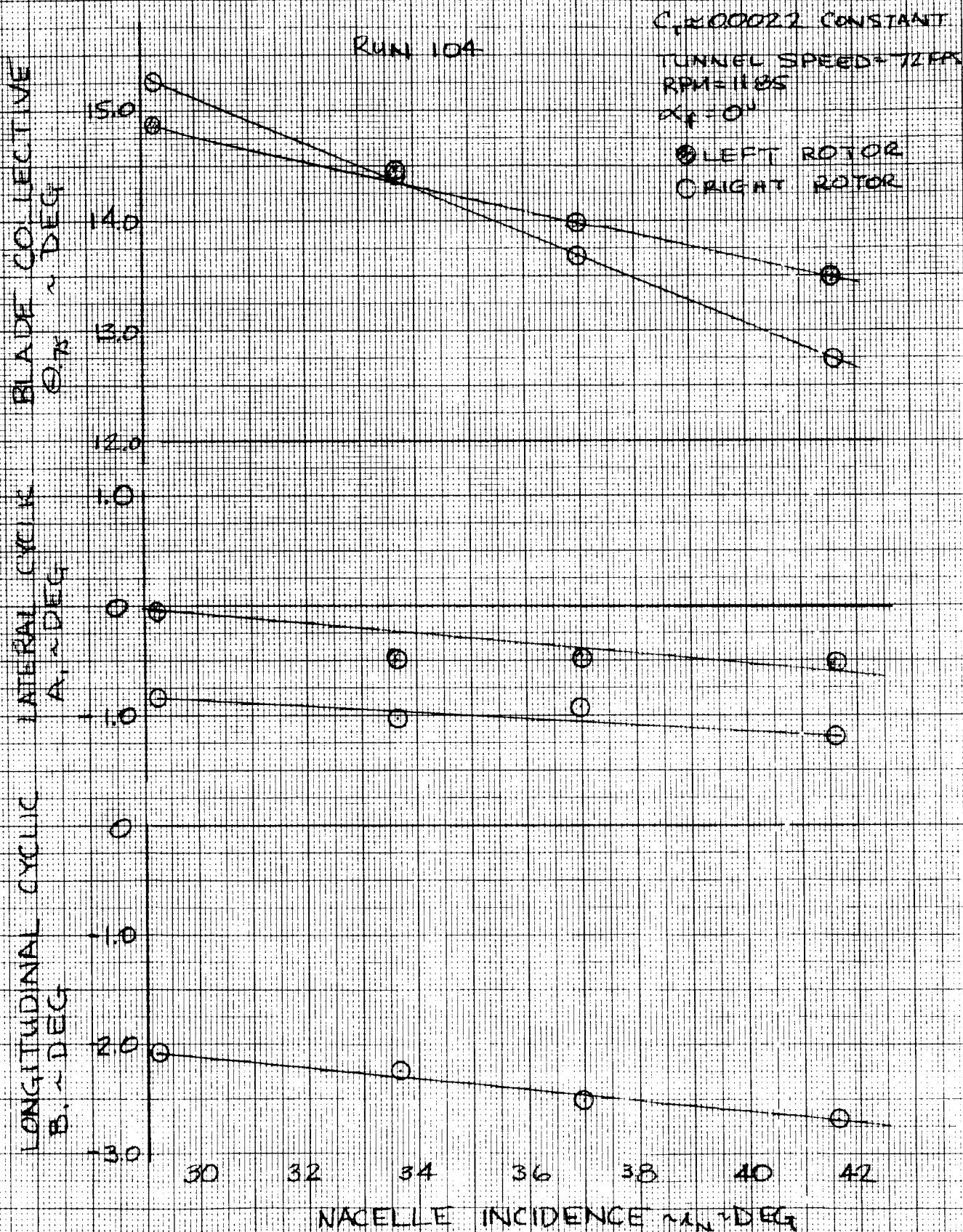
CYCLIC REQUIRED TO MINIMIZE BLADE LOADS
DURING NACELLE INCIDENCE SWEEP

Figure 257

EFFECT OF LONGITUDINAL CYCLIC IN TRANSITION ON ALTERNATING BLADE LOADS

RUN 107

RIGHT ROTOR
RPM 1185
TUNNEL SPEED 72 FPS
 $\alpha = 0^\circ$
 $\gamma_N = 41.6^\circ$
 $\beta = 140^\circ$
 $\alpha_s = 43^\circ$
FULL SCALE
EQUIVALENT = 90 KTS
SPEED

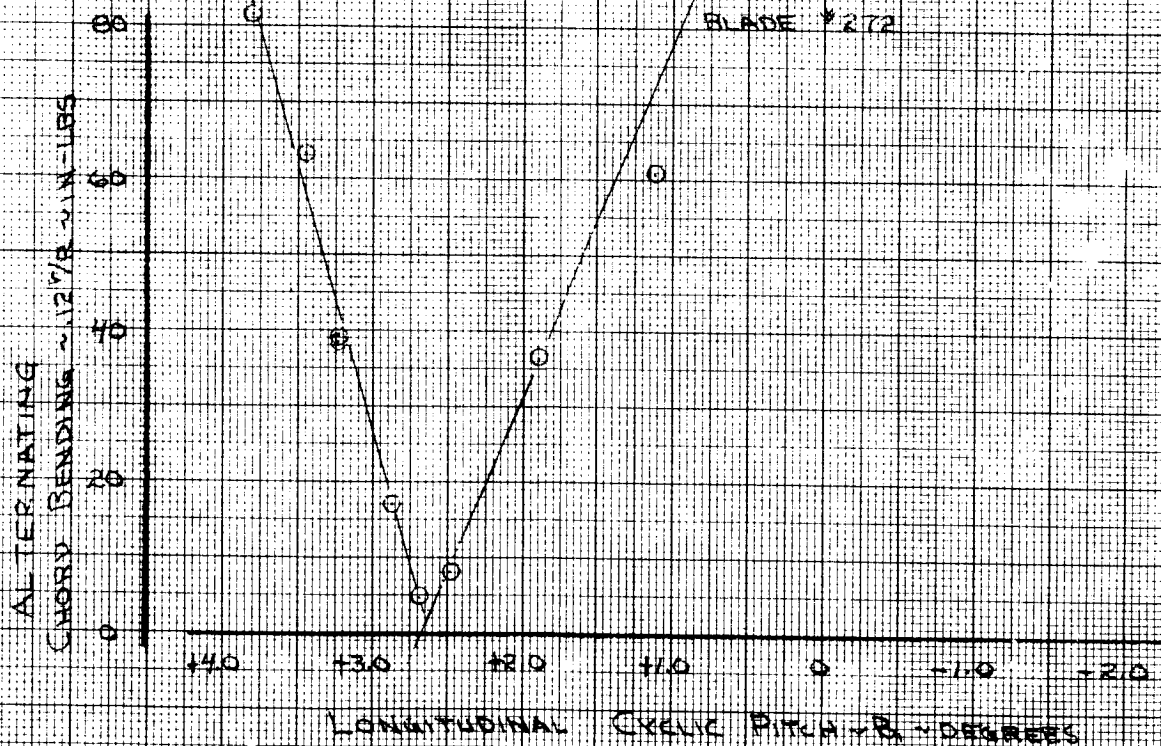
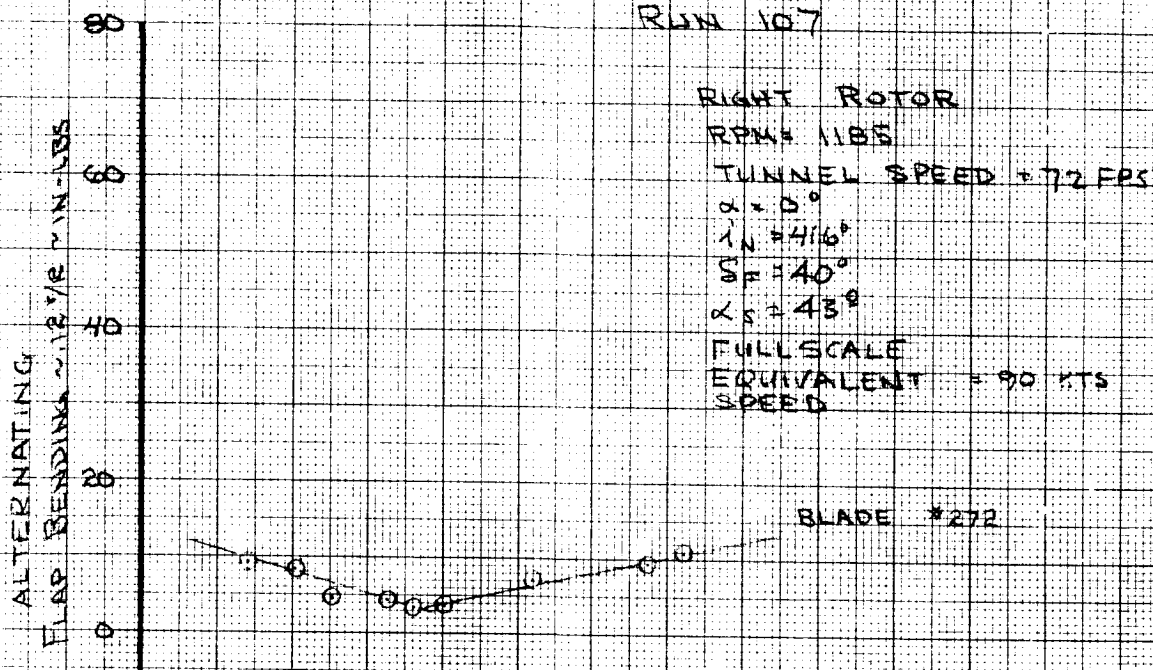


Figure 258

EFFECT OF LATERAL CYCLIC IN TRANSITION ON ALTERNATING BLADE LOADS

RUN 108

RIGHT ROTOR

RPM = 1185

TUNNEL SPEED = 72 FPS

$\alpha = 0^\circ$

$\alpha_0 = 41.6^\circ$

$\alpha_s = 43^\circ$

$\alpha_c = 40^\circ$

FULL SCALE

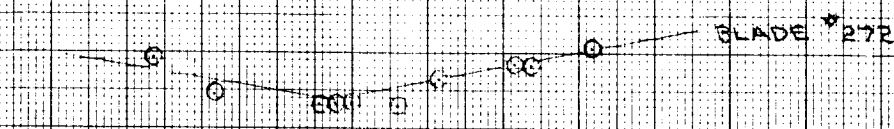
EQUIVALENT

SPEED

90 KTS

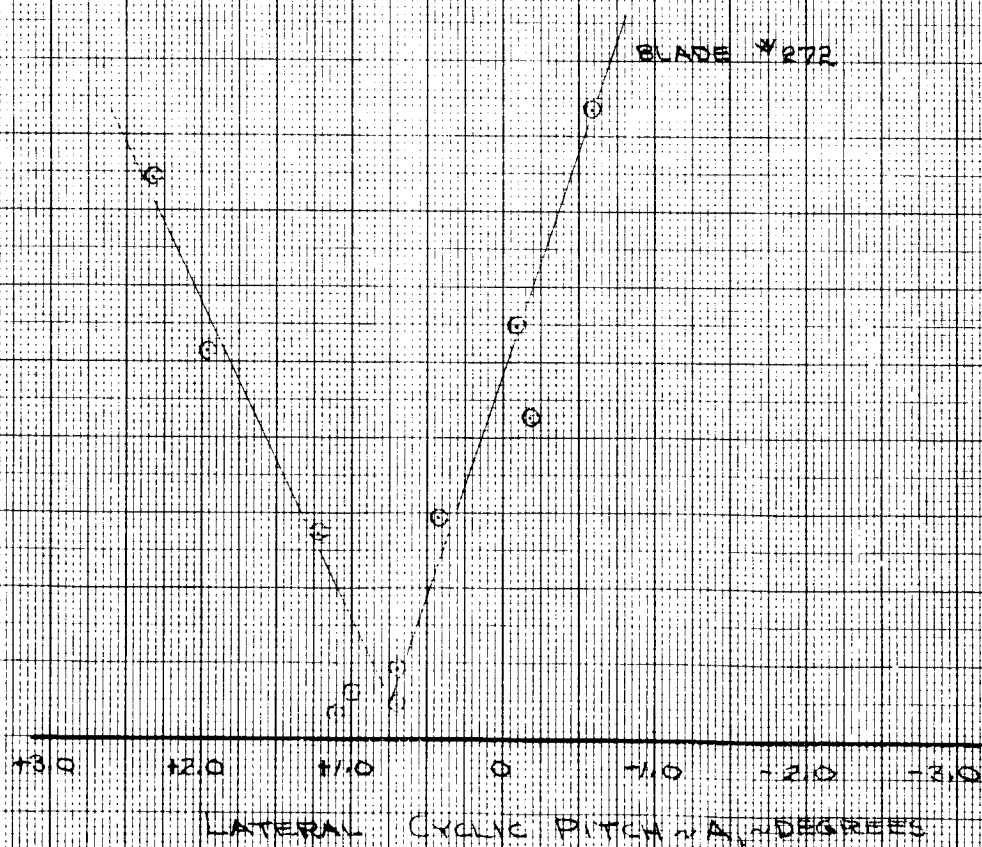
FLAP BENDING ~ 12 1/2 IN-LBS

60
40
20
0



CHORD BENDING ~ 12 1/2 IN-LBS

80
60
40
20
0



LATERAL CYCLIC PITCH ~ α ~ DEGREES

Figure 259

6.3 CRUISE BLADE LOADS

6.3.1 Attitude Effects

The variation of blade root bending moments with angle of attack are given in Figure 260 for tunnel speeds of 113 ft/sec to 162 ft/sec. It is significant to note that the angle of attack for minimum blade loads increases with tunnel speed as was indicated in Reference 6. As the speed is increased the minimum blade loads increase as a function of the speed squared (V^2), or advance ratio squared (μ^2). The rate of change of blade loads with angle of attack also increases at approximately a μ^2 trend for both chord and flap bending moments.

Blade load data obtained from yaw angle investigation is presented in Figure 261 and is representative of an isolated rotor since the lift does not vary during the yaw sweep. The minimum value of blade loads is obviously the same as for the pitch but the variation of alternating blade load with yaw angle is approximately 25 percent lower than that defined for pitch angle in Figure 260. This indicates that lift increases the blade load variation with attitude. As a further verification of this, the flap deflection effect on blade loads is presented in Figure 262.

6.3.2 Effects of Forward Speed

As indicated in Figure 260 the minimum blade loads appear to increase as a function of speed squared. To get further verification of this, speed sweeps were made and the blade load data was presented in Figure 263 and 264 with dynamic pressure as the primary variable since it is a unique quantity that is a function of

velocity squared. This shows a very linear trend to achieve the minimum blade loads for each speed while maintaining zero degrees fuselage angle of attack is presented in Figure 265. This shows increasing cyclic is required as speed is increased. This is consistent with the increasing angle of attack for minimum blade loads trends indicated in Figure 260.

6.3.3 Cyclic Pitch Effects

Cyclic pitch investigations were made in the cruise mode to define the effectiveness of this rotor control and as baseline information to be utilized in shaping and phasing of the low rate feedback system. Figure 266 presents the longitudinal cyclic effects which reduces the alternating blade chord bending moments 44 in-lbs/degree at 162 ft/sec tunnel speed. This is 70 percent more effective than angle of attack. Figure 267 presents the effects of lateral cyclic and this also is 70 percent more effective than the yaw angle. Utilizing cyclic manually to simulate the low rate cyclic feedback, an angle of attack run was made and is compared with a similar run with fixed cyclic in Figure 268. The run with cyclic varying has almost no change in blade loads. The longitudinal and lateral cyclic associated with these blade loads is presented in Figure 269. Imposed on Figure 268 is the blade load comparison of test and prediction and it shows good agreement with the change due to angle of attack but there is a load shift for the minimum blade loads.

EFFECT OF FORWARD SPEED IN CRUISE ON ALTERNATING BLADE LOADS

ALTERNATING
BLADE FLAP BENDING-MOMENTS
12.4 % $\frac{1}{2}$

80
40
0

SYM	RUN	TUNNEL SPEED
○	77	113m
□	80	113m
△	83	139m
◇	86	139m
▽	89	162m

NOTE
RPM = 830
 $\lambda_{0.5} = 0$
 $S_{\theta} = 0$
BLADE 272

ALTERNATING
BLADE CHORD BENDING-MOMENTS
12.4 % $\frac{1}{2}$

100
80
60
40
20
0

SHAFT ANGLE OF ATTACK $\alpha_{0.5}$ DEGREES

Figure 260

EFFECT OF FUSELAGE YAW ANGLE ON ALTERNATING BLADE LOADS

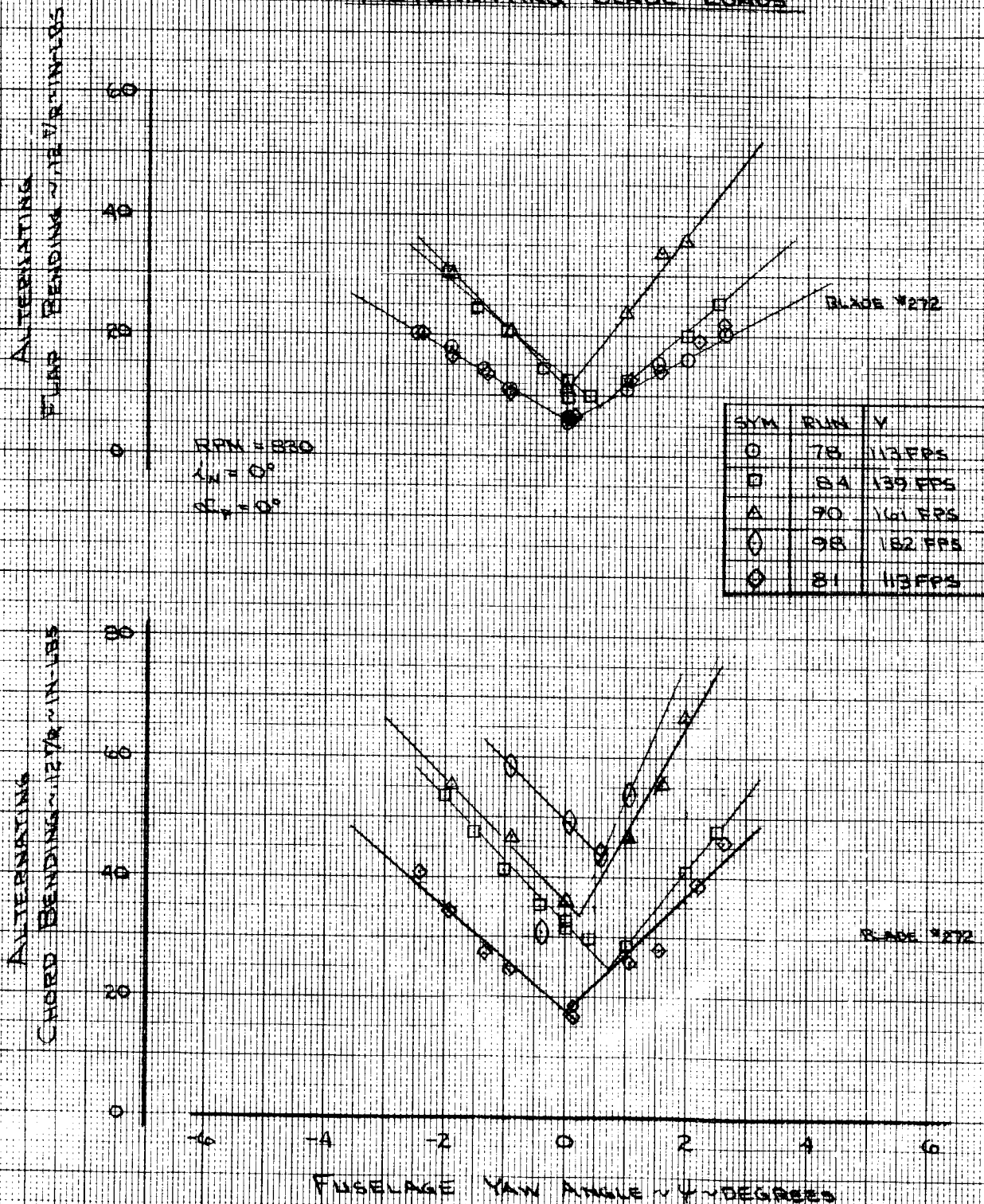


Figure 261

EFFECT OF FLAP DEFLECTION ON ALTERNATING BLADE LOADS CRUISE

$\mu = 0$
 $V = 113 \text{ FPS}$

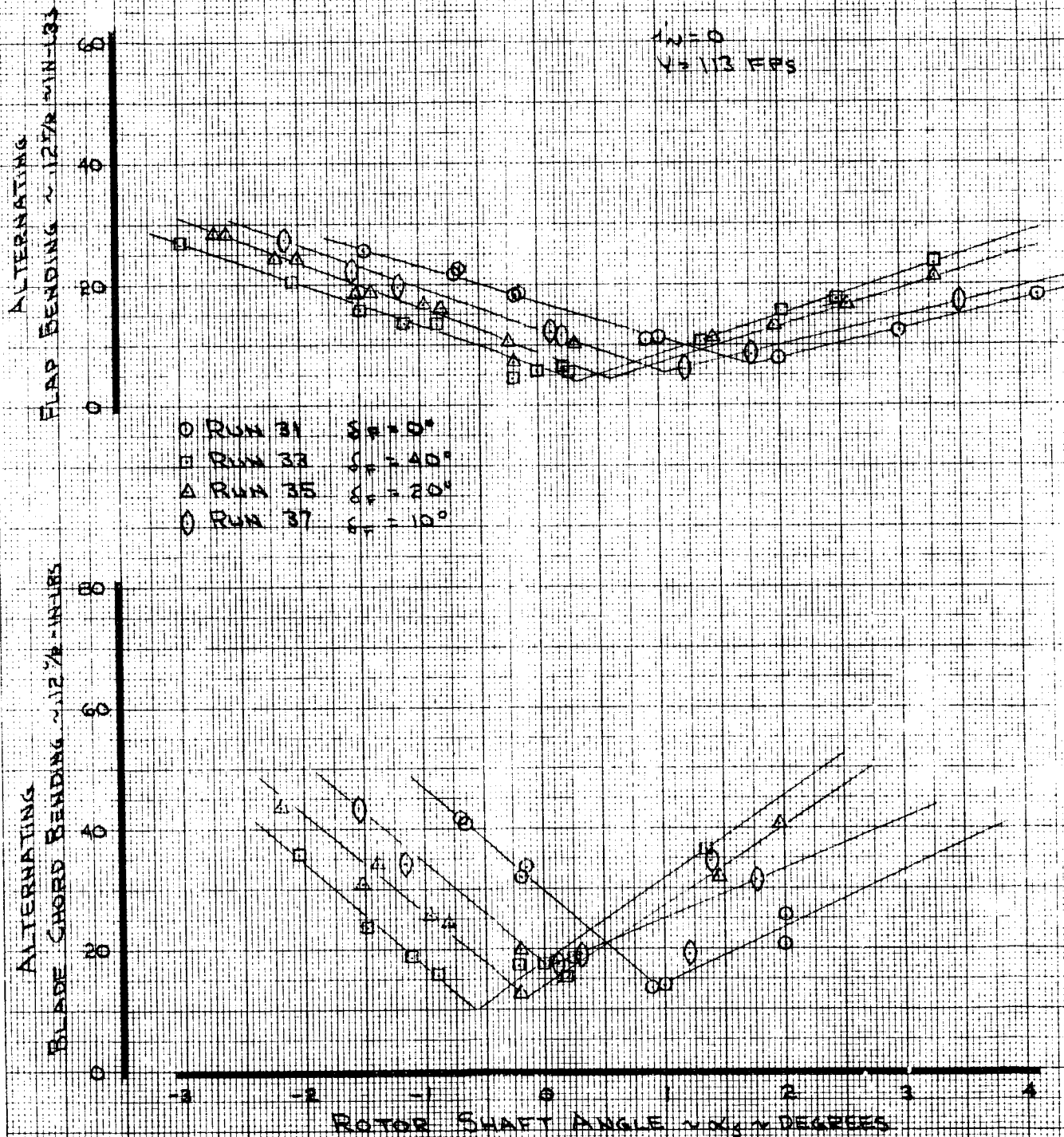


Figure 262

EFFECT OF TUNNEL DYNAMIC PRESSUREON
ALTERNATING BLADE LOADS

RIGHT ROTOR

NOTES:

1. 830 RPM

2. 9 SWEEP

3. MODEL C 0, 0

4. ALTERNATING VALUES.

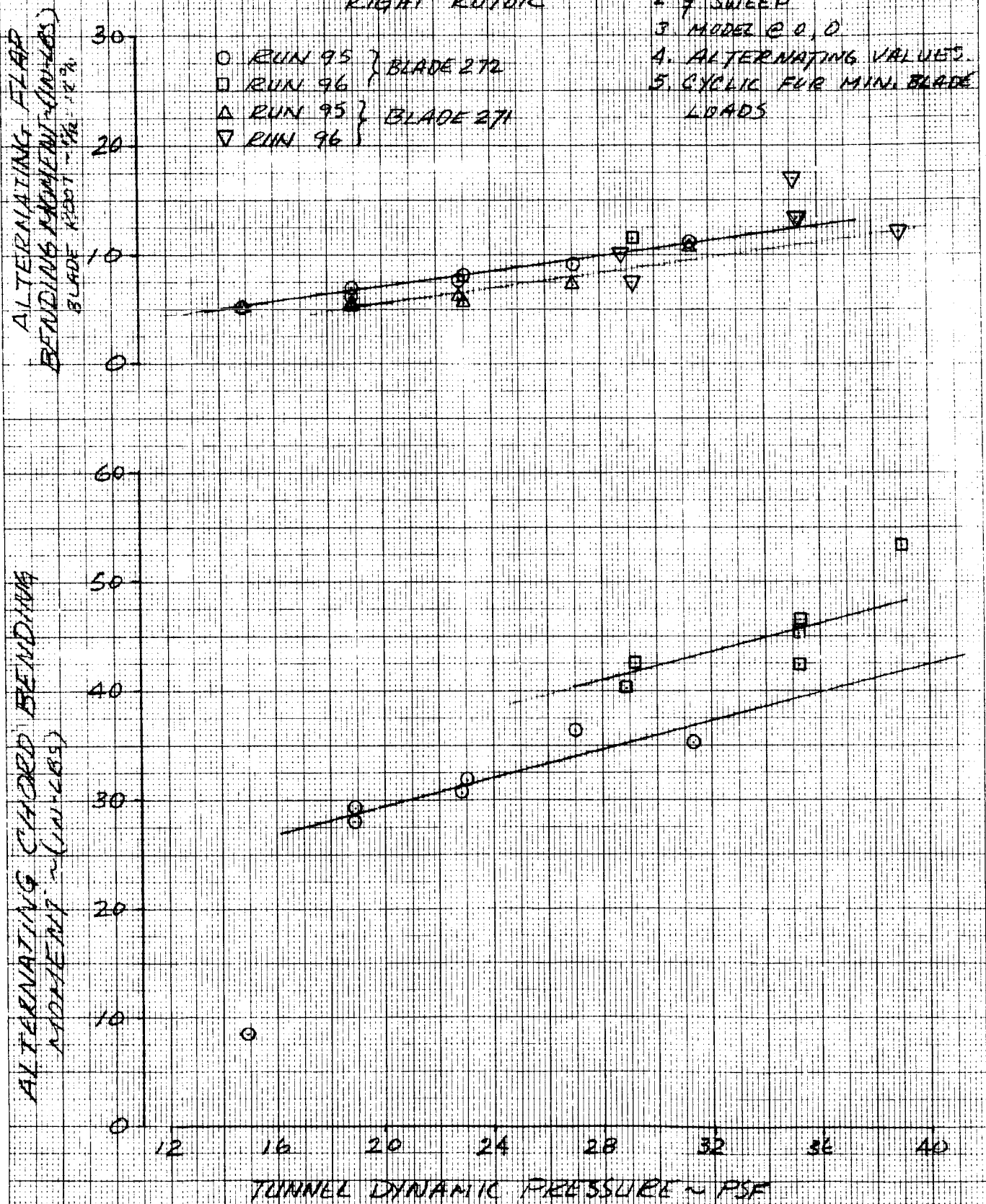
5. CYCLIC FOR MIN. BLADE
LOADS

Figure 263

LEFT ROTOR

NOTES

1. 830 RPM
2. 9 SNEEP
3. MODEL @ 0.0
4. ALTERNATING VALUES
5. CYCLE FOR MIN. BLADE LOADS

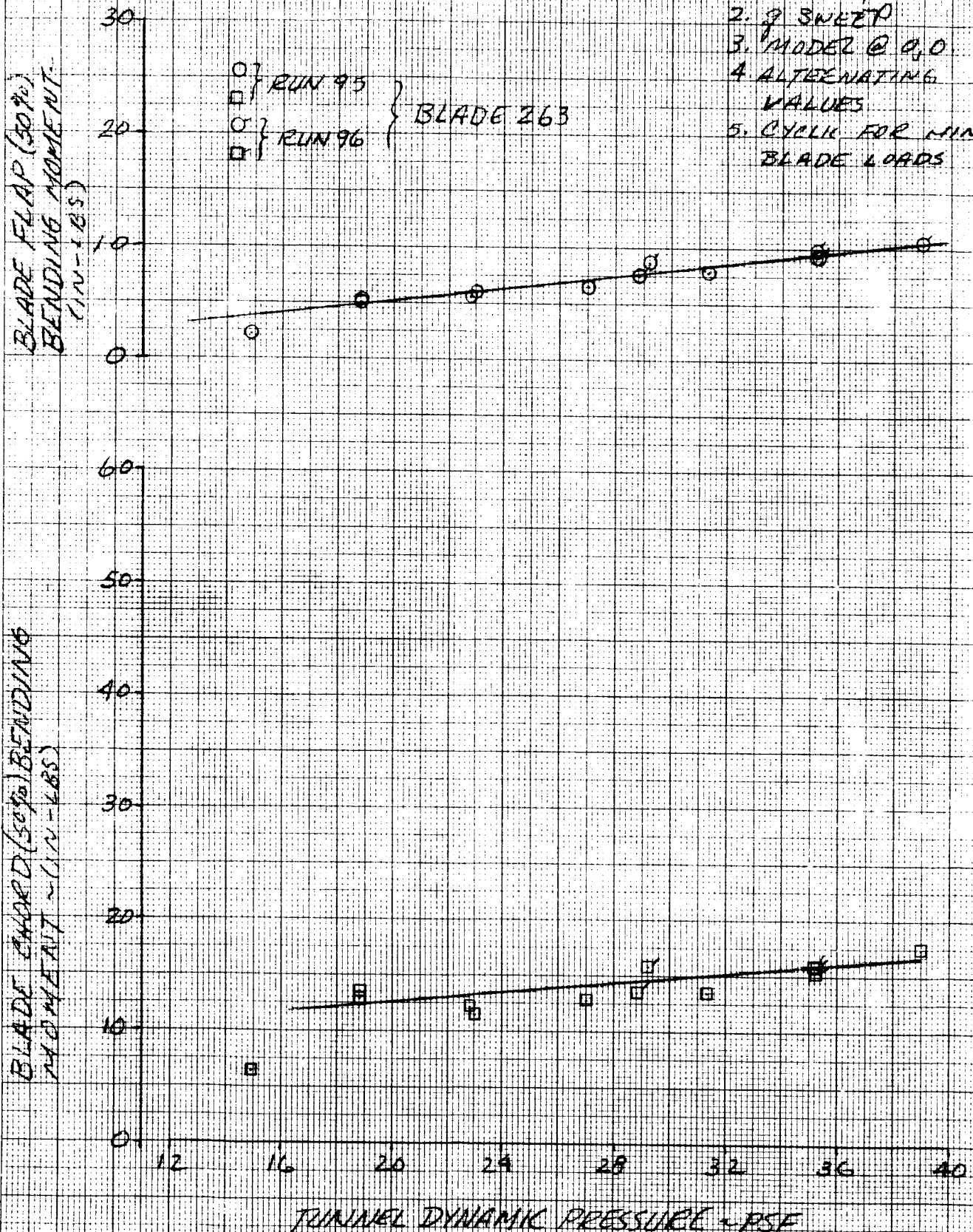


Figure 264

CYCLIC REQUIRED TO MINIMIZE BLADE LOADS
FROM 71 TO 183 FPS TUNNEL SPEED

(FULL SCALE EQUIVALENT SPEED 90 TO 235 KTS)

 $\alpha_A = 0^\circ$

830 RPM

 $\alpha = 0^\circ$

O LEFT ROTOR

O RIGHT ROTOR

RUN 95 + 96

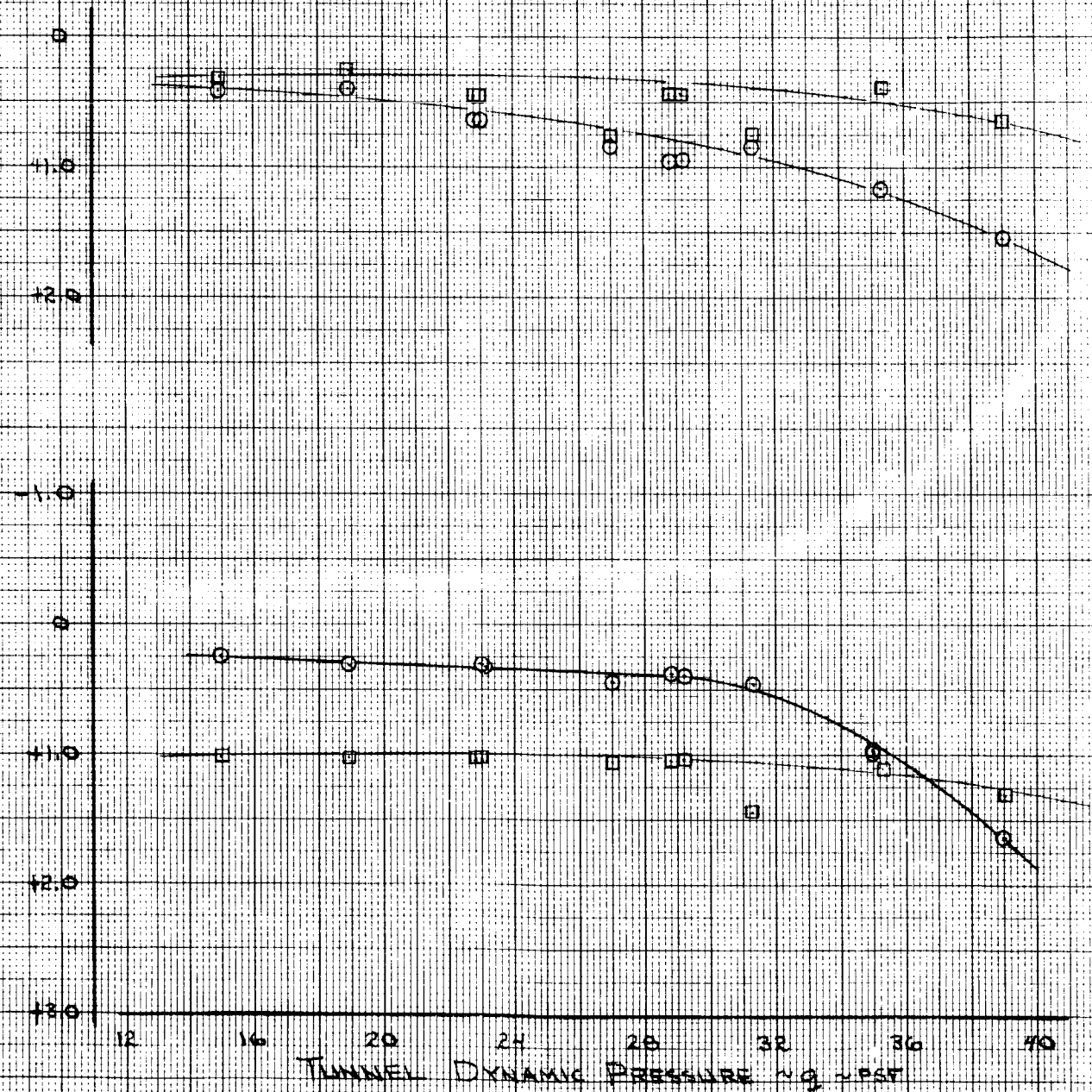
LONGITUDINAL PITCH α_L - DEGREESLATERAL PITCH α_A - DEGREES

Figure 265

EFFECT OF LONGITUDINAL CYCLIC IN CRUISE ON ALTERNATING BLADE LOADS

ALTERNATING
FLAP BENDING 1/2 IN - LBS

80
60
40
20
0

RIGHT ROTOR

RUN 92

RPM = 830
TUNNEL SPEED 161 FPS
 $\alpha = 0^\circ$
 $\alpha_2 = 0^\circ$
 $S_F = 0$
FULL SCALE
EQUIVALENT = 200 KTS
SPEED

BLADE #272

ALTERNATING
CHORD BENDING 1/2 IN - LBS

80
60
40
20
0

BLADE #272

-3.0 -2.0 -1.0 0 1.0 2.0 3.0

LONGITUDINAL CYCLIC PITCH - DEGREES

Figure 266

EFFECT OF LATERAL CYCLIC IN CRUISE ON ALTERNATING BLADE LOADS

RUN 91

RIGHT ROTOR

RPM = 830

TUNNEL SPEED = 161 F

 $\alpha = 0^\circ$ $\mu = 0^\circ$ $S_r = 0^\circ$

FULL SCALE

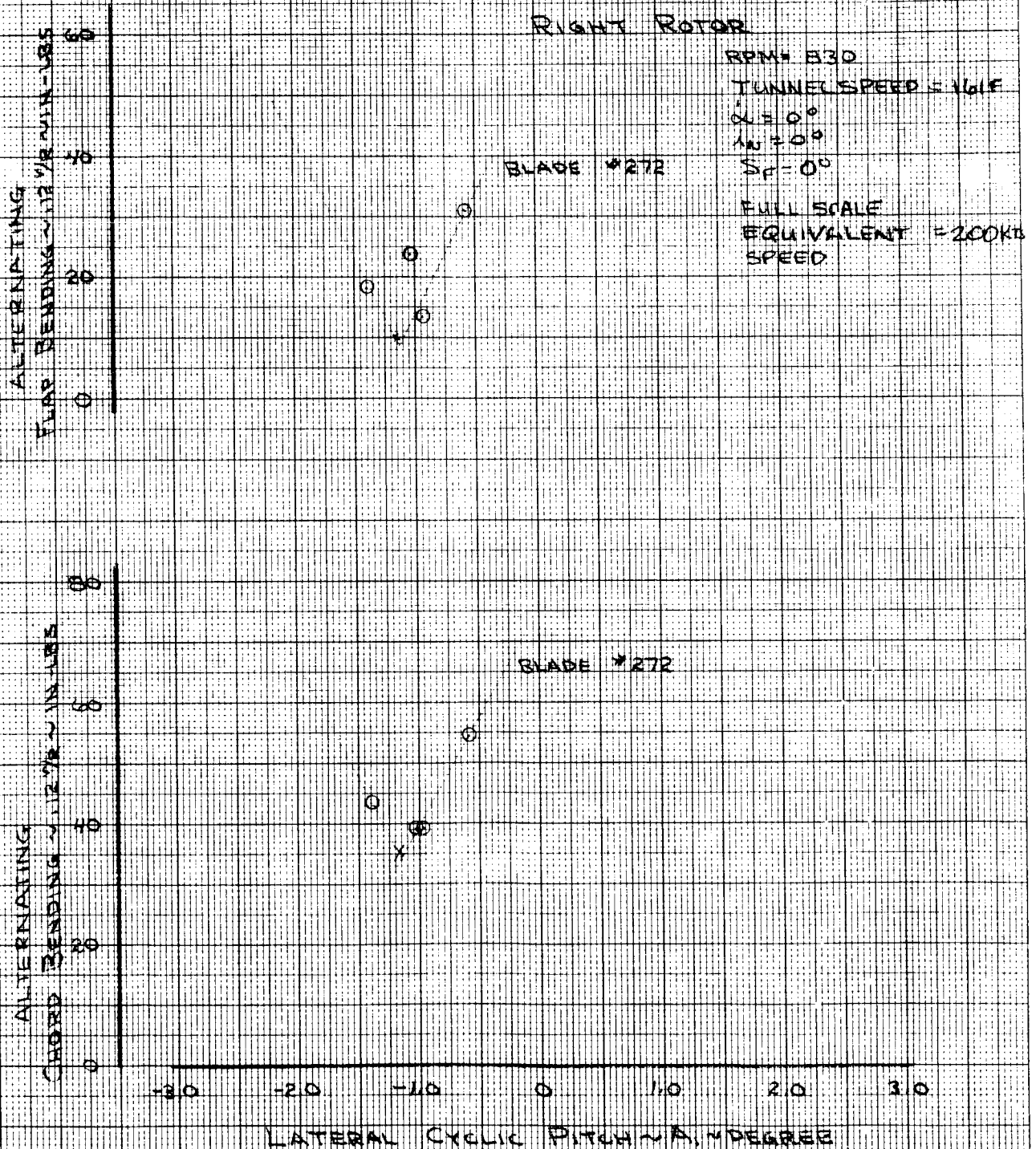
EQUIVALENT = 200 KTS
SPEED

Figure 267

EFFECT OF CYCLIC ON ALTERNATING BLADE LOADS IN CRUISE

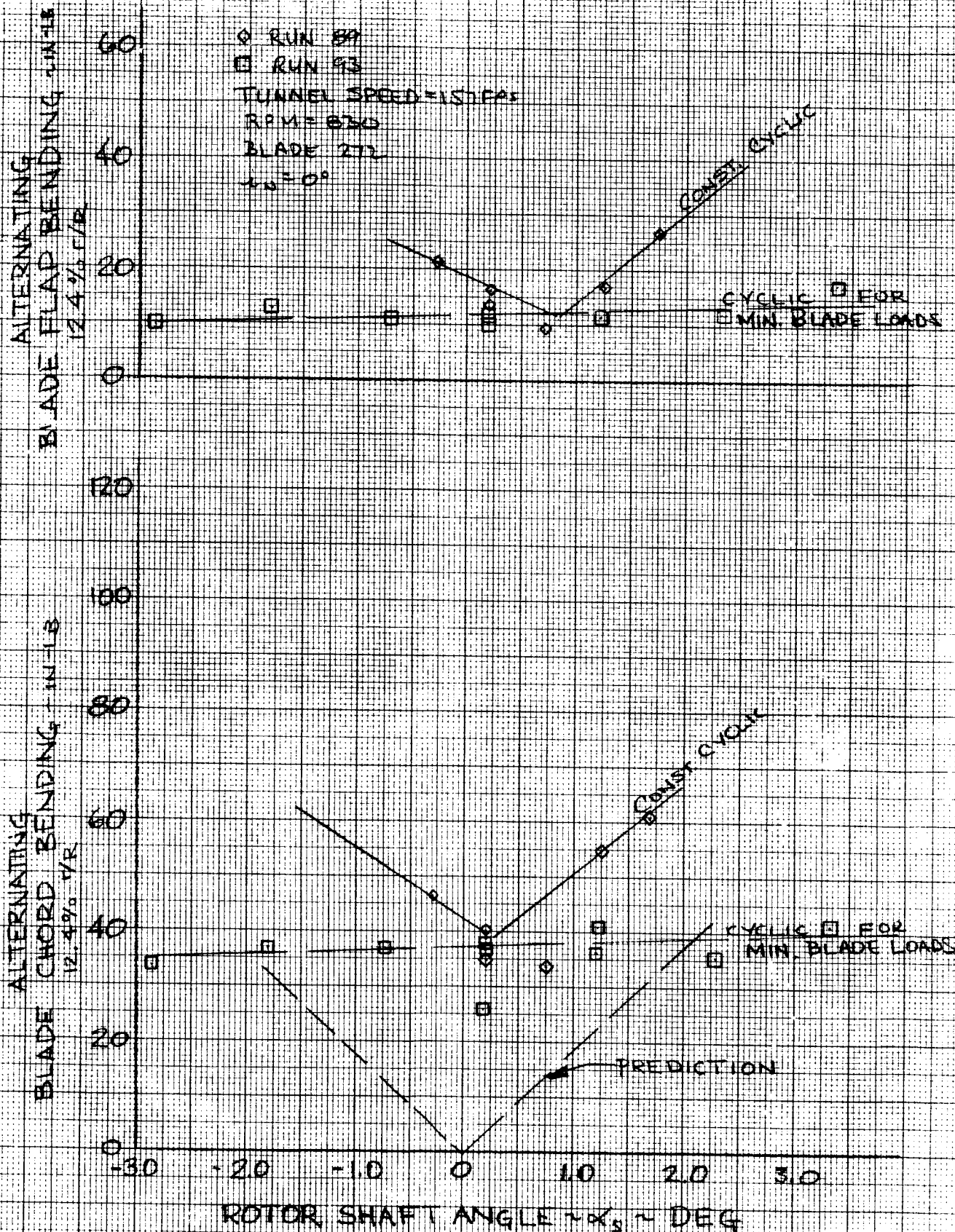


FIGURE 268

CYCLIC REQUIRED TO MINIMIZE BLADE LOADS
AT TUNNEL CRUISE SPEED = 161 FPS
(FULL SCALE EQUIVALENT SPEED = 200 KTS)

RUN 93

 $N_R = 830 \text{ RPM}$

O LEFT ROTOR

□ RIGHT ROTOR

RUN 89

 $N_R = 830 \text{ RPM}$

● LEFT ROTOR

■ RIGHT ROTOR

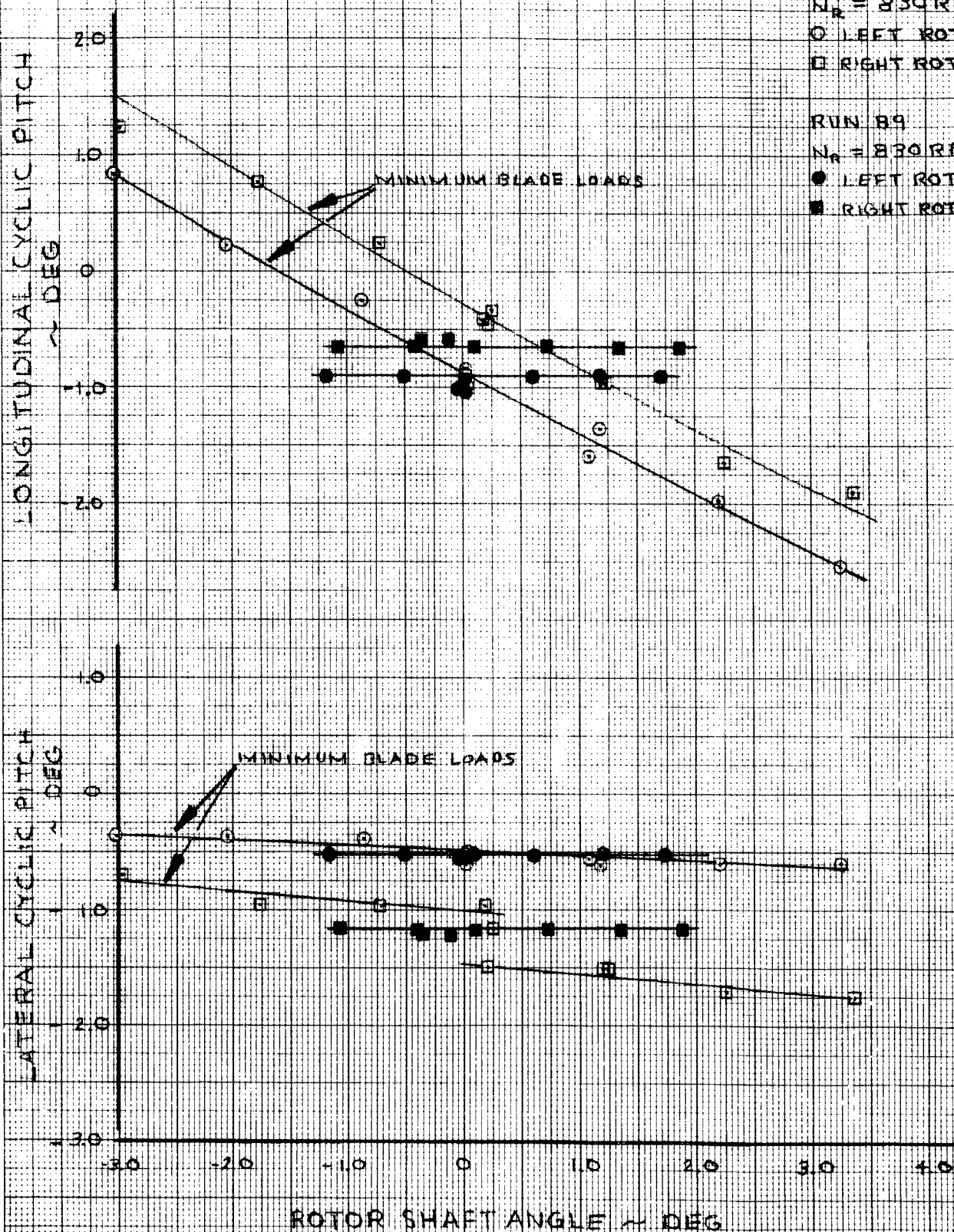


Figure 269

7.0 DYNAMICS

This section discusses the dynamic characteristics of the model and the aeroelastic testing accomplished during this program directed at Objective 9 in Section 2.0. The testing accomplished in cruise and transition is supplemented by some data acquired during the hover checkout. In the following sections, the test data is scaled up to full scale for rapid comparison with the research aircraft, where applicable.

7.1 MODEL FREQUENCIES

The wind tunnel model was designed and fabricated to be a dynamic representation of the Model 222 Tilt Rotor Research Aircraft as it was defined in Reference 1. As a result of meeting some of the more stringent requirements, the model was significantly overweight, 178 lbs as compared a required 122 lbs. Stiffness of the wing-nacelle junction was approximately 45 percent of the requirements as indicated from the deflection data presented in Figure B-14. These two items caused the wind tunnel model to be significantly different than the currently proposed Model 222 and the pedestal mount introduced additional modes that also alter the dynamic characteristics of the model. To establish a configuration definition, it is necessary to obtain the model frequencies. These are presented in the following table.

This data was obtained from static disturbance tests ("bangs and tweaks") on the model without rotor blades mounted on the pedestal in the wind tunnel test section. The current configuration of the Model 222 as defined in Reference 7 is also shown in Table 12 to provide some insight into the difference between this aircraft and the wind tunnel model.

TABLE 12. MODEL FREQUENCIES

Item	Model Frequencies Converted to Full Scale			Full Scale Aircraft Frequencies
	$i_N=0^\circ$	$i_N=45^\circ$	$i_N=90^\circ$	
Wing				
Vertical Bending	2.58	2.70	2.72	3.60
Chord Bending	3.56	3.60	3.62	6.86
Torsion	6.67	6.55	6.97	6.10
Model on Pedestal				
Pitch	3.72			---
Roll	1.30			---
Yaw	1.21			---
Horizontal Stabilizer				
Vertical Bending	13.85			13.5
Vertical Stabilizer				
Lateral Bending	13.2			14.0

NOTES:

1. Static Blade Frequencies are presented in Table 11.
2. Full Scale Frequency = $\frac{\text{Model Frequency}}{2.15}$

7.2 AEROELASTIC STABILITY AND DAMPING

Aeroelastic data and correlation from the 1/4.622 model test are presented in this section. Analytical predictions and test data were obtained in the cruise, hover and transition modes and the figures have all been converted to full scale equivalent parameters. It should be noted that the 1/4.622 scale model is substantially different from the proposed Model 222 and the stand upon which the model was mounted introduced additional modes which significantly altered the dynamic behavior of the model. The result was a model with considerably lower full scale equivalent frequencies than the proposed Model 222. This accounts for the difference in the whirl flutter boundaries (i.e., 360 knots for 1/4.622 scale model and 490 knots proposed Model 222 at 386 rpm) and the shift of the air resonance region into the model operating regime. The correlation between predicted model behavior and test data shown in the following figures, indicates that the analysis is slightly conservative in lightly damped regions and near instabilities but show excellent correlation with the test data. A description of the differences between the 1/4.622 scale model and the proposed Model 222 research aircraft frequencies is contained in Table 12.

7.2.1 Cruise

The predicted cruise aeroelastic stability boundaries are shown in Figure 270 along with the test data. All of the conditions tested were found to be stable and as seen in the figure fall within the region predicted to be stable. At cruise rotor speed (386 rpm) the model was taken up to 236 knots equivalent full scale with no indication of instability. At 90 knots the rotor speed was

increased to hover rpm (551). Figure 271 shows the predicted and test measured damping in the air resonance mode. The test data shows the same trend as the predictions with the predictions being on the conservative side in the region with the least damping.

7.2.2 Hover

Figure 272 shows the predicted coupled frequency spectrum (full scale equivalent) for hover. In hover a resonance problem occurs when the lower blade lag and wing chordwise bending frequencies coalesce. This occurs at a rotor speed of 520 rpm as shown in Figure 272.

The damping in this resonance mode for the same rpm region is shown in Figure 273. An instability in the region of this coalescence is predicted with its onset occurring about 35 rpm ahead of the coalescence. The peak of instability is just about at the coalescent rpm and the model becomes more stable as the frequencies move apart. This instability was encountered during the test. It occurred at about 510 rpm as shown by the data point on Figure 273. This is just 10 rpm lower than the coalescent value which indicates the predictions show less damping for a wider span of rpm and are thus conservative.

7.2.3 Transition

The predicted coupled frequency spectrum is shown in Figure 274 for a nacelle incidence angle of 45 degrees and ninety knots forward speed for a rotor speed sweep. For this case the coalescence of the lower lag mode and both the vertical bending and chordwise bending are potential instabilities. They occur at approximately

475 and 540 rpm respectively as shown in Figure 274. The predicted damping over this range is shown in Figure 275 and shows slight instabilities in the regions of these two coalescences. The test data is also plotted in Figure 275 and shows the predicted damping is conservative in the region of instability. The model was approaching an unstable condition at about 500 rpm which is about 20 rpm above the predicted value.

It should be noted that in the cruise mode the lower blade lag mode couples with the wing vertical bending to produce the air resonance instability. In hover the lag mode couples with wing chord bending. In transition, the tilted nacelle causes large amounts of coupling between the two wing modes so that both of the predicted instability peaks are highly coupled modes, making it hard to justify putting a label on them. This same coupling is probably the reason for the discrepancy between test and predicted damping at the lower rpm.

$\frac{1}{4}$ SCALE MODEL
FULL SCALE DATA
CRUISE STABILITY BOUNDARIES
PREDICTED WITH ACTUAL MODEL FREQUENCIES
 $\alpha = 0^\circ$

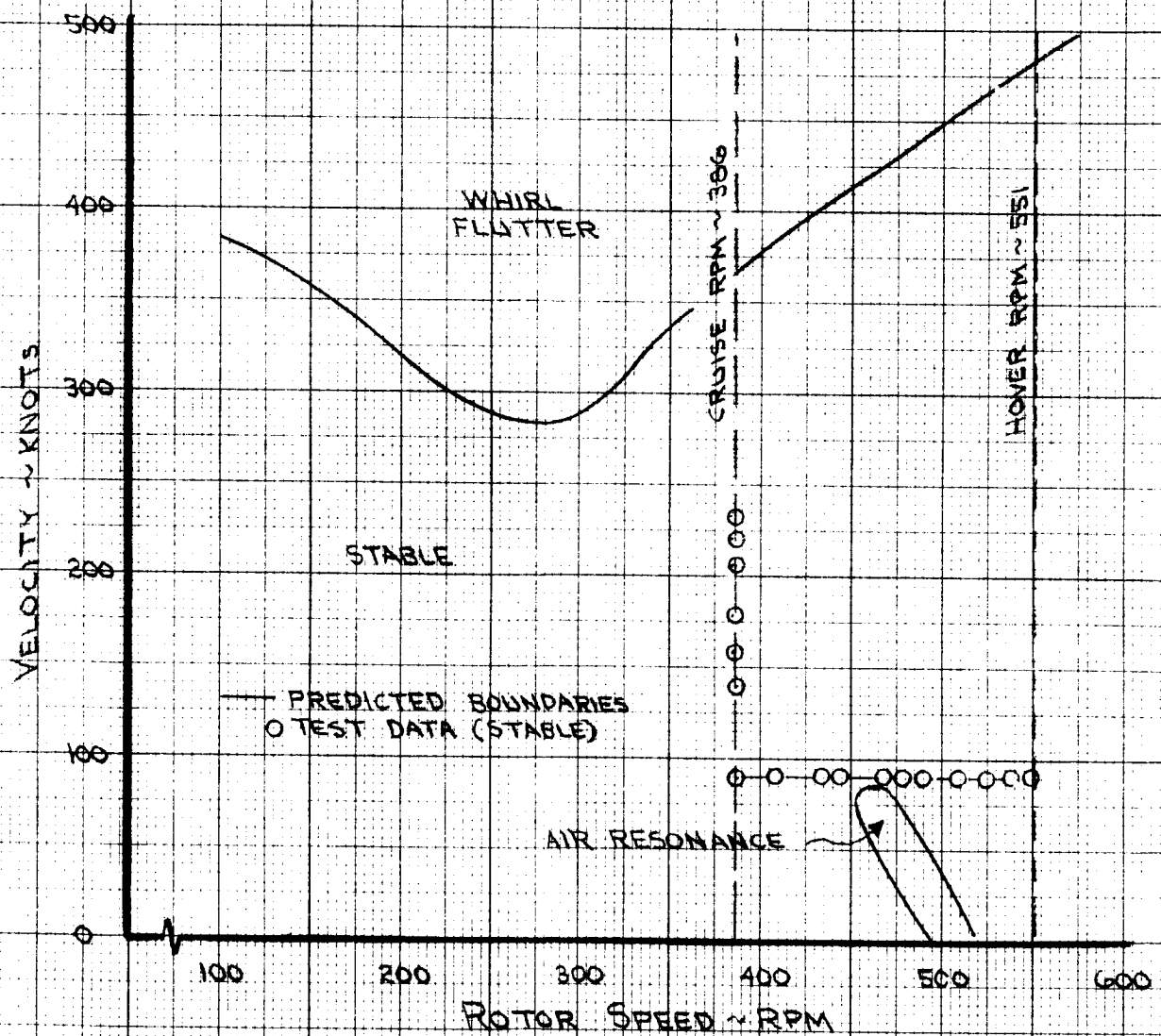


Figure 270

1/4.622 SCALE MODEL
FULL SCALE PARAMETERS
CRUISE
FORWARD SPEED 90 KNOTS
DAMPING IN AIR RESONANCE MODE
 $\alpha_N = 0^\circ$

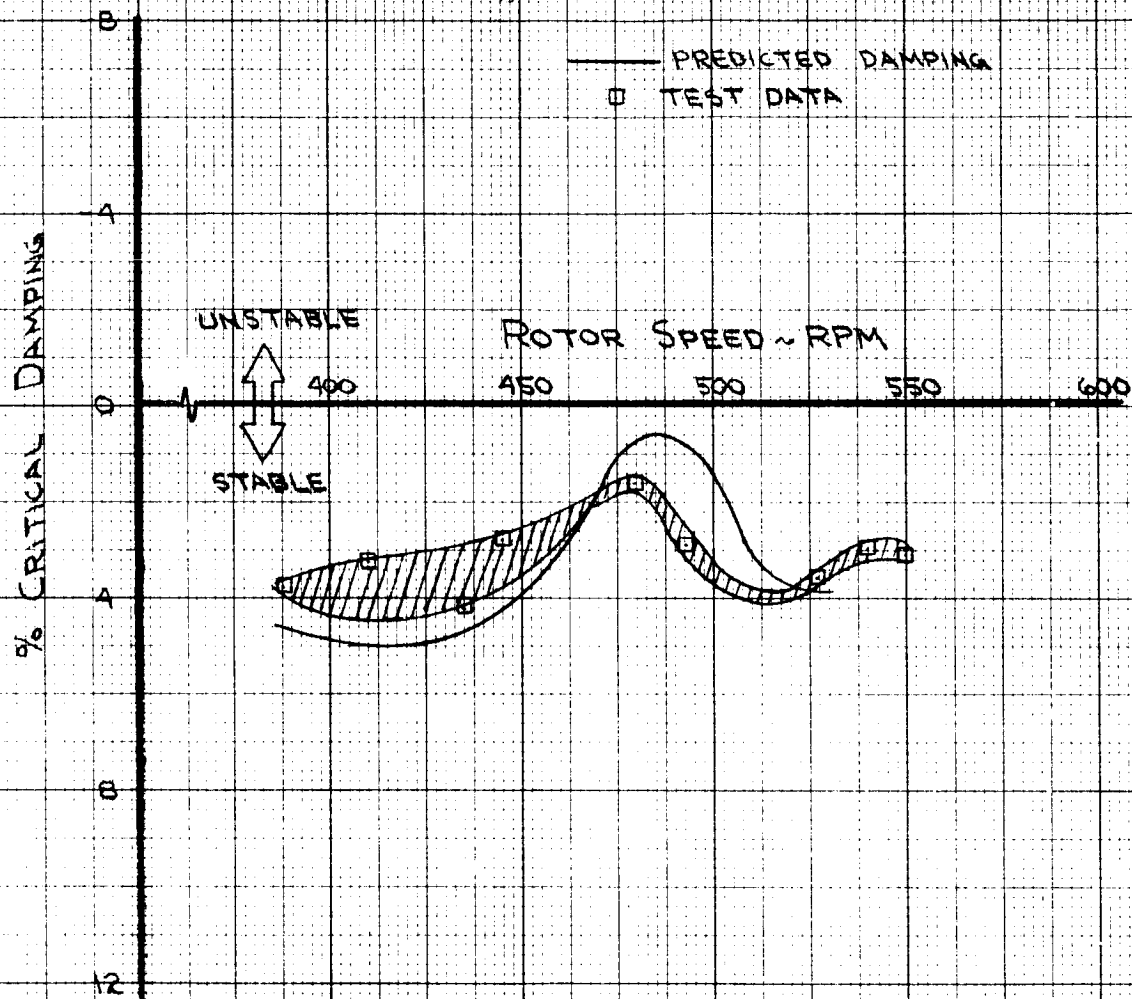


Figure 271

1/4.622 SCALE MODEL
FULL SCALE PARAMETERS
HOVER
PREDICTED COUPLED FREQUENCIES
 $L \approx 90$ DEGREES

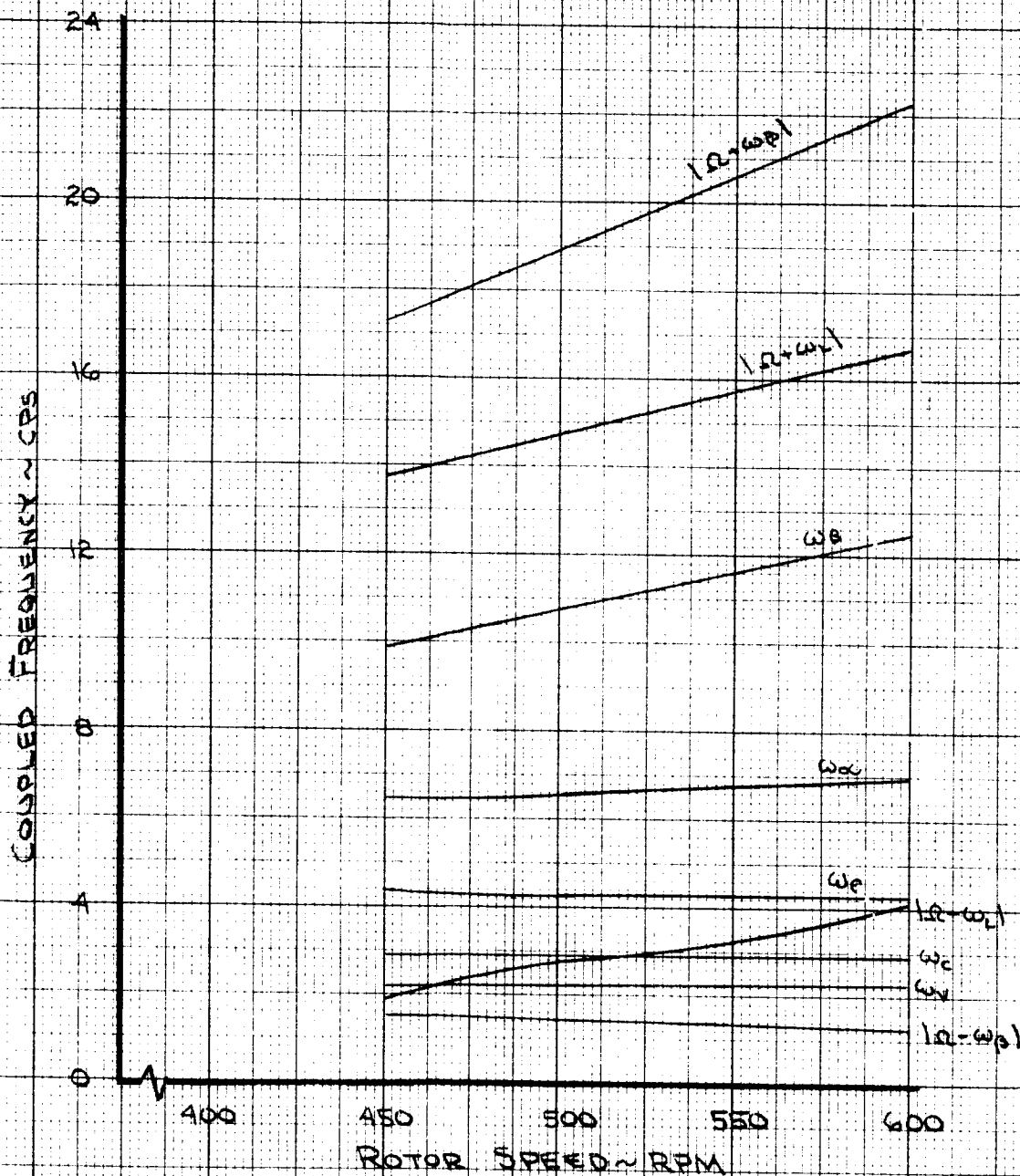


Figure 272

1/4.622 SCALE MODEL
FULL SCALE PARAMETERS
HOVER
DAMPING IN RESONANCE MODE
 $\tau_N = 90^\circ$

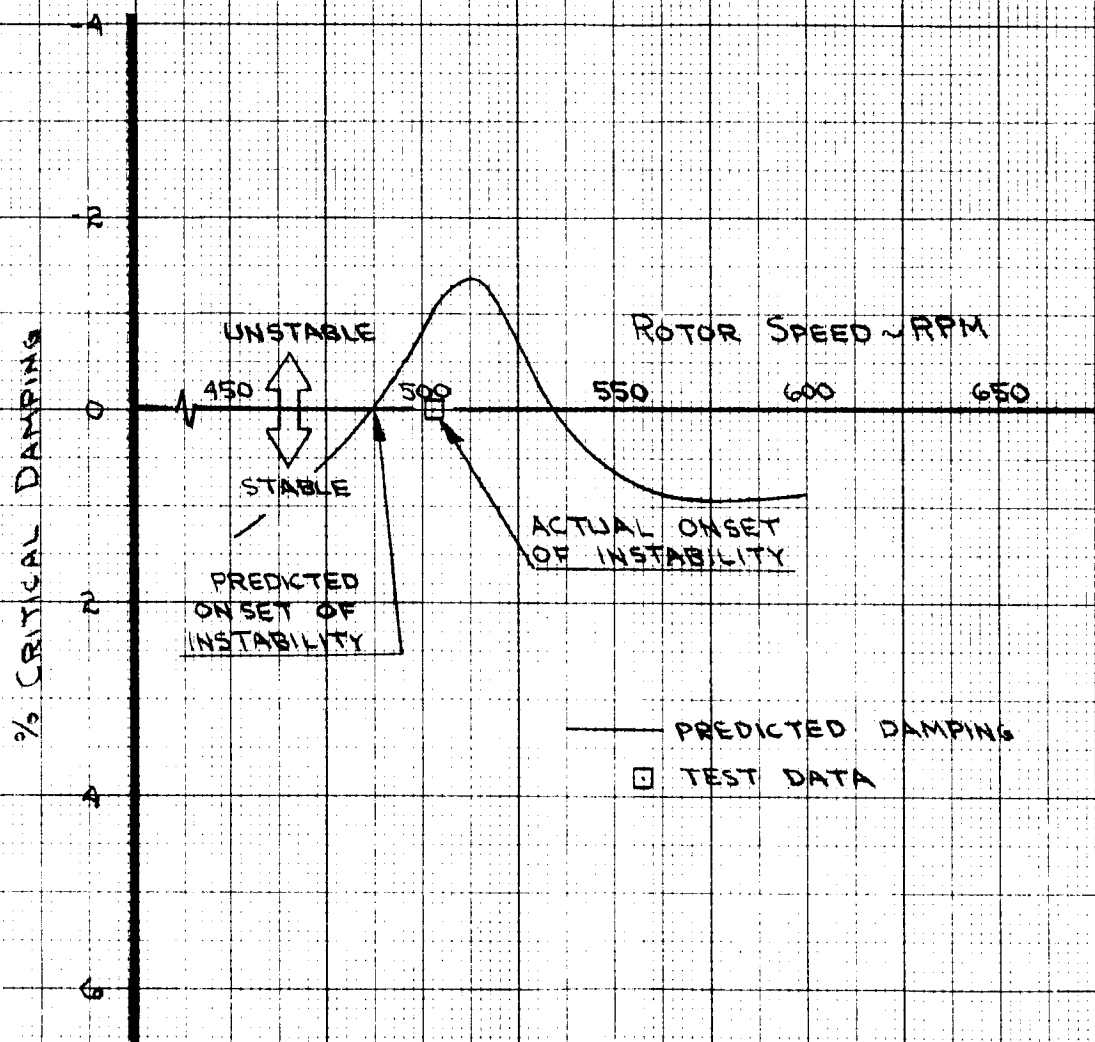


Figure 273

1/4 G22 SCALE MODEL
FULL SCALE PARAMETERS
14745°
FORWARD SPEED 90 KNOTS
DAMPING IN RESONANCE MODE

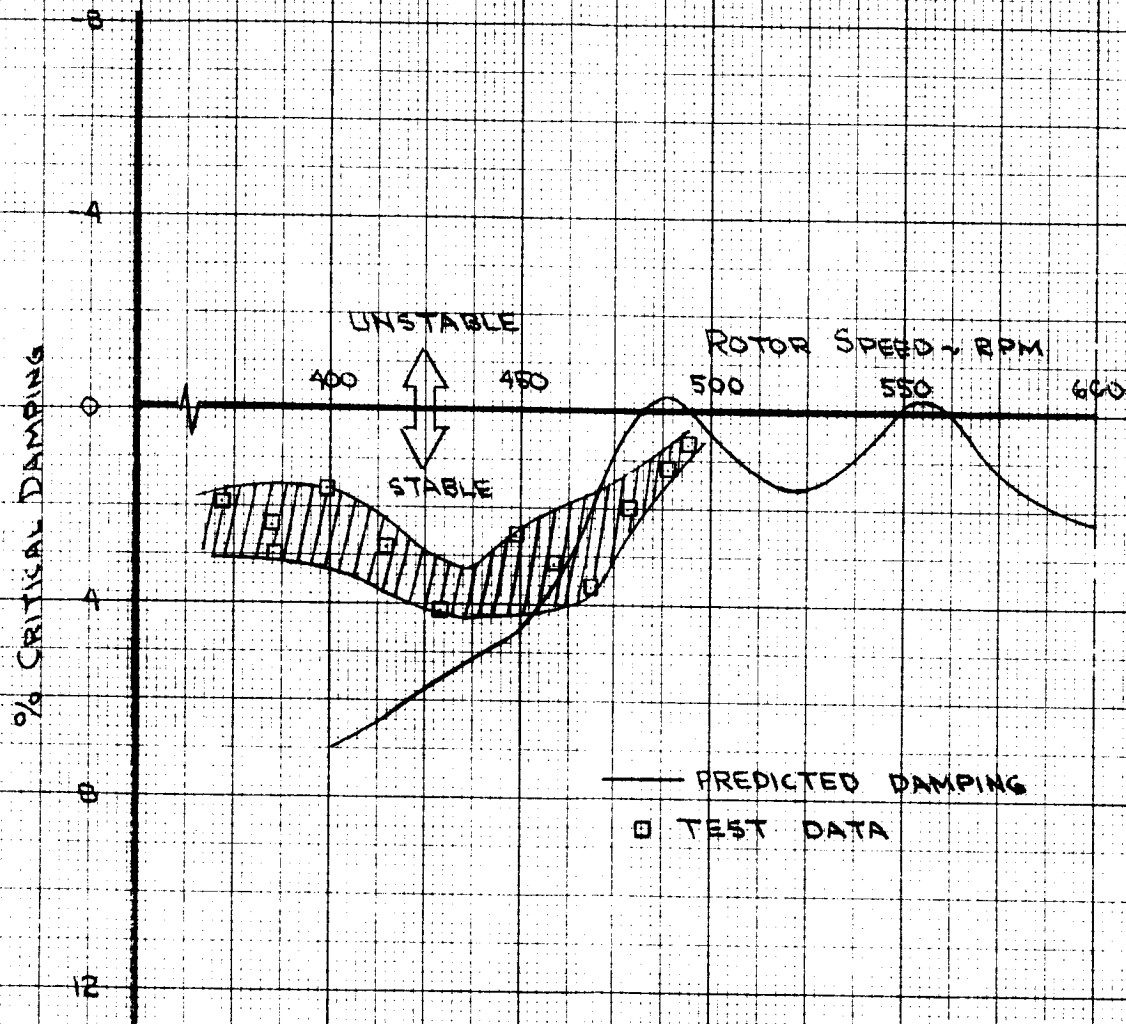


Figure 274

1/4 G22 SCALE MODEL
FULL SCALE PARAMETERS
 $\alpha_N = 45^\circ$
 $V_{FWO} = 90 \text{ KTS}$
COUPLED FREQUENCIES FROM ANALYSIS

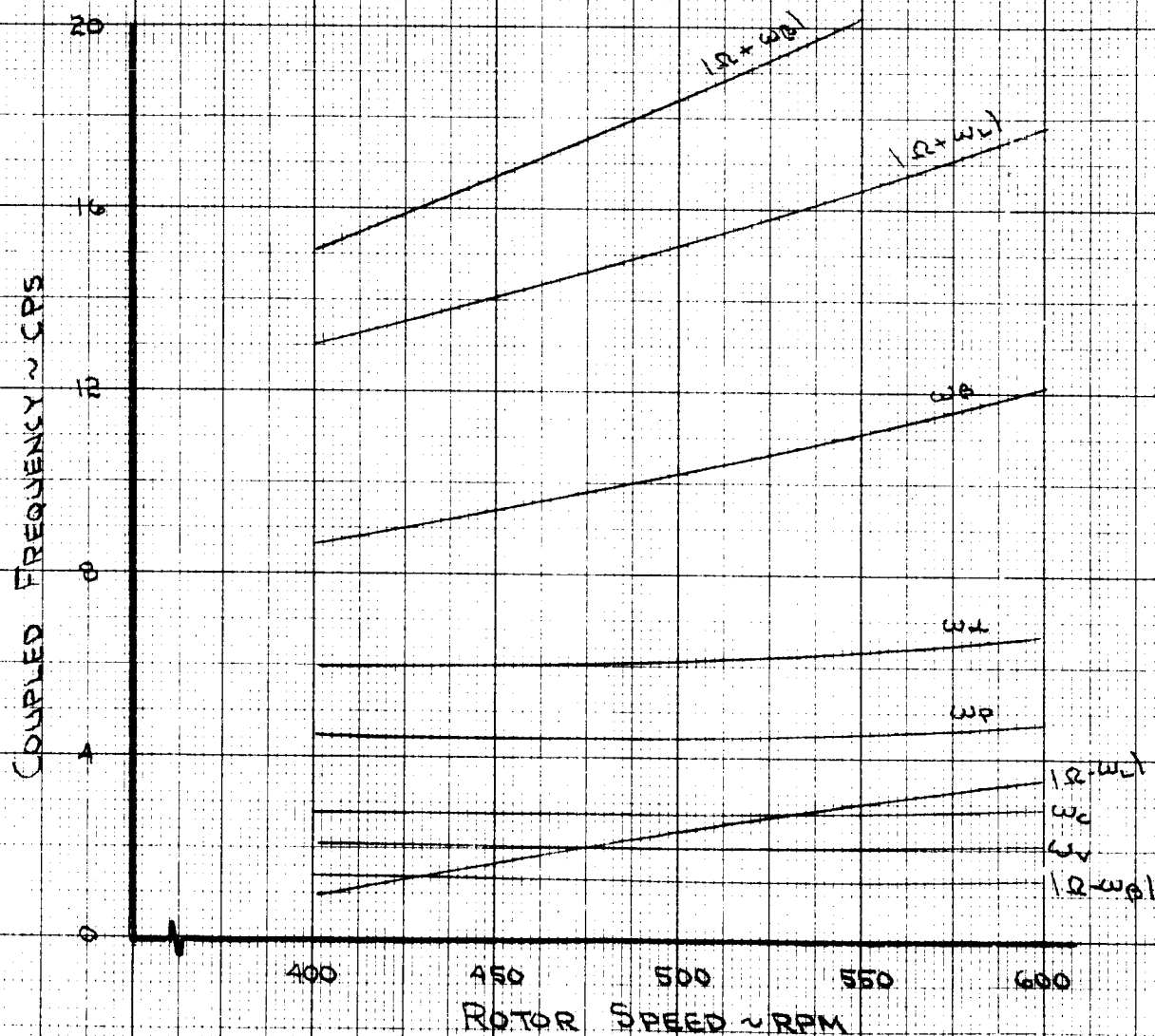


Figure 275

8.0 CONCLUSIONS AND RECOMMENDATIONS

The data analysis performed in this report provides the following conclusions:

1. Rotor performance matches predictions well.
2. Horizontal tail contribution to longitudinal stability is 15% higher than predicted.
3. Vertical tail contribution is the same as predicted.
4. Elevator effectiveness is 17% less than predicted.
5. Rudder effectiveness is as predicted.
6. Rotor control derivatives with lateral cyclic are close to the D-88 predictions. Longitudinal cyclic derivatives are significantly affected by wing/rotor interferences effects.
7. The rotor derivatives with collective are approximately the same as the D-88 predictions.
8. Alternating blade load variation with angle of attack was the same as the D-88 prediction.
9. Owing to numerous areas of poor fairing, especially in the nacelle and wing/fuselage fairing, no valid drag data could be obtained.
10. The model control system did not provide sufficiently positive or accurate control to permit further testing.
This must be changed before further testing of the model.

Recommendations that have been developed from the test program and data analysis are:

1. Define the modifications to the model required to complete Phase 0, I and II testing.

2. Define the source of funding and implement these modifications.

3. Conduct Phase 0, I and II test programs.

Items 1 and 2 have been completed, but the funding of Phase 0, I and II testing have not been provided.

9.0 REFERENCES

1. Preliminary Design of Research Aircraft, Volume II of V/STOL Tilt Rotor Aircraft Study NASA CR 114438, March 1972.
2. D-88 Computer Program Document, D222-10054-1.
3. Wind Tunnel Test of a Powered Tilt Rotor Performance Model; J. P. Magee, et al, AFFDL-TR-71-62, October 1971.
4. USAF Stability and Control DATCOM; Hoak, D. E., dated August 1968.
5. Prop/Rotor Dynamic Derivative Program C41; User Report D21010116-1.
6. Feedback Control Tests on a Windmilling 2.81 foot Diameter Soft-in-Plane Hingeless Tilt Rotor in the Cruise Mode, B. Fry, et al, D222-10047-1, October 1972.
7. Structural Loads and Dynamics Volume III Study of V/STOL Tilt Rotor Research Aircraft Program (Phase I), January 1973.

APPENDIX A - RUN LOG

The following tabulation summarizes the test runs made during the contract testing. Initial checkout and exploratory test runs were made on the company sponsored funding.

The testing includes the following runs:

- 1-16 End to end system check
 (no nacelle fairings)

- 17-39 Complete model with non-aerodynamic nacelle
 fairings in cruise regime

- 40-63 Complete model with non-aerodynamic nacelle
 fairings minus rotor blades in cruise and
 transition regime

- 64-72 Complete model with new nacelle fairings
 minus rotor blades in cruise and transition
 regime

- 73-76 Complete model with new nacelle fairings
 minus rotor blades and horizontal and
 vertical tail in cruise and transition regime

- 77-119 Complete model with new nacelle fairings in
 cruise and transition regime

- 120-121 Complete model with new nacelle fairings minus
 horizontal and vertical tail in cruise regime

[illegible]

PREP.	CHK.	APPR	RUN NO.	CONFIGURATION	TYPE OF RUN	WT. TARE RUN	RPM	g	On R/L deg	R ₁ /B ₁ deg R	R ₂ /B ₂ deg L	ΔB/Δg deg	in deg	DATE / TIME
			3	MODEL ON PEDESTAL			300	0	10/10		0	0	90	9/23/72
			4				300	0	10/10	0/0	0/0	0	90	
			5				300	0	10/10	0/0	0/0	0	90	
			6		5% TBA		300 → 1000	0	5/10	0/0	0/0	0	90	9/25/72
			7				300 → 1100	0	10/10	0/0	0/0	0	90	
			8				300	0	10/10	0/0	0/0	0	90	

T.P. 20 ALL CYCLIC = 0

RUN 3

1/4

SCALE M-222
HOVER CHECKOUT

DATA PT.	8	9	10	11	12	13	14	15	16	17	18	19	20	21	22	23	24	25	26	27	28	29	30	31
A ₁ -RT	0	0	0	0	0	0	0	0	0	0	2L	2R	4R	0	0	0	0	0	0	0	0	0	0	0
B ₁ -RT	0	2A	4A	2A	0	2F	4F	2F	0	0	0	0	0	0	0	0	0	0	2R	4R	2R	2L	4L	2L
A ₁ -L	0	0	0	0	0	0	0	0	0	0	0	0	0	0	0	0	0	0	0	0	0	0	0	0
B ₁ -L	0	0	0	0	0	0	0	0	0	0	0	0	0	0	2A	4A	2A	2F	4F	0	0	0	0	0
Δ ₁₅ R	12	10	10	10	10	10	10	10	10	10	10	10	10	10	10	10	10	10	10	10	10	10	10	10
Δ ₁₅ R	12	10	10	10	10	10	10	10	10	10	10	10	10	10	10	10	10	10	10	10	10	10	10	10

MODEL NEAR TUNNEL FLOOR FOR RUNS 3-5

6. CHECKOUT, TRACK AND BALANCE
SHUT DOWN TO CLEAN UP RPM READOUT.
SHUT DOWN AT 1000 RPM TO INVESTIGATE HAZEL BALANCE SATURATION OF R.M. BOTH ROTORS. DOUBLED THE SENSITIVITY OF R/M BOTH ROTORS.

7. RUN TO INVESTIGATE MODEL BEHAVIOR AT HIGHER RPM - AT 1100 RPM EXPERIENCED A DIVERGENT INSTABILITY - NO DAMAGE

BYWT
104

[illegible]

PREP.		RUN NO.	CONFIGURATION	TYPE OF RUN	WT. TARE RUN	α°/ψ	δ_F°	$\delta_R^{\circ}/\delta_E^{\circ}$	$\delta_E^{\circ}/\delta_R^{\circ}$	ψ°/RPM	i_N°	$\theta_{.75}$	A_1	B_1	C_T	DATE / TIME OF TEST
CHK.	APPR															
		11	MODEL ON PEDESTAL, NO NAC. FRG.	ELEV PWR	11	0/0	0	0/VAR	0/0	2.0/830	0	16	0*	0*	.008	9/27/72
		12	✓	✓	✓	✓	✓	VAR/0	✓	✓	✓	16	✓	✓	✓	✓
		13	✓	✓	✓	✓	✓	0/0	✓	✓	✓	VAR	✓	✓	VAR	✓
		14	✓	✓	✓	✓	✓	-	✓	✓	✓	✓	✓	✓	✓	✓
		15	-	-	✓	0/0	0	-	✓	2.0/830	0	19	0	0	-	✓
		16	✓	✓	✓	0/0	0	✓	✓	VAR/VAR	0	VAR	0	0	.0016	✓
		17	COMPLETE ✓	✓	✓	0/0	0	0/0	0/0	15/830	0	32*	VAR	VAR	.0016	✓
		18	✓	✓	✓	VAR/0	0	0/0	0/0	15/830	0	32	CONST	CONST	✓	✓
		19			✓	0/0	0	0/0	0/0	✓	✓	✓	✓	✓	✓	✓
		20			✓	0/0	0	0/0	0/0	✓	✓	✓	✓	✓	✓	✓

11.	* A ₁ B ₁ SET FOR MIN BLADE LOADS.	0.75	FOR C _T = .008	- 16° (L)	η ⁰ = +10 → -25
12.	✓	✓	✓	✓	δ _R =
13.	C _T SWEEP C _T .004 → .01 / .002			L.H. NAC. SE 100°	STEADY @ .08 →
14.	PITCH SWEEP: ∇ α _B = -10 to +14 BY Δ ⁰ OF 2 DEG.				
15.	□ CYCLIC PITCH SWEEP TO BLADE LOAD ALLOWABLES				
16.	SNUBBERS FROM WING TIPS TO FLOOR. INCREMENTAL RUN TO TEST CONDITION OF q = 15.0 : C _T = .016 RPM = 830.				
17.	SNUBBERS OFF. * θ ₇₅ = 32° FOR C _T = .006 TO REDUCE BLADE LOADS TO MINIMUM. POWER TEMP AND Q LIMIT @ α = +9.			α _B = 0, 2, 4, 6, 8, -2°, -4, -6°	CYCLIC RESET @ EACH α _B
18.	REPEAT OF 17 WITH A CONSTANT CYCLIC PITCH				
19.	▽ YAW SWEEP BY Δ ⁰ OF 1 deg				
20.	▽ ELEVATOR SWEEP Δ ⁰ OF 5 deg. * STARTED BVWT 105 AFTER RUN 16				

1/4 SCALE M-222
PHASE 1 TEST

BYWT
105 *

PREP.	CHK.	APPR.	RUN NO.	CONFIGURATION	TYPE OF TARE RUN	WT. TARE RUN	Q_B	δ_F	δ_R	δ_S	δ_A	δ_{RPM}	i_N	θ_{15}	A_1	B_1	C_T	DATE / TIME
			21	Model on Pedestal	Photo Sweep	17	0%	0	0/40	0%	0%	15/830	0	32	0	0	0	8-27-72
			22		Yaw Sweep	17	0%	-	-	-	-	-	-	-	-	-	-	
			23		Roller Sweep	17	0%	-	0%	-	-	-	-	-	-	-	-	
			24		Pitch Sweep	17	0%	0	20%	-	-	-	-	-	-	-	-	10-2-72
			25		-	17	-	-	-	-	-	-	-	-	-	-	-	
			26		Yaw Sweep	17	0%	-	-	-	-	-	-	-	-	-	-	
			27		A_1 Sweep	17	0%	-	0%	-	-	-	-	-	5	0	-	
			28		Pitch Sweep	17	0%	-	-	-	-	-	-	-	.5	0	-	
			29		Yaw Sweep	17	0%	-	-	-	-	-	-	-	-	-	-	
			30		B_1 Sweep	17	0%	-	-	-	-	-	-	-	0	0	0	

NO	DATA THIS RUN	YAW SWEEP	A_1 SWEEP ON EACH ROTOR INDIVIDUALLY	PITCH SWEEP	Yaw SWEEP	B_1 SWEEP ON EACH ROTOR INDIVIDUALLY
24	NO DATA THIS RUN					
26	2					
27	5					
28	1					
29	2					
30	6					

1/4 SCALE M-222
PHASE 1 TEST

BVWT
105

PREP.	CHK.	APPR	RUN NO.	CONFIGURATION	TYPE OF TARE RUN	WT. OF TARE RUN	$\frac{d\alpha}{dt} \%$	δ_F	$\frac{\delta_k}{\delta_e}$	$\frac{\delta_j}{\delta_g}$	$\frac{Q}{RPM}$	\dot{W}	θ_{ys}	A_i	B_i	C_T	DATE / TIME
			31	MODEL ON PEDESTAL	PITCH SWEEP		$\nabla 0$	0	0	0	15 / 83	0	32	0	1.0	.002	10-2-72
			32		YAW SWEEP		$\nabla 0$	0	0	0	-	-	-	-	-	-	
			33				$\nabla 0$	40	-	-	-	-	-	-	0	-	
			34				$\nabla 0$	40	-	-	-	-	-	-	-	-	
			35				$\nabla 0$	20	-	-	-	-	-	-	-	-	
			36				$\nabla 0$	20	-	-	-	-	-	-	-	-	
			37				$\nabla 0$	10	-	-	-	-	-	-	-	-	
			38				$\nabla 0$	0	-	-	-	8	34	*	*	* .002	
			39				$\nabla 0$	0	-	-	-	8	34	*	*	* .002	

31 ∇ PITCH SWEEP

32 ∇ YAW SWEEP

33 PITCH SWEEP WITH ALL FLAPS SET AT 40°

34 YAW SWEEP WITH ALL FLAPS SET AT 40°

35 FLAP SETTINGS FOR D.P. 1-6 WERE INCORRECTLY SET - POT'S ARE SLIPPING.

~~36~~ PITCH SWEEP WITH ALL FLAPS SET AT 20°

36 YAW SWEEP WITH ALL FLAPS SET AT 20°

38 & 39 A_i & B_i SET TO MINIMIZE BLADE LOADS AT δθ = 0.

BY WT 105

[illegible]

40	1	PITCH SWEEP -14 TO +18
41	2	3 SWEEP 15 TO 35 FUSELAGE CENTER SECTION WAS COMING LOOSE-DOWN TO RETAPE
42	3	REPEAT OF RUN 41 9 SWEEP 15 TO 50 P.S.F
43		ADDED A TRIPPER STRIP TO THE L.E. OF THE WING (1/2 INCH WIDE MASKING TAPE)
	4	8 SWEEP 15 TO 50. LIFT AT A 8=30 WAS 30 LB LESS THAN THAT OF RUN 42. WOT FOR RUN 42 WAS TAKEN AT $d_B = 0$ FOR THIS RUN WOT WAS TAKEN AT $d_B = 0$
44		REMOVED TRIPPER STRIP. WOT RECORDED AT $d_B = 0$ THE LIFT NOW AGREES WITH THAT OF RUN 43. THE TRIPPER STRIP ACTUALLY DECREASED THE WING LIFT.
45	5	YAW SWEEP $\pm 15^\circ$ THE COMPUTER PRINTOUT OF YAW ANGLE IS A FACTOR OF 10/3.28 TOO LOW
46		ELEVATOR SWEEP +10 TO $\pm 25^\circ$
47	6	PITCH SWEEP -14 TO +18

1/4 SCALE M-222

PHASE 1 TEST

BYWT
105

PREP.	CHK.	APPR.	REVISD	DATE	RUN NO.	CONFIGURATION	TYPE OF RUN	WT. TARE RUN	$\dot{\alpha}$ %	$\dot{\delta}_F$	$\frac{\dot{\delta}_F}{\dot{\delta}_E}$	$\frac{\dot{\delta}_F}{\dot{\delta}_A}$	$\frac{\dot{\delta}_F}{RPM}$	$\dot{\alpha}_N$	$\dot{\alpha}_S$	A _i	B _i	C _T	DATE / TIME
					4-8	MODEL ON POSTAL-NO BLADES	YAW SWEEP	17	0	0	0/10	0/0	15/0	0	0	-	-	-	10-3-72
					4-9	OLD NOBLE FAIRINGS	PITCH SWEEP	17	0	0	0/0	0/0	15/0	0	0	-	-	-	
					50		PITCH SWEEP	17	0	0	0/0	0/0	15/0	0	0	-	-	-	
					51		YAW SWEEP	17	0	0	0/0	0/0	15/0	0	0	-	-	-	
					52		FLAP SWEEP	17	0	0	0/0	0/0	15/0	0	0	-	-	-	10-4-72
					53		PITCH SWEEP	17	0	10	0/0	0/0	15/0	0	0	-	-	-	
					54		YAW SWEEP	17	0	10	0/0	0/0	15/0	0	0	-	-	-	
					55		PITCH SWEEP	17	0	20	0/0	0/0	15/0	0	0	-	-	-	
					56		YAW SWEEP	17	0	20	0/0	0/0	15/0	0	0	-	-	-	10/5/72
					57		YAW SWEEP	17	0	20	0/0	0/0	15/0	0	0	-	-	-	

4-8 ∇ YAW SWEEP $\pm 15^\circ$
 4-9 ∇ RUDDER SWEEP $\pm 30^\circ$
 50 ∇ PITCH SWEEP $\pm 15^\circ$
 51 ∇ YAW SWEEP $\pm 15^\circ$
 52 ∇ FLAP ANGLE SWEEP 0 to 60°
 53 ∇ PITCH SWEEP -14 TO 71°
 54 ∇ YAW SWEEP $\pm 15^\circ$
 55 ∇ PITCH SWEEP 0 to -14 THEN MODEL WOULD NOT PITCH UP DOWN TO TROUBLESHOOT
 56 REPEAT RUN 55. $\alpha_0 = 0, -4, -8, -10, -12, -14, 0, 4, 8, 10, 12, 14$ $\alpha_{STALL} 10^\circ$
 57 ψ SWEEP $\pm 15^\circ$

1/4 SCALE M-222
PHASE I TEST

BVWT
105

PREP.	CHK.	APPR	RUN NO.	CONFIGURATION	TYPE OF RUN	WT. TARE RUN	$\frac{d\beta}{\psi}$	δ_F	$\frac{\delta_F}{\delta_E}$	$\frac{\delta_F}{\delta_A}$	$\frac{g}{rpm}$	i_N°	θ_{15}°	A°	B°	C_T	DATE / TIME
			58	MODEL ON PEDISTAL - NO BLADES	PITCH SWEEP		$\frac{0}{0}$	40	$\frac{0}{0}$	$\frac{0}{0}$	13	0	-	-	-	-	10-5-72
			59	" " " "	PITCH SWEEP		$\frac{0}{0}$	40	$\frac{0}{0}$	$\frac{0}{0}$	13	0	-	-	-	-	"
			60	" " " "	PITCH SWEEP		$\frac{0}{0}$	40	$\frac{0}{0}$	$\frac{0}{0}$	13	0	-	-	-	-	"
			61	" " " "	PITCH SWEEP		$\frac{0}{0}$	0	$\frac{0}{0}$	$\frac{0}{0}$	16	0	-	-	-	-	"
			62	" " " "	PITCH SWEEP		$\frac{0}{0}$	0	$\frac{0}{0}$	$\frac{0}{0}$	15	8	-	-	-	-	"
			63	" " " "	PITCH SWEEP		$\frac{0}{0}$	0	$\frac{0}{0}$	$\frac{0}{0}$	15	8	-	-	-	-	"
			64	Model on Pedestal - New Nac. Cover - No Blade Sweep	PITCH SWEEP	64	$\frac{0}{0}$	0	$\frac{0}{0}$	$\frac{0}{0}$	15	0	-	-	-	-	10-6-72
			65	" " " "	PITCH SWEEP		$\frac{0}{0}$	0	$\frac{0}{0}$	$\frac{0}{0}$	15	0	-	-	-	-	"
			66	" " " "	PITCH SWEEP		$\frac{0}{0}$	20	$\frac{0}{0}$	$\frac{0}{0}$	15	0	-	-	-	-	"

58 ∇ PITCH SWEEP.
59 REPEAT OF RUN 58.
60 ∇ YAW SWEEP.
61 ∇ PITCH SWEEP.
62 ∇ PITCH SWEEP.
63 ∇ YAW SWEEP.
64 NEW NACELLE COVERS ∇ PITCH SWEEP
65 ∇ ROLL POWER SWEEP @ INBD. FLAP = 0
66 ∇ SAME ROLL POWER SWEEP WITH INBD. FLAP (LIR) = +20°
[BAD AF (BAL) DRIFT AT TP 15]

$\delta_{SL} = 0, 5, 10, 20, 30, 40, 45, 25, 0$; $\delta_{A_k} = RT$ OUTBD. FLP. = 0, 5, 10, 15, 20, 10, 0;
(δ_{AL}, δ_{SR}) = (0, 0), (5, -7.5), (10, -15), (12.5, -20), (15, -26), (17.5, -34), (20, -45), (15, -26), (10, -15), (5, -7.5), (0, 0)

1/4 SCALE M-222
PHASE 1 TEST

BYWT
105

PREP.	CHK.	APPR.	REVIS	DATE	RUN NO.	CONFIGURATION	TYPE OF RUN	WT. TARE RUN	α_0 / ψ_0	δF	$\delta \epsilon / \delta E$	$\delta \epsilon / \delta A$	δ / mm	i_N	θ_{25}	A, B, C _T	DATE / TIME
					67	Model on Pedestal - New Nuc. Cover - No Blade	PITCH SWEEP	64	$\nabla 0$	0	0/0	45/20R	15/0	0	-	-	10-6-72
					68	✓	YAW SWEEP	✓	0/0	0	✓	✓	✓	✓	-	-	✓
					69	✓	PITCH SWEEP	69	$\nabla 0$	40	✓	✓	6/0	45	-	-	✓
					70	✓	YAW SWEEP	✓	0/0	✓	✓	✓	✓	✓	-	-	✓
					71	✓	PITCH SWEEP	✓	$\nabla 0$	40	✓	0/0	✓	✓	-	-	✓
					72	✓	YAW SWEEP	✓	0/0	✓	✓	✓	✓	✓	-	-	✓
					73	Model on Pedestal - New Nuc. - No Blade - No Tail	PITCH SWEEP	73	$\nabla 0$	✓	✓	✓	✓	✓	-	-	✓
					74	✓	YAW SWEEP	✓	0/0	✓	✓	✓	✓	✓	-	-	✓
					75	✓	PITCH SWEEP	75	$\nabla 0$	0	✓	✓	15/0	0	-	-	✓
					76	✓	YAW SWEEP	✓	0/0	0	✓	✓	15/0	0	-	-	✓

67 ∇ PITCH SWEEP
 68 ∇ YAW SWEEP
 69 ∇ PITCH SWEEP
 70 ∇ YAW SWEEP
 71 ∇ PITCH SWEEP
 72 ∇ YAW SWEEP
 73 ∇ PITCH SWEEP, VERTICAL & HORIZONTAL TAILS OFF, STRAKES ON
 74 ∇ YAW SWEEP
 75 ∇ PITCH SWEEP
 76 ∇ YAW SWEEP

BVWT
105

PREP.	CHK.	APPR	RUN NO.	CONFIGURATION	TYPE OF RUN	WT. TARE RUN	$\delta\phi/\phi$	$\delta\phi$	$\delta\phi/\delta\phi$	$\delta\phi/\delta\phi$	ϕ/kpm	ϕ	ϕ_{15}	A ₁	B ₁	C _T	DATE / TIME
			77	MODEL ON PERISTAL NEW NMC CURETS	PITCH SWEEP	17	∇	0	0%	0%	13/830	0	33	*	*	017	10-10-72
			78		YAW SWEEP	17	∇	0	0%	0%	15/830	0	33	*	*	017	-
			79		CHECK RUN	17	∇	0	0%	0%	0/30	0	33	0	0	-	-
			80		PITCH SWEEP	17	∇	0	0%	0%	13/830	0	33	*	*	017	10-11-72
			81		YAW SWEEP	17	∇	0	0%	0%	15/830	0	33	*	*	017	-
			82		-	-	-	-	-	-	-	-	-	-	-	-	-
			83		PITCH SWEEP	17	∇	0	0%	0%	22/830	0	38	*	*	017	-
			84		YAW SWEEP	17	∇	0	0%	0%	22/830	0	38	*	*	017	-
			85		-	17	-	0	0%	0%	22/830	0	38	-	-	-	10-12-72
			86		PITCH SWEEP	17	∇	0	0%	0%	22/830	0	38	*	*	017	10-12-72
77 ∇ PITCH SWEEP * A ₁ AND B ₁ SET TO GIVE MINIMUM BLADE LOADS AT $\phi_B = 0$																	
78 ∇ YAW SWEEP																	
79 CHECK RUN																	
80 PITCH SWEEP CYCLIC SHAKE AT $\phi = 15$																	
81 YAW SWEEP																	
82 NO DATA																	
83 ∇ PITCH SWEEP INCLUDING CYCLIC SHAKE AT ϕ OF 165, 18, 20 & 22																	
84 ∇ YAW SWEEP																	
85 NO DATA - HARD OVER ON L/H LAT. CYCLIC-EMERGENCY SHUT DOWN.																	
86 ∇ PITCH SWEEP																	
															BYWT 105		

	NO	DATA	LOST	C.B	AT	DC	S/H	26C
49-						12.4%		

PREP.	CHK.	APPR	RUN NO.	CONFIGURATION	TYPE OF TARE RUN	WT. TARE RUN	$\frac{dF}{dp}$	$\frac{dF}{dE}$	$\frac{dF}{dA}$	$\frac{R}{RPM}$	θ_{75}	A _i	B _i	C _T	DATE / TIME
			95	MODEL ON PEDISTAL-NEW MAX. COVERS	SWEEP	17	0	0	0	VARY	0	*	*	015	10-13-72
			96	✓ - - - - -	-	17	0	0	0	VARY	0	*	*	019	-
			97		SWEEP	17	0	0	0	VARY	0	*	*	-	-
			98		YAW SWEEP	17	0	0	0	37.6	0	*	*	-	-
			99		A _i SWEEP	17	0	0	0	37.6	0	*	*	-	-
			100	✓ - - - -	8 th RPM	17	0	0	0	VARY	0	*	*	022	10-16-72

* CYCLICS SET FOR MIN. BLADE LOADS

95,96 SE SHAKE AT 7th 15, 19, 23, 27, 31, 35, 39

AT 8=39 LH θ_{75} MOVED FROM 47 TO 34 RESULTING IN A N
EMERGENCY SHUT DOWN.

97 8 SWEEP TO 37.6 PSF, SE SHAKE AT 37.6

✓ PITCH SWEEP AT 37.6

98 ✓ YAW SWEEP

99 ✓ A_i SWEEP

100 ✓ 8 SWEEP FROM 15 TO 6 PSF WITH RPM SET AT 830
THEN RPM SWEEP FROM 830 TO 1185 WITH 8 = 6 PSF.

SE SHAKE AT EACH DATA PT. FREQUENCIES OF SHAKE AT
3 AND 4.75 NR.

BYWT
105

PREP.	CHK.	APPR	REVISD	DATE	DATE / TIME	B ₁ CT	A ₁	θ ₁₅	i _N	g / RPM	δ ₁ / δ _A	δ ₁ / δ _E	δ ₁ / δ _F	δ ₁ / δ _ψ	WT. TARE RUN	TYPE OF RUN	CONFIGURATION	RUN NO.
					10-17-72	* .022	*	14	30	6 / 1185	0 / 0	0 / 0	30	0 / 0	17	PITCH SWEEP	MODEL ON PEDSTAL-NEW MAC. COVERS	101
					- - -	* .022	*	12	30	6 / 1185	0 / 0	0 / 0	45	0 / 0	69	YAW SWEEP	- - -	102
					- - -	* .022	*	12	45	VARY	0 / 0	0 / 0	45	0 / 0	69	YAW SWEEP	- - -	103
					10-18-72	* .022	*	13	45	6 / 1185	0 / 0	0 / 0	40	0 / 0	69	PITCH SWEEP	- - -	104
					- - -	* .022	*	13	45	6 / 1185	0 / 0	0 / 0	40	0 / 0	69	YAW SWEEP	- - -	105
					- - -	* .022	*	13	45	6 / 1185	0 / 0	0 / 0	40	0 / 0	69	YAW SWEEP	- - -	106
					- - -	* .022	*	13	45	6 / 1185	0 / 0	0 / 0	40	0 / 0	69	YAW SWEEP	- - -	107
					- - -	* .022	*	13	45	6 / 1185	0 / 0	0 / 0	40	0 / 0	69	YAW SWEEP	- - -	108
					- - -	* .022	*	13	45	6 / 1185	0 / 0	0 / 0	40	0 / 0	69	YAW SWEEP	- - -	109
					- - -	* .022	*	13	45	6 / 1185	0 / 0	0 / 0	40	0 / 0	69	PITCH SWEEP	- - -	110

* CYCLIC SET TO GIVE MINIMUM BLADE LOADS AT $\alpha_B = 0$

101 ∇ PITCH SWEEP WITH δ_E SHAKE

102 ∇ YAW SWEEP AT $\alpha_B = 0$ AND α_B SWEEP AT $\psi = 0$, δ_E SHAKE DURING THE α_B SWEEP.

103 THIS RUN WAS TO DEFINE % CRITICAL DAMPING AS A FUNCTION OF δ AND RPM. THE DAMPING WAS ZERO AT RPM = 1085, $\delta = 5.1$ PSF

104 SWEEP FROM 30 TO 45° WITH δ_E SHAKE THEN PITCH SWEEP.

105 ∇ YAW SWEEP

106 δ_S R/H SIDE SWEEP THEN δ_A L/H SWEEP THEN BOTH δ_S R/H AND δ_A L/H SWEEP PER SCHEDULE.

107 ∇ B₁ SWEEP

108 ∇ A₁ SWEEP

109 DIFFERENTIAL θ_{15} SWEEP WITH * L/H CT = 0.017 AND R/H = 0.018 AT $\alpha_B = 0$

110 ∇ PITCH SWEEP

BVWT
105

PREP.	CHK.	APPR	RUN NO.	CONFIGURATION	TYPE OF RUN	WT. TARE RUN	$\frac{d\phi}{dt}$	$\frac{d\delta}{dt}$	$\frac{d\epsilon}{dt}$	$\frac{d\gamma}{dt}$	$\frac{d\alpha}{dt}$	$\frac{d\beta}{dt}$	$\frac{d\gamma}{dt}$	$\frac{d\delta}{dt}$	$\frac{d\epsilon}{dt}$	$\frac{d\gamma}{dt}$	$\frac{d\delta}{dt}$	$\frac{d\epsilon}{dt}$	$\frac{d\gamma}{dt}$	$\frac{d\delta}{dt}$	$\frac{d\epsilon}{dt}$	DATE / TIME
			111	MODEL ON PEDestal NEW NAC. COVERS	Pitch SWEEP	69	0	40	0	0	0	0	0	0	0	0	0	0	0	0	0	10-18-72
			112	" " " " " "	YAW SWEEP	69	0	40	0	0	0	0	0	0	0	0	0	0	0	0	0	"
			113	" " " " " "	PITCH	✓	0	40	0	0	0	0	0	0	0	0	0	0	0	0	0	"
			114	" " " " " "	YAW SWEEP	✓	0	40	0	0	0	0	0	0	0	0	0	0	0	0	0	"
			115	" " " " " "	"	✓	0	40	0	0	0	0	0	0	0	0	0	0	0	0	0	"
			116	" " " " " "	SE SWEEP	✓	0	40	0	0	0	0	0	0	0	0	0	0	0	0	0	"
			117	" " " " " "	PITCH SWEEP	✓	0	30	0	0	0	0	0	0	0	0	0	0	0	0	0	"
			118	" " " " " "	"	✓	0	20	0	0	0	0	0	0	0	0	0	0	0	0	0	"
			119	" " " " " "	"	✓	0	20	0	0	0	0	0	0	0	0	0	0	0	0	0	"

** DIFFERENTIAL CYCLIC L/H B, AFT R/H B, FWD (IC ROTAR																						
111 TIP PLANE TILT) DIFFERENTIAL ϕ_{75} L/H AT CT = .027 AND																						
R/H AT CT = .018 AT $\alpha_B = 0$																						
✓ PITCH SWEEP																						
112 SAME A, B, AND ϕ_{75} SETUP AS FOR RUN 111																						
✓ YAW SWEEP.																						
113 SAME A, B, AND ϕ_{75} SETUP AS FOR RUN 111 ALSO																						
δ_3 R/H = 45° AND δ_A L/H = 20°																						
✓ PITCH SWEEP																						
114 SAME AS RUN 113 FOR A, B, ϕ_{75} , δ_3 , AND δ_A																						
✓ YAW SWEEP																						
115 SAME AS RUN 114																						
✓ YAW SWEEP, A, B, ϕ_{75} , δ_3 , AND δ_A SAME AS RUN 114																						
116 SAME AS RUN 114																						
✓ SE SWEEP, A, B, ϕ_{75} , δ_3 , AND δ_A SAME AS RUN 114																						
117 SAME AS RUN 114																						
✓ PITCH SWEEP (118 AND 119 DATA N.G.) 2H ϕ_{75} A, B, GREEP																						

FORM 49510 (3/70)

APPENDIX B - DEFLECTION TESTS

A limited amount of model deflection data was obtained from testing with the model installed on the pedestal in the wind tunnel test section. Deflection measurements were made from supports set on the fixed ground plane which was composed of four by eight sheets of one-inch thick plywood supported at four foot intervals. This mounting allowed the floor to be extremely flexible, hampering the deflection tests and in some instances inducing spurious errors in the test results. This appendix presents the test results for each major section of the model.

Wing

Wing flapwise deflections due to wing lift, rotor normal force and rotor pitching moment are shown in Figures B-1 through B-5. This data shows that the wing vertical stiffness of the model is less than the design value by approximately 20%.

The wing chordwise deflections due to rotor thrust in the cruise mode indicate the chordwise stiffness is much less than the design value, as shown in Figure B-6. However, if the same deflection data for a 40-pound thrust load is plotted versus wing station as shown in Figure B-7, it can be seen that the wing chord stiffness was equal to the design value when the motion of the total model on the pedestal is

The wing torsional deflection due to rotor normal force, rotor pitching moment and rotor thrust, as shown in Figures B-8 through B-12, show the wing torsional stiffness to be slightly greater than the design stiffness.

Rotor

The rotor disc rotations due to rotor pitching moment and rotor normal force, as shown in Figures B-13 through B-19, indicate the total nacelle pitch stiffness to be approximately one-half the design stiffness.

Rotor disc deflections due to rotor yawing moments and rotor side force are shown in Figures B-20 through B-25. There are no design values for comparison with this test data.

Fuselage and Pedestal Mount

Additional deflection data on the model fuselage pitch and roll were used in calculating model pitch and roll stiffness on the pedestal support. The model pitch stiffness is 3240 inch-pounds/degree. The model roll stiffness is 3700 inch-pounds/degree. A lateral stiffness of the model on the pedestal of 1030 pounds/inch was determined from deflection data.

The deflection data was used in determining the angular deflections shown in the table on the next page. These angular deflections were used in the data reduction program for the fuselage and nacelle balances to determine for each test point the actual rotor shaft angle and fuselage pitch angle.

ANGULAR DEFLECTIONS

NACELLE INCIDENCE					
ITEM	RESULTING FROM	DESIGNATION	$i_N=0$	$i_N=45^\circ$	$i_N=90^\circ$
Rotor Disc	Rotor Normal Force	$\partial \alpha / \partial NF$	0.04°/LB	0.0525°/LB	0.075°/LB
	Rotor Pitching Moment	$\partial \alpha / \partial PM$	0.0061°/INLB	0.0061°/INLB	0.0061°/INLB
	Rotor Thrust	$\partial \alpha / \partial T$	-0.0025°/LB	-0.0025°/LB	0
	Rotor Side Force	$\partial \psi / \partial SF$	0.018°/LB	0.018°/LB	0.018°/LB
	Rotor Yawing Moment	$\partial \psi / \partial YM$	0.00262°/INLB	0.00238°/INLB	0.00275°/INLB
	Wing Lift per Semispan	$\partial \alpha / \partial L$	0.00215°/LB	0.00215°/LB	0.00215°/LB
	Wing Drag per Semispan	$\partial \alpha / \partial D$	0	0	0
	Wing Pitching Moment per Semispan	$\partial \alpha / \partial M$	0.000938°/INLB	0.000938°/INLB	0.000938°/INLB
Wing	Rotor Normal Force	$\partial \alpha / \partial NF$	0.0095°/LB	0.0095°/LB	0.0095°/LB
	Rotor Pitching Moment	$\partial \alpha / \partial PM$	0.000938°/INLB	0.000938°/INLB	0.000938°/INLB
	Rotor Thrust	$\partial \alpha / \partial T$ @ Wingtip	-0.00196°/LB		
		α @ mid Semispan	-0.00163°/LB		
	Wing Lift per Semispan	$\partial \alpha / \partial L$	0.00215°/LB	0.00215°/LB	0.00215°/LB
	Wing Drag per Semispan	$\partial \alpha / \partial D$	0	0	0
	Wing Pitching Moment per Semispan	$\partial \alpha / \partial M$	0.000938°/INLB	0.000938°/INLB	0.000938°/INLB

DEFLECTION TEST

WING DEFLECTION DUE TO WINGLIFT

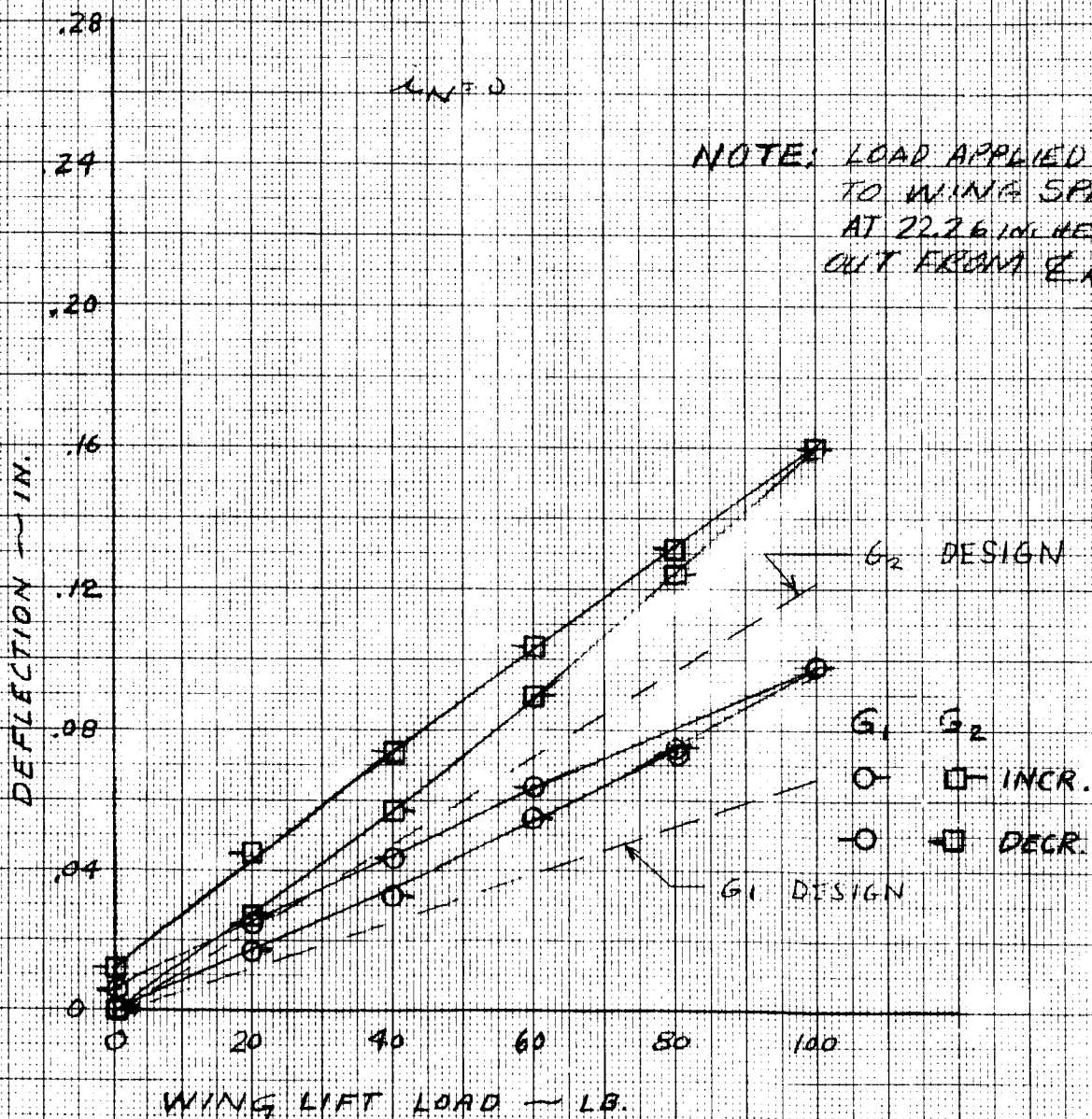
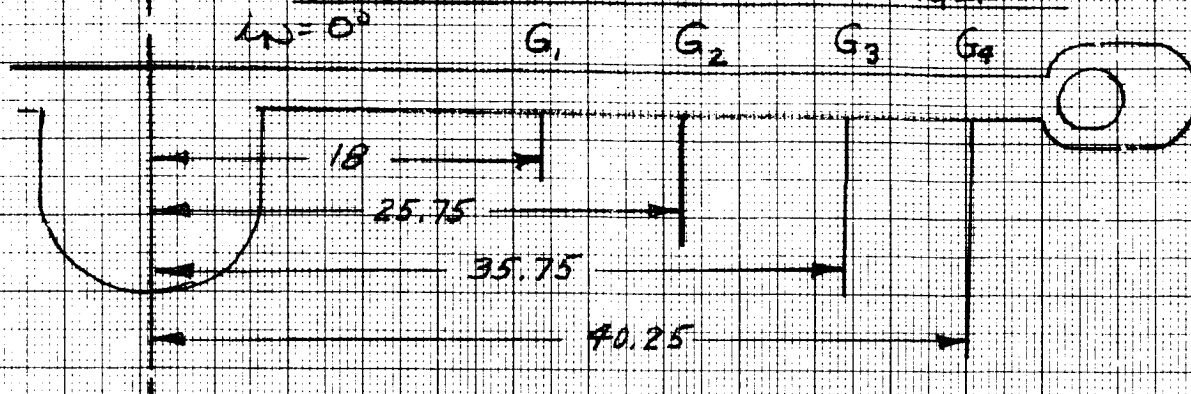


Figure B1

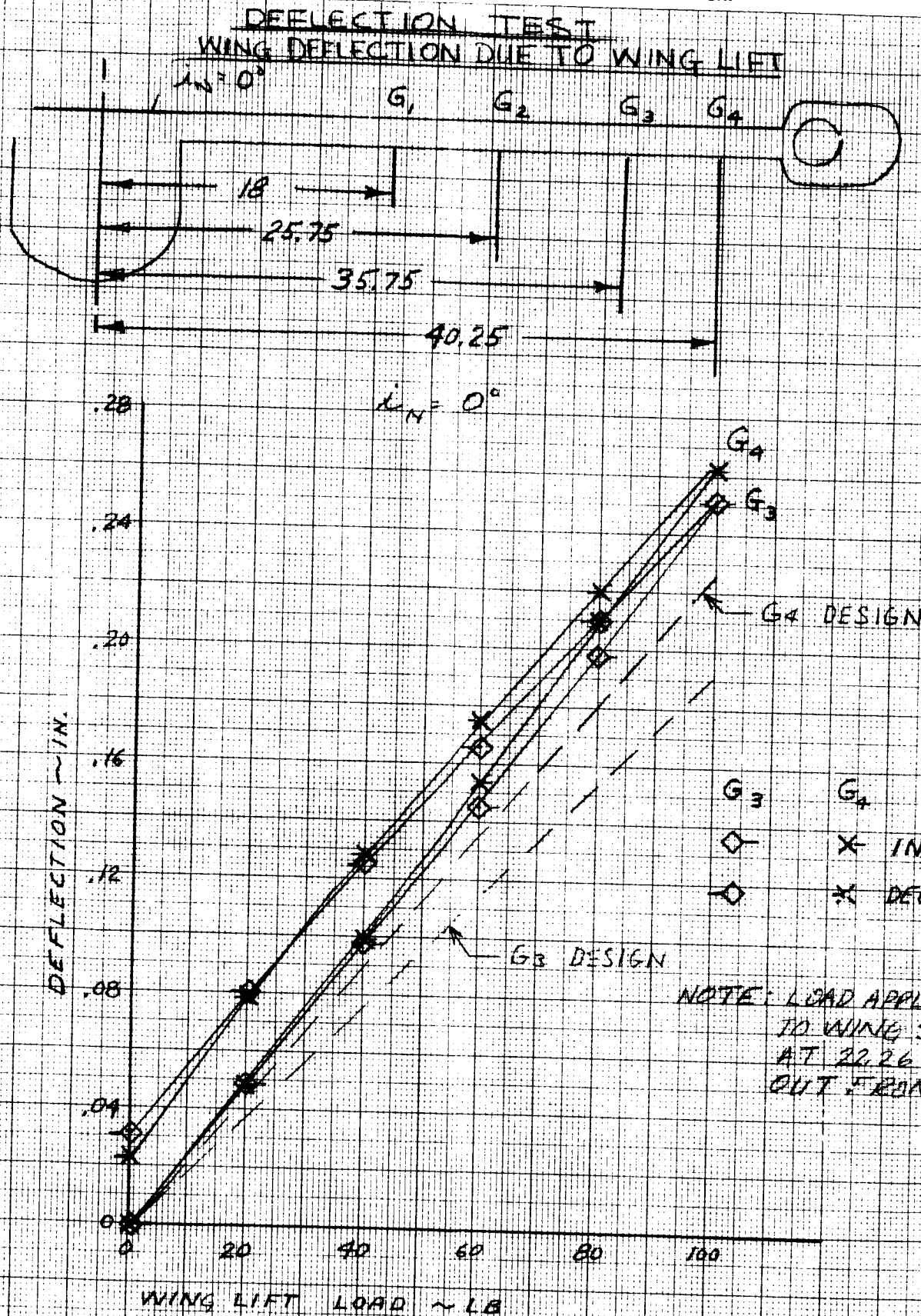


Figure B2

DEFLECTION TEST

WING DEFLECTIONS DUE TO ROTOR NORMAL FORCE

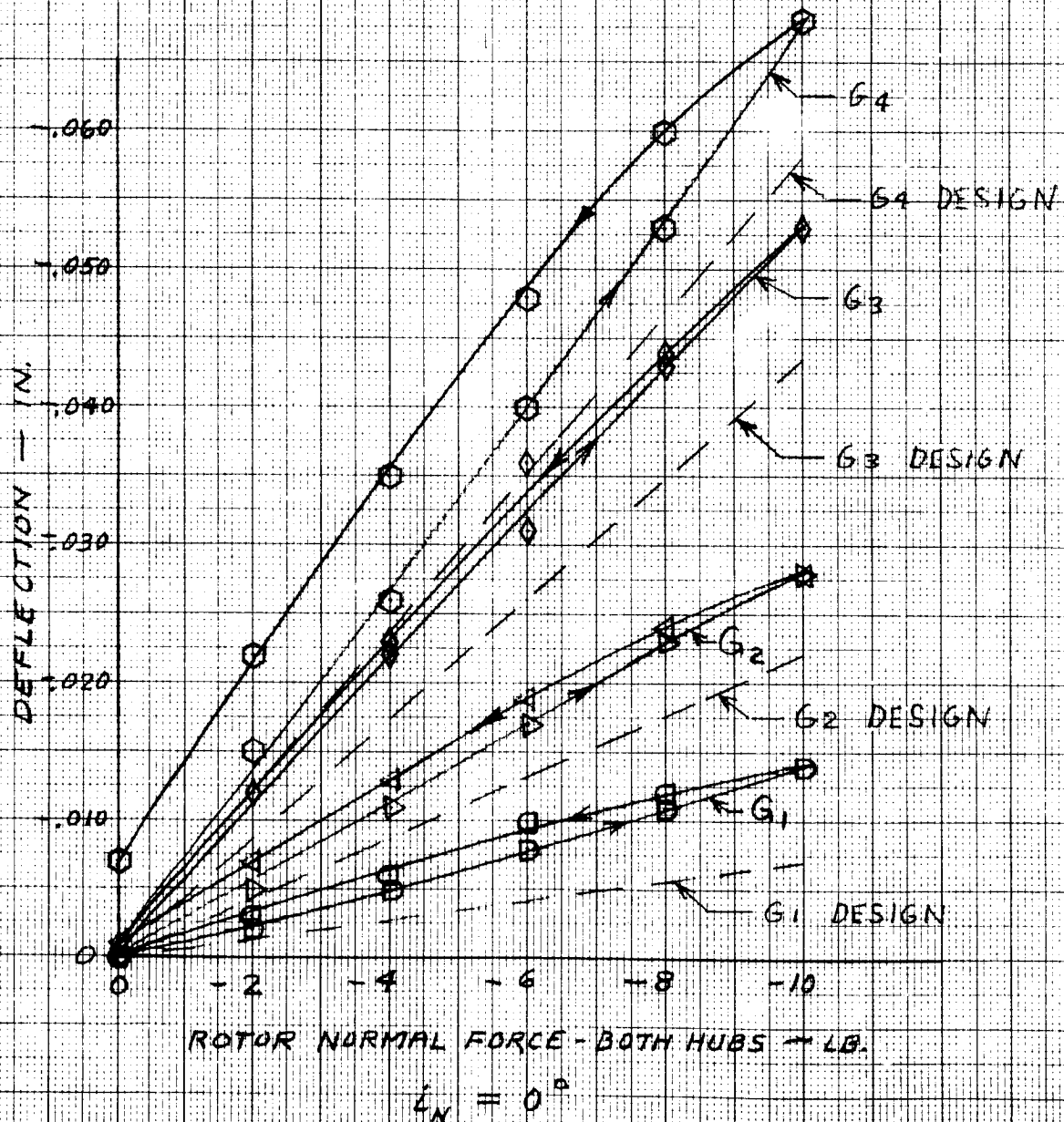
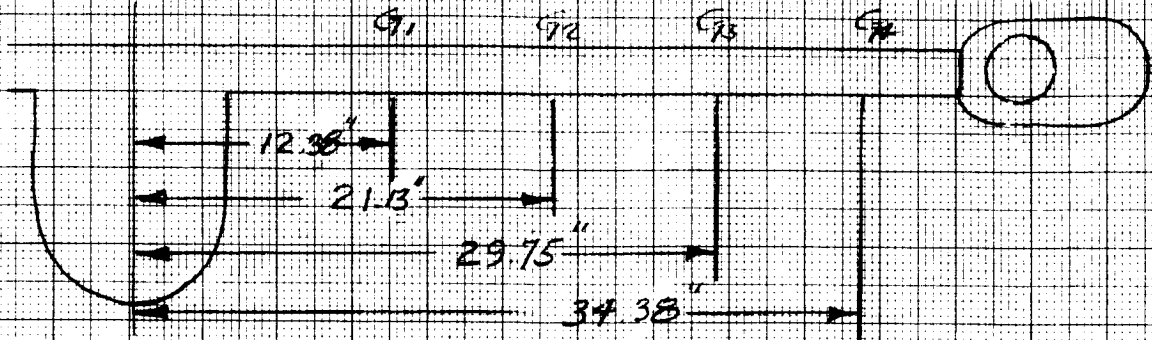
 $\alpha_N = 0^\circ$ 

Figure B3

DEFLECTION TEST WING DEFLECTION DUE TO ROTOR NORMAL FORCE

$i_N = 45^\circ$

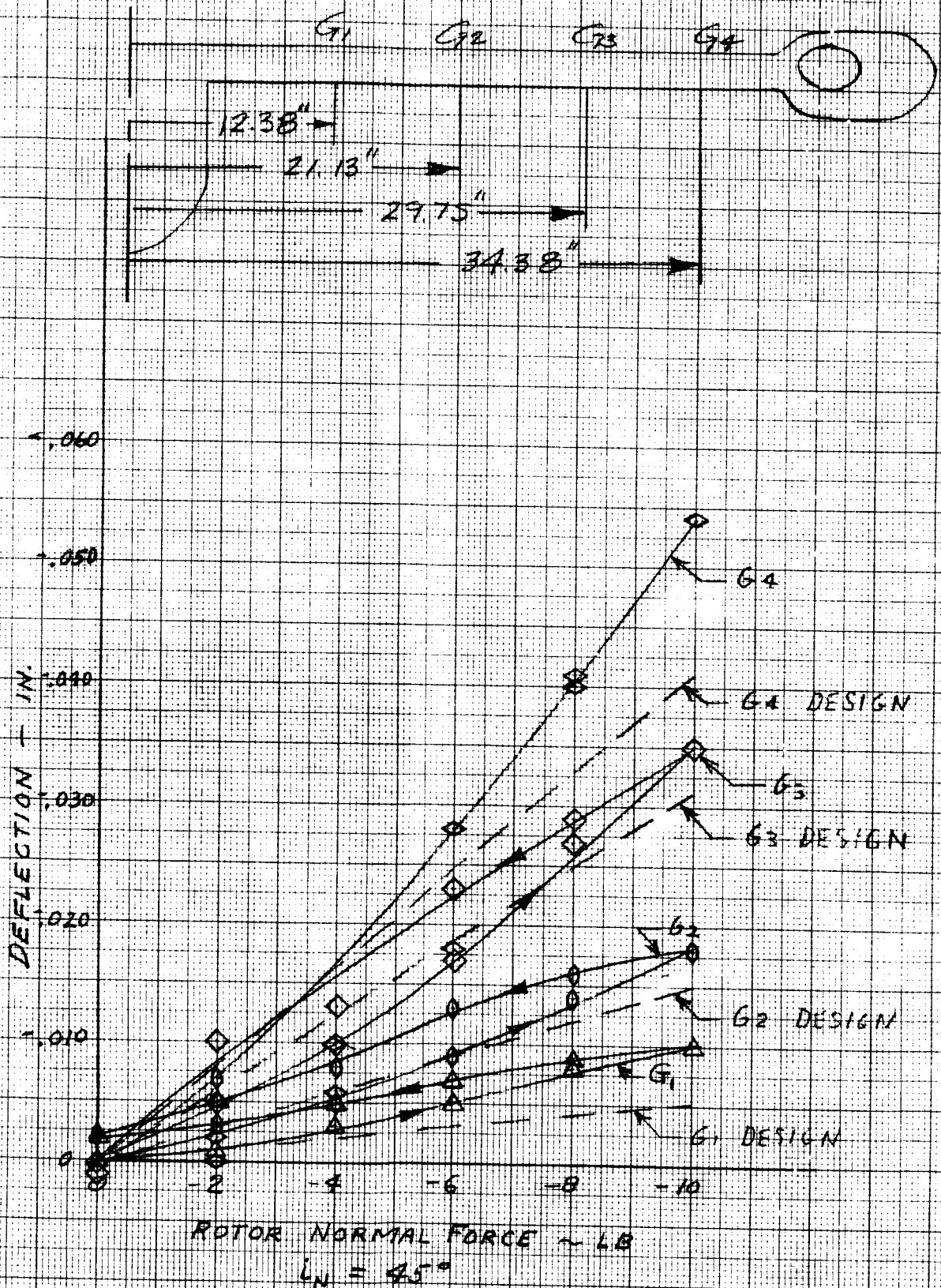


Figure B4

DEFLECTION TEST WING DEFLECTION DUE TO ROTOR PITCHING MOMENT

$$\alpha_N = 0^\circ$$

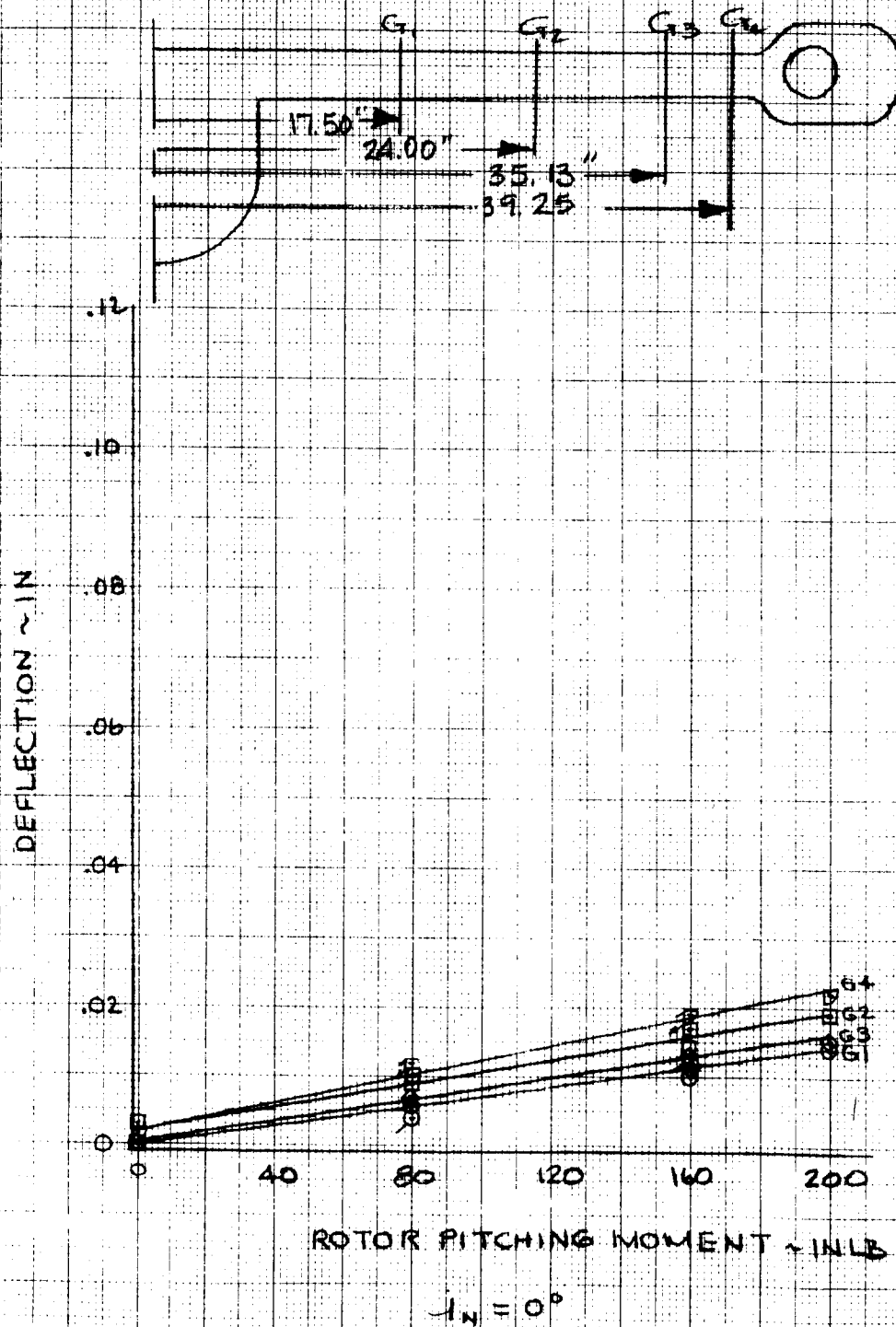


Figure B5

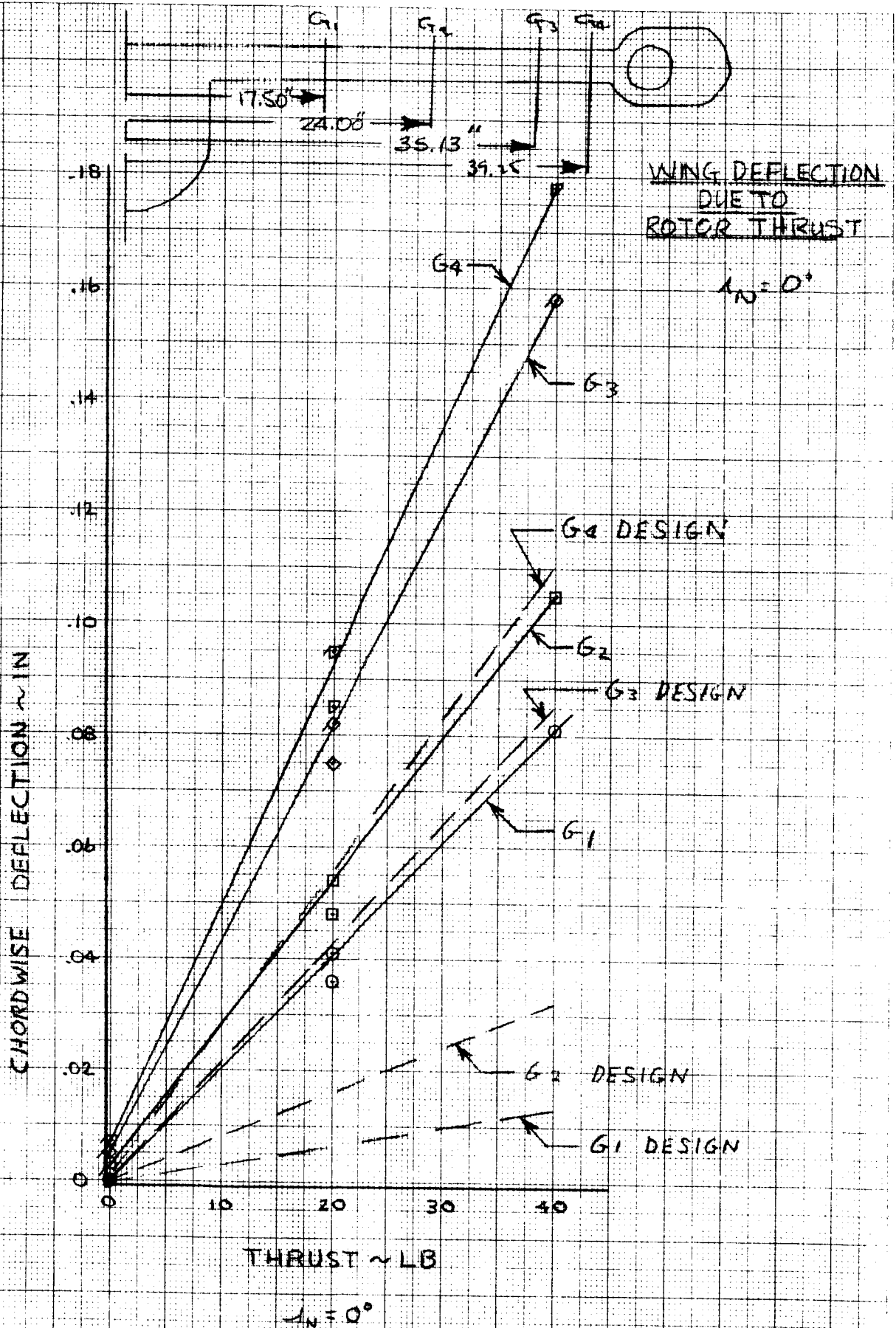


Figure B6

MODEL 222

WING CHORDWISE DEFLECTIONS WITH 40# ROTOR THRUST

 $\alpha = 0^\circ$

CHORDWISE DEFLECTION - INCHES

TEST

DESIGN

DEFLECTION OF MODEL
ON PEDESTAL SUPPORT

WING STATION - INCHES

Figure B7

DEFLECTION TEST

WING ROTATION DUE TO ROTOR NORMAL FORCE

$$\alpha_N = 0^\circ$$

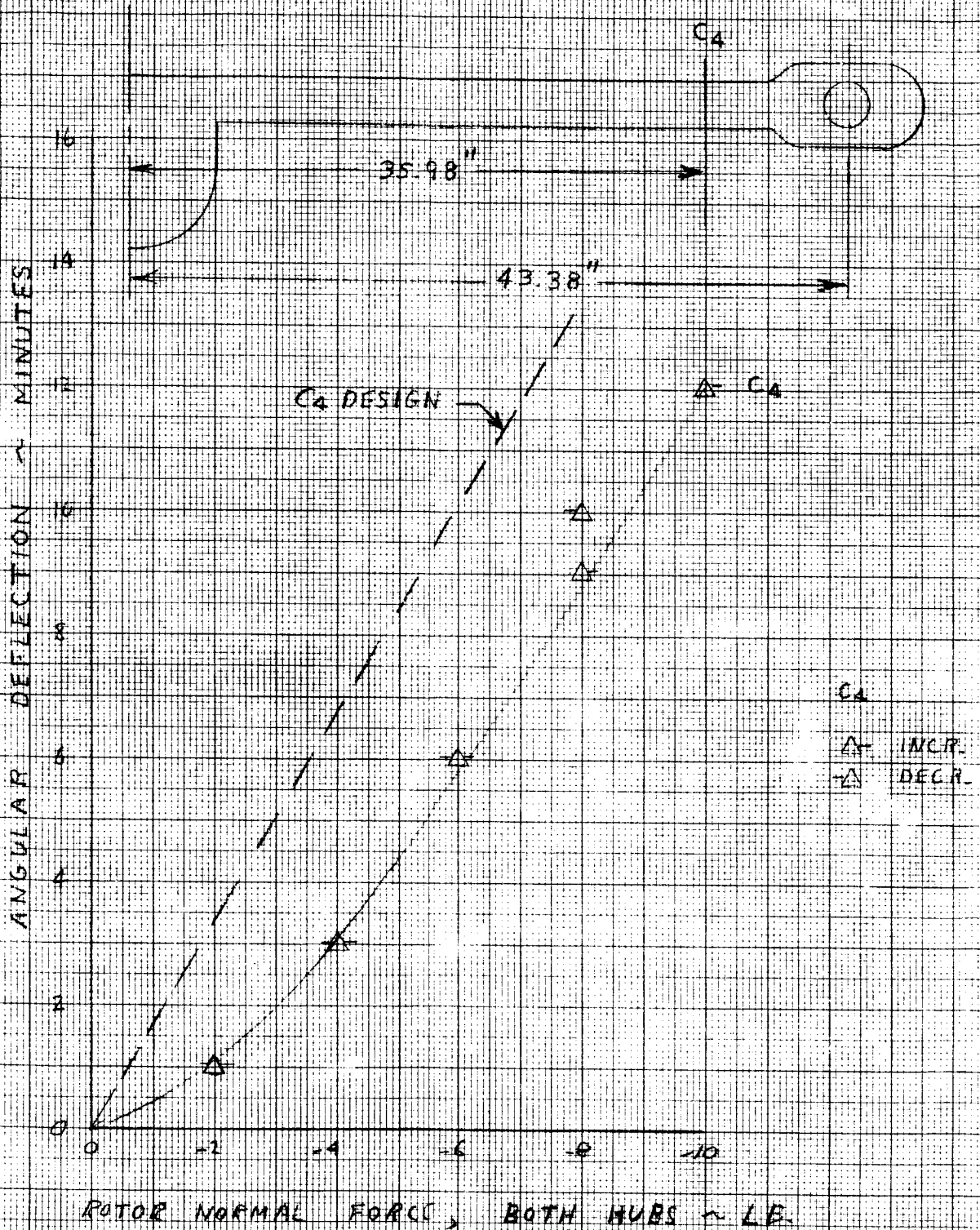


Figure B8

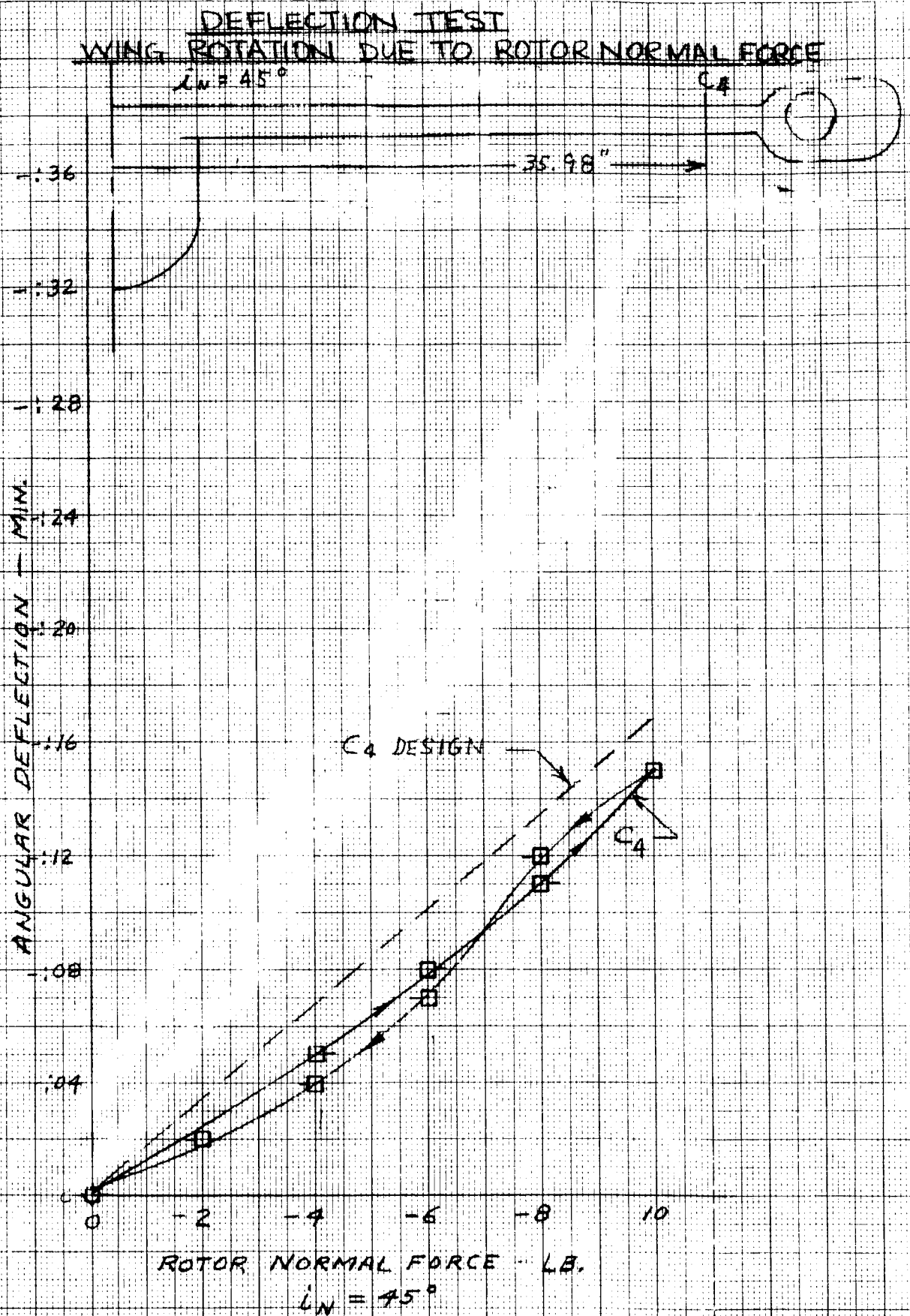
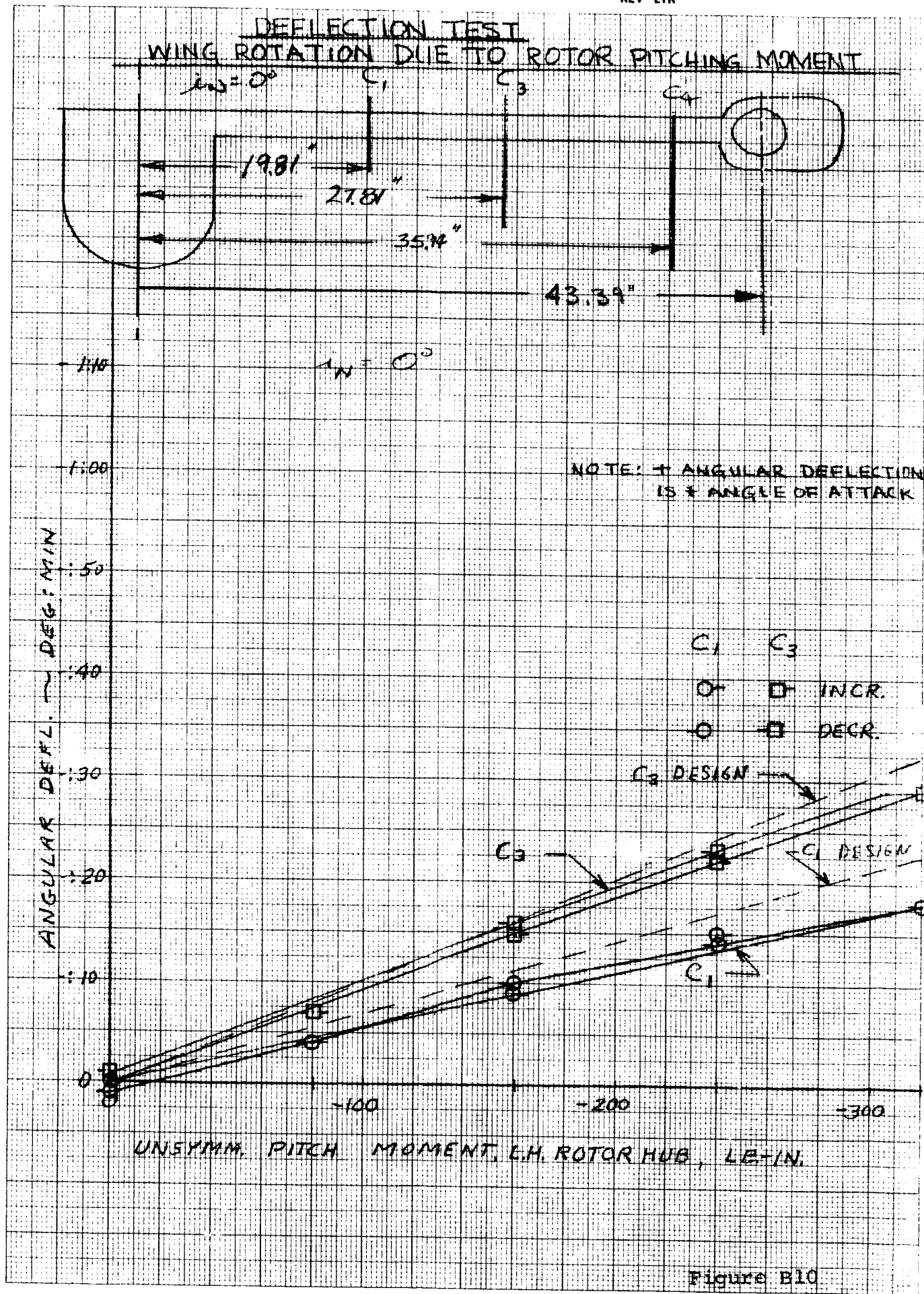


Figure B9



DEFLECTION TEST

WING ROTATION DUE TO ROTOR PITCHING MOMENT

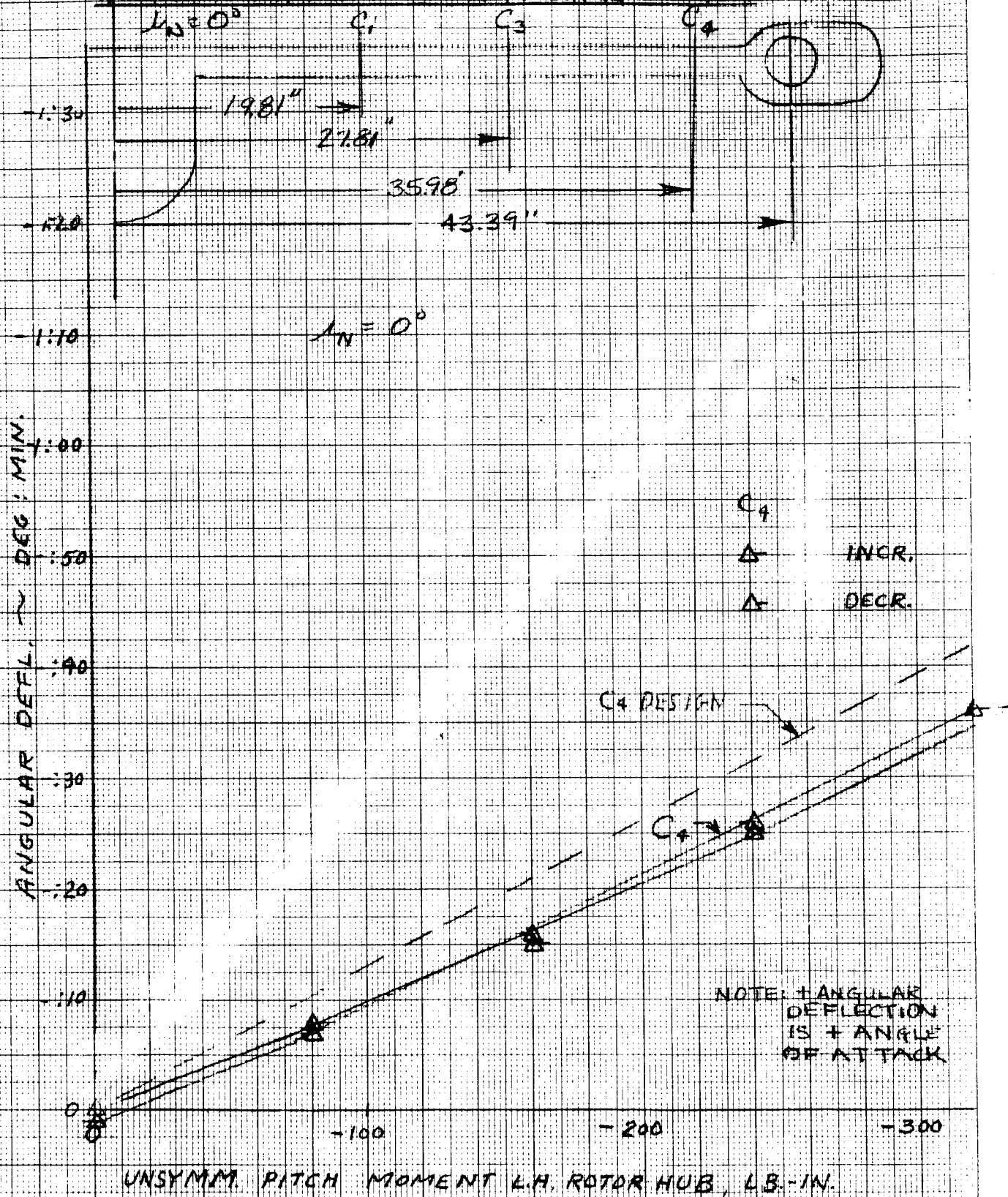


Figure B11

DEFLECTION TEST
WING ROTATION DUE TO ROTOR THRUST
 $\lambda_w = 0$

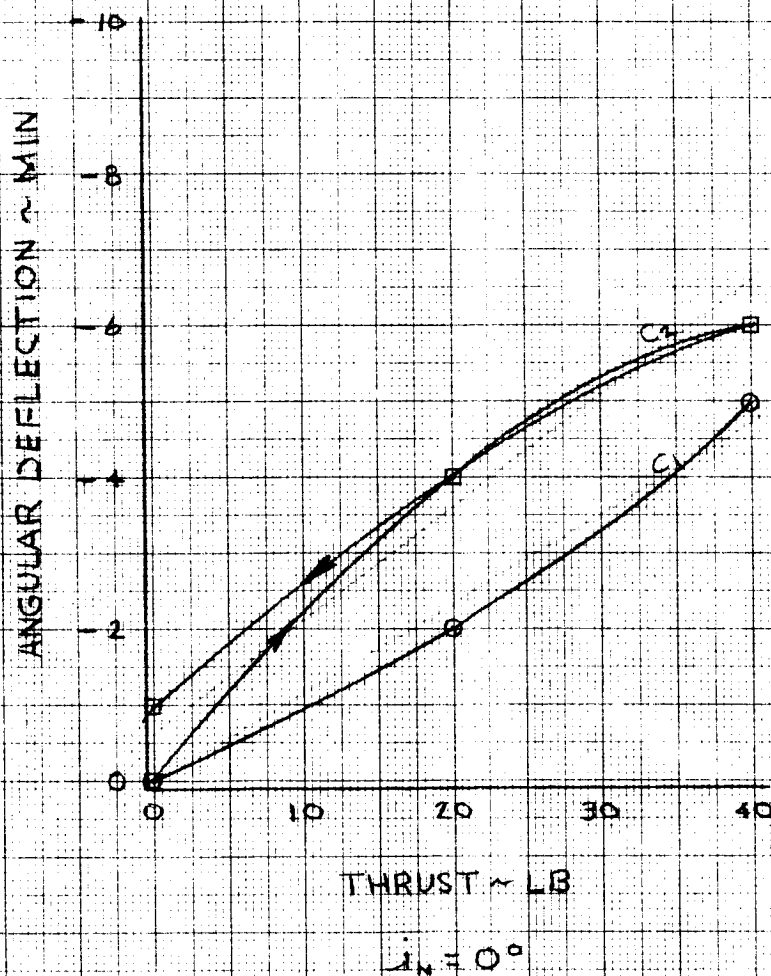
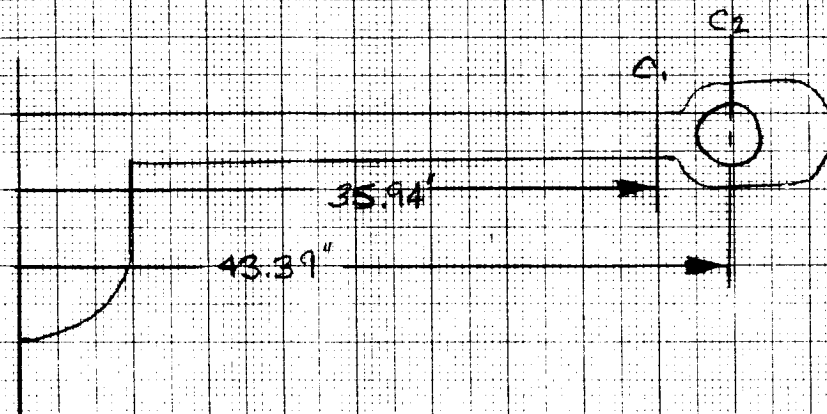
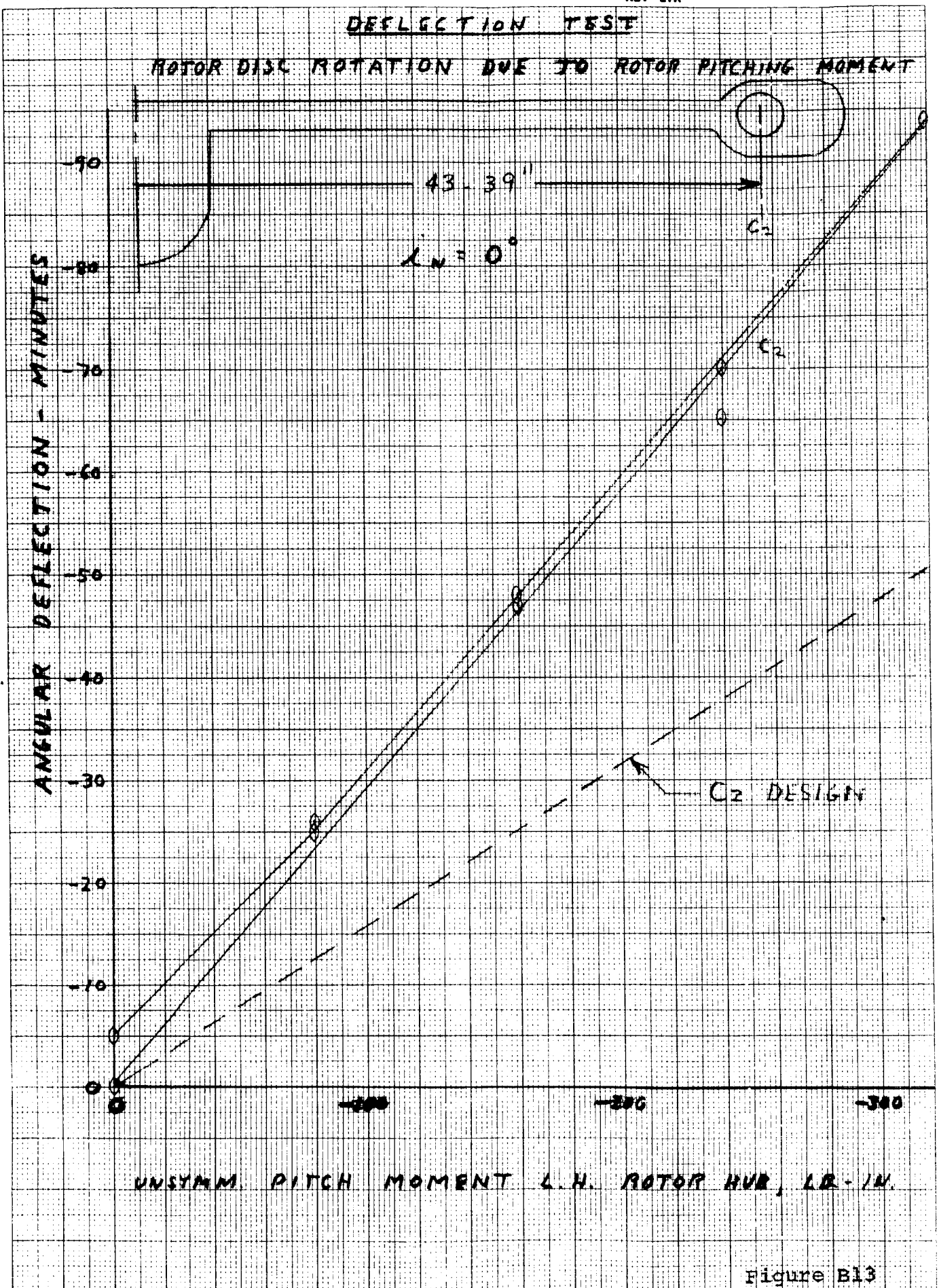
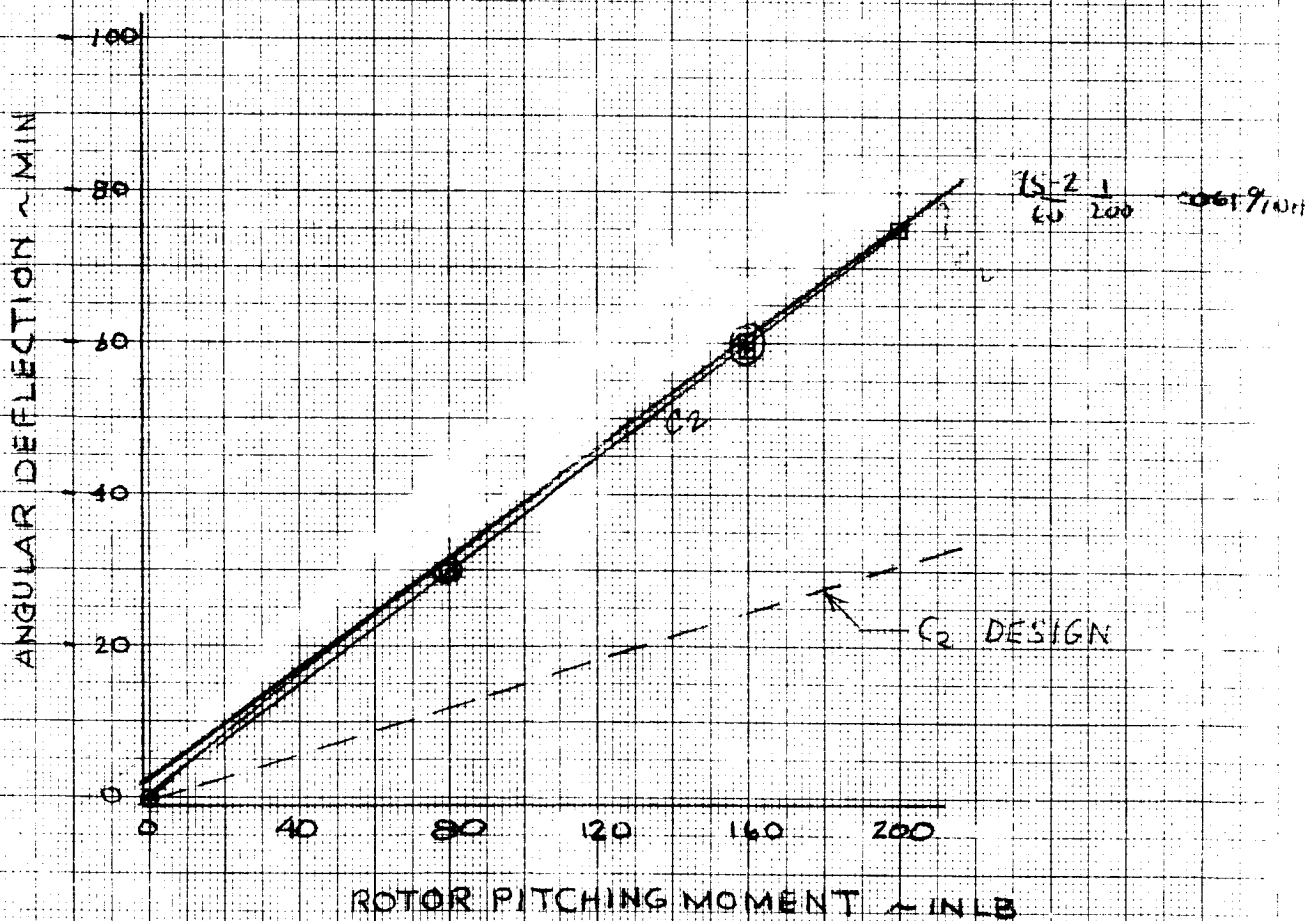
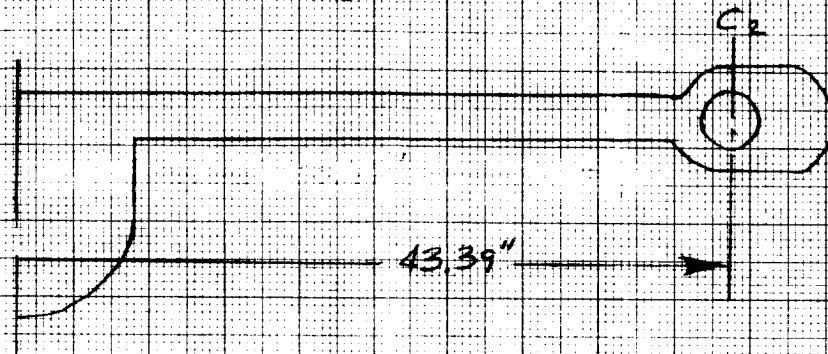


Figure B12



DEFLECTION TEST ROTOR DISC ROTATION DUE TO ROTOR PITCHING MOMENT

$\lambda_H = 0^\circ$



$\lambda_H = 0^\circ$

Figure B14

DEFLECTION TEST ROTOR DISC ROTATION DUE TO ROTOR PITCHING MOMENT

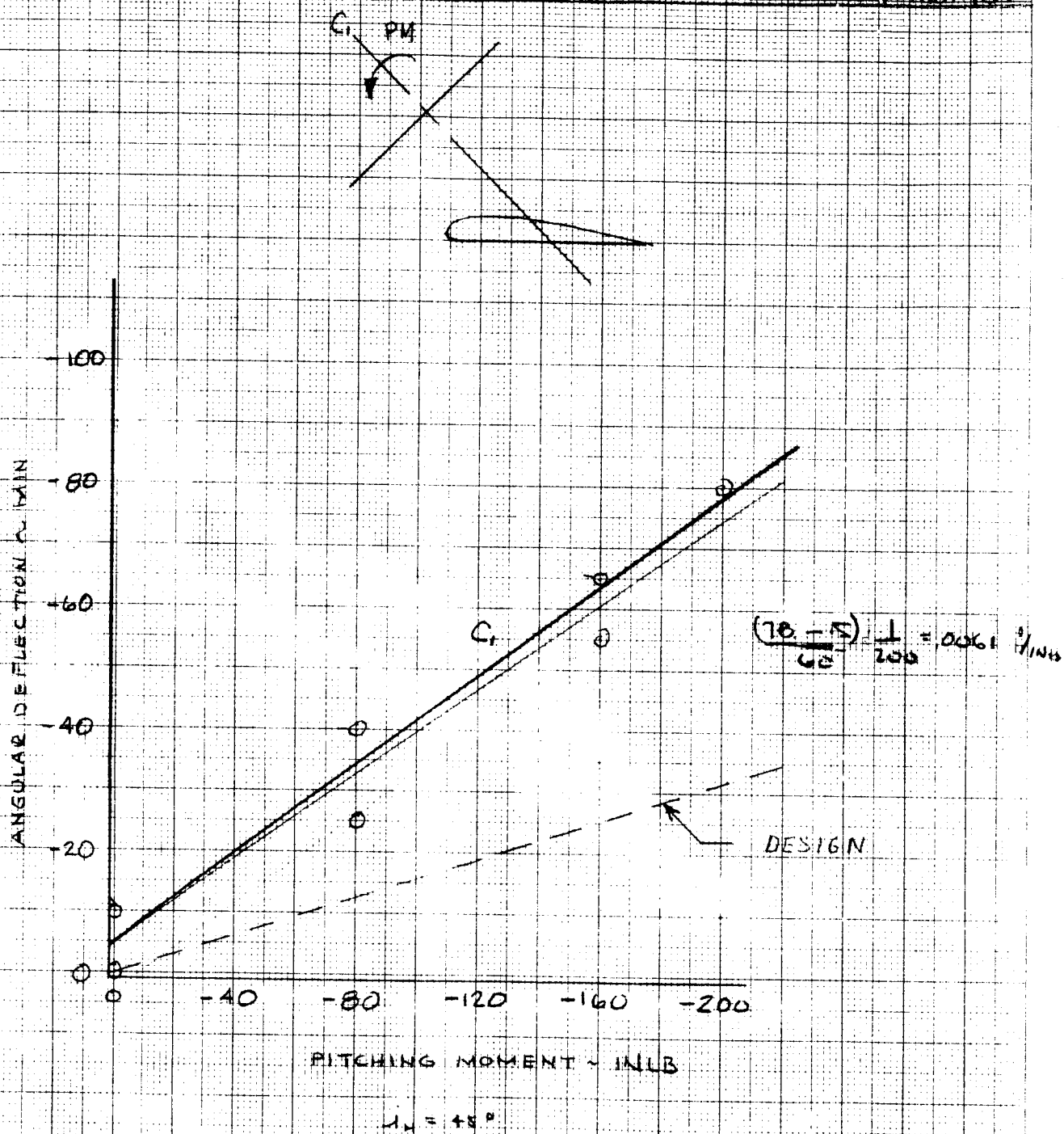
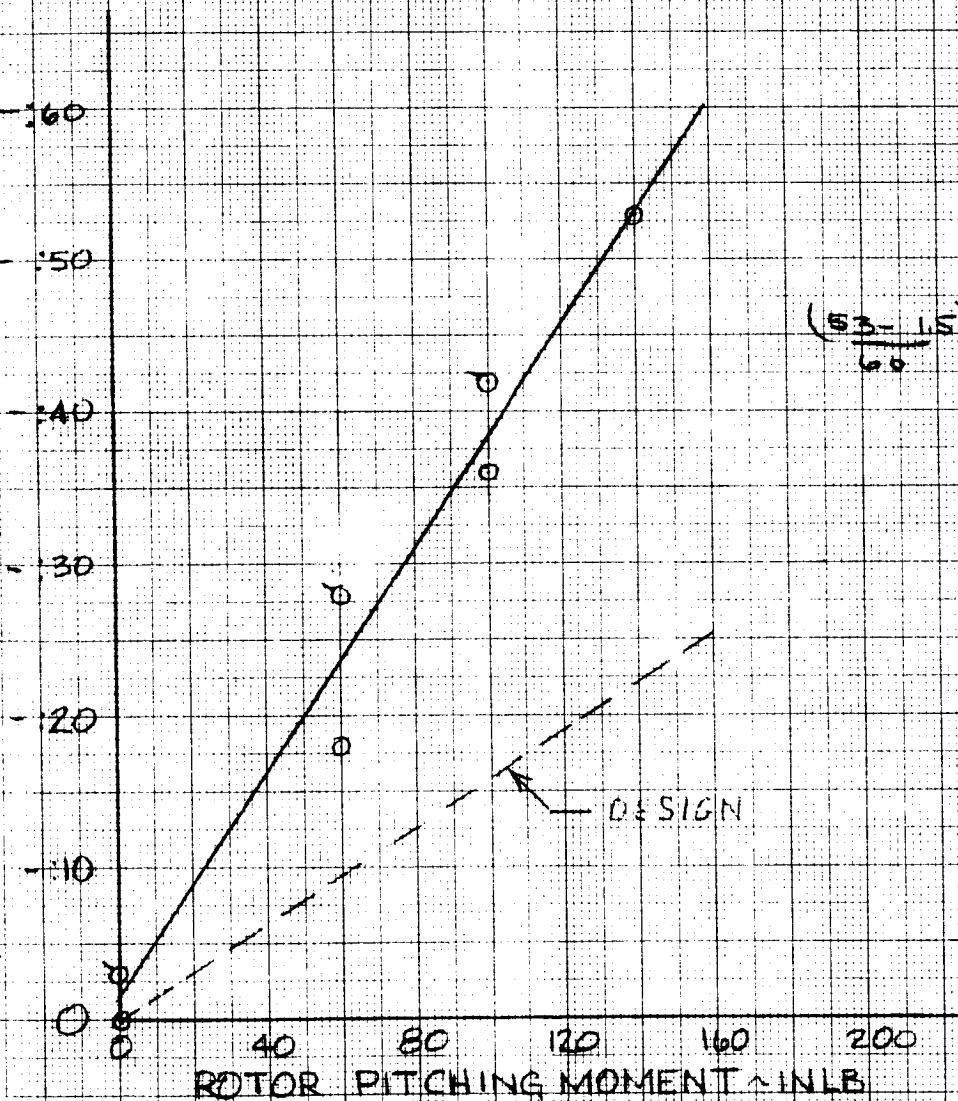


Figure B15

DEFLECTION TEST ROTOR DISC ROTATION DUE TO ROTOR PITCHING MOMENT

$\lambda_N = 90^\circ$

C. ANGULAR DEFLECTION OF ROTOR HUB



$\lambda_N = 90^\circ$

Figure B16

DEFLECTION TESTROTOR DISC ROTATION DUE TO ROTOR NORMAL FORCE

$$\angle_N = 0^\circ$$

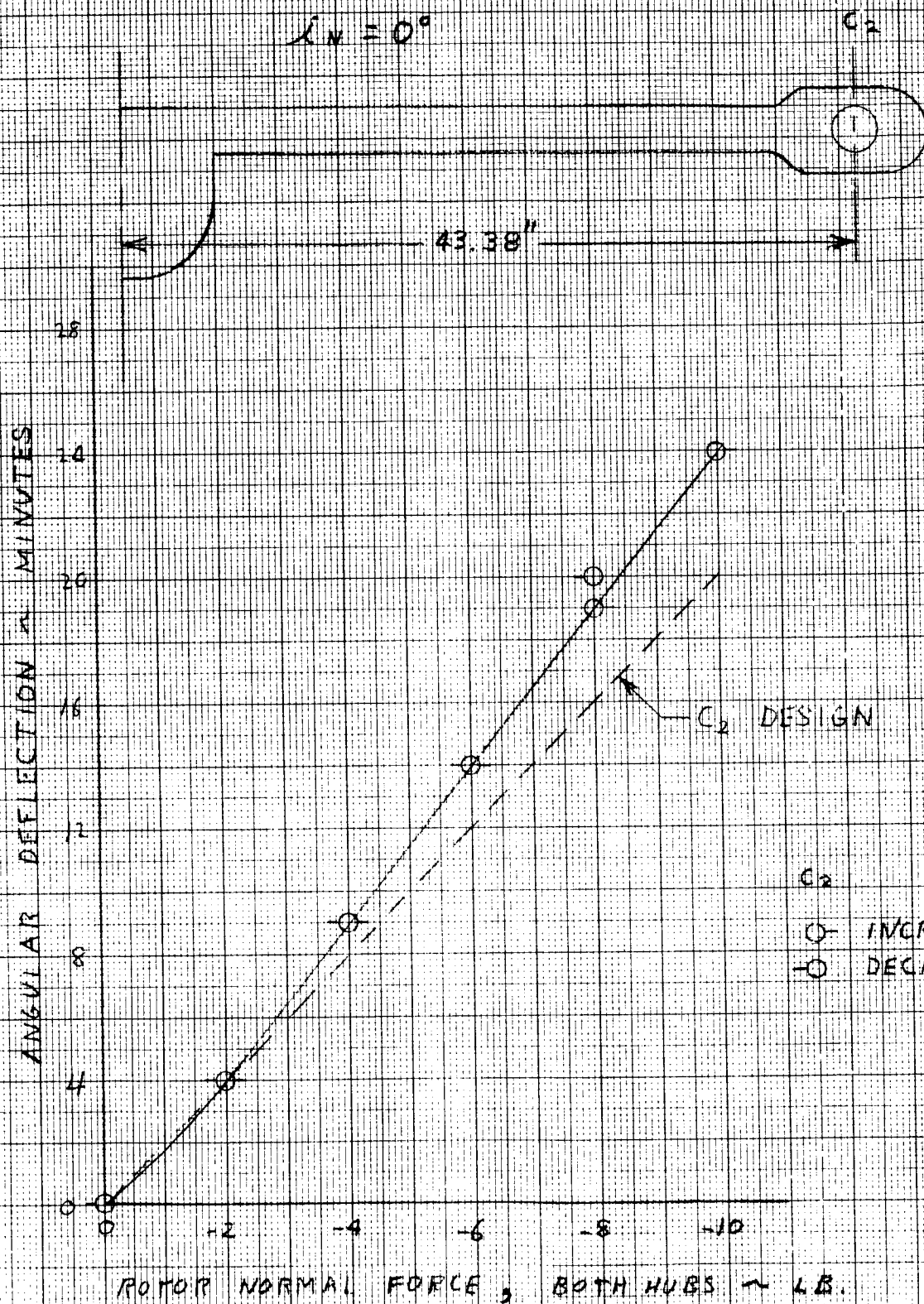


Figure B17

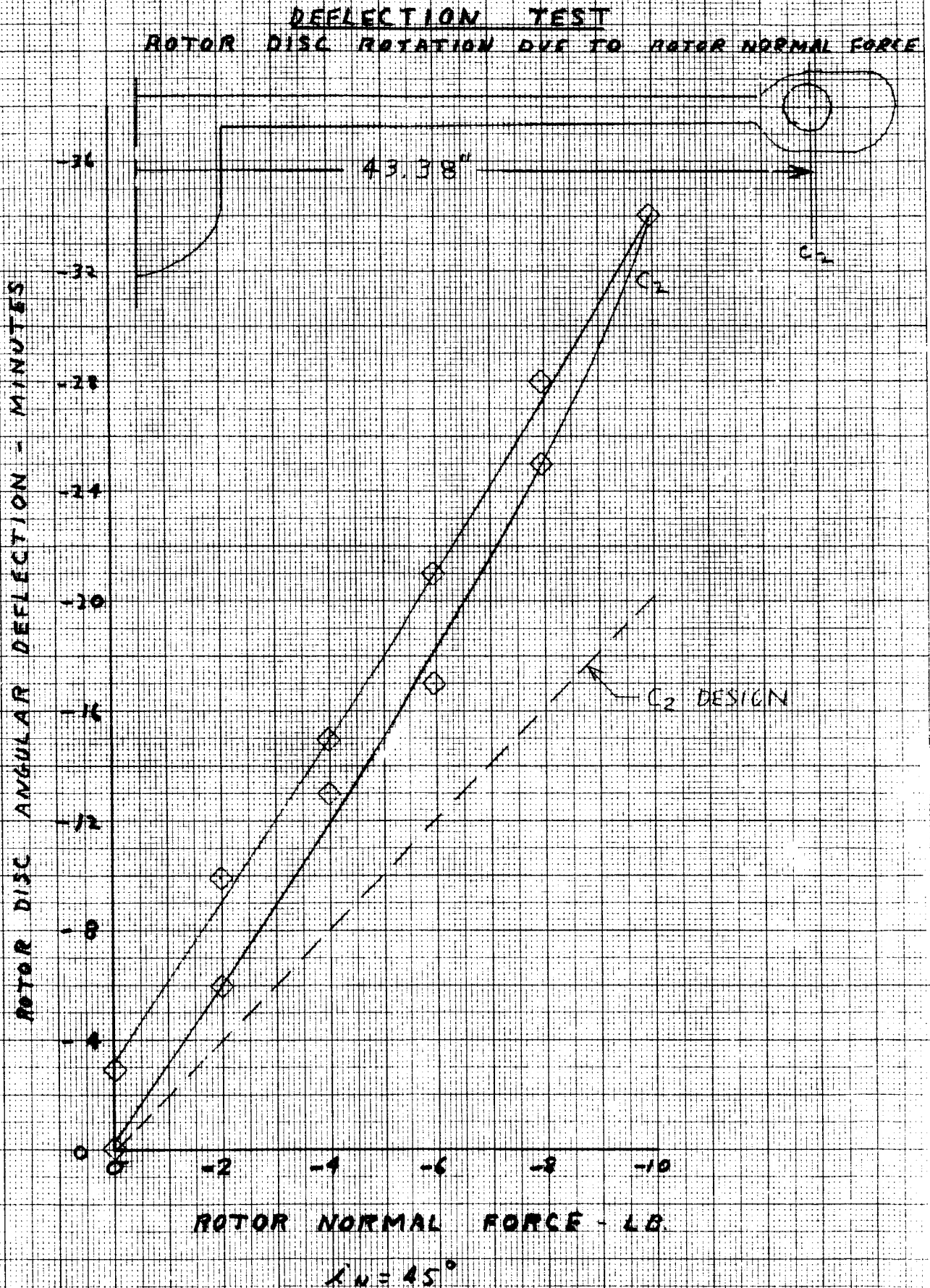


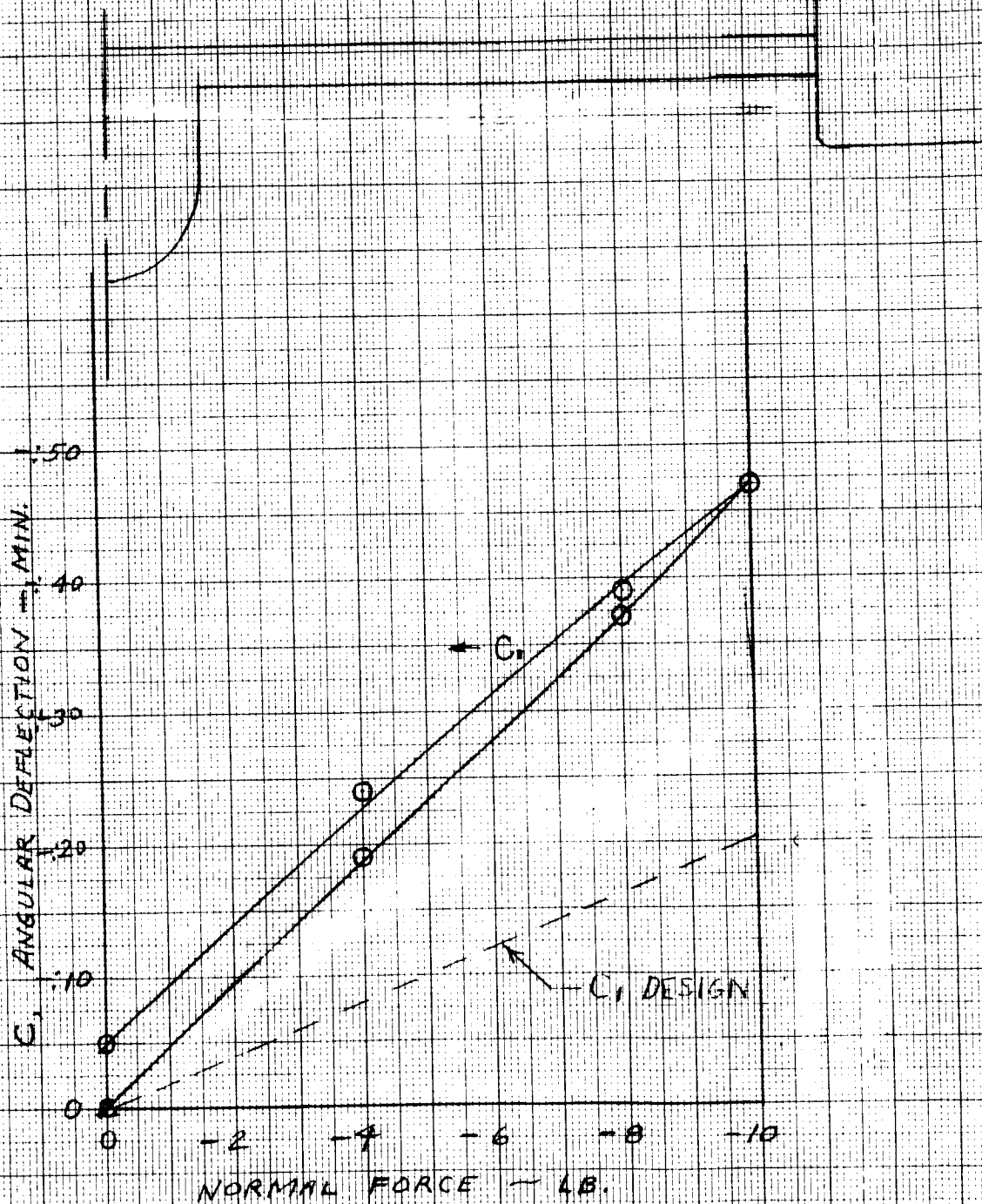
Figure B18

DEFLECTION TEST ROTOR DISC ROTATION DUE TO ROTOR NORMAL FORCE

$\lambda = 90^\circ$

⊙ NF

C_1



$\lambda_N = 90^\circ$

Figure B19

DEFLECTION TEST ROTOR DISC DEFLECTION DUE TO ROTOR YAWING MOMENT

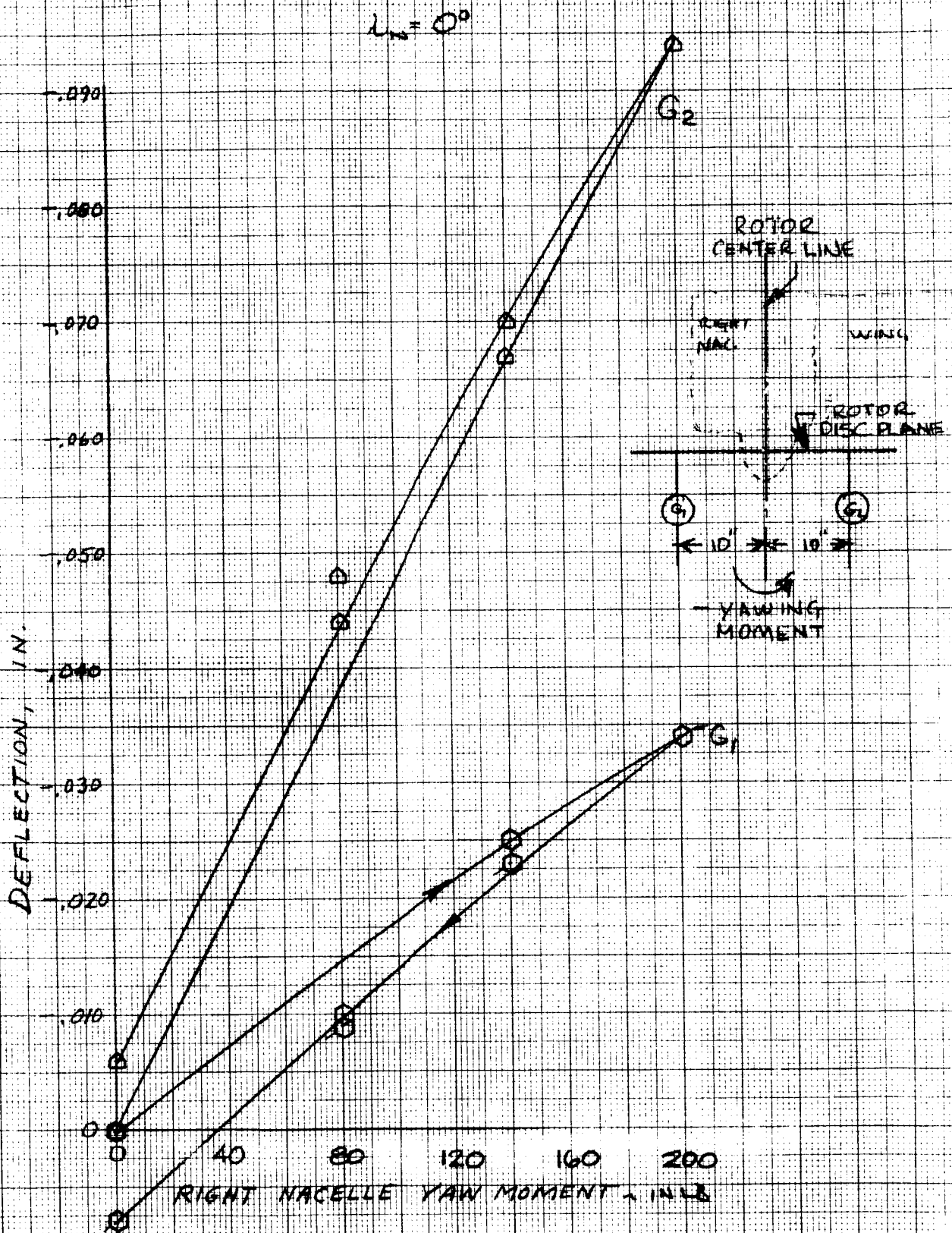
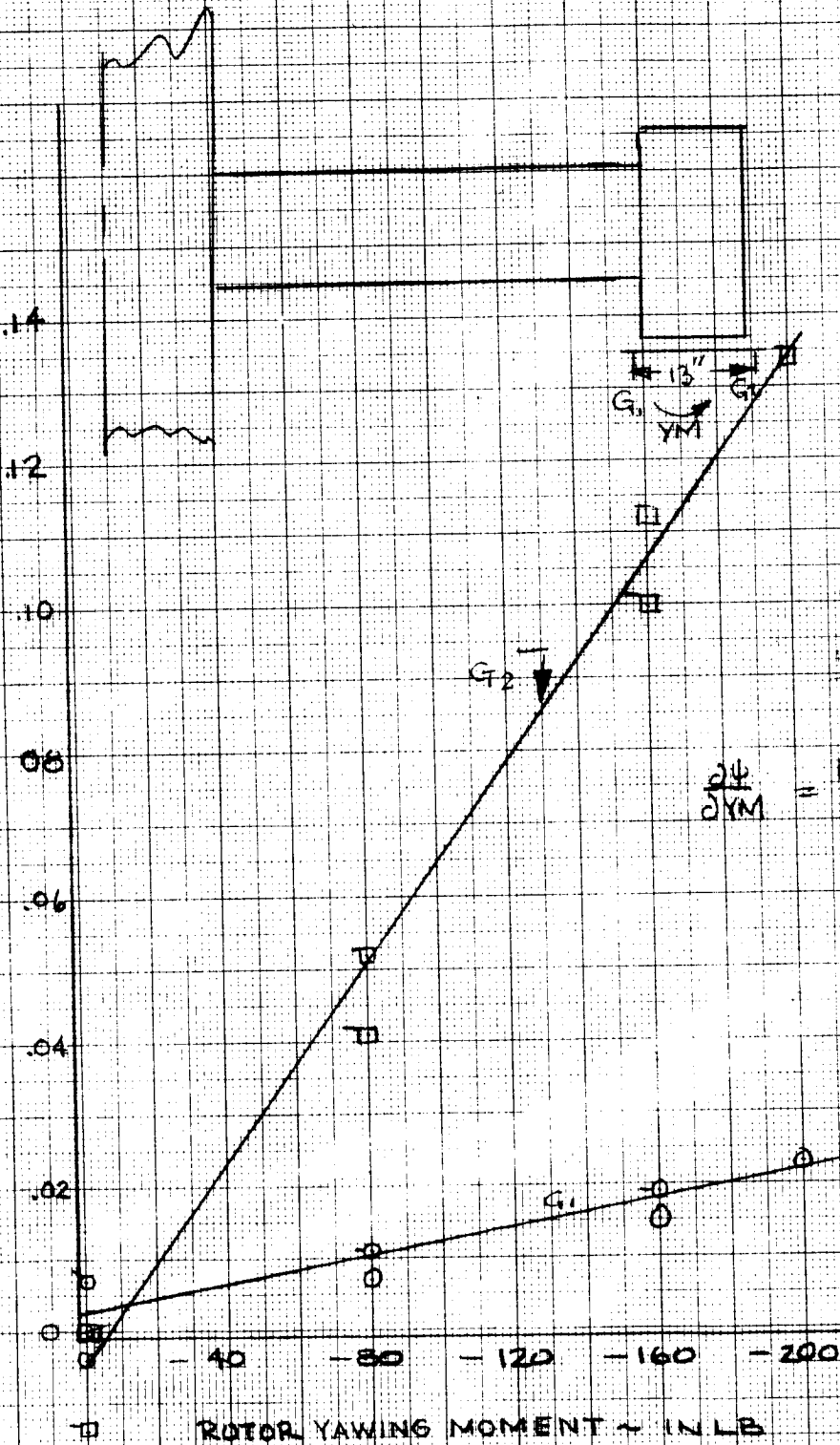


Figure B20

DEFLECTION TEST ROTOR DISC DEFLECTION DUE TO ROTOR YAWING MOMENT

$\alpha_N = 0^\circ$

DEFLECTION OF ROTOR DISC PLANE IN



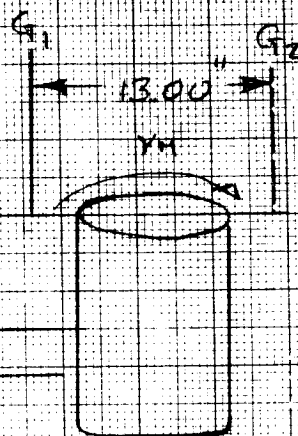
$$\frac{\partial \psi}{\partial Y_M} = \frac{(119) 573}{13.0} \cdot \frac{1}{200} = 0.0026 \%$$

LEFT NAC $\alpha_N = 0^\circ$

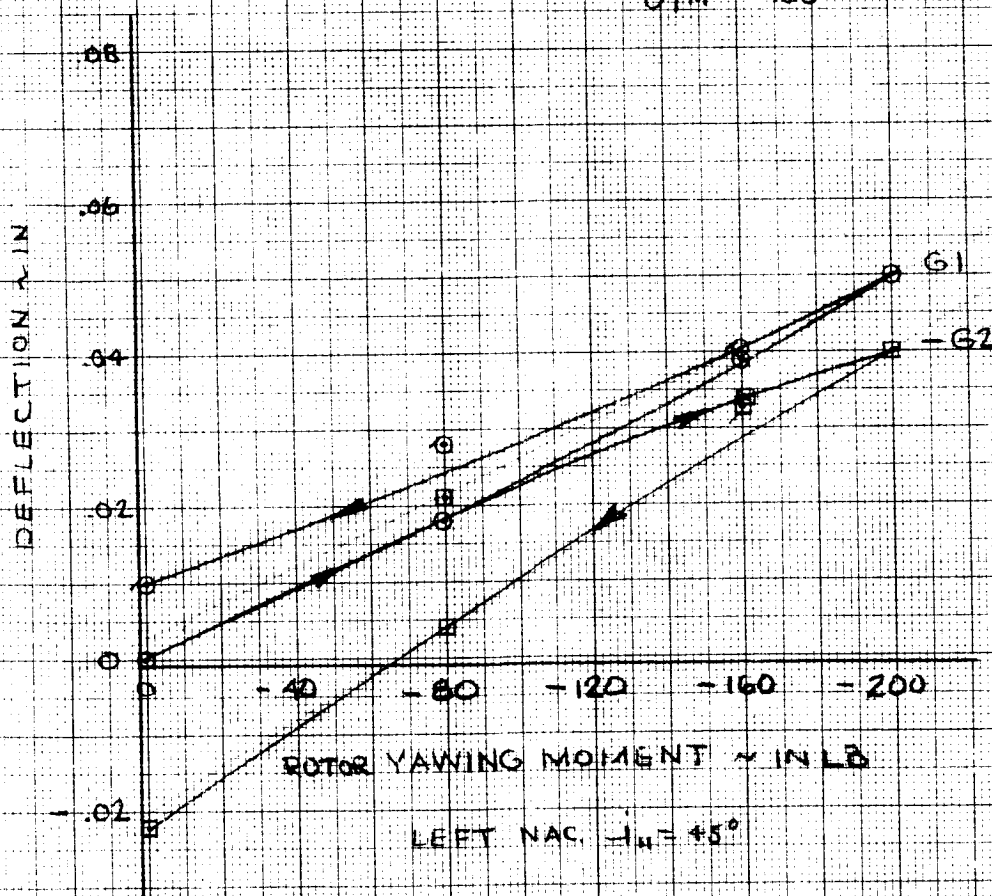
Figure B21

DEFLECTION TEST ROTOR DISC ROTATION DUE TO ROTOR YAWING MOMENT

$\alpha = 45^\circ$



$$\frac{d\psi}{dY_M} = \frac{(0.000148) 523}{13.0} \cdot \frac{1}{200} = 0.00238 \text{ } ^\circ/\text{IN LB}$$



LEFT NAC. $\alpha = 45^\circ$

Figure B22

DEFLECTION TEST

ROTOR DISC ROTATION DUE TO ROTOR YAWING MOMENT

$i_N = 90^\circ$

YM

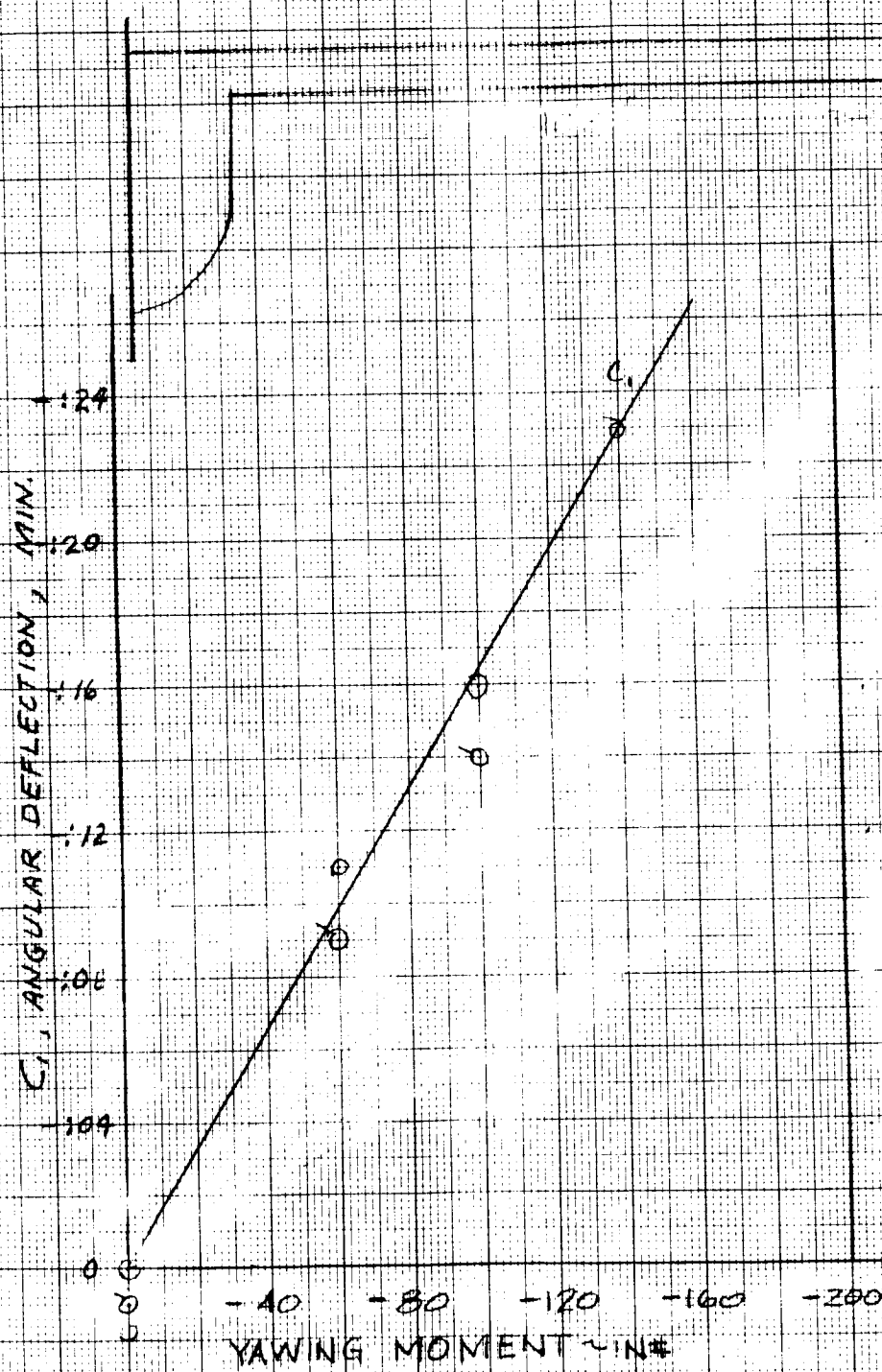
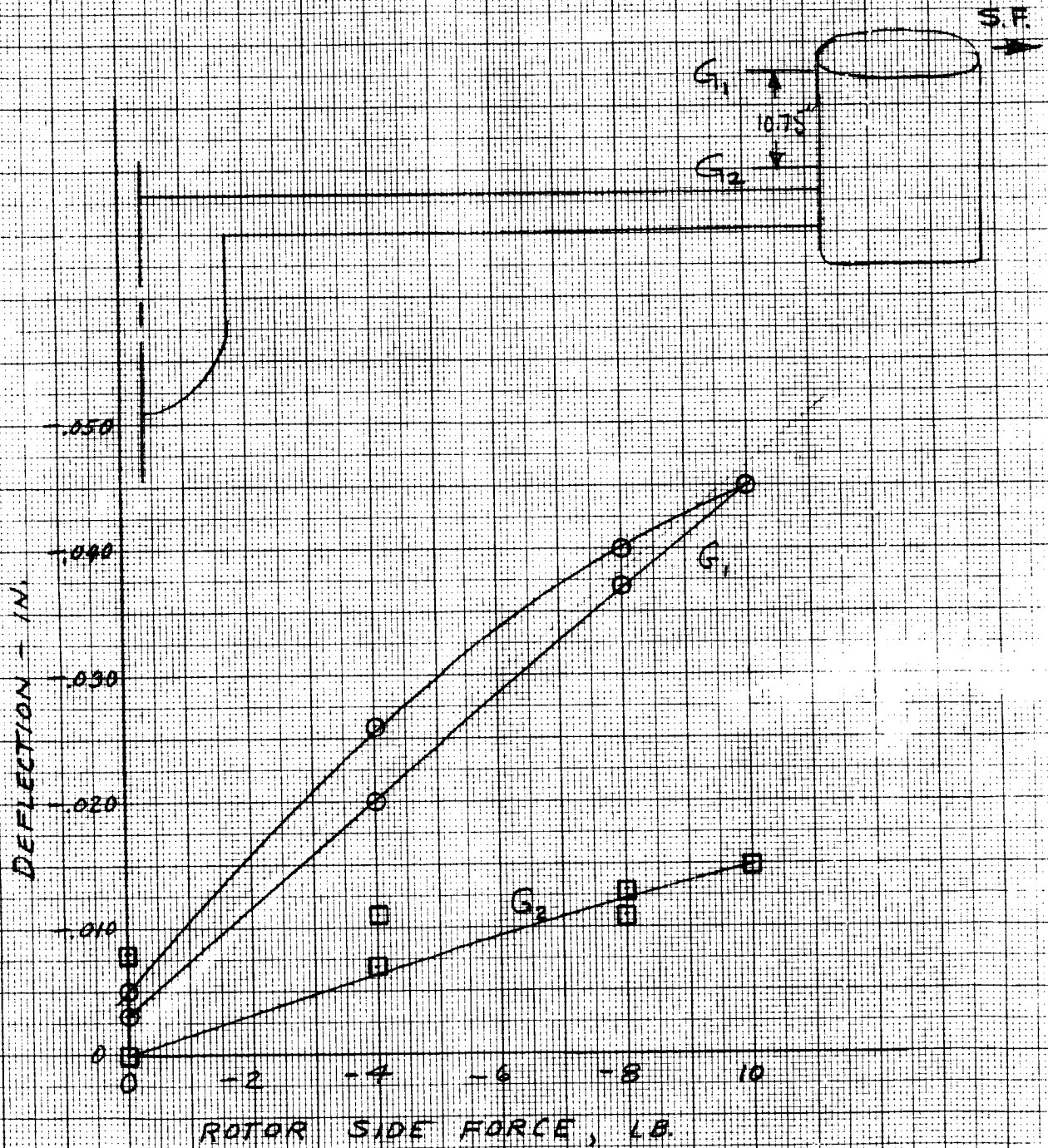


Figure B23

EUGENE DIETZGEN CO.
NO. 340R-MP DIETZGEN GRAPH PAPER
MADE IN U.S.A.
MILLIMETER

DEFLECTION TEST
NACELLE DEFLECTION DUE TO ROTOR SIDE FORCE
 $\alpha_N = 45^\circ$



$\alpha_N = 45^\circ$

Figure B24

EUGENE DIETZGEN CO.
MADE IN U.S.A.
NO. 340R-MP DIETZGEN GRAPH PAPER
MILLIMETER

DEFLECTION TEST ROTOR DISC PLANE ROTATION DUE TO ROTOR SIDE FORCE

$L_N = 90^\circ$

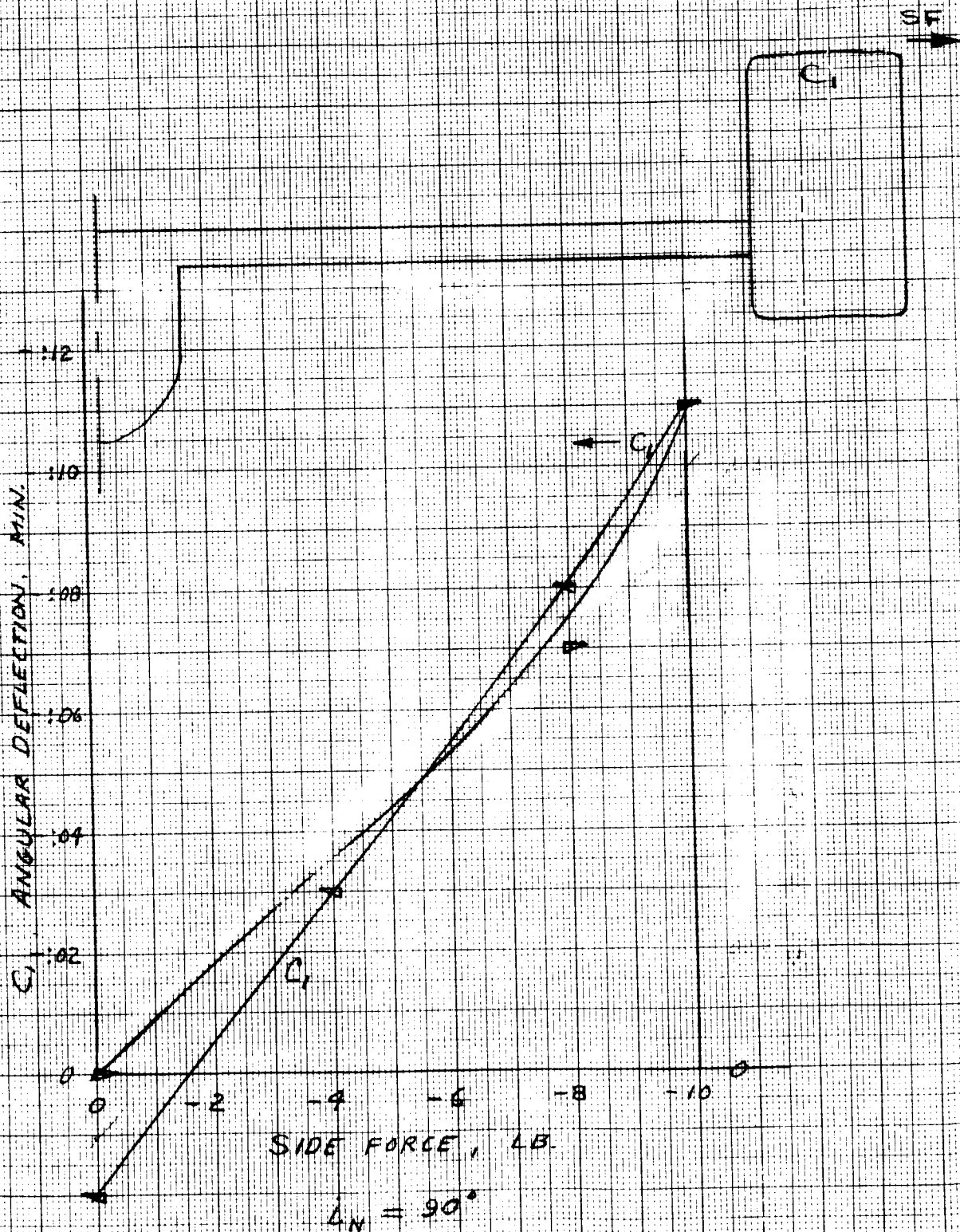


Figure B25

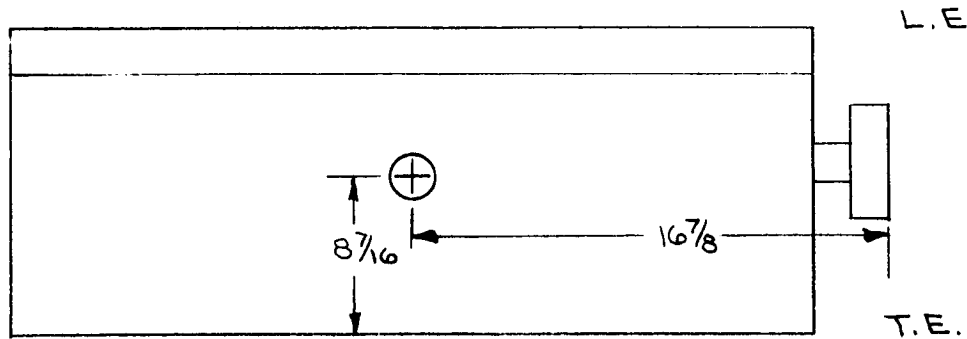
APPENDIX C - MODEL WEIGHT, BALANCE AND INERTIA

The weight, balance and inertia of model components were determined experimentally during the model assembly phase. Inertias were determined for movable control surfaces and nacelles only. Model symmetry was assumed and therefore only one of each hand component was determined.

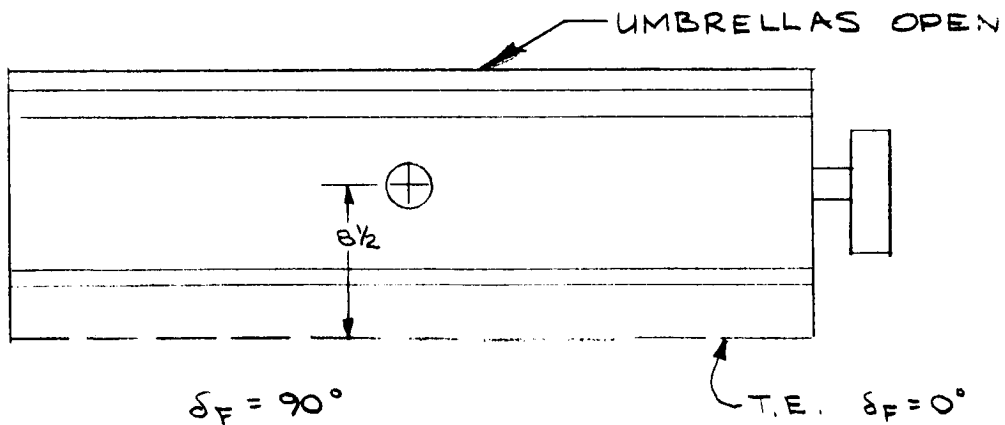
The weight and balance of the wing for the cruise and hover mode are shown in Figure C-1. The fuselage weight and balance are shown in Figure C-2. The weight, balance and inertia of the nacelle, horizontal tail, vertical tail and wing flap are shown in Figures C-3 through C-6 respectively.

WING WEIGHT & BALANCE

LEFT WING WEIGHT = 15.80LB



CRUISE MODE
 $\delta_F = 0^\circ$



$\delta_F = 90^\circ$

HOVER MODE

Figure C1

FUSELAGE + WINGS + HORIZONTAL TAIL - MOTOR - WING BOXES	= 82.82
BALSA	= -2.59
	<u>80.23</u>
WING FITTING	= -1.09
	<u>79.14</u>
FUSE. SHELLS	5.02
MOTOR & GEAR BOX	<u>25.39</u>
	109.55
- WING	<u>25.44</u>
	84.11
- H. TAIL	<u>3.02</u>
FUSELAGE	= 81.09

FUSELAGE C.G. = $4\frac{21}{32}$ " FROM CENTER FRAME AFT EDGE

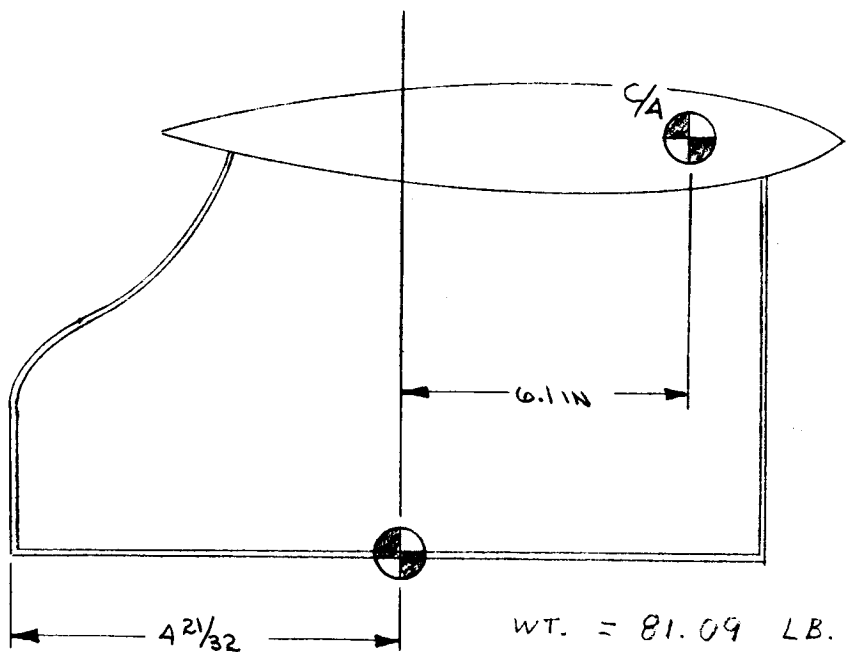
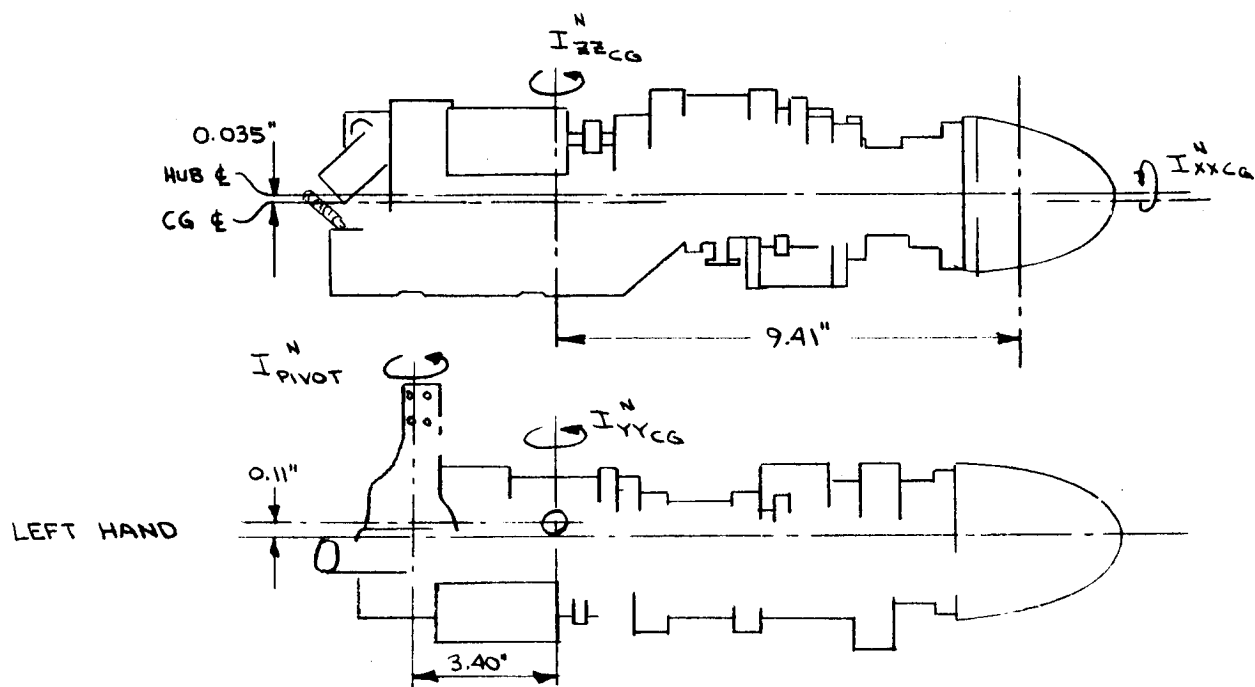


Figure C2

1/4 SCALE MODEL 222
NACELLES



NACELLE WEIGHT (NO COVER OR BLADES) : 29.49 LB
SLIP RING ASSY 0.31 LB
SPINNER 0.22 LB

$$I_{XXCG}^N = 0.2309 \text{ LB IN SEC}^2$$

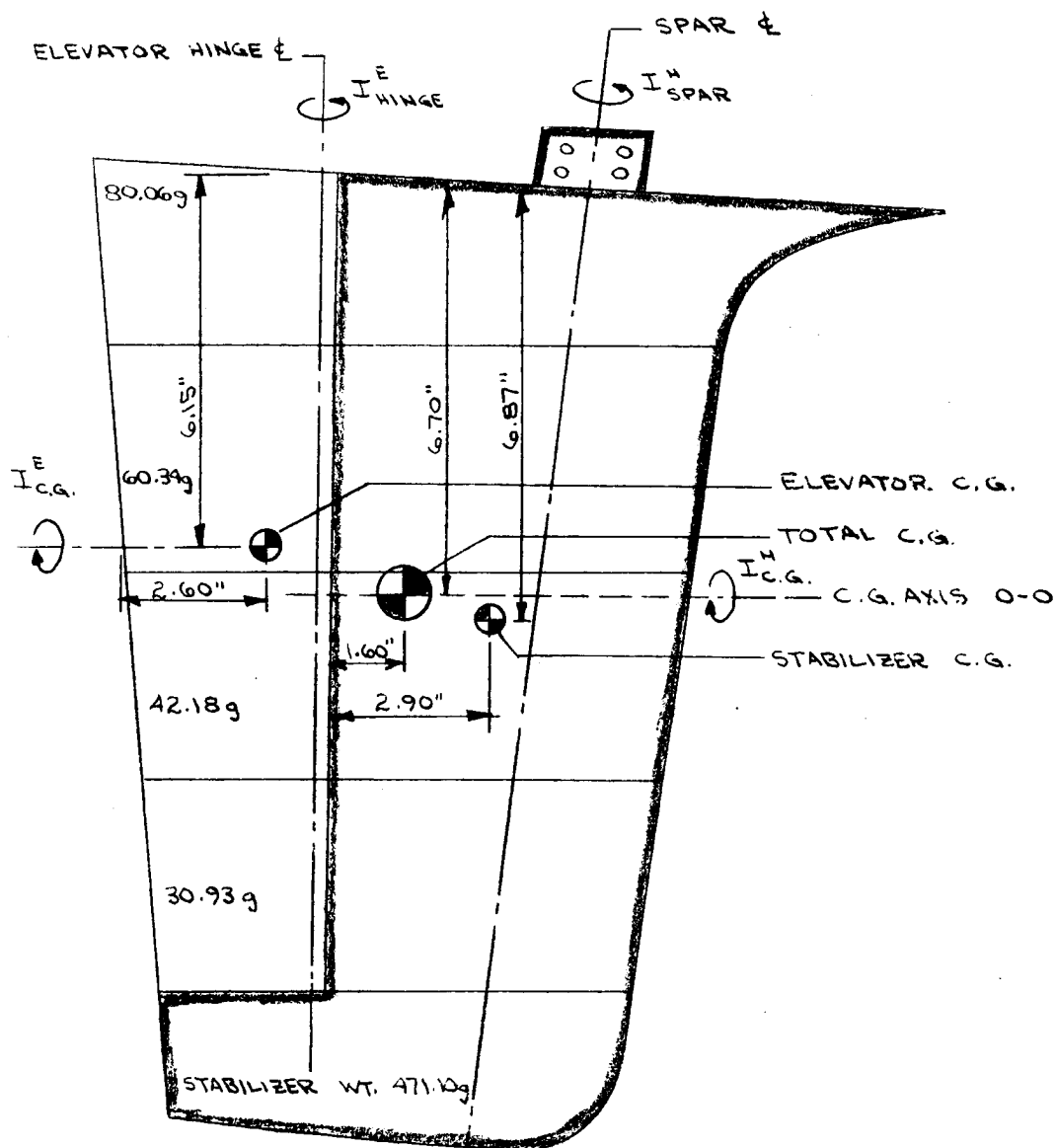
$$I_{YYCG}^N = 1.9658 \text{ LB IN SEC}^2$$

$$I_{ZZCG}^N = 1.9658 \text{ LB IN SEC}^2$$

$$I_{PIVOT}^N = 2.8481 \text{ LB IN SEC}^2$$

Figure C3

1/4 SCALE MODEL 222
HORIZONTAL STABILIZER



STABILIZER WT 471.10 g
ELEVATOR WT 213.56 g
TOTAL WT 684.66 g

INERTIAS

ELEVATOR ALONE

$$I_{HINGE}^E = 0.002286 \text{ IN-LB SEC}^2$$

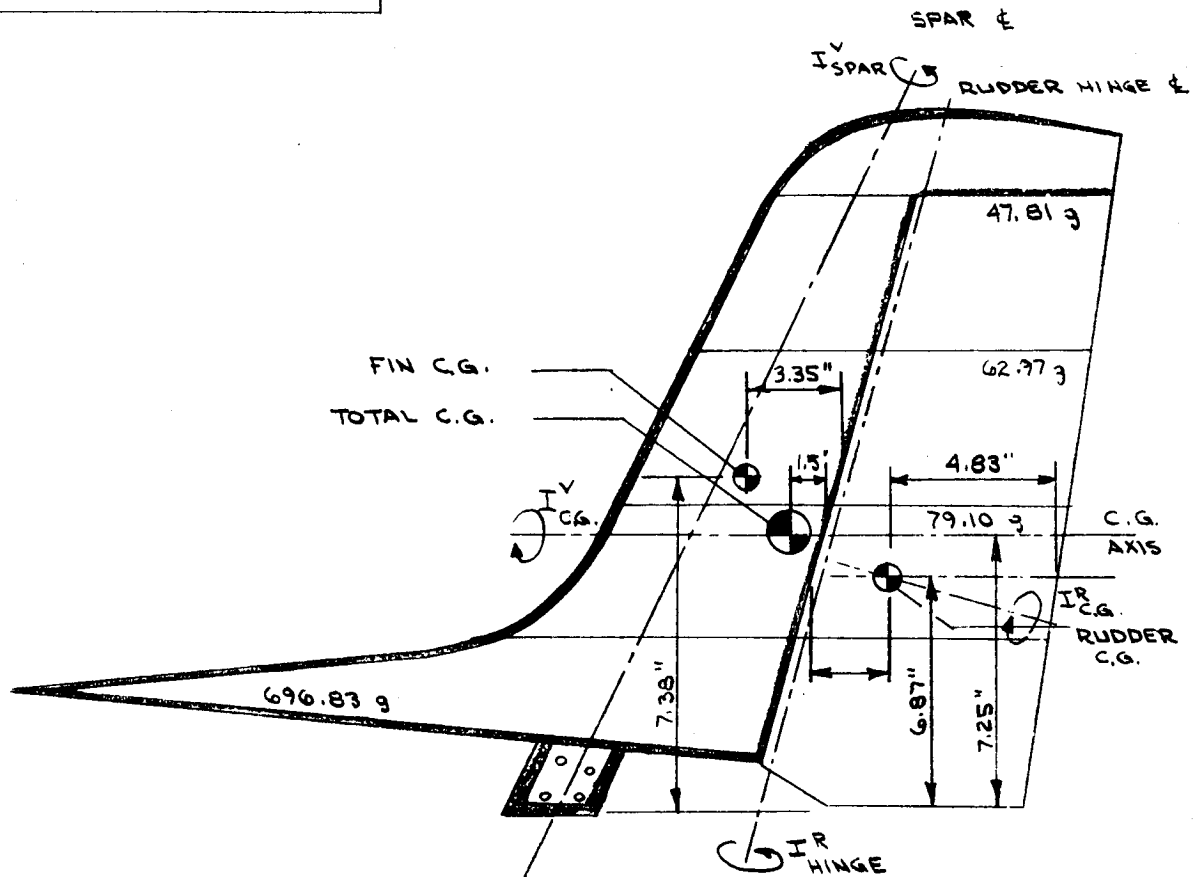
$$I_{C.G.}^E = 0.02352 \text{ IN-LB SEC}^2$$

ASSEMBLY

$$I_{SPAR}^H = 0.03777 \text{ IN-LB SEC}^2$$

$$I_{C.G.}^H = 0.09155 \text{ IN-LB SEC}^2$$

1/4 SCALE MODEL 222
VERTICAL STABILIZER



PIN WT	696.83 g
RUDDER WT	294.68 g
TOTAL WT	991.51 g

INERTIAS

RUDDER ALONE

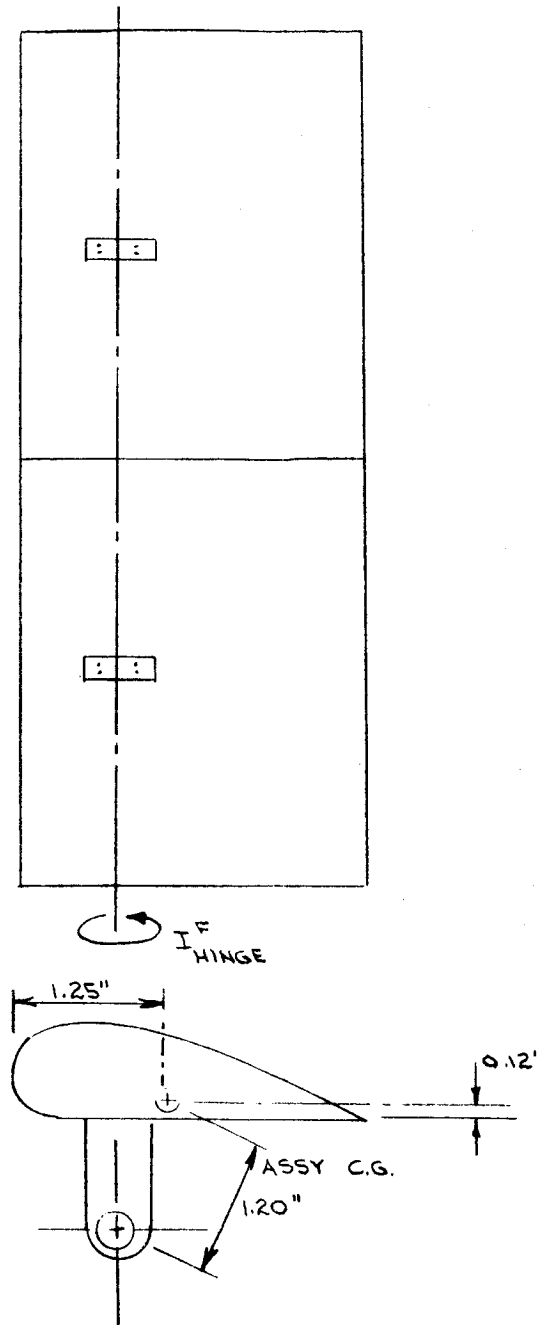
I_{HINGE}^R	= 0.01370 IN LB SEC ²
I_{CG}^R	= 0.04755 IN LB SEC ²

ASSEMBLY

I_{SPAR}^V	= 0.14462 IN LB SEC ²
I_{CG}^V	= 0.05857 IN LB SEC ²

Figure C5

1/4 SCALE MODEL 222
FLAPS



WEIGHT OF 2-PANEL ASSEMBLY (4 PANELS PER WING) = 221.5 g

$$I_{\text{HINGE}}^F = 0.008007 \text{ IN-LB SEC}^2$$

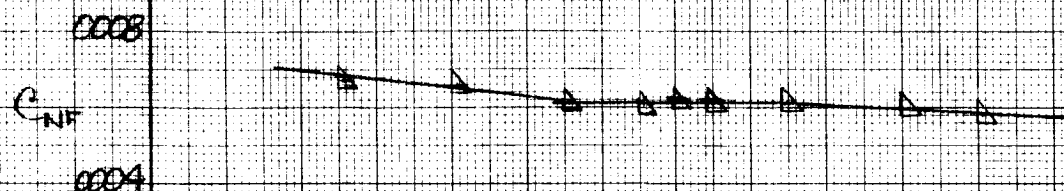
Figure C6

APPENDIX D - ROTOR HUB TARES

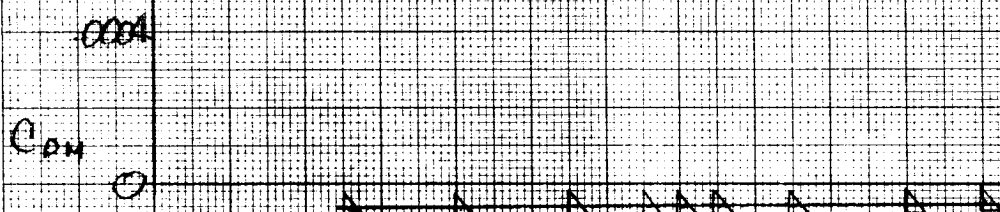
During the testing with rotor blades off, data was recorded on the nacelle balances. This would provide the contribution to the rotor forces and moments that is made by the spinner - or hub. Tare values are necessary to establish the contribution made by the rotor blades which is required for comparison with theory. Figures D-1 through D-4 are for mid-transition with the nacelle incidence at 45 degrees and the forces and moments are nondimensionalized into rotor coefficients based on a rotor speed of 1185 RPM. Figures D-5 through D-8 are for cruise with a nacelle incidence of zero and a rotor speed of 830 RPM.

ROTOR HUB TARES TRANSITION

ROTOR NORMAL FORCE COEFFICIENT



ROTOR PITCHING MOMENT COEFFICIENT



ROTOR SIDE FORCE COEFFICIENT

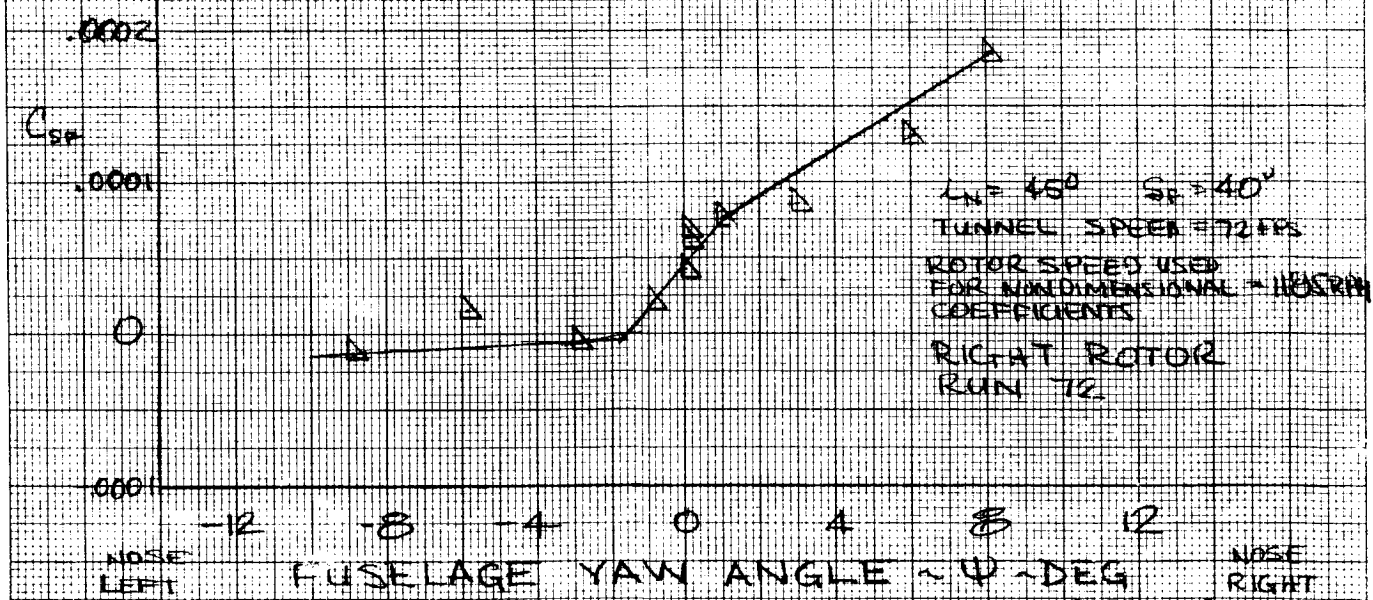


Figure D1

ROTOR HUB TARES
TRANSITIONROTOR THRUST COEFFICIENT

0.000

 C_T

0

-0.0010

$L_N = 45^\circ$ $S_c = 40^\circ$
TUNNEL SPEED USED
FOR NONDIMENSIONAL = 1180 RPM
COEFFICIENTS
RIGHT ROTOR
RUN 72

ROTOR YAWING MOMENT COEFFICIENT

.0004

 C_{YM}

0

-.0004

NOSE
LEFT

-12

8

-4

0

4

8

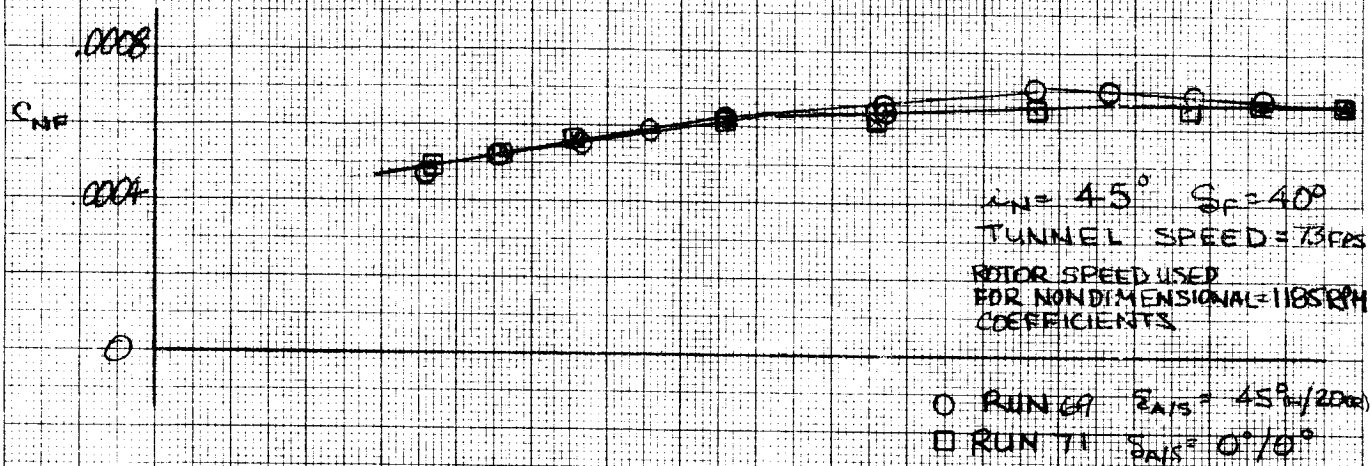
12

NOSE
RIGHTFUSELAGE YAW ANGLE $\sim \psi \sim \text{DEG}$

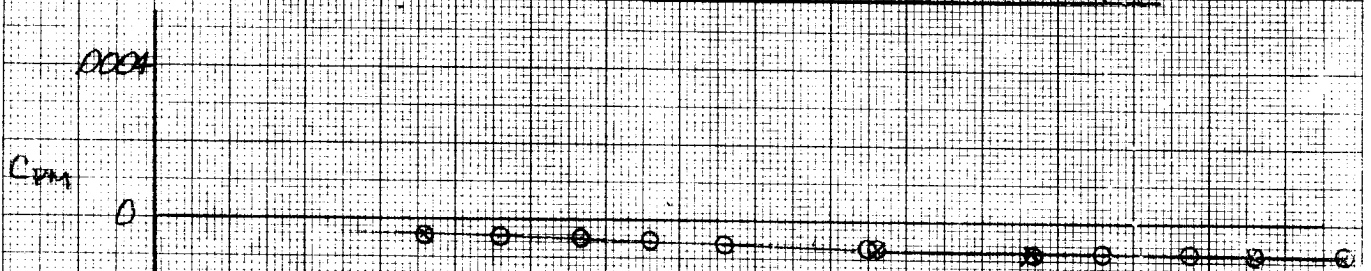
Figure D2

ROTOR HUB TARES
TRANSITION

ROTOR NORMAL FORCE COEFFICIENT



ROTOR PITCHING MOMENT COEFFICIENT



ROTOR SIDE FORCE COEFFICIENT

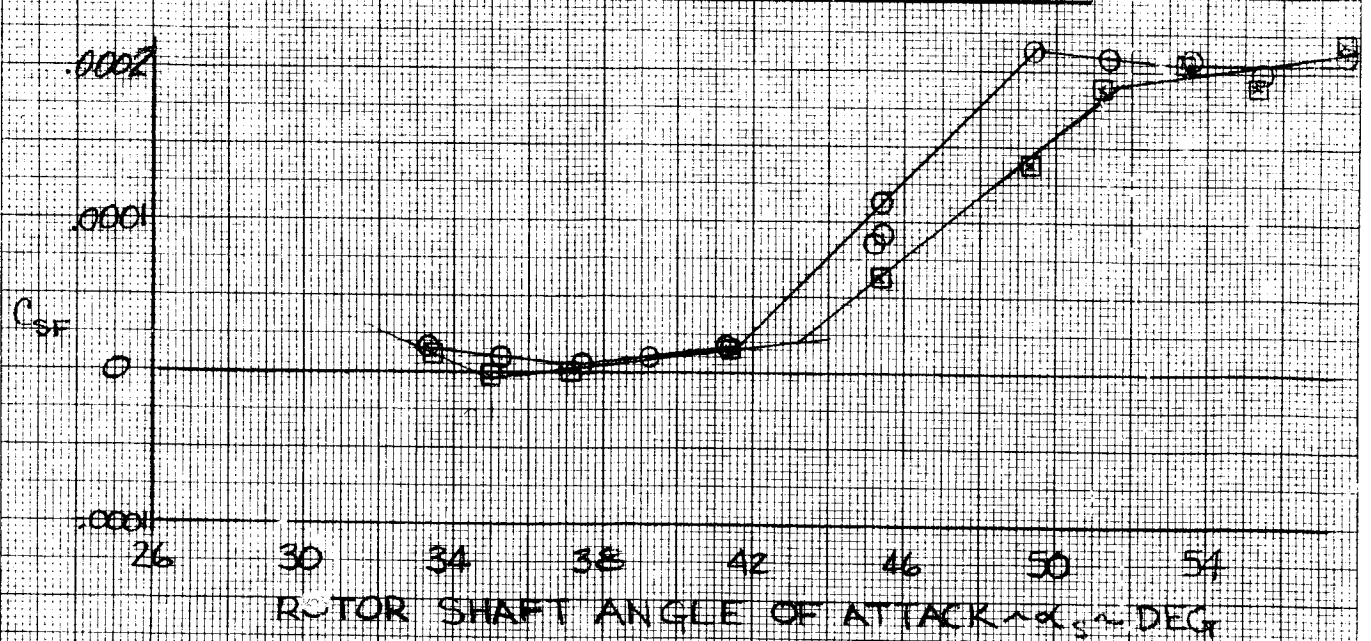


Figure D3

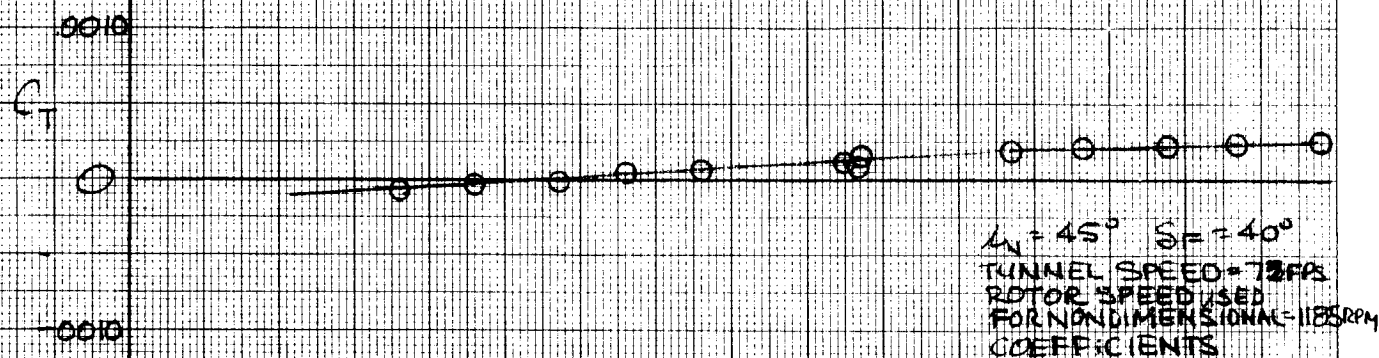
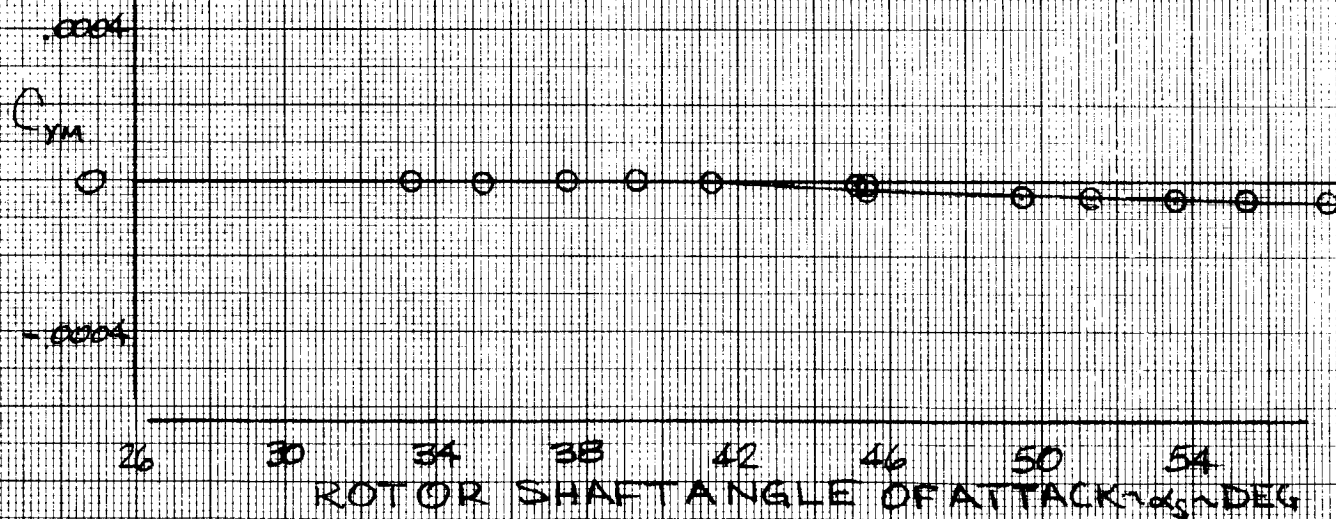
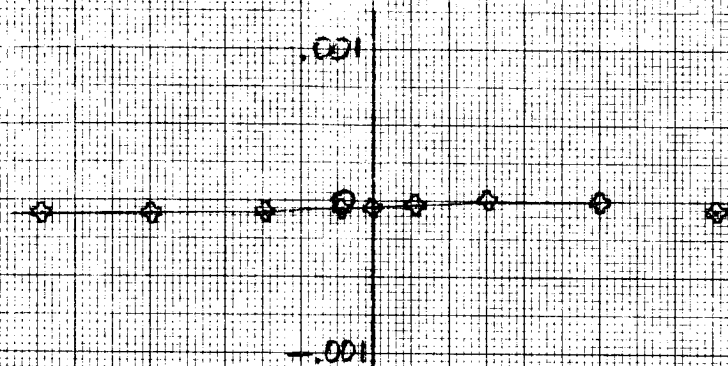
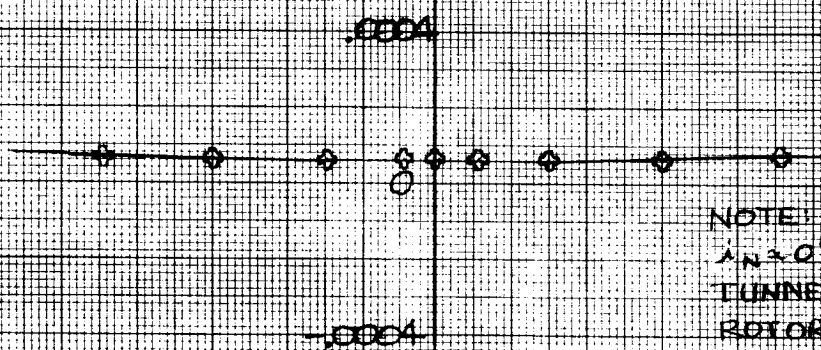
ROTOR HUB TARES
TRANSITIONROTOR THRUST COEFFICIENTROTOR YAWING MOMENT COEFFICIENT

Figure D4

ROTOR HUB TARES
CRUISE
ROTOR NORMAL FORCE COEFFICIENT

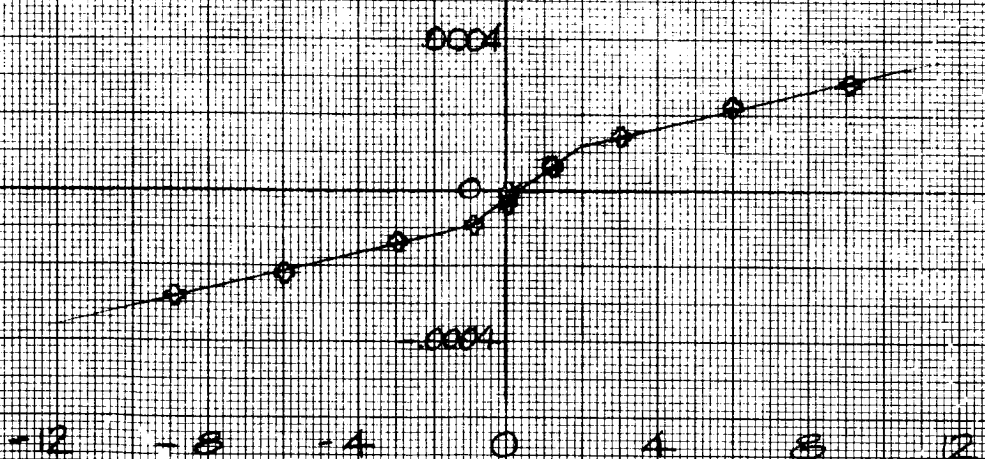


ROTOR PITCHING MOMENT COEFFICIENT



NOTE:
 $\lambda = 0.0$
TUNNEL SPEED = 113 FPS
ROTOR SPEED USED
FOR NONDIMENSIONAL = 83 RPM
COEFFICIENTS
RUN 76
RIGHT ROTOR

ROTOR SIDE FORCE COEFFICIENT



FUSELAGE YAW ANGLE ψ - DEG

Figure D5

ROTOR HUB TARES

CRUISE

NOTE

$\lambda_N = 0^\circ$

TUNNEL SPEED = 113 FPS

ROTOR SPEED USED

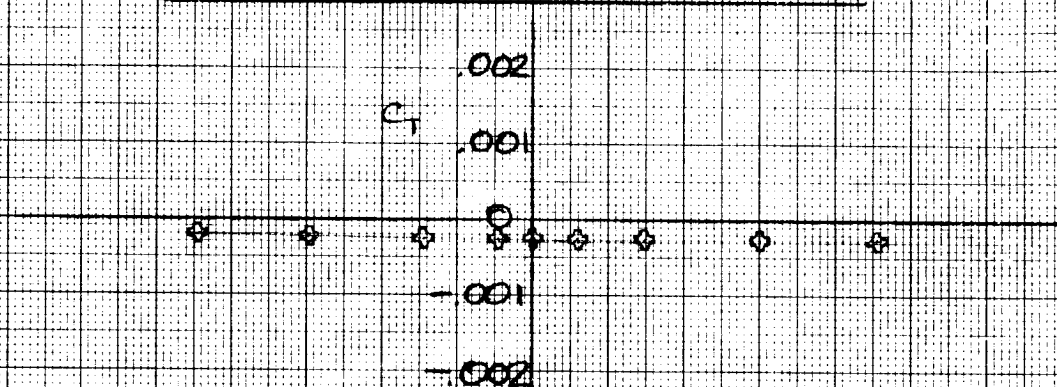
FOR NONDIMENSIONAL = 0.30 RPM

COEFFICIENTS

RUN 76

RIGHT ROTOR

ROTOR THRUST COEFFICIENT



ROTOR YAWING MOMENT COEFFICIENT

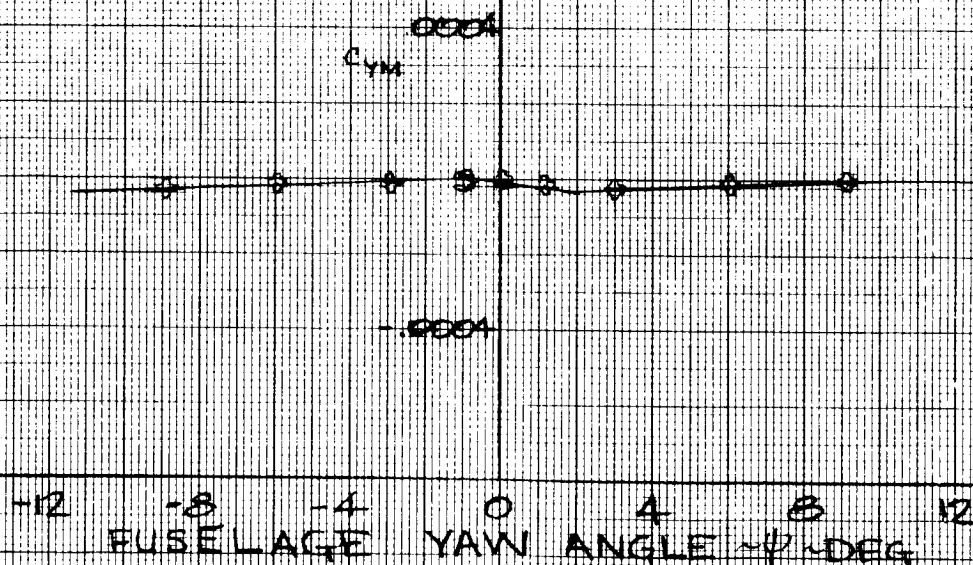
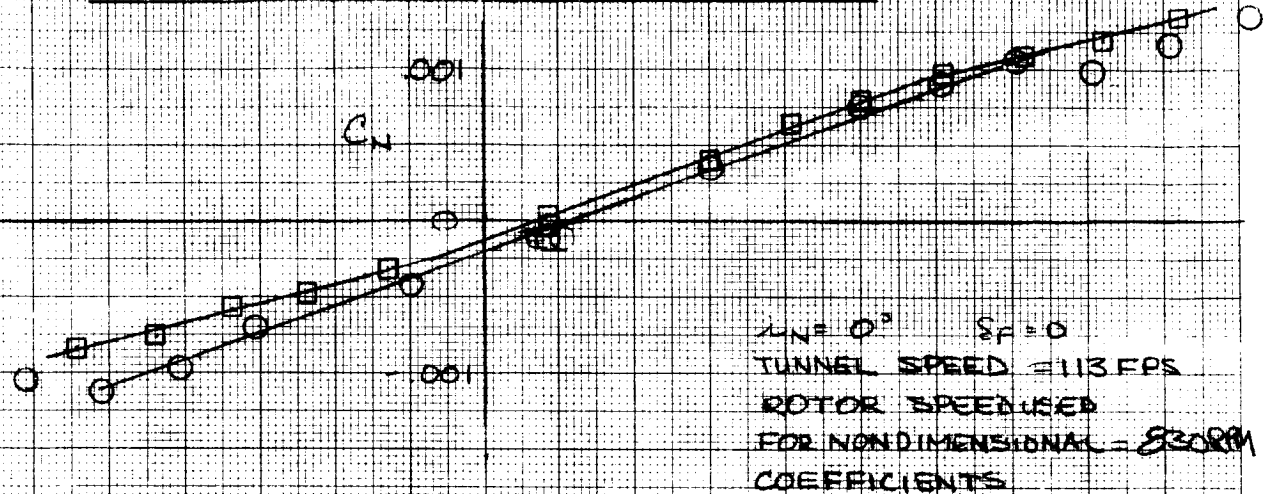


Figure D6

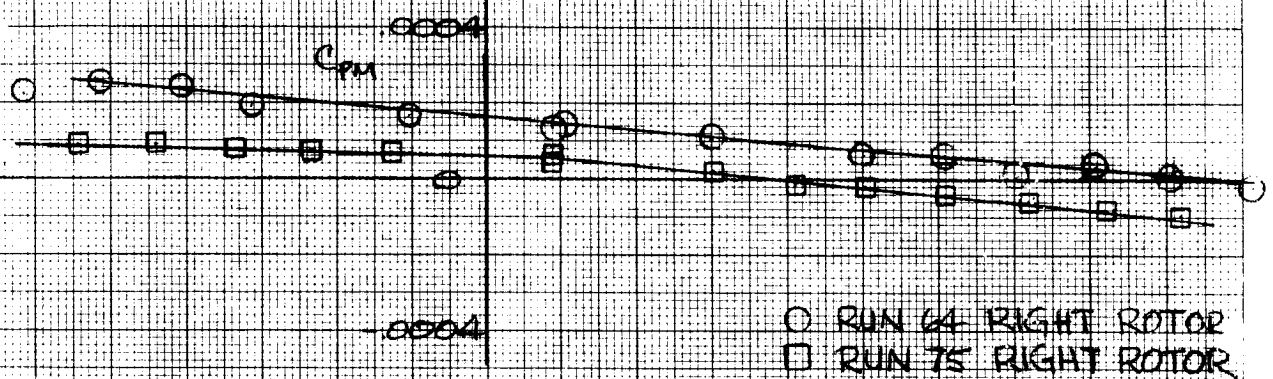
ROTOR HUB TARES

CRUISE

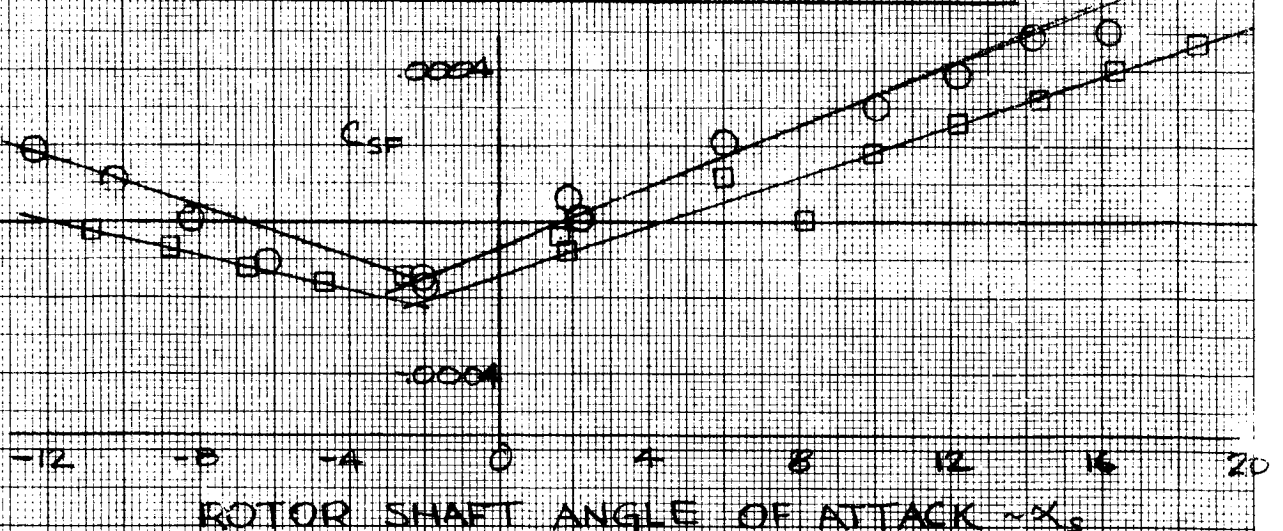
ROTOR NORMAL FORCE COEFFICIENT



ROTOR PITCHING MOMENT COEFFICIENT



ROTOR SIDE FORCE COEFFICIENT



ROTOR SHAFT ANGLE OF ATTACK α_0

Figure D7

ROTOR HUB TARES

CRUISE

TUNNEL SPEED = 113 FPS
 ROTOR SPEED USED
 FOR NONDIMENSIONAL
 COEFFICIENTS
 RIGHT ROTOR
 $S_c = 0^\circ$
 $L_w = 0^\circ$

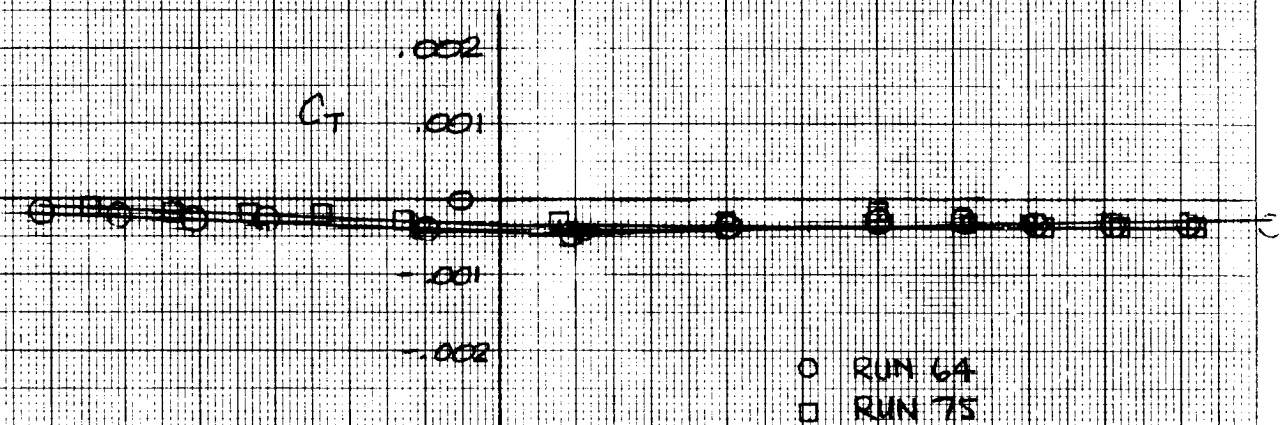
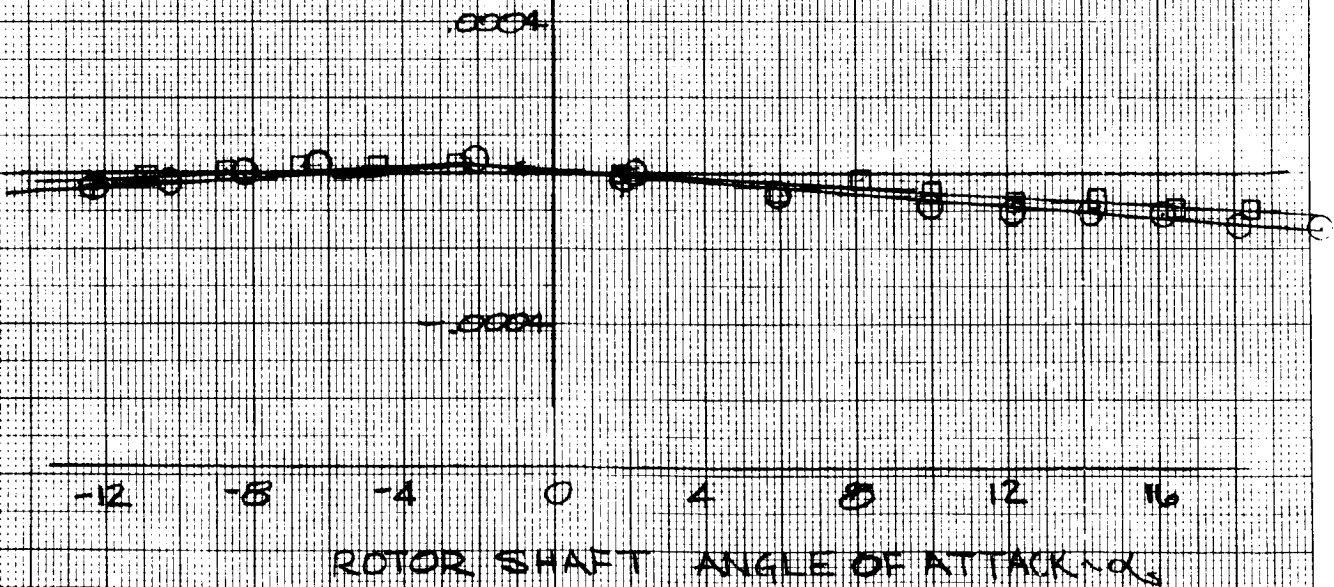
ROTOR THRUST COEFFICIENTROTOR YAWING MOMENT COEFFICIENT

Figure D8

APPENDIX E - RESULTS OF THE FLOW VISUALIZATION TESTS OF THE
1/4.622 SCALE MODEL 222 - BVWT 096

(Ref. Boeing Vertol IMO 8-7445-2-65,
dated April 24, 1972.)

This appendix is a reprint of a Boeing-Vertol interoffice memorandum that summarizes the flow visualization testing performed on a wooden pattern of the 1/4.622 Model 222. The reference number is IOM 8-7445-2-65, dated April 24 1972.

SUMMARY

A flow visualization test was conducted on the wooden pattern of the 1/4.622 scale Model 222 tilt rotor aircraft in the Boeing-Vertol wind tunnel on March 11, 1972. The model was installed, 12 flow visualization runs made and the model was removed in 12 hours.

Testing was conducted to examine the flow at the wing/fuselage junction and the tail and to develop filleting that would eliminate separation over the normal attitude range in cruise.

Final filleting with clay was done at seven degrees fuselage attitude to provide a minimum amount of separation. Seven degrees fuselage attitude results in a nine degree wing angle of attack which is the beginning of insipient wing stall. With this fillet a pressure survey was made at the tail with the fuselage attitude at zero degrees. Test data indicated a uniform velocity distribution laterally. The wing downwash was observed at approximately 2 inches above the horizontal tail plane. This confirms the prediction made using the methods presented in TR648 for the center of the wake and dynamic pressure loss in the wake. As a final check, yaw sweeps were performed to examine the flow at the wing/fuselage

junction and at the vertical stabilizer. This showed a small amount of rough flow on the fuselage and the vertical stabilizer at 15 degrees of yaw but not of major consequence.

Test Objectives

The objectives of this flow visualization test on the wooden pattern of 1/4.622 Froude scale Model 222 was to examine the flow at the wing/fuselage junction and provide filleting that will eliminate any potential separation up to insipient stall. Also to examine the downwash flow uniformity and dynamic pressure loss at the location of the horizontal tail. Testing was performed to accomplish each of these objectives.

Test Scope

Enclosure E-1 presents a detail run summary of this test, BVWT 096. The nomenclature used in the table is as follows:

q_{PSF} - Nominal tunnel dynamic pressure
 α°_{FUS} - Fuselage angle of attack
 ψ_{FUS} - Fuselage yaw angle (+ nose right)
Horiz. Tail - Horizontal tail on or off the model
Tuft Grid - Tuft grid at the tail
BLR - Boundary Layer Rake

Included is a description of the changes made to the model and any detail information relative to the position of the boundary layer rake. At the end of Enclosure E-1 is the definition of the probe positions in the boundary layer rake and the location relative to the horizontal stabilizer.

Model and Instrumentation

The model utilized in this test was the wooden pattern of the 1/4.622 Froude scale Model 222. The components were as follows:

Fuselage with sponsons and strakes

Horizontal tail

Vertical tail

Wing section

The wing section was a 6 foot span and did not include the nacelles for this test. The fuselage wing and tail were tufted to provide visualization of the flow and a tuft grid was installed at the aft end of the fuselage. A pressure rake was placed at the quarter chord of the horizontal tail to define the lateral and vertical pressure distribution.

Test Results

The flow visualization testing was performed using tufts attached to the fuselage, wing and tail to examine the characteristics of the flow. Enclosures E-2 through E-7 provide a summary of the key test runs by presenting a top and side view of the model indicating the areas of undesirable flow characteristics. Enclosure E-2, presenting the first run, shows that there is a large area of rough flow at the leading and trailing edges of the wing with the model at zero degrees angle of attack. Clay was added to build up these areas for Run 2. Flow was slightly improved and more clay was added for Run 3. Enclosure E-3 indicates that the fillets were adequate for zero degrees. The model was then pitched to 10° and as indicated

on Enclosure E-4 there is a large area of separated flow on the aft portion of the wing and fuselage. This attitude results in 12 degrees wing angle of attack and is well into the insipient stall regime. The attitude was reduced to 7° for Run 5 which is the beginning of insipient stall. Clay was added to reduce the separated regions at the leading and trailing edge and Run 6 was performed. Separation was reduced but more buildup was required. To facilitate testing, the fillets at the trailing edge of the wing were built up more on the right side than on the left to provide simultaneous testing of two different configurations. The leading edge was also built up and Run 7 was performed. Enclosure E-5 presents these results, indicating that the separation was almost completely eliminated at the leading edge and the trailing edge fillet on the right side eliminated the separation. This configuration of fillets provided acceptable flow.

An examination of yawed flight was then made at zero degrees fuselage attitude. Enclosures E-6 and E-7 present the 15° nose left and 15° nose right flight condition. There is a minimum amount of slightly rough flow on the leading edge of the vertical stabilizer and on the top of the fuselage at the beginning of the dorsal fin. This final fillet arrangement provided acceptable flow and will be included in the dynamic wind tunnel model.

Runs 8, 9 and 10 were the pressure surveys at 19.5, 50 and 77.5 percent of the tail semispan. A tabulation of the manometer board reading is presented in Enclosure E-8. Enclosure E-9 presents the variation of local dynamic pressure to tunnel free stream dynamic

pressure ratio ($\Delta P/q$) with height at the three semispan locations. There are two regions where a pressure loss occurs on the most in-board survey; the lower one being the separated flow generated by the model mount spilling off the end of the strake. The upper one is the wing wake and can be seen in the three surveys. The location and the dynamic pressure loss of the wing wake confirm the prediction made using the method presented in NACA TR648. The wing wake back in the region of the tail is 2.8 inches below the wing trailing edge and results in a dynamic pressure loss of 12% of the free stream q . It is significant to note that the flow distribution laterally is uniform. This can be seen in Enclosure E-10 which presents the data of Enclosure E-9 superimposed on an isometric drawing of the fuselage and horizontal tail.

RUN SUMMARY

BVWT-096

CONFIGURATION

	TYPE WT. OF TARE RUN	α_{FUS}	α_{TUF}	HORIZ. TAIL GRID	BLR	PHOTOS	DATE / TIME
1	TUFT	7.6	0°	ON	OUT	TOP SIDE	11 MAR
2	✓	✓	✓	✓	✓	✓	✓
3	✓	✓	✓	✓	✓	✓	✓
4	✓	✓	✓	✓	✓	✓	✓
5	✓	✓	+10°	OFF IN	✓	✓	✓
6	✓	✓	+7°	✓	✓	✓	✓
7	✓	✓	✓	✓	✓	✓	✓
8	✓	✓	0°	✓	IN	MANO-BOARD	✓
9	✓	✓	✓	✓	✓	✓	✓
10	✓	✓	✓	✓	✓	✓	✓

1) BASIC MODEL WITH TUFTS ; NO CLAY

2) BUILD-UP WITH ADDITIONAL CLAY AT L.E. & T.E. OF WING / FUSELAGE INTERSECTION

3) ADD MORE CLAY AS RUN 2

4) REMOVE HORIZ. TAIL, ADD TUFT GRID, MODEL TO $\alpha = +10^\circ$

5) MODEL TO $+7^\circ$

6) ADD MORE CLAY AS RUN 2 ; FAIR INTO VERT. FIN

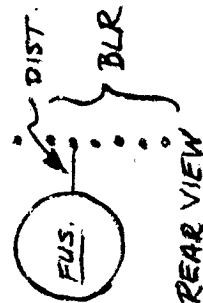
7) CROWN ON T.E. FILLET

8) BLR PROBE 1.5" FROM FUSELAGE ON HORIZ. STAB AXIS (FLOOR W.L. = 0.0")

BLR PROBE @ VERT. W.L. (PROBE #70) = 72.625" ; HORIZ. STAB. AXIS @ W.L. = 81.375"
L.E. PROBES @ 3/4 OF HORIZ. STAB.

9) BLR PROBE 8.0" FROM FUSELAGE

10) BLR PROBE 14.0" FROM FUSELAGE



RUN SUMMARY

RUN NO.	CONFIGURATION	TYPE WT. OF TARE RUN	PSF	TUFT	HORIZ TUFT	BLR	PHOTOS		DATE / TIME
							TOP	SIDE	
11	MODEL 222			TUFT - 7.6	0° - 15° CFF OUT	OUT	✓	✓	11 MAR
12	✓	✓	✓	✓	✓	✓	✓	✓	✓

- 1) BLR REMOVED, MODEL YAWED, NOSE LEFT -15°
- 2) MODEL YAWED, NOSE RIGHT +15°

BLR PROBE POSITIONS

PROBE NO	DIST. FROM PROBE No. 41	T/S W.L. ~ IN.	POS. N.
41	0	92.625	
42	1.00"	91.625	
43	1.80"	90.825	
44	2.80"	89.825	
45	3.60"	89.025	
46	4.80"	87.825	
47	6.00"	86.625	
48	7.00"	85.625	
49	8.00"	84.625	
50	9.00"	83.625	
51	10.00"	82.625	
52	11.00"	81.625	
53	12.00"	80.625	
54	16.00"	76.625	
55	18.00"	74.625	
56	20.00"	72.625	

BLR PROBES READ
MANOMETER FLUID
MERRIAM OIL - S.G. = .827
4.3 psf / IN. OIL

← HORIZ. STAB. AXIS @ W.L. = 81.375"

$$\alpha_f = 0^\circ$$

$$i_w = 2^\circ$$

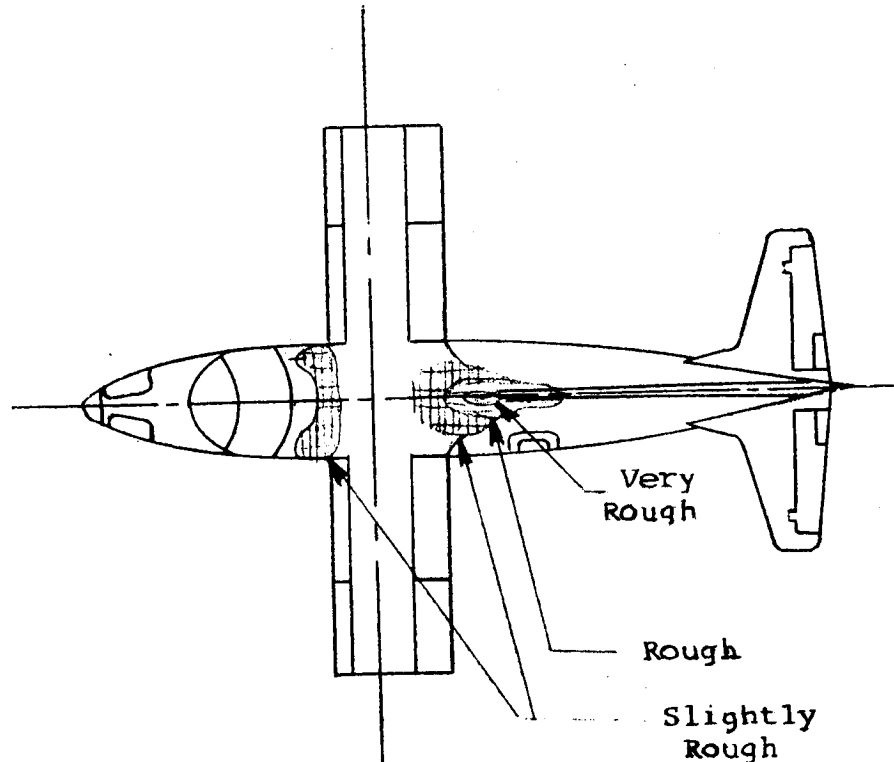
$$\psi = 2^\circ$$


Tunnel V=80 FPS

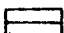
Enclosure E2

D222-10053-1

NO FAIRING




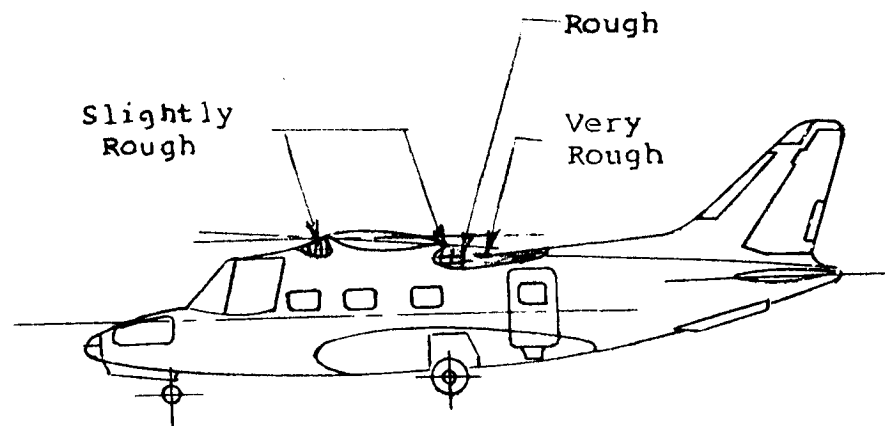
 Separated

 Intermittent Separation

 Very Rough

 Rough

 Slightly Rough



MODEL 222 INITIAL FLOW SURVEY AT 0° FUSELAGE ATTITUDE

RUN 3

$\alpha_f = 0^\circ$

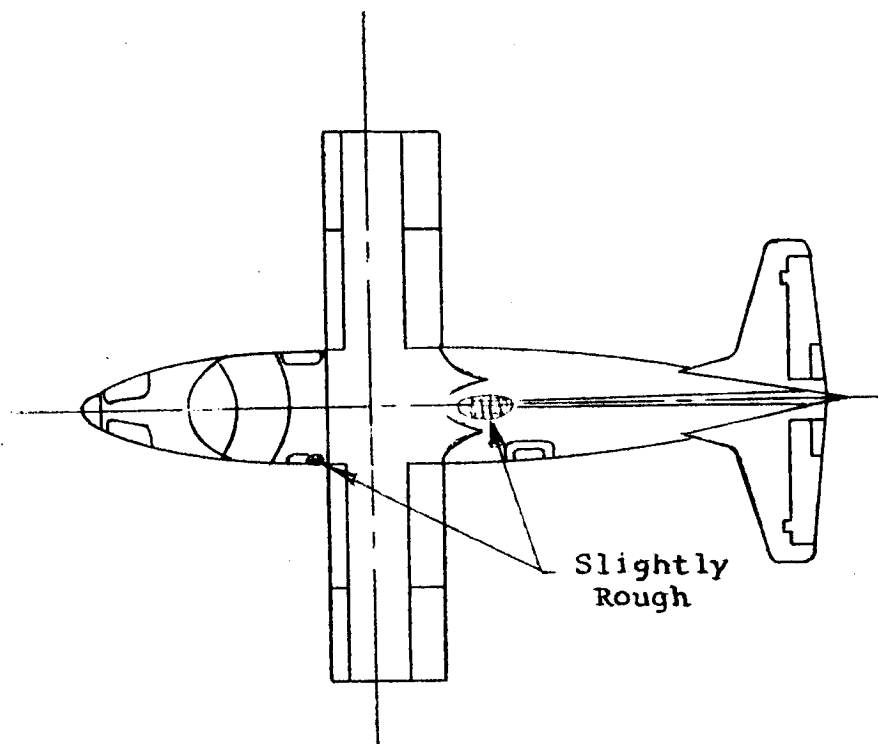
$i_w = 2^\circ$

$\psi = 0^\circ$

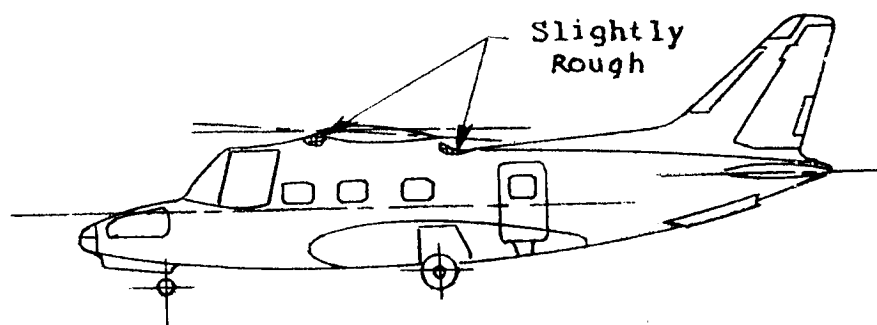
Tunnel V = 80 FPS

Enclosure E3

D222-10053-1



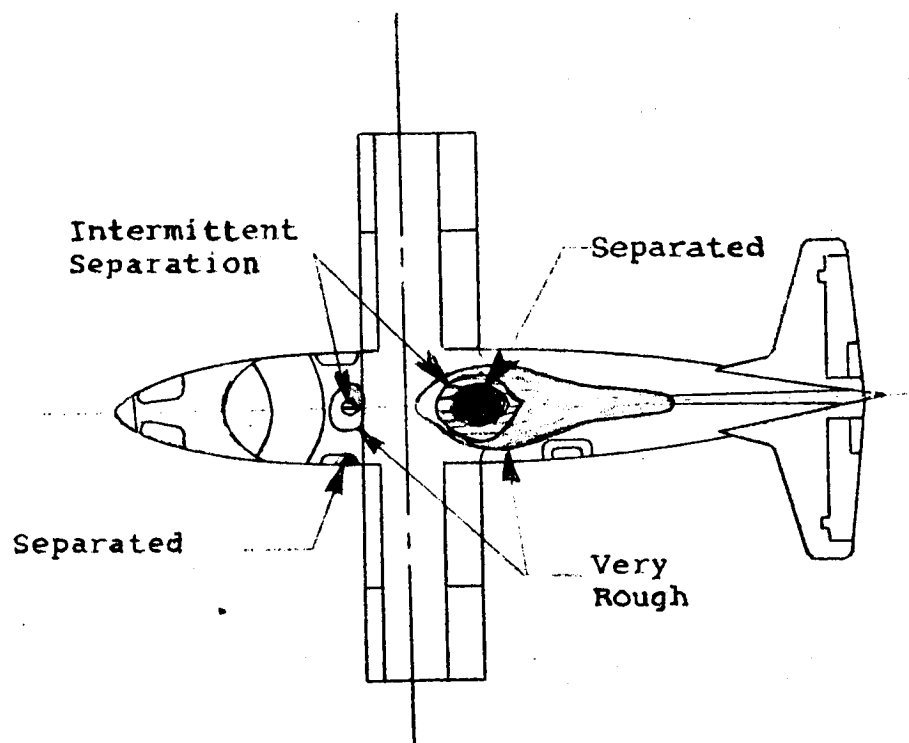
-  Separated
-  Intermittent Separation
-  Very Rough
-  Rough
-  Slightly Rough


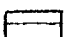

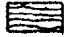



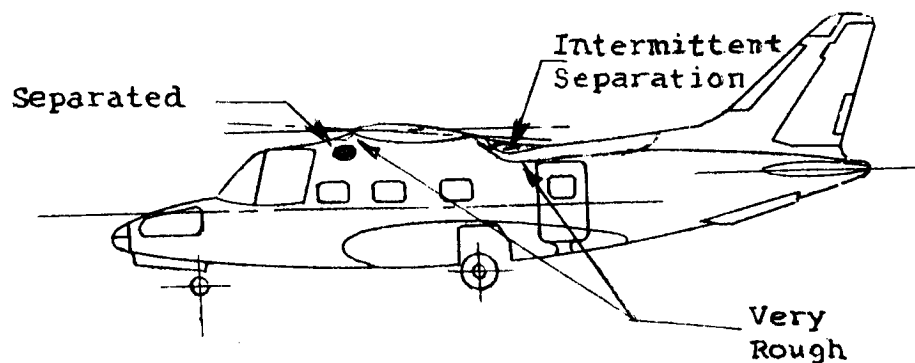
MODEL 222 FLOW SURVEY AT 10° FUSELAGE ATTITUDE
MODIFIED FILLET OF RUN 3

$\alpha_f = 10^\circ$ $i_w = 2^\circ$ $\psi = 0^\circ$

Tunnel V = 80 FPS



-  Separated
-  Intermittent Separation
-  Very Rough
-  Rough
-  Slightly Rough

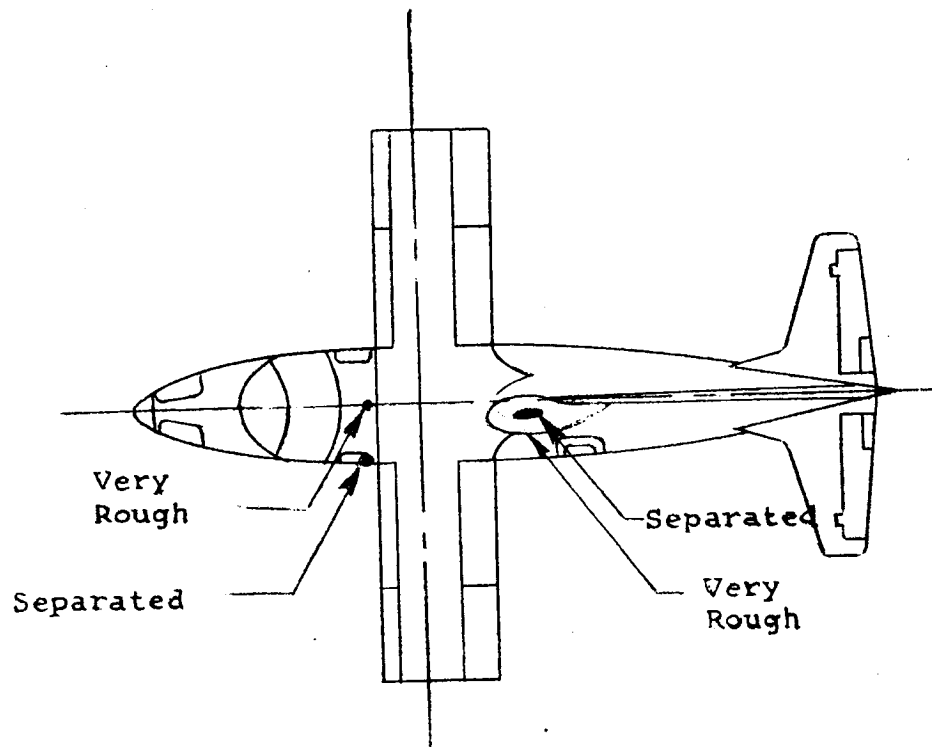



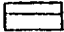
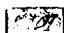
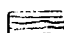
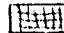
MODEL 222 FLOW SURVEY AT 10° FUSELAGE ATTITUDE
MODIFIED FILLET OF RUN 3

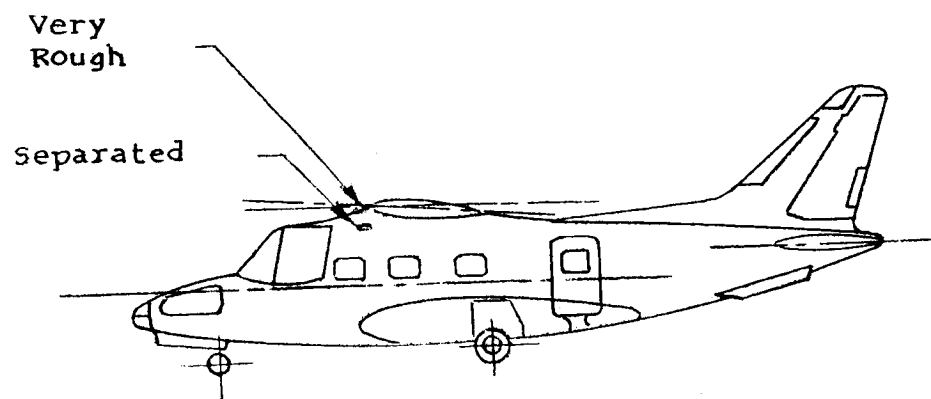
RUN 7
 $\alpha_f = 7^\circ$
 $i_w = 2^\circ$
 $\psi = 0^\circ$
 Tunnel V = 80 FPS

Enclosure E 5

D222-10053-1

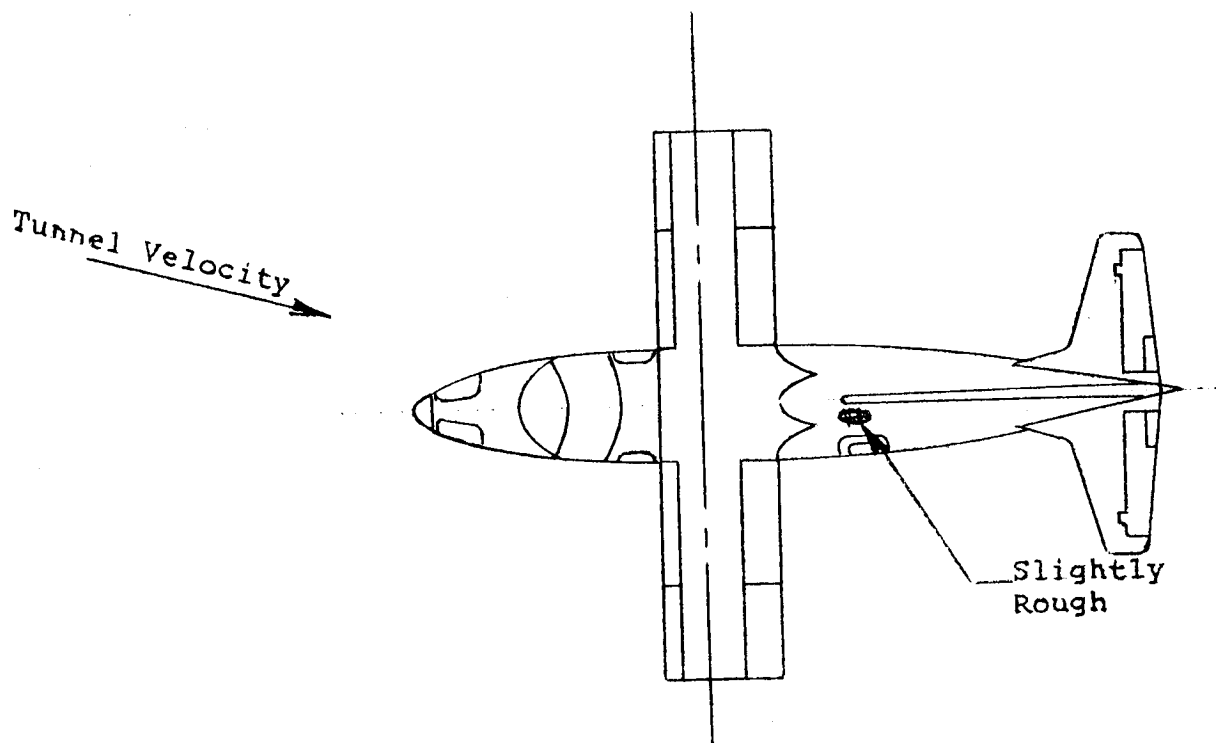



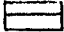

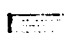
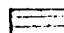
-  Separated
-  Intermittent Separation
-  Very Rough
-  Rough
-  Slightly Rough

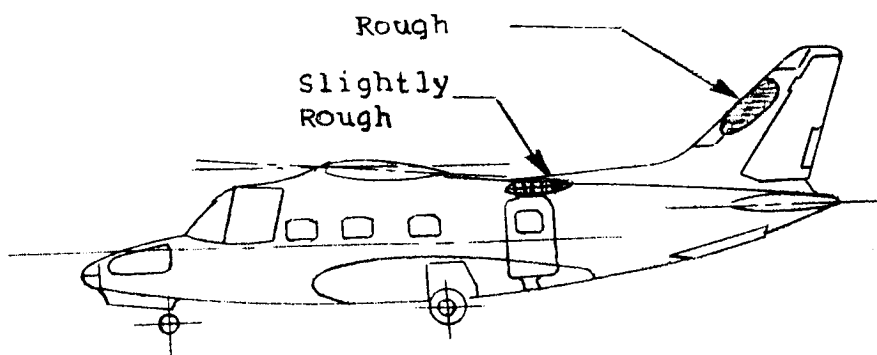


MODEL 222 FLOW SURVEY AT 7° FUSELAGE ATTITUDE
 FINAL FILLET MODIFICATION

RUN 11
NOSE LEFT
 $\alpha = 0^\circ$
 $i_w = 2^\circ$
 $\psi = -15^\circ$
Tunnel V=80 FPS

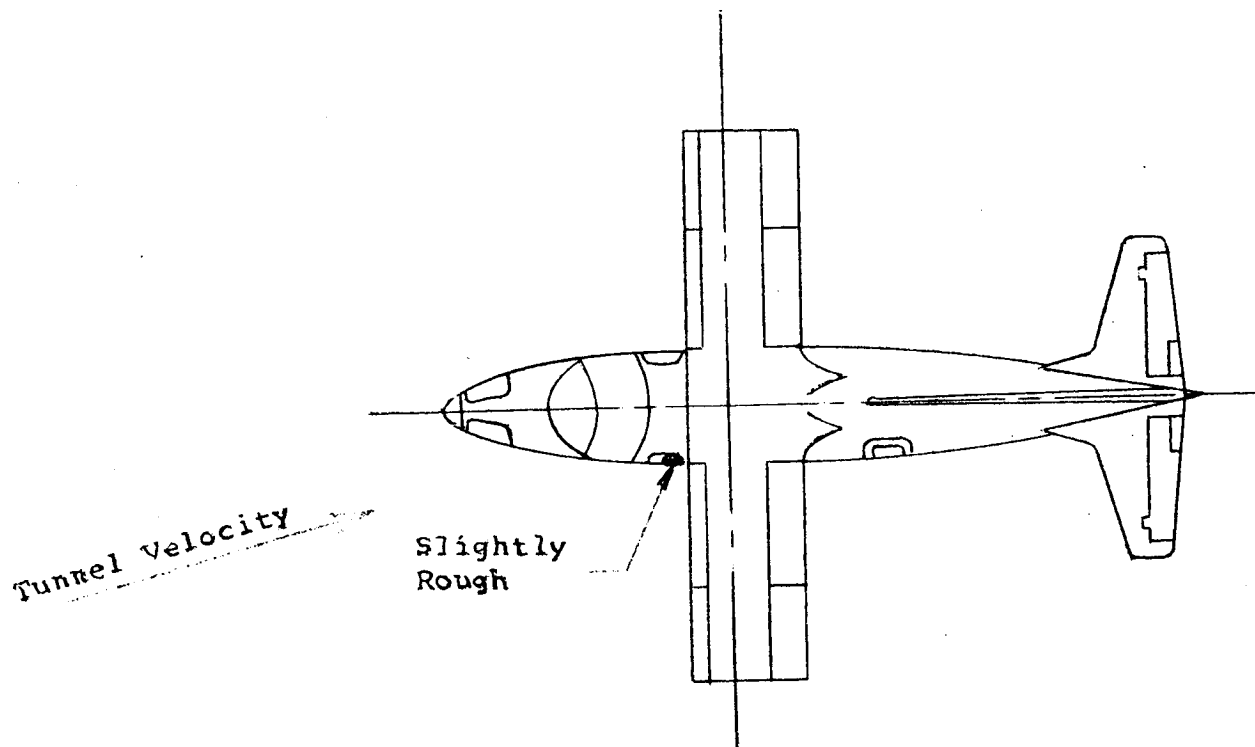



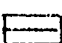
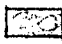
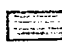
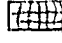
-  Separated
-  Intermittent Separation
-  Very Rough
-  Rough
-  Slightly Rough

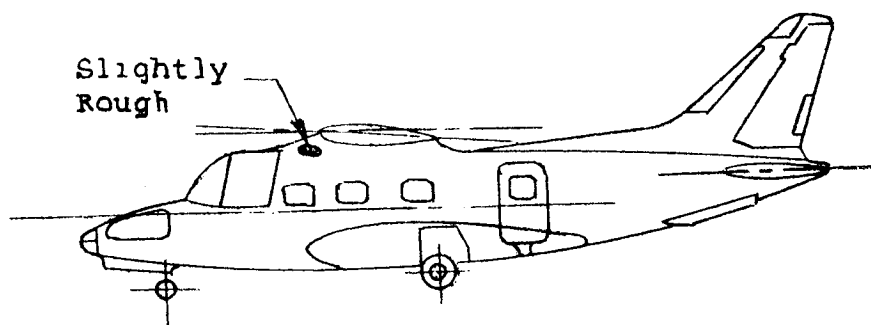


MODEL 222 FLOW SURVEY AT 0° FUSELAGE ATTITUDE
15° NOSE LEFT YAW
FILLET MODIFICATION

RUN 12
 NOSE RIGHT
 $\alpha_f = 0^\circ$
 $i_w = 2^\circ$
 $\psi = 15^\circ$
 Tunnel V = 80 FPS



-  Separated
-  Intermittent Separation
-  Very Rough
-  Rough
-  Slightly Rough



MODEL 222 FLOW SURVEY AT 0° FUSELAGE ATTITUDE
 15° NOSE RIGHT YAW
 FINAL FILLET MODIFICATION

BVWT 096 PRESSURE SURVEY AT TAIL

Enclosure E5
D222-10053-1

RUN 8			RUN 9			RUN 10		
PROBE IDENT	Δ INCHES OF FLUID	$\Delta P/q$	Δ INCHES OF FLUID	$\Delta P/q$		Δ INCHES OF FLUID	$\Delta P/q$	Δ HEIGHT ABOVE TAIL C/4
		$q = 9.6$		$q = 9.90$			$q = 9.90$	
TOTAL	2.25	1.00	2.30	1.00		2.30	1.00	
41	2.25	1.000	2.30	1.000		2.25	0.977	+11.25
46	2.25	1.000	2.30	1.000		2.20	0.956	+10.25
50	2.25	1.000	2.30	1.000		2.25	0.977	+9.45
55	2.25	1.000	2.25	0.977		2.20	0.956	+8.45
57	2.25	1.000	2.25	0.977		2.25	0.977	+7.55
59	2.25	1.000	2.25	0.977		2.20	0.956	+6.45
61	2.25	1.000	2.25	0.977		2.25	0.977	+5.25
62	2.25	1.000	2.25	0.977		2.15	0.935	+4.25
63	2.10	0.934	2.05	0.891		2.10	0.912	+3.25
64	2.0	0.889	2.0	0.869		1.95	0.847	+2.25
65	2.15	0.956	2.25	0.977		2.15	0.935	+1.25
66	2.2	0.977	2.30	1.000		2.20	0.956	+0.25
67	2.15	0.956	2.30	1.000		2.20	0.956	+0.75
68	1.65	0.733	2.30	1.000		2.20	0.956	-4.75
69	2.15	0.956	2.30	1.000		2.15	0.935	-6.75
70	2.20	0.977	2.30	1.000		2.25	0.977	-8.75
LOCATION OF BL R INCHES			8.0 IN OUT FROM A/C			14.0 IN OUT FROM A/C		
PERCENT OF TAIL SEMISPAN			.50 $bt/2$.75 $bt/2$		
1.5 IN OUT FROM A/C								
.195 $bt/2$								

MANOMETER FLUID - 4.3 PSF / IN
SURVEY MEASURED AT C/4 MAC OF
HORIZONTAL TAIL

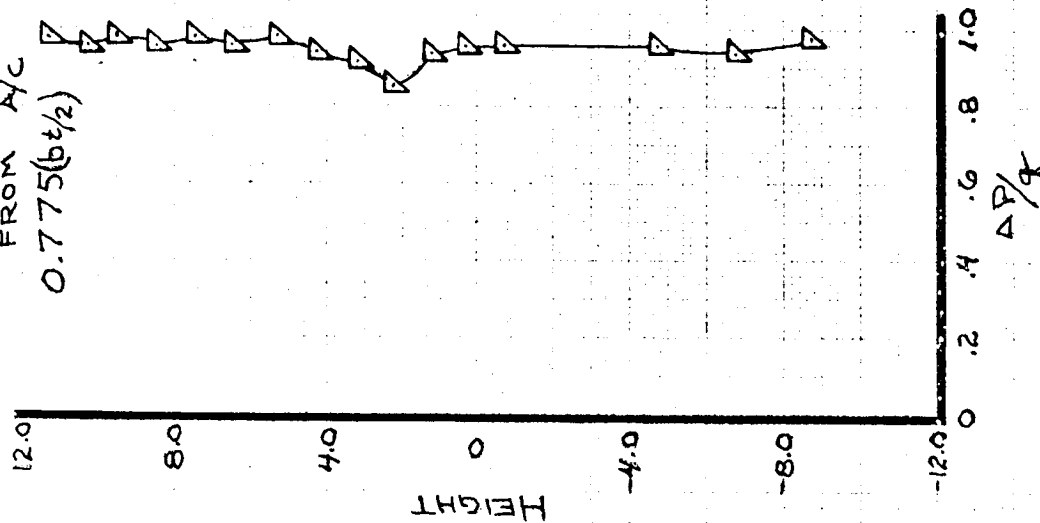
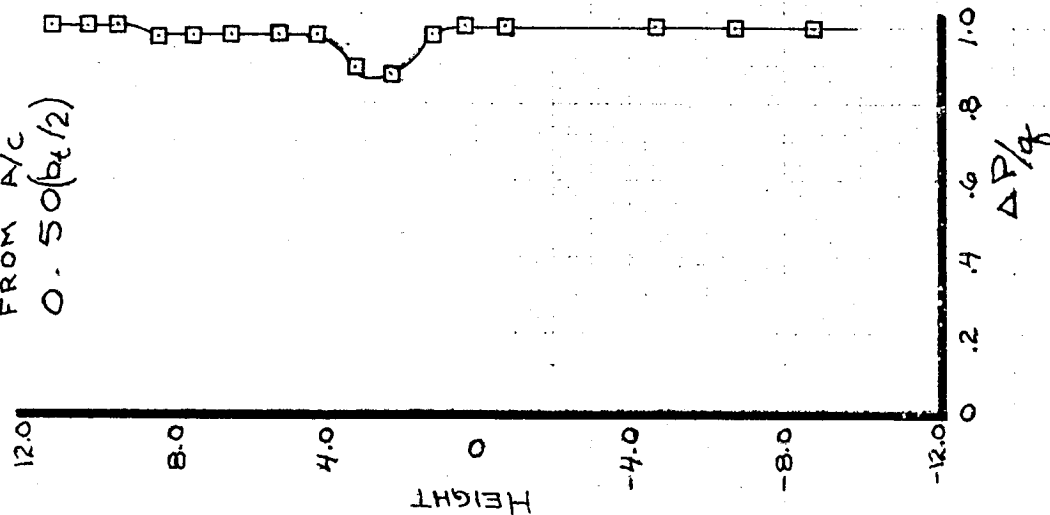
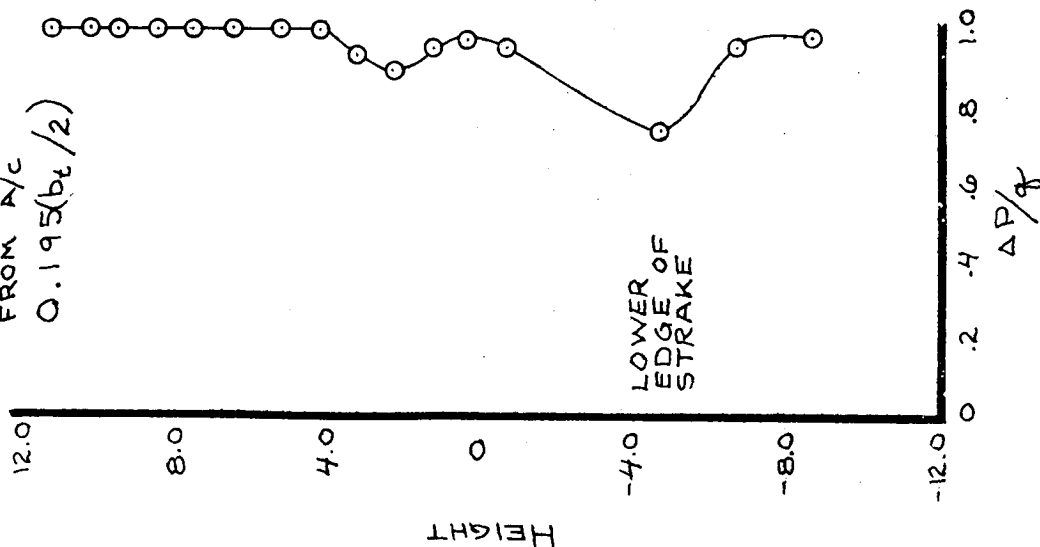
PRESSURE SURVEY AT TAIL PLANE

$\alpha_f = 0^\circ$ $\alpha_w = 2^\circ$

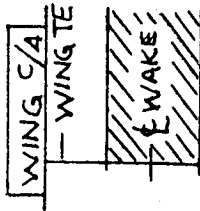
RUN 8
1.5 IN. OUT
FROM A/C
0.195($b_t/2$)

RUN 9
8.0 IN. OUT
FROM A/C
0.50($b_t/2$)

RUN 10
14.0 IN. OUT
FROM A/C
0.775($b_t/2$)



PREDICTION
OF WAKE
POSITION
PER TR 648



NOTE: SURVEY MEASURED
AT C/4 MAC FOR
HORIZ. TAIL

PRESSURE SURVEY
AT TAIL PLANE

$\alpha = 0^\circ$

$\alpha = 2^\circ$

$i_w = 1^\circ$

$\epsilon =$

HORIZONTAL PLANE

DOWNWASH

WING

